

ACTUACIONES

FUNDAMENTALS  
AERODYNAMICS



**FUNDAMENTALS  
OF  
AERODYNAMICS  
JOHN D. ANDERSON, JR.**



FUNDAMENTALS  
of  
AERODYNAMICS

# FUNDAMENTALS OF AERODYNAMICS/ANDERSON

# SO FM McGRAW-HILL



## FUNDAMENTALS AERODYNAMICS JOHN D. ANDERSON

INTRODUCTORY COMPRESSIBLE FLOW: With Historical Perspective  
**John D. Anderson, Jr.**, University of Maryland  
480 pages, (0-07-001654-2)

A clearly written book includes full treatment of such modern topics as computational fluid dynamics, high temperature flows, and time invariant technique, which has revolutionized the analysis of mixed sonic-supersonic flows. It also covers the classical material—starting with fundamental governing equations of inviscid fluid dynamics, and using these equations in the study of normal and oblique shock motion and conical flows. Throughout, special historical sections and near the related technical material give students a unique historical perspective on the field.

INTRODUCTION TO FLIGHT: Its Engineering and History  
**John D. Anderson, Jr.**, University of Maryland  
432 pages, (0-07-001637-2)

is a comprehensive introduction to aerospace engineering from a technological and an historical point of view. Topics covered include low speed and high speed aerodynamics; the evolution of wind tunnels; airplane performance; stability and control; supercritical flows; astronautics and propulsion; and the development of the first solid rocket engines. Both SI and U.S. Customary units are used, enabling readers to become proficient in both systems.

SUPERFLUID FLUID MECHANICS  
**Walter R. Nelson**, University of Notre Dame  
(available Fall, 1984), (0-07-046218-6)  
Designed for courses in flight mechanics, flight dynamics, or stability and control, this book includes interesting discussions of developments in the history of flight mechanics, numerous problems and exercises, review material on aerodynamics, automatic control theory and ordinary differential equations.

McGraw-Hill Book Company  
Publishers of the *Need for Knowledge*®  
1221 Avenue of the Americas  
New York 10020

**FUNDAMENTALS  
OF  
AERODYNAMICS**

## ABOUT THE AUTHOR

and enjoyable  
chum of  
no prior  
ics in general or  
The author  
d informal style  
immediately  
llenging field of  
necessary elements  
or calculus  
Chapters 1  
l, incompressible  
cover inviscid,  
Chapters 15 and  
ome basic

*tional fluid*  
within various  
of the  
matics. With the  
fluid dynamics  
dynamics,  
ment and pure  
ly indispensable  
ists. Thus, such  
vortex panel  
characteristics,  
solutions are  
s they naturally

w acquaints  
aspects of the  
the flight  
readers to an  
applications to  
nle,  
planetary entry

resting  
such topics as  
lation theory of  
rounded the  
peed  
inence of  
Kutta,

**John D. Anderson, Jr.** has published more than seventy articles in the areas of high temperature gasdynamics, applied aerodynamics, computational fluid dynamics, and hypersonic aerodynamics. He is also the author of *Introduction to Flight: Its Engineering and History* (1978), *Modern Compressible Flow: With Historical Perspective* (1982), and *Gasdynamic Lasers, An Introduction* (1976).

From 1966 to 1973, Dr. Anderson was Chief of the Hypersonics Group, Aerophysics Division, at the U.S. Naval Ordnance Laboratory in Maryland. From 1973 to 1980, he served as Chairman of the Department of Aerospace Engineering of the University of Maryland at College Park; and since 1980 he has pursued his teaching and research there full time as Professor of Aerospace Engineering.

John D. Anderson, Jr. is a member of the American Physical Society and the American Society for Engineering Education. He is an Associate Fellow of the American Institute of Aeronautics and Astronautics. In 1975 he was chosen as an Outstanding Educator of America and won the Engineering Sciences Award of the Washington Academy of Sciences. He has been designated by the University of Maryland as a Distinguished Scholar/Teacher. Dr. Anderson received his Ph.D. in Aeronautical and Astronautical Engineering from Ohio State University.

Here is an understandable and enjoyable treatment of the entire spectrum of aerodynamics. It assumes no prior knowledge of fluid dynamics in general or aerodynamics in particular. The author writes in a clear, direct, and informal style that speaks to readers and immediately arouses interest in the challenging field of aerodynamics.

A compact review of the necessary elements of vector algebra and vector calculus appears early in the book. Chapters 1 through 6 deal with inviscid, incompressible flow; chapters 7 through 14 cover inviscid, compressible flow; and in chapters 15 and 16, the author introduces some basic elements of viscous flow.

An introduction to computational fluid dynamics is incorporated within various chapters as an integral part of the beginning study of aerodynamics. With the emergence of computational fluid dynamics as a third dimension in aerodynamics, complimenting pure experiment and pure theory, this material is really indispensable to prospective aerodynamicists. Thus, such subjects as the source and vortex panel techniques, the method of characteristics, and explicit finite-difference solutions are introduced and discussed as they naturally arise.

A chapter on hypersonic flow acquaints readers with some specific aspects of the extreme high-speed end of the flight spectrum. It also introduces readers to an area with important current applications to the design of the space shuttle, hypervelocity missiles, and planetary entry vehicles.

Many chapters end with interesting historical notes that discuss such topics as the development of the circulation theory of lift, the excitement which surrounded the early development of high-speed aerodynamics, and the importance of Bernoulli, Euler, d'Alembert, Kutta,

**John D.**  
more than  
high tem-  
perature  
aerodyna-  
mics.  
He is also  
*Flight: Its  
Modern C-  
Perspectiv-  
An Introd.*

From 1961  
of the Hy-  
Division, C-  
Laborator  
1980, he s-  
Departme  
the Univer  
and since  
and respec-  
Aerospac

John D. An-  
American I  
American S  
Education, I  
American I  
Astronautic  
Outstanding  
the Enginee  
Washington  
been design  
Maryland a  
Teacher, Dr  
Aeronautics  
from Ohio

## ALSO FROM McGRAW-HILL

MODERN COMPRESSIBLE FLOW: With Historical Perspective  
**John D. Anderson, Jr.**, University of Maryland  
1982, 480 pages, (0-07-001654-2)

This clearly written book includes full treatment of such modern topics as computational fluid dynamics, high temperature flows, and time dependent technique, which has revolutionized the analysis of mixed subsonic-supersonic flows. It also covers the classical material—starting with fundamental governing equations of inviscid fluid dynamics, and then using these equations in the study of normal and oblique shock wave motion and conical flows. Throughout, special historical sections placed near the related technical material give students a unique historical perspective on the field.

INTRODUCTION TO FLIGHT: Its Engineering and History  
**John D. Anderson, Jr.**, University of Maryland  
1978, 432 pages, (0-07-001637-2)

Here is a comprehensive introduction to aerospace engineering from both a technological and an historical point of view. Topics covered include low speed and high speed aerodynamics; the evolution of wind tunnels; airplane performance; stability and control; supercritical airfoils; astronautics and propulsion; and the development of the first jet and rocket engines. Both SI and U.S. Customary units are used, enabling readers to become proficient in both systems.

ATMOSPHERIC FLIGHT MECHANICS  
**Robert Nelson**, University of Notre Dame  
1985 (available Fall, 1984), (0-07-046218-6)

Designed for courses in flight mechanics, flight dynamics, or stability and control, this book includes interesting discussions of developments in the history of flight mechanics, numerous problems and exercises, and review material on aerodynamics, automatic control theory and ordinary differential equations.

McGraw-Hill Book Company  
Serving the Need for Knowledge®  
1221 Avenue of the Americas  
New York, New York 10020

ISBN 0-07-001656-9

---

# FUNDAMENTALS OF AERODYNAMICS

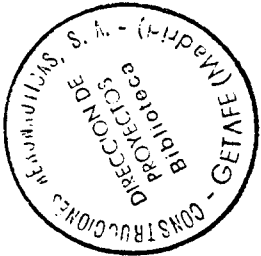
---

**John D. Anderson, Jr.**  
*Professor of Aerospace Engineering  
University of Maryland*

**McGraw-Hill Book Company**

New York St. Louis San Francisco Auckland Bogotá Hamburg  
Johannesburg London Madrid Mexico Montreal New Delhi  
Panama Paris São Paulo Singapore Sydney Tokyo Toronto

## CONTENTS



ix

### Preface

### Chapter 1 Aerodynamics: Some Introductory Thoughts

1.1	Importance of Aerodynamics: Historical Examples	1
1.2	Aerodynamics: Classification and Practical Objectives	7
1.3	Road Map for This Chapter	10
1.4	Some Fundamental Aerodynamic Variables	10
1.5	Aerodynamic Forces and Moments	12
1.6	Center of Pressure	19
1.7	Dimensional Analysis: The Buckingham Pi Theorem	21
1.8	Flow Similarity	27
1.9	Fluid Statics: Buoyancy Force	29
1.10	Types of Flow	34
1.11	Historical Note: The Illusive Center of Pressure	40
1.12	Summary Problems	43

### Chapter 2 Aerodynamics: Some Fundamental Principles and Equations

2.1	Introduction and Road Map	47
2.2	Review of Vector Relations	48
2.3	Models of the Fluid: Control Volumes and Fluid Elements	60
2.4	Continuity Equation	63
2.5	Momentum Equation	68
2.6	An Application of the Momentum Equation: Drag of a Two-Dimensional Body	73
2.7	Energy Equation	78
2.8	Interim Summary	83
2.9	Substantial Derivative	83
2.10	Fundamental Equations in Terms of the Substantial Derivative Pathlines and Streamlines of a Flow	86
2.11	Angular Velocity, Vorticity, and Strain	88
2.12	Angular Velocity, Vorticity, and Strain	92

This book was set in Times Roman by Beacon Graphics Corporation.

The editor was Susan Hazlett;

the production supervisor was Phil Galea.

The drawings were done by J & R Services, Inc.

The cover was designed by James Handloser.

Halliday Lithograph Corporation was printer and binder.

### FUNDAMENTALS OF AERODYNAMICS

Copyright © 1984 by McGraw-Hill, Inc. All rights reserved. Printed in the United States of America. Except as permitted under the United States Copyright Act of 1976, no part of this publication may be reproduced or distributed in any form or by any means, or stored in a data base or retrieval system, without the prior written permission of the publisher.

1234567890H A L H A L 89876543

ISBN 0-07-001656-7

Library of Congress Cataloging in Publication Data

Anderson, John David.

Fundamentals of aerodynamics.

Includes bibliographical references and index.

1. Aerodynamics. I. Title.

TL570.A677 1984 629.132'3 83-12031

ISBN 0-07-001656-9

iii

<p><b>Chapter 1</b></p> <p>1.1 Circulation 1.2 Stream Function 1.3 Velocity Potential 1.4 Relationship between the Stream Function and Velocity Potential 1.5 Summary Problems</p> <p>98 101 105 106 107</p>	<p>1.6 Incompressible Flow over Finite Wings 1.7 Problems</p> <p>226 228</p>	<p>1.8 CONTENTS v</p>
<p><b>Chapter 2</b></p> <p>2.1 Introduction and Road Map 2.2 Bernoulli's Equation 2.3 Incompressible Flow in a Duct: The Venturi and Low-Speed Wind Tunnel 2.4 Pitot Tube: Measurement of Airspeed 2.5 Pressure Coefficient 2.6 Condition on Velocity for Incompressible Flow 2.7 Governing Equation for Irrotational, Incompressible Flow: Laplace's Equation 2.8 Interim Summary 2.9 Uniform Flow: Our First Elementary Flow 2.10 Source Flow: Our Second Elementary Flow 2.11 Combination of a Uniform Flow with a Source and Sink 2.12 Doublet Flow: Our Third Elementary Flow 2.13 Nonlifting Flow over a Circular Cylinder 2.14 Vortex Flow: Our Fourth Elementary Flow 2.15 Lifting Flow over a Cylinder 2.16 The Kutta-Joukowski Theorem and the Generation of Lift 2.17 Nonlifting Flows over Arbitrary Bodies: The Numerical Source Panel Method 2.18 Historical Note: Bernoulli and Euler — The Origins of Theoretical Fluid Dynamics 2.19 Historical Note: d'Alembert and His Paradox 2.20 Summary Problems</p> <p>111 112 114 118 126 129 130 131 135 135 138 142 145 147 152 155 164 166 176 180 181 184 186 186 187 190</p>	<p>2.12 Incompressible Flow 2.13 Problems</p> <p>229 229</p>	
<p><b>Chapter 3</b></p> <p>3.1 Fundamentals of Inviscid, Incompressible Flow 3.2 Introduction and Road Map 3.3 Bernoulli's Equation 3.4 Incompressible Flow in a Duct: The Venturi and Low-Speed Wind Tunnel 3.5 Pitot Tube: Measurement of Airspeed 3.6 Condition on Velocity for Incompressible Flow 3.7 Governing Equation for Irrotational, Incompressible Flow: Laplace's Equation 3.8 Interim Summary 3.9 Uniform Flow: Our First Elementary Flow 3.10 Source Flow: Our Second Elementary Flow 3.11 Combination of a Uniform Flow with a Source and Sink 3.12 Doublet Flow: Our Third Elementary Flow 3.13 Nonlifting Flow over a Circular Cylinder 3.14 Vortex Flow: Our Fourth Elementary Flow 3.15 Lifting Flow over a Cylinder 3.16 The Kutta-Joukowski Theorem and the Generation of Lift 3.17 Nonlifting Flows over Arbitrary Bodies: The Numerical Source Panel Method 3.18 Historical Note: Bernoulli and Euler — The Origins of Theoretical Fluid Dynamics 3.19 Historical Note: d'Alembert and His Paradox 3.20 Summary Problems</p> <p>111 112 114 118 126 129 130 131 135 135 138 142 145 147 152 155 164 166 176 180 181 184 186 186 187 190</p>	<p>3.12 Incompressible Flow 3.13 Problems</p> <p>229 229</p>	
<p><b>Chapter 4</b></p> <p>4.1 Incompressible Flow over Airfoils 4.2 Airfoil Nomenclature 4.3 Airfoil Characteristics 4.4 Philosophy of Theoretical Solutions for Low-Speed Flow over Airfoils: The Vortex Sheet 4.5 The Kutta Condition 4.6 Kelvin's Circulation Theorem and the Starting Vortex 4.7 Classical Thin Airfoil Theory: The Symmetric Airfoil 4.8 The Cambered Airfoil 4.9 Lifting Flows over Arbitrary Bodies: The Vortex Panel Numerical Method 4.10 Modern Low-Speed Airfoils 4.11 Historical Note: Kutta, Joukowski, and the Circulation Theory of Lift</p> <p>194 198 202 204 212 217 222</p>	<p>4.12 Incompressible Flow 4.13 Problems</p> <p>229 229</p>	
<p><b>Chapter 5</b></p> <p>5.1 Introduction: Downwash and Induced Drag 5.2 The Vortex Filament, the Biot-Savart Law, and Helmholtz's Vortex Theorems 5.3 Prandtl's Classical Lifting-Line Theory 5.4 A Numerical Nonlinear Lifting-Line Method 5.5 Lifting-Surface Theory; Vortex Lattice Numerical Method 5.6 Historical Note: Lanchester and Prandtl — The Early Development of Finite-Wing Theory 5.7 Historical Note: Prandtl — The Man 5.8 Summary Problems</p> <p>234 237 258 261 267 270 273 275</p>	<p>5.12 Incompressible Flow 5.13 Problems</p> <p>229 229</p>	
<p><b>Chapter 6</b></p> <p>6.1 Introduction 6.2 Three-Dimensional Source 6.3 Three-Dimensional Doublet 6.4 Flow over a Sphere 6.5 General Three-Dimensional Flows: Panel Techniques 6.6 Summary Problems</p> <p>276 276 277 279 280 283 285 286</p>	<p>6.12 Incompressible Flow 6.13 Problems</p> <p>229 229</p>	
<p><b>Chapter 7</b></p> <p>7.1 Compressible Flow: Some Preliminary Aspects 7.2 Introduction 7.3 A Brief Review of Thermodynamics 7.4 Definition of Compressibility 7.5 Governing Equations for Inviscid, Compressible Flow 7.6 Definition of Total (Stagnation) Conditions 7.7 Some Aspects of Supersonic Flow: Shock Waves 7.8 Summary Problems</p> <p>287 287 289 297 299 301 305 308 311</p>	<p>7.12 Compressible Flow 7.13 Problems</p> <p>229 229</p>	
<p><b>Chapter 8</b></p> <p>8.1 Normal Shock Waves and Related Topics 8.2 Introduction 8.3 The Basic Normal Shock Equations 8.4 Speed of Sound 8.5 Special Forms of the Energy Equation 8.6 When Is a Flow Compressible? 8.7 Calculation of Normal Shock-wave Properties 8.8 Measurement of Velocity in a Compressible Flow 8.9 Summary Problems</p> <p>313 313 315 318 323 328 329 336 339</p>	<p>8.12 Normal Shock Waves 8.13 Problems</p> <p>229 229</p>	

<b>Chapter 9</b>	OblIQUE SHOCK AND EXPANSION WAVES	
9.1	Introduction	343
9.2	OblIQUE Shock Relations	343
9.3	Supersonic Flow over Wedges and Cones	347
9.4	Shock Interactions and Reflections	357
9.5	Detached Shock Wave in Front of a Blunt Body	359
9.6	Prandtl-Meyer Expansion Waves	362
9.7	Shock-Expansion Theory: Applications to Supersonic Airfoils	364
9.8	Historical Note: Ernst Mach—A Biographical Sketch	370
9.9	Summary	372
	Problems	374
		375

<b>Chapter 10</b>	COMPRESSIBLE FLOW THROUGH NOZZLES, DIFFUSERS, AND WIND TUNNELS	
10.1	Introduction	377
10.2	Governing Equations for Quasi-One-Dimensional Flow	377
10.3	Nozzle Flows	378
10.4	Diffusers	387
10.5	Supersonic Wind Tunnels	397
10.6	Summary	399
	Problems	404
		405

<b>Chapter 11</b>	SUBSONIC COMPRESSIBLE FLOW OVER AIRFOILS: LINEAR THEORY	
11.1	Introduction	407
11.2	The Velocity Potential Equation	407
11.3	The Linearized Velocity Potential Equation	409
11.4	Prandtl-Glauert Compressibility Correction	412
11.5	Improved Compressibility Corrections	412
11.6	Critical Mach Number	421
11.7	Drag-Divergence Mach Number: The Sound Barrier	423
11.8	The Area Rule	427
11.9	The Supercritical Airfoil	428
11.10	Historical Note: High-Speed Airfoils—Early Research and Development	430
11.11	Historical Note: Richard T. Whitcomb—Architect of the Area Rule and the Supercritical Wing	433
11.12	Summary	437
	Problems	438
		440

<b>Chapter 12</b>	LINEARIZED SUPersonic FLOW	
12.1	Introduction	441
12.2	Derivation of the Linearized Supersonic Pressure Coefficient Formula	441
12.3	Application to Supersonic Airfoils	442
12.4	Summary	445
	Problems	448

<b>Chapter 9</b>	OBLIQUE SHOCK AND EXPANSION WAVES	
9.1	Introduction	343
9.2	OBLIQUE Shock Relations	343
9.3	Supersonic Flow over Wedges and Cones	347
9.4	Shock Interactions and Reflections	357
9.5	Detached Shock Wave in Front of a Blunt Body	359
9.6	Prandtl-Meyer Expansion Waves	362
9.7	Shock-Expansion Theory: Applications to Supersonic Airfoils	364
9.8	Historical Note: Ernst Mach—A Biographical Sketch	370
9.9	Summary	372
	Problems	374
		375

<b>Chapter 13</b>	INTRODUCTION TO NUMERICAL TECHNIQUES FOR NONLINEAR SUPERSONIC FLOW	
13.1	Introduction: Philosophy of Computational Fluid Dynamics	450
13.2	Elements of the Method of Characteristics	450
13.3	Supersonic Nozzle Design	452
13.4	Elements of Finite-Difference Methods	459
13.5	The Time-Dependent Technique: Application to Supersonic Blunt Bodies	462
13.6	Summary	477
	Problems	478
		479

<b>Chapter 14</b>	ELEMENTS OF HYPERSONIC FLOW	
14.1	Introduction	479
14.2	Qualitative Aspects of Hypersonic Flow	479
14.3	Newtonian Theory	483
	Problems	487
<b>Chapter 15</b>	INTRODUCTION TO THE FUNDAMENTAL PRINCIPLES AND EQUATIONS OF VISCOUS FLOW	
15.1	Introduction	488
15.2	Qualitative Aspects of Viscous Flow	488
15.3	Viscosity and Thermal Conduction	489
15.4	The Navier-Stokes Equations	496
15.5	The Viscous Flow Energy Equation	501
15.6	Similarity Parameters	504
15.7	Solutions of Viscous Flows	508
15.8	Summary	512
	Problems	514
		516
<b>Chapter 16</b>	INTRODUCTION TO BOUNDARY LAYERS	
16.1	Introduction	517
16.2	Boundary Layer Properties	517
16.3	The Boundary Layer Equations	519
16.4	Incompressible Flow over a Flat Plate: The Blasius Solution	525
16.5	Compressible Flow over a Flat Plate	528
16.6	Results for Turbulent Boundary Layers	534
16.7	Final Comments	538
16.8	Summary	540
	Problems	542

<b>Appendices</b>		
A	Isentropic Flow Properties	543
B	Normal Shock Properties	543
C	Prandtl-Meyer Function and Mach Angle	548
References		552
Index		554

## PREFACE

This book is for students—to be read, understood, and enjoyed. It is consciously written in a clear, informal, and direct style designed to *talk* to the reader and to gain his or her immediate interest in the challenging and yet beautiful discipline of aerodynamics. The explanation of each topic is carefully constructed to make sense to the reader. Moreover, the structure of each chapter is highly organized in order to keep the reader aware of where we are, where we were, and where we are going. Too frequently the student of aerodynamics loses sight of what is trying to be accomplished; to avoid this, we attempt to keep the reader informed of our intent at all times. For example, virtually each chapter contains a road map—a block diagram designed to keep the reader well aware of the proper flow of ideas and concepts. The use of such chapter road maps is one of the unique features of this book. Also, to help organize the reader's thoughts, there are special summary sections at the end of most chapters.

The material in this book is at the level of college juniors and seniors in aerospace or mechanical engineering. It assumes no prior knowledge of fluid dynamics in general, or aerodynamics in particular. It does assume a familiarity with differential and integral calculus, as well as the usual physics background common to most students of science and engineering. Also, the language of vector analysis is used liberally; a compact review of the necessary elements of vector algebra and vector calculus is given in Chap. 2 in such a fashion that it can either educate or refresh the reader, whichever may be the case for each individual.

This book is designed for a 1-year course in aerodynamics. Chapters 1 to 6 constitute a solid semester emphasizing inviscid, incompressible flow. Chapters 7 to 14 occupy a second semester dealing with inviscid, compressible flow. Finally, Chaps. 15 and 16 introduce some basic elements of viscous flow, mainly to serve as a contrast to and comparison with the inviscid flows treated throughout the bulk of the text. This book contains several unique features:

1. The use of chapter road maps to help organize the material in the mind of the reader, as discussed earlier.
2. An introduction to computational fluid dynamics as an integral part of the beginning study of aerodynamics. Computational fluid dynamics (CFD) has recently

become a third dimension in aerodynamics, complimenting the previously existing dimensions of pure experiment and pure theory. It is absolutely necessary that the modern student of aerodynamics be introduced to some of the basic ideas of CFD — he or she will most certainly come face to face with either its "machinery" or its results after entering the professional ranks of practicing aerodynamicists. Hence, such subjects as the source and vortex panel techniques, the method of characteristics, and explicit finite-difference solutions are introduced and discussed as they naturally arise during the course of our discussions. In particular, Chap. 13 is devoted exclusively to numerical techniques, couched at a level suitable to an introductory aerodynamics text.

3. A short chapter is devoted entirely to hypersonic flow. Although hypersonics is at one extreme end of the flight spectrum, it has current important applications to the design of the space shuttle, hypervelocity missiles, and planetary entry vehicles. Therefore, hypersonic flow deserves some attention in any modern presentation of aerodynamics. This is the purpose of Chap. 14.

4. Historical notes are placed at the end of many of the chapters. This follows in the tradition of the author's previous books, *Introduction to Flight: Its Engineering and History* (McGraw-Hill, 1978), and *Modern Compressible Flow: With Historical Perspective* (McGraw-Hill, 1982). Although aerodynamics is a rapidly evolving subject, its foundations are deeply rooted in the history of science and technology. It is important for the modern student of aerodynamics to have an appreciation for the historical origin of the tools of the trade. Therefore, this book addresses such questions as who were Bernoulli, Euler, d'Alembert, Kutta, Joukowski, and Prandtl; how was the circulation theory of lift developed; and what excitement surrounded the early development of high-speed aerodynamics? The author wishes to thank various members of the staff of the National Air and Space Museum of the Smithsonian Institution for opening their extensive files for some of the historical research behind these history sections. Also, a constant biographical reference was the *Dictionary of Scientific Biography*, edited by C. C. Gillespie, Charles Scribner's Sons, New York, 1980. This is a 16-volume set of books which is a valuable source of biographic information on the leading scientists in history.

Present book in both senior-level courses in incompressible and compressible flow. On the other hand, the present book is entirely self-contained; no prior familiarity with aerodynamics on the part of the reader is assumed. All basic principles and concepts are introduced and developed from their beginnings.

The author wishes to thank his students for many stimulating discussions on the subject of aerodynamics — discussions which ultimately resulted in the present book. Special thanks go to two of the author's graduate students, Tae-Hwan Cho and Kevin Bowcutt, who provided illustrative results from the source and vortex panel techniques. Of course, all of the author's efforts would have gone for naught if it had not been for the excellent preparation of the typed manuscript by Ms. Sue Osborn.

Finally, special thanks go to two institutions: (1) the University of Maryland for

providing a challenging intellectual atmosphere in which the author has basked for the past 9 years and (2) the Anderson household — Sarah-Allen, Katherine, and Elizabeth — who have been patient and understanding while their husband and father was in his ivory tower.

*John D. Anderson, Jr.*

This book has developed from the author's experience in teaching both incompressible and compressible flow to undergraduate students at the University of Maryland. Such courses require careful attention to the structure and sequence of the presentation of basic material, and to the manner in which sophisticated subjects are described to the uninitiated reader. This book meets the author's needs at Maryland; it is hoped that it will also meet the needs of others, both in the formal atmosphere of the classroom and in the informal pleasure of self-study.

Readers who are already familiar with the author's *Introduction to Flight* will find the present book to be a logical sequel. Many of the aerodynamic concepts first introduced in the most elementary sense in *Introduction to Flight* are revisited and greatly expanded in the present book. For example, at Maryland, *Introduction to Flight* is used in a sophomore-level introductory course, followed by the material of the

## AERODYNAMICS: SOME INTRODUCTORY THOUGHTS

*The term "aerodynamics" is generally used for problems arising from flight and other topics involving the flow of air.*

*Ludwig Prandtl, 1949*

*Aerodynamics: The dynamics of gases, especially of atmospheric interactions with moving objects.*

*The American Heritage  
Dictionary of the English  
Language, 1969*

### 1.1 IMPORTANCE OF AERODYNAMICS: HISTORICAL EXAMPLES

On August 8, 1588, the waters of the English Channel churned with the gyrations of hundreds of warships. The great Spanish Armada had arrived to carry out an invasion of Elizabethan England and was met head-on by the English fleet under the command of Sir Francis Drake. The Spanish ships were large and heavy; they were packed with soldiers and carried formidable cannons that fired 50-lb round shot that could devastate any ship of that era. In contrast, the English ships were smaller and lighter; they carried no soldiers and were armed with lighter, shorter-range cannons. The balance of power in Europe hinged on the outcome of this naval encounter. King Philip II of Catholic Spain was attempting to squash Protestant England's rising influence in the political and religious affairs of Europe; in turn, Queen Elizabeth I was attempting to defend the very existence of England as a sovereign state. In fact, on that crucial day in 1588, when the English floated six fire ships into the Spanish formation and then drove headlong into the ensuing confusion, the future history of Europe was in the balance. In the final outcome, the heavier, sluggish, Spanish ships were no match for the faster, more maneuverable, English craft, and by that evening the Spanish Armada lay in disarray, no longer a threat to England. This naval battle is of particular importance because it was the first in history to be fought by ships on both sides powered completely by sail.

(in contrast to earlier combinations of oars and sail) and it taught the world that political power was going to be synonymous with naval power. In turn, naval power was going to depend greatly on the speed and maneuverability of ships. To increase the speed of a ship, it is important to reduce the resistance created by the water flow around the ship's hull. Suddenly, the drag on ship hulls became an engineering problem of great interest, thus giving impetus to the study of fluid mechanics.

This impetus hit its stride almost a century later, when, in 1687, Isaac Newton (1642–1727) published his famous *Principia*, in which the entire second book was devoted to fluid mechanics. Newton encountered the same difficulty as others before him, namely, that the analysis of fluid flow is conceptually more difficult than the dynamics of solid bodies. A solid body is usually geometrically well defined, and its motion is therefore relatively easy to describe. On the other hand, a fluid is a "squishy" substance, and in Newton's time it was difficult to decide even how to qualitatively model its motion, let alone obtain quantitative relationships. Newton considered a fluid flow as a uniform, rectilinear stream of particles, much like a cloud of pellets from a shotgun blast. As sketched in Fig. 1.1, Newton assumed that upon striking a surface inclined at an angle  $\theta$  to the stream, the particles would transfer their normal momentum to the surface but their tangential momentum would be preserved. Hence, after collision with the surface, the particles would then move along the surface. This led to an expression for the hydrodynamic force on the surface which varies as  $\sin^2 \theta$ . This is Newton's famous sine-squared law (described in detail in Chap. 14). Although its accuracy left much to be desired, its simplicity led to wide application in naval architecture. Later, in 1777, a series of experiments were carried out by Jean Le Rond d'Alembert (1717–1783), under the support of the French government, in order to measure the resistance of ships in canals. The results showed that "the rule that for oblique planes resistance varies with the sine square of the angle of incidence holds good only for angles between 50 and 90 degrees and must be abandoned for lesser angles." Also, in 1781, Leonhard Euler (1707–1783) pointed out the physical inconsistency of Newton's model (Fig. 1.1) consisting of a rectilinear stream of particles impacting without warning on a surface. In contrast to this model, Euler noted that the fluid moving toward a body "before reaching the latter, bends its direction and its velocity so that

when it reaches ... body it flows past it along the surface, and exercises no other force on the body except the pressure corresponding to the single points of contact." Euler went on to present a formula for resistance which attempted to take into account the shear stress distribution along the surface, as well as the pressure distribution. This expression became proportional to  $\sin^2 \theta$  for large incidence angles, whereas it was proportional to  $\sin \theta$  at small incidence angles. Euler noted that such a variation was in reasonable agreement with the ship-hull experiments carried out by d'Alembert. This early work in fluid dynamics has now been superseded by modern concepts and techniques. (However, amazingly enough, Newton's sine-squared law has found new application in very high speed aerodynamics, to be discussed in Chap. 14.) The major point here is that the rapid rise in the importance of naval architecture after the sixteenth century made fluid dynamics an important science, occupying the minds of Newton, d'Alembert, and Euler, among many others. Today, the modern ideas of fluid dynamics, presented in this book, are still driven in part by the importance of reducing hull drag on ships.

Consider a second historical example. The scene shifts to Kill Devil Hills, 4 mi south of Kitty Hawk, North Carolina. It is summer of 1901, and Wilbur and Orville Wright are struggling with their second major glider design, the first being a stunning failure the previous year. The airfoil shape and wing design of their glider are based on aerodynamic data published in the 1890s by the great German aviation pioneer Otto Lilienthal (1848–1896) and by Samuel Pierpont Langley (1834–1906), secretary of the Smithsonian Institution—the most prestigious scientific position in the United States at that time. Because their first glider in 1900 produced no meaningful lift, the Wright brothers have increased the wing area from 165 to 290 ft<sup>2</sup> and have increased the wing camber (a measure of the airfoil curvature—the larger the camber, the more "arched" is the thin airfoil shape) by almost a factor of 2. But something is still wrong. In Wilbur's words, the glider's "lifting capacity seemed scarcely one-third of the calculated amount." Frustration sets in. The glider is not performing even close to their expectations, although it is designed on the basis of the best available aerodynamic data. On August 20, the Wright brothers dispairingly pack themselves aboard a train going back to Dayton, Ohio. On the ride back, Wilbur mutters that "nobody will fly for a thousand years." However, one of the hallmarks of the Wrights is perseverance, and within weeks of returning to Dayton, they decide on a complete departure from their previous approach. Wilbur later wrote that "having set out with absolute faith in the existing scientific data, we were driven to doubt one thing after another, until finally after two years of experiment, we cast it all aside, and decided to rely entirely upon our own investigations." Since their 1901 glider was of poor aerodynamic design, the Wrights set about determining what constitutes good aerodynamic design. In the fall of 1901, they design and build a 6-ft-long, 16-in square wind tunnel powered by a two-bladed fan connected to a gasoline engine. An original photograph of the Wrights' tunnel in their Dayton bicycle shop is shown in Fig. 1.2a. In this wind tunnel they test over 200 different wing and airfoil shapes, including flat plates, curved plates, rounded leading edges, rectangular and curved planforms, and various monoplane and multiplane configurations. A sample of their test models is shown in Fig. 1.2b. The aerodynamic data is taken logically and carefully. It shows a major departure from the existing "state-of-the-art" data. Armed with their new aerodynamic information, the

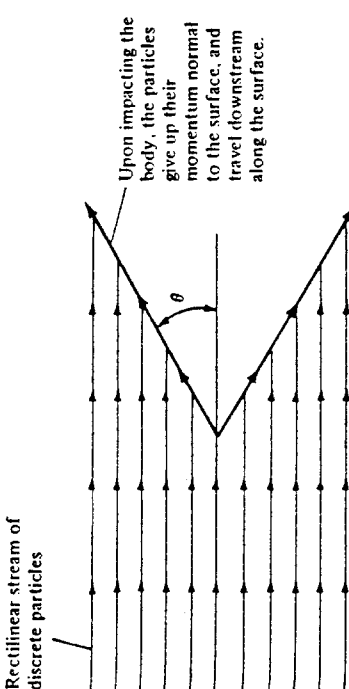


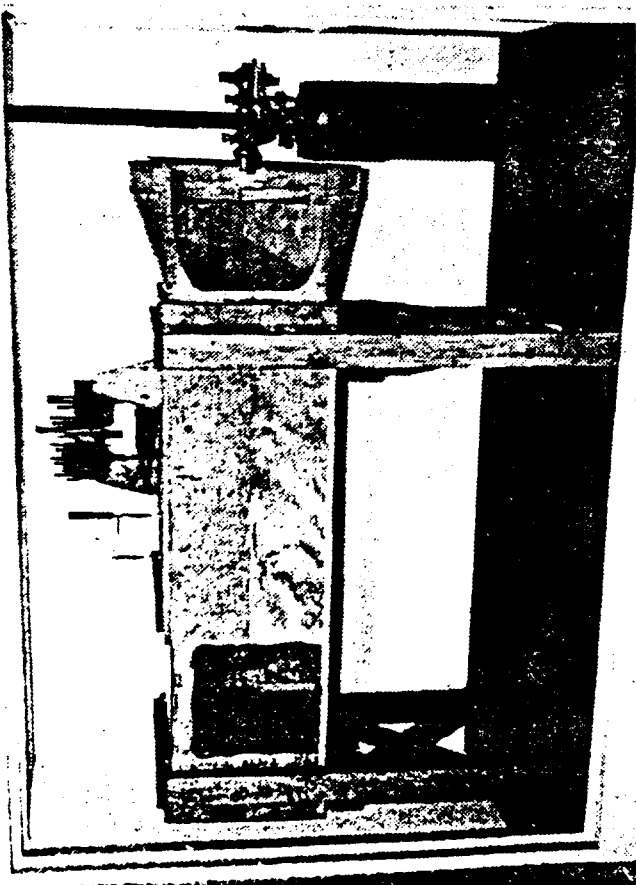
Figure 1.1 Isaac Newton's model of fluid flow in the year 1687. This model was widely adopted in the seventeenth and eighteenth centuries but was later found to be conceptually inaccurate for most fluid flows.

Wrights design a new glider in the spring of 1902. The airfoil is much more efficient; the camber is reduced considerably, and the location of the maximum rise of the airfoil is moved closer to the front of the wing. The most obvious change, however, is that the ratio of the length of the wing (wingspan) to the distance from the front to the rear of the airfoil (chord length) is increased from 3 to 6. The success of this glider during the summer and fall of 1902 is astounding; Orville and Wilbur accumulate over a thousand flights during this period. In contrast to the previous year, the Wrights return to Dayton flushed with success and devote all their subsequent efforts to powered flight. The rest is history.

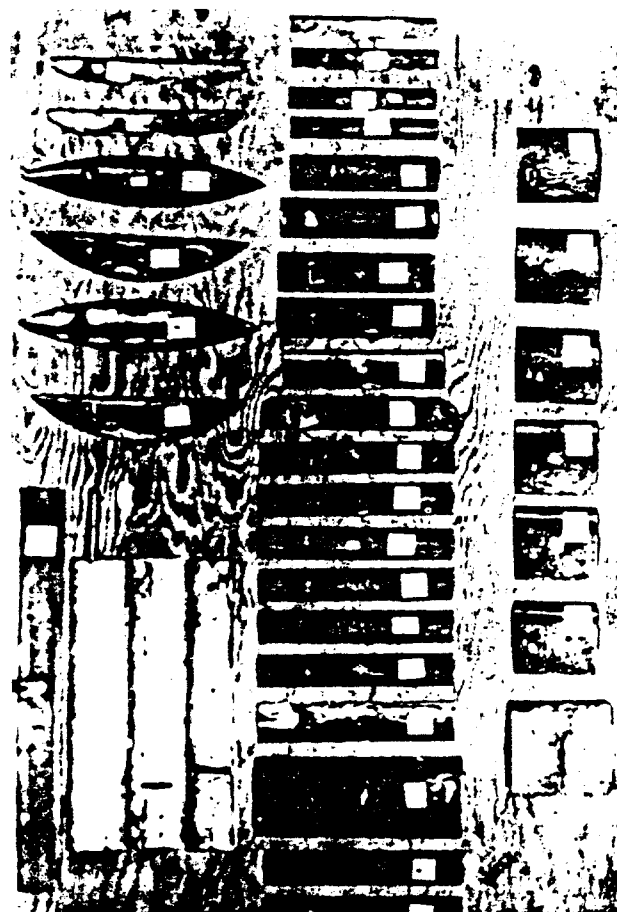
The major point here is that good aerodynamics was vital to the ultimate success of the Wright brothers and, of course, to all subsequent successful airplane designs up to the present day. The importance of aerodynamics to successful manned flight goes without saying, and a major thrust of this book is to present the aerodynamic fundamentals that govern such flight.

Consider a third historical example of the importance of aerodynamics, this time as it relates to rockets and space flight. High-speed, supersonic flight had become a dominant feature of aerodynamics by the end of World War II. By this time, aerodynamicists appreciated the advantages of using slender, pointed body shapes to reduce the drag of supersonic vehicles. The more pointed and slender the body, the weaker the shock wave attached to the nose, and hence the smaller the wave drag. Consequently, the German V-2 rocket used during the last stages of World War II had a pointed nose, and all short-range rocket vehicles flown during the next decade followed suit. Then, in 1953, the first hydrogen bomb was exploded by the United States. This immediately spurred the development of long-range intercontinental ballistic missiles (ICBMs) to deliver such bombs. These vehicles were designed to fly outside the region of the earth's atmosphere for distances of 5000 mi or more and to reenter the atmosphere at suborbital speeds of from 20,000 to 22,000 ft/s. At such high velocities, the aerodynamic heating of the reentry vehicle becomes severe, and this heating problem dominated the minds of high-speed aerodynamicists. Their first thinking was conventional — a sharp-pointed, slender reentry body. Efforts to minimize aerodynamic heating centered on the maintenance of laminar boundary layer flow on the vehicle's surface; such laminar flow produces far less heating than turbulent flow (discussed in Chaps. 15 and 16). However, nature much prefers turbulent flow, and reentry vehicles are no exception. Therefore, the pointed-nose reentry body was doomed to failure because it would burn up in the atmosphere before reaching the earth's surface.

However, in 1951, one of those major breakthroughs that come very infrequently in engineering was created by H. Julian Allen at the NACA Ames Aeronautical Laboratory — he introduced the concept of the *blunt* reentry body. His thinking was based by the following concepts. At the beginning of reentry, near the outer edge of the atmosphere, the vehicle has a large amount of kinetic energy due to its high velocity and a large amount of potential energy due to its high altitude. However, by the time the vehicle reaches the surface of the earth, its velocity is relatively small and its altitude is zero; hence, it has virtually no kinetic or potential energy. Where has all the energy gone? The answer is that it has gone into (1) heating the body and (2) heating the airflow around the body. This is illustrated in Fig. 1.3. Here, the shock wave from the nose of



(a)



(b) Figure 1.2 (a) Wind tunnel designed, built, and used by the Wright brothers in Dayton, Ohio, during 1901–1902. (b) Wing models tested by the Wright brothers in their wind tunnel during 1901–1902.

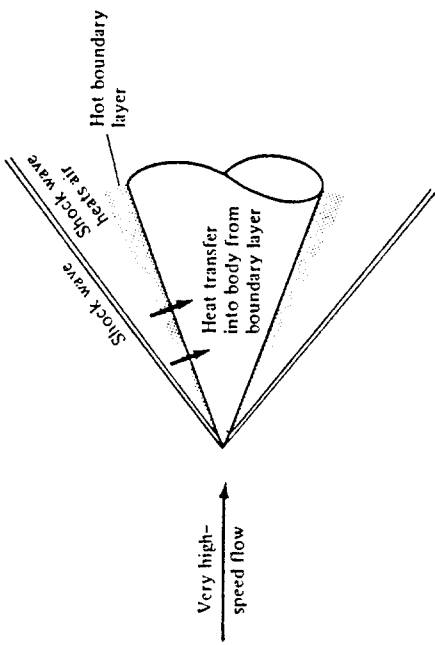


Figure 1.3 Energy of reentry goes into heating both the body and the air around the body.

the vehicle heats the airflow around the vehicle; at the same time, the vehicle is heated by the intense frictional dissipation within the boundary layer on the surface. Allen reasoned that if more of the total reentry energy could be dumped into the airflow, then less would be available to be transferred to the vehicle itself in the form of heating. In turn, the way to increase the heating of the airflow is to create a stronger shock wave at the nose, i.e., to use a blunt-nosed body. The contrast between slender and blunt reentry bodies is illustrated in Fig. 1.4. This was a stunning conclusion — to minimize aerodynamic heating, you actually want a blunt rather than a slender body. The result was so important that it was bottled up in a secret government document. Moreover, because it was so foreign to contemporary intuition, the blunt-reentry-body concept was accepted only gradually by the technical community. Over the next few years, additional aerodynamic analyses and experiments confirmed the validity of blunt reentry bodies. By 1955, Allen was publicly recognized for his work, receiving the Sylvanus Albert Reed Award of the Institute of the Aeronautical Sciences (now the American Institute of Aeronautics and Astronautics). Finally, in 1958, his work was made available to the public in the pioneering document NACA Report 1381 entitled "A Study of the Motion and Aerodynamic Heating of Ballistic Missiles Entering the Earth's Atmosphere at High Supersonic Speeds." Since Harvey Allen's early work, all successful reentry bodies, from the first Atlas ICBM to the manned Apollo lunar capsule, have been blunt. Incidentally, Allen went on to distinguish himself in many other areas, becoming the director of the NASA Ames Research Center in 1965, and retiring in 1970. His work on the blunt reentry body is an excellent example of the importance of aerodynamics to space vehicle design.

In summary, the purpose of this section has been to underscore the importance of aerodynamics in historical context. The goal of this book is to introduce the fundamentals of aerodynamics and to give the reader a much deeper insight to many technical applications in addition to the few described above. Aerodynamics is also a subject of intellectual beauty, composed and drawn by many great minds over the centuries. If you are challenged and interested by these thoughts, or even the least bit curious,

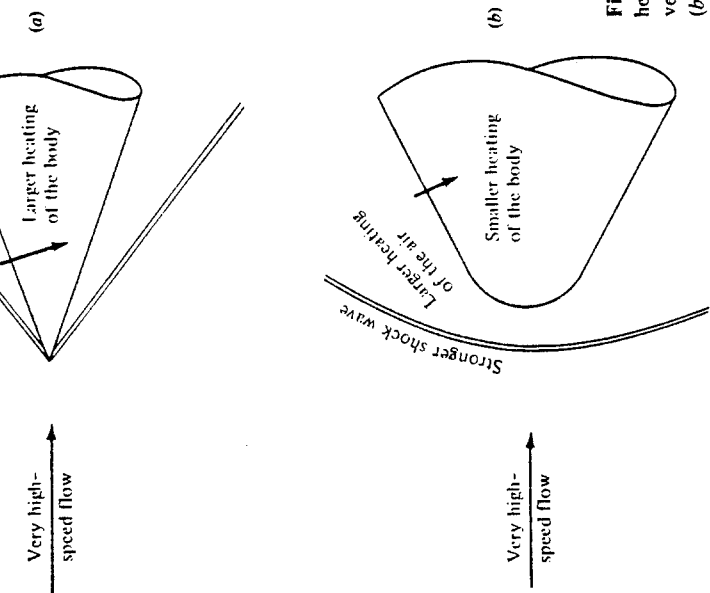


Figure 1.4 Contrast of aerodynamic heating for slender and blunt reentry vehicles. (a) Slender reentry body. (b) Blunt reentry body.

## 1.2 AERODYNAMICS: CLASSIFICATION AND PRACTICAL OBJECTIVES

A distinction between solids, liquids, and gases can be made in a simplistic sense as follows. Put a solid object inside a larger, closed container. The solid object will not change; its shape and boundaries will remain the same. Now put a liquid inside the container. The liquid will change its shape to conform to that of the container and will take on the same boundaries as the container up to the maximum depth of the liquid. Now put a gas inside the container. The gas will completely fill the container, taking on the same boundaries as the container.

The word "fluid" is used to denote either a liquid or a gas. A more technical distinction between a solid and a fluid can be made as follows. When a force is applied tangentially to the surface of a solid, the solid will experience a *finite* deformation, and the tangential force per unit area — the shear stress — will usually be proportional to the amount of deformation. In contrast, when a tangential shear stress is applied to the surface of a fluid, the fluid will experience a *continuously increasing* deformation, and the shear stress usually will be proportional to the rate of change of the deformation.

The most fundamental distinction between solids, liquids, and gases is at the atomic and molecular level. In a solid, the molecules are packed so closely together that their nuclei and electrons form a rigid geometric structure, "glued" together by powerful intermolecular forces. In a liquid, the spacing between molecules is larger, and although intermolecular forces are still strong they allow enough movement of the molecules to give the liquid its "fluidity." In a gas, the spacing between molecules is much larger (for air at standard conditions, the spacing between molecules is, on the average, about 10 times the molecular diameter). Hence, the influence of intermolecular forces is much weaker, and the motion of the molecules occurs rather freely throughout the gas. This movement of molecules in both gases and liquids leads to similar physical characteristics, the characteristics of a fluid — quite different from those of a solid. Therefore, it makes sense to classify the study of the dynamics of both liquids and gases under the same general heading, called *fluid dynamics*. On the other hand, certain differences exist between the flow of liquids and the flow of gases; also, different species of gases (say, N<sub>2</sub>, He, etc.) have different properties. Therefore, fluid dynamics is subdivided into three areas as follows:

- Hydrodynamics — flow of liquids
- Gas dynamics — flow of gases
- Aerodynamics — flow of air

These areas are by no means mutually exclusive; there are many similarities and identical phenomena between them. Also, the word "aerodynamics" has taken on a popular usage that sometimes covers the other two areas. As a result, this author tends to interpret the word "aerodynamics" very liberally, and its use throughout this book does *not* always limit our discussions just to air.

Aerodynamics is an applied science with many practical applications in engineering. No matter how elegant an aerodynamic theory may be, or how mathematically complex a numerical solution may be, or how sophisticated an aerodynamic experiment may be, all such efforts are usually aimed at one or more of the following practical objectives:

1. The prediction of forces and moments on, and heat transfer to, bodies moving through a fluid (usually air). For example, we are concerned with the generation of lift, drag, and moments on airfoils, wings, fuselages, engine nacelles, and, most importantly, whole airplane configurations. We want to estimate the wind force on buildings, ships, and other surface vehicles. We are concerned with the hydrodynamic forces on surface ships, submarines, and torpedoes. We need to be able to calculate the aerodynamic heating of flight vehicles ranging from the supersonic transport to a planetary probe entering the atmosphere of Jupiter. These are but a few examples.
2. Determination of flows moving internally through ducts. We wish to calculate and measure the flow properties inside rocket and air-breathing jet engines and to calculate the engine thrust. We need to know the flow conditions in the test section of a wind tunnel. We must know how much fluid can flow through pipes under

various conditions. A recent, very interesting application of aerodynamics is high-energy chemical and gas-dynamic lasers (see Ref. 1), which are nothing more than specialized wind tunnels that can produce extremely powerful laser beams. Fig. 1.5 is a photograph of an early gas-dynamic laser designed in the late 1960s.

The applications in item 1 come under the heading of *external aerodynamics* since they deal with external flows over a body. In contrast, the applications in item 2 involve *internal aerodynamics* because they deal with flows internally within ducts. In external aerodynamics, in addition to forces, moments, and aerodynamic heating associated with a body, we are frequently interested in the details of the flow field away from the body. For example, the communication blackout experienced by the space shuttle during a portion of its reentry trajectory is due to a concentration of free electrons in the hot shock layer around the body. We need to calculate the variation of electron density throughout such flow fields. Another example is the propagation of shock waves in a supersonic flow; for instance, does the shock wave from the wing of a supersonic airplane impinge upon and interfere with the tail surfaces? Yet another example is the flow associated with the strong vortices trailing downstream from the wing tips of large subsonic airplanes such as the Boeing 747. What are the properties of these vortices, and how do they affect smaller aircraft which happen to fly through them?

The above is just a sample of the myriad applications of aerodynamics. One purpose of this book is to provide the reader with the technical background necessary to fully understand the nature of such practical aerodynamic applications.

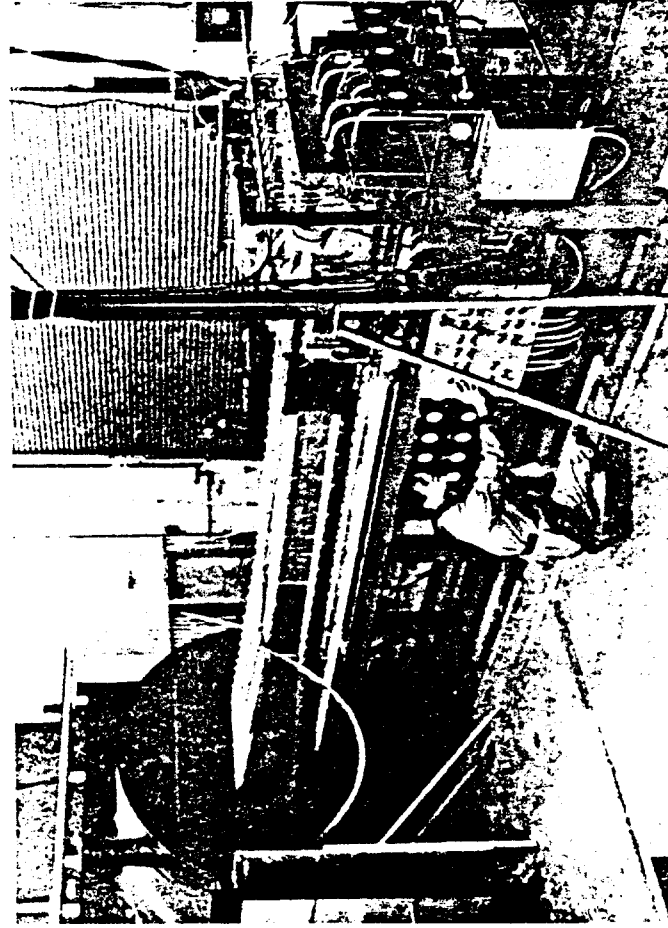


Figure 1.5 A CO<sub>2</sub>-N<sub>2</sub> gas-dynamic laser, circa 1969. (Courtesy of the Avco Everett Research Laboratory.)

### 1.3 ROAD MAP FOR THIS CHAPTER

When learning a new subject, it is important for you to know where you are, where you are going, and how you can get there. Therefore, at the beginning of each chapter in this book, a road map will be given to help guide you through the material of that chapter and to help you obtain a perspective as to how the material fits within the general framework of aerodynamics. For example, a road map for Chap. 1 is given in Fig. 1.6. You will want to frequently refer back to these road maps as you progress through the individual chapters. When you reach the end of each chapter, look back over the road map to see where you started, where you are now, and what you learned in between.

### 1.4 SOME FUNDAMENTAL AERODYNAMIC VARIABLES

A prerequisite to understanding physical science and engineering is simply learning the vocabulary used to describe concepts and phenomena. Aerodynamics is no exception. Throughout this book, and throughout your working career, you will be adding to your technical vocabulary list. Let us start by defining four of the most frequently used words in aerodynamics: "pressure," "density," "temperature," and "flow velocity."<sup>†</sup>

Consider a surface immersed in a fluid. The surface can be a real, solid surface such as the wall of a duct or the surface of a body; it can also be a free surface which we simply imagine drawn somewhere in the middle of the fluid. Also, keep in mind that the molecules of the fluid are constantly in motion. *Pressure* is the normal force per unit area exerted on a surface due to the time rate of change of momentum of the gas molecules impacting on (or crossing) that surface. It is important to note that even though pressure is defined as force "per unit area," you do not need a surface that is exactly 1 ft<sup>2</sup> or 1 m<sup>2</sup> to talk about pressure. In fact, pressure is usually defined as a *point* property in the fluid or a *point* on a solid surface and can vary from one point to another. To see this more clearly, consider a point *B* in a volume of fluid. Let

$$dA = \text{elemental area at } B$$

$$dF = \text{force on one side of } dA \text{ due to pressure}$$

Then, the pressure at point *B* in the fluid is defined as

$$p = \lim \left( \frac{dF}{dA} \right) \quad dA \rightarrow 0$$

The pressure *p* is the limiting form of the force per unit area, where the area of interest has shrunk to nearly zero at the point *B*.<sup>‡</sup> Clearly you can see that pressure is a *point* property and can have a different value from one point to another in the fluid.

<sup>†</sup>A basic introduction to these quantities is given on pages 35–39 of Ref. 2.

<sup>‡</sup>Strictly speaking, *dA* can never achieve the limit of zero, because there would be no molecules at point *B* in that case. The above limit should be interpreted as *dA* approaching a very small value, near zero in terms of our macroscopic thinking, but sufficiently larger than the average spacing between molecules on

Some introductory aerodynamic concepts.

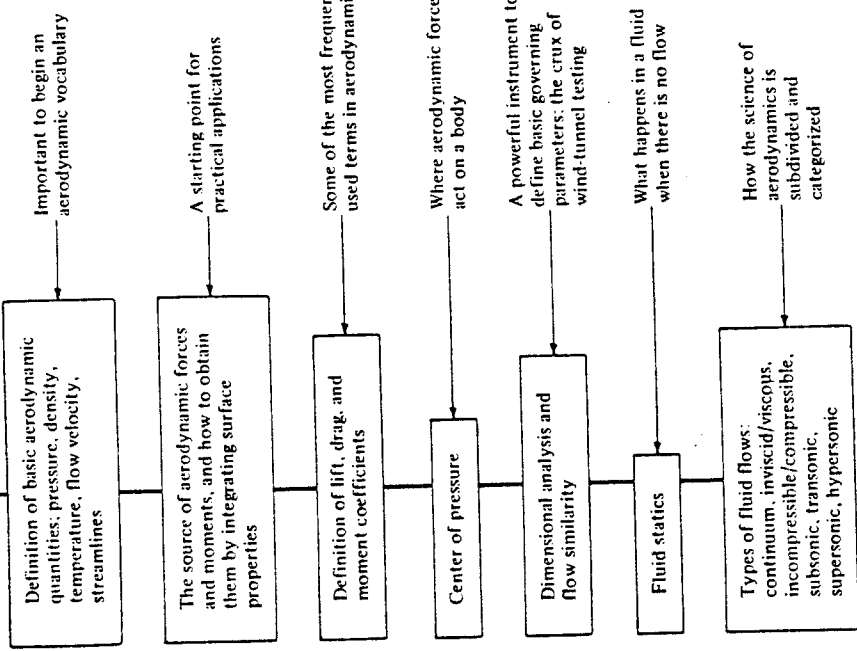


Figure 1.6 Road map for Chap. 1.

Another important aerodynamic variable is *density*, defined as the mass per unit volume. Analogous to our discussion on pressure, the definition of density does not require an actual volume of 1 ft<sup>3</sup> or 1 m<sup>3</sup>. Rather, it is a *point property* that can vary from point to point in the fluid. Again, consider a point *B* in the fluid. Let

$$dv = \text{elemental volume around } B$$

$$dm = \text{mass of fluid inside } dv$$

Then, the density at point *B* is

$$\rho = \lim \frac{dm}{dv} \quad dv \rightarrow 0$$

Therefore, the density *p* is the limiting form of the mass per unit volume, where the volume of interest has shrunk to nearly zero around point *B*. (Note that *dv* cannot

achieve the value of zero for the reason discussed in the footnote concerning  $dA$  in the definition of pressure.)

*Temperature* takes on an important role in high-speed aerodynamics (introduced in Chap. 7). The temperature  $T$  of a gas is directly proportional to the average kinetic energy of the molecules of the fluid. In fact, if  $KE$  is the mean molecular kinetic energy, then temperature is given by  $KE = \frac{1}{2} kT$ , where  $k$  is the Boltzmann constant. Hence, we can qualitatively visualize a high-temperature gas as one in which the molecules and atoms are randomly rattling about at high speeds, whereas in a low-temperature gas, the random motion of the molecules is relatively slow. Temperature is also a point property, which can vary from point to point in the gas.

The principal focus of aerodynamics is fluids in motion. Hence, flow velocity is an extremely important consideration. The concept of the velocity of a fluid is slightly more subtle than that of a solid body in motion. Consider a solid object in translational motion, say, moving at 30 m/s. Then all parts of the solid are simultaneously translating at the same 30 m/s. In contrast, a fluid is a "squishy" substance, and for a fluid in motion, one part of the fluid may be traveling at a different velocity than another part. Hence, we have to adopt a certain perspective, as follows. Consider the flow of air over an airfoil, as shown in Fig. 1.7. Lock your eyes on a specific, infinitesimally small element of mass in the gas, called a *fluid element*, and watch this element move with time. Both the speed and direction of this fluid element can vary as it moves from point to point in the gas. Now, fix your eyes on a specific fixed point in space, say point  $B$  in Fig. 1.7. *Flow velocity* can now be defined as follows: The velocity of a flowing gas at any fixed point  $B$  in space is the velocity of an infinitesimally small fluid element as it sweeps through  $B$ . The flow velocity  $\mathbf{V}$  has both magnitude and direction; hence, it is a vector quantity. This is in contrast to  $p$ ,  $\rho$ , and  $T$ , which are scalar variables. The scalar magnitude of  $\mathbf{V}$  is frequently used and is denoted by  $V$ . Again, we emphasize that velocity is a point property and can vary from point to point in the flow.

Referring again to Fig. 1.7, a moving fluid element traces out a fixed path in space. As long as the flow is steady, i.e., as long as it does not fluctuate with time, this path is called a *streamline* of the flow. Drawing the streamlines of the flow field is an important way of visualizing the motion of the gas; we will frequently be sketching the streamlines of the flow about various objects. A more rigorous discussion of streamlines is given in Chap. 2.

## 1.5 AERODYNAMIC FORCES AND MOMENTS

At first glance, the generation of the aerodynamic force on a giant Boeing 747 may seem complex, especially in light of the complicated three-dimensional flow field over the wings, fuselage, engine nacelles, tail, etc. Similarly, the aerodynamic resistance on an automobile traveling at 55 mi/h on the highway involves a complex interaction of the body, the air, and the ground. However, in these and all other cases, the aerodynamic forces and moments on the body are due to only two basic sources:

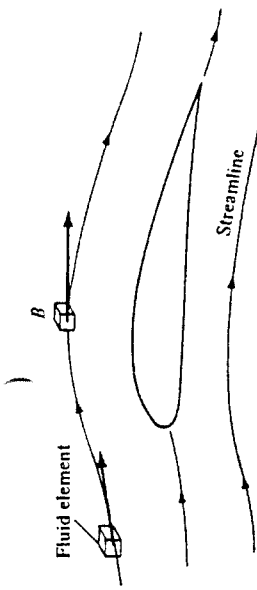


Figure 1.7 Illustration of flow velocity and streamlines.

### 1. Pressure distribution over the body surface

### 2. Shear stress distribution over the body surface

No matter how complex the body shape may be, the aerodynamic forces and moments on the body are due entirely to the above two basic sources. The *only* mechanisms nature has for communicating a force to a body moving through a fluid are pressure and shear stress distributions on the body surface. Both pressure  $p$  and shear stress  $\tau$  have dimensions of force per unit area (pounds per square foot or newtons per square meter). As sketched in Fig. 1.8,  $p$  acts *normal* to the surface, and  $\tau$  acts *tangential* to the surface. Shear stress is due to the "tugging action" on the surface, which is caused by friction between the body and the air (and is studied in great detail in Chaps. 15 and 16).

The net effect of the  $p$  and  $\tau$  distributions integrated over the complete body surface is a resultant aerodynamic force  $R$  and moment  $M$  on the body, as sketched in Fig. 1.9. In turn, the resultant  $R$  can be split into components, two sets of which are shown in Fig. 1.10. In Fig. 1.10,  $V_x$  is the *relative wind*, defined as the flow velocity far ahead of the body. The flow far away from the body is called the *freestream*, and hence  $V_x$  is also called the freestream velocity. In Fig. 1.10, by definition,

$$L \equiv \text{lift} \equiv \text{component of } R \text{ perpendicular to } V_x$$

$$D \equiv \text{drag} \equiv \text{component of } R \text{ parallel to } V_x$$

The chord  $c$  is the linear distance from the leading edge to the trailing edge of the body. Sometimes,  $R$  is split into components perpendicular and parallel to the chord, as also shown in Fig. 1.10. By definition,

$$N \equiv \text{normal force} \equiv \text{component of } R \text{ perpendicular to } c$$

$$A \equiv \text{axial force} \equiv \text{component of } R \text{ parallel to } c$$

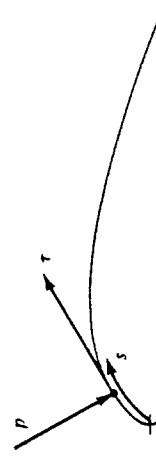


Figure 1.8 Illustration of pressure and shear stress on an aerodynamic surface.

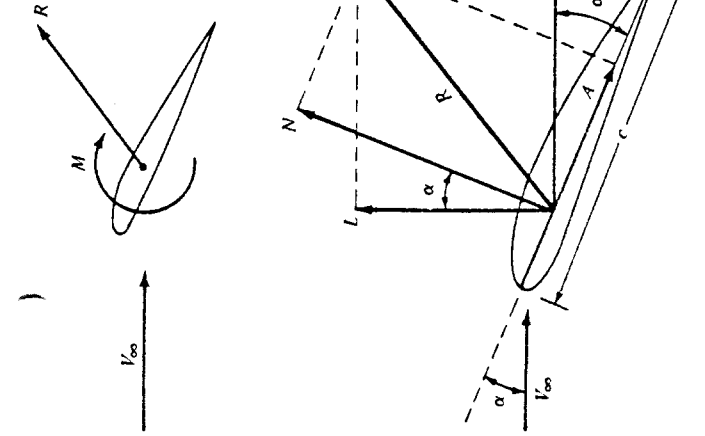


Figure 1.9 Resultant aerodynamic force and moment on the body.

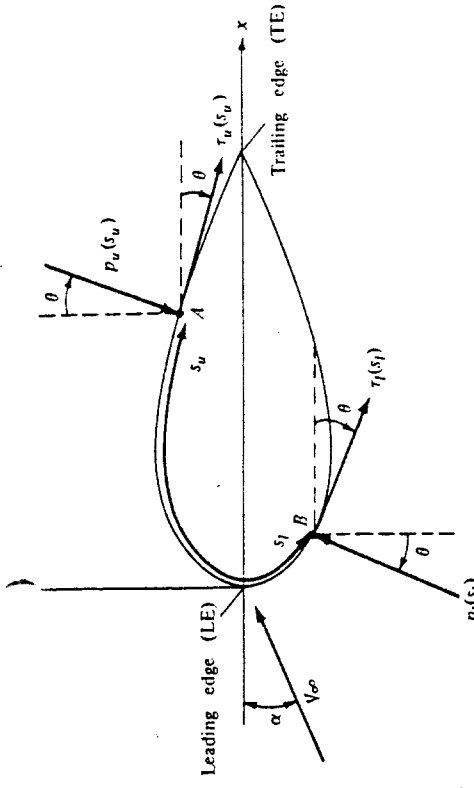


Figure 1.11 Nomenclature for the integration of pressure and shear stress distributions over a two-dimensional body surface.

Figure 1.10 Resultant aerodynamic force and the components into which it splits.

The angle of attack  $\alpha$  is defined as the angle between  $c$  and  $V_x$ . Hence,  $\alpha$  is also the angle between  $L$  and  $N$ , and between  $D$  and  $A$ . The geometrical relation between these two sets of components is, from Fig. 1.10,

$$L = N \cos \alpha - A \sin \alpha \quad (1.1)$$

$$D = N \sin \alpha + A \cos \alpha \quad (1.2)$$

Let us examine in more detail the integration of the pressure and shear stress distributions to obtain the aerodynamic forces and moments. Consider the two-dimensional body sketched in Fig. 1.11. The chord line is drawn horizontally, and hence, the relative wind is inclined relative to the horizontal by the angle of attack  $\alpha$ . An  $xy$  coordinate system is oriented parallel and perpendicular, respectively, to the chord. The distance from the leading edge measured along the body surface to an arbitrary point  $A$  on the upper surface is  $s_u$ ; similarly, the distance to an arbitrary point  $B$  on the lower surface is  $s_l$ . The pressure and shear stress on the upper surface are denoted by  $p_u$  and  $\tau_u$ , respectively; both  $p_u$  and  $\tau_u$  are functions of  $s_u$ . Similarly,  $p_l$  and  $\tau_l$  are the corresponding quantities on the lower surface and are functions of  $s_l$ . At a given point, the pressure is normal to the surface and is oriented at an angle  $\theta$  relative to the perpendicular; shear stress is tangential to the surface and is oriented at the same angle  $\theta$  relative to the horizontal. In Fig. 1.11, the sign convention for  $\theta$  is positive when measured clockwise from the vertical line to the direction of  $p$  and from the horizontal line to the direction of  $\tau$ . In Fig. 1.11, all thetas are shown in their positive direction. Now consider the two-dimensional shape in Fig. 1.11 as a cross section of

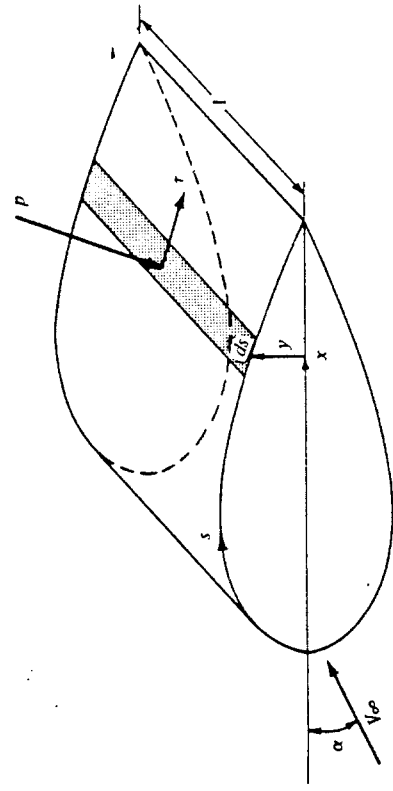


Figure 1.12 Aerodynamic force on an element of the body surface.

$$\begin{aligned} dN'_i &= p_i ds_i \cos \theta - \tau_i ds_i \sin \theta & (1.5) \\ dA'_i &= p_i ds_i \sin \theta + \tau_i ds_i \cos \theta & (1.6) \end{aligned}$$

In Eqs. (1.3) to (1.6), the positive directions of  $N'$  and  $A'$  are those shown in Fig. 1.10. In these equations, the positive clockwise convention for  $\theta$  must be followed. For example, consider again Fig. 1.11. Near the leading edge of the body, where the slope of the upper body surface is positive,  $\tau$  is inclined upward, and hence it gives a positive contribution to  $N'$ . For an upward inclined  $\tau$ ,  $\theta$  would be counterclockwise, hence negative. Therefore, in Eq. (1.3),  $\sin \theta$  would be negative, making the shear stress term (the last term) a positive value, as it should be in this instance. Hence, Eqs. (1.3) to (1.6) hold in general (for both the forward and rearward portions of the body) as long as the above sign convention for  $\theta$  is consistently applied.

The total normal and axial forces *per unit span* are obtained by integrating Eqs. (1.3) to (1.6) from the leading edge (LE) to the trailing edge (TE).

$$\begin{aligned} N' &= - \int_{LE}^{TE} (p_u \cos \theta + \tau_u \sin \theta) ds_u + \int_{LE}^{TE} (p_l \cos \theta - \tau_l \sin \theta) ds_l & (1.7) \\ A' &= \int_{LE}^{TE} (-p_u \sin \theta + \tau_u \cos \theta) ds_u + \int_{LE}^{TE} (p_l \sin \theta + \tau_l \cos \theta) ds_l & (1.8) \end{aligned}$$

In turn, the total lift and drag per unit span can be obtained by inserting Eqs. (1.7) and (1.8) into (1.1) and (1.2); note that Eqs. (1.1) and (1.2) hold for forces on an arbitrarily shaped body (unprimed) and for the forces per unit span (primed).

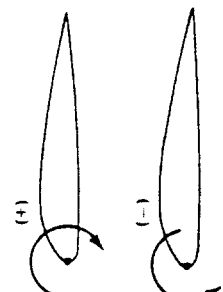
The aerodynamic moment exerted on the body depends on the point about which moments are taken. Consider moments taken about the leading edge. By convention, moments which tend to increase  $\alpha$  (pitch up) are positive, and moments which tend to decrease  $\alpha$  (pitch down) are negative. This convention is illustrated in Fig. 1.13. Returning again to Figs. 1.11 and 1.12, the moment per unit span about the leading edge due to  $p$  and  $\tau$  on the elemental area  $dS$  on the upper surface is

$$\begin{aligned} dM'_u &= (p_u \cos \theta + \tau_u \sin \theta) x ds_u \\ &\quad + (-p_l \sin \theta + \tau_l \cos \theta) y ds_u & (1.9) \end{aligned}$$

On the bottom surface,

$$\begin{aligned} dM'_l &= (-p_l \cos \theta + \tau_l \sin \theta) x ds_l \\ &\quad + (p_l \sin \theta + \tau_l \cos \theta) y ds_l & (1.10) \end{aligned}$$

In Eqs. (1.9) and (1.10), note that the same sign convention for  $\theta$  applies as before and that  $y$  is a positive number above the chord and a negative number below the chord.



Integrating Eqs. (1.9) and (1.10) from the leading to the trailing edges, we obtain for the moment about the leading edge per unit span:

$$\begin{aligned} M'_{LE} &= \int_{LE}^{TE} [(p_u \cos \theta + \tau_u \sin \theta)x - (p_l \sin \theta - \tau_l \cos \theta)y] ds_y \\ &\quad + \int_{LE}^{TE} [(-p_l \cos \theta + \tau_l \sin \theta)x + (p_l \sin \theta + \tau_l \cos \theta)y] ds_y & (1.11) \end{aligned}$$

In Eqs. (1.7), (1.8), and (1.11),  $\theta$ ,  $x$ , and  $y$  are known functions of  $s$  for a given body shape. Hence, if  $p_u$ ,  $p_l$ ,  $\tau_u$ , and  $\tau_l$  are known as functions of  $s$  (from theory or experiment), the integrals in these equations can be evaluated. Clearly, Eqs. (1.7), (1.8), and (1.11) demonstrate the principle stated earlier, namely, that *the source of the aerodynamic lift, drag, and moments on a body are the pressure and shear stress distributions integrated over the body*. A major goal of theoretical aerodynamics is to calculate  $p(s)$  and  $\tau(s)$  for a given body shape and freestream conditions, thus yielding the aerodynamic forces and moments via Eqs. (1.7), (1.8), and (1.11).

As our discussions of aerodynamics progress, it will become clear that there are quantities of an even more fundamental nature than the aerodynamic forces and moments themselves. These are *dimensionless force and moment coefficients*, defined as follows. Let  $\rho_\infty$  and  $V_\infty$  be the density and velocity, respectively, in the freestream, far ahead of the body. We define a dimensional quantity called the *freestream dynamic pressure* as

$$q_\infty \equiv \frac{1}{2} \rho_\infty V_\infty^2$$

The dynamic pressure has the units of pressure (i.e., pounds per square foot or newtons per square meter). In addition, let  $S$  be a reference area and  $l$  be a reference length. The dimensionless force and moment coefficients are defined as follows:

$$\begin{aligned} \text{Lift coefficient} & C_L \equiv \frac{L}{q_\infty S} \\ \text{Drag coefficient} & C_D \equiv \frac{D}{q_\infty S} \\ \text{Normal force coefficient} & C_N \equiv \frac{N}{q_\infty S} \\ \text{Axial force coefficient} & C_A \equiv \frac{A}{q_\infty S} \\ \text{Moment coefficient} & C_M \equiv \frac{M}{q_\infty S l} \end{aligned}$$

In the above coefficients, the reference area  $S$  and reference length  $l$  are chosen to pertain to the given geometric body shape; for different shapes,  $S$  and  $l$  may be different things. For example, for an airplane wing,  $S$  is the planform area, and  $l$  is the mean chord length, as illustrated in Fig. 1.14a. However, for a sphere,  $S$  is the cross-sectional area, and  $l$  is the diameter, as shown in Fig. 1.14b. The particular choice of reference area and length is not critical; however, when using force and moment coefficient data, you must always know what reference quantities the particular data are based upon.

Figure 1.13 Sign convention for aerodynamic moments

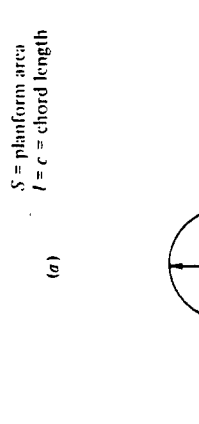
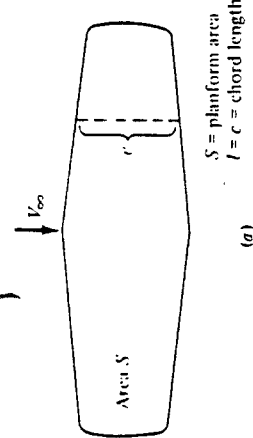


Figure 1.14 Some reference areas and lengths.

The symbols in capital letters listed above, that is,  $C_l$ ,  $C_D$ ,  $C_M$ ,  $C_N$ , and  $C_\alpha$ , denote the force and moment coefficients for a complete three-dimensional body such as an airplane or a finite wing. In contrast, for a two-dimensional body, such as given in Figs. 1.11 and 1.12, the forces and moments are per unit span. For these two-dimensional bodies, it is conventional to denote the aerodynamic coefficients by lower-case letters, e.g.,

$$c_l \equiv \frac{L'}{q_x c} \quad c_d \equiv \frac{D'}{q_x c} \quad c_m \equiv \frac{M'}{q_x c^2}$$

where the reference area  $S = c(1) = c$ .

Two additional dimensionless quantities of immediate use are

$$\text{Pressure coefficient } C_p \equiv \frac{p - p_\infty}{q_x} \quad (1.12)$$

Skin friction coefficient

$$c_f \equiv \frac{\tau}{q_x} \quad (1.13)$$

where  $p_\infty$  is the freestream pressure.

The most useful forms of Eqs. (1.7), (1.8), and (1.11) are in terms of the dimensionless coefficients introduced above. From the geometry shown in Fig. 1.15,

$$dx = ds \cos \theta \quad (1.14)$$

$$dy = -(ds \sin \theta) \quad (1.15)$$

$$S = c(1) \quad (1.16)$$

Substituting Eqs. (1.12) and (1.13) into Eqs. (1.7), (1.8), and (1.11), dividing by  $q_x$ , and further dividing by  $S$  in the form of Eq. (1.14), we obtain the following integral forms for the force and moment coefficients:

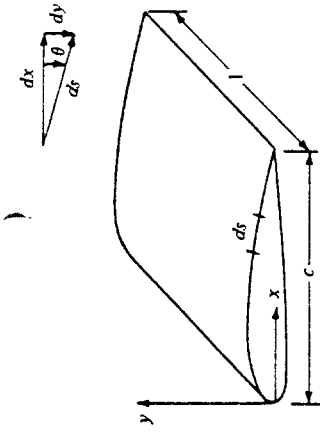


Figure 1.15 Geometrical relationship of differential lengths.

$$c_n = \frac{1}{c} \left[ \int_0^c (C_{p,l} - C_{p,u}) dx + \int_{l_E}^{l_E} (c_{f,u} + c_{f,l}) dy \right] \quad (1.15)$$

$$c_d = \frac{1}{c} \left[ \int_{l_E}^{l_E} (C_{p,u} - C_{p,l}) dy + \int_0^c (c_{f,u} + c_{f,l}) dx \right] \quad (1.16)$$

$$c_m = \frac{1}{c^2} \left[ \int_0^c (C_{p,u} - C_{p,l}) x dx - \int_{l_E}^{l_E} (c_{f,u} + c_{f,l}) x dy \right. \\ \left. + \int_{l_E}^{l_E} (C_{p,u} - C_{p,l}) y dy + \int_0^c (c_{f,u} + c_{f,l}) y dx \right] \quad (1.17)$$

The simple algebraic steps are left as an exercise for the reader. When evaluating the integrals with respect to  $y$ , keep in mind from Fig. 1.15 and Eq. (1.13) that  $dy$  is a negative quantity when the body surface slopes downward and is positive when the body surface slopes upward.

The lift and drag coefficients can be obtained from Eqs. (1.1) and (1.2) cast in coefficient form:

$$c_l = c_n \cos \alpha - c_d \sin \alpha \quad (1.18)$$

$$c_d = c_n \sin \alpha + c_d \cos \alpha \quad (1.19)$$

Integral forms for  $c_l$  and  $c_d$  are obtained by substituting Eqs. (1.15) and (1.16) into (1.18) and (1.19).

It is important to note from Eqs. (1.15) through (1.19) that the aerodynamic force and moment coefficients can be obtained by integrating the pressure and skin friction coefficients over the body. This is a common procedure in both theoretical and experimental aerodynamics. In addition, although our derivations have used a two-dimensional body, an analogous development can be presented for three-dimensional bodies—the geometry and equations only get more complex and involved—the principle is the same.

## 1.6 CENTER OF PRESSURE

From Eqs. (1.7) and (1.8), we see that the normal and axial forces on the body are due to the distributed loads imposed by the pressure and shear stress distributions. More

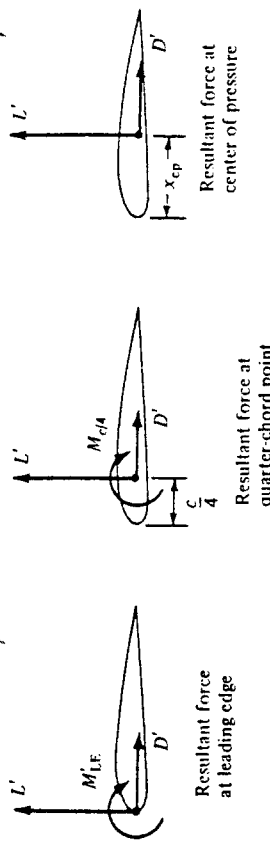


Figure 1.17 Equivalent ways of specifying the force and moment system on an airfoil.

over, these distributed loads generate a moment about the leading edge, as given by Eq. (1.11). *Question:* If the aerodynamic force on a body is specified in terms of a resultant single force,  $R$ , or its components such as  $N$  and  $A$ , where on the body should this resultant be placed? The answer is that the resultant force should be located on the body such that it produces the same effect as the distributed loads. For example, the distributed load on a two-dimensional body such as an airfoil produces a moment about the leading edge given by Eq. (1.11); therefore,  $N'$  and  $A'$  must be placed on the airfoil at such a location to generate the same moment about the leading edge. If  $A'$  is placed on the chord line as shown in Fig. 1.16, then  $N'$  must be located a distance  $x_{cp}$  downstream of the leading edge such that

$$M'_{LE} = -(x_{cp})N' \quad (1.20)$$

$$x_{cp} = -\frac{M'_{LE}}{N'} \quad (1.21)$$

In Fig. 1.16, the direction of the curled arrow illustrating  $M'_{LE}$  is drawn in the positive (pitch-up) sense. (From Sec. 1.5, recall the standard convention that aerodynamic moments are positive if they tend to increase the angle of attack.) Examining Fig. 1.16, a positive  $N'$  creates a negative (pitch-down) moment about the leading edge. This is consistent with the negative sign in Eq. (1.20). Therefore, in Fig. 1.16, the actual moment about the leading edge is negative and, hence, is in a direction opposite to the curled arrow shown.

In Fig. 1.16 and Eq. (1.20),  $x_{cp}$  is defined as the *center of pressure*. It is the location where the resultant of a distributed load effectively acts on the body. If moments were taken about the center of pressure, the integrated effect of the distributed loads would be zero. Hence, an alternate definition of the center of pressure is that point on the body about which the aerodynamic moment is zero.

In cases where the angle of attack of the body is small,  $\sin \alpha \approx 0$  and  $\cos \alpha \approx 1$ ; hence, from Eq. (1.1),  $L' \approx N'$ . Thus, Eq. (1.20) becomes

$$x_{cp} \approx -\frac{M'_{LE}}{L'} \quad (1.21)$$

Examine Eqs. (1.20) and (1.21). As  $N'$  and  $L'$  decrease,  $x_{cp}$  increases. As the forces approach zero, the center of pressure moves to infinity. For this reason, the center of pressure is not always a convenient concept in aerodynamics. However, this is no problem. To define the force-and-moment system due to a distributed load on a body, the resultant force can be placed at *any* point on the body, as long as the value of the

moment about that point is also given. For example, Fig. 1.17 illustrates three equivalent ways of specifying the force-and-moment system on an airfoil. In the left figure, the resultant is placed at the leading edge, with a finite value of  $M'_{LE}$ . In the middle figure, the resultant is placed at the quarter-chord point, with a finite value of  $M'_{c4}$ . In the right figure, the resultant is placed at the center of pressure, with a zero moment about that point. By inspection of Fig. 1.17, the quantitative relation between these cases is

$$M'_{LE} = -\frac{c}{4} L' + M'_{c4} = -x_{cp} L' \quad (1.22)$$

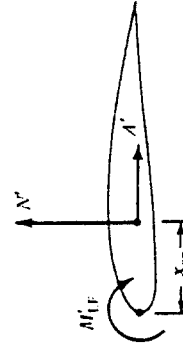
## 1.7 DIMENSIONAL ANALYSIS: THE BUCKINGHAM PI THEOREM

The aerodynamic forces and moments on a body, and the corresponding force and moment coefficients, have been defined and discussed in Sec. 1.5. *Question:* What physical quantities determine the variation of these forces and moments? The answer can be found from the powerful method of *dimensional analysis*, which is introduced in this section.<sup>†</sup>

Consider a body of given shape at a given angle of attack, for example, the airfoil sketched in Fig. 1.10. The resultant aerodynamic force is  $R$ . On a physical, intuitive basis, we expect  $R$  to depend on

1. Freestream velocity  $V_\infty$ .
2. Freestream density  $\rho_\infty$ .
3. Viscosity of the fluid. We have seen that shear stress  $\tau$  contributes to the aerodynamic forces and moments. In turn, in Chap. 15 we will see that  $\tau$  is proportional to the velocity gradients in the flow. For example, if the velocity gradient is given by  $\partial u / \partial y$ , then  $\tau = \mu \cdot \partial u / \partial y$ . The constant of proportionality is the viscosity coefficient  $\mu$ . Hence, let us represent the influence of viscosity on aerodynamic forces and moments by the freestream viscosity coefficient  $\mu_\infty$ .
4. The size of the body, represented by some chosen reference length. In Fig. 1.10, the convenient reference length is the chord length  $c$ .

Figure 1.16 Center of pressure for an airfoil.



<sup>†</sup>For a more elementary treatment of dimensional analysis, see chap. 5 of Ref. 2.

5. The compressibility of the fluid. The technical definition of compressibility is given in Chap. 7. For our present purposes, let us just say that compressibility is related to the variation of density throughout the flow field, and certainly the aerodynamic forces and moments should be sensitive to any such variation. In turn, compressibility is related to the speed of sound,  $a$ , in the fluid, as shown in Chap. 8.<sup>†</sup> Therefore, let us represent the influence of compressibility on aerodynamic forces and moments by the freestream speed of sound,  $a_{\infty}$ .

In light of the above, and without any a priori knowledge about the variation of  $R$ , we can use common sense to write

$$R = f(\rho_{\infty}, V_{\infty}, c, \mu_{\infty}, a_{\infty}) \quad (1.23)$$

Equation (1.23) is a general functional relation, and as such is not very practical for the direct calculation of  $R$ . In principle, we could mount the given body in a wind tunnel, incline it at the given angle of attack, and then systematically measure the variation of  $R$  due to variations of  $\rho_{\infty}$ ,  $V_{\infty}$ ,  $c$ ,  $\mu_{\infty}$ , and  $a_{\infty}$ , taken one at a time. By cross-plotting the vast bulk of data thus obtained, we might be able to extract a precise functional relation for Eq. (1.23). But it would be hard work, and would certainly be costly in terms of a huge amount of required wind tunnel time. Fortunately, we can simplify the problem and considerably reduce our time and effort, by first employing the method of dimensional analysis. This method will define a set of dimensionless parameters which govern the aerodynamic forces and moments; this set will considerably reduce the number of independent variables as presently occurs in Eq. (1.23).

Dimensional analysis is based on the obvious fact that in an equation dealing with the real physical world, each term must have the same dimensions. For example, if

$$\psi + \eta + \zeta = \phi$$

is a physical relation, then  $\psi$ ,  $\eta$ ,  $\zeta$ , and  $\phi$  must have the same dimensions. Otherwise, we would be adding apples and oranges. The above equation can be made dimensionless by dividing by any one of the terms, say  $\phi$ .

$$\frac{\psi}{\phi} + \frac{\eta}{\phi} + \frac{\zeta}{\phi} = 1$$

These ideas are formally embodied in the Buckingham pi theorem, stated below without derivation. (See Ref. 3, pages 21–28, for such a derivation.)

**Buckingham pi theorem** Let  $K$  equal the number of fundamental dimensions required to describe the physical variables. (In mechanics, all physical variables can be expressed in terms of the dimensions of mass, length, and time; hence,  $K = 3$ .) Let  $P_1, P_2, \dots, P_N$  represent  $N$  physical variables in the physical relation

$$f_1(P_1, P_2, \dots, P_N) = 0 \quad (1.24)$$

Then, the physical relation Eq. (1.24) may be reexpressed as a relation of  $(N - K)$

<sup>†</sup>Common experience tells us that sound waves propagate through air at some finite velocity, much slower than the speed of light; you see a flash of lightning in the distance, and hear the thunder moments later. The speed of sound is an important physical quantity in aerodynamics and is discussed in detail in Sec. 8.1.

dimension. ) products (called  $\Pi$  products),

$$f_2(\Pi_1, \Pi_2, \dots, \Pi_{N-K}) = 0 \quad (1.25)$$

where each  $\Pi$  product is a dimensionless product of an arbitrarily selected set of  $K$  physical variables plus one other physical variable. Let  $P_1, P_2, \dots, P_K$  be the arbitrarily selected set of  $K$  physical variables. Then

$$\begin{aligned} \Pi_1 &= f_3(P_1, P_2, \dots, P_K, P_{K+1}) \\ \Pi_2 &= f_4(P_1, P_2, \dots, P_K, P_{K+2}) \\ &\vdots \\ \Pi_{N-K} &= f_5(P_1, P_2, \dots, P_K, P_N) \end{aligned} \quad (1.26)$$

Returning to our consideration of the aerodynamic force on a given body at a given angle of attack, Eq. (1.23) can be written in the form of Eq. (1.24),

$$g(R, \rho_{\infty}, V_{\infty}, c, \mu_{\infty}, a_{\infty}) = 0 \quad (1.27)$$

Following the Buckingham pi theorem, the fundamental dimensions are

$m$  = dimensions of mass

$l$  = dimension of length

$t$  = dimension of time

Hence,  $K = 3$ . The physical variables and their dimensions are

$$[R] = m l t^{-2}$$

$$[\rho_{\infty}] = m l^{-3}$$

$$[V_{\infty}] = l t^{-1}$$

$$[c] = l$$

$$[\mu_{\infty}] = m l^{-1} t^{-1}$$

$$[a_{\infty}] = l t^{-1}$$

Hence,  $N = 6$ . In the above, the dimensions of the force  $R$  are obtained from Newton's second law, force = mass  $\times$  acceleration; hence,  $[R] = \mu_{\infty} m l t^{-2}$ . The dimensions of  $\mu_{\infty}$  are obtained from its definition, e.g.,  $\mu_{\infty} = \tau / (\partial u / \partial y)$ , and from Newton's second law.

(Show for yourself that  $[\mu_{\infty}] = m l^{-1} t^{-1}$ .) Choose  $\rho_{\infty}$ ,  $V_{\infty}$ , and  $c$  as the arbitrarily selected set of  $K$  physical variables. Then, Eq. (1.27) can be reexpressed in terms of  $N - K = 6 - 3 = 3$  dimensionless  $\Pi$  products in the form of Eq. (1.25),

$$\Pi_1(\Pi_2, \Pi_3) = 0 \quad (1.28)$$

From Eq. (1.26), these  $\Pi$  products are

$$\Pi_1 = f_3(\rho_{\infty}, V_{\infty}, c, R) \quad (1.29a)$$

$$\Pi_2 = f_4(\rho_{\infty}, V_{\infty}, c, \mu_{\infty}) \quad (1.29b)$$

$$\Pi_3 = f_5(\rho_{\infty}, V_{\infty}, c, a_{\infty}) \quad (1.29c)$$

For the time being, concentrate on  $\Pi_1$  from Eq. (1.29a). Note that

$$\Pi_1 = \rho_s^d V_s^b c^e R \quad (1.30)$$

where  $d$ ,  $b$ , and  $e$  are exponents to be found. In dimensional terms, Eq. (1.30) is

$$[\Pi_1] = (ml^{-1})^d (l^{-1})^b (ml^{-1})^e \quad (1.31)$$

Because  $\Pi_1$  is dimensionless, the right side of Eq. (1.31) must also be dimensionless. This means that the exponents of  $m$  must add to zero, and similarly for the exponents of  $l$  and  $t$ . Hence,

$$d + 1 = 0$$

$$-3d + b + e + 1 = 0$$

$$-b - 2 = 0$$

Solving the above equations, we find that  $d = -1$ ,  $b = -2$ , and  $e = -2$ . Substituting these values into Eq. (1.30), we have

$$\Pi_1 = R \rho_s^{-1} V_s^{-2} c^{-2} \quad (1.32)$$

$$\Pi_1 = \frac{R}{\rho_s V_s^2 c^2}$$

The quantity  $R/\rho_s V_s^2 c^2$  is a dimensionless parameter in which  $c^2$  has the dimensions of an area. We can replace  $c^2$  with any reference area we wish (such as the planform area of a wing,  $S$ ), and  $\Pi_1$  will still be dimensionless. Moreover, we can multiply  $\Pi_1$  by a pure number, and it will still be dimensionless. Thus, from Eq. (1.32),  $\Pi_1$  can be redefined as

$$\Pi_1 = \frac{R}{4\rho_s V_s^2 S} = \frac{R}{q_s S} \quad (1.33)$$

Hence,  $\Pi_1$  is a force coefficient,  $C_R$ , as defined in Sec. 1.5. In Eq. (1.33),  $S$  is a reference area germane to the given body shape.

The remaining  $\Pi$  products can be found as follows. From Eq. (1.29b), assume

$$\Pi_2 = \rho_s V_s^h c^i \mu' \quad (1.34)$$

Paralleling the above analysis,

$$[\Pi_2] = (ml^{-1})^h (l^{-1})^i (ml^{-1})^j \quad (1.35)$$

Hence,

$$1 + j = 0$$

$$-3 + h + i - j = 0$$

$$-h - j = 0$$

Thus,  $j = -1$ ,  $h = 1$ , and  $i = 1$ . Substitution into Eq. (1.34) gives

$$\Pi_2 = \frac{\rho_s V_s^h c}{\mu_s} \quad (1.35)$$

The dimensionless combination in Eq. (1.35) is defined as the freestream  $Reynolds$  number  $Re = \rho_s V_s c / \mu_s$ . The Reynolds number is physically a measure of the ratio of inertia forces to viscous forces in a flow and is one of the most powerful parameters in fluid dynamics. Its importance is emphasized in Chaps. 15 and 16.

Returning to Eq. (1.29c), assume

$$\Pi_3 = V_s \rho_s^k c^l a_s^m \quad (1.36)$$

$$[\Pi_3] = (ll^{-1})^k (ml^{-1})^l (lt^{-1})^m$$

For  $m$ :

$$1 - 3k + r + s = 0$$

$$-1 - s = 0$$

For  $t$ :

Hence,  $k = 0$ ,  $s = -1$ , and  $r = 0$ . Substituting into Eq. (1.36), we have

$$\Pi_3 = \frac{V_s}{a_s} \quad (1.37)$$

The dimensionless combination in Eq. (1.37) is defined as the freestream *Mach number*  $M = V_s/a_s$ . The Mach number is the ratio of the flow velocity to the speed of sound; it is a powerful parameter in the study of gas dynamics. Its importance is emphasized in subsequent chapters.

The results of our dimensional analysis may be organized as follows. Inserting Eqs. (1.33), (1.35), and (1.37) into (1.28), we have

$$f_2 \left( \frac{R}{4\rho_s V_s^2 S}, \frac{\rho_s V_s c}{\mu_s}, \frac{V_s}{a_s} \right) = 0$$

or

$$f_2(C_R, Re, M_s) = 0 \quad (1.38)$$

This is an important result! Compare Eqs. (1.23) and (1.38). In Eq. (1.23),  $R$  is expressed as a general function of five independent variables. However, our dimensional analysis has shown that

1.  $R$  can be expressed in terms of a dimensionless force coefficient,  $C_R = R/\rho_s V_s^2 S$ .
2.  $C_R$  is a function of only  $Re$  and  $M_s$ , from Eq. (1.38).

Therefore, by using the Buckingham pi theorem, we have reduced the number of independent variables from five in Eq. (1.23) to two in Eq. (1.38). Now, if we wish to run a series of wind-tunnel tests for a given body at a given angle of attack, we need only to vary Reynolds number and Mach number in order to obtain data for the direct formulation of  $R$  through Eq. (1.38). With a small amount of analysis, we have saved a huge amount of effort and wind-tunnel time. More importantly, we have defined two dimensionless parameters,  $Re$  and  $M_s$ , which govern the flow. They are called *similarity parameters*, for reasons to be discussed in the following section. Other similarity parameters are introduced as our aerodynamic discussions progress.

Since the lift and drag are components of the resultant force, corollaries to Eq. (1.38) are

$$C_L = f_1(\text{Re}, M_\infty) \quad (1.39)$$

$$C_D = f_2(\text{Re}, M_\infty) \quad (1.40)$$

Moreover, a relation similar to Eq. (1.23) holds for the aerodynamic moments, and dimensional analysis yields

$$C_M = f_3(\text{Re}, M_\infty) \quad (1.41)$$

Keep in mind that the above analysis was for a given body shape at a given angle of attack,  $\alpha$ . If  $\alpha$  is allowed to vary, then  $C_L$ ,  $C_D$ , and  $C_M$  will in general depend on the value of  $\alpha$ . Hence, Eqs. (1.39) to (1.41) can be generalized to

$C_L = f_{10}(\text{Re}, M_\infty, \alpha)$
$C_D = f_{11}(\text{Re}, M_\infty, \alpha)$
$C_M = f_{12}(\text{Re}, M_\infty, \alpha)$

Equations (1.42) to (1.44) assume a given body shape. Much of theoretical and experimental aerodynamics is focused on obtaining explicit expressions for Eqs. (1.42) to (1.44) for specific body shapes. This is one of the practical applications of aerodynamics mentioned in Sec. 1.2, and it is one of the major thrusts of this book.

For mechanical problems that also involve thermodynamics and heat transfer, the temperature, specific heat, and thermal conductivity of the fluid, as well as the temperature of the body surface (wall temperature), must be added to the list of physical variables, and the unit of temperature (say, kelvin or degree Rankine) must be added to the list of fundamental dimensions. For such cases, dimensional analysis yields additional dimensionless products such as heat transfer coefficients, and additional similarity parameters such as the ratio of specific heat at constant pressure to that at constant volume  $c_p/c_v$ , the ratio of wall temperature to freestream temperature  $T_w/T_\infty$ , and the Prandtl number  $Pr = \mu_\infty c_p/k_\infty$ , where  $k_\infty$  is the thermal conductivity of the freestream.<sup>†</sup> Thermodynamics is essential to the study of compressible flow (Chaps. 7 to 14), and heat transfer is part of the study of viscous flow (Chaps. 15 and 16). Hence, these additional similarity parameters will be emphasized when they appear logically in our subsequent discussions. For the time being, however, Mach number and Reynolds number will suffice as the dominant similarity parameters for our present considerations.

<sup>†</sup>The specific heat of a fluid is defined as the amount of heat added to a system,  $\delta q$ , per unit increase in temperature,  $c_v = \delta q/dT$  if  $\delta q$  is added at constant volume, and similarly for  $c_p$ , if  $\delta q$  is added at constant pressure. Specific heats are discussed in detail in Sec. 7.2. The thermal conductivity relates heat flux to temperature gradients in the fluid. For example, if  $\dot{q}_x$  is the heat transferred in the  $x$  direction per second per unit area and  $\partial T/\partial x$  is the temperature gradient in the  $x$  direction, then thermal conductivity  $k$  is defined by  $\dot{q}_x = -k(\partial T/\partial x)$ . Thermal conductivity is discussed in detail in Sec. 15.3.

## 1.8 FLOW SIMILARITY

Consider two different flow fields over two different bodies. By definition, different flows are *geometrically similar* if

1. The streamline patterns are geometrically similar.
2. The distributions of  $V/V_\infty$ ,  $p/p_\infty$ ,  $T/T_\infty$ , etc., throughout the flow field are the same when plotted against common nondimensional coordinates.
3. The force coefficients are the same.

Actually, item 3 is a consequence of item 2; if the nondimensional pressure and shear stress distributions over different bodies are the same, then the nondimensional force coefficients will be the same.

The definition of dynamic similarity was given above. *Question:* What are the criteria to ensure that two flows are dynamically similar? The answer comes from the results of the dimensional analysis in Sec. 1.7. Two flows will be dynamically similar if

1. The bodies and any other solid boundaries are geometrically similar for both flows.
2. The similarity parameters are the same for both flows.

So far, we have emphasized two similarity parameters,  $\text{Re}$  and  $M_\infty$ . For many aerospace applications, these are by far the dominant similarity parameters. Therefore, in a limited sense, but applicable to many problems, we can say that flows over geometrically similar bodies at the same Mach and Reynolds numbers are dynamically similar, and hence the lift, drag, and moment coefficients will be identical for the bodies. This is a key point in the validity of wind-tunnel testing. If a scale model of a flight vehicle is tested in a wind tunnel, the measured lift, drag, and moment coefficients will be the same as for free flight as long as the Mach and Reynolds numbers of the wind-tunnel test-section flow are the same as for the free-flight case. As we will see in subsequent chapters, this statement is not quite precise because there are other similarity parameters that influence the flow. In addition, differences in freestream turbulence between the wind tunnel and free flight can have an important effect on  $C_D$  and the maximum value of  $C_L$ . However, direct simulation of the free-flight  $\text{Re}$  and  $M_\infty$  is the primary goal of many wind-tunnel tests.

**Example 1.1** Consider the flow over two circular cylinders, one having four times the diameter of the other, as shown in Fig. 1.18. The flow over the smaller cylinder has a freestream density, velocity, and temperature given by  $\rho_1$ ,  $V_1$ , and  $T_1$ , respectively. The flow over the larger cylinder has a freestream density, velocity, and temperature given by  $\rho_2$ ,  $V_2$ , and  $T_2$ , respectively, where  $\rho_2 = \rho_1/4$ ,  $V_2 = 2V_1$ , and  $T_2 = 4T_1$ . Assume that both  $\mu$  and  $a$  are proportional to  $T^{1/2}$ . Show that the two flows are dynamically similar.

**SOLUTION** Since  $\mu \propto \sqrt{T}$  and  $a \propto \sqrt{T}$ , then

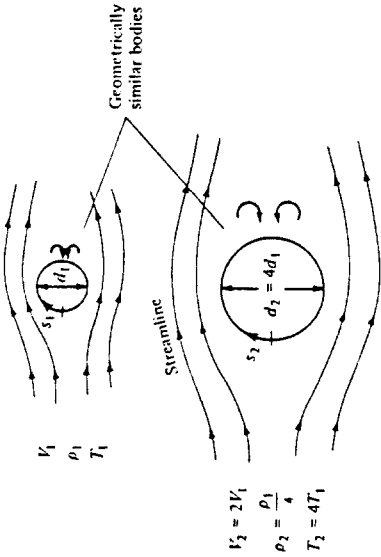


Figure 1.18 Example of dynamic flow similarity. Note that as part of the definition of dynamic similarity, the streamlines (lines along which the flow velocity is tangent at each point) are geometrically similar between the two flows.

$$\frac{\mu_2}{\mu_1} = \sqrt{\frac{T_2}{T_1}} = \sqrt{\frac{4T_1}{T_1}} = 2$$

$$\frac{a_2}{a_1} = \sqrt{\frac{T_2}{T_1}} = 2$$

and

By definition,

$$M_1 = \frac{V_1}{a_1}$$

$$M_2 = \frac{V_2}{a_2} = \frac{2V_1}{2a_1} = \frac{V_1}{a_1} = M_1$$

and

$$Re_1 = \frac{\rho_1 V_1 d_1}{\mu_1}$$

$$Re_2 = \frac{\rho_2 V_2 d_2}{\mu_2} = \frac{(\rho_1/4)(2V_1)(4d_1)}{2\mu_1} = \frac{\rho_1 V_1 d_1}{\mu_1} = Re_1$$

Hence, the Reynolds numbers are the same. Since the two bodies are geometrically similar and  $M_\infty$  and  $Re$  are the same, we have satisfied all the criteria; the two flows are dynamically similar. In turn, as a consequence of being similar flows, we know from the definition that

1. The streamline patterns around the two cylinders are geometrically similar.
2. The nondimensional pressure, temperature, density, velocity, etc., distributions are the same around the two cylinders. This is shown schematically in Fig. 1.19.

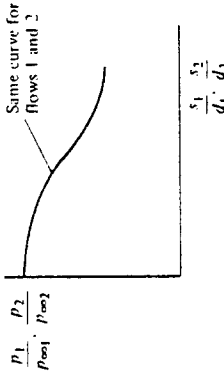


Figure 1.19 One aspect of the definition of dynamically similar flows. The nondimensional flow variable distributions are the same.

where the nondimensional pressure distribution  $p/p_\infty$  is shown as a function of the nondimensional surface distance,  $s/d$ . It is the same curve for both bodies.

3. The drag coefficients for the two bodies are the same. Here,  $C_D = D/qS$ , where  $S = \pi d^2/4$ . As a result of the flow similarity,  $C_{D1} = C_{D2}$ . (Note: Examining Fig. 1.18, the lift on the cylinders is zero because the flow is symmetrical about the horizontal axis through the center of the cylinder. The pressure distribution over the top is the same as over the bottom, and they cancel each other in the vertical direction. Therefore, drag is the only aerodynamic force on the body.)

## 1.9 FLUID STATICS: BUOYANCY FORCE

In aerodynamics, we are concerned about fluids in motion, and the resulting forces and moments on bodies due to such motion. However, in this section we consider the special case of *no* fluid motion, i.e., *fluid statics*. A body immersed in a fluid will still experience a force even if there is no relative motion between the body and the fluid. Let us see why.

To begin, we must first consider the force on an element of fluid itself. Consider a stagnant fluid above the  $xz$  plane as shown in Fig. 1.20. The vertical direction is given by  $y$ . Consider an infinitesimally small fluid element with sides of length  $dx$ ,  $dy$ , and  $dz$ . There are two types of forces acting on this fluid element: pressure forces from the surrounding fluid exerted on the surface of the element, and the gravity force due to the

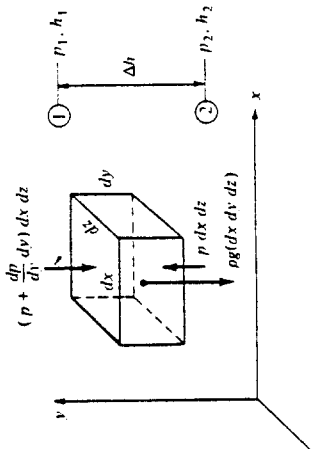


Figure 1.20 Forces on a fluid element in a stagnant fluid.

weight of the fluid inside the element. Consider forces in the  $y$  direction. The pressure on the bottom surface of the element is  $p$ , and hence the force on the bottom face is  $p(dx dz)$  in the upward direction, as shown in Fig. 1.20. The pressure on the top surface of the element will be slightly different than the pressure on the bottom because the top surface is at a different location in the fluid. Let  $dp/dy$  denote the rate of change of  $p$  with respect to  $y$ . Then the pressure exerted on the top surface will be  $p + (dp/dy) dy$ , and the pressure force on the top of the element will be  $[p + (dp/dy) dy](dx dz)$  in the downward direction, as shown in Fig. 1.20. Hence, letting upward force be positive:

$$\begin{aligned} \text{Net pressure force} &= p(dx dz) - \left( p + \frac{dp}{dy} dy \right) (dx dz) \\ &= -\frac{dp}{dy} (dx dy dz) \end{aligned}$$

Let  $\rho$  be the mean density of the fluid element. The total mass of the element is  $\rho(dx dy dz)$ . Therefore,

$$\text{Gravity force} = -\rho(dx dy dz)g$$

where  $g$  is the acceleration of gravity. Since the fluid element is stationary (in equilibrium), the sum of the forces exerted on it must be zero.

$$-\frac{dp}{dy} (dx dy dz) - g\rho(dx dy dz) = 0$$

$$\text{or } \frac{dp}{dy} = -g\rho dy \quad (1.45)$$

Eq. (1.45) is called the *hydrostatic equation*; it is a differential equation which relates the change in pressure,  $dp$ , in a fluid with a change in vertical height,  $dy$ .

The net force on the element acts only in the vertical direction. The pressure forces on the front and back faces are equal and opposite and hence cancel; the same is true for the left and right faces. Also, the pressure forces shown in Fig. 1.20 act at the center of the top and bottom faces, and the center of gravity is at the center of the elemental volume (assuming the fluid is homogeneous); hence the forces in Fig. 1.20 are collinear, and as a result there is no moment on the element.

Equation (1.45) governs the variation of atmospheric properties as a function of altitude in the air above us. It is also used to estimate the properties of other planetary atmospheres such as for Venus, Mars, and Jupiter. The use of Eq. (1.45) in the analysis and calculation of the "standard atmosphere" is given in detail in Ref. 2; hence it will not be repeated here.

Let the fluid be a liquid, for which we can assume  $\rho$  is constant. Consider points 1 and 2 separated by the vertical distance  $\Delta h$  as sketched on the right side of Fig. 1.20. The pressure and  $y$  locations at these points are  $p_1, h_1$ , and  $p_2, h_2$ , respectively. Integrating Eq. (1.45) between points 1 and 2, we have

$$\int_{p_1}^{p_2} dp = -\rho g \int_{h_1}^{h_2} dy$$

$$\text{or } p_2 - p_1 = -\rho g(h_2 - h_1) = \rho g \Delta h \quad (1.46)$$

where  $\Delta h = h_2 - h_1$ . Equation (1.46) can be more conveniently expressed as

$$p_2 + \rho gh_2 = p_1 + \rho gh_1$$

$$\text{or } p + \rho gh = \text{constant} \quad (1.47)$$

Note that in Eqs. (1.46) and (1.47), increasing values of  $h$  are in the positive (upward)  $y$  direction.

A simple application of Eq. (1.47) is the calculation of the pressure distribution on the walls of a container holding a liquid, and open to the atmosphere at the top. This is illustrated in Fig. 1.21, where the top of the liquid is at a height  $h$ . The atmospheric pressure  $p_a$  is impressed on the top of the liquid; hence the pressure at  $h_1$  is simply  $p_a$ . Applying Eq. (1.47) between the top (where  $h = h_1$ ) and an arbitrary height  $h$ , we have

$$p + \rho gh = p_1 + \rho gh_1 = p_a + \rho gh_1$$

$$\text{or } p = p_a + \rho g(h_1 - h) \quad (1.48)$$

Equation (1.48) gives the pressure distribution on the vertical sidewall of the container as a function of  $h$ . Note that the pressure is a *linear* function of  $h$ , as sketched on the right of Fig. 1.21, and that  $p$  increases with depth below the surface.

Another simple and very common application of Eq. (1.47) is the liquid-filled U-tube manometer used for measuring pressure differences, as sketched in Fig. 1.22. The manometer is usually made from hollow glass tubing bent in the shape of the letter U. Imagine that we have an aerodynamic body immersed in an air flow (such as in a wind tunnel), and we wish to use a manometer to measure the surface pressure at point  $b$  on the body. A small pressure orifice (hole) at point  $b$  is connected to one side of the manometer via a long (usually flexible) pressure tube. The other side of the manometer is open to the atmosphere, where the pressure  $p_a$  is a known value. The U tube is partially filled with a liquid of known density  $\rho$ . The tops of the liquid on the left and right sides of the U tube are at points 1 and 2, with heights  $h_1$  and  $h_2$ , respectively. The body surface pressure  $p_b$  is transmitted through the pressure tube and impressed on the top of the liquid at point 1. The atmospheric pressure  $p_a$  is impressed

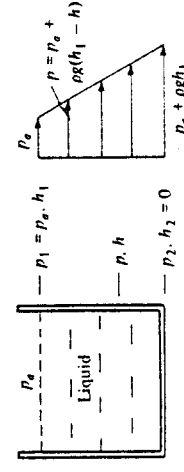


Figure 1.21 Hydrostatic pressure distribution on the walls of a container.

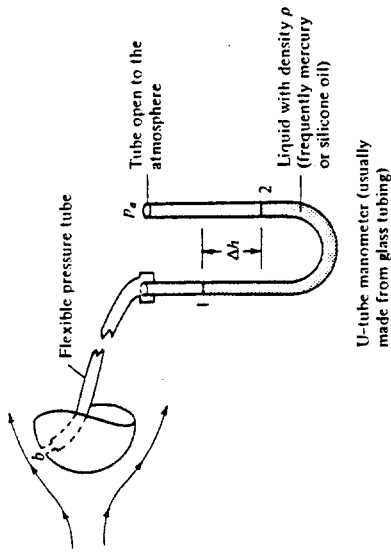


Figure 1.22 The use of a U-tube manometer.

on the top of the liquid at point 2. Because in general  $p_b \neq p_a$ , the tops of the liquid will be at different heights, i.e., the two sides of the manometer will show a displacement  $\Delta h = h_1 - h_2$  of the fluid. We wish to obtain the value of the surface pressure at point  $b$  on the body by reading the value of  $\Delta h$  from the manometer. From Eq. (1.47) applied between points 1 and 2:

$$\begin{aligned} p_b + \rho g h_1 &= p_a + \rho g h_2 \\ p_b &= p_a - \rho g (h_1 - h_2) \\ p_b &= p_a - \rho g \Delta h \end{aligned} \quad (1.49)$$

In Eq. (1.49),  $p_a$ ,  $\rho$ , and  $g$  are known, and  $\Delta h$  is read from the U tube, thus allowing  $p_b$  to be measured.

At the beginning of this section, we stated that a solid body immersed in a fluid will experience a force even if there is no relative motion between the body and the fluid. We are now in a position to derive an expression for this force, henceforth called the *buoyancy force*. We will consider a body immersed in either a stagnant gas or liquid, hence  $\rho$  can be a variable. For simplicity, consider a rectangular body of unit width, length  $l$ , and height  $(h_1 - h_2)$ , as shown in Fig. 1.23. Examining Fig. 1.23, we see that the vertical force  $F$  on the body due to the pressure distribution over the surface is

$$F = (p_2 - p_1)l(1) \quad (1.50)$$

There is no horizontal force because the pressure distributions over the vertical faces of the rectangular body lead to equal and opposite forces which cancel each other. In Eq. (1.50), an expression for  $p_2 - p_1$  can be obtained by integrating the hydrostatic equation, Eq. (1.45), between the top and bottom faces.

$$p_2 - p_1 = \int_{p_1}^{p_2} dp = - \int_{h_2}^{h_1} \rho g dy = \int_{h_2}^{h_1} \rho g dy$$

Substituting this result into Eq. (1.50), we obtain for the buoyancy force,

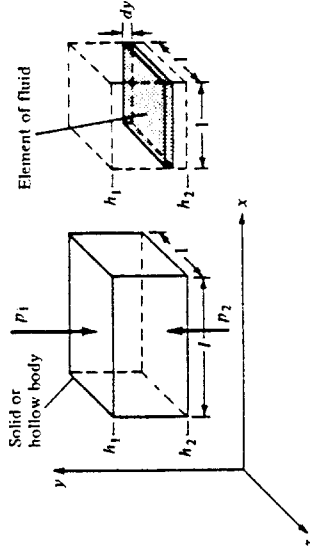


Figure 1.23 Source of the buoyancy force on a body immersed in a fluid.

$$F = l(1) \int_{h_2}^{h_1} \rho g dy \quad (1.51)$$

Consider the physical meaning of the integral in Eq. (1.51). The weight of a small element of fluid of height  $dy$  and width and length of unity as shown at the right of Fig. 1.23 is  $\rho g dy$  (1)(1). In turn, the weight of a column of fluid with a base of unit area and a height  $(h_1 - h_2)$  is

$$\int_{h_2}^{h_1} \rho g dy$$

which is precisely the integral in Eq. (1.51). Moreover, if we place  $l$  of these fluid columns side by side, we would have a volume of fluid equal to the volume of the body on the left of Fig. 1.23, and the weight of this total volume of fluid would be

$$l \int_{h_2}^{h_1} \rho g dy$$

which is precisely the right-hand side of Eq. (1.51). Therefore, Eq. (1.51) states in words that

$$\text{Buoyance force} = \frac{\text{weight of fluid}}{\text{on body}} = \frac{\text{displaced by body}}$$

We have just proved the well-known *Archimedes principle*, first advanced by the Greek scientist, Archimedes of Syracuse (287–212 B.C.). Although we have used a rectangular body to simplify our derivation, the Archimedes principle holds for bodies of any general shape. (See Prob. 1.14 at the end of this chapter.) Also, note from our derivation that the Archimedes principle holds for both gases and liquids, and does not require that the density be constant.

The density of liquids is usually several orders of magnitude larger than the density of gases; for example, for water  $\rho = 10^3 \text{ kg/m}^3$ , whereas for air  $\rho = 1.23 \text{ kg/m}^3$ . Therefore, a given body will experience a buoyancy force a thousand times greater

in water than in air. Obviously, for naval vehicles buoyancy force is all important, whereas for airplanes it is negligible. On the other hand, lighter-than-air vehicles, such as blimps and hot-air balloons, rely on buoyancy force for sustentation; they obtain sufficient buoyancy force simply by displacing huge volumes of air. For most problems in aerodynamics, however, buoyancy force is so small that it can be readily neglected.

### 1.10 TYPES OF FLOW

An understanding of aerodynamics, like that of any other physical science, is obtained through a "building-block" approach — we dissect the discipline, form the parts into nice, polished blocks of knowledge, and then later attempt to reassemble the blocks to form an understanding of the whole. An example of this process is the way that different types of aerodynamic flows are categorized and visualized. Although nature has no trouble setting up the most detailed and complex flow with a whole spectrum of interacting physical phenomena, we must attempt to understand such flows by modeling them with less detail, and neglecting some of the (hopefully) less significant phenomena. As a result, a study of aerodynamics has evolved into a study of numerous and distinct types of flow. The purpose of this section is to itemize and contrast these types of flow, and to briefly describe their most important physical phenomena.

### Continuum versus Free Molecule Flow

Consider the flow over a body, say, for example, a circular cylinder of diameter  $d$ . Also, consider the fluid to consist of individual molecules, which are moving about in random motion. The mean distance that a molecule travels between collisions with neighboring molecules is defined as the *mean-free path*  $\lambda$ . If  $\lambda$  is orders of magnitude smaller than the scale of the body measured by  $d$ , then the flow appears to the body as a continuous substance. The molecules impact the body surface so frequently that the body cannot distinguish the individual molecular collisions, and the surface feels the fluid as a continuous medium. Such flow is called *continuum flow*. The other extreme is where  $\lambda$  is on the same order as the body scale; here the gas molecules are spaced so far apart (relative to  $d$ ) that collisions with the body surface occur only infrequently, and the body surface can feel distinctly each molecular impact. Such flow is called *free molecular flow*. For manned flight, vehicles such as the space shuttle encounter free molecular flow at the extreme outer edge of the atmosphere, where the air density is so low that  $\lambda$  becomes on the order of the shuttle size. There are intermediate cases, where flows can exhibit some characteristics of both continuum and free molecule flows; such flows are generally labeled "low-density flows" in contrast to continuum flow. By far, the vast majority of practical aerodynamic applications involve continuum flows. Low-density and free molecule flows are just a small part of the total spectrum of aerodynamics. Therefore, in this book we will always deal with continuum flow; i.e., we will always treat the fluid as a continuous medium.

### Inviscid versus Viscous Flow

A major facet of a gas or liquid is the ability of the molecules to move rather freely, as explained in Sec. 1.2. When the molecules move, even in a very random fashion, they obviously transport their mass, momentum, and energy from one location to another in the fluid. This transport on a molecular scale gives rise to the phenomena of mass diffusion, viscosity (friction), and thermal conduction. Such "transport phenomena" will be discussed in detail in Chap. 15. For our purposes here, we need only to recognize that all real flows exhibit the effects of these transport phenomena; such flows are called *viscous flows*. In contrast, a flow that is assumed to involve no friction, thermal conduction, or diffusion is called an *inviscid flow*. Inviscid flows do not truly exist in nature; however, there are many practical aerodynamic flows (more than you would think) where the influence of transport phenomena is small, and we can *model* the flow as being inviscid. For this reason, more than 70 percent of this book (Chaps. 3 to 14) deals with inviscid flows.

Theoretically, inviscid flow is approached in the limit as the Reynolds number goes to infinity (to be proved in Chap. 16). However, for practical problems, many flows with high but finite  $Re$  can be assumed to be inviscid. For such flows, the influence of friction, thermal conduction, and diffusion is limited to a very thin region adjacent to the body surface (the boundary layer, to be defined in Chap. 16), and the remainder of the flow outside this thin region is essentially inviscid. This division of the flow into two regions is illustrated in Fig. 1.24. Hence, the material discussed in Chaps. 3 to 14 applies to the flow outside the boundary layer. For flows over slender bodies, such as the airfoil sketched in Fig. 1.24, inviscid theory adequately predicts the pressure distribution and lift on the body and gives a valid representation of the streamlines and flow field away from the body. However, because friction (shear stress) is a major source of aerodynamic drag, inviscid theories by themselves cannot adequately predict total drag.

In contrast, there are some flows that are dominated by viscous effects. For example, if the airfoil in Fig. 1.24 is inclined to a high incidence angle to the flow (high angle of attack), then the boundary layer will tend to separate from the top surface, and a large wake is formed downstream. The separated flow is sketched at the top of Fig. 1.25; it is characteristic of the flow field over a "stalled" airfoil. Separated flow also dominates the aerodynamics of blunt bodies, such as the cylinder at the bottom of Fig. 1.25. Here, the flow expands around the front face of the cylinder, but separates from the surface on the rear face, forming a rather fat wake downstream. The types of

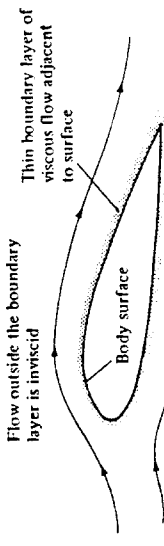


Figure 1.24 The division of a flow into two regions: (1) the thin viscous boundary layer adjacent to the body surface and (2) the inviscid flow outside the boundary layer.

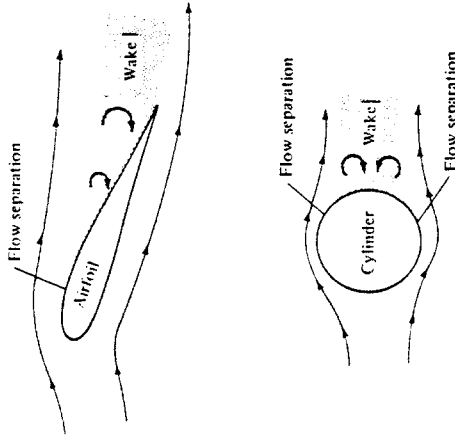


Figure 1.25 Examples of viscous-dominated flow.

flow illustrated in Fig. 1.25 are dominated by viscous effects; no inviscid theory can independently predict the aerodynamics of such flows. They require the inclusion of viscous effects, to be presented in Chaps. 15 and 16.

### Incompressible versus Compressible Flows

A flow in which the density  $\rho$  is constant is called *incompressible*. In contrast, a flow where the density is variable is called *compressible*. A more precise definition of compressibility will be given in Chap. 7. For our purposes here, we will simply note that all flows, to a greater or lesser extent, are compressible; truly incompressible flow, where the density is precisely constant, does not occur in nature. However, analogous to our discussion of inviscid flow, there are a number of aerodynamic problems that can be modeled as being incompressible without any detrimental loss of accuracy. For example, the flow of homogeneous liquids is treated as incompressible, and hence most problems involving hydrodynamics assume  $\rho = \text{constant}$ . Also, the flow of gases at low Mach number is essentially incompressible; for  $M < 0.3$ , it is always safe to assume  $\rho = \text{constant}$ . (We will prove this in Chap. 8.) This was the flight regime of all airplanes from the Wright brothers' first flight in 1903 to just prior to World War II. It is still the flight regime of most small, general aviation aircraft of today. Hence, there exists a large bulk of aerodynamic experimental and theoretical data for incompressible flows. Such flows are the subject of Chaps. 3 to 6. On the other hand, high-speed flow (near Mach 1 and above) must be treated as compressible; for such flows  $\rho$  can vary over wide latitudes. Compressible flow is the subject of Chaps. 7 to 14.

### Mach Number Regimes

Of all the ways of subdividing and describing different aerodynamic flows, the distinction based on Mach number is probably the most prevalent. If  $M$  is the local Mach number at an arbitrary point in a flow field, then by definition the flow is locally

Subsonic if  $M < 1$   
Sonic if  $M = 1$   
Supersonic if  $M > 1$

Looking at the whole flow field simultaneously, four different speed regimes can be identified using Mach number as the criterion.

1. *Subsonic flow* ( $M < 1$  everywhere). A flow field is defined as *subsonic* if the Mach number is less than 1 at every point. Subsonic flows are characterized by smooth streamlines (no discontinuity in slope), as sketched in Fig. 1.26a. Moreover, since the flow velocity is everywhere less than the speed of sound, disturbances in the flow (say the sudden deflection of the trailing edge of the airfoil in Fig. 1.26a) propagate both upstream and downstream, and are felt throughout

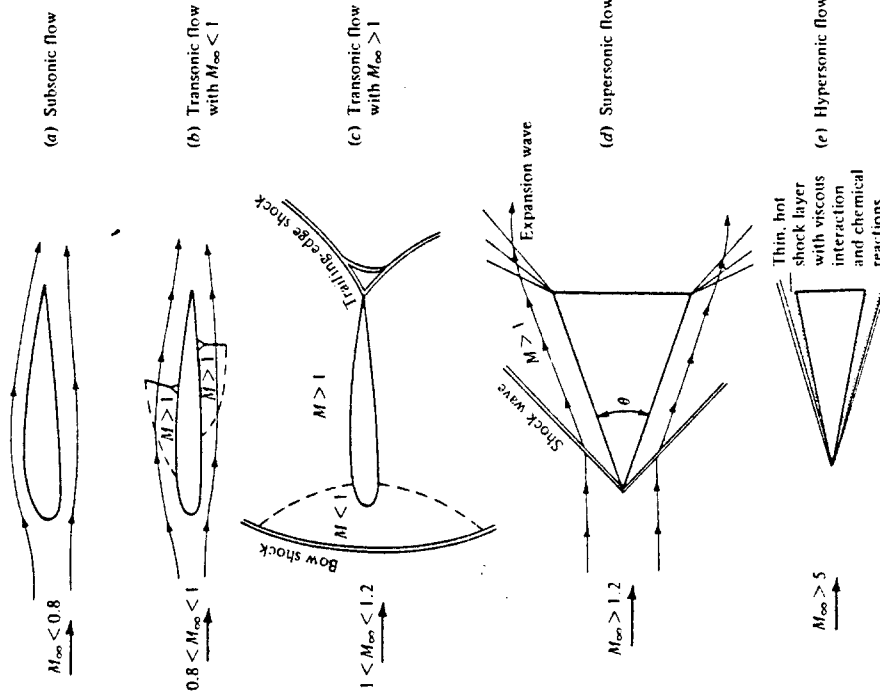


Figure 1.26 Different regimes of flow.

the entire flow field. Note that a freestream Mach number,  $M_\infty$ , less than 1 does not guarantee a totally subsonic flow over the body. In expanding over an aerodynamic shape, the flow velocity increases above the freestream value, and if  $M_\infty$  is close enough to 1, the local Mach number may become supersonic in certain regions of the flow. This gives rise to a rule of thumb that  $M_\infty < 0.8$  for subsonic flow over slender bodies. For blunt bodies,  $M_\infty$  must be even lower to insure totally subsonic flow. (Again, emphasis is made that the above is just a loose rule of thumb, and should not be taken as a precise quantitative definition.) Also, we will show later that incompressible flow is a special limiting case of subsonic flow where  $M \rightarrow 0$ .

2. *Transonic flow* (mixed regions where  $M < 1$  and  $M > 1$ ). As stated above, if  $M_\infty$  is subsonic but is near unity, the flow can become locally supersonic ( $M > 1$ ). This is sketched in Fig. 1.26b, which shows pockets of supersonic flow over both the top and bottom surfaces of the airfoil, terminated by weak shock waves behind which the flow becomes subsonic again. Moreover, if  $M_\infty$  is increased slightly above unity, a bow shock wave is formed in front of the body; behind this shock wave the flow is locally subsonic, as shown in Fig. 1.26c. This subsonic flow subsequently expands to a low supersonic value over the airfoil. Weak shock waves are usually generated at the trailing edge, sometimes in a "fishtail" pattern as shown in Fig. 1.26c. The flow fields shown in Fig. 1.26b and c are characterized by mixed subsonic-supersonic flows, and are dominated by the physics of both types of flows. Hence, such flow fields are called *transonic flows*. Again, as a rule of thumb for slender bodies, transonic flows occur for freestream Mach numbers in the range  $0.8 < M_\infty < 1.2$ .

3. *Supersonic flow* ( $M > 1$  everywhere). A flow field is defined as *supersonic* if the Mach number is greater than 1 at every point. Supersonic flows are frequently characterized by the presence of shock waves across which the flow properties and streamlines change discontinuously (in contrast to the smooth, continuous variations in subsonic flows). This is illustrated in Fig. 1.26d for supersonic flow over a sharp-nosed wedge; the flow remains supersonic behind the oblique shock wave from the tip. Also shown are distinct expansion waves which are common in supersonic flow. (Again, the listing of  $M_\infty > 1.2$  is strictly a rule of thumb. For example, in Fig. 1.26d, if  $\theta$  is made large enough, the oblique shock wave will detach from the tip of the wedge, and will form a strong, curved bow shock ahead of the wedge with a substantial region of subsonic flow behind the wave. Hence, the totally supersonic flow sketched in Fig. 1.26d is destroyed if  $\theta$  is too large for a given  $M_\infty$ . This shock detachment phenomenon can occur at any value of  $M_\infty > 1$ , but the value of  $\theta$  at which it occurs increases as  $M_\infty$  increases. In turn, if  $\theta$  is made infinitesimally small, the flow field in Fig. 1.26d holds for  $M_\infty \geq 1.0$ . These matters will be considered in detail in Chap. 9. However, the above discussion clearly shows that the listing of  $M_\infty > 1.2$  in Fig. 1.26d is a very tenuous rule of thumb, and should not be taken literally.) In a supersonic flow, because the local flow velocity is greater than the speed of sound, disturbances created at some point in the flow can *not* work their way upstream (in contrast to subsonic flow). This property is one of the most significant physical differences between subsonic and

supersonic flows. It is the basic reason why shock waves occur in supersonic flows, but do not occur in steady subsonic flow. We will come to appreciate this difference more fully in Chaps. 7 to 14.

4. *Hypersonic flow* (very high supersonic speeds). Refer again to the wedge in Fig. 1.26d. Assume  $\theta$  is a given, fixed value. As  $M_\infty$  increases above 1, the shock wave moves closer to the body surface. Also, the strength of the shock wave increases, leading to higher temperatures in the region between the shock and the body (the shock layer). If  $M_\infty$  is sufficiently large, the shock layer becomes very thin, and interactions between the shock wave and the viscous boundary layer on the surface occur. Also, the shock layer temperature becomes high enough that chemical reactions occur in the air. The  $O_2$  and  $N_2$  molecules are torn apart; i.e., the gas molecules dissociate. When  $M_\infty$  becomes large enough such that viscous interaction and/or chemically reacting effects begin to dominate the flow (Fig. 1.26e), the flow field is called *hypersonic*. (Again, a somewhat arbitrary but frequently used rule of thumb for hypersonic flow is  $M_\infty > 5$ .) Hypersonic aerodynamics received a great deal of attention during the period 1955–1970 because atmospheric entry vehicles encounter the atmosphere at Mach numbers between 2.5 (ICBMs) and 36 (the Apollo lunar return vehicle). Today, hypersonic aerodynamics is just part of the whole spectrum of realistic flight speeds. Some basic elements of hypersonic flow are treated in Chap. 14.

In summary, we attempt to organize our study of aerodynamic flows according to one or more of the various categories discussed in this section. The block diagram in Fig. 1.27 is presented to help emphasize these categories, and to show how they are

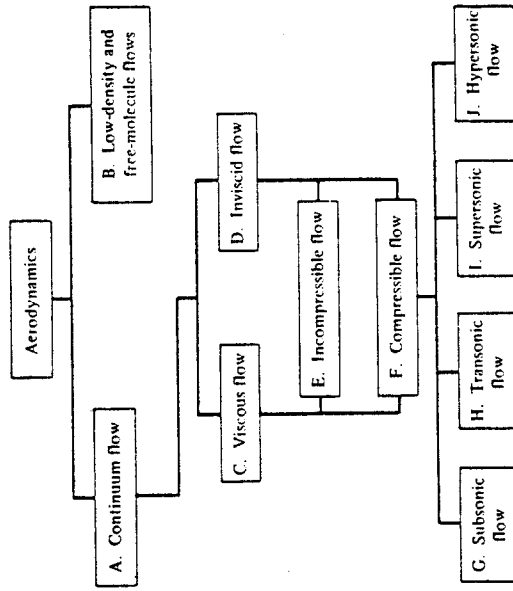


Figure 1.27 Block diagram categorizing the types of aerodynamic flows.

related. Indeed, Fig. 1.27 serves as a road map for this entire book. All the material to be covered in subsequent chapters fits into these blocks, which are lettered for easy reference. For example, Chap. 2 contains discussions of some fundamental aerodynamic principles and equations which fit into both blocks C and D. Chapters 3 to 6 fit into blocks D and E, Chap. 7 fits into blocks D and F, and so on. As we proceed with our development of aerodynamics, we will frequently refer to Fig. 1.27 in order to help put specific, detailed material in proper perspective relative to the whole of aerodynamics.

### 1.11 HISTORICAL NOTE: THE ILLUSIVE CENTER OF PRESSURE

The center of pressure of an airfoil was an important matter during the development of aeronautics. It was recognized in the nineteenth century that, for a heavier-than-air machine to fly at stable equilibrium conditions (e.g., straight and level flight), the moment about the vehicle's center of gravity must be zero (see chapter 7 of Ref. 2). The wing lift acting at the center of pressure, which is generally a distance away from the center of gravity, contributes substantially to this moment. Hence, the understanding and prediction of the center of pressure was felt to be absolutely necessary in order to design a vehicle with proper equilibrium. On the other hand, the early experimenters had difficulty measuring the center of pressure, and much confusion reigned. Let us examine this matter further.

The first experiments to investigate the center of pressure of a lifting surface were conducted by the Englishman George Cayley (1773–1857) in 1808. Cayley was the inventor of the modern concept of the airplane, namely, a vehicle with fixed wings, a fuselage, and a tail. He was the first to conceptually separate the functions of lift and propulsion; prior to Cayley, much thought had gone into ornithopters — machines that flapped their wings for both lift and thrust. Cayley rejected this idea, and in 1799, on a silver disk now in the collection of the Science Museum in London, he inscribed a sketch of a rudimentary airplane with all the basic elements we recognize today. Cayley was an active, inventive, and long-lived man, who conducted numerous pioneering aerodynamic experiments and fervently believed that powered, heavier-than-air, manned flight was inevitable. (See chapter 1 of Ref. 2 for an extensive discussion of Cayley's contributions to aeronautics.)

In 1808, Cayley reported on experiments of a winged model which he tested as a glider and as a kite. His comments on the center of pressure are as follows:

By an experiment made with a large kite formed of an hexagon with wings extended from it, all so constructed as to present a hollow curve to the current, I found that when loaded nearly to 1 lb to a foot and  $\frac{1}{2}$ , it required the center of gravity to be suspended so as to leave the anterior and posterior portions of the surface in the ratio of 3 to 7. But as this included the tail operating with a double leverage behind, I think such hollow surfaces relieve about an equal pressure on each part, when they are divided in the ratio of 5 to 12, 5 being the anterior portion. It is really surprising to find so great a difference, and it obliges the center of gravity of flying machines to be much forwarder of the center of bulk (the centroid) than could be supposed a priori.

Here, Cayley is saying that the center of pressure is 5 units from the leading edge and 12 units from the trailing edge; that is,  $x_{cp} = \frac{5}{12}c$ . Later, he states in addition: "I tried a small square sail in one plane, with the weight nearly the same, and I could not perceive that the center-of-resistance differed from the center of bulk." That is, Cayley is stating that the center of pressure in this case is  $\frac{1}{2}c$ .

There is no indication from Cayley's notes that he recognized that center-of-pressure moves when the lift, or angle of attack, is changed. However, there is no doubt that he was clearly concerned with the location of the center of pressure and its effect on aircraft stability.

The center of pressure on a flat surface inclined at a small angle to the flow was studied by Samuel P. Langley during the period 1887–1896. Langley was the secretary of the Smithsonian at that time, and devoted virtually all his time and much of the Smithsonian's resources to the advancement of powered flight. Langley was a highly respected physicist and astronomer, and he approached the problem of powered flight with the systematic and structured mind of a scientist. Using a whirling arm apparatus as well as scores of rubber-band powered models, he collected a large bulk of aerodynamic information with which he subsequently designed a full-scale aircraft. The efforts of Langley to build and fly a successful airplane resulted in two dismal failures in which his machine fell into the Potomac River — the last attempt being just 9 days before the Wright brothers' historic first flight on December 17, 1903. In spite of these failures, the work of Langley helped in many ways to advance powered flight. (See chapter 1 of Ref. 2 for more details.)

Langley's observations on the center of pressure for a flat surface inclined to the flow are found in the *Langley Memoir on Mechanical Flight, Part I, 1887 to 1896*, by Samuel P. Langley, and published by the Smithsonian Institution in 1911 — 5 years after Langley's death. In this paper, Langley states:

The center-of-pressure in an advancing inclined plane in soaring flight is always in advance of the center of figure, and moves forward as the angle-of-inclination of the sustaining surfaces diminishes, and, to a less extent, as horizontal flight increases in velocity. These facts furnish the elementary ideas necessary in discussing the problem of equilibrium, whose solution is of the most vital importance to successful flight.

The solution would be comparatively simple if the position of the center-of-pressure could be accurately known beforehand, but how difficult the solution is may be realized from a consideration of one of the facts just stated, namely, that the position of the center-of-pressure in horizontal flight shifts with velocity of the flight itself.

Here, we see that Langley is fully aware that the center of pressure moves over a lifting surface, but that its location is hard to pin down. Also, he notes the correct variation for a flat plate, namely, that  $x_{cp}$  moves forward as the angle of attack decreases. However, he is puzzled by the behavior of  $x_{cp}$  for a curved (cambered) airfoil. In his own words:

Later experiments conducted under my direction indicate that upon the curved surfaces I employed, the center-of-pressure moves forward with an increase in the angle of elevation, and backward with a decrease, so that it may lie even behind the center of the surface. Since for some surfaces the

center-of-pressure moves backward, and for others forward, it would seem that there might be some other surface for which it will be fixed.

Here, Langley is noting the totally opposite behavior of the travel of the center of pressure on a cambered airfoil in comparison to a flat surface, and is indicating ever so slightly some of his frustration in not being able to explain his results in a rational scientific way.

Three-hundred-and-fifty miles to the west of Langley, in Dayton, Ohio, Orville and Wilbur Wright were also experimenting with airfoils. As described in Sec. 1.1, the Wrights had constructed a small wind tunnel in their bicycle shop with which they conducted aerodynamic tests on hundreds of different airfoil and wing shapes during the fall, winter, and spring of 1901–1902. Clearly, the Wrights had an appreciation of the center of pressure, and their successful airfoil design used on the 1903 Wright Flyer is a testimonial to their mastery of the problem. Interestingly enough, in the written correspondence of the Wright brothers, only one set of results for the center of pressure can be found. This appears in Wilbur's notebook, dated July 25, 1905, in the form of a table and a graph. The graph is shown in Fig. 1.28 — the original form as plotted by Wilbur. Here, the center of pressure, given in terms of the percentage of distance from the leading edge, is plotted versus angle of attack. The data for two airfoils are given, one with large curvature (maximum height to chord ratio =  $\frac{1}{2}$ ) and one with more moderate curvature (maximum height to chord ratio =  $\frac{1}{8}$ ). These results show the now

familiar travel of the center of pressure for a curved airfoil, namely that  $x_{cp}$  moves forward as the angle of attack is increased, at least for small to moderate values of  $\alpha$ . However, the most forward excursion of  $x_{cp}$  in Fig. 1.28 is 33 percent behind the leading edge — the center of pressure is always behind the quarter-chord point.

The first practical airfoil theory, valid for thin airfoils, was developed by Ludwig Prandtl and his colleagues at Göttingen, Germany, during the period just prior to and during World War I. This thin airfoil theory is described in detail in Chap. 4. The result for the center of pressure for a curved (cambered) airfoil is given by Eq. (4.66), and shows that  $x_{cp}$  moves forward as the angle of attack (hence  $c_l$ ) increases, and that it is always behind the quarter-chord point for finite, positive values of  $c_l$ . This theory, in concert with more sophisticated wind-tunnel measurements that were being made during the period 1915–1925, finally brought the understanding and prediction of the location of the center of pressure for a cambered airfoil well into focus.

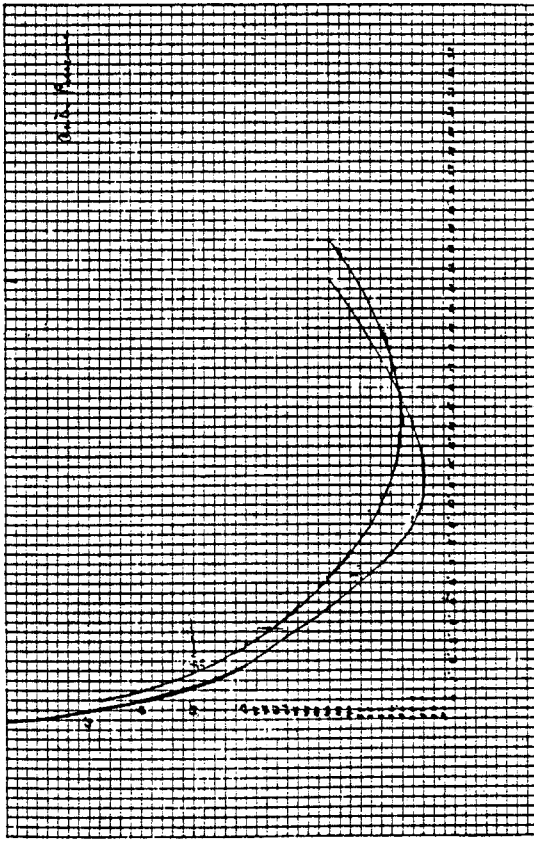
Because  $x_{cp}$  makes such a large excursion over the airfoil as the angle of attack is varied, its importance as a basic and practical airfoil property has diminished. Beginning in the early 1930s, the National Advisory Committee for Aeronautics (NACA), at its Langley Memorial Aeronautical Laboratory in Virginia, measured the properties of several systematically designed families of airfoils — airfoils which became a standard in aeronautical engineering. These NACA airfoils are discussed in Secs. 4.2 and 4.3. Instead of giving the airfoil data in terms of lift, drag, and center of pressure, the NACA chose the alternate systems of reporting lift, drag, and moments about either the quarter-chord point or the aerodynamic center. These are totally appropriate alternative methods of defining the force and moment system on an airfoil, as discussed in Sec. 1.6 and illustrated in Fig. 1.17. As a result, the center of pressure is rarely given as part of modern airfoil data. On the other hand, for three-dimensional bodies, such as slender projectiles and missiles, the location of the center of pressure still remains an important quantity, and modern missile data frequently include  $x_{cp}$ . Therefore, a consideration of center of pressure still retains its importance when viewed over the whole spectrum of flight vehicles.

## 1.12 SUMMARY

Refer again to the road map for Chap. 1 given in Fig. 1.6. Read again each block in this diagram as a reminder of the material we have covered. If you feel uncomfortable about some of the concepts, or if your memory is slightly "foggy" on certain points, go back and reread the pertinent sections until you have mastered the material.

This chapter has been primarily qualitative, emphasizing definitions and basic concepts. However, some of the more important quantitative relations are summarized below.

**Figure 1.28** Wright brothers' measurements of the center of pressure as a function of angle of attack for a curved (cambered) airfoil. Center of pressure is plotted on the ordinate in terms of percentage distance along the chord from the leading edge. This figure shows the actual data as hand plotted by Wilbur Wright, which appears in Wilbur's notebook dated July 25, 1905.



The normal, axial, lift, drag, and moment coefficients for an aerodynamic body can be obtained by integrating the pressure and skin friction coefficients over the body surface from the leading to the trailing edge. For a two-dimensional body:

## PROBLEMS

$$c_n = \frac{1}{c} \left[ \int_0^{LE} (C_{r,u} - C_{r,v}) dx + \int_{LE}^{\infty} (c_{f,u} + c_{f,v}) dy \right] \quad (1.15)$$

$$c_a = \frac{1}{c} \left[ \int_{LE}^E (C_{r,u} - C_{r,v}) dy + \int_0^E (c_{f,u} + c_{f,v}) dx \right] \quad (1.16)$$

$$c_{m,LE} = \frac{1}{c^2} \left[ \int_0^c (C_{r,u} - C_{r,v}) x dx - \int_{LE}^E (c_{f,u} + c_{f,v}) x dy \right. \\ \left. + \int_{LE}^E (C_{r,u} - C_{r,v}) y dy + \int_0^c (c_{f,u} + c_{f,v}) y dx \right] \quad (1.17)$$

$$c_l = c_n \cos \alpha - c_a \sin \alpha \quad (1.18)$$

$$c_d = c_n \sin \alpha + c_a \cos \alpha \quad (1.19)$$

The center of pressure is obtained from

$$x_{cp} = -\frac{M_{LE}}{N} \approx -\frac{M_{LE}}{L} \quad (1.20) \text{ and } (1.21)$$

The criteria for two or more flows to be dynamically similar are

1. The bodies and any other solid boundaries must be geometrically similar.
2. The similarity parameters must be the same. Two important similarity parameters are Mach number  $M = V/c$  and Reynolds number  $Re = \rho V c / \mu$ .

If two or more flows are dynamically similar, then the force coefficients  $C_L$ ,  $C_D$ , etc., are the same.

In fluid statics, the governing equation is the hydrostatic equation:

$$dp = -\gamma g dy \quad (1.45)$$

For a constant density medium, this integrates to

$$p + \rho g h = \text{constant} \quad (1.47)$$

$$\text{or } p_1 + \rho g h_1 = p_2 + \rho g h_2$$

Such equations govern, among other things, the operation of a manometer, and also lead to Archimedes' principle that the buoyancy force on a body immersed in a fluid is equal to the weight of the fluid displaced by the body.

- 1.1** For most gases at standard or near standard conditions, the relationship between pressure, density, and temperature is given by the perfect gas equation of state:  $p = \rho R T$ , where  $R$  is the specific gas constant. For air at near standard conditions,  $R = 287 \text{ J/(kg} \cdot \text{K)}$  in the International System of Units and  $R = 1716 \text{ ft} \cdot \text{lb}/(\text{slug} \cdot ^\circ\text{R})$  in the English Engineering System of Units. (More details on the perfect gas equation of state are given in Chap. 7.) Using the above information, consider the following two cases:
- (a) At a given point on the wing of a Boeing 727, the pressure and temperature of the air are  $1.9 \times 10^4 \text{ N/m}^2$  and  $203 \text{ K}$ , respectively. Calculate the density at this point.
  - (b) At a point in the test section of a supersonic wind tunnel, the pressure and density of the air are  $1058 \text{ lb/ft}^2$  and  $1.23 \times 10^{-3} \text{ slug/ft}^3$ , respectively. Calculate the temperature at this point.
- 1.2** Starting with Eqs. (1.7), (1.8), and (1.11), derive in detail Eqs. (1.15), (1.16), and (1.17).
- 1.3** Consider an infinitely thin flat plate of chord  $c$  at an angle of attack  $\alpha$  in a supersonic flow. The pressures on the upper and lower surfaces are different but constant over each surface; that is,  $p_u(x) = c_1$  and  $p_l(x) = c_2$ , where  $c_1$  and  $c_2$  are constants and  $c_2 > c_1$ . Ignoring the shear stress, calculate the location of the center of pressure.
- 1.4** Consider an infinitely thin flat plate with a 1-m chord at an angle of attack of  $10^\circ$  in a supersonic flow. The pressure and shear stress distributions on the upper surfaces are given by  $p_u = 4 \times 10^4 (x - 1)^2 + 5.4 \times 10^4$ ,  $p_l = 2 \times 10^4 (x - 1)^7 + 1.73 \times 10^4$ ,  $\tau_u = 288x^{-0.2}$ , and  $\tau_l = 731x^{-0.1}$ , respectively, where  $x$  is the distance from the leading edge in meters and  $p$  and  $\tau$  are in newtons per square meter. Calculate the normal and axial forces, the lift and drag, moments about the leading edge, and moments about the quarter chord, all per unit span. Also, calculate the location of the center of pressure.
- 1.5** Consider an airfoil at  $12^\circ$  angle of attack. The normal and axial force coefficients are 1.2 and 0.03, respectively. Calculate the lift and drag coefficients.
- 1.6** Consider an NACA 2412 airfoil (the meaning of the number designations for standard NACA airfoil shapes is discussed in Chap. 4). The following is a tabulation of the lift, drag, and moment coefficients about the quarter chord for this airfoil, as a function of angle of attack.

$\alpha$ (degrees)	$c_l$	$c_d$	$C_m, \text{at } 4$
-2.0	0.05	0.006	-0.042
0	0.25	0.006	-0.040
2.0	0.44	0.006	-0.038
4.0	0.64	0.007	-0.036
6.0	0.85	0.0075	-0.036
8.0	1.08	0.0092	-0.036
10.0	1.26	0.0115	-0.034
12.0	1.43	0.0150	-0.030
14.0	1.56	0.0186	-0.025

From this table, plot on graph paper the variation of  $x_{cp}/c$  as a function of  $\alpha$ .

- 1.7** The drag on the hull of a ship depends in part on the height of the water waves produced by the hull. The potential energy associated with these waves therefore depends on the acceleration of gravity,  $g$ . Hence, we can state that the wave drag on the hull is  $D = f(N, V, c, g)$  where  $c$  is a length scale associated with the hull, say, the maximum width of the hull. Define the drag coefficient as  $C_D = D/gc^2$ . Also, define a similarity parameter called the *Froude number*,  $Fr = V/\sqrt{gc}$ . Using Buckingham's pi theorem, prove that  $C_D = f(Pr)$ .
- 1.8** The shock waves on a vehicle in supersonic flight cause a component of drag called supersonic wave drag,  $D_{sw}$ . Define the wave-drag coefficient as  $C_{D,sw} = D_{sw}/q_s S$ , where  $S$  is a suitable reference area for the body. In supersonic flight, the flow is governed in part by its thermodynamic properties, given by the specific

heats at constant pressure,  $C_p$ , and at constant volume,  $C_v$ . Define the ratio  $C_p/C_v = \gamma$ . Using Buckingham's pi theorem, show that  $C_{D,\infty} = f(M_\infty, \gamma)$ . Neglect the influence of friction.

**1.9** Consider two different flows over geometrically similar airfoil shapes, one airfoil being twice the size of the other. The flow over the smaller airfoil has freestream properties given by  $T_\infty = 200\text{ K}$ ,  $\rho_\infty = 1.21\text{ kg/m}^3$ , and  $V_\infty = 100\text{ m/s}$ . The flow over the larger airfoil is described by  $T_\infty = 800\text{ K}$ ,  $\rho_\infty = 1.739\text{ kg/m}^3$ , and  $V_\infty = 200\text{ m/s}$ . Assume that both  $\mu$  and  $\alpha$  are proportional to  $T^{1/2}$ . Are the two flows dynamically similar?

**1.10** Consider a Lear jet flying at a velocity of  $250\text{ m/s}$  at an altitude of  $10\text{ km}$ , where the density and temperature are  $0.414\text{ kg/m}^3$  and  $223\text{ K}$ , respectively. Consider also a one-fifth scale model of the Lear jet being tested in a wind tunnel in the laboratory. The pressure in the test section of the wind tunnel is  $1\text{ atm} = 1.01 \times 10^5\text{ N/m}^2$ . Calculate the necessary velocity, temperature, and density of the airflow in the wind-tunnel test section such that the lift and drag coefficients are the same for the wind-tunnel model and the actual airplane in flight. Note: The relation between pressure, density, and temperature is given by the equation of state described in Prob. 1.1.

**1.11** A U-tube mercury manometer is used to measure the pressure at a point on the wing of a wind-tunnel model. One side of the manometer is connected to the model, and the other side is open to the atmosphere. Atmospheric pressure and the density of liquid mercury are  $1.01 \times 10^5\text{ N/m}^2$  and  $1.36 \times 10^4\text{ kg/m}^3$ , respectively. When the displacement of the two columns of mercury is  $20\text{ cm}$ , with the high column on the model side, what is the pressure on the wing?

**1.12** The German Zeppelins of World War I were dirigibles with the following typical characteristics: volume =  $15,000\text{ m}^3$  and maximum diameter =  $14.0\text{ m}$ . Consider a Zeppelin flying at a velocity of  $30\text{ m/s}$  at a standard altitude of  $10000\text{ m}$  (look up the corresponding density in any standard altitude table). The Zeppelin is at a small angle of attack such that its lift coefficient is  $0.05$  (based on the maximum cross-sectional area). The Zeppelin is flying in straight-and-level flight with no acceleration. Calculate the total weight of the Zeppelin.

**1.13** Consider a circular cylinder in a hypersonic flow, with its axis perpendicular to the flow. Let  $\phi$  be the angle measured between radii drawn to the leading edge (the stagnation point) and to any arbitrary point on the cylinder. The pressure coefficient distribution along the cylindrical surface is given by  $C_p = 2 \cos^2 \phi$  for  $0 \leq \phi \leq \pi/2$  and  $3\pi/2 \leq \phi \leq 2\pi$  and  $C_p = 0$  for  $\pi/2 \leq \phi \leq 3\pi/2$ . Calculate the drag coefficient for the cylinder, based on projected frontal area of the cylinder.

**1.14** Derive Archimedes' principle using a body of general shape.

To be a good craftsman, one must have good tools and know how to use them effectively. Similarly, a good aerodynamicist must have good aerodynamic tools and must know how to use them for a variety of applications. The purpose of this chapter is "tool-building"; we develop some of the concepts and equations which are vital to the study of aerodynamic flows. However, please be cautioned: A craftsman usually derives his or her pleasure from the works of art created with the *use* of the tools; the actual building of the tools themselves is sometimes considered a mundane chore. You may derive a similar feeling here. As we proceed to build our aerodynamic tools, you may wonder from time to time why such tools are necessary and what possible value they may have in the solution of practical problems. But rest assured that every aerodynamic tool we develop in this and subsequent chapters is important for the analysis and understanding of practical problems to be discussed later. So, as we move through this chapter, do not get lost or disoriented; rather, as we develop each tool, simply put it away in the store box of your mind for future use.

To help you keep track of our tool building, and to give you some orientation, the road map in Fig. 2.1 is provided for your reference. As we progress through each section of this chapter, use Fig. 2.1 to help you maintain a perspective of our work. You

## AERODYNAMICS: SOME FUNDAMENTAL PRINCIPLES AND EQUATIONS

*There is so great a difference between a fluid and a collection of solid particles that the laws of pressure and of equilibrium of fluids are very different from the laws of the pressure and equilibrium of solids.*

*Jean Le Rond d'Alembert. 1768*

*The principle is most important, not the detail.*

*Theodore von Karman, 1954*

### 2.1 INTRODUCTION AND ROAD MAP

### Aerodynamic tools

Basic flow equations  
(containing the fundamental physics of flows)

Review of vector relations  
(for convenience in expressing the aerodynamic tools)

Continuity equation

Momentum equation

Energy equation

Substantial derivative

Streamline

Vorticity

Circulation

Stream function

Velocity potential

The solution of practical aerodynamic problems

### Some Vector Algebra

Consider a vector quantity  $\mathbf{A}$ ; both its magnitude and direction are given by the arrow labeled  $\mathbf{A}$  in Fig. 2.2. The absolute magnitude of  $\mathbf{A}$  is  $|\mathbf{A}|$ , and is a scalar quantity. The *unit vector*  $\mathbf{n}$ , defined by  $\mathbf{n} = \mathbf{A}/|\mathbf{A}|$ , has a magnitude of unity and a direction equal to that of  $\mathbf{A}$ . Let  $\mathbf{B}$  represent another vector. The *vector addition* of  $\mathbf{A}$  and  $\mathbf{B}$  yields a third vector,  $\mathbf{C}$ ,

$$\mathbf{A} + \mathbf{B} = \mathbf{C} \quad (2.1)$$

which is formed by connecting the tail of  $\mathbf{A}$  with the head of  $\mathbf{B}$ , as shown in Fig. 2.2. Now consider  $-\mathbf{B}$ , which is equal in magnitude to  $\mathbf{B}$ , but opposite in direction. The vector subtraction of  $\mathbf{B}$  from  $\mathbf{A}$  yields vector  $\mathbf{D}$

$$\mathbf{A} - \mathbf{B} = \mathbf{D} \quad (2.2)$$

which is formed by connecting the tail of  $\mathbf{A}$  with the head of  $-\mathbf{B}$ , as shown in Fig. 2.2.

There are two forms of vector multiplication. Consider two vectors  $\mathbf{A}$  and  $\mathbf{B}$  at an angle  $\theta$  to each other, as shown in Fig. 2.2. The *scalar product* (dot product) of the two vectors  $\mathbf{A}$  and  $\mathbf{B}$  is defined as

$$\begin{aligned} \mathbf{A} \cdot \mathbf{B} &\equiv |\mathbf{A}| |\mathbf{B}| \cos \theta \\ &= \text{magnitude of } \mathbf{A} \times \text{magnitude of the component of } \mathbf{B} \text{ along the direction of } \mathbf{A} \end{aligned} \quad (2.3)$$

Note that the scalar product of two vectors is a scalar. In contrast, the *vector product* (cross product) of the two vectors  $\mathbf{A}$  and  $\mathbf{B}$  is defined as

$$\mathbf{A} \times \mathbf{B} \equiv (|\mathbf{A}| |\mathbf{B}| \sin \theta) \mathbf{e} = \mathbf{G} \quad (2.4)$$

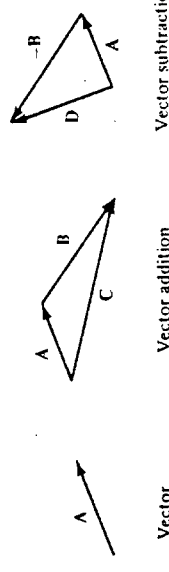
where  $\mathbf{G}$  is perpendicular to the plane of  $\mathbf{A}$  and  $\mathbf{B}$  and in a direction which obeys the "right-hand rule." (Rotate  $\mathbf{A}$  into  $\mathbf{B}$ , as shown in Fig. 2.2. Now curl the fingers of your right hand in the direction of the rotation. Your right thumb will be pointing in the

Figure 2.1 Road map for Chap. 2.

will note that Fig. 2.1 is full of strange-sounding terms, such as "substantial derivative," "circulation," and "velocity potential." However, when you finish this chapter, and you look back at Fig. 2.1, all these terms will be second nature to you.

## 2.2 REVIEW OF VECTOR RELATIONS

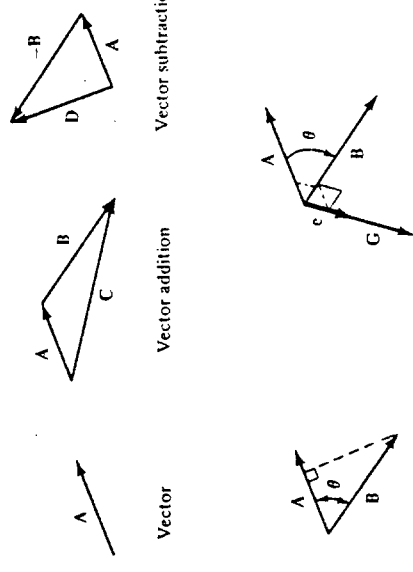
Aerodynamics is full of quantities that have both magnitude and direction, such as force and velocity. These are *vector quantities*, and as such, the mathematics of aerodynamics is most conveniently expressed in vector notation. The purpose of this section is to set forth the basic relations we need from vector algebra and vector calculus. If you are familiar with vector analysis, this section will serve as a concise review. If you are not conversant with vector analysis, this section will help you establish some vector notation, and will serve as a skeleton from which you can fill in more information from the many existing texts on vector analysis (see, for example, Refs. 4 to 6).



Vector product

Scalar product

Figure 2.2 Vector diagrams.



direction of  $\mathbf{G}$ .) In Eq. (2.4),  $\mathbf{e}$  is a unit vector in the direction of  $\mathbf{G}$ , as also shown in Fig. 2.2. Note that the vector product of two vectors is a vector.

### Typical Orthogonal Coordinate Systems

To describe mathematically the flow of fluid through three-dimensional space, we have to prescribe a three-dimensional coordinate system. The geometry of some aerodynamic problems best fits a rectangular space, whereas others are mainly cylindrical in nature, and yet others may have spherical properties. Therefore, we have interest in the three most common orthogonal coordinate systems: cartesian, cylindrical, and spherical. These systems are described below. (An orthogonal coordinate system is one where all three coordinate directions are mutually perpendicular. It is interesting to note that some modern numerical solutions of fluid flows utilize nonorthogonal coordinate spaces; moreover, for some numerical problems the coordinate system is allowed to evolve and change during the course of the solution. These so-called adaptive grid techniques are beyond the scope of this book. See Ref. 7 for details.)

A *cartesian coordinate system* is shown in Fig. 2.3a. The  $x$ ,  $y$ , and  $z$  axes are mutually perpendicular, and  $\mathbf{i}$ ,  $\mathbf{j}$ , and  $\mathbf{k}$  are unit vectors in the  $x$ ,  $y$ , and  $z$  directions, respectively. An arbitrary point  $P$  in space is located by specifying the three coordinates ( $x$ ,  $y$ ,  $z$ ). The point can also be located by the *position vector*  $\mathbf{r}$ , where

$$\mathbf{r} = xi + yj + zk$$

If  $\mathbf{A}$  is a given vector in cartesian space, it can be expressed as

$$\mathbf{A} = A_x \mathbf{i} + A_y \mathbf{j} + A_z \mathbf{k}$$

where  $A_x$ ,  $A_y$ , and  $A_z$  are the scalar components of  $\mathbf{A}$  along the  $x$ ,  $y$ , and  $z$  directions, respectively, as shown in Fig. 2.3b.

A *cylindrical coordinate system* is shown in Fig. 2.4a. A "phantom" cartesian system is also shown with dashed lines to help visualize the figure. The location of point

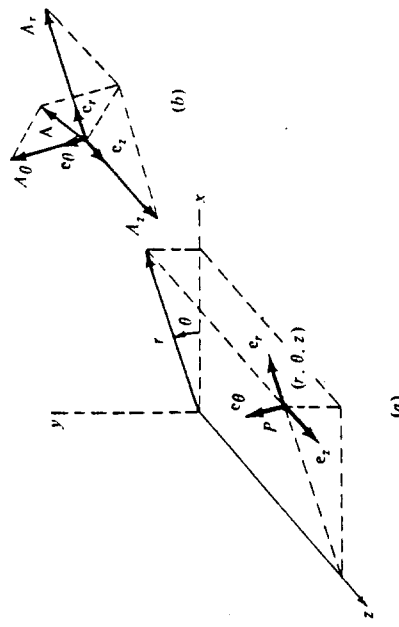


Figure 2.4 Cylindrical coordinates.

$P$  in space is given by three coordinates  $(r, \theta, z)$ , where  $r$  and  $\theta$  are measured in the  $xy$  plane shown in Fig. 2.4a. The  $r$  coordinate direction is the direction of increasing  $r$ , holding  $\theta$  and  $z$  constant;  $\mathbf{e}_r$  is the unit vector in the  $r$  direction. The  $\theta$  coordinate direction is the direction of increasing  $\theta$ , holding  $r$  and  $z$  constant;  $\mathbf{e}_\theta$  is the unit vector in the  $\theta$  direction. The  $z$  coordinate direction is the direction of increasing  $z$ , holding  $r$  and  $\theta$  constant;  $\mathbf{e}_z$  is the unit vector in the  $z$  direction. If  $\mathbf{A}$  is a given vector in cylindrical space, then

$$\mathbf{A} = A_r \mathbf{e}_r + A_\theta \mathbf{e}_\theta + A_z \mathbf{e}_z$$

where  $A_r$ ,  $A_\theta$ , and  $A_z$  are the scalar components of  $\mathbf{A}$  along the  $r$ ,  $\theta$ , and  $z$  directions, respectively, as shown in Fig. 2.4b. The relationship, or *transformation*, between cartesian and cylindrical coordinates can be obtained from inspection of Fig. 2.4a, namely,

$$\begin{aligned} x &= r \cos \theta \\ y &= r \sin \theta \\ z &= z \end{aligned} \tag{2.5}$$

or inversely,

$$\begin{aligned} r &= \sqrt{x^2 + y^2} \\ \theta &= \arctan \frac{y}{x} \\ z &= z \end{aligned} \tag{2.6}$$

$$z = z$$

A *spherical coordinate system* is shown in Fig. 2.5a. Once again, a phantom cartesian system is shown with dashed lines. (However, for clarity in the picture, the  $z$  axis is drawn vertically, in contrast to Figs. 2.3 and 2.4.) The location of point  $P$  in space is given by the three coordinates  $(r, \theta, \Phi)$ , where  $r$  is the distance of  $P$  from the

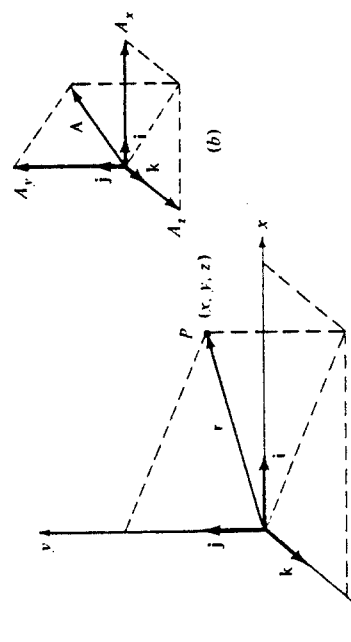


Figure 2.3 Cartesian coordinates.

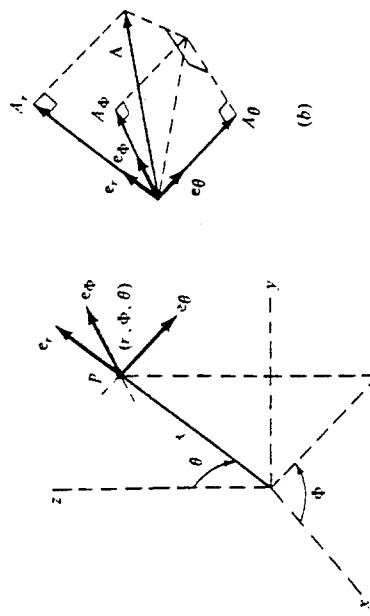


Figure 2.5 Spherical coordinates.

origin,  $\theta$  is the angle measured from the  $z$  axis and is in the  $rz$  plane, and  $\phi$  is the angle measured from the  $x$  axis and is in the  $xy$  plane. The  $r$  coordinate direction is the direction of increasing  $r$ , holding  $\theta$  and  $\phi$  constant;  $\mathbf{e}_r$  is the unit vector in the  $r$  direction. The  $\theta$  coordinate direction is the direction of increasing  $\theta$ , holding  $r$  and  $\phi$  constant;  $\mathbf{e}_\theta$  is the unit vector in the  $\theta$  direction. The  $\phi$  coordinate direction is the direction of increasing  $\phi$ , holding  $r$  and  $\theta$  constant;  $\mathbf{e}_\phi$  is the unit vector in the  $\phi$  direction. The unit vectors  $\mathbf{e}_r$ ,  $\mathbf{e}_\theta$ , and  $\mathbf{e}_\phi$  are mutually perpendicular. If  $\mathbf{A}$  is a given vector in spherical space, then

$$\mathbf{A} = A_r \mathbf{e}_r + A_\theta \mathbf{e}_\theta + A_\phi \mathbf{e}_\phi$$

where  $A_r$ ,  $A_\theta$ , and  $A_\phi$  are the scalar components of  $\mathbf{A}$  along the  $r$ ,  $\theta$ , and  $\phi$  directions, respectively, as shown in Fig. 2.5b. The transformation between cartesian and spherical coordinates is obtained from inspection of Fig. 2.5a, namely,

$$\begin{aligned} x &= r \sin \theta \cos \phi \\ y &= r \sin \theta \sin \phi \\ z &= r \cos \theta \end{aligned} \quad (2.7)$$

or inversely,

$$\begin{aligned} r &= \sqrt{x^2 + y^2 + z^2} \\ \theta &= \arccos \frac{z}{r} = \arccos \frac{z}{\sqrt{x^2 + y^2 + z^2}} \\ \phi &= \arccos \frac{x}{\sqrt{x^2 + y^2}} \end{aligned} \quad (2.8)$$

Cylindrical coordinates. Let

$$\begin{aligned} \mathbf{A} &= A_r \mathbf{e}_r + A_\theta \mathbf{e}_\theta + A_z \mathbf{e}_z \\ \mathbf{B} &= B_r \mathbf{e}_r + B_\theta \mathbf{e}_\theta + B_z \mathbf{e}_z \end{aligned} \quad (2.9)$$

(2.10)

## Scalar and Vector Fields

A scalar quantity given as a function of coordinate space and time  $t$  is called a *scalar field*. For example, pressure, density, and temperature are scalar quantities, and

$$\begin{aligned} p &= p_1(x, y, z, t) = p_2(r, \theta, z, t) = p_3(r, \theta, \Phi, t) \\ \rho &= \rho_1(x, y, z, t) = \rho_2(r, \theta, z, t) = \rho_3(r, \theta, \Phi, t) \\ T &= T_1(x, y, z, t) = T_2(r, \theta, z, t) = T_3(r, \theta, \Phi, t) \end{aligned}$$

are scalar fields for pressure, density, and temperature, respectively. Similarly, a vector quantity given as a function of coordinate space and time is called a *vector field*. For example, velocity is a vector quantity, and

$$\mathbf{V} = V_x \mathbf{i} + V_y \mathbf{j} + V_z \mathbf{k}$$

where

$$\begin{aligned} V_x &= V_x(x, y, z, t) \\ V_y &= V_y(x, y, z, t) \\ V_z &= V_z(x, y, z, t) \end{aligned}$$

is the vector field for  $\mathbf{V}$  in cartesian space. Analogous expressions can be written for vector fields in cylindrical and spherical space. In many theoretical aerodynamic problems, the above scalar and vector fields are the unknowns to be obtained in a solution for a flow with prescribed initial and boundary conditions.

## Scalar and Vector Products

The scalar and vector products defined by Eqs. (2.3) and (2.4), respectively, can be written in terms of the components of each vector as follows.

Cartesian coordinates. Let

$$\begin{aligned} \mathbf{A} &= A_x \mathbf{i} + A_y \mathbf{j} + A_z \mathbf{k} \\ \mathbf{B} &= B_x \mathbf{i} + B_y \mathbf{j} + B_z \mathbf{k} \\ \mathbf{A} \cdot \mathbf{B} &= A_x B_x + A_y B_y + A_z B_z \end{aligned} \quad (2.9)$$

and

Then

and

$$\mathbf{A} \times \mathbf{B} = \begin{bmatrix} i & j & k \\ A_x & A_y & A_z \\ B_x & B_y & B_z \end{bmatrix} = i(A_y B_z - A_z B_y) + j(A_z B_x - A_x B_z) + k(A_x B_y - A_y B_x) \quad (2.10)$$

Then  $\mathbf{A} \cdot \mathbf{B} = A_r B_r + A_\theta B_\theta + A_\Phi B_\Phi$  (2.11)

$$\text{and } \mathbf{A} \times \mathbf{B} = \begin{vmatrix} \mathbf{e}_r & \mathbf{e}_\theta & \mathbf{e}_\Phi \\ A_r & A_\theta & A_\Phi \\ B_r & B_\theta & B_\Phi \end{vmatrix} \quad (2.12)$$

Spherical coordinates. Let

$$\mathbf{A} = A_r \mathbf{e}_r + A_\theta \mathbf{e}_\theta + A_\Phi \mathbf{e}_\Phi$$

$$\mathbf{B} = B_r \mathbf{e}_r + B_\theta \mathbf{e}_\theta + B_\Phi \mathbf{e}_\Phi$$

$$\text{and } \mathbf{A} \cdot \mathbf{B} = A_r B_r + A_\theta B_\theta + A_\Phi B_\Phi \quad (2.13)$$

$$\text{and } \mathbf{A} \times \mathbf{B} = \begin{vmatrix} \mathbf{e}_r & \mathbf{e}_\theta & \mathbf{e}_\Phi \\ A_r & A_\theta & A_\Phi \\ B_r & B_\theta & B_\Phi \end{vmatrix} \quad (2.14)$$

### Gradient of a Scalar Field

We now begin a review of some elements of vector calculus. Consider a scalar field  $p = p(x, y, z) = p(r, \theta, z) = p(r, \theta, \Phi)$

The *gradient* of  $p$ ,  $\nabla p$ , at a given point in space is defined as a vector such that

1. Its magnitude is the maximum rate of change of  $p$  per unit length of the coordinate space at the given point.
2. Its direction is that of the maximum rate of change of  $p$  at the given point.

For example, consider a two-dimensional pressure field in cartesian space as sketched in Fig. 2.6. The solid curves are lines of constant pressure; i.e., they connect points in the pressure field which have the same value of  $p$ . Such lines are called *isolines*. Consider an arbitrary point  $(x, y)$  in Fig. 2.6. If we move away from this point in an arbitrary direction,  $p$  will, in general, change because we are moving to another location in space. Moreover, there will be some direction from this point along which  $p$  changes the most over a unit length in that direction. This defines the *direction of the gradient* of  $p$  and is identified in Fig. 2.6. The magnitude of  $\nabla p$  is the rate of change of  $p$  per unit length in that direction. Both the magnitude and direction of  $\nabla p$

### Divergence of a Vector Field

Consider a vector field,

$$\mathbf{V} = \mathbf{V}(x, y, z) = \mathbf{V}(r, \theta, z) = \mathbf{V}(r, \theta, \Phi)$$

In the above,  $\mathbf{V}$  can represent any vector quantity. However, for practical purposes, and to aid in physical interpretation, consider  $\mathbf{V}$  to be the flow velocity. Also, visualize a

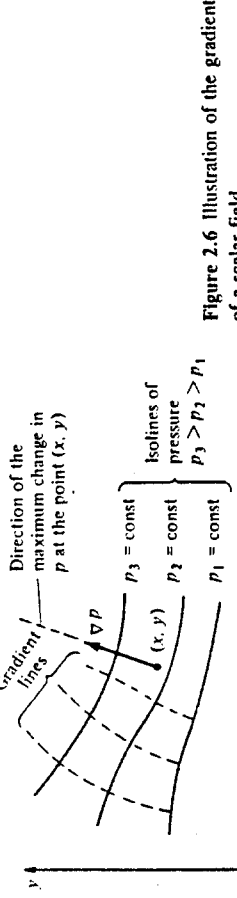
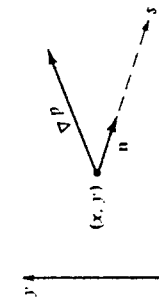


Figure 2.7 Sketch for the directional derivative.

small fluid element of fixed mass moving along a streamline with velocity  $\mathbf{V}$ . As the fluid element moves through space, its volume will, in general, change. In Sec. 2.3 we prove that the time rate of change of the volume of a moving fluid element of fixed mass, per unit volume of that element, is equal to the *divergence* of  $\mathbf{V}$ , denoted by  $\nabla \cdot \mathbf{V}$ . The divergence of a vector is a scalar quantity; it is one of two ways that the derivative of a vector field can be defined. In different coordinate systems, we have

$$\text{Cartesian: } \mathbf{V} = \mathbf{V}(x, y, z) = V_x \mathbf{i} + V_y \mathbf{j} + V_z \mathbf{k}$$

$$\nabla \cdot \mathbf{V} = \frac{\partial V_x}{\partial x} + \frac{\partial V_y}{\partial y} + \frac{\partial V_z}{\partial z} \quad (2.19)$$

$$\text{Cylindrical: } \mathbf{V} = \mathbf{V}(r, \theta, z) = V_r \mathbf{e}_r + V_\theta \mathbf{e}_\theta + V_z \mathbf{e}_z$$

$$\nabla \cdot \mathbf{V} = \frac{1}{r} \frac{\partial}{\partial r} (r V_r) + \frac{1}{r} \frac{\partial V_\theta}{\partial \theta} + \frac{\partial V_z}{\partial z} \quad (2.20)$$

$$\text{Spherical: } \mathbf{V} = \mathbf{V}(r, \theta, \Phi) = V_r \mathbf{e}_r + V_\theta \mathbf{e}_\theta + V_\Phi \mathbf{e}_\Phi$$

$$\nabla \cdot \mathbf{V} = \frac{1}{r^2} \frac{\partial}{\partial r} (r^2 V_r) + \frac{1}{r \sin \theta} \frac{\partial}{\partial \theta} (V_\theta \sin \theta) + \frac{1}{r \sin \theta} \frac{\partial V_\Phi}{\partial \Phi} \quad (2.21)$$

### Line Integrals

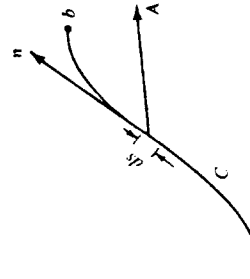
Consider a vector field

$$\mathbf{A} = \mathbf{A}(x, y, z) = \mathbf{A}(r, \theta, z) = \mathbf{A}(r, \theta, \Phi)$$

Also, consider a curve  $C$  in space connecting two points  $a$  and  $b$  as shown on the left side of Fig. 2.8. Let  $d\mathbf{s}$  be an elemental length of the curve, and  $\mathbf{n}$  be a unit vector tangent to the curve. Define the vector  $d\mathbf{s} = \mathbf{n} ds$ . Then, the *line integral* of  $A$  along curve  $C$  from point  $a$  to point  $b$  is

$$\int_a^b \mathbf{A} \cdot d\mathbf{s} \quad (2.22)$$

If the curve  $C$  is closed, as shown at the right of Fig. 2.8, then the line integral is given by



Although  $\mathbf{V}$  can be any vector quantity, again consider  $\mathbf{V}$  to be the flow velocity. Once again visualize a fluid element moving along a streamline. It is possible for this fluid element to be rotating with an angular velocity  $\boldsymbol{\omega}$  as it translates along the streamline. In Sec. 2.9 we prove that  $\boldsymbol{\omega}$  is equal to one-half of the *curl* of  $\mathbf{V}$ , where the curl of  $\mathbf{V}$  is denoted by  $\nabla \times \mathbf{V}$ . The curl of  $\mathbf{V}$  is a vector quantity; it is the alternate way that the derivative of a vector field can be defined, the first being  $\nabla \cdot \mathbf{V}$  (see Sec. 2.2, Divergence of a Vector Field). In different coordinate systems, we have

$$\text{Cartesian: } \mathbf{V} = V_x \mathbf{i} + V_y \mathbf{j} + V_z \mathbf{k}$$

$$\nabla \times \mathbf{V} = \begin{vmatrix} \mathbf{i} & \mathbf{j} & \mathbf{k} \\ \frac{\partial}{\partial x} & \frac{\partial}{\partial y} & \frac{\partial}{\partial z} \\ V_x & V_y & V_z \end{vmatrix} = \mathbf{i} \left( \frac{\partial V_z}{\partial y} - \frac{\partial V_y}{\partial z} \right) + \mathbf{j} \left( \frac{\partial V_x}{\partial z} - \frac{\partial V_z}{\partial x} \right) + \mathbf{k} \left( \frac{\partial V_y}{\partial x} - \frac{\partial V_x}{\partial y} \right) \quad (2.23)$$

Figure 2.8 Sketch for line integrals.

$$\oint_C \mathbf{A} \cdot d\mathbf{s}$$

where the *counterclockwise* direction around  $C$  is considered positive. (The positive direction around a closed curve is, by convention, that direction you would move such that the area enclosed by  $C$  is always on your left.)

### Surface Integrals

Consider an open surface  $S$  bounded by the closed curve  $C$ , as shown in Fig. 2.9. At point  $P$  on the surface, let  $dS$  be an elemental area of the surface and  $\mathbf{n}$  be a unit vector normal to the surface. The orientation of  $\mathbf{n}$  is in the direction according to the right-hand rule for movement along  $C$ . (Curl the fingers of your right hand in the direction of movement around  $C$ ; your thumb will then point in the general direction of  $\mathbf{n}$ .) Define a vector elemental area as  $d\mathbf{S} = \mathbf{n} dS$ . In terms of  $d\mathbf{S}$ , the *surface integral* over the surface  $S$  can be defined in three ways:

$$\iint_S p d\mathbf{S} = \text{surface integral of a scalar } p \text{ over the open surface } S \text{ (the result is a vector)}$$

$$\iint_S \mathbf{A} \cdot d\mathbf{S} = \text{surface integral of a vector } \mathbf{A} \text{ over the open surface } S \text{ (the result is a scalar)}$$

$$\iint_S \mathbf{A} \times d\mathbf{S} = \text{surface integral of a vector } \mathbf{A} \text{ over the open surface } S \text{ (the result is a vector)}$$

If the surface  $S$  is *closed* (e.g., the surface of a sphere or a cube),  $\mathbf{n}$  points out of the surface, away from the enclosed volume, as shown in Fig. 2.10. The surface integrals over the closed surface are

$$\iint_S p d\mathbf{S} \quad \iint_S \mathbf{A} \cdot d\mathbf{S} \quad \iint_S \mathbf{A} \times d\mathbf{S}$$

### Volume Integrals

Consider a volume  $V$  in space. Let  $\rho$  be a scalar field in this space. The *volume integral* over the volume  $V$  of the quantity  $\rho$  is written as

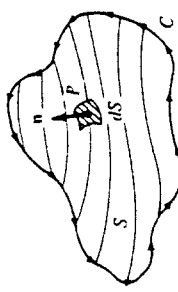


Figure 2.9 Sketch for surface integrals. The three-dimensional surface area  $S$  is bounded by the closed curve  $C$ .

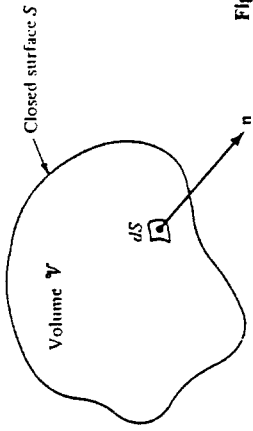


Figure 2.10 Volume  $V$  enclosed by the closed surface  $S$ .

$$\iiint_V \rho dV = \text{volume integral of a scalar } \rho \text{ over the volume } V \text{ (the result is a scalar)}$$

Let  $\mathbf{A}$  be a vector field in space. The volume integral over the volume  $V$  of the quantity  $\mathbf{A}$  is written as

$$\iiint_V \mathbf{A} dV = \text{volume integral of a vector } \mathbf{A} \text{ over the volume } V \text{ (the result is a vector)}$$

### Relations between Line, Surface, and Volume Integrals

Consider again the open area  $S$  bounded by the closed curve  $C$ , as shown in Fig. 2.9. Let  $\mathbf{A}$  be a vector field. The line integral of  $\mathbf{A}$  over  $C$  is related to the surface integral of  $\mathbf{A}$  over  $S$  by *Stokes' theorem*:

$$\oint_C \mathbf{A} \cdot d\mathbf{s} = \iint_S (\nabla \times \mathbf{A}) \cdot d\mathbf{S} \quad (2.25)$$

Consider again the volume  $V$  enclosed by the closed surface  $S$ , as shown in Fig. 2.10. The surface and volume integrals of the vector field  $\mathbf{A}$  are related through the *divergence theorem*

$$\iint_S \mathbf{A} \cdot d\mathbf{S} = \iiint_V (\nabla \cdot \mathbf{A}) dV \quad (2.26)$$

If  $p$  represents a scalar field, a vector relationship analogous to Eq. (2.26) is given by the *gradient theorem*:

$$\iint_S p d\mathbf{S} = \iiint_V \nabla p dV \quad (2.27)$$

### Summary

This section has provided a concise review of those elements of vector analysis which we will use as tools in our subsequent discussions. Make certain to review these tools until you feel comfortable with them, especially the relations in boxes.

## 2.3 MODELS OF THE FLUID: CONTROL VOLUMES AND FLUID ELEMENTS

Aerodynamics is a fundamental science, steeped in physical observation. As you proceed through this book, make every effort to gradually develop a “physical feel” for the material. An important virtue of all successful aerodynamics (indeed, of all successful engineers and scientists) is that they have good “physical intuition,” based on thought and experience, which allows them to make reasonable judgments on difficult problems. Although this chapter is full of equations and (seemingly) esoteric concepts, now is the time for you to start developing this physical feel.

With this section, we begin to build the basic equations of aerodynamics. There is a certain philosophical procedure involved with the development of these equations, as follows:

1. Invoke three fundamental physical principles which are deeply entrenched in our macroscopic observations of nature, namely,
  - a. Mass is conserved, i.e., mass can be neither created nor destroyed.
  - b. Newton’s second law: force = mass × acceleration.
  - c. Energy is conserved; it can only change from one form to another.
2. Determine a suitable *model* of the fluid. Remember that a fluid is a squishy substance, and therefore it is usually more difficult to describe than a well-defined solid body. Hence, we have to adopt a reasonable model of the fluid to which we can apply the fundamental principles stated in item 1.
3. Apply the fundamental physical principles listed in item 1 to the model of the fluid determined in item 2 in order to obtain mathematical equations which properly describe the physics of the flow. In turn, use these fundamental equations to analyze any particular aerodynamic flow problem of interest.

In this section, we concentrate on item 2, namely, we ask the question: What is a suitable model of the fluid? How do we visualize this squishy substance in order to apply the three fundamental physical principles to it? There is no single answer to this question; rather, three different models have been used successfully throughout the modern evolution of aerodynamics. They are (1) finite control volume, (2) infinitesimal fluid element, and (3) molecular. Let us examine what these models involve and how they are applied.

### Finite Control Volume Approach

Consider a general flow field as represented by the streamlines in Fig. 2.11. Let us imagine a closed volume drawn within a *finite* region of the flow. This volume defines

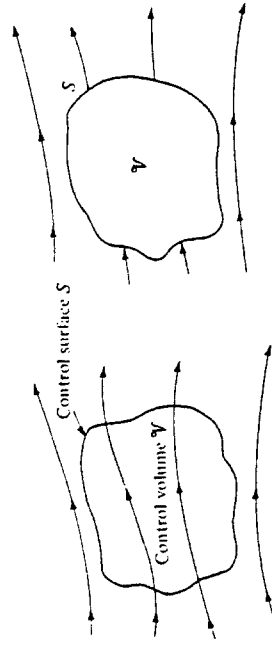


Figure 2.11 Finite control volume approach.  
Finite control volume moving  
fixed in space with the  
fluid moving through it

Figure 2.11 Finite control volume approach.

a *control volume*,  $V$ , and a *control surface*,  $S$ , is defined as the closed surface which bounds the control volume. The control volume may be *fixed* in space with the fluid moving through it, as shown at the left of Fig. 2.11. Alternatively, the control volume may be moving with the fluid such that the same fluid particles are always inside it, as shown at the right of Fig. 2.11. In either case, the control volume is a reasonably large, finite region of the flow. The fundamental physical principles are applied to the fluid inside the control volume, and to the fluid crossing the control surface (if the control volume is fixed in space). Therefore, instead of looking at the whole flow field at once, with the control volume model we limit our attention to just the fluid in the finite region of the volume itself.

### Infinitesimal Fluid Element Approach

Consider a general flow field as represented by the streamlines in Fig. 2.12. Let us imagine an infinitesimally small fluid element in the flow, with a differential volume  $dV$ . The fluid element is infinitesimal in the same sense as differential calculus; however, it is large enough to contain a huge number of molecules so that it can be viewed as a continuous medium. The fluid element may be fixed in space with the fluid moving

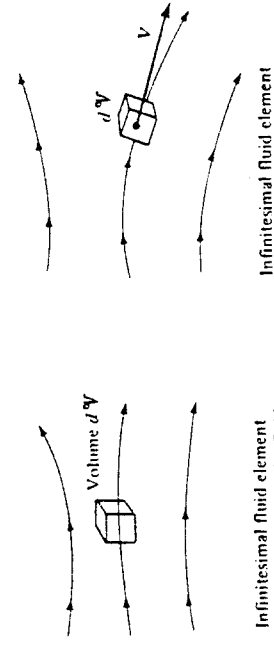


Figure 2.12 Infinitesimal fluid element approach.  
Infinite fluid element  
moving along a streamline with  
the velocity v equal to the  
local flow velocity at each point

Figure 2.12 Infinitesimal fluid element approach.

through it, as shown at the left of Fig. 2.12. Alternatively, it may be moving along a streamline with velocity  $\mathbf{V}$  equal to the flow velocity at each point. Again, instead of looking at the whole flow field at once, the fundamental physical principles are applied to just the fluid element itself.

### Molecular Approach

In actuality, of course, the motion of a fluid is a ramification of the mean motion of its atoms and molecules. Therefore, a third model of the flow can be a microscopic approach wherein the fundamental laws of nature are applied directly to the atoms and molecules, using suitable statistical averaging to define the resulting fluid properties. This approach is in the purview of *kinetic theory*, which is a very elegant method with many advantages in the long run. However, it is beyond the scope of the present book. In summary, although many variations on the theme can be found in different texts for the derivation of the general equations of fluid flow, the flow model can usually be categorized under one of the approaches described above.

In the equations to follow, the divergence of velocity,  $\nabla \cdot \mathbf{V}$ , occurs frequently. Before leaving this section, let us prove the statement made earlier (Sec. 2.2) that  $\nabla \cdot \mathbf{V}$  is physically the time rate of change of the volume of a moving fluid element of fixed mass per unit volume of that element. Consider a control volume moving with the fluid (the case shown on the right of Fig. 2.11). This control volume is always made up of the same fluid particles as it moves with the flow; hence, its mass is fixed, invariant with time. However, its volume  $\delta V$  and control surface  $S$  are changing with time as it moves to different regions of the flow where different values of  $\rho$  exist. That is, this moving control volume of fixed mass is constantly increasing or decreasing its volume and is changing its shape, depending on the characteristics of the flow. This control volume is shown in Fig. 2.13 at some instant in time. Consider an infinitesimal element of the surface  $dS$  moving at the local velocity  $\mathbf{V}$ , as shown in Fig. 2.13. The change in the volume of the control volume  $\Delta V$ , due to just the movement of  $dS$  over a time increment  $\Delta t$  is, from Fig. 2.13, equal to the volume of the long, thin cylinder with base area  $dS$  and altitude  $(\mathbf{V} \Delta t) \cdot \mathbf{n}$ ; that is,

$$\Delta V = [(\mathbf{V} \Delta t) \cdot \mathbf{n}] dS = (\mathbf{V} \Delta t) \cdot dS \quad (2.28)$$

Over the time increment  $\Delta t$ , the total change in volume of the whole control volume is equal to the summation of Eq. (2.28) over the total control surface. In the limit as  $dS \rightarrow 0$ , the sum becomes the surface integral

$$\text{or}$$

$$\frac{D(\delta V)}{Dt} = (\nabla \cdot \mathbf{V}) \delta V$$

$$\frac{D(\delta V)}{Dt} = \iint_S (\nabla \cdot \mathbf{V}) dS \quad (2.32)$$

Examine Eq. (2.32). It states that  $\nabla \cdot \mathbf{V}$  is physically the *time rate of change of the volume of a moving fluid element, per unit volume*. Hence, the interpretation of  $\nabla \cdot \mathbf{V}$ , first given in Sec. 2.2, Divergence of a Vector Field, is now proved.

### 2.4 CONTINUITY EQUATION

In Sec. 2.3 we discussed several models which can be used to study the motion of a fluid. Following the philosophy set forth at the beginning of Sec. 2.3, we now apply the fundamental physical principles to such models. Unlike the above derivation of the physical significance of  $\nabla \cdot \mathbf{V}$  wherein we used the model of a moving finite control volume, we now employ the model of a *fixed* finite control volume as sketched on the left side of Fig. 2.11. Here, the control volume is fixed in space, with the flow moving

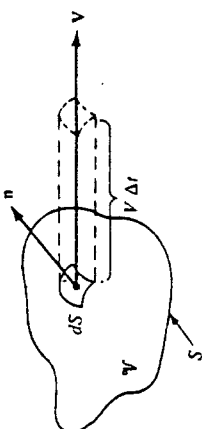


Figure 2.13 Moving control volume used for the physical interpretation of the divergence of velocity.

through it. Unlike our previous derivation, the volume  $V$  and control surface  $S$  are now constant with time, and the mass of fluid contained within the control volume can change as a function of time (due to unsteady fluctuations of the flow field).

Before starting the derivation of the fundamental equations of aerodynamics, we must examine a concept vital to those equations, namely, the concept of *mass flow*. Consider a given area  $A$  arbitrarily oriented in a flow field as shown in Fig. 2.14. In Fig. 2.14, we are looking at an edge view of area  $A$ . Let  $A$  be small enough such that the flow velocity  $\mathbf{V}$  is uniform across  $A$ . Consider the fluid elements with velocity  $\mathbf{V}$  that pass through  $A$ . In time  $dt$  after crossing  $A$ , they have moved a distance  $\mathbf{V} dt$  and have swept out the shaded volume shown in Fig. 2.14. This volume is equal to the base area  $A$  times the height of the cylinder,  $V_n dt$ , where  $V_n$  is the component of velocity normal to  $A$ , i.e.,

$$\text{Volume} = (V_n dt)A \quad (2.33)$$

The mass inside the shaded volume is, therefore,

$$\text{Mass} = \rho(V_n dt)A \quad (2.33)$$

This is the mass that has swept past  $A$  in time  $dt$ . By definition, the *mass flow* through  $A$  is the mass crossing  $A$  per second (e.g., newtons per second, slugs per second). Let  $\dot{m}$  denote mass flow. From Eq. (2.33),

$$\dot{m} = \frac{\rho(V_n dt)A}{dt} \quad (2.34)$$

or

$$\boxed{\dot{m} = \rho V_n A} \quad (2.34)$$

Equation (2.34) demonstrates that mass flow through  $A$  is given by the product  $\text{Area} \times \text{density} \times \text{component of flow velocity normal to the area}$ .

A related concept is that of *mass flux*, defined as the mass flow *per unit area*. From Eq. (2.34),

$$\boxed{\text{Mass flux} = \frac{\dot{m}}{A} = \rho V_n} \quad (2.35)$$

Typical units of mass flux are  $\text{kg}/(\text{s} \cdot \text{m}^2)$  and  $\text{slug}/(\text{s} \cdot \text{ft}^2)$ .

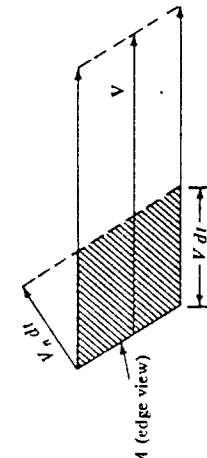


Figure 2.14 Sketch for discussion of mass flow through area  $A$  in a flow field.

The concepts of mass flow and mass flux are important. Note from Eq. (2.35) that mass flux across a surface is equal to the product of density times the component of velocity perpendicular to the surface. Many of the equations of aerodynamics involve products of density and velocity. For example, in cartesian coordinates,  $\mathbf{V} = V_x \mathbf{i} + V_y \mathbf{j} + V_z \mathbf{k} = u\mathbf{i} + v\mathbf{j} + w\mathbf{k}$ , where  $u$ ,  $v$ , and  $w$  denote the  $x$ ,  $y$ , and  $z$  components of velocity, respectively. (The use of  $u$ ,  $v$ , and  $w$  rather than  $V_x$ ,  $V_y$ , and  $V_z$  to symbolize the  $x$ ,  $y$ , and  $z$  components of velocity is quite common in aerodynamic literature; we henceforth adopt the  $u$ ,  $v$ , and  $w$  notation.) In many of the equations of aerodynamics, you will find the products  $\rho u$ ,  $\rho v$ , and  $\rho w$ ; always remember that these products are the mass fluxes in the  $x$ ,  $y$ , and  $z$  directions, respectively. In a more general sense, if  $V$  is the magnitude of velocity in an arbitrary direction, the product  $\rho V$  is physically the mass flux (mass flow per unit area) across an area oriented perpendicular to the direction of  $V$ .

We are now ready to apply our first physical principle to a finite control volume fixed in space.

**Physical principle** Mass can be neither created or destroyed.

Consider a flow field wherein all properties vary with spatial location and time, e.g.,  $\rho = \rho(x, y, z, t)$ . In this flow field, consider the fixed finite control volume shown in Fig. 2.15. At a point on the control surface, the flow velocity is  $\mathbf{V}$  and the vector elemental surface area is  $dS$ . Also,  $dV$  is an elemental volume inside the control volume. Applied to this control volume, the above physical principle means

$$\text{Net mass flow out of control volume } S = \frac{\text{time rate of decrease of mass inside control volume } S}{\text{volume through surface } S} \quad (2.36a)$$

or

$$B = C \quad (2.36b)$$

where  $B$  and  $C$  are just convenient symbols for the left and right sides, respectively, of Eq. (2.36a). First, let us obtain an expression for  $B$  in terms of the quantities shown in Fig. 2.15. From Eq. (2.34), the elemental mass flow across the area  $dS$  is

$$\rho V_n dS = \rho \mathbf{V} \cdot d\mathbf{S}$$

Examining Fig. 2.15, note that by convention,  $d\mathbf{S}$  always points in a direction *out of* the control volume. Hence, when  $\mathbf{V}$  also points out of the control volume (as shown in Fig. 2.15), the product  $\rho \mathbf{V} \cdot d\mathbf{S}$  is *positive*. Moreover, when  $\mathbf{V}$  points out of the

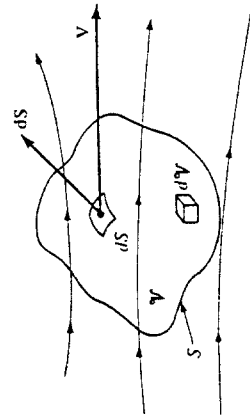


Figure 2.15 Finite control volume fixed in space.

control volume, the mass flow is physically leaving the control volume; i.e., it is an *outflow*. Hence, a positive  $\rho \mathbf{V} \cdot d\mathbf{S}$  denotes an outflow. In turn, when  $\mathbf{V}$  points into the control volume,  $\rho \mathbf{V} \cdot d\mathbf{S}$  is *negative*. Moreover, when  $\mathbf{V}$  points inward, the mass flow is physically entering the control volume; i.e., it is an *inflow*. Hence, a negative  $\rho \mathbf{V} \cdot d\mathbf{S}$  denotes an *inflow*. The *net* mass flow *out* of the entire control surface  $S$  is the summation over  $S$  of the elemental mass flows. In the limit, this becomes a surface integral, which is physically the left side of Eqs. (2.36a and b), i.e.,

$$B = \oint_S \rho \mathbf{V} \cdot d\mathbf{S} \quad (2.37)$$

Now consider the right side of Eqs. (2.36a and b). The mass contained within the elemental volume  $dV$  is

$$\rho dV$$

Hence, the total mass inside the control volume is

$$\iiint_V \rho dV$$

The time rate of *increase* of mass inside  $V$  is then

$$\frac{\partial}{\partial t} \iiint_V \rho dV$$

In turn, the time rate of *decrease* of mass inside  $V$  is the negative of the above; i.e.,

$$-\frac{\partial}{\partial t} \iiint_V \rho dV = C \quad (2.38)$$

Thus, substituting Eqs. (2.37) and (2.38) into (2.36b), we have

$$\oint_S \rho \mathbf{V} \cdot d\mathbf{S} = -\frac{\partial}{\partial t} \iiint_V \rho dV$$

$$\boxed{\frac{\partial}{\partial t} \iiint_V \rho dV + \oint_S \rho \mathbf{V} \cdot d\mathbf{S} = 0} \quad (2.39)$$

Equation (2.39) is the final result of applying the physical principle of the conservation of mass to a finite control volume fixed in space. Equation (2.39) is called the *continuity equation*. It is one of the most fundamental equations of fluid dynamics.

Note that Eq. (2.39) expresses the continuity equation in integral form. We will have numerous opportunities to use this form; it has the advantage of relating aerodynamic phenomena over a finite region of space without being concerned about the details of precisely what is happening at a given distinct point in the flow. On the other hand, there are many times when we are concerned with the details of a flow and we want to have equations which relate flow properties at a *given point*. In such a case,

the integral form as expressed in Eq. (2.39) is not particularly useful. However, Eq. (2.39) can be reduced to another form which does relate flow properties at a given point, as follows. To begin with, since the control volume used to obtain Eq. (2.39) is fixed in space, the limits of integration are also fixed. Hence, the time derivative can be placed inside the volume integral, and Eq. (2.39) can be written as

$$\iiint_V \frac{\partial \rho}{\partial t} dV + \oint_S \rho \mathbf{V} \cdot d\mathbf{S} = 0 \quad (2.40)$$

Applying the divergence theorem, Eq. (2.26), the right-hand term of Eq. (2.40) can be expressed as

$$\oint_S \rho (\mathbf{V} \cdot d\mathbf{S}) = \iiint_V \nabla \cdot (\rho \mathbf{V}) dV \quad (2.41)$$

Substituting Eq. (2.41) into (2.40),

$$\begin{aligned} & \iiint_V \left[ \frac{\partial \rho}{\partial t} + \nabla \cdot (\rho \mathbf{V}) \right] dV = 0 \\ \text{or} \quad & \iiint_V \left[ \frac{\partial \rho}{\partial t} dV + \iiint_V \nabla \cdot (\rho \mathbf{V}) dV \right] dV = 0 \end{aligned} \quad (2.42)$$

Examine the integrand of Eq. (2.42). If the integrand were a finite number, then Eq. (2.42) would require that the integral over part of the control volume be equal and opposite in sign to the integral over the remainder of the control volume, such that the net integration would be zero. However, the finite control volume is *arbitrarily* drawn in space; there is no reason to expect cancellation of one region by the other. Hence, the only way for the integral in Eq. (2.42) to be zero for an arbitrary control volume is for the integrand to be zero at *all* points within the control volume. Thus, from Eq. (2.42), we have

$$\boxed{\frac{\partial \rho}{\partial t} + \nabla \cdot (\rho \mathbf{V}) = 0} \quad (2.43)$$

Equation (2.43) is the continuity equation in the form of a partial differential equation. This equation relates the flow field variables at a *point in the flow*, as opposed to Eq. (2.39), which deals with a finite space.

It is important to keep in mind that Eqs. (2.39) and (2.43) are equally valid statements of the physical principle of conservation of mass. They are mathematical representations, but always remember that they speak words — they say that mass can be neither created nor destroyed.

Note that in the derivation of the above equations, the only assumption about the nature of the fluid is that it is a continuum. Therefore, Eqs. (2.39) and (2.43) hold in general for the three-dimensional, unsteady flow of any type of fluid, inviscid or viscous, compressible or incompressible. (Note: It is important to keep track of all assumptions which are used in the derivation of any equation because they tell you the

Limitations on the final result and, therefore, prevent you from using an equation for a situation in which it is not valid. In all our future derivations, develop the habit of noting all assumptions that go with the resulting equations.)

It is important to emphasize the difference between unsteady and steady flows. In an *unsteady* flow, the flow field variables are a function of both spatial location and time, e.g.,

$$\rho = \rho(x, y, z, t)$$

This means that if you lock your eyes on one fixed point in space, the density at that point will change with time. Such unsteady fluctuations can be caused by time-varying boundaries (e.g., an airfoil pitching up and down with time or the supply valves of a wind tunnel being turned off and on). Equations (2.39) and (2.43) hold for such unsteady flows. On the other hand, the vast majority of practical aerodynamic problems involve *steady* flow. Here, the flow field variables are a function of spatial location only, e.g.,

$$\rho = \rho(x, y, z)$$

This means that if you lock your eyes on a fixed point in space, the density at that point will be a fixed value, invariant with time. For steady flow,  $\partial/\partial t = 0$ , and hence Eqs. (2.39) and (2.43) reduce to

$$\oint_S \rho \mathbf{v} \cdot d\mathbf{S} = 0 \quad (2.44)$$

$$\nabla \cdot (\rho \mathbf{v}) = 0 \quad (2.45)$$

## 2.5 MOMENTUM EQUATION

Newton's second law is frequently written as

$$\mathbf{F} = m \mathbf{a} \quad (2.46)$$

where  $\mathbf{F}$  is the force exerted on a body of mass  $m$  and  $\mathbf{a}$  is the acceleration. However, a more general form of Eq. (2.46) is

$$\mathbf{F} = \frac{d}{dt} (m \mathbf{V}) \quad (2.47)$$

which reduces to Eq. (2.46) for a body of constant mass. In Eq. (2.47),  $m \mathbf{V}$  is the momentum of a body of mass  $m$ . Equation (2.47) represents the second fundamental principle upon which theoretical fluid dynamics is based.

**Physical principle** Force = time rate of change of momentum.

We will apply this principle [in the form of Eq. (2.47)] to the model of a finite control volume fixed in space as sketched in Fig. 2.15. Our objective is to obtain expressions for both the left and right sides of Eq. (2.47) in terms of the familiar flow-field variables  $p$ ,  $\rho$ ,  $\mathbf{V}$ , etc. First, let us concentrate on the left side of Eq. (2.47), i.e., obtain an expression for  $\mathbf{F}$ , which is the force exerted on the fluid as it flows through the control volume. This force comes from two sources:

1. *Body forces*: gravity, electromagnetic forces, or any other forces which "act at a distance" on the fluid inside  $V$
2. *Surface forces*: pressure and shear stress acting on the control surface  $S$

Let  $\mathbf{f}$  represent the net body force per unit mass exerted on the fluid inside  $V$ . The body force on the elemental volume  $dV$  in Fig. 2.15 is therefore

$$\rho \mathbf{f} dV$$

and the total body force exerted on the fluid in the control volume is the summation of the above over the volume  $V$ ,

$$\text{Body force} = \iiint_V \rho \mathbf{f} dV \quad (2.48)$$

The elemental surface force due to pressure acting on the element of area  $dS$  is

$$-p d\mathbf{S}$$

where the negative sign indicates that the force is in the direction opposite of  $dS$ . That is, the control surface is experiencing a pressure force which is directed into the control volume and which is due to the pressure from the surroundings, and examination of Fig. 2.15 shows that such an inward-directed force is in the direction opposite of  $dS$ . The complete pressure force is the summation of the elemental forces over the entire control surface

$$\text{Pressure force} = -\iint_S p d\mathbf{S} \quad (2.49)$$

In a viscous flow, the shear and normal viscous stresses also exert a surface force. A detailed evaluation of these viscous stresses is not warranted at this stage of our discussion. Let us simply recognize this effect by letting  $\mathbf{F}_{\text{viscous}}$  denote the total viscous force exerted on the control surface. We are now ready to write an expression for the left-hand side of Eq. (2.47). The total force experienced by the fluid as it is sweeping through the fixed control volume is given by the sum of Eqs. (2.48) and (2.49) and  $\mathbf{F}_{\text{viscous}}$ .

$$\mathbf{F} = \iiint_V \rho \mathbf{f} dV - \iint_S p d\mathbf{S} + \mathbf{F}_{\text{viscous}} \quad (2.50)$$

Now consider the right side of Eq. (2.47). The time rate of change of momentum of the fluid as it sweeps through the fixed control volume is the sum of two terms:

$$\begin{aligned} \text{Net flow of momentum out} \\ \text{of control volume across surface } S &= G \end{aligned} \quad (2.51a)$$

Time rate of change of momentum due to  
unsteady fluctuations of flow properties inside  $\mathcal{V} \equiv H$  (2.51b)

Consider the term denoted by  $G$  in Eq. (2.51a). The flow has a certain momentum as it enters the control volume in Fig. 2.15, and in general it has a different momentum as it leaves the control volume (due in part to the force  $F$  that is exerted on the fluid as it is sweeping through  $\mathcal{V}$ ). The *net* flow of momentum *out* of the control volume across the surface  $S$  is simply this outflow minus the inflow of momentum across the control surface. This change in momentum is denoted by  $G$ , as noted above. To obtain an expression for  $G$ , recall that the mass flow across the elemental area  $dS$  is  $(\rho \mathbf{V} \cdot d\mathbf{S})$ ; hence, the flow of momentum per second across  $dS$  is

$$(\rho \mathbf{V} \cdot d\mathbf{S}) \mathbf{V} \quad (2.52)$$

The net flow of momentum out of the control volume through  $S$  is the summation of the above elemental contributions, namely,

$$G = \oint_S (\rho \mathbf{V} \cdot d\mathbf{S}) \mathbf{V} \quad (2.52)$$

In Eq. (2.52), recall that positive values of  $(\rho \mathbf{V} \cdot d\mathbf{S})$  represent mass flow out of the control volume, and negative values represent mass flow into the control volume. Hence, in Eq. (2.52) the integral over the whole control surface is a combination of positive contributions (outflow of momentum) and negative contributions (inflow of momentum), with the resulting value of the integral representing the net outflow of momentum. If  $G$  has a positive value, there is more momentum flowing out of the control volume per second than flowing in; conversely, if  $G$  has a negative value, there is more momentum flowing into the control volume per second than flowing out.

Now consider  $H$  from Eq. (2.51b). The momentum of the fluid in the elemental volume  $d\mathcal{V}$  shown in Fig. 2.15 is

$$(\rho d\mathcal{V}) \mathbf{V}$$

The momentum contained at any instant inside the control volume is therefore

$$\iiint_V \rho \mathbf{V} d\mathcal{V}$$

and its time rate of change due to unsteady flow fluctuations is

$$H = \frac{\partial}{\partial t} \iiint_V \rho \mathbf{V} d\mathcal{V} \quad (2.53)$$

Combining Eqs. (2.52) and (2.53), we obtain an expression for the total time rate of change of momentum of the fluid as it sweeps through the fixed control volume, which in turn represents the right-hand side of Eq. (2.47)

$$\frac{d}{dt} (m \mathbf{V}) = G + H = \iint_S (\rho \mathbf{V} \cdot d\mathbf{S}) \mathbf{V} + \frac{\partial}{\partial t} \iiint_V \rho \mathbf{V} d\mathcal{V} \quad (2.54)$$

Hence, from Eqs. (2.50) and (2.54), Newton's second law,

$$\frac{d}{dt} (m \mathbf{V}) = \mathbf{F}$$

applied to a fluid flow is

$$\boxed{\frac{\partial}{\partial t} \iiint_V \rho \mathbf{V} d\mathcal{V} + \iint_S (\rho \mathbf{V} \cdot d\mathbf{S}) \mathbf{V} = - \oint_S \rho \mathbf{V} d\mathbf{S} + \iiint_V \rho \mathbf{f} d\mathcal{V} + \mathbf{F}_{\text{viscous}}} \quad (2.55)$$

Equation (2.55) is the momentum equation in integral form. Note that it is a vector equation. Just as in the case of the integral form of the continuity equation, Eq. (2.55) has the advantage of relating aerodynamic phenomena over a finite region of space without being concerned with the details of precisely what is happening at a given distinct point in the flow. This advantage is illustrated in Sec. 2.6.

From Eq. (2.55), we now proceed to a partial differential equation which relates flow-field properties at a point in space. Such an equation is a counterpart to the differential form of the continuity equation given in Eq. (2.43). Apply the gradient theorem, Eq. (2.27), to the first term on the right side of Eq. (2.55).

$$-\oint_S \rho \mathbf{V} d\mathbf{S} = - \iiint_V \nabla \rho \mathbf{V} d\mathcal{V} \quad (2.56)$$

Also, because the control volume is fixed, the time derivative in Eq. (2.55) can be placed inside the integral. Hence, Eq. (2.55) can be written as

$$\iiint_V \frac{\partial (\rho \mathbf{V})}{\partial t} d\mathcal{V} + \iint_S (\rho \mathbf{V} \cdot d\mathbf{S}) \mathbf{V} = - \iiint_V \nabla \rho \mathbf{V} d\mathcal{V} + \iiint_V \rho \mathbf{f} d\mathcal{V} + \mathbf{F}_{\text{viscous}} \quad (2.57)$$

Recall that Eq. (2.57) is a vector equation. It is convenient to write this equation as three scalar equations. Using cartesian coordinates, where

$$\mathbf{V} = u\mathbf{i} + v\mathbf{j} + w\mathbf{k}$$

the  $x$  component of Eq. (2.57) is

$$\iiint_V \frac{\partial (\rho u)}{\partial t} d\mathcal{V} + \iint_S (\rho \mathbf{V} \cdot d\mathbf{S}) u = - \iiint_V \frac{\partial \rho}{\partial x} d\mathcal{V} + \iiint_V \rho f_x d\mathcal{V} + (F_x)_{\text{viscous}} \quad (2.58)$$

[Note: In Eq. (2.58), the product  $(\rho \mathbf{V} \cdot d\mathbf{S})$  is a scalar and, therefore, has no components.] Apply the divergence theorem, Eq. (2.26), to the surface integral on the left side of Eq. (2.58):

$$\oint\limits_S (\rho V \cdot dS) u = \oint\limits_V (\rho u V) \cdot dS = \oint\limits_V \nabla \cdot (\rho u V) dV \quad (2.59)$$

Substituting Eq. (2.59) into Eq. (2.58), we have

$$\oint\limits_V \left[ \frac{\partial(\rho u)}{\partial t} + \nabla \cdot (\rho u V) + \frac{\partial p}{\partial x} - \rho f_x - (\mathcal{F}_x)_{viscous} \right] dV = 0 \quad (2.60)$$

where  $(\mathcal{F}_x)_{viscous}$  denotes the proper form of the  $x$  component of the viscous shear stresses when placed inside the volume integral (this form will be obtained explicitly in Chap. 15). For the same reasons as stated in Sec. 2.4, the integrand in Eq. (2.60) is identically zero at all points in the flow; hence,

$$\frac{\partial(\rho u)}{\partial t} + \nabla \cdot (\rho u V) = -\frac{\partial p}{\partial x} + \rho f_x + (\mathcal{F}_x)_{viscous} \quad (2.61a)$$

Equation (2.61a) is the  $x$  component of the momentum equation in differential form. Returning to Eq. (2.57), and writing the  $y$  and  $z$  components, we obtain in a similar fashion,

$$\frac{\partial(\rho v)}{\partial t} + \nabla \cdot (\rho v V) = -\frac{\partial p}{\partial y} + \rho f_y + (\mathcal{F}_y)_{viscous} \quad (2.61b)$$

$$\frac{\partial(\rho w)}{\partial t} + \nabla \cdot (\rho w V) = -\frac{\partial p}{\partial z} + \rho f_z + (\mathcal{F}_z)_{viscous} \quad (2.61c)$$

where the subscripts  $y$  and  $z$  on  $f$  and  $\mathcal{F}$  denote the  $y$  and  $z$  components of the body and viscous forces, respectively. Equations (2.61a to c) are the scalar  $x$ ,  $y$ , and  $z$  components of the momentum equation, respectively; they are partial differential equations which relate flow-field properties at any point in the flow.

Note that Eqs. (2.55) and (2.61a to c) apply to the unsteady, three-dimensional flow of any fluid, compressible or incompressible, viscous or inviscid. Specialized to a steady ( $\partial/\partial t = 0$ ), inviscid ( $\mathbf{F}_{viscous} = 0$ ) flow with no body forces ( $\mathbf{f} = 0$ ), these equations become:

$$\oint\limits_S (\rho V \cdot dS) V = -\oint\limits_S p dS \quad (2.62)$$

$$\boxed{\begin{aligned} \nabla \cdot (\rho u V) &= -\frac{\partial p}{\partial x} \\ \nabla \cdot (\rho v V) &= -\frac{\partial p}{\partial y} \\ \nabla \cdot (\rho w V) &= -\frac{\partial p}{\partial z} \end{aligned}} \quad (2.63a)$$

$$\text{and} \quad \boxed{\begin{aligned} \frac{\partial(\rho u)}{\partial t} + \nabla \cdot (\rho u V) + \frac{\partial p}{\partial x} - \rho f_x - (\mathcal{F}_x)_{viscous} \end{aligned}} \quad (2.63b)$$

$$\boxed{\begin{aligned} \frac{\partial(\rho v)}{\partial t} + \nabla \cdot (\rho v V) + \frac{\partial p}{\partial y} - \rho f_y - (\mathcal{F}_y)_{viscous} \end{aligned}} \quad (2.63c)$$

Since most of the material in Chaps. 3 through 14 assumes steady, inviscid flow with no body forces, we will have frequent occasion to use the momentum equation in the forms of Eqs. (2.62) and (2.63a to c).

The momentum equations for an inviscid flow [such as Eqs. (2.63a to c)] are called the *Euler equations*. The momentum equations for a viscous flow [such as Eqs. (2.61a to c)] are called the *Navier-Stokes equations*. We will encounter this terminology in subsequent chapters.

## 2.6 AN APPLICATION OF THE MOMENTUM EQUATION: DRAG OF A TWO-DIMENSIONAL BODY

We briefly interrupt our orderly development of the fundamental equations of fluid dynamics in order to examine an important application of the integral form of the momentum equation. During the 1930s and 1940s, the National Advisory Committee for Aeronautics (NACA) measured the lift and drag characteristics of a series of systematically designed airfoil shapes (discussed in detail in Chap. 4). These measurements were carried out in a specially designed wind tunnel where the wing models spanned the entire test section, i.e., the wing tips were butted against both sidewalls of the wind tunnel. This was done in order to establish two-dimensional (rather than three-dimensional) flow over the wing, thus allowing the properties of an airfoil (rather than a finite wing) to be measured. The distinction between the aerodynamics of airfoils and that of finite wings is made in Chaps. 4 and 5. The important point here is that because the wings were mounted against both sidewalls of the wind tunnel, the NACA did not use a conventional force balance to measure the lift and drag. Rather, the lift was obtained from the pressure distributions on the *ceiling and floor* of the tunnel (above and below the wing), and the drag was obtained from measurements of the flow velocity *downstream* of the wing. These measurements may appear to be a strange way to measure the aerodynamic force on a wing. Indeed, how are these measurements related to lift and drag? What is going on here? The answers to these questions are addressed in this section; they involve an application of the fundamental momentum equation in integral form, and they illustrate a basic technique that is frequently used in aerodynamics.

Consider a two-dimensional body in a flow, as sketched in Fig. 2.16. A control volume is drawn around this body, as given by the dashed lines in Fig. 2.16. The control volume is bounded by

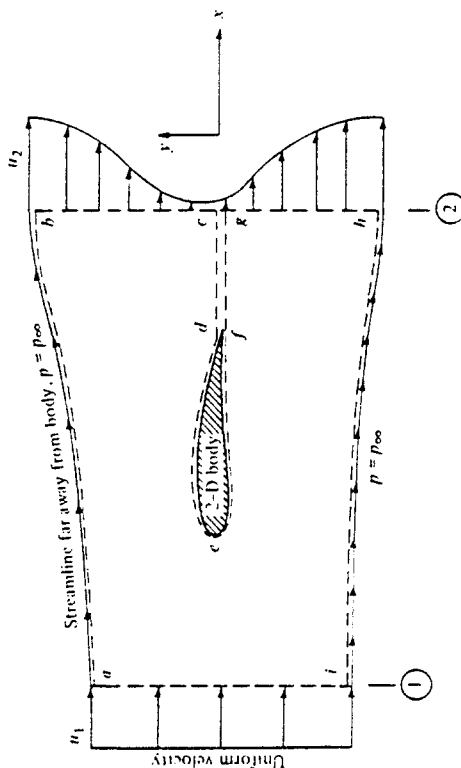


Figure 2.16 Control volume for obtaining drag on a two-dimensional body.

1. The upper and lower streamlines far above and below the body (*ab* and *hi*, respectively).
2. Lines perpendicular to the flow velocity far ahead of and behind the body (*cdefg*).
3. A cut that surrounds and wraps the surface of the body (*abhi*).

The entire control volume is *abhiabcdefgabhi*. The width of the control volume in the *z* direction (perpendicular to the page) is unity. Stations 1 and 2 are inflow and outflow stations, respectively.

Assume that the contour *abhi* is far enough from the body such that the pressure is everywhere the same on *abhi* and equal to the freestream pressure  $p = p_\infty$ . Also assume that the inflow velocity  $u_1$  is uniform across *ai* (as it would be in a freestream, or a test section of a wind tunnel). The outflow velocity  $u_2$  is *not* uniform across *bh*, because the presence of the body has created a wake at the outflow station. However, assume that both  $u_1$  and  $u_2$  are in the *x* direction; hence,  $u_1 = \text{constant}$  and  $u_2 = f(y)$ .

Consider the surface forces on the control volume. They stem from two contributions:

1. The pressure distribution over the surface *abhi*,

$$-\iint_{abhi} p \, dS$$

2. The surface force on *def* created by the presence of the body,

In the list above, the surface shear stress on *ab* and *hi* has been neglected. Also, note that in Fig. 2.16 the cuts *cd* and *f'g'* are taken adjacent to each other; hence, any shear stress or pressure distribution on one is equal and opposite to that on the other, i.e., the

surface forces on *cd* and *fg'* cancel each other. Also note that the surface force on *def* is the *equal and opposite reaction* to the shear stress and pressure distribution created by the flow over the surface of the body. To see this more clearly, examine Fig. 2.17. On the left is shown the flow over the body. As explained in Sec. 1.5, the moving fluid exerts pressure and shear stress distributions over the body surface which create a resultant aerodynamic force per unit span  $\mathbf{R}'$  on the body. In turn, by Newton's third law, the body exerts equal and opposite pressure and shear stress distributions on the flow, i.e., on the part of the control surface bounded by *def*. Hence, the body exerts a force  $-\mathbf{R}'$  on the control surface, as shown on the right of Fig. 2.17. With the above in mind, the total surface force on the entire control volume is

$$\text{Surface force} = - \iint_{abhi} p \, dS - \mathbf{R}' \quad (2.64)$$

Moreover, this is the *total* force on the control volume shown in Fig. 2.16 because the volumetric body force is negligible.

Consider the integral form of the momentum equation as given by Eq. (2.55). The right-hand side of this equation is physically the force on the fluid moving through the control volume. For the control volume in Fig. 2.16, this force is simply the expression given by Eq. (2.64). Hence, using Eq. (2.55), with the right-hand side given by Eq. (2.64), we have

$$\frac{\partial}{\partial t} \iiint_V \rho \mathbf{V} \, dV + \iint_S (\rho \mathbf{V} \cdot \mathbf{dS}) \mathbf{V} = - \iint_{abhi} p \, dS - \mathbf{R}' \quad (2.65)$$

Assuming steady flow, Eq. (2.65) becomes

$$\mathbf{R}' = - \iint_S (\rho \mathbf{V} \cdot \mathbf{dS}) \mathbf{V} - \iint_{abhi} p \, dS \quad (2.66)$$

Equation (2.66) is a vector equation. Consider again the control volume in Fig. 2.16. Take the *x* component of Eq. (2.66), noting that the inflow and outflow velocities  $u_1$  and  $u_2$  are in the *x* direction and the *x* component of  $\mathbf{R}'$  is the aerodynamic drag per unit span  $D'$ .

$$D' = - \iint_S (\rho \mathbf{V} \cdot \mathbf{dS}) u - \iint_{abhi} (p \, dS), \quad (2.67)$$



Flow exerts  $p$  and  $r$  on the surface of the body, giving a resultant aerodynamic force  $\mathbf{R}$   
Equal and opposite reaction: body exerts a surface force on the section of the control volume *def* that equals  $-\mathbf{R}$

Figure 2.17 Equal and opposite reactions on a body and adjacent section of control surface.

In Eq. (2.67), the last term is the component of the pressure force in the  $x$  direction. [The expression  $(p/dS)$ , is the  $x$  component of the pressure force exerted on the elemental area  $dS$  of the control surface.] Recall that the boundaries of the control volume *abhi* are chosen far enough from the body such that  $p$  is constant along these boundaries. For a constant pressure,

$$\iint_{\text{abhi}} (p \, dS)_x = 0 \quad (2.68)$$

because, looking along the  $x$  direction in Fig. 2.16, the pressure force on *abhi* pushing toward the right exactly balances the pressure force pushing toward the left. This is true no matter what the shape of *abhi* is, as long as  $p$  is constant along the surface (for proof of this statement, see Prob. 2.3). Therefore, substituting Eq. (2.68) into (2.67),

$$D' = - \iint_{\text{abhi}} (\rho \mathbf{V} \cdot d\mathbf{S})_u \quad (2.69)$$

Evaluating the surface integral in Eq. (2.69), note from Fig. 2.16 that

1. The sections, *ab*, *hi*, and *df*, are streamlines of the flow. Since by definition  $\mathbf{V}$  is parallel to the streamlines and  $d\mathbf{S}$  is perpendicular to the control surface, along these sections  $\mathbf{V}$  and  $d\mathbf{S}$  are perpendicular vectors, and hence,  $\mathbf{V} \cdot d\mathbf{S} = 0$ . As a result, the contributions of *ab*, *hi*, and *df* to the integral in Eq. (2.69) are zero.
2. The cuts *cd* and *fg* are adjacent to each other. The mass flux out of one is identically the mass flux into the other. Hence, the contributions of *cd* and *fg* to the integral in Eq. (2.69) cancel each other.

As a result, the only contributions to the integral in Eq. (2.69) come from sections *ai* and *bh*. These sections are oriented in the  $y$  direction. Also, the control volume has unit depth in the  $z$  direction (perpendicular to the page). Hence, for these sections,  $dS = dy(1)$ . The integral in Eq. (2.69) becomes

$$\iint_{\text{abhi}} (\rho \mathbf{V} \cdot d\mathbf{S})_u = - \int_a^b \rho_1 u_1^2 dy + \int_h^b \rho_2 u_2^2 dy \quad (2.70)$$

Note that the minus sign in front of the first term on the right-hand side of Eq. (2.70) is due to  $\mathbf{V}$  and  $d\mathbf{S}$  being in opposite directions along *ai* (station 1 is an inflow boundary); in contrast,  $\mathbf{V}$  and  $d\mathbf{S}$  are in the same direction over *bh* (station 2 is an outflow boundary), and hence the second term has a positive sign.

Before going further with Eq. (2.70), consider the integral form of the continuity equation for steady flow, Eq. (2.44). Applied to the control volume in Fig. 2.16, Eq. (2.44) becomes

$$\begin{aligned} & - \int_i^a \rho_1 u_1 dy + \int_h^b \rho_2 u_2 dy = 0 \\ \text{or} \quad & \int_i^a \rho_1 u_1 dy = \int_h^b \rho_2 u_2 dy \end{aligned} \quad (2.71)$$

In Eq. (2.67), the last term is the component of the pressure force in the  $x$  direction. [The expression  $(p/dS)$ , is the  $x$  component of the pressure force exerted on the elemental area  $dS$  of the control surface.] Recall that the boundaries of the control volume *abhi* are chosen far enough from the body such that  $p$  is constant along these boundaries. For a constant pressure,

$$\iint_{\text{abhi}} (p \, dS)_x = 0 \quad (2.68)$$

because, looking along the  $x$  direction in Fig. 2.16, the pressure force on *abhi* pushing toward the right exactly balances the pressure force pushing toward the left. This is true no matter what the shape of *abhi* is, as long as  $p$  is constant along the surface (for proof of this statement, see Prob. 2.3). Therefore, substituting Eq. (2.68) into (2.67),

$$D' = \iint_{\text{abhi}} \rho_2 u_2 (u_1 - u_2) dy \quad (2.69)$$

Equation (2.74) is the desired result of this section; it expresses the drag of a body in terms of the known freestream velocity  $u_1$  and the flow-field properties  $\rho_2$  and  $u_2$ , across a vertical station downstream of the body. These downstream properties can be measured in a wind tunnel, and the drag per unit span of the body,  $D'$ , can be obtained by evaluating the integral in Eq. (2.74) numerically, using the measured data for  $\rho_2$  and  $u_2$  as a function of  $y$ .

Examine Eq. (2.74) more closely. The quantity  $u_1 - u_2$  is the velocity decrement at a given  $y$  location. That is, because of the drag on the body, there is a wake that trails downstream of the body. In this wake, there is a loss in flow velocity  $u_1 - u_2$ . The quantity  $\rho_2 u_2$  is simply the mass flux; when multiplied by  $u_1 - u_2$ , it gives the decrement in momentum. Therefore, the integral in Eq. (2.74) is physically the decrement in momentum flow that exists across the wake, and from Eq. (2.74), this wake momentum decrement is equal to the drag on the body.

For incompressible flow,  $\rho = \text{constant}$  and is known. For this case, Eq. (2.74) becomes

$$D' = \rho \int_h^b u_2 (u_1 - u_2) dy \quad (2.75)$$

Equation (2.75) is the answer to the questions posed at the beginning of this section. It shows how a measurement of the velocity distribution across the wake of a body can yield the drag. These velocity distributions are conventionally measured with a Pitot rake, such as shown in Fig. 2.18. This is nothing more than a series of Pitot tubes attached to a common stem, which allows the simultaneous measurement of velocity across the wake. (The principle of the Pitot tube as a velocity-measuring instrument is discussed in Chap. 3. See also pages 94–108 of Ref. 2 for an introductory discussion on Pitot tubes.)

The result embodied in Eq. (2.75) illustrates the power of the integral form of the momentum equation; it relates drag on a body located at some position in the flow to the flow-field variables at a completely different location.

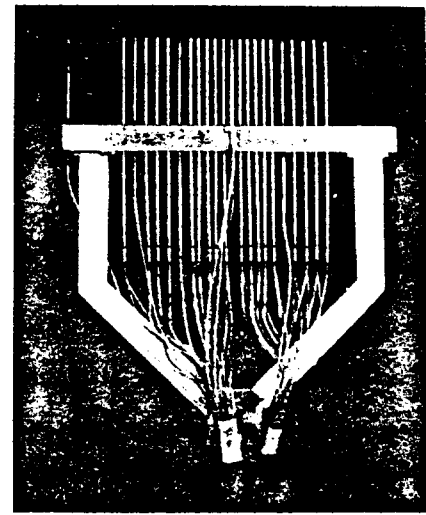


Figure 2.18 A Pitot rake for wake surveys. (Courtesy of the University of Maryland Aerodynamic Laboratory.)

At the beginning of this section, it was mentioned that lift on a two-dimensional body can be obtained by measuring the pressures on the ceiling and floor of a wind tunnel, above and below the body. This relation can be established from the integral form of the momentum equation in a manner analogous to that used to establish the drag relation; the derivation is left as a homework problem.

## 2.7 ENERGY EQUATION

For an incompressible flow, where  $\rho$  is constant, the primary flow-field variables are  $p$  and  $\mathbf{V}$ . The continuity and momentum equations obtained earlier are two equations in terms of the two unknowns  $p$  and  $\mathbf{V}$ . Hence, for a study of incompressible flow, the continuity and momentum equations are sufficient tools to do the job.

However, for a compressible flow,  $\rho$  is an additional variable, and therefore we need an additional fundamental equation to complete the system. This fundamental relation is the energy equation, to be derived in this section. In the process, two additional flow-field variables arise, namely, the internal energy  $e$  and temperature  $T$ . Additional equations must also be introduced for these variables, as will be mentioned later in this section.

The material discussed in this section is germane to the study of compressible flow. For those readers interested only in the study of incompressible flow for the time being, you may bypass this section and return to it at a later stage.

**Physical principle** Energy can be neither created nor destroyed; it can only change in form.

This physical principle is embodied in the first law of thermodynamics. A brief review of thermodynamics is given in Chap. 7. Thermodynamics is essential to the study of compressible flow; however, at this stage we will only introduce the first law, and we defer any substantial discussion of thermodynamics until Chap. 7, where we begin to concentrate on compressible flow.

Consider a fixed amount of matter contained within a closed boundary. This matter defines the *system*. Because the molecules and atoms within the system are constantly in motion, the system contains a certain amount of energy. For simplicity, let the system contain a unit mass; in turn, denote the internal energy per unit mass by  $e$ .

The region outside the system defines the *surroundings*. Let an incremental amount of heat,  $\delta q$ , be added to the system from the surroundings. Also, let  $\delta w$  be the work done on the system by the surroundings. (The quantities  $\delta q$  and  $\delta w$  are discussed in more detail in Chap. 7.) Both heat and work are forms of energy, and when added to the system, they change the amount of internal energy in the system. Denote this change of internal energy by  $de$ . From our physical principle that energy is conserved, we have for the system

$$\delta q + \delta w = de \quad (2.76)$$

Equation (2.76) is a statement of the first law of thermodynamics.

Let us apply the first law to the fluid flowing through the fixed control volume shown in Fig. 2.15. Let

$$B_1 = \text{rate of heat added to fluid inside control volume from surroundings}$$

$$B_2 = \text{rate of work done on fluid inside control volume}$$

$$B_3 = \text{rate of change of energy of fluid as it flows through control volume}$$

From the first law,

$$B_1 + B_2 = B_3 \quad (2.77)$$

Note that each term in Eq. (2.77) involves the *time rate* of energy change; hence, Eq. (2.77) is, strictly speaking, a *power* equation. However, because it is a statement of the fundamental principle of conservation of energy, the equation is conventionally termed the "energy equation." We continue this convention here.

First, consider the rate of heat transferred to or from the fluid. This can be visualized as volumetric heating of the fluid inside the control volume due to absorption of radiation originating outside the system or the local emission of radiation by the fluid itself, if the temperature inside the control volume is high enough. In addition, there may be chemical combustion processes taking place inside the control volume, such as fuel-air combustion in a jet engine. Let this volumetric rate of heat addition per unit mass be denoted by  $\dot{q}$ . Typical units for  $\dot{q}$  are  $\text{J/s} \cdot \text{kg}$  or  $\text{lbf/s} \cdot \text{slug}$ . Examining Fig. 2.15, the mass contained within an elemental volume is  $\rho dV$ ; hence, the rate of heat addition to this mass is  $\dot{q}(\rho dV)$ . Summing over the complete control volume, we obtain

$$\text{Rate of volumetric heating} = \iiint_V \dot{q} \rho dV \quad (2.78)$$

In addition, if the flow is viscous, heat can be transferred into the control volume by means of thermal conduction and mass diffusion across the control surface. At this stage, a detailed development of these viscous heat-addition terms is not warranted; they are considered in detail in Chap. 15. Rather, let us denote the rate of heat addition

to the control volume due to viscous effects simply by  $\dot{Q}_{\text{viscous}}$ . Therefore, in Eq. (2.77), the total rate of heat addition is given by Eq. (2.78) plus  $\dot{Q}_{\text{viscous}}$ :

$$B_1 = \iiint_V q\rho dV + \dot{Q}_{\text{viscous}} \quad (2.79)$$

Before considering the rate of work done on the fluid inside the control volume, consider a simpler case of a solid object in motion, with a force  $\mathbf{F}$  being exerted on the object, as sketched in Fig. 2.19. The position of the object is measured from a fixed origin by the radius vector  $\mathbf{r}$ . In moving from position  $\mathbf{r}_1$  to  $\mathbf{r}_2$  over an interval of time  $d\tau$ , the object is displaced through  $d\mathbf{r}$ . By definition, the work done on the object in time  $d\tau$  is  $\mathbf{F} \cdot d\mathbf{r}$ . Hence, the time rate of doing work is simply  $\mathbf{F} \cdot d\mathbf{r}/d\tau$ . However, we can state that

$$\text{Rate of doing work on moving body} = \mathbf{F} \cdot \mathbf{V}$$

In words, the rate of work done on a moving body is equal to the product of its velocity and the component of force in the direction of the velocity.

This result leads to an expression for  $B_2$ , as follows. Consider the elemental area  $dS$  of the control surface in Fig. 2.15. The pressure force on this elemental area is  $-p dS$ . From the above result, the rate of work done on the fluid passing through  $dS$  with velocity  $\mathbf{V}$  is  $(-p dS) \cdot \mathbf{V}$ . Hence, summing over the complete control surface,

$$\text{Rate of work done on fluid inside } V \text{ due to pressure force on } S = - \iiint_S (-p dS) \cdot \mathbf{V} \quad (2.80)$$

In addition, consider an elemental volume,  $dV$ , inside the control volume, as shown in Fig. 2.15. Recalling that  $\mathbf{f}$  is the body force per unit mass, the rate of work done on the elemental volume due to the body force is  $(\rho \mathbf{f} dV) \cdot \mathbf{V}$ . Summing over the complete control volume,

$$\text{Rate of work done on fluid inside } V \text{ due to body forces} = \iiint_V (\rho \mathbf{f} dV) \cdot \mathbf{V} \quad (2.81)$$

If the flow is viscous, the shear stress on the control surface will also perform work on the fluid as it passes across the surface. Once again, a detailed development of this term is deferred until Chap. 15. Let us denote this contribution simply by  $\dot{W}_{\text{viscous}}$ . Then the total rate of work done on the fluid inside the control volume is the sum of Eqs. (2.80) and (2.81) and  $\dot{W}_{\text{viscous}}$ .

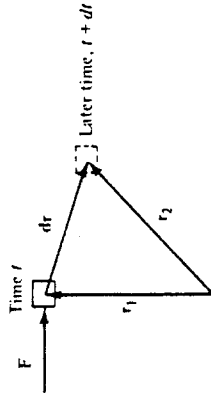


Figure 2.19 Schematic for the rate of doing work by a force  $\mathbf{F}$  exerted on a moving body.

$$B_2 = - \iiint_V \rho \mathbf{V} \cdot dS + \iiint_V \rho(\mathbf{f} \cdot \mathbf{V}) dV + \dot{W}_{\text{viscous}} \quad (2.77)$$

To visualize the energy inside the control volume, recall that in the first law of thermodynamics as stated in Eq. (2.76), the internal energy  $e$  is due to the random motion of the atoms and molecules inside the system. Equation (2.76) is written for a stationary system. However, the fluid inside the control volume in Fig. 2.15 is not stationary; it is moving at the local velocity  $\mathbf{V}$  with a consequent kinetic energy per unit mass of  $V^2/2$ . Hence, the energy per unit mass of the moving fluid is the sum of both internal and kinetic energies,  $e + V^2/2$ . This sum is called the *total energy* per unit mass.

We are now ready to obtain an expression for  $B_3$ , the rate of change of total energy of the fluid as it flows through the control volume. Keep in mind that mass flows into the control volume of Fig. 2.15 bringing with it a certain total energy; at the same time mass flows out of the control volume taking with it a generally different amount of total energy. The elemental mass flow across  $dS$  is  $\rho \mathbf{V} \cdot dS$ , and therefore, the elemental flow of total energy across  $dS$  is  $(\rho \mathbf{V} \cdot dS)(e + V^2/2)$ . Summing over the complete control surface,

$$\text{Net rate of flow of total energy across control surface} = \iiint_S (\rho \mathbf{V} \cdot dS) \left( e + \frac{V^2}{2} \right) \quad (2.83)$$

In addition, if the flow is unsteady, there is a time rate of change of total energy inside the control volume due to the transient fluctuations of the flow-field variables. The total energy contained in the elemental volume  $dV$  is  $\rho(e + V^2/2)dV$ , and hence the total energy inside the complete control volume at any instant in time is

$$\iiint_V \rho \left( e + \frac{V^2}{2} \right) dV$$

Therefore,

$$\text{Time rate of change of total energy inside } V \text{ due to transient variations} = \frac{\partial}{\partial t} \iiint_V \rho \left( e + \frac{V^2}{2} \right) dV \quad (2.84)$$

In turn,  $B_3$  is the sum of Eqs. (2.83) and (2.84):

$$B_3 = \frac{\partial}{\partial t} \iiint_V \rho \left( e + \frac{V^2}{2} \right) dV + \iiint_V (\rho \mathbf{V} \cdot dS) \left( e + \frac{V^2}{2} \right) \quad (2.85)$$

Repeating the physical principle stated at the beginning of this section, the rate of heat added to the fluid plus the rate of work done on the fluid is equal to the rate of change of total energy of the fluid at it flows through the control volume; i.e., *energy is conserved*. In turn, these words can be directly translated into an equation by combining Eqs. (2.77), (2.79), (2.82), and (2.85):

$$\oint \dot{q}p dV + \dot{Q}_{viscous} dV = \oint pV \cdot dS + \oint_V \rho(\mathbf{f} \cdot \mathbf{V}) dV + \dot{W}_{viscous}$$

$$= \frac{\partial}{\partial t} \oint_V \rho \left( e + \frac{V^2}{2} \right) dV + \oint_S \rho \left( e + \frac{V^2}{2} \right) \mathbf{V} \cdot d\mathbf{S}$$

(2.86)

Equation (2.86) is the energy equation in integral form; it is essentially the first law of thermodynamics applied to a fluid flow.

For the sake of completeness, note that if a shaft penetrates the control surface in Fig. 2.15, driving some power machinery located inside the control volume (say, a compressor of a jet engine), then the rate of work delivered by the shaft,  $\dot{W}_{shaft}$ , must be added to the left side of Eq. (2.86). In addition, if the size of the control volume were so large that changes in height  $z$  were important, then the potential energy per unit mass,  $gz$ , must be added to the total energy; i.e., total energy would be  $e + V^2/2 + gz$ , rather than just  $e + V^2/2$ , as appears in Eq. (2.86). However, for the aerodynamic problems considered in this book, shaft work is not treated, and changes in potential energy are always negligible. Therefore, these effects have been intentionally not included in Eq. (2.86).

Following the approach established in Secs. 2.4 and 2.5, we can obtain a partial differential equation for total energy from the integral form given in Eq. (2.86). Applying the divergence theorem to the surface integrals in Eq. (2.86), collecting all terms inside the same volume integral, and setting the integrand equal to zero, we obtain

$$\frac{\partial}{\partial t} \left[ \rho \left( e + \frac{V^2}{2} \right) \right] + \nabla \cdot \left[ \rho \left( e + \frac{V^2}{2} \right) \mathbf{V} \right] = \rho \dot{q} - \nabla \cdot (p \mathbf{V}) + \rho (\mathbf{f} \cdot \mathbf{V})$$

$$+ \dot{Q}'_{viscous} + \dot{W}'_{viscous}$$

(2.87)

where  $\dot{Q}'_{viscous}$  and  $\dot{W}'_{viscous}$  represent the proper forms of the viscous terms, to be obtained in Chap. 15. Equation (2.87) is a partial differential equation which relates the flow field variables at a given point in space.

If the flow is steady ( $\partial/\partial t = 0$ ), inviscid ( $\dot{Q}'_{viscous} = 0$  and  $\dot{W}'_{viscous} = 0$ ), adiabatic (no heat addition,  $\dot{q} = 0$ ), without body forces ( $\mathbf{f} = 0$ ), then Eqs. (2.86) and (2.87) reduce to

$$\oint_S \rho \left( e + \frac{V^2}{2} \right) \mathbf{V} \cdot d\mathbf{S} = - \oint_S p \mathbf{V} \cdot d\mathbf{S}$$

(2.88)

Equations (2.88) and (2.89) are discussed and applied at length beginning with Chap. 7.

With the energy equation, we have introduced another unknown flow-field variable,  $e$ . We now have three equations, continuity, momentum, and energy, which involve four dependent variables,  $\rho$ ,  $p$ ,  $\mathbf{V}$ , and  $e$ . A fourth equation can be obtained from a thermodynamic state relation for  $e$  (see Chap. 7). If the gas is calorically perfect, then

$$e = c_v T \quad (2.90)$$

where  $c_v$  is the specific heat at constant volume. Equation (2.90) introduces temperature as yet another dependent variable. However, the system can be completed by using the perfect gas equation of state

$$p = \rho RT \quad (2.91)$$

where  $R$  is the specific gas constant. Therefore, the continuity, momentum, and energy equations, along with Eqs. (2.90) and (2.91) are five independent equations for the five unknowns,  $\rho$ ,  $p$ ,  $\mathbf{V}$ ,  $e$ , and  $T$ . The matter of a perfect gas and related equations of state are reviewed in detail in Chap. 7; Eqs. (2.90) and (2.91) are presented here only to round out our development of the fundamental equations of fluid flow.

## 2.8 INTERIM SUMMARY

At this stage, let us pause and think about the various equations we have developed. Do not fall into the trap of seeing these equations as just a jumble of mathematical symbols that, by now, might look all the same to you. Quite the contrary, these equations speak words: for example, Eqs. (2.39), (2.43), (2.44), and (2.45) all say that mass is conserved; Eqs. (2.55), (2.61a to c), (2.62), and (2.63a to c) are statements of Newton's second law applied to a fluid flow; Eqs. (2.86) to (2.89) say that energy is conserved. It is very important to be able to see the physical principles behind these equations. When you look at an equation, try to develop the ability to see past a collection of mathematical symbols and, instead, to read the physics that the equation represents.

The equations listed above are fundamental to all of aerodynamics. Take the time to go back over them. Become familiar with the way they are developed, and make yourself comfortable with their final forms. In this way, you will find our subsequent aerodynamic applications that much easier to understand.

Also, note our location on the road map shown in Fig. 2.1. We have finished the items on the left branch of the map—we have obtained the basic flow equations containing the fundamental physics of fluid flow. We now start with the branch on the right, which is a collection of useful concepts helpful in the application of the basic flow equations.

## 2.9 SUBSTANTIAL DERIVATIVE

Consider a small fluid element moving through a flow field, as shown in Fig. 2.20. The velocity field is given by  $\mathbf{V} = u\mathbf{i} + v\mathbf{j} + w\mathbf{k}$ , where

$$\nabla \cdot [\rho \left( e + \frac{V^2}{2} \right) \mathbf{V}] = -\nabla \cdot (p \mathbf{V}) \quad (2.89)$$

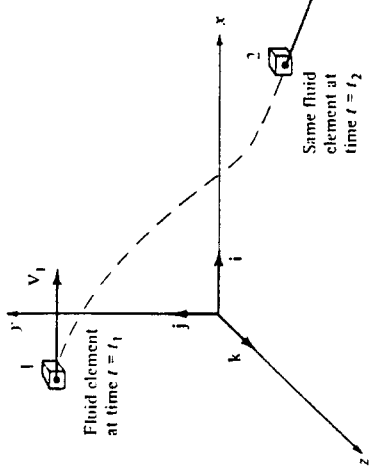


Figure 2.20 Fluid element moving in a flow field—illustration for the substantial derivative.

$$u = u(x, y, z, t)$$

$$v = v(x, y, z, t)$$

$$w = w(x, y, z, t)$$

In addition, the density field is given by

$$\rho = \rho(x, y, z, t)$$

At time  $t_1$ , the fluid element is located at point 1 in the flow (see Fig. 2.20), and its density is

$$\rho_1 = \rho(x_1, y_1, z_1, t_1)$$

At a later time,  $t_2$ , the same fluid element has moved to a different location in the flow field, such as point 2 in Fig. 2.20. At this new time and location, the density of the fluid element is

$$\rho_2 = \rho(x_2, y_2, z_2, t_2)$$

Since  $\rho = \rho(x, y, z, t)$ , we can expand this function in a Taylor series about point 1 as follows:

$$\begin{aligned} \rho_2 &= \rho_1 + \left(\frac{\partial \rho}{\partial x}\right)_1 (x_2 - x_1) + \left(\frac{\partial \rho}{\partial y}\right)_1 (y_2 - y_1) + \left(\frac{\partial \rho}{\partial z}\right)_1 (z_2 - z_1) \\ &\quad + \left(\frac{\partial \rho}{\partial t}\right)_1 (t_2 - t_1) + \text{higher-order terms} \end{aligned}$$

Dividing by  $t_2 - t_1$ , and ignoring the higher-order terms, we have

$$\frac{\rho_2 - \rho_1}{t_2 - t_1} = \left(\frac{\partial \rho}{\partial x}\right)_1 \frac{x_2 - x_1}{t_2 - t_1} + \left(\frac{\partial \rho}{\partial y}\right)_1 \frac{y_2 - y_1}{t_2 - t_1} + \left(\frac{\partial \rho}{\partial z}\right)_1 \frac{z_2 - z_1}{t_2 - t_1} + \left(\frac{\partial \rho}{\partial t}\right)_1 \quad (2.92)$$

Consider the physical meaning of the left side of Eq. (2.92). The term  $(\rho_2 - \rho_1)/(t_2 - t_1)$  is the *average* time rate of change in density of the fluid element as it moves from point 1 to point 2. In the limit, as  $t_2$  approaches  $t_1$ , this term becomes

$$\lim_{t_2 \rightarrow t_1} \frac{\rho_2 - \rho_1}{t_2 - t_1} = \frac{D\rho}{Dt}$$

Here,  $D\rho/Dt$  is a symbol for the *instantaneous* time rate of change of density of the fluid element as it moves through point 1. By definition, this symbol is called the *substantial derivative*  $D/Dt$ . Note that  $D\rho/Dt$  is the time rate of change of density of a given *fluid element* as it moves through space. Here, our eyes are locked on the fluid element as it is moving, and we are watching the density of the element change as it moves through point 1. This is different from  $(\partial \rho / \partial t)_1$ , which is physically the time rate of change of density at the *fixed* point 1. For  $(\partial \rho / \partial t)_1$ , we fix our eyes on the stationary point 1, and watch the density change due to transient fluctuations in the flow field. Thus,  $D\rho/Dt$  and  $\partial \rho / \partial t$  are physically and numerically different quantities.

Returning to Eq. (2.92), note that

$$\lim_{t_2 \rightarrow t_1} \frac{x_2 - x_1}{t_2 - t_1} \equiv u$$

$$\lim_{t_2 \rightarrow t_1} \frac{y_2 - y_1}{t_2 - t_1} \equiv v$$

$$\lim_{t_2 \rightarrow t_1} \frac{z_2 - z_1}{t_2 - t_1} \equiv w$$

Thus, taking the limit of Eq. (2.92) as  $t_2 \rightarrow t_1$ , we obtain

$$\frac{D\rho}{Dt} = u \frac{\partial \rho}{\partial x} + v \frac{\partial \rho}{\partial y} + w \frac{\partial \rho}{\partial z} + \frac{\partial \rho}{\partial t} \quad (2.93)$$

Examine Eq. (2.93) closely. From it, we can obtain an expression for the substantial derivative in cartesian coordinates:

$$\frac{D}{Dt} = \frac{\partial}{\partial t} + u \frac{\partial}{\partial x} + v \frac{\partial}{\partial y} + w \frac{\partial}{\partial z} \quad (2.94)$$

$$\nabla \equiv i \frac{\partial}{\partial x} + j \frac{\partial}{\partial y} + k \frac{\partial}{\partial z} \quad (2.95)$$

Furthermore, in cartesian coordinates, the vector operator  $\nabla$  is defined as

$$\boxed{\frac{D}{Dt} \equiv \frac{\partial}{\partial t} + (\mathbf{V} \cdot \nabla)}$$

Hence, Eq. (2.94) can be written as

Equation (2.95) represents a definition of the substantial derivative in vector notation; thus, it is valid for any coordinate system.

Focusing on Eq. (2.95), we once again emphasize that  $D/Dt$  is the substantial derivative, which is physically the time rate of change following a moving fluid ele-

ment;  $\partial/\partial t$  is called the *local derivative*, which is physically the time rate of change at a fixed point;  $\mathbf{V} \cdot \nabla$  is called the *convective derivative*, which is physically the time rate of change due to the movement of the fluid element from one location to another in the flow field where the flow properties are spatially different. The substantial derivative applies to any flow-field variable, for example,  $D\rho/Dt$ ,  $DT/Dt$ ,  $Du/Dt$ . For example,

$$\frac{DT}{Dt} = \frac{\partial T}{\partial t} + (\mathbf{V} \cdot \nabla)T = \frac{\partial T}{\partial t} + u \frac{\partial T}{\partial x} + v \frac{\partial T}{\partial y} + w \frac{\partial T}{\partial z} \quad (2.96)$$

local convective derivative

Again, Eq. (2.96) states physically that the temperature of the fluid element is changing as the element sweeps past a point in the flow because at that point the flow-field temperature itself may be fluctuating with time (the local derivative) and because the fluid element is simply on its way to another point in the flow field where the temperature is different (the convective derivative).

Consider an example which will help to reinforce the physical meaning of the substantial derivative. Imagine that you are hiking in the mountains, and you are about to enter a cave. The temperature inside the cave is cooler than outside. Thus, as you walk through the mouth of the cave, you feel a temperature decrease—this is analogous to the convective derivative in Eq. (2.96). However, imagine that, at the same time, a friend throws a snowball at you such that the snowball hits you just at the same instant you pass through the mouth of the cave. You will feel an additional, but momentary, temperature drop when the snowball hits you—this is analogous to the local derivative in Eq. (2.96). The net temperature drop you feel as you walk through the mouth of the cave is therefore a combination of both the act of moving into the cave, where it is cooler, and being struck by the snowball at the same instant—this net temperature drop is analogous to the substantial derivative in Eq. (2.96).

## 2.10 FUNDAMENTAL EQUATIONS IN TERMS OF THE SUBSTANTIAL DERIVATIVE

In this section, we express the continuity, momentum, and energy equations in terms of the substantial derivative. In the process, we make use of the following vector identity:

$$\nabla \cdot (\rho \mathbf{V}) \equiv \rho \nabla \cdot \mathbf{V} + \mathbf{V} \cdot \nabla \rho \quad (2.97)$$

In words, this identity states that the divergence of a scalar times a vector is equal to the scalar times the divergence of the vector plus the dot product of the vector and the gradient of the scalar.

First, consider the continuity equation given in the form of Eq. (2.43).

$$\frac{\partial \rho}{\partial t} + \nabla \cdot (\rho \mathbf{V}) = 0 \quad (2.43)$$

Using the vector identity given by Eq. (2.97), Eq. (2.43) becomes

$$\frac{D\rho}{Dt} + \rho \nabla \cdot \mathbf{V} = 0 \quad (2.104a)$$

$$\frac{\partial \rho}{\partial t} + \mathbf{V} \cdot \nabla \rho + \rho \nabla \cdot \mathbf{V} = 0 \quad (2.98)$$

However, the sum of the first two terms of Eq. (2.98) is the substantial derivative of  $\rho$  [see Eq. (2.95)]. Thus, from Eq. (2.98),

$$\frac{D\rho}{Dt} + \rho \nabla \cdot \mathbf{V} = 0 \quad (2.99)$$

Equation (2.99) is the continuity equation written in terms of the substantial derivative. Next, consider the  $x$  component of the momentum equation given in the form of Eq. (2.61a).

$$\frac{\partial(\rho u)}{\partial t} + \nabla \cdot (\rho u \mathbf{V}) = -\frac{\partial p}{\partial x} + \rho f_x + (\mathcal{F}_x)_{viscous} \quad (2.61a)$$

The first terms can be expanded as

$$\frac{\partial(\rho u)}{\partial t} = \rho \frac{\partial u}{\partial t} + u \frac{\partial \rho}{\partial t} \quad (2.100)$$

In the second term of Eq. (2.61a), treat the scalar quantity as  $u$  and the vector quantity as  $\rho \mathbf{V}$ . Then, the term can be expanded using the vector identity in Eq. (2.97).

$$\nabla \cdot (\rho u \mathbf{V}) \equiv \nabla \cdot [u(\rho \mathbf{V})] = u \nabla \cdot (\rho \mathbf{V}) + (\rho \mathbf{V}) \cdot \nabla u \quad (2.101)$$

Substituting Eqs. (2.100) and (2.101) into (2.61a);

$$\rho \frac{\partial u}{\partial t} + u \frac{\partial \rho}{\partial t} + u \nabla \cdot (\rho \mathbf{V}) + (\rho \mathbf{V}) \cdot \nabla u = -\frac{\partial p}{\partial x} + \rho f_x + (\mathcal{F}_x)_{viscous}$$

or

$$\rho \frac{\partial u}{\partial t} + u \left[ \frac{\partial \rho}{\partial t} + \nabla \cdot (\rho \mathbf{V}) \right] + (\rho \mathbf{V}) \cdot \nabla u = -\frac{\partial p}{\partial x} + \rho f_x + (\mathcal{F}_x)_{viscous} \quad (2.102)$$

Examine the two terms inside the square brackets; they are precisely the left side of the continuity equation, Eq. (2.43). Since the right side of Eq. (2.43) is zero, the sum inside the square brackets is zero. Hence, Eq. (2.102) becomes

$$\rho \frac{\partial u}{\partial t} + \rho \mathbf{V} \cdot \nabla u = -\frac{\partial p}{\partial x} + \rho f_x + (\mathcal{F}_x)_{viscous}$$

or

$$\rho \left( \frac{\partial u}{\partial t} + \mathbf{V} \cdot \nabla u \right) = -\frac{\partial p}{\partial x} + \rho f_x + (\mathcal{F}_x)_{viscous} \quad (2.103)$$

Examine the two terms inside the parenthesis in Eq. (2.103); their sum is precisely the substantial derivative  $Du/Dt$ . Hence, Eq. (2.103) becomes

In a similar manner, Eq. (2.61b and c) yield

$$\boxed{\frac{Dv}{Dt} = -\frac{\partial p}{\partial y} + \rho f_y + (\mathcal{F}_y)_{viscous}} \quad (2.104b)$$

$$\boxed{\frac{Dw}{Dt} = -\frac{\partial p}{\partial z} + \rho f_z + (\mathcal{F}_z)_{viscous}} \quad (2.104c)}$$

Equations (2.104a to c) are the  $x$ ,  $y$ , and  $z$  components of the *momentum equation* written in terms of the substantial derivative. Compare these equations with Eqs. (2.61a to c). Note that the right sides of both sets of equations are unchanged; only the left sides are different.

In an analogous fashion, the energy equation given in the form of Eq. (2.87) can be expressed in terms of the substantial derivative. The derivation is left as a homework problem; the result is

$$\boxed{\frac{D(e + V'/2)}{Dt} = \rho \dot{q} - \nabla \cdot (p \mathbf{V}) + \rho(\mathbf{f} \cdot \mathbf{V}) + \dot{Q}'_{viscous} + \dot{W}'_{viscous}} \quad (2.105)}$$

Again, the right-hand sides of Eqs. (2.87) and (2.105) are the same; only the form of the left sides is different.

In modern aerodynamics, it is conventional to call the form of Eqs. (2.43), (2.61a to c), and (2.87) the *conservation form* of the fundamental equations (sometimes these equations are labeled as the *divergence form* because of the divergence terms on the left side.) In contrast, the form of Eqs. (2.99), (2.104a to c), and (2.105), which deals with the substantial derivative on the left side, is called the *nonconservation form*. Both forms are equally valid statements of the fundamental principles, and in most cases there is no particular reason to chose one form over the other. The nonconservation form is frequently found in textbooks and in aerodynamic theory. However, for the numerical solution of some aerodynamic problems, the conservation form sometimes leads to more accurate results. Hence, the distinction between the conservation form and the nonconservation form has become important in the modern discipline of computational fluid dynamics. (See Ref. 7 for more details.)

## 2.11 PATHLINES AND STREAMLINES OF A FLOW

In addition to knowing the density, pressure, temperature, and velocity fields, in aerodynamics we like to draw pictures of "where the flow is going." To accomplish this, we construct diagrams of pathlines and/or streamlines of the flow. The distinction between pathlines and streamlines is described in this section.

Consider an unsteady flow with a velocity field given by  $\mathbf{V} = \mathbf{V}(x, y, z, t)$ . Also consider an infinitesimal fluid element moving through the flow field, say, element A as shown in Fig. 2.21a. Element A passes through point 1. Let us trace the path of

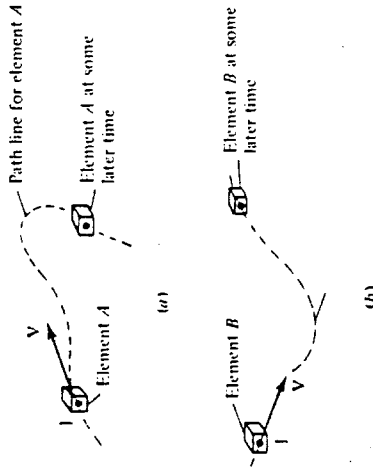


Figure 2.21 Pathlines for two different fluid elements passing through the same point in space: unsteady flow.

element A as it moves downstream from point 1, as given by the dashed line in Fig. 2.21a. Such a path is defined as the *pathline* for element A. Now, trace the path of another fluid element, say, element B as shown in Fig. 2.21b. Assume that element B also passes through point 1, but at some different time than element A. The pathline of element B is given by the dashed line in Fig. 2.21b. Because the flow is unsteady, the velocity at point 1 (and at all other points of the flow) changes with time. Hence, the pathlines of elements A and B are different curves in Fig. 2.21a and b. In general, for *unsteady* flow, the pathlines for different fluid elements passing through the same point are not the same.

In Sec. 1.4, the concept of a streamline was introduced in a somewhat heuristic manner. Let us be more precise here. By definition, a *streamline* is a curve whose tangent at any point is in the direction of the velocity vector at that point. Streamlines are illustrated in Fig. 2.22. The streamlines are drawn such that their tangents at every point along the streamline are in the same direction as the velocity vectors at those points. If the flow is unsteady, the streamline pattern is different at different times because the velocity vectors are fluctuating with time in both magnitude and direction.

In general, streamlines are different than pathlines. You can visualize a pathline as a time-exposure photograph of a given fluid element, whereas a streamline pattern is like a single frame of a motion picture of the flow. In an unsteady flow, the streamline pattern changes; hence each "frame" of the motion picture is different.

However, for the case of *steady flow* (which applies to most of the applications in this book), the magnitude and direction of the velocity vectors at all points are fixed, invariant with time. Hence, the pathlines for different fluid elements going through the

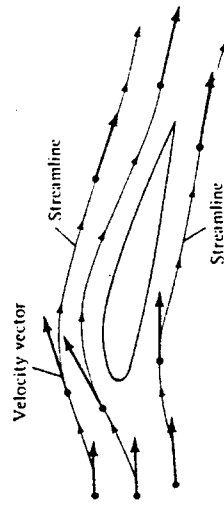


Figure 2.22 Streamlines.

same point are the same. Moreover, the pathlines and streamlines are identical. Therefore, in steady flow, there is no distinction between pathlines and streamlines; they are the same curves in space. This fact is reinforced in Fig. 2.23, which illustrates the fixed, time-invariant streamline (pathline) through point 1. In Fig. 2.23, a given fluid element passing through point 1 traces the same pathline. Since the velocity vector is tangent to the pathline at all points on the pathline for all times, the pathline is also a streamline. For the remainder of this book, we deal mainly with the concept of streamlines rather than pathlines; however, always keep in mind the distinction described above.

**Question:** Given the velocity field of a flow, how can we obtain the mathematical equation for a streamline? Obviously, the streamline illustrated in Fig. 2.23 is a curve in space, and hence it can be described by the equation  $f(x, y, z) = 0$ . How can we obtain this equation? To answer this question, let  $ds$  be a directed element of the streamline, such as shown at point 2 in Fig. 2.23. The velocity at point 2 is  $\mathbf{V}$ , and by definition of a streamline,  $\mathbf{V}$  is parallel to  $ds$ . Hence, from the definition of the vector cross product [see Eq. (2.4)],

$$ds \times V = 0 \quad (2.106)$$

Equation (2.106) is a valid equation for a streamline. To put it in a more recognizable form, expand Eq. (2.106) in cartesian coordinates:

$$ds = dx \mathbf{i} + dy \mathbf{j} + dz \mathbf{k}$$

$$\mathbf{V} = u\mathbf{i} + v\mathbf{j} + w\mathbf{k}$$

$$ds \times V = \begin{vmatrix} \mathbf{i} & \mathbf{j} & \mathbf{k} \\ dx & dy & dz \\ u & v & w \end{vmatrix} = i(vw - vdz) + j(u dz - wd x) + k(v dx - u dy) = 0 \quad (2.107)$$

Since the vector given by Eq. (2.107) is zero, its components must each be zero.

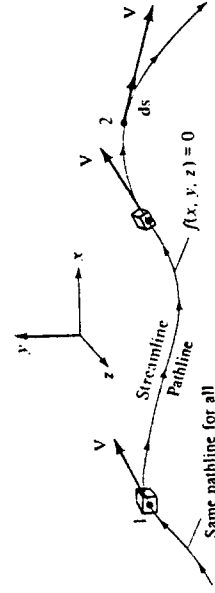


Figure 2.23 For steady flow, streamlines and pathlines are the same.

$$\boxed{\begin{aligned} w dy - v dz &= 0 & (2.108a) \\ u dz - w dx &= 0 & (2.108b) \\ v dx - u dy &= 0 & (2.108c) \end{aligned}}$$

Equations (2.108a to c) are differential equations for the streamline. Knowing  $u$ ,  $v$ , and  $w$  as functions of  $x$ ,  $y$ , and  $z$ , Eqs. (2.108a to c) can be integrated to yield the equation for the streamline:  $f(x, y, z) = 0$ .

To reinforce the physical meaning of Eqs. (2.108a to c), consider a streamline in two dimensions, as sketched in Fig. 2.24a. The equation of this streamline is  $y = f(x)$ . Hence, at point 1 on the streamline, the slope is  $dy/dx$ . However,  $\mathbf{V}$ , with  $x$  and  $y$  components  $u$  and  $v$ , respectively, is tangent to the streamline at point 1. Thus, the slope of the streamline is also given by  $v/u$ , as shown in Fig. 2.24. Therefore,

$$\boxed{\frac{dy}{dx} = \frac{v}{u}} \quad (2.109)$$

Equation (2.109) is a differential equation for a streamline in two dimensions. From Eq. (2.109),

$$v dx - u dy = 0$$

which is precisely Eq. (2.108c). Therefore, Eqs. (2.108a to c) and (2.109) simply state mathematically that the velocity vector is tangent to the streamline. A concept related to streamlines is that of a streamtube. Consider an arbitrary closed curve  $C$  in three-dimensional space, as shown in Fig. 2.24b. Consider the streamlines which pass through all points on  $C$ . These streamlines form a tube in space as sketched in Fig. 2.24b; such a tube is called a *streamtube*. For example, the walls of an ordinary garden hose form a streamtube for the water flowing through the hose.

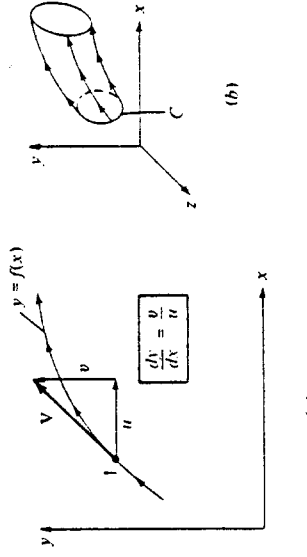


Figure 2.24 (a) Equation of a streamline in two-dimensional cartesian space. (b) Sketch of a streamtube in three-dimensional space.

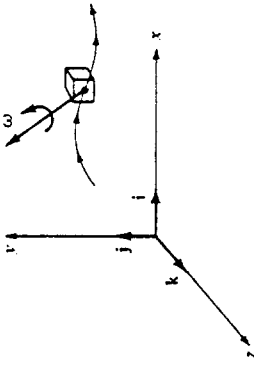


Figure 2.27 Angular velocity of a fluid element in three-dimensional space.

Now consider line  $AB$ . The  $x$  component of the velocity at point  $A$  at time  $t$  is  $u$ , as shown in Fig. 2.26. Because point  $B$  is a distance  $dy$  from point  $A$ , the horizontal component of velocity of point  $B$  at time  $t$  is  $u + (\partial u / \partial y) dy$ . By reasoning similar to that above, the net displacement in the  $x$  direction of  $B$  relative to  $A$  over the time increment  $\Delta t$  is  $[(\partial u / \partial y) dy] \Delta t$ , as shown in Fig. 2.26. Hence,

$$\tan(-\Delta\theta_1) = \frac{[(\partial u / \partial y) dy] \Delta t}{dy} = \frac{\partial u}{\partial y} \Delta t \quad (2.112)$$

Since  $-\Delta\theta_1$  is small, Eq. (2.112) reduces to

$$\Delta\theta_1 = -\frac{\partial u}{\partial y} \Delta t \quad (2.113)$$

Consider the angular velocities of lines  $AB$  and  $AC$ , defined as  $d\theta_1/dt$  and  $d\theta_2/dt$ , respectively. From Eq. (2.113), we have

$$\frac{d\theta_1}{dt} = \lim_{\Delta t \rightarrow 0} \frac{\Delta\theta_1}{\Delta t} = -\frac{\partial u}{\partial y} \quad (2.114)$$

From Eq. (2.111), we have

$$\frac{d\theta_2}{dt} = \lim_{\Delta t \rightarrow 0} \frac{\Delta\theta_2}{\Delta t} = \frac{\partial v}{\partial x} \quad (2.115)$$

By definition, the angular velocity of the fluid element as seen in the  $xy$  plane is the average of the angular velocities of lines  $AB$  and  $AC$ . Let  $\omega_r$  denote this angular velocity. Therefore, by definition,

$$\omega_r = \frac{1}{2} \left( \frac{d\theta_1}{dt} + \frac{d\theta_2}{dt} \right) \quad (2.116)$$

Combining Eqs. (2.114) to (2.116),

$$\omega_r = \frac{1}{2} \left( \frac{\partial v}{\partial x} - \frac{\partial u}{\partial y} \right) \quad (2.117)$$

In the above discussion, we have considered motion in the  $xy$  plane only. However, the fluid element is generally moving in three-dimensional space, and its angular velocity is a vector  $\omega$  that is orientated in some general direction, as shown in Fig. 2.27. In Eq. (2.117), we have obtained only the component of  $\omega$  in the  $z$  direction; this explains the subscript  $r$  in Eqs. (2.116) and (2.117). The  $x$  and  $y$  components of  $\omega$  can be obtained in a similar fashion. The resulting angular velocity of the fluid element in three-dimensional space is

$$\tan \Delta\theta_2 = \frac{[(\partial v / \partial x) dx] \Delta t}{dx} = \frac{\partial v}{\partial x} \Delta t \quad (2.110)$$

Since  $\Delta\theta_2$  is a small angle,  $\tan \Delta\theta_2 \approx \Delta\theta_2$ . Hence, Eq. (2.110) reduces to

$$\Delta\theta_2 = \frac{\partial v}{\partial x} \Delta t \quad (2.111)$$

Now consider line  $AB$ . The  $x$  component of the velocity at point  $A$  at time  $t$  is  $u$ , as shown in Fig. 2.26. Because point  $B$  is a distance  $dy$  from point  $A$ , the horizontal component of velocity of point  $B$  at time  $t$  is  $u + (\partial u / \partial y) dy$ . By reasoning similar to that above, the net displacement in the  $x$  direction of  $B$  relative to  $A$  over the time increment  $\Delta t$  is  $[(\partial u / \partial y) dy] \Delta t$ , as shown in Fig. 2.26. Hence,

$$\tan(-\Delta\theta_1) = \frac{[(\partial u / \partial y) dy] \Delta t}{dy} = \frac{\partial u}{\partial y} \Delta t \quad (2.112)$$

Since  $-\Delta\theta_1$  is small, Eq. (2.112) reduces to

$$\Delta\theta_1 = -\frac{\partial u}{\partial y} \Delta t \quad (2.113)$$

Consider the angular velocities of lines  $AB$  and  $AC$ , defined as  $d\theta_1/dt$  and  $d\theta_2/dt$ , respectively. From Eq. (2.113), we have

$$\frac{d\theta_1}{dt} = \lim_{\Delta t \rightarrow 0} \frac{\Delta\theta_1}{\Delta t} = -\frac{\partial u}{\partial y} \quad (2.114)$$

From Eq. (2.111), we have

$$\frac{d\theta_2}{dt} = \lim_{\Delta t \rightarrow 0} \frac{\Delta\theta_2}{\Delta t} = \frac{\partial v}{\partial x} \quad (2.115)$$

By definition, the angular velocity of the fluid element as seen in the  $xy$  plane is the average of the angular velocities of lines  $AB$  and  $AC$ . Let  $\omega_r$  denote this angular velocity. Therefore, by definition,

$$\omega_r = \frac{1}{2} \left( \frac{d\theta_1}{dt} + \frac{d\theta_2}{dt} \right) \quad (2.116)$$

Combining Eqs. (2.114) to (2.116),

$$\omega_r = \frac{1}{2} \left( \frac{\partial v}{\partial x} - \frac{\partial u}{\partial y} \right) \quad (2.117)$$

In the above discussion, we have considered motion in the  $xy$  plane only. However, the fluid element is generally moving in three-dimensional space, and its angular velocity is a vector  $\omega$  that is orientated in some general direction, as shown in Fig. 2.27. In Eq. (2.117), we have obtained only the component of  $\omega$  in the  $z$  direction; this explains the subscript  $r$  in Eqs. (2.116) and (2.117). The  $x$  and  $y$  components of  $\omega$  can be obtained in a similar fashion. The resulting angular velocity of the fluid element in three-dimensional space is

$$\omega = \omega_r \mathbf{i} + \omega_x \mathbf{j} + \omega_y \mathbf{k} \quad (2.118)$$

Equation (2.118) is the desired result; it expresses the angular velocity of the fluid element in terms of the velocity field, or more precisely, in terms of derivatives of the velocity field.

The angular velocity of a fluid element plays an important role in theoretical aerodynamics, as we shall soon see. However, the expression  $2\omega$  appears frequently, and therefore, we define a new quantity, *vorticity*, which is simply twice the angular velocity. Denote vorticity by the vector  $\xi$ :

$$\xi \equiv 2\omega$$

Hence, from Eq. (2.118),

$$\xi = \left( \frac{\partial w}{\partial y} - \frac{\partial v}{\partial z} \right) \mathbf{i} + \left( \frac{\partial u}{\partial z} - \frac{\partial w}{\partial x} \right) \mathbf{j} + \left( \frac{\partial v}{\partial x} - \frac{\partial u}{\partial y} \right) \mathbf{k} \quad (2.119)$$

Recall Eq. (2.22) for  $\nabla \times \mathbf{V}$  in cartesian coordinates. Since  $u$ ,  $v$ , and  $w$  denote the  $x$ ,  $y$ , and  $z$  components of velocity, respectively, note that the right sides of Eqs. (2.22) and (2.119) are identical. Hence, we have the important result that

$$\xi = \nabla \times \mathbf{v} \quad (2.120)$$

In a velocity field, the curl of the velocity is equal to the vorticity.

The above leads to two important definitions:

1. If  $\nabla \times \mathbf{V} \neq 0$  at every point in a flow, the flow is called *rotational*. This implies that the fluid elements have a finite angular velocity.
2. If  $\nabla \times \mathbf{V} = 0$  at every point in a flow, the flow is called *irrotational*. This implies that the fluid elements have no angular velocity; rather, their motion through space is a pure translation.

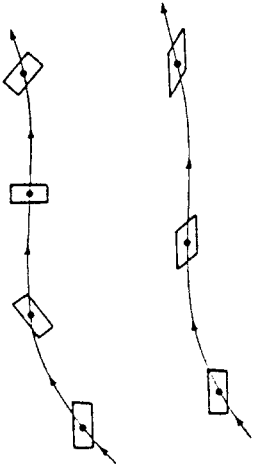


Figure 2.28 Fluid elements in a rotational flow.

The case of rotational flow is illustrated in Fig. 2.28. Here, fluid elements moving along two different streamlines are shown in various modes of rotation. In contrast, the case of irrotational flow is illustrated in Fig. 2.29. Here, the upper streamline shows a fluid element where the angular velocities of two intersecting sides are zero. The lower streamline shows a fluid element where the angular velocities of two intersecting sides are finite but equal and opposite to each other, and so their sum is identically zero. In both cases, the angular velocity of the fluid element is zero; i.e., the flow is irrotational.

If the flow is two-dimensional (say, in the  $xy$  plane), then from Eq. (2.119),

$$\xi = \xi \mathbf{k} = \left( \frac{\partial v}{\partial x} - \frac{\partial u}{\partial y} \right) \mathbf{k} \quad (2.121)$$

Also, if the flow is irrotational,  $\xi = 0$ . Hence, from Eq. (2.121),

$$\boxed{\frac{\partial v}{\partial x} - \frac{\partial u}{\partial y} = 0} \quad (2.122)$$

Equation (2.122) is the *condition of irrotationality for two-dimensional flow*. We will have frequent occasion to use Eq. (2.122). Why is it so important to make a distinction between rotational and irrotational flows? The answer becomes blatantly obvious as we progress in our study of aerodynamics; we find that irrotational flows are much easier to analyze than rotational flows. However, irrotational flow may at first glance appear to be so special that its applications are limited. Amazingly enough, such is not the case. There are a large number of practical aerodynamic problems where the flow field is essentially irrotational, e.g., the supersonic flow over airfoils, the supersonic flow over slender bodies at

small angle of attack, and the subsonic-supersonic flow through nozzles. For such cases, there is generally a thin boundary layer of viscous flow immediately adjacent to the surface; in this viscous region the flow is highly rotational. As a result, the study of irrotational flow is an important aspect of aerodynamics.

Return to the fluid element shown in Fig. 2.26. Let the angle between sides  $AB$  and  $AC$  be denoted by  $\kappa$ . As the fluid element moves through the flow field,  $\kappa$  will change. In Fig. 2.26, at time  $t$ ,  $\kappa$  is initially  $90^\circ$ . At time  $t + \Delta t$ ,  $\kappa$  has changed by the amount  $\Delta\kappa$ , where

$$\Delta\kappa = -\Delta\theta_2 - (-\Delta\theta_1) \quad (2.123)$$

By definition, the *strain* of the fluid element as seen in the  $xy$  plane is the change in  $\kappa$ , where positive strain corresponds to a *decreasing*  $\kappa$ . Hence, from Eq. (2.123),

$$\text{Strain} = -\Delta\kappa = \Delta\theta_2 - \Delta\theta_1 \quad (2.124)$$

In viscous flows (to be discussed in Chaps. 15 and 16), the time rate of strain is an important quantity. Denote the time rate of strain by  $\epsilon_{xy}$ , where in conjunction with Eq. (2.124)

$$\epsilon_{xy} \equiv -\frac{d\kappa}{dt} = \frac{d\theta_2}{dt} - \frac{d\theta_1}{dt} \quad (2.125)$$

Substituting Eqs. (2.114) and (2.115) into (2.125), we have

$$\epsilon_{xy} = \frac{\partial v}{\partial x} + \frac{\partial u}{\partial y} \quad (2.126a)$$

In the  $yz$  and  $zx$  planes, by a similar derivation the strain is, respectively,

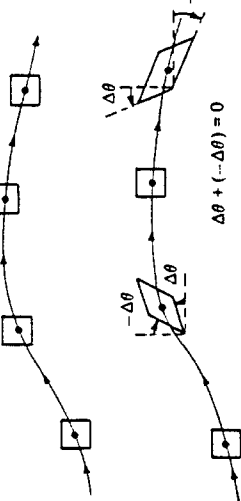
$$\epsilon_{yz} = \frac{\partial w}{\partial y} + \frac{\partial v}{\partial z} \quad (2.126b)$$

$$\epsilon_{zx} = \frac{\partial u}{\partial z} + \frac{\partial w}{\partial x} \quad (2.126c)$$

Note that angular velocity (hence, vorticity) and time rate of strain depend solely on the velocity derivatives of the flow field. These derivatives can be displayed in a matrix as follows:

$$\begin{bmatrix} \frac{\partial u}{\partial x} & \frac{\partial u}{\partial y} & \frac{\partial u}{\partial z} \\ \frac{\partial v}{\partial x} & \frac{\partial v}{\partial y} & \frac{\partial v}{\partial z} \\ \frac{\partial w}{\partial x} & \frac{\partial w}{\partial y} & \frac{\partial w}{\partial z} \end{bmatrix}$$

Figure 2.29 Fluid elements in an irrotational flow.



The sum of the diagonal terms is simply equal to  $\nabla \cdot \mathbf{V}$ , which from Sec. 2.3 is equal to the time rate of change of volume of a fluid element; hence, the diagonal terms

represent the *dilatation* of a fluid element. The off-diagonal terms are cross derivatives which appear in Eqs. (2.118), (2.119), and (2.126a to c). Hence, the off-diagonal terms are associated with rotation and strain of a fluid element.

In summary, in this section we have examined the rotation and deformation of a fluid element moving in a flow field. The angular velocity of a fluid element and the corresponding vorticity at a point in the flow are concepts which are useful in the analysis of both inviscid and viscous flows; in particular, the absence of vorticity — irrotational flow — greatly simplifies the analysis of the flow, as we will see. We take advantage of this simplification in much of our treatment of inviscid flows in subsequent chapters. On the other hand, we do not make use of the time rate of strain until we discuss viscous flow, beginning with Chap. 15.

**Example 2.2** For the velocity field given in Example 2.1, calculate the vorticity.

#### SOLUTION

$$\begin{aligned} \boldsymbol{\xi} = \nabla \times \mathbf{V} &= \begin{vmatrix} \mathbf{i} & \mathbf{j} & \mathbf{k} \\ \frac{\partial}{\partial x} & \frac{\partial}{\partial y} & \frac{\partial}{\partial z} \\ u & v & w \end{vmatrix} = \begin{vmatrix} \mathbf{i} & \mathbf{j} & \mathbf{k} \\ \frac{\partial}{\partial x} & \frac{\partial}{\partial y} & \frac{\partial}{\partial z} \\ \frac{y}{x^2+y^2} & \frac{-x}{x^2+y^2} & 0 \end{vmatrix} \\ &= [0 - 0] - j[0 - 0] \\ &\quad + k \left[ \frac{(x^2+y^2)(-1) + x(2x)}{x^2+y^2} - \frac{(x^2+y^2) - y(2y)}{x^2+y^2} \right] \\ &= 0\mathbf{i} + 0\mathbf{j} + 0\mathbf{k} = \mathbf{0} \end{aligned}$$

The flow field is irrotational at every point except at the origin, where  $x^2 + y^2 = 0$ .

## 2.13 CIRCULATION

You are reminded again that this is a tool-building chapter. Taken individually, each aerodynamic tool we have developed so far may not be particularly exciting. However, taken collectively, these tools allow us to obtain solutions for some very practical and exciting aerodynamic problems.

In this section we introduce a tool which is fundamental to the calculation of aerodynamic lift, namely, *circulation*. This tool was used independently by Frederick Lanchester (1878–1946) in England, Wilhelm Kutta (1867–1944) in Germany, and Nikolai Joukowski (1847–1921) in Russia to create a breakthrough in the theory of aerodynamic lift at the turn of the twentieth century. The relationship between circulation and lift and the historical circumstances surrounding this breakthrough are discussed in Chaps. 3 and 4. The purpose of this section is only to define circulation and relate it to vorticity.

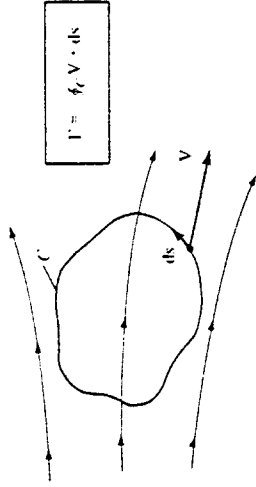


Figure 2.30 Definition of circulation.

Consider a closed curve  $C$  in a flow field, as sketched in Fig. 2.30. Let  $\mathbf{V}$  and  $d\mathbf{s}$  be the velocity and directed line segment, respectively, at a point on  $C$ . The circulation, denoted by  $\Gamma$ , is defined as

$$\Gamma = - \oint_C \mathbf{v} \cdot d\mathbf{s} \quad (2.127)$$

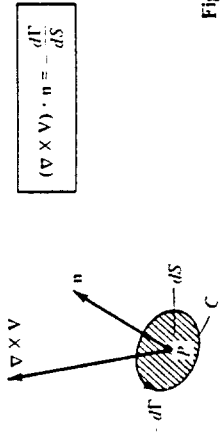
The circulation is simply the negative of the line integral of velocity around a closed curve in the flow; it is a kinematic property depending only on the velocity field and the choice of the curve  $C$ . As discussed in Sec. 2.2, Line Integrals, by mathematical convention the positive sense of the line integral is counterclockwise. However, in aerodynamics, it is convenient to consider a positive circulation as being clockwise. Hence, a minus sign appears in the definition given by Eq. (2.127) to account for the positive-counterclockwise sense of the integral and the positive-clockwise sense of circulation.<sup>f</sup>

The use of the word “circulation” to label the integral in Eq. (2.127) may be somewhat misleading because it leaves a general impression of something moving around in a loop. Indeed, according to the *American Heritage Dictionary of the English Language*, the first definition given to the word “circulation” is “movement in a circle or circuit.” However, in aerodynamics, circulation has a very precise technical meaning, namely, Eq. (2.127). It does *not* necessarily mean that the fluid elements are moving around in circles within this flow field — a common early misconception of new students of aerodynamics. Rather, when circulation exists in a flow, it simply means that the line integral in Eq. (2.127) is finite. For example, if the airfoil in Fig. 2.22 is generating lift, the circulation taken around a closed curve enclosing the airfoil will be finite, although the fluid elements are by no means executing circles around the airfoil (as clearly seen from the streamlines sketched in Fig. 2.22).

Circulation is also related to vorticity as follows. Refer back to Fig. 2.9, which shows an open surface bounded by the closed curve  $C$ . Assume that the surface is in a flow field and the velocity at point  $P$  is  $\mathbf{V}$ , where  $P$  is any point on the surface (including any point on curve  $C$ ). From Stokes' theorem [Eq. (2.25)],

<sup>f</sup>Some books do not use the minus sign in the definition of circulation. In such cases, the positive sense of both the line integral and  $\Gamma$  is in the same direction. This causes no problem as long as the reader is aware of the convention used in a particular book or paper.

$$\Gamma \equiv - \oint_C \mathbf{v} \cdot d\mathbf{s} = - \iint_S (\nabla \times \mathbf{v}) \cdot d\mathbf{s}$$
(2.128)



Hence, the circulation about a curve  $C$  is equal to the vorticity integrated over any open surface bounded by  $C$ . This leads to the immediate result that if the flow is *irrotational* everywhere within the *contour of integration* (i.e., if  $\nabla \times \mathbf{V} = 0$  over any surface bounded by  $C$ ), then  $\Gamma = 0$ . A related result is obtained by letting the curve  $C$  shrink to an infinitesimal size, and denoting the circulation around this infinitesimally small curve by  $d\Gamma$ . Then, in the limit as  $C$  becomes infinitesimally small, Eq. (2.128) yields

$$d\Gamma = -(\nabla \times \mathbf{v}) \cdot d\mathbf{s} = -(\nabla \times \mathbf{v}) \cdot \mathbf{n} dS$$

$$(\nabla \times \mathbf{v}) \cdot \mathbf{n} = - \frac{d\Gamma}{dS}$$
(2.129)

or

$$(\nabla \times \mathbf{v}) \cdot \mathbf{n} = - \frac{d\Gamma}{dS}$$

where  $dS$  is the infinitesimal area enclosed by the infinitesimal curve  $C$ . Referring to Fig. 2.31, Eq. (2.129) states that at a point  $P$  in a flow, the component of vorticity normal to  $dS$  is equal to the negative of the "circulation per unit area," where the circulation is taken around the boundary of  $dS$ .

**Example 2.3** For the velocity field given in Example 2.1, calculate the circulation around a circular path of radius 5 m. Assume that  $u$  and  $v$  given in Example 2.1 are in units of meters per second.

**SOLUTION** Since we are dealing with a circular path, it is easier to work this problem in polar coordinates, where  $x = r \cos \theta$ ,  $y = r \sin \theta$ ,  $x^2 + y^2 = r^2$ ,  $V_r = u \cos \theta + v \sin \theta$ , and  $V_\theta = -u \sin \theta + v \cos \theta$ . Therefore,

$$\begin{aligned} u &= \frac{y}{x^2 + y^2} = \frac{r \sin \theta}{r^2} = \frac{\sin \theta}{r} \\ v &= -\frac{x}{x^2 + y^2} = -\frac{r \cos \theta}{r^2} = -\frac{\cos \theta}{r} \\ V_r &= \frac{\sin \theta}{r} \cos \theta + \left(-\frac{\cos \theta}{r}\right) \sin \theta = -\frac{1}{r} \\ V_\theta &= -\frac{\sin \theta}{r} \sin \theta + \left(-\frac{\cos \theta}{r}\right) \cos \theta = -\frac{1}{r} \end{aligned}$$

$$\begin{aligned} \mathbf{V} \cdot d\mathbf{s} &= (V_r \mathbf{e}_r + V_\theta \mathbf{e}_\theta) \cdot (dr \mathbf{e}_r + r d\theta \mathbf{e}_\theta) \\ &= V_r dr + r V_\theta d\theta = 0 + r \left(-\frac{1}{r}\right) d\theta = -d\theta \\ &= V_r dr + r V_\theta d\theta = - \int_0^{2\pi} -d\theta = [2\pi \text{ m/s}] \end{aligned}$$
(2.132)

Hence

Figure 2.31 Relation between vorticity and circulation.

Note that we never used the 5-m diameter of the circular path; in this case the value of  $\Gamma$  is independent of the diameter of the path.

## 2.14 STREAM FUNCTION

In this section, we consider two-dimensional steady flow. Recall from Sec. 2.11 that the differential equation for a streamline in such a flow is given by Eq. (2.109), repeated below

$$\frac{dy}{dx} = \frac{v}{u}$$
(2.109)

If  $u$  and  $v$  are known functions of  $x$  and  $y$ , then Eq. (2.109) can be integrated to yield the algebraic equation for a streamline

$$f(x, y) = c$$
(2.130)

where  $c$  is an arbitrary constant of integration, with different values for different streamlines. In Eq. (2.130), denote the function of  $x$  and  $y$  by the symbol  $\bar{\psi}$ . Hence, Eq. (2.130) is written as

$$\bar{\psi}(x, y) = c$$
(2.131)

The function  $\bar{\psi}(x, y)$  is called the *streamfunction*. From Eq. (2.131) we see that the equation for a streamline is given by *setting the stream function equal to a constant*, i.e.,  $c_1$ ,  $c_2$ ,  $c_3$ , etc. Two different streamlines are illustrated in Fig. 2.32; streamlines  $ab$  and  $cd$  are given by  $\bar{\psi} = c_1$  and  $\bar{\psi} = c_2$ , respectively.

There is a certain arbitrariness in Eqs. (2.130) and (2.131) via the arbitrary constant of integration  $c$ . Let us define the stream function more precisely in order to reduce this arbitrariness. Referring to Fig. 2.32, let us define the numerical value of  $\bar{\psi}$  such that the difference  $\Delta \bar{\psi}$  between  $\bar{\psi} = c_2$  for streamline  $cd$  and  $\bar{\psi} = c_1$  for streamline  $ab$  is equal to the mass flow between the two streamlines. Since Fig. 2.32 is a two-dimensional flow, the mass flow between two streamlines is defined *per unit depth perpendicular to the page*. That is, in Fig. 2.32 we are considering the mass flow inside a streamtube bounded by streamlines  $ab$  and  $cd$ , with a rectangular cross-sectional area equal to  $\Delta n$  times a unit depth perpendicular to the page. Here,  $\Delta n$  is the normal distance between  $ab$  and  $cd$ , as shown in Fig. 2.32. Hence, mass flow between streamlines  $ab$  and  $cd$  per unit depth perpendicular to the page is

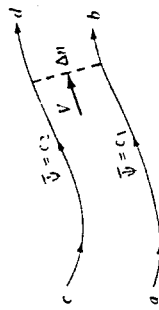


Figure 2.32 Different streamlines are given by different values of the stream function.

The above definition does not completely remove the arbitrariness of the constant of integration in Eqs. (2.130) and (2.131), but it does make things a bit more precise. For example, consider a given two-dimensional flow field. Choose one streamline of the flow, and give it an arbitrary value of the stream function, say  $\bar{\psi} = c_1$ . Then, the value of the stream function for any other streamline in the flow, say  $\bar{\psi} = c_2$ , is fixed by the definition given in Eq. (2.132). Which streamline you choose to designate as  $\bar{\psi} = c_1$  and what numerical value you give  $c_1$  usually depend on the geometry of the given flow field, as we see in Chap. 3.

The equivalence between  $\bar{\psi} = \text{constant}$  designating a streamline, and  $\Delta \bar{\psi}$  equaling mass flow (per unit depth) between streamlines, is natural. For a steady flow, the mass flow inside a given streamtube is constant along the tube; the mass flow across any cross section of the tube is the same. Since by definition  $\Delta \bar{\psi}$  is equal to this mass flow, then  $\Delta \bar{\psi}$  itself is constant for a given streamtube. In Fig. 2.32, if  $\bar{\psi}_1 = c_1 + \Delta \bar{\psi}$  is also constant streamline on the bottom of the streamtube, then  $\bar{\psi}_2 = c_2 = c_1 + \Delta \bar{\psi}$  is also constant along the top of the streamtube. Since by definition of a streamtube (see Sec. 2.11) the upper boundary of the streamtube is a streamline itself, then  $\bar{\psi}_2 = c_2 = \text{constant}$  must designate this streamline.

We have yet to develop the most important property of the stream function, namely, that derivatives of  $\bar{\psi}$  yield the flow-field velocities. To obtain this relationship, consider again the streamlines *ab* and *cd* in Fig. 2.32. Assume that these streamlines are close together (i.e., assume  $n$  is small), such that the flow velocity  $V$  is a constant value across  $\Delta n$ . The mass flow through the streamtube per unit depth perpendicular to the page is

$$\begin{aligned}\Delta \bar{\psi} &\equiv \rho V \Delta n \quad (1) \\ \frac{\Delta \bar{\psi}}{\Delta n} &= \rho V \\ \text{or} \\ \text{Consider the limit of Eq. (2.133) as } \Delta n \rightarrow 0.\end{aligned}$$

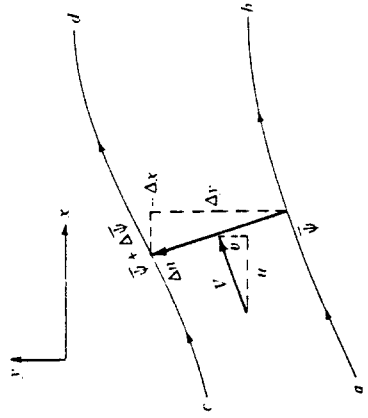


Figure 2.33 Mass flow through  $\Delta n$  is the sum of the mass flows through  $\Delta y$  and  $-\Delta x$ .

$$\text{Mass flow} = \Delta \bar{\psi} = \rho V \Delta n = \rho u \Delta y + \rho v (-\Delta x) \quad (2.135)$$

Letting *cd* approach *ab*, Eq. (2.135) becomes in the limit

$$d\bar{\psi} = \rho u dy - \rho v dx \quad (2.136)$$

However, since  $\bar{\psi} = \bar{\psi}(x, y)$ , the chain rule of calculus states

$$d\bar{\psi} = \frac{\partial \bar{\psi}}{\partial x} dx + \frac{\partial \bar{\psi}}{\partial y} dy \quad (2.137)$$

Comparing Eqs. (2.136) and (2.137), we have

$$\boxed{\begin{aligned}\rho u &= \frac{\partial \bar{\psi}}{\partial y} \\ \rho v &= -\frac{\partial \bar{\psi}}{\partial x}\end{aligned}}$$

Equations (2.138a and *b*) are important. If  $\bar{\psi}(x, y)$  is known for a given flow field, then at any point in the flow the products  $\rho u$  and  $\rho v$  can be obtained by differentiating  $\bar{\psi}$  in the directions normal to  $n$  and  $v$ , respectively.

If Fig. 2.33 were to be redrawn in terms of polar coordinates, then a similar derivation yields

$$\boxed{\begin{aligned}\rho V_r &= \frac{1}{r} \frac{\partial \bar{\psi}}{\partial \theta} \\ \rho V_\theta &= -\frac{\partial \bar{\psi}}{\partial r}\end{aligned}}$$

Equation (2.134) states that if we know  $\bar{\psi}$ , then we can obtain the product  $(\rho V)$  by differentiating  $\bar{\psi}$  in the direction *normal* to  $V$ . To obtain a practical form of Eq. (2.134) for cartesian coordinates, consider Fig. 2.33. Notice that the directed normal distance  $\Delta n$  is equivalent first to moving upward in the  $y$  direction by the amount  $\Delta y$  and then to the left in the negative  $x$  direction by the amount  $-\Delta x$ . Due to conservation of mass, the mass flow through  $\Delta n$  (per unit depth) is equal to the sum of the mass flows through  $\Delta y$  and  $-\Delta x$  (per unit depth).

Such a derivation is left as a homework problem.

Note that the dimensions of  $\bar{\psi}$  are equal to mass flow per unit depth perpendicular to the page. That is, in SI units,  $\bar{\psi}$  is in terms of kilograms per second per meter perpendicular to the page, or simply  $\text{kg}/(\text{s} \cdot \text{m})$ .

The stream function  $\bar{\psi}$  defined above applies to both compressible and incompressible flow. Now consider the case of incompressible flow only, where  $\rho = \text{constant}$ . Equation (2.134) can be written as

$$V = \frac{\partial(\bar{\psi}/\rho)}{\partial n} \quad (2.140)$$

We define a new stream function, for incompressible flow only, as  $\psi \equiv \bar{\psi}/\rho$ . Then Eq. (2.140) becomes

$$V = \frac{\partial\psi}{\partial n}$$

and Eqs. (2.138) and (2.139) become

$$u = \frac{\partial\psi}{\partial y} \quad (2.141a)$$

$$v = -\frac{\partial\psi}{\partial x} \quad (2.141b)$$

$$V_r = \frac{1}{r} \frac{\partial\psi}{\partial\theta} \quad (2.142a)$$

$$V_\theta = -\frac{\partial\psi}{\partial r} \quad (2.142b)$$

and

The incompressible stream function  $\psi$  has characteristics analogous to its more general compressible counterpart  $\bar{\psi}$ . For example, since  $\bar{\psi}(x, y) = c$  is the equation of a streamline, and since  $\rho$  is a constant for incompressible flow, then  $\psi(x, y) \equiv \bar{\psi}/\rho = \text{constant}$  is also the equation for a streamline (for incompressible flow only). In addition, since  $\Delta\bar{\psi}$  is mass flow between two streamlines (per unit depth perpendicular to the page), and since  $\rho$  is mass per unit volume, then physically  $\Delta\psi = \Delta\bar{\psi}/\rho$  represents the *volume flow* (per unit depth) between two streamlines. In SI units,  $\Delta\psi$  is expressed as cubic meters per second per meter perpendicular to the page, or simply  $\text{m}^2/\text{s}$ . In summary, the concept of the stream function is a powerful tool in aerodynamics, for two primary reasons. Assuming that  $\bar{\psi}(x, y)$  [or  $\psi(x, y)$ ] is known through the two-dimensional flow field, then

1.  $\bar{\psi} = \text{constant}$  (or  $\psi = \text{constant}$ ) gives the equation of a streamline.
2. The flow velocity can be obtained by differentiating  $\bar{\psi}$  (or  $\psi$ ), as given by Eqs. (2.138) and (2.139) for compressible flow and Eqs. (2.141) and (2.142) for incompressible flow.

We have not yet discussed how  $\bar{\psi}(x, y)$  [or  $\psi(x, y)$ ] can be obtained in the first place; we are assuming that it is known. The actual determination of the stream function for various problems is discussed in Chap. 3.

## 2.15 VELOCITY POTENTIAL

Recall from Sec. 2.12 that an irrotational flow is defined as a flow where the vorticity is zero at every point. From Eq. (2.120), for an irrotational flow,

$$\xi = \nabla \times \mathbf{V} = 0 \quad (2.143)$$

Consider the following vector identity: if  $\phi$  is a scalar function, then

$$\nabla \times (\nabla\phi) = 0 \quad (2.144)$$

i.e., the curl of the gradient of a scalar function is identically zero. Comparing Eqs. (2.143) and (2.144), we see that

$$\boxed{\mathbf{V} = \nabla\phi} \quad (2.145)$$

Equation (2.145) states that for an *irrotational* flow, there exists a scalar function  $\phi$  such that the velocity is given by the gradient of  $\phi$ . We denote  $\phi$  as the *velocity potential*.  $\phi$  is a function of the spatial coordinates, i.e.,  $\phi = \phi(x, y, z)$ , or  $\phi = \phi(r, \theta, z)$ , or  $\phi = \phi(r, \theta, \Phi)$ . From the definition of the gradient in cartesian coordinates given by Eq. (2.16), we have from Eq. (2.145)

$$ui + vj + wk = \frac{\partial\phi}{\partial x} \mathbf{i} + \frac{\partial\phi}{\partial y} \mathbf{j} + \frac{\partial\phi}{\partial z} \mathbf{k} \quad (2.146)$$

The coefficients of like unit vectors must be the same on both sides of Eq. (2.146). Thus, in cartesian coordinates,

$$\boxed{u = \frac{\partial\phi}{\partial x} \quad v = \frac{\partial\phi}{\partial y} \quad w = \frac{\partial\phi}{\partial z}} \quad (2.147)$$

In a similar fashion, from the definition of the gradient in cylindrical and spherical coordinates given by Eqs. (2.17) and (2.18), we have, in cylindrical coordinates,

$$V_r = \frac{\partial\phi}{\partial r} \quad V_\theta = \frac{1}{r} \frac{\partial\phi}{\partial\theta} \quad V_z = \frac{\partial\phi}{\partial z} \quad (2.148)$$

and in spherical coordinates,

$$V_r = \frac{\partial\phi}{\partial r} \quad V_\theta = \frac{1}{r \sin\theta} \frac{\partial\phi}{\partial\theta} \quad V_\Phi = \frac{1}{r \sin\theta} \frac{\partial\phi}{\partial\Phi} \quad (2.149)$$

The velocity potential is analogous to the stream function in the sense that derivatives of  $\phi$  yield the flow-field velocities. However, there are distinct differences between  $\phi$  and  $\bar{\psi}$  (or  $\psi$ ):

1. The flow-field velocities are obtained by differentiating  $\phi$  in the same direction as the velocities [see Eqs. (2.147) to (2.149)], whereas  $\bar{\psi}$  (or  $\psi$ ) is differentiated normal to the velocity direction [see Eqs. (2.138) and (2.139), or Eqs. (2.141) and (2.142)].

2. The velocity potential is defined for irrotational flow only. In contrast, the stream function can be used in either rotational or irrotational flows.
  3. The velocity potential applies to three-dimensional flows, whereas the stream function is defined for two-dimensional flows only.<sup>†</sup>
- When a flow field is irrotational, hence allowing a velocity potential to be defined, there is a tremendous simplification. Instead of dealing with the velocity components (say,  $u$ ,  $v$ , and  $w$ ) as unknowns, hence requiring three equations for these three unknowns, we can instead deal with the velocity potential as one unknown, therefore requiring the solution of only one equation for the flow field. Once  $\phi$  is known for a given problem, the velocities are obtained directly from Eqs. (2.147) to (2.149). This is why, in theoretical aerodynamics, we make a distinction between irrotational and rotational flows and why the analysis of irrotational flows is simpler than that of rotational flows.

Because irrotational flows can be described by the velocity potential  $\phi$ , such flows are called *potential flows*.

In this section, we have not yet discussed how  $\phi$  can be obtained in the first place; we are assuming that it is known. The actual determination of  $\phi$  for various problems is discussed in Chaps. 3, 6, 11, and 12.

## 2.16 RELATIONSHIP BETWEEN THE STREAM FUNCTION AND VELOCITY POTENTIAL

In Sec. 2.15, we demonstrated that for an irrotational flow,  $\mathbf{V} = \nabla\phi$ . At this stage, take a moment and review some of the nomenclature introduced in Sec. 2.2 for the gradient of a scalar field. We see that a line of constant  $\phi$  is an isoline of  $\phi$ ; since  $\phi$  is the velocity potential, we give this isoline a specific name, *equipotential line*. In addition, a line drawn in space such that  $\nabla\phi$  is tangent at every point is defined as a gradient line; however, since  $\nabla\phi = \mathbf{V}$ , this gradient line is a *streamline*. In turn, from Sec. 2.14, a streamline is a line of constant  $\bar{\psi}$  (for a two-dimensional flow). Because gradient lines and isolines are perpendicular (see Sec. 2.2, Gradient of a Scalar Field), then equipotential lines ( $\phi = \text{constant}$ ) and streamlines ( $\bar{\psi} = \text{constant}$ ) are mutually perpendicular.

To illustrate this result more clearly, consider a two-dimensional, irrotational, incompressible flow in cartesian coordinates. For a streamline,  $\psi(x, y) = \text{constant}$ .

Hence, the differential of  $\psi$  along the streamline is zero; i.e.,

$$d\psi = \frac{\partial\psi}{\partial x} dx + \frac{\partial\psi}{\partial y} dy = 0 \quad (2.150)$$

From Eqs. (2.141a and b), Eq. (2.150) can be written as

$$d\psi = -v dx + u dy = 0 \quad (2.151)$$

<sup>†</sup> $\bar{\psi}$  (or  $\phi$ ) can be defined for axisymmetric flows, such as the flow over a cone at zero degrees angle of attack. However, for such flows, only two spatial coordinates are needed to describe the flow field (see Chap. 6).

Solve Eq. (2.151) for  $dy/dx$ , which is the slope of the  $\psi = \text{constant}$  line, i.e., the slope of the streamline.

$$\left( \frac{dy}{dx} \right)_{\psi=\text{const}} = \frac{v}{u} \quad (2.152)$$

Similarly, for an equipotential line,  $\phi(x, y) = \text{constant}$ . Along this line,

$$d\phi = \frac{\partial\phi}{\partial x} dx + \frac{\partial\phi}{\partial y} dy = 0 \quad (2.153)$$

From Eq. (2.147), Eq. (2.153) can be written as

$$d\phi = u dx + v dy = 0 \quad (2.154)$$

Solving Eq. (2.154) for  $dy/dx$ , which is the slope of the  $\phi = \text{constant}$  line, i.e., the slope of the equipotential line,

$$\left( \frac{dy}{dx} \right)_{\phi=\text{const}} = -\frac{u}{v} \quad (2.155)$$

Combining Eqs. (2.152) and (2.155),

$$\left( \frac{dy}{dx} \right)_{\phi=\text{const}} = -\frac{1}{(dy/dx)_{\phi=\text{const}}} \quad (2.156)$$

Equation (2.156) shows that the slope of a  $\psi = \text{constant}$  line is the negative reciprocal of the slope of a  $\phi = \text{constant}$  line, i.e., streamlines and equipotential lines are mutually perpendicular.

## 2.17 SUMMARY

Return to the road map for this chapter, as given in Fig. 2.1. We have now covered both the left and right branches of this map and are ready to launch into the solution of practical aerodynamic problems in subsequent chapters. Look at each block in Fig. 2.1; let your mind flash over the important equations and concepts represented by each block. If the flashes are dim, return to the appropriate sections of this chapter and review the material until you feel comfortable with these aerodynamic tools.

For your convenience, the most important results are summarized below.

### Basic Flow Equations

*Continuity equation*

$$\frac{\partial}{\partial t} \iiint_V \rho dV + \iint_S \rho \mathbf{V} \cdot d\mathbf{S} = 0 \quad (2.39)$$

$$\frac{\partial \rho}{\partial t} + \nabla \cdot (\rho \mathbf{V}) = 0 \quad (2.43)$$

$$\frac{D\rho}{Dt} + \rho \nabla \cdot \mathbf{V} = 0 \quad (2.99)$$

or

$$\frac{\partial}{\partial t} \iiint_V \rho \mathbf{V} dV + \iint_S (\rho \mathbf{V} \cdot d\mathbf{S}) V = - \iint_S p d\mathbf{S} + \iint_V \rho f dV + F_{viscous} \quad (2.55)$$

$$\text{or } \frac{\partial(\rho u)}{\partial t} + \nabla \cdot (\rho u \mathbf{V}) = - \frac{\partial p}{\partial x} + \rho f_x + (\mathcal{F}_x)_{viscous} \quad (2.61a)$$

$$\frac{\partial(\rho v)}{\partial t} + \nabla \cdot (\rho v \mathbf{V}) = - \frac{\partial p}{\partial y} + \rho f_y + (\mathcal{F}_y)_{viscous} \quad (2.61b)$$

$$\frac{\partial(\rho w)}{\partial t} + \nabla \cdot (\rho w \mathbf{V}) = - \frac{\partial p}{\partial z} + \rho f_z + (\mathcal{F}_z)_{viscous} \quad (2.61c)$$

$$\rho \frac{Du}{Dt} = - \frac{\partial p}{\partial x} + \rho f_x + (\mathcal{F}_x)_{viscous} \quad (2.104a)$$

$$\rho \frac{Dv}{Dt} = - \frac{\partial p}{\partial y} + \rho f_y + (\mathcal{F}_y)_{viscous} \quad (2.104b)$$

$$\rho \frac{Dw}{Dt} = - \frac{\partial p}{\partial z} + \rho f_z + (\mathcal{F}_z)_{viscous} \quad (2.104c)$$

*Energy equation*

$$\begin{aligned} & \frac{\partial}{\partial t} \iiint_V \rho \left( e + \frac{V^2}{2} \right) dV + \iint_S \rho \left( e + \frac{V^2}{2} \right) \mathbf{V} \cdot d\mathbf{S} \\ &= \iint_V \dot{q} \rho dV + \dot{Q}_{viscous} - \iint_S p \mathbf{V} \cdot d\mathbf{S} \\ &+ \iint_V \rho (\mathbf{f} \cdot \mathbf{V}) dV + \dot{W}_{viscous} \end{aligned} \quad (2.86)$$

$$\text{or } \frac{\partial}{\partial t} \left[ \rho \left( e + \frac{V^2}{2} \right) \right] + \nabla \cdot \left[ \rho \left( e + \frac{V^2}{2} \right) \mathbf{V} \right] = \rho \dot{q} - \nabla \cdot (p \mathbf{V}) + \rho (\mathbf{f} \cdot \mathbf{V}) + \dot{Q}'_{viscous} + \dot{W}'_{viscous} \quad (2.87)$$

$$\rho \frac{D(e + V^2/2)}{Dt} = \rho \dot{q} - \nabla \cdot (p \mathbf{V}) + \rho (\mathbf{f} \cdot \mathbf{V}) + \dot{Q}'_{viscous} + \dot{W}'_{viscous} \quad (2.105)$$

*Substantial derivative*

$$\frac{D}{Dt} \equiv \frac{\partial}{\partial t} + (\mathbf{V} \cdot \nabla) \quad (2.95)$$

local convective derivative

A streamline is a curve whose tangent at any point is in the direction of the velocity vector at that point. The equation of a streamline is given by

$$ds \times \mathbf{V} = 0 \quad (2.106)$$

or, in cartesian coordinates,

$$w dy - v dz = 0 \quad (2.108a)$$

$$u dz - w dx = 0 \quad (2.108b)$$

$$v dx - u dy = 0 \quad (2.108c)$$

The vorticity  $\xi$  at any given point is equal to twice the angular velocity of a fluid element  $\omega$ , and both are related to the velocity field by

$$\xi = 2\omega = \nabla \times \mathbf{V} \quad (2.120)$$

When  $\nabla \times \mathbf{V} \neq 0$ , the flow is rotational. When  $\nabla \times \mathbf{V} = 0$ , the flow is irrotational.

Circulation  $\Gamma$  is related to lift and is defined as

$$\Gamma \equiv - \oint_C \mathbf{V} \cdot d\mathbf{s} \quad (2.127)$$

Circulation is also related to vorticity via

$$\Gamma \equiv - \oint_C \mathbf{V} \cdot d\mathbf{s} = - \iint_S (\nabla \times \mathbf{V}) \cdot d\mathbf{S} \quad (2.128)$$

$$\text{or } (\nabla \times \mathbf{V}) \cdot \mathbf{n} = - \frac{d\Gamma}{dS} \quad (2.129)$$

The stream function  $\bar{\psi}$  is defined such that  $\bar{\psi}(x, y) = \text{constant}$  is the equation of a streamline and the difference in the stream function between two streamlines,  $\Delta \bar{\psi}$ , is equal to the mass flow between the streamlines. As a consequence of this definition, in cartesian coordinates,

$$\rho u = \frac{\partial \bar{\psi}}{\partial y} \quad (2.138a)$$

$$\rho v = - \frac{\partial \bar{\psi}}{\partial x} \quad (2.138b)$$

and in cylindrical coordinates,

$$\rho V_r = \frac{1}{r} \frac{\partial \bar{\psi}}{\partial \theta} \quad (2.139a)$$

$$\rho V_\theta = - \frac{\partial \bar{\psi}}{\partial r} \quad (2.139b)$$

For incompressible flow,  $\psi \equiv \bar{\psi}/\rho$  is defined such that  $\psi(x, y) = \text{constant}$  denotes a streamline and  $\Delta\psi$  between two streamlines is equal to the volume flow between these streamlines. As a consequence of this definition, in cartesian coordinates,

$$u = \frac{\partial \psi}{\partial y} \quad (2.141a)$$

$$v = - \frac{\partial \psi}{\partial x} \quad (2.141b)$$

and in cylindrical coordinates,

$$V_r = \frac{1}{r} \frac{\partial \psi}{\partial \theta} \quad (2.142a)$$

$$V_\theta = - \frac{\partial \psi}{\partial r} \quad (2.142b)$$

The stream function is valid for both rotational and irrotational flows, but it is restricted to two-dimensional flows only.

The velocity potential  $\phi$  is defined for irrotational flows only, such that

$$\mathbf{V} \equiv \nabla \phi \quad (2.145)$$

In cartesian coordinates,

$$u = \frac{\partial \phi}{\partial x} \quad v = \frac{\partial \phi}{\partial y} \quad w = \frac{\partial \phi}{\partial z} \quad (2.147)$$

In cylindrical coordinates,

$$V_r = \frac{\partial \phi}{\partial r} \quad V_\theta = \frac{1}{r} \frac{\partial \phi}{\partial \theta} \quad V_z = \frac{\partial \phi}{\partial z} \quad (2.148)$$

In spherical coordinates,

$$V_r = \frac{\partial \phi}{\partial r} \quad V_\theta = \frac{1}{r} \frac{\partial \phi}{\partial \theta} \quad V_\Phi = \frac{1}{r \sin \theta} \frac{\partial \phi}{\partial \Phi} \quad (2.149)$$

An irrotational flow is called a potential flow.

## PROBLEMS

- 2.1 Consider a body of arbitrary shape. If the pressure distribution over the surface of the body is constant, prove that the resultant pressure force on the body is zero. (Recall that this fact was used in Eq. (2.68).)
- 2.2 Consider an airfoil in a wind tunnel (i.e., a wing that spans the entire test section). Prove that the lift per unit span can be obtained from the pressure distributions on the top and bottom walls of the wind tunnel (i.e., from the pressure distributions on the walls above and below the airfoil).

- 2.3 Consider a velocity field where the  $x$  and  $y$  components of velocity are given by  $u = cx/(x^2 + y^2)$  and  $v = cy/(x^2 + y^2)$ , where  $c$  is a constant. Obtain the equations of the streamlines.
- 2.4 Consider a velocity field where the  $x$  and  $y$  components of velocity are given by  $u = cy/(x^2 + y^2)$  and  $v = -cx/(x^2 + y^2)$ , where  $c$  is a constant. Obtain the equations of the streamlines.

- 2.5 Consider a velocity field where the radial and tangential components of velocity are  $V_r = 0$  and  $V_\theta = cr$ , respectively, where  $c$  is a constant. Obtain the equations of the streamlines.
- 2.6 Consider a velocity field where the  $x$  and  $y$  components of velocity are given by  $u = cx$  and  $v = -cy$ , where  $c$  is a constant. Obtain the equations of the streamlines.

- 2.7 The velocity field given in Prob. 2.3 is called *source flow*. For source flow, calculate:
- The time rate of change of the volume of a fluid element per unit volume
  - The vorticity

- Hint:* It is simpler to convert the velocity components into polar coordinates and deal with a polar coordinate system.

- 2.8 The velocity field given in Prob. 2.4 is called *vortex flow*. For vortex flow, calculate:
- The time rate of change of the volume of a fluid element per unit volume
  - The vorticity

- Hint:* Again, for convenience use polar coordinates.

- 2.9 Is the flow field given in Prob. 2.5 irrotational? Prove your answer.

- 2.10 Consider a flow field in polar coordinates, where the stream function is given as  $\psi = \psi(r, \theta)$ . Starting with the concept of mass flow between two streamlines, derive Eqs. (2.139a and b).

- 2.11 Assuming the velocity field given in Prob. 2.6 pertains to an incompressible flow, calculate the stream function and velocity potential. Using your results, show that lines of constant  $\phi$  are perpendicular to lines of constant  $\psi$ .

A line of constant  $\phi$  is an equipotential line. Equipotential lines are perpendicular to streamlines (for two-dimensional irrotational flows).

## CHAPTER THREE

### FUNDAMENTALS OF INVISCID, INCOMPRESSIBLE FLOW

*Theoretical fluid dynamics, being a difficult subject, is for convenience, commonly divided into two branches, one treating of frictionless or perfect fluids, the other treating of viscous or imperfect fluids. The frictionless fluid has no existence in nature, but is hypothesized by mathematicians in order to facilitate the investigation of important laws and principles that may be approximately true of viscous or natural fluids.*

*Albert F. Zahm, 1912  
(Professor of aerodynamics, and  
developer of the first aeronautical  
laboratory in a U.S. university. The  
Catholic University of America)*

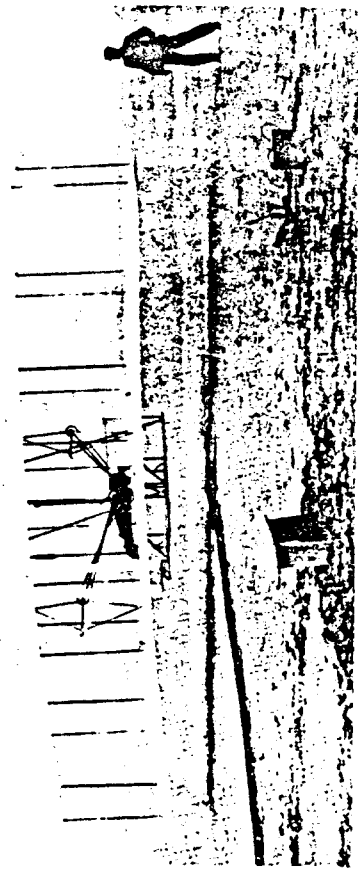


Figure 3.1 Historic photograph of the first successful heavier-than-air powered manned flight, achieved by the Wright brothers on December 17, 1903.

described by *incompressible flow*. As a result, a huge bulk of experimental and theoretical aerodynamic results was acquired over the 40-year period beginning with the Wright Flyer — results which applied to incompressible flow. Today, we are still very interested in incompressible aerodynamics because most modern general aviation aircraft still fly at speeds below 300 mi/h; a typical light general aviation airplane is shown in Fig. 3.3. In addition to low-speed aeronautical applications, the principles of incompressible flow apply to the flow of fluids, e.g., water flow through pipes, the motion of submarines and ships through the ocean, the design of wind turbines (the modern term for windmills), and many other important applications.

### 3.1 INTRODUCTION AND ROAD MAP

The world of practical aviation was born on December 17, 1903, when, at 10:35 A.M., and in the face of cold, stiff, dangerous winds, Orville Wright piloted the Wright Flyer on its historic 12-s., 120-ft first flight. Figure 3.1 shows a photograph of the Wright Flyer at the instant of lift-off, with Wilbur Wright running along the right side of the machine, supporting the wing tip so that it will not drag the sand. This photograph is the most important picture in aviation history; the event it depicts launched the profession of aeronautical engineering into the mainstream of the twentieth century.<sup>†</sup>

The flight velocity of the Wright Flyer was about 30 mi/h. Over the ensuing decades, the flight velocities of airplanes steadily increased. By means of more powerful engines and attention to drag reduction, the flight velocities of airplanes rose to approximately 300 mi/h just prior to World War II. Figure 3.2 shows a typical fighter airplane of the immediate pre-World War II era. From an aerodynamic point of view, at air velocities between 0 and 300 mi/h the air density remains essentially constant, varying by only a few percent. Hence, the aerodynamics of the family of airplanes spanning the period between the two photographs shown in Figs. 3.1 and 3.2 could be

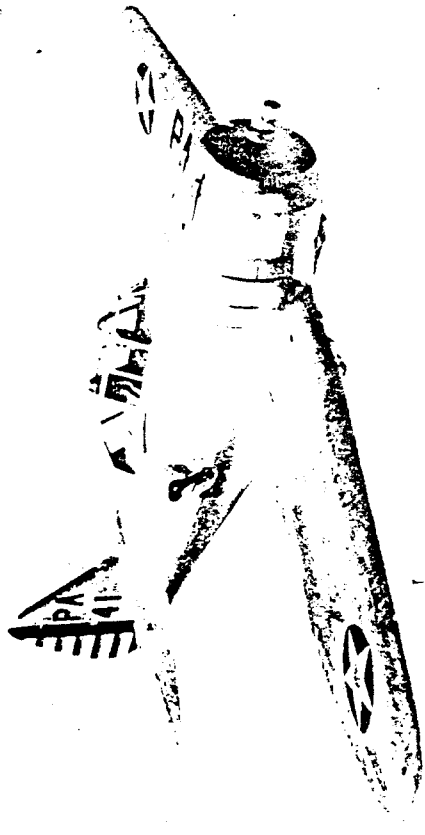


Figure 3.2 The Seversky P-35. (Courtesy of the U.S. Air Force.)

<sup>†</sup> See Ref. 2 for historical details leading to the first flight by the Wright brothers.



Figure 3.3 The Beechcraft Bonanza F33A. (Courtesy of Beechcraft.)

For all the above reasons, the study of incompressible flow is as relevant today as it was at the time of the Wright brothers. Therefore, Chaps. 3 to 6 deal exclusively with incompressible flow. Moreover, for the most part, we ignore any effects of friction, thermal conduction, or diffusion; i.e., we deal with *inviscid* incompressible flow in these chapters.<sup>†</sup> Looking at our spectrum of aerodynamic flows as shown in Fig. 1.27, the material contained in Chaps. 3 to 6 falls within the combined blocks *D* and *E*.

The purpose of this chapter is to establish some fundamental relations applicable to inviscid, incompressible flows and to discuss some simple but important flow fields and applications. The material in this chapter is then used as a launching pad for the airfoil theory of Chap. 4 and the finite wing theory of Chap. 5.

A road map for this chapter is given in Fig. 3.4. There are three main avenues:

- (1) a development of Bernoulli's equation, with some straightforward applications;
- (2) a discussion of Laplace's equation, which is the governing equation for inviscid, incompressible, irrotational flow; (3) the presentation of some elementary flow patterns, how they can be superimposed to synthesize both the nonlifting and lifting flow over a circular cylinder, and how they form the basis of a general numerical technique, called the *panel technique*, for the solution of flows over bodies of general shape. As you progress through this chapter, occasionally refer to this road map so that you can maintain your orientation and see how the various sections are related.

### 3.2 BERNOULLI'S EQUATION

As will be portrayed in Sec. 3.18, the early part of the eighteenth century saw the flowering of theoretical fluid dynamics, paced by the work of Johann and Daniel

<sup>†</sup> An inviscid, incompressible fluid is sometimes called an *ideal fluid*, or *perfect fluid*. This terminology will not be used here because of the confusion it sometimes causes with "ideal gases" or "perfect gases" from thermodynamics. This author prefers to use the more precise descriptor "inviscid, incompressible flow," rather than ideal fluid or perfect fluid.

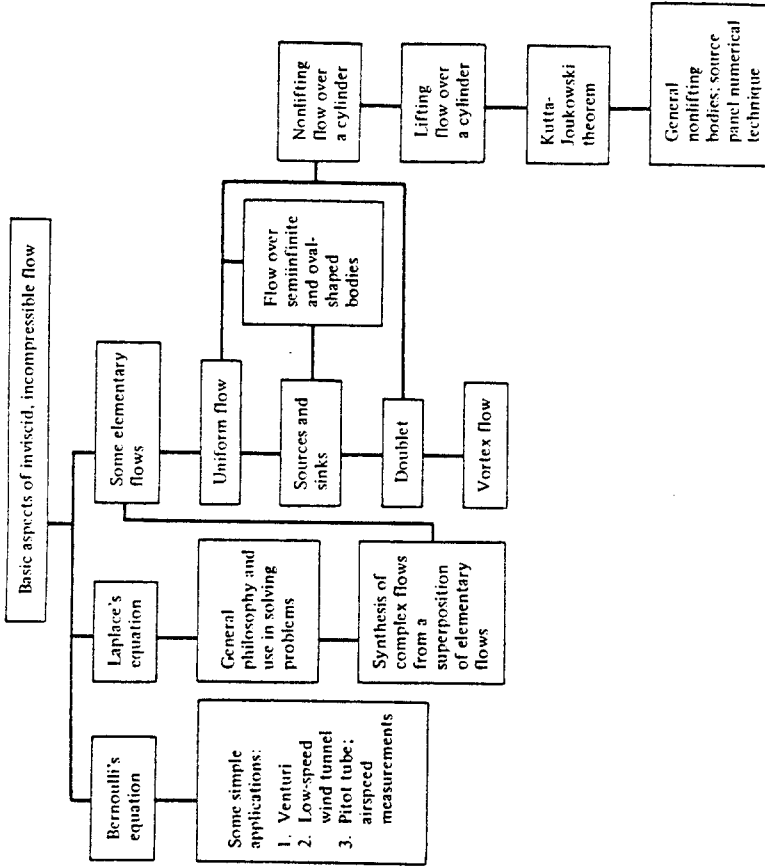


Figure 3.4 Road map for Chap. 3.

Bernoulli and, in particular, by Leonhard Euler. It was at this time that the relation between pressure and velocity in an inviscid, incompressible flow was first understood. The resulting equation is

$$p + \frac{1}{2} \rho V^2 = \text{const}$$

This equation is called *Bernoulli's equation*, although it was first presented in the above form by Euler (see Sec. 3.18). Bernoulli's equation is probably the most famous equation in fluid dynamics, and the purpose of this section is to derive it from the general equations discussed in Chap. 2.

Consider the *x* component of the momentum equation given by Eq. (2.104a). For an inviscid flow with no body forces, this equation becomes

$$\rho \frac{Du}{Dt} = - \frac{\partial p}{\partial x}$$

$$\rho \frac{\partial u}{\partial t} + \rho u \frac{\partial u}{\partial x} + \rho v \frac{\partial u}{\partial y} + \rho w \frac{\partial u}{\partial z} = - \frac{\partial p}{\partial x}$$

For steady flow,  $\partial u / \partial t = 0$ . Equation (3.1) is then written as

$$u \frac{\partial u}{\partial x} + v \frac{\partial u}{\partial y} + w \frac{\partial u}{\partial z} = -\frac{1}{\rho} \frac{\partial p}{\partial x} \quad (3.2)$$

Multiply Eq. (3.2) by  $dx$ :

$$u \frac{\partial u}{\partial x} dx + v \frac{\partial u}{\partial y} dx + w \frac{\partial u}{\partial z} dx = -\frac{1}{\rho} \frac{\partial p}{\partial x} dx \quad (3.3)$$

Consider the flow along a streamline in three-dimensional space. The equation of a streamline is given by Eqs. (2.108a to c). In particular, substituting

$$u dz - w dx = 0 \quad (2.108b)$$

$$v dx - u dy = 0 \quad (2.108c)$$

and

into Eq. (3.3), we have

$$u \frac{\partial u}{\partial x} dx + u \frac{\partial u}{\partial y} dy + u \frac{\partial u}{\partial z} dz = -\frac{1}{\rho} \frac{\partial p}{\partial x} dx \quad (3.4)$$

$$u \left( \frac{\partial u}{\partial x} dx + \frac{\partial u}{\partial y} dy + \frac{\partial u}{\partial z} dz \right) = -\frac{1}{\rho} \frac{\partial p}{\partial x} dx \quad (3.5)$$

Recall from calculus that given a function  $u = u(x, y, z)$ , the differential of  $u$  is

$$du = \frac{\partial u}{\partial x} dx + \frac{\partial u}{\partial y} dy + \frac{\partial u}{\partial z} dz$$

This is exactly the term in parentheses in Eq. (3.5). Hence, Eq. (3.5) is written as

$$u du = -\frac{1}{\rho} \frac{\partial p}{\partial x} dx \quad (3.6)$$

$$\frac{1}{2} d(u^2) = -\frac{1}{\rho} \frac{\partial p}{\partial x} dx \quad (3.7)$$

or

$$\frac{1}{2} d(v^2) = -\frac{1}{\rho} \frac{\partial p}{\partial y} dy \quad (3.8)$$

In a similar fashion, starting from the  $y$  component of the momentum equation given by Eq. (2.104b), specializing to an inviscid, steady flow, and applying the result to flow along a streamline, Eqs. (2.108a and c), we have

$$\frac{1}{2} d(w^2) = -\frac{1}{\rho} \frac{\partial p}{\partial z} dz \quad (3.9)$$

Similarly, from the  $z$  component of the momentum equation, Eq. (2.104c), we obtain

$$\frac{1}{2} d(u^2) = -\frac{1}{\rho} \frac{\partial p}{\partial x} dx \quad (3.8)$$

Adding Eqs. (3.6) through (3.8),

$$\frac{1}{2} d(u^2 + v^2 + w^2) = -\frac{1}{\rho} \left( \frac{\partial p}{\partial x} dx + \frac{\partial p}{\partial y} dy + \frac{\partial p}{\partial z} dz \right) \quad (3.9)$$

However,

$$u^2 + v^2 + w^2 = V^2 \quad (3.10)$$

$$\text{and} \quad \frac{\partial p}{\partial x} dx + \frac{\partial p}{\partial y} dy + \frac{\partial p}{\partial z} dz = dp \quad (3.11)$$

Substituting Eqs. (3.10) and (3.11) into (3.9), we have

$$\frac{1}{2} d(V^2) = -\frac{dp}{\rho} \quad (3.12)$$

or

or

Equation (3.12) is called *Euler's equation*. It applies to an inviscid flow with no body forces, and it relates the change in velocity along a streamline  $dV$  to the change in pressure  $dp$  along the same streamline.

Equation (3.12) takes on a very special and important form for incompressible flow. In such a case,  $\rho = \text{constant}$ , and Eq. (3.12) can be easily integrated between any two points 1 and 2 along a streamline. From Eq. (3.12), with  $\rho = \text{constant}$ , we have

$$\int_{p_1}^{p_2} dp = -\rho \int_{V_1}^{V_2} V dV$$

$$p_2 - p_1 = -\rho \left( \frac{V_2^2}{2} - \frac{V_1^2}{2} \right)$$

$$p_1 + \frac{1}{2} \rho V_1^2 = p_2 + \frac{1}{2} \rho V_2^2 \quad (3.13)$$

Equation (3.13) is *Bernoulli's equation*, which relates  $p_1$  and  $V_1$  on a streamline to  $p_2$  and  $V_2$  at another point 2 on the same streamline. Equation (3.13) can also be written as

$$p + \frac{1}{2} \rho V^2 = \text{const} \quad \text{along a streamline} \quad (3.14)$$

In the derivation of Eqs. (3.13) and (3.14), no stipulation has been made as to whether the flow is rotational or irrotational — these equations hold along a streamline in either case. For a general, rotational flow, the value of the constant in Eq. (3.14) will change from one streamline to the next. However, if the flow is irrotational, then Bernoulli's equation holds between any two points in the flow, not necessarily just on the same streamline. For an irrotational flow, the constant in Eq. (3.14) is the same for all streamlines, and

$$p + \frac{1}{2} \rho V^2 = \text{const} \quad \text{throughout the flow} \quad (3.15)$$

The proof of this statement is given as Prob. 3.1.

The physical significance of Bernoulli's equation is obvious from Eqs. (3.13) to (3.15); namely, *when the velocity increases, the pressure decreases, and when the velocity decreases, the pressure increases.*

Note that Bernoulli's equation was derived from the momentum equation; hence, it is a statement of Newton's second law for an inviscid, incompressible flow with no body forces. However, note that the dimensions of Eqs. (3.13) to (3.15) are energy per unit volume ( $\frac{1}{2}\rho V^2$  is the kinetic energy per unit volume). Hence, Bernoulli's equation is also a relation for mechanical energy in an incompressible flow; it states that the work done on a fluid by pressure forces is equal to the change in kinetic energy of the flow. Indeed, Bernoulli's equation can be derived from the general energy equation, such as Eq. (2.105). This derivation is left to the reader. The fact that Bernoulli's equation can be interpreted as either Newton's second law or an energy equation simply illustrates that the energy equation is redundant for the analysis of inviscid, incompressible flow. For such flows, the continuity and momentum equations suffice. (You may wish to review the opening comments of Sec. 2.7 on this same subject.) The strategy for solving most problems in inviscid, incompressible flow is as follows:

1. Obtain the velocity field from the governing equations. These equations, appropriate for an inviscid, incompressible flow, are discussed in Secs. 3.6 and 3.7.
2. Once the velocity field is known, obtain the pressure field from Bernoulli's equation.

However, before treating the general approach to the solution of such flows (Sec. 3.7), several applications of the continuity equation and Bernoulli's equation are made to flows in ducts (Sec. 3.3) and to the measurement of airspeed using a Pitot tube (Sec. 3.4).

**Example 3.1** Consider an airfoil in a flow at standard sea-level conditions with a freestream velocity of 50 m/s. At a given point on the airfoil, the pressure is  $0.9 \times 10^5 \text{ N/m}^2$ . Calculate the velocity at this point.

**SOLUTION** At standard sea-level conditions,  $\rho_\infty = 1.23 \text{ kg/m}^3$  and  $p_\infty = 1.01 \times 10^5 \text{ N/m}^2$ . Hence,

$$V = \sqrt{\frac{2(p_\infty - p)}{\rho} + \frac{1}{2}\rho V_\infty^2} = \sqrt{\frac{2(1.01 - 0.9) \times 10^5}{1.23} + \frac{1}{2}(1.23)(50)^2}$$

$V = 139.4 \text{ m/s}$

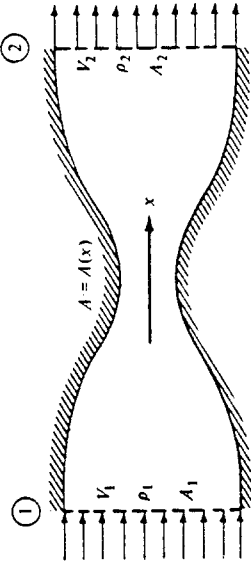


Figure 3.5 Quasi-one-dimensional flow in a duct.

sections which vary in area from one location to another. The flow through such a duct is three-dimensional and, strictly speaking, should be analyzed by means of the full three-dimensional conservation equations derived in Chap. 2. However, in many applications, the variation of area  $A = A(x)$  is moderate, and for such cases it is reasonable to assume that the flow-field properties are uniform across any cross section, and, hence, vary only in the  $x$  direction. In Fig. 3.5, uniform flow is sketched at station 1, and another but different uniform flow is shown at station 2. Such flow, where the area changes as a function of  $x$  and all the flow-field variables are assumed to be functions of  $x$  only, i.e.,  $A = A(x)$ ,  $V = V(x)$ ,  $p = p(x)$ , etc., is called *quasi-one-dimensional flow*. Although such flow is only an approximation of the truly three-dimensional flow in ducts, the results are sufficiently accurate for many aerodynamic applications. Such quasi-one-dimensional flow calculations are frequently used in engineering. They are the subject of this section.

Consider the integral form of the continuity equation written below:

$$\oint \rho dV + \oint \rho V \cdot dS = 0 \quad (2.39)$$

For steady flow, this becomes

$$\oint \frac{\partial}{\partial t} \oint_V \rho dV + \oint_S \rho V \cdot dS = 0 \quad (3.16)$$

$$\iint_A \rho V \cdot dS = 0 \quad (3.17)$$

Apply Eq. (3.16) to the duct shown in Fig. 3.5, where the control volume is bounded by  $A_1$  on the left,  $A_2$  on the right, and the upper and lower walls of the duct. Hence, Eq. (3.16) is

$$\iint_{A_1} \rho V \cdot dS + \iint_{A_2} \rho V \cdot dS + \iint_{\text{wall}} \rho V \cdot dS = 0 \quad (3.18)$$

Along the walls, the flow velocity is tangent to the wall. Since by definition  $dS$  is perpendicular to the wall, then along the wall,  $V \cdot dS = 0$ , and the integral over the wall surface is zero; i.e., in Eq. (3.17),

Consider the flow through a duct, such as that sketched in Fig. 3.5. In general, the duct will be a three-dimensional shape, such as a tube with elliptical or rectangular cross

At station 1, the flow is uniform across  $A_1$ . Noting that  $d\mathbf{S}$  and  $\mathbf{V}$  are in opposite directions at station 1 ( $d\mathbf{S}$  always points *out* of the control volume by definition), we have in Eq. (3.17)

$$\iint_{A_1} \rho \mathbf{V} \cdot d\mathbf{S} = -\rho A_1 V_1 \quad (3.19)$$

At station 2, the flow is uniform across  $A_2$ , and since  $d\mathbf{S}$  and  $\mathbf{V}$  are in the same direction, we have in Eq. (3.17)

$$\iint_{A_2} \rho \mathbf{V} \cdot d\mathbf{S} = \rho A_2 V_2 \quad (3.20)$$

Substituting Eqs. (3.18) to (3.20) into (3.17), we obtain

$$-\rho_1 A_1 V_1 + \rho_2 A_2 V_2 + 0 = 0$$

$$\boxed{\rho_1 A_1 V_1 = \rho_2 A_2 V_2} \quad (3.21)$$

Equation (3.21) is the quasi-one-dimensional continuity equation; it applies to both compressible and incompressible flow.<sup>t</sup> In physical terms, it states that the mass flow through the duct is constant (i.e., what goes in must come out). Compare Eq. (3.21) with Eq. (2.34) for mass flow.

Consider *incompressible* flow only, where  $\rho = \text{constant}$ . In Eq. (3.21),  $\rho_1 = \rho_2$ , and we have

$$\boxed{A_1 V_1 = A_2 V_2} \quad (3.22)$$

Equation (3.22) is the quasi-one-dimensional continuity equation for incompressible flow. In physical terms, it states that the volume flow (cubic feet per second or cubic meters per second) through the duct is constant. From Eq. (3.22), we see that if the area decreases along the flow (convergent duct), the velocity increases; conversely, if the area increases (divergent duct), the velocity decreases. These variations are shown in Fig. 3.6; they are fundamental consequences of the incompressible continuity equation, and you should fully understand them. Moreover, from Bernoulli's equation, Eq. (3.15), we see that when the velocity increases in a convergent duct, the pressure decreases; conversely, when the velocity decreases in a divergent duct, the pressure increases. These pressure variations are also shown in Fig. 3.6.

Consider the incompressible flow through a convergent-divergent duct, shown in Fig. 3.7. The flow enters the duct with velocity  $V_1$  and pressure  $p_1$ . The velocity increases in the convergent portion of the duct, reaching a maximum value  $V_2$  at the minimum area of the duct. This minimum area is called the *throat*. Also in the convergent section, the pressure decreases, as sketched in Fig. 3.7. At the throat, the pressure reaches a minimum value,  $p_2$ . In the divergent section downstream of the throat, the velocity decreases, and the pressure increases. The duct shown in Fig. 3.7

<sup>t</sup> For a simpler, more rudimentary derivation of Eq. (3.21), see chapter 4 of Ref. 2. In the present discussion, we have established a more rigorous derivation of Eq. (3.21), consistent with the general integral form of the continuity equation.

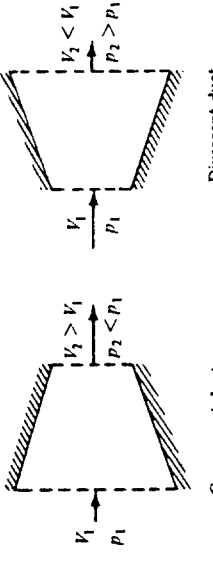


Figure 3.6 Incompressible flow in a duct.

is called a *venturi*; it is a device which finds many applications in engineering, and its use dates back more than a century. Its primary characteristic is that the pressure  $p_2$  is lower at the throat than the ambient pressure  $p_1$  outside the venturi. This pressure difference  $p_1 - p_2$  is used to advantage in several applications. For example, in the carburetor of your automobile engine, there is a venturi through which the incoming air is mixed with fuel. The fuel line opens into the venturi at the throat. Because  $p_2$  is less than the surrounding ambient pressure  $p_1$ , the pressure difference  $p_1 - p_2$  helps to force the fuel into the airstream and mix it with the air downstream of the throat.

In an application closer to aerodynamics, a venturi can be used to measure air-speeds. Consider a venturi with a given inlet-to-throat-area ratio  $A_1/A_2$ , as shown in Fig. 3.7. Assume that the venturi is inserted into an airstream that has an unknown velocity  $V_1$ . We wish to use the venturi to measure this velocity. With regard to the venturi itself, the most direct quantity that can be measured is the pressure difference  $p_1 - p_2$ . This can be accomplished by placing a small hole (a pressure tap) in the wall of the venturi at both the inlet and the throat and connecting the pressure leads (tubes) from these holes across a differential pressure gage, or to both sides of a U-tube manometer (see Sec. 1.9). In such a fashion, the pressure difference  $p_1 - p_2$  can be

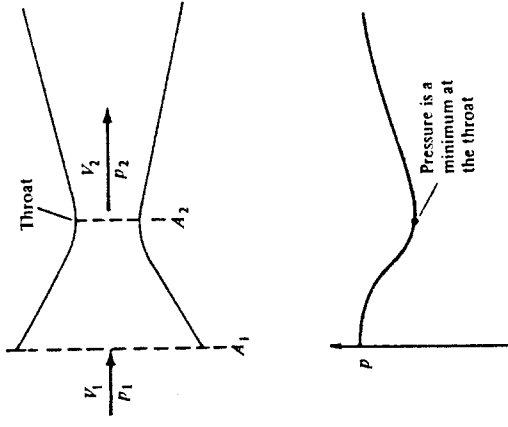


Figure 3.7 Flow through a venturi.

obtained directly. This measured pressure difference can be related to the unknown velocity  $V_1$  as follows. From Bernoulli's equation, Eq. (3.13), we have

$$V_1^2 = \frac{2}{\rho} (p_2 - p_1) + V_2^2 \quad (3.23)$$

From the continuity equation Eq. (3.22), we have

$$V_2 = \frac{A_1}{A_2} V_1 \quad (3.24)$$

Substituting Eq. (3.24) into (3.23),

$$V_1^2 = \frac{2}{\rho} (p_2 - p_1) + \left( \frac{A_1}{A_2} \right)^2 V_1^2 \quad (3.25)$$

Solving Eq. (3.25) for  $V_1$ , we obtain

$$V_1 = \sqrt{\frac{2(p_1 - p_2)}{\rho[(A_1/A_2)^2 - 1]}} \quad (3.26)$$

Equation (3.26) is the desired result; it gives the inlet air velocity  $V_1$  in terms of the measured pressure difference  $p_1 - p_2$  and the known density  $\rho$  and area ratio  $A_1/A_2$ . In this fashion, a venturi can be used to measure air speeds. Indeed, historically the first practical airspeed indicator on an airplane was a venturi used by the French Captain A. Eleve in January, 1911, more than 7 years after the Wright brothers' first powered flight. Today, the most common airspeed-measuring instrument is the Pitot tube (to be discussed in Sec. 3.4); however, the venturi is still found on some general-aviation airplanes, including home-built and simple experimental aircraft.

Another application of incompressible flow in a duct is the low-speed wind tunnel. The desire to build ground-based experimental facilities designed to produce flows of air in the laboratory which simulate actual flight in the atmosphere dates back to 1871, when Francis Wenham in England built and used the first wind tunnel in history.<sup>†</sup> From that date to the mid-1930s, almost all wind tunnels were designed to produce air flows with velocities from 0 to 250 mi/h. Such low-speed wind tunnels are still much in use today, along with a complement of transonic, supersonic, and hypersonic tunnels. The principles developed in this section allow us to examine the basic aspects of low-speed wind tunnels, as follows.

In essence, a low-speed wind tunnel is a large venturi where the airflow is driven by a fan connected to some type of motor drive. The wind-tunnel fan blades are similar to airplane propellers and are designed to draw the airflow through the tunnel circuit. The wind tunnel may be open circuit, where the air is drawn in the front directly from the atmosphere and exhausted out the back, again directly to the atmosphere, as shown in Fig. 3.8a; or the wind tunnel may be closed circuit, where the air from the exhaust is returned directly to the front of the tunnel via a closed duct forming a loop, as shown

<sup>†</sup> For a discussion on the history of wind tunnels, see chapter 4 of Ref. 2.

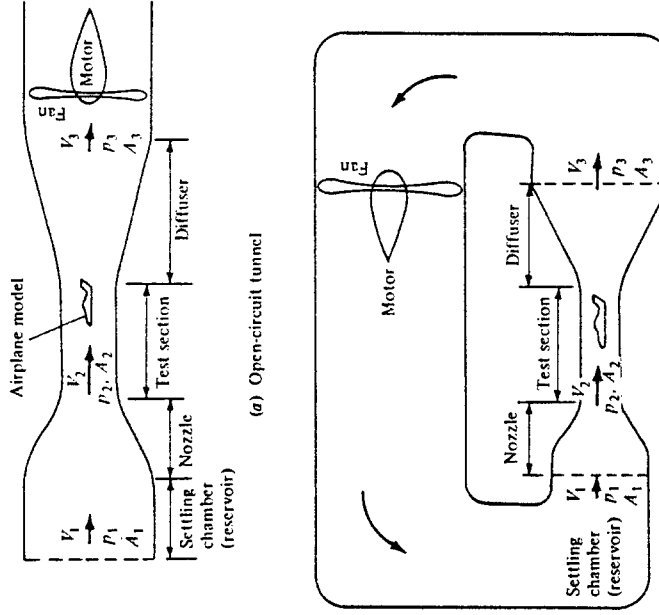


Figure 3.8 (a) Open-circuit tunnel. (b) Closed-circuit tunnel.

in Fig. 3.8b. In either case, the airflow with pressure  $p_1$  enters the nozzle at a low velocity  $V_1$ , where the area is  $A_1$ . The nozzle converges to a smaller area  $A_2$  at the test section, where the velocity has increased to  $V_2$  and the pressure has decreased to  $p_2$ . After flowing over an aerodynamic model (which may be a model of a complete airplane or part of an airplane such as a wing, tail, engine, or nacelle), the air passes into a diverging duct called a *diffuser*, where the area increases to  $A_3$ , the velocity decreases to  $V_3$ , and the pressure increases to  $p_3$ . From the continuity equation (3.22), the test-section air velocity is

$$V_2 = \frac{A_1}{A_2} V_1 \quad (3.27)$$

In turn, the velocity at the exit of the diffuser is

$$V_3 = \frac{A_2}{A_3} V_2 \quad (3.28)$$

The pressure at various locations in the wind tunnel is related to the velocity by Bernoulli's equation.

$$p_1 + \frac{1}{2}\rho V_1^2 = p_2 + \frac{1}{2}\rho V_2^2 = p_3 + \frac{1}{2}\rho V_3^2 \quad (3.29)$$

The basic factor that controls the air velocity in the test section of a given low-speed wind tunnel is the pressure difference  $p_1 - p_2$ . To see this more clearly, rewrite Eq. (3.29) as

$$V_2^2 = \frac{2}{\rho} (p_1 - p_2) + V_1^2 \quad (3.30)$$

From Eq. (3.27),  $V_1 = (A_1/A_2)V_2$ . Substituting into the right-hand side of Eq. (3.30), we have

$$V_2^2 = \frac{2}{\rho} (p_1 - p_2) + \left(\frac{A_2}{A_1}\right)^2 V_2^2 \quad (3.31)$$

Solving Eq. (3.31) for  $V_2$ , we obtain

$$V_2 = \sqrt{\frac{2(p_1 - p_2)}{\rho[1 - (A_2/A_1)^2]}} \quad (3.32)$$

The area ratio  $A_2/A_1$  is a fixed quantity for a wind tunnel of given design. Moreover, the density is a known constant for incompressible flow. Therefore, Eq. (3.32) demonstrates conclusively that the test-section velocity  $V_2$  is governed by the pressure difference  $p_1 - p_2$ . The fan driving the wind-tunnel flow creates this pressure difference by doing work on the air. When the wind-tunnel operator turns the "control knob" of the wind tunnel and adjusts the power to the fan, he or she is essentially adjusting the pressure difference  $p_1 - p_2$  and, in turn, adjusting the velocity via Eq. (3.32).

In low-speed wind tunnels, the most convenient method of measuring the pressure difference  $p_1 - p_2$ , hence of measuring  $V_2$  via Eq. (3.32), is by means of a manometer as discussed in Sec. 1.9. In Eq. (1.49), the density is the density of the liquid in the manometer (*not* the density of the air in the tunnel). The product of density and the acceleration of gravity  $g$  in Eq. (1.49) is the weight per unit volume of the manometer fluid. Denote this weight per unit volume by  $w$ . Referring to Eq. (1.49), if the side of the manometer associated with  $p_a$  is connected to a pressure tap in the settling chamber of the wind tunnel, where the pressure is  $p_1$ , and if the other side of the manometer (associated with  $p_b$ ) is connected to a pressure tap in the test section, where the pressure is  $p_2$ , then from Eq. (1.49),

$$p_1 - p_2 = w \Delta h$$

where  $\Delta h$  is the difference in heights of the liquid between the two sides of the manometer. In turn, Eq. (3.32) can be expressed as

$$V_2 = \sqrt{\frac{2w \Delta h}{\rho[1 - (A_2/A_1)^2]}}$$

In many low-speed wind tunnels, the test section is vented to the surrounding atmosphere by means of slots in the wall; in others, the test section is not a duct at all, but rather an open area between the nozzle exit and the diffuser inlet. In both cases, the pressure in the surrounding atmosphere is impressed on the test-section flow; hence,

$p_2 = 1$  atm. (In subsonic flow, a jet which is dumped freely into the surrounding air takes on the same pressure as the surroundings; in contrast, a supersonic free jet may have completely different pressures than the surrounding atmosphere, as we see in Chap. 10.)

Keep in mind that the basic equations used in this section have certain limitations—we are assuming a quasi-one-dimensional inviscid flow. Such equations can sometimes lead to misleading results when the neglected phenomena are in reality important. For example, if  $A_3 = A_1$  (inlet area of the tunnel is equal to the exit area), then Eqs. (3.27) and (3.28) yield  $V_3 = V_1$ . In turn, from Eq. (3.29),  $p_3 = p_1$ ; i.e., there is no pressure difference across the entire tunnel circuit. If this were true, the tunnel would run without the application of any power—we would have a perpetual motion machine. In reality, there are losses in the airflow due to friction at the tunnel walls and drag on the aerodynamic model in the test section. Bernoulli's equation, Eq. (3.29), does not take such losses into account. (Review the derivation of Bernoulli's equation in Sec. 3.2; note that viscous effects are neglected.) Thus, in an actual wind tunnel, there is a pressure loss due to viscous and drag effects, and  $p_3 < p_1$ . The function of the wind-tunnel motor and fan is to add power to the airflow in order to increase the pressure of the flow coming out of the diffuser so that it can be exhausted into the atmosphere (Fig. 3.8a) or returned to the inlet of the nozzle at the higher pressure  $p_1$  (Fig. 3.8b).

**Example 3.2** Consider a venturi with a throat-to-inlet area ratio of 0.8 mounted in a flow at standard sea-level conditions. If the pressure difference between the inlet and the throat is  $7 \text{ lb}/\text{ft}^2$ , calculate the velocity of the flow at the inlet.

**SOLUTION** At standard sea-level conditions,  $\rho = 0.002377 \text{ slug}/\text{ft}^3$ . Hence,

$$V_1 = \sqrt{\frac{2(p_1 - p_2)}{\rho[(A_1/A_2)^2 - 1]}} = \sqrt{\frac{2(7)}{(0.002377)[(\frac{1}{0.8})^2 - 1]}} = \boxed{102.3 \text{ ft/s}}$$

**Example 3.3** Consider a low-speed subsonic wind tunnel with a 12/1 contraction ratio for the nozzle. If the flow in the test section is at standard sea-level conditions with a velocity of  $50 \text{ m/s}$ , calculate the height difference in a U-tube mercury manometer with one side connected to the nozzle inlet and the other to the test section.

**SOLUTION** At standard sea level,  $\rho = 1.23 \text{ kg}/\text{m}^3$ . From Eq. (3.32),

$$p_1 - p_2 = \frac{1}{2} \rho V_2^2 \left[ 1 - \left( \frac{A_2}{A_1} \right)^2 \right] = \frac{1}{2} (50)^2 (1.23) \left[ 1 - \left( \frac{1}{12} \right)^2 \right] = 1527 \text{ N/m}^2$$

However,  $p_1 - p_2 = w \Delta h$ . The density of liquid mercury is  $1.36 \times 10^4 \text{ kg}/\text{m}^3$ . Hence,

$$w = (1.36 \times 10^4 \text{ kg}/\text{m}^3)(9.8 \text{ m/s}^2) = 1.33 \times 10^5 \text{ N/m}^2$$

$$\Delta h = \frac{p_1 - p_2}{w} = \frac{1527}{1.33 \times 10^4} = \boxed{0.01148 \text{ m}}$$

### 3.4 PITOT TUBE: MEASUREMENT OF AIRSPEED

In 1732, the Frenchman Henri Pitot was busy trying to measure the flow velocity of the Seine River in Paris. One of the instruments he used was his own invention — a strange-looking tube bent into an L shape, as shown in Fig. 3.9. Pitot oriented one of the open ends of the tube so that it faced directly into the flow. In turn, he used the pressure inside this tube to measure the water flow velocity. This was the first time in history that a proper measurement of fluid velocity was made, and Pitot's invention has carried through to the present day as the *Pitot tube* — one of the most common and frequently used instruments in any modern aerodynamic laboratory. Moreover, a Pitot tube is the most common device for measuring flight velocities of airplanes. The purpose of this section is to describe the basic principle of the Pitot tube.<sup>†</sup>

Consider a flow with pressure  $p_1$  moving with velocity  $V_1$ , as sketched at the left of Fig. 3.9. Let us consider the significance of the pressure  $p_1$  more closely. In Sec. 1.4, the pressure is associated with the time rate of change of momentum of the gas molecules impacting on or crossing a surface; i.e., pressure is clearly related to the motion of the molecules. This motion is very random, with molecules moving in all directions with various velocities. Now imagine that you hop on a fluid element of the flow and ride with it at the velocity  $V_1$ . The gas molecules, because of their random motion, will still bump into you, and you will feel the pressure  $p_1$  of the gas. We now give this pressure a specific name: the *static* pressure. Static pressure is a measure of the purely random motion of molecules in the gas; it is the pressure you feel when you ride along with the gas at the local flow velocity. All pressures used in this book so far have been static pressures; the pressure  $p$  appearing in all our previous equations has

<sup>†</sup> See chapter 4 of Ref. 2 for a detailed discussion of the history of the Pitot tube, how Pitot used it to overturn a basic theory in civil engineering, how it created some controversy in engineering, and how it finally found application in aeronautics.

been the static pressure. In engineering, whenever a reference is made to "pressure" without further qualification, that pressure is always interpreted as the *static* pressure. Furthermore, consider a boundary of the flow, such as a wall, where a small hole is drilled perpendicular to the surface. The plane of the hole is parallel to the flow, as shown at point A in Fig. 3.9. Because the flow moves over the opening, the pressure felt at point A is due only to the random motion of the molecules; i.e., at point A, the static pressure is measured. Such a small hole in the surface is called a *static pressure orifice*, or a *static pressure tap*.

In contrast, consider that a Pitot tube is now inserted into the flow, with an open end facing directly into the flow. That is, the plane of the opening of the tube is perpendicular to the flow, as shown at point B in Fig. 3.9. The other end of the Pitot tube is connected to a pressure gage, such as point C in Fig. 3.9; i.e., the Pitot tube is closed at point C. For the first few milliseconds after the Pitot tube is inserted into the flow, the gas will rush into the open end and will fill the tube. However, the tube is closed at point C; there is no place for the gas to go, and hence after a brief period of adjustment, the gas inside the tube will stagnate, i.e., the gas velocity inside the tube will go to zero. Indeed, the gas will eventually pile up and stagnate *everywhere* inside the tube, including at the open mouth at point B. As a result, the streamline of the flow that impinges directly at the open face of the tube (streamline DB in Fig. 3.9) sees this face as an obstruction to the flow. The fluid elements along streamline DB slow down as they get closer to the Pitot tube and go to zero velocity right at point B. Any point in a flow where  $V = 0$  is called a *stagnation point* of the flow; hence, point B at the open face of the Pitot tube is a stagnation point, where  $V_B = 0$ . In turn, from Bernoulli's equation we know the pressure increases as the velocity decreases. Hence,  $p_B > p_1$ . The pressure at a stagnation point is called the *stagnation pressure*, or *total* pressure, denoted by  $p_0$ . Hence, at point B,  $p_B = p_0$ .

From the above discussion, we see that two types of pressure can be defined for a given flow: static pressure, which is the pressure you feel by moving with the flow at its local velocity  $V_1$ , and total pressure, which is the pressure that the flow achieves when the velocity is reduced to zero. In aerodynamics, the distinction between total and static pressure is important; we have discussed this distinction at some length, and you should make yourself comfortable with the above paragraphs before proceeding further. (Further elaboration on the meaning and significance of total and static pressure will be made in Chap. 7.)

How is the Pitot tube used to measure flow velocity? To answer this question, first note that the total pressure  $p_0$  exerted by the flow at the tube inlet (point B) is impressed throughout the tube (there is no flow inside the tube); hence, the pressure everywhere inside the tube is  $p_0$ . Therefore, the pressure gage at point C reads  $p_0$ . This measurement, in conjunction with a measurement of the static pressure  $p_1$  at point A, yields the difference between total and static pressure,  $p_0 - p_1$ , and it is this pressure *difference* which allows the calculation of  $V_1$  via Bernoulli's equation. In particular, apply Bernoulli's equation between point A, where the pressure and velocity are  $p_1$  and  $V_1$ , respectively, and point B, where the pressure and velocity are  $p_0$  and  $V = 0$ , respectively.

$$p_A + \frac{1}{2} \rho V_1^2 = p_B + \frac{1}{2} \rho V_B^2$$

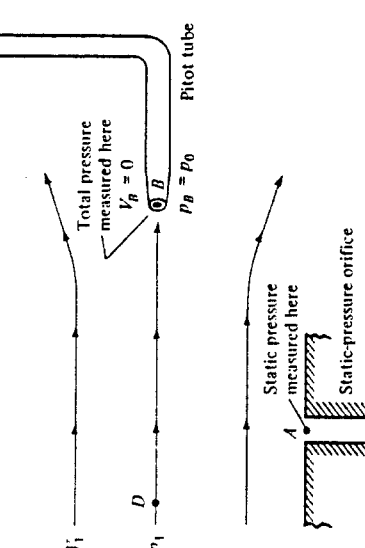


Figure 3.9 Pitot tube and a static pressure orifice.

$$(3.33) \quad p_1 + \frac{1}{2} \rho V_1^2 = p_0 + 0$$

or  
Solving Eq. (3.33) for  $V_1$ , we have

$$(3.34) \quad V_1 = \sqrt{\frac{2(p_0 - p_1)}{\rho}}$$

Equation (3.34) allows the calculation of velocity simply from the measured difference between total and static pressure. The total pressure  $p_0$  is obtained from the Pitot tube, and the static pressure  $p_1$  is obtained from a suitably placed static pressure tap.

It is possible to combine the measurement of both total and static pressure in one instrument, a *Pitot-static probe*, as sketched in Fig. 3.10. A Pitot-static probe measures  $p_0$  at the nose of the probe and  $p_1$  at a suitably placed static pressure tap on the probe surface downstream of the nose.

In Eq. (3.33), the term  $\frac{1}{2} \rho V^2$  is called the *dynamic pressure* and is denoted by the symbol  $q_1$ . The grouping  $\frac{1}{2} \rho V^2$  is called the *dynamic pressure by definition* and is used in all flows, incompressible to hypersonic.

$$q = \frac{1}{2} \rho V^2$$

However, for incompressible flow, the dynamic pressure has special meaning; it is precisely the difference between total and static pressure. Repeating Eq. (3.33),

$$(3.35) \quad p_1 + \frac{1}{2} \rho V_1^2 = p_0$$

$$q_1 = p_0 - p_1$$

$$\text{or} \quad p_1 + q_1 = p_0$$

$$\text{or} \quad q_1 = p_0 - p_1$$

It is important to keep in mind that Eq. (3.35) comes from Bernoulli's equation, and thus holds for *incompressible flow only*. For compressible flow, where Bernoulli's equation is not valid, the pressure difference  $p_0 - p_1$  is *not* equal to  $q_1$ . Moreover, Eq. (3.34) is valid for incompressible flow only. The velocities of compressible flows, both subsonic and supersonic, can be measured by means of a Pitot tube, but the equations are different from Eq. (3.34). (Velocity measurements in subsonic and supersonic compressible flows are discussed in Chap. 8.)

At this stage, it is important to repeat that Bernoulli's equation holds for incompressible flow only, and therefore any result derived from Bernoulli's equation also

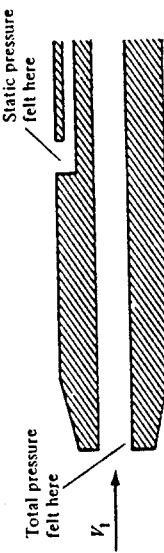


Figure 3.10 Pitot-static probe.

holds for incompressible flow only, such as Eqs. (3.26), (3.32), (3.34). Experience has shown that some students when first introduced to aerodynamics seem to adopt Bernoulli's equation as the gospel and tend to use it for all applications, including many cases where it is not valid. Hopefully, the repetitive warnings given above will squelch such tendencies.

**Example 3.4** An airplane is flying at standard sea level. The measurement obtained from a Pitot tube mounted on the wing tip reads 2190 lb/ft<sup>2</sup>. What is the velocity of the airplane?

**SOLUTION** Standard sea-level pressure is 2116 lb/ft<sup>2</sup>. From Eq. (3.34), we have

$$V_1 = \sqrt{\frac{2(p_0 - p_1)}{\rho}} = \sqrt{\frac{2(2190 - 2116)}{0.002377}} = 250 \text{ ft/s}$$

### 3.5 PRESSURE COEFFICIENT

Pressure, by itself, is a dimensional quantity, e.g., pounds per square foot, newtons per square meter. However, in Secs. 1.7 and 1.8, we established the usefulness of certain dimensionless parameters such as  $M$ ,  $Re$ ,  $C_L$ . It makes sense, therefore, that a dimensionless pressure would also find use in aerodynamics. Such a quantity is the *pressure coefficient*  $C_p$ , first introduced in Sec. 1.5 and defined as

$$(3.36) \quad C_p = \frac{p - p_\infty}{q_\infty}$$

where

$$q_\infty = \frac{1}{2} \rho_\infty V_\infty^2$$

The definition given in Eq. (3.36) is just that—a definition. It is used throughout aerodynamics, from incompressible to hypersonic flow. In the aerodynamic literature, it is very common to find pressures given in terms of  $C_p$  rather than the pressure itself. Indeed, pressure coefficient is another similarity parameter than can be added to the list started in Secs. 1.7 and 1.8.

For *incompressible flow*,  $C_p$  can be expressed in terms of velocity only. Consider the flow over an aerodynamic body immersed in a freestream with pressure  $p_\infty$  and velocity  $V_\infty$ . Pick an arbitrary point in the flow where the pressure and velocity are  $p$  and  $V$ , respectively. From Bernoulli's equation,

$$(3.37) \quad p_\infty + \frac{1}{2} \rho V_\infty^2 = p + \frac{1}{2} \rho V^2$$

or

$$p - p_\infty = \frac{1}{2} \rho (V_\infty^2 - V^2)$$

Substituting Eq. (3.37) into (3.36),

$$C_p = \frac{p - p_\infty}{q_\infty} = \frac{\frac{1}{2} \rho (V_\infty^2 - V^2)}{\frac{1}{2} \rho V_\infty^2}$$

$$C_p = 1 - \left( \frac{V}{V_s} \right)^2 \quad (3.38)$$

or

which is precisely Eq. (3.39).

Equation (3.38) is a useful expression for the pressure coefficient; however, note that the form of Eq. (3.38) holds for incompressible flow only.

Note from Eq. (3.38) that the pressure coefficient at a stagnation point (where  $V = 0$ ) in an incompressible flow is always equal to 1.0. This is the highest allowable value of  $C_p$  anywhere in the flow field. (For compressible flows,  $C_p$  at a stagnation point is greater than 1.0, as shown in Chap. 14.) Also, keep in mind that in regions of the flow where  $V > V_s$  or  $p < p_s$ ,  $C_p$  will be a negative value.

**Example 3.5** Consider an airfoil in a flow with a freestream velocity of 150 ft/s. The velocity at a given point on the airfoil is 225 ft/s. Calculate the pressure coefficient at this point.

SOLUTION

$$C_p = 1 - \left( \frac{V}{V_s} \right)^2 = 1 - \left( \frac{225}{150} \right)^2 = [-1.25]$$

### 3.6 CONDITION ON VELOCITY FOR INCOMPRESSIBLE FLOW

Consulting our chapter road map in Fig. 3.4, we have completed the left branch dealing with Bernoulli's equation. We now begin a more general consideration of incompressible flow, given by the center branch in Fig. 3.4. However, before introducing Laplace's equation, it is important to establish a basic condition on velocity in an incompressible flow, as follows.

First, consider the physical definition of incompressible flow, namely,  $\rho =$  constant. Since  $\rho$  is the mass per unit volume and  $\rho$  is constant, then a fluid element of fixed mass moving through an incompressible flow field must also have a fixed, constant volume. Recall Eq. (2.32), which shows that  $\nabla \cdot \mathbf{V}$  is physically the time rate of change of the volume of a moving fluid element per unit volume. However, for an incompressible flow, we have just stated that the volume of a fluid element is constant [e.g., in Eq. (2.32),  $D(\delta V)/Dt \equiv 0$ ]. Therefore, for an incompressible flow,

$$\boxed{\nabla \cdot \mathbf{V} = 0} \quad (3.39)$$

The fact that the divergence of velocity is zero for an incompressible flow can also be shown directly from the continuity equation, Eq. (2.43).

$$\frac{\partial p}{\partial t} + \nabla \cdot \rho \mathbf{V} = 0 \quad (2.43)$$

For incompressible flow,  $\rho =$  constant. Hence,  $\partial p/\partial t = 0$  and  $\nabla \cdot (\rho \mathbf{V}) = \rho \nabla \cdot \mathbf{V}$ . Equation (2.43) then becomes

$$\boxed{0 + \rho \nabla \cdot \mathbf{V} = 0}$$

$$\nabla \cdot \mathbf{V} = 0$$

or

which is precisely Eq. (3.39).

### 3.7 GOVERNING EQUATION FOR IRROTATIONAL, INCOMPRESSIBLE FLOW: LAPLACE'S EQUATION

We have seen in Sec. 3.6 that the principle of mass conservation for an incompressible flow can take the form of Eq. (3.39):

$$\boxed{\nabla \cdot \mathbf{V} = 0} \quad (3.39)$$

In addition, for an irrotational flow we have seen in Sec. 2.15 that a velocity potential  $\phi$  can be defined such that [from Eq. (2.145)]

$$\boxed{\mathbf{V} = \nabla \phi} \quad (2.145)$$

Therefore, for a flow that is both incompressible and irrotational, Eqs. (3.39) and (2.145) can be combined to yield

$$\boxed{\nabla \cdot (\nabla \phi) = 0} \quad (3.39)$$

or

$$\boxed{\nabla^2 \phi = 0} \quad (3.40)$$

Equation (3.40) is *Laplace's equation*—one of the most famous and extensively studied equations in mathematical physics. Solutions of Laplace's equation are called *harmonic functions*, for which there is a huge bulk of existing literature. Therefore, it is most fortuitous that incompressible, irrotational flow is described by Laplace's equation, for which numerous solutions exist and are well understood.

For convenience, Laplace's equation is written below in terms of the three common orthogonal coordinate systems employed in Sec. 2.2.

*Cartesian coordinates:*  $\phi = \phi(x, y, z)$

$$\nabla^2 \phi = \frac{\partial^2 \phi}{\partial x^2} + \frac{\partial^2 \phi}{\partial y^2} + \frac{\partial^2 \phi}{\partial z^2} = 0 \quad (3.41)$$

*Cylindrical coordinates:*  $\phi = \phi(r, \theta, z)$

$$\nabla^2 \phi = \frac{1}{r} \frac{\partial}{\partial r} \left( r \frac{\partial \phi}{\partial r} \right) + \frac{1}{r^2} \frac{\partial^2 \phi}{\partial \theta^2} + \frac{\partial^2 \phi}{\partial z^2} = 0 \quad (3.42)$$

*Spherical coordinates:*  $\phi = \phi(r, \theta, \Phi)$

$$\nabla^2 \phi = \frac{1}{r^2 \sin \theta} \left[ \frac{\partial}{\partial r} \left( r^2 \sin \theta \frac{\partial \phi}{\partial r} \right) + \frac{\partial}{\partial \theta} \left( \sin \theta \frac{\partial \phi}{\partial \theta} \right) + \frac{\partial}{\partial \Phi} \left( \frac{1}{\sin \theta} \frac{\partial \phi}{\partial \Phi} \right) \right] = 0 \quad (3.43)$$

Recall from Sec. 2.14 that, for a two-dimensional incompressible flow, a stream function  $\psi$  can be defined such that, from Eqs. (2.141a and b),

$$u = \frac{\partial \psi}{\partial y} \quad (2.141a)$$

$$v = -\frac{\partial \psi}{\partial x} \quad (2.141b)$$

From the continuity equation,  $\nabla \cdot \mathbf{V} = 0$ , expressed in cartesian coordinates:

$$\nabla \cdot \mathbf{V} = \frac{\partial u}{\partial x} + \frac{\partial v}{\partial y} = 0 \quad (3.44)$$

Substituting Eqs. (2.141a and b) into (3.44),

$$\frac{\partial}{\partial x} \left( \frac{\partial \psi}{\partial y} \right) + \frac{\partial}{\partial y} \left( -\frac{\partial \psi}{\partial x} \right) = \frac{\partial^2 \psi}{\partial x \partial y} - \frac{\partial^2 \psi}{\partial y \partial x} = 0 \quad (3.45)$$

Since mathematically  $\partial^2 \psi / \partial x \partial y = \partial^2 \psi / \partial y \partial x$ , we see from Eq. (3.45) that  $\psi$  automatically satisfies the continuity equation. *Indeed, the very definition and use of  $\psi$  is a statement of the conservation of mass, and Eqs. (2.141a and b) therefore can be used in place of the continuity equation itself.* If, in addition, the incompressible flow is irrotational, we have from the irrotationality condition stated in Eq. (2.122)

$$\frac{\partial v}{\partial x} - \frac{\partial u}{\partial y} = 0 \quad (2.122)$$

Substituting Eqs. (2.141a and b) into (2.122),

$$\frac{\partial}{\partial x} \left( -\frac{\partial \psi}{\partial x} \right) - \frac{\partial}{\partial y} \left( \frac{\partial \psi}{\partial y} \right) = 0 \quad (3.46)$$

or

$$\boxed{\frac{\partial^2 \psi}{\partial x^2} + \frac{\partial^2 \psi}{\partial y^2} = 0}$$

which is Laplace's equation. Therefore, the stream function also satisfies Laplace's equation, along with  $\phi$ . From Eqs. (3.40) and (3.46), we make the following obvious and important conclusions:

1. Any irrotational, incompressible flow has a velocity potential and stream function (for two-dimensional flow) that both satisfy Laplace's equation.
2. Conversely, any solution of Laplace's equation represents the velocity potential or stream function (two-dimensional) for an irrotational, incompressible flow.

Note that Laplace's equation is a second-order linear partial differential equation. The fact that it is *linear* is particularly important, because the sum of any particular solutions of a linear differential equation is also a solution of the equation. For example, if  $\phi_1, \phi_2, \dots, \phi_n$  represent  $n$  separate solutions of Eq. (3.40), then the sum

$$\phi = \phi_1 + \phi_2 + \dots + \phi_n$$

is also a solution of Eq. (3.40). Since irrotational, incompressible flow is governed by Laplace's equation and Laplace's equation is linear, we conclude that a *complicated flow pattern for an irrotational, incompressible flow can be synthesized by adding together a number of elementary flows which are also irrotational and incompressible*. Indeed, this establishes the grand strategy for the remainder of our discussions on inviscid, incompressible flow. We develop flow-field solutions for several different elementary flows, which by themselves may not seem to be practical flows in real life. However, we then proceed to add (i.e., superimpose) these elementary flows in different ways such that the resulting flow fields do pertain to practical problems.

Before proceeding further, consider the irrotational, incompressible flow fields over different aerodynamic shapes, such as a sphere, cone, or airplane wing. Clearly, each flow is going to be distinctly different; the streamlines and pressure distribution over a sphere are quite different from those over a cone. However, these different flows are all governed by the same equation, namely,  $\nabla^2 \phi = 0$ . How, then, do we obtain different flows for the different bodies? The answer is found in the *boundary conditions*. Although the governing equation for the different flows is the same, the boundary conditions for the equation must conform to the different geometric shapes and, hence, yield different flow-field solutions. Boundary conditions are therefore of vital concern in aerodynamic analysis. Let us examine the nature of boundary conditions further.

Consider the external aerodynamic flow over a stationary body, such as the airfoil sketched in Fig. 3.11. The flow is bounded by (1) the freestream flow which occurs (theoretically) an infinite distance away from the body, and (2) the surface of the body itself. Therefore, two sets of boundary conditions apply, as follows.

### Infinity Boundary Conditions

Far away from the body (toward infinity), in all directions, the flow approaches the uniform freestream conditions. Let  $V_\infty$  be aligned with the  $x$  direction as shown in Fig. 3.11. Hence, at infinity,

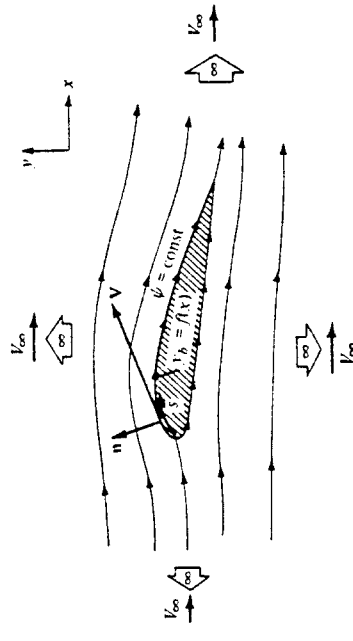


Figure 3.11 Boundary conditions at infinity and on a body: inviscid flow.

$$u = \frac{\partial \phi}{\partial x} = \frac{\partial \psi}{\partial y} = V_x \quad (3.47a)$$

$$v = \frac{\partial \phi}{\partial y} = -\frac{\partial \psi}{\partial x} = 0 \quad (3.47b)$$

Equations (3.47a and b) are the *boundary conditions on velocity at infinity*. They apply at an infinite distance from the body in all directions, above and below, and to the left and right of the body, as indicated in Fig. 3.11.

### Wall Boundary Conditions

If the body in Fig. 3.11 has a solid surface, then it is impossible for the flow to penetrate the surface. Instead, if the flow is viscous, the influence of friction between the fluid and the solid surface creates a zero velocity at the surface. Such viscous flows are discussed in Chaps. 15 and 16. In contrast, for inviscid flows the velocity at the surface can be finite, but because the flow cannot penetrate the surface, the velocity vector must be *tangent* to the surface. This "wall tangency" condition is illustrated in Fig. 3.11, which shows  $\mathbf{V}$  tangent to the body surface. If the flow is tangent to the surface, then the component of velocity *normal* to the surface must be zero. Let  $\mathbf{n}$  be a unit vector normal to the surface as shown in Fig. 3.11. The wall boundary condition can be written as

$$\mathbf{V} \cdot \mathbf{n} = (\nabla \phi) \cdot \mathbf{n} = 0 \quad (3.48a)$$

$$\frac{\partial \phi}{\partial n} = 0 \quad (3.48b)$$

or

$$\frac{\partial \psi}{\partial s} = 0 \quad (3.48c)$$

Equation (3.48a or b) gives the boundary condition for velocity at the wall; it is expressed in terms of  $\phi$ . If we are dealing with  $\psi$  rather than  $\phi$ , then the wall boundary condition is

$$\psi_{\text{surface}} = \psi_{y=y_b} = \text{const} \quad (3.48d)$$

is an alternative expression for the boundary condition given in Eq. (3.48c). If we are dealing with neither  $\phi$  nor  $\psi$ , but rather with the velocity components  $u$  and  $v$  themselves, then the wall boundary condition is obtained from the equation of a streamline Eq. (2.109), evaluated at the body surface, i.e.,

$$\frac{dy_b}{dx} = \left( \frac{v}{u} \right)_{\text{surface}} \quad (3.48e)$$

Equation (3.48e) states simply that the body surface is a streamline of the flow. The form given in Eq. (3.48e) for the flow tangency condition at the body surface is used for all inviscid flows, incompressible to hypersonic, and does not depend on the formulation of the problem in terms of  $\phi$  or  $\psi$  (or  $\bar{\psi}$ ).

### 3.8 INTERIM SUMMARY

Reflecting on our previous discussions, the general approach to the solution of irrotational, incompressible flows can be summarized as follows:

1. Solve Laplace's equation for  $\phi$  [Eq. (3.40)] or  $\psi$  [Eq. (3.46)] along with the proper boundary conditions [such as Eqs. (3.47) and (3.48)]. These solutions are usually in the form of a sum of elementary solutions (to be discussed in the following sections).
2. Obtain the flow velocity from  $\mathbf{V} = \nabla \phi$  or  $u = \partial \phi / \partial y$  and  $v = -\partial \phi / \partial x$ .
3. Obtain the pressure from Bernoulli's equation,  $p + \frac{1}{2} \rho V^2 = p_\infty + \frac{1}{2} \rho V_\infty^2$ , where  $p_\infty$  and  $V_\infty$  are known freestream conditions.

Since  $\mathbf{V}$  and  $p$  are the primary dependent variables for an incompressible flow, steps 1 to 3 are all that we need to solve a given problem as long as the flow is incompressible and irrotational.

### 3.9 UNIFORM FLOW: OUR FIRST ELEMENTARY FLOW

In this section, we present the first of a series of elementary incompressible flows which later will be superimposed to synthesize more complex incompressible flows. For the remainder of this chapter and in Chap. 4, we deal with two-dimensional steady flows; three-dimensional steady flows are treated in Chaps. 5 and 6.

Consider a uniform flow with velocity  $V_\infty$  oriented in the positive  $x$  direction, as sketched in Fig. 3.12. It is easily shown (see Prob. 3.8) that a uniform flow is a physically possible incompressible flow (i.e., it satisfies  $\nabla \cdot \mathbf{V} = 0$ ) and that it is irrotational (i.e., it satisfies  $\nabla \times \mathbf{V} = 0$ ). Hence, a velocity potential for uniform flow

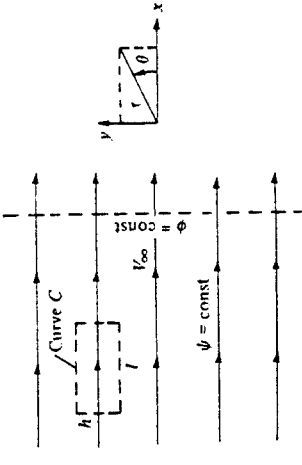


Figure 3.12 Uniform flow.

can be obtained such that  $\nabla\phi = \mathbf{V}$ . Examining Fig. 3.12, and recalling Eq. (2.147), we have

$$\frac{\partial\phi}{\partial x} = u = V_\infty \quad (3.49a)$$

$$\frac{\partial\phi}{\partial y} = v = 0 \quad (3.49b)$$

and

Integrating Eq. (3.49a) with respect to  $x$ , we have

$$\phi = V_\infty x + f(y) \quad (3.50)$$

where  $f(y)$  is a function of  $y$  only. Integrating Eq. (3.49b) with respect to  $y$ , we obtain

$$\phi = \text{const} + g(x) \quad (3.51)$$

where  $g(x)$  is a function of  $x$  only. In Eqs. (3.50) and (3.51),  $\phi$  is the same function; hence, by comparing these equations,  $g(x)$  must be  $V_\infty x$ , and  $f(y)$  must be constant. Thus,

$$\phi = V_\infty x + \text{const} \quad (3.52)$$

Note that in a practical aerodynamic problem, the actual value of  $\phi$  is not significant; rather,  $\phi$  is always used to obtain the velocity by differentiation, i.e.,  $\nabla\phi = \mathbf{V}$ . Since the derivative of a constant is zero, we can drop the constant from Eq. (3.52) without any loss of rigor. Hence, Eq. (3.52) can be written as

$$\boxed{\phi = V_\infty x} \quad (3.53)$$

Equation (3.53) is the velocity potential for a uniform flow with velocity  $V_\infty$  oriented in the positive  $x$  direction. Note that the derivation of Eq. (3.53) does not depend on the assumption of incompressibility; it applies to any uniform flow, compressible or incompressible.

Consider the incompressible stream function  $\psi$ . From Fig. 3.12 and Eqs. (2.141a and b), we have

$$\frac{\partial\psi}{\partial y} = u = V_\infty \quad (3.54a)$$

$$\frac{\partial\psi}{\partial x} = -v = 0 \quad (3.54b)$$

Integrating Eq. (3.54a) with respect to  $y$  and Eq. (3.54b) with respect to  $x$ , and comparing the results, we obtain

$$\boxed{\psi = V_\infty y} \quad (3.55)$$

Equation (3.55) is the stream function for an incompressible uniform flow oriented in the positive  $x$  direction.

From Sec. 2.14, the equation of a streamline is given by  $\psi = \text{constant}$ . Therefore, from Eq. (3.55), the streamlines for the uniform flow are given by  $\psi = V_\infty y = \text{constant}$ . Because  $V_\infty$  is itself constant, the streamlines are thus given mathematically as  $y = \text{constant}$ , i.e., as lines of constant  $y$ . This result is consistent with Fig. 3.12, which shows the streamlines as horizontal lines, i.e., as lines of constant  $y$ . Also note from Eq. (3.53) that the equipotential lines are lines of constant  $x$ , as shown by the dashed line in Fig. 3.12. Consistent with our discussion in Sec. 2.16, note that the lines of  $\psi = \text{constant}$  and  $\phi = \text{constant}$  are mutually perpendicular.

Equations (3.53) and (3.55) can be expressed in terms of polar coordinates, where  $x = r \cos \theta$  and  $y = r \sin \theta$ , as shown in Fig. 3.12. Hence,

$$\boxed{\phi = V_\infty r \cos \theta} \quad (3.56)$$

$$\boxed{\psi = V_\infty r \sin \theta} \quad (3.57)$$

Consider the circulation in a uniform flow. The definition of circulation is given by

$$\Gamma \equiv - \oint_C \mathbf{v} \cdot d\mathbf{s} \quad (2.127)$$

Let the closed curve  $C$  in Eq. (2.127) be the rectangle shown at the left of Fig. 3.12;  $h$  and  $l$  are the lengths of the vertical and horizontal sides, respectively, of the rectangle. Then

$$\oint_C \mathbf{v} \cdot d\mathbf{s} = -V_\infty l - 0(h) + V_\infty l + 0(h) = 0$$

or

$$\Gamma = 0 \quad (3.58)$$

Equation (3.58) is true for any arbitrary closed curve in the uniform flow. To show this, note that  $\mathbf{V}_\infty$  is constant in both magnitude and direction, and hence,

$$\Gamma = - \oint_C \mathbf{v} \cdot d\mathbf{s} = - \mathbf{V}_\infty \cdot \oint_C d\mathbf{s} = \mathbf{V}_\infty \cdot \mathbf{0} = 0$$

because the line integral of  $d\mathbf{s}$  around a closed curve is identically zero. Therefore, from Eq. (3.58), we state that *circulation around any closed curve in a uniform flow is zero*.

The above result is consistent with Eq. (2.128), which states that

$$\Gamma = - \iint_S (\nabla \times \mathbf{V}) \cdot d\mathbf{S} \quad (2.128)$$

We stated earlier that a uniform flow is irrotational, i.e.,  $\nabla \times \mathbf{V} = 0$  everywhere. Hence, Eq. (2.128) yields  $\Gamma = 0$ .

Note that Eqs. (3.53) and (3.55) satisfy Laplace's equation [see Eq. (3.41)], which can be easily proved by simple substitution. Therefore, uniform flow is a viable elementary flow for use in building more complex flows.

**3.10 SOURCE FLOW: OUR SECOND ELEMENTARY FLOW**

Consider a two-dimensional, incompressible flow where all the streamlines are straight lines emanating from a central point,  $O$ , as shown at the left of Fig. 3.13. Moreover, let the velocity along each of the streamlines vary inversely with distance from point  $O$ . Such a flow is called a *source flow*. Examining Fig. 3.13, the velocity components in the radial and tangential directions are  $V_r$  and  $V_\theta$ , respectively, where  $V_z = 0$ . The coordinate system in Fig. 3.13 is a cylindrical coordinate system, with the  $z$  axis perpendicular to the page. (Note that polar coordinates are simply the cylindrical coordinates  $r$  and  $\theta$  confined to a single plane given by  $z = \text{constant}$ .) It is easily shown (see Prob. 3.9) that (1) source flow is a physically possible incompressible flow, i.e.,  $\nabla \cdot \mathbf{V} = 0$ , at every point *except* the origin, where  $\nabla \cdot \mathbf{V}$  becomes infinite, and (2) source flow is *irrotational* at every point.

In a source flow, the streamlines are directed *away from* the origin, as shown at the left of Fig. 3.13. The opposite case is that of a *sink flow*, where by definition the streamlines are directed *toward* the origin, as shown at the right of Fig. 3.13. For sink flow, the streamlines are still radial lines from a common origin, along which the flow velocity varies inversely with distance from point  $O$ . Indeed, a sink flow is simply a negative source flow.

The flows in Fig. 3.13 have an alternate, somewhat philosophical interpretation. Consider the origin, point  $O$ , as a *discrete* source or sink. Moreover, interpret the radial flow surrounding the origin as simply being *induced* by the presence of the discrete source or sink at the origin (much like a magnetic field is induced in the space surrounding a current-carrying wire). Recall that, for a source flow,  $\nabla \cdot \mathbf{V} = 0$  everywhere except at the origin, where it is infinite. Thus, the origin is a *singular point*, and we can interpret this singular point as a discrete source or sink of a given strength, with a corresponding induced flow field about the point. This interpretation is very convenient and is used frequently. Other types of singularities, such as doublets and vortices, are introduced in subsequent sections. Indeed, the irrotational, incompressible flow field about an arbitrary body can be visualized as a flow induced by a proper distribution of such singularities over the surface of the body. This concept is fundamental to many theoretical solutions of incompressible flow over airfoils and other aerodynamic shapes, and it is the very heart of modern numerical techniques for the

solution of such flows. You will obtain a greater appreciation for the concept of distributed singularities for the solution of incompressible flow in Chaps. 4 through 6. At this stage, however, simply visualize a discrete source (or sink) as a singularity that induces the flows shown in Fig. 3.13.

Let us look more closely at the velocity field induced by a source or sink. By definition, the velocity is inversely proportional to the radial distance  $r$ . As stated earlier, this velocity variation is a physically possible flow, because it yields  $\nabla \cdot \mathbf{V} = 0$ . Moreover, it is the *only* such velocity variation for which the relation  $\nabla \cdot \mathbf{V} = 0$  is satisfied for the radial flows shown in Fig. 3.13. Hence,

$$V_r = \frac{c}{r} \quad (3.59a)$$

$$V_\theta = 0 \quad (3.59b)$$

and

where  $c$  is a constant. The value of the constant is related to the volume flow from the source, as follows. In Fig. 3.13, consider a depth of length  $l$  perpendicular to the page, i.e., a length  $l$  along the  $z$  axis. This is sketched in three-dimensional perspective in Fig. 3.14. In Fig. 3.14, we can visualize an entire line of sources along the  $z$  axis, of which the source at  $O$  is just part. Therefore, in a two-dimensional flow, the discrete source, sketched in Fig. 3.13, is simply a single point on the line source shown in Fig. 3.14. The two-dimensional flow shown in Fig. 3.13 is the same in any plane perpendicular to the  $z$  axis, i.e., for any plane given by  $z = \text{constant}$ . Consider the mass flow across the surface of the cylinder of radius  $r$  and height  $l$  as shown in Fig. 3.14. The elemental mass flow across the surface element  $dS$  shown in Fig. 3.14 is  $\rho \mathbf{V} \cdot d\mathbf{S} = \rho V_r (r d\theta) l$ . Hence, noting that  $V_r$  is the same value at any  $\theta$  location for the fixed radius  $r$ , the total mass flow across the surface of the cylinder is

$$\dot{m} = \int_0^{2\pi} \rho V_r (r d\theta) l = \rho l V_r \int_0^{2\pi} d\theta = 2\pi l \rho V_r \quad (3.60)$$

Since  $\rho$  is defined as the mass per unit volume and  $\dot{m}$  is mass per second, then  $\dot{m}/\rho$  is the volume flow per second. Denote this rate of volume flow by  $\dot{V}$ . Thus, from Eq. (3.60), we have

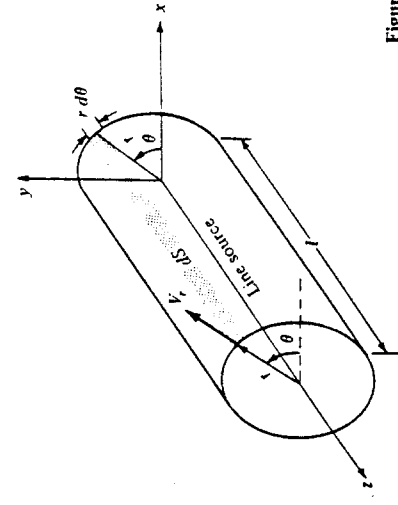


Figure 3.14 Volume flow rate from a line source.

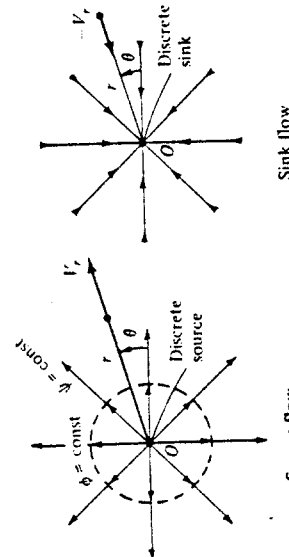


Figure 3.13 Source and sink flow.

$$\dot{V} = \frac{\dot{m}}{\rho} = 2\pi r V_r \quad (3.61)$$

Moreover, the rate of volume flow per unit length along the cylinder is  $\dot{V}/l$ . Denote this volume flow rate per unit length (which is the same as per unit depth perpendicular to the page in Fig. 3.13) as  $\Lambda$ . Hence, from Eq. (3.61), we obtain

$$\Lambda = \frac{\dot{V}}{l} = 2\pi r V_r \quad (3.62)$$

or

$$V_r = \frac{\Lambda}{2\pi r} \quad (3.63)$$

Hence, comparing Eqs. (3.59a) and (3.62), we see that the constant in Eq. (3.59a) is  $c = \Lambda/2\pi$ . In Eq. (3.62),  $\Lambda$  defines the *source strength*; it is physically the rate of volume flow from the source, per unit depth perpendicular to the page of Fig. 3.13.

Typical units of  $\Lambda$  are square meters per second or square feet per second. In Eq. (3.62), a positive value of  $\Lambda$  represents a source, whereas a negative value represents a sink.

The velocity potential for a source can be obtained as follows. From Eqs. (2.148), (3.59b), and (3.62),

$$\frac{\partial \phi}{\partial r} = V_r = \frac{\Lambda}{2\pi r} \quad (3.63)$$

$$\text{and } \frac{1}{r} \frac{\partial \phi}{\partial \theta} = V_\theta = 0 \quad (3.64)$$

Integrating Eq. (3.63) with respect to  $r$ , we have

$$\phi = \frac{\Lambda}{2\pi} \ln r + f(\theta) \quad (3.65)$$

Integrating Eq. (3.64) with respect to  $\theta$ , we have

$$\phi = \text{const} + f(r) \quad (3.66)$$

Comparing Eqs. (3.65) and (3.66), we see that  $f(r) = (\Lambda/2\pi) \ln r$  and  $f(\theta) = \text{const}$ . As explained in Sec. 3.9, the constant can be dropped without loss of rigor, and hence, Eq. (3.65) yields

$$\phi = \frac{\Lambda}{2\pi} \ln r \quad (3.67)$$

Equation (3.67) is the velocity potential for a two-dimensional source flow. The stream function can be obtained as follows. From Eqs. (2.142a and b), (3.59b), and (3.62),

$$\frac{1}{r} \frac{\partial \psi}{\partial \theta} = V_r = \frac{\Lambda}{2\pi r} \quad (3.68)$$

$$-\frac{\partial \psi}{\partial r} = V_\theta = 0 \quad (3.69)$$

Integrating Eq. (3.68) with respect to  $\theta$ , we obtain

$$\psi = \frac{\Lambda}{2\pi} \theta + f(r) \quad (3.70)$$

Integrating Eq. (3.69) with respect to  $r$ , we have

$$\psi = \text{const} + f(\theta) \quad (3.71)$$

Comparing Eqs. (3.70) and (3.71) and dropping the constant, we have

$$\boxed{\psi = \frac{\Lambda}{2\pi} \theta} \quad (3.72)$$

Equation (3.72) is the stream function for a two-dimensional source flow.

The equation of the streamlines can be obtained by setting Eq. (3.72) equal to a constant:

$$\boxed{\psi = \frac{\Lambda}{2\pi} \theta = \text{const}} \quad (3.73)$$

From Eq. (3.73), we see that  $\theta = \text{constant}$ , which, in polar coordinates, is the equation of a straight line from the origin. Hence, Eq. (3.73) is consistent with the picture of the source flow sketched in Fig. 3.13. Moreover, Eq. (3.67) gives an equipotential line as  $r = \text{constant}$ , i.e., a circle with its center at the origin, as shown by the dashed line in Fig. 3.13. Once again, we see that streamlines and equipotential lines are mutually perpendicular.

To evaluate the circulation for source flow, recall that  $\nabla \times \mathbf{V} = 0$  everywhere. In turn, from Eq. (2.128)

$$\Gamma = - \iint_C (\nabla \times \mathbf{V}) \cdot d\mathbf{S} = 0$$

for any closed curve  $C$  chosen in the flow field. Hence, as in the case of uniform flow discussed in Sec. 3.9, there is no circulation associated with the source flow.

It is straightforward to show that Eqs. (3.67) and (3.72) satisfy Laplace's equation, simply by substitution into  $\nabla^2 \phi = 0$  and  $\nabla^2 \psi = 0$  written in terms of cylindrical coordinates [see Eq. (3.42)]. Therefore, source flow is a viable elementary flow for use in building more complex flows.

Consider a polar coordinate system with a source of strength  $\Lambda$  located at the origin. Superimpose on this flow a uniform stream with velocity  $V_\infty$  moving from left to right, as sketched in Fig. 3.15. The stream function for the resulting flow is the sum of Eqs. (3.57) and (3.72):

$$\psi = V_\infty r \sin \theta + \frac{\Lambda}{2\pi} \theta \quad (3.74)$$

Since both Eqs. (3.57) and (3.72) are solutions of Laplace's equation, we know that Eq. (3.74) also satisfies Laplace's equation, i.e., Eq. (3.74) describes a viable irrotational, incompressible flow. The streamlines of the combined flow are obtained from Eq. (3.74) as

$$\psi = V_\infty r \sin \theta + \frac{\Lambda}{2\pi} \theta = \text{const} \quad (3.75)$$

The resulting streamline shapes from Eq. (3.75) are sketched at the right of Fig. 3.15. The source is located at point  $D$ . The velocity field is obtained by differentiating Eq. (3.75),

$$V_r = \frac{1}{r} \frac{\partial \psi}{\partial \theta} = V_\infty \cos \theta + \frac{\Lambda}{2\pi} \quad (3.76)$$

$$V_\theta = - \frac{\partial \psi}{\partial r} = - V_\infty \sin \theta \quad (3.77)$$

and

Note from Sec. 3.10 that the radial velocity from a source is  $\Lambda/2\pi r$ , and from Sec. 3.9 the component of the freestream velocity in the radial direction is  $V_\infty \cos \theta$ . Hence, Eq. (3.76) is simply the direct sum of the two velocity fields—a result which is consistent with the linear nature of Laplace's equation. Therefore, not only can we add the values of  $\phi$  or  $\psi$  to obtain more complex solutions, we can add their derivatives, i.e., the velocities, as well.

The stagnation points in the flow can be obtained by setting Eqs. (3.76) and (3.77) equal to zero.

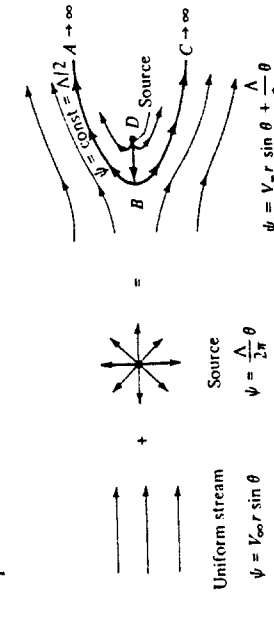


Figure 3.15 Superposition of a uniform flow and a source: flow over a semi-infinite body.

$$V_x \cos \theta + \frac{\Lambda}{2\pi r} = 0 \quad (3.78)$$

$$V_x \sin \theta = 0 \quad (3.79)$$

Solving for  $r$  and  $\theta$ , we find that one stagnation point exists, located at  $(r, \theta) = (\Lambda/2\pi V_\infty, \pi)$ , which is labeled as point  $B$  in Fig. 3.15. That is, the stagnation point is a distance  $(\Lambda/2\pi V_\infty)$  directly upstream of the source. From this result, the distance  $DB$  clearly grows smaller if  $V_\infty$  is increased and larger if  $\Lambda$  is increased—trends that also make sense based on intuition. For example, looking at Fig. 3.15, you would expect that as the source strength is increased, keeping  $V_\infty$  the same, the stagnation point  $B$  will be blown further upstream. Conversely, if  $V_\infty$  is increased, keeping the source strength the same, the stagnation point will be blown further downstream.

If the coordinates of the stagnation point at  $B$  are substituted into Eq. (3.75), we obtain

$$\psi = V_\infty \frac{\Lambda}{2\pi V_\infty} \sin \pi + \frac{\Lambda}{2\pi} \pi = \text{const}$$

$$\psi = \frac{\Lambda}{2} = \text{const}$$

Hence, the streamline that goes through the stagnation point is described by  $\psi = \Lambda/2$ . This streamline is shown as curve  $ABC$  in Fig. 3.15.

Examining Fig. 3.15, we now come to an important conclusion. Since we are dealing with inviscid flow, where the velocity at the surface of a solid body is tangent to the body, then any streamline of the combined flow at the right of Fig. 3.15 could be replaced by a solid surface of the same shape. In particular, consider the streamline  $ABC$ . Because it contains the stagnation point at  $B$ , the streamline  $ABC$  is a *dividing streamline*, i.e., it separates the fluid coming from the freestream and the fluid emanating from the source. All the fluid outside  $ABC$  is from the freestream, and all the fluid inside  $ABC$  is from the source. Therefore, as far as the freestream is concerned, the entire region inside  $ABC$  could be replaced with a solid body of the same shape, and the external flow, i.e., the flow from the freestream, would not feel the difference. The streamline  $\psi = \Lambda/2$  extends downstream to infinity, forming a semi-infinite body. Therefore, we are led to the following important interpretation. If we want to construct the flow over a solid semi-infinite body described by the curve  $ABC$  as shown in Fig. 3.15, then all we need to do is take a uniform stream with velocity  $V_\infty$  and add to it a source of strength  $\Lambda$  at point  $D$ . The resulting superposition will then represent the flow over the prescribed solid semi-infinite body of shape  $ABC$ . This illustrates the practicality of adding elementary flows to obtain a more complex flow over a body of interest.

The superposition illustrated in Fig. 3.15 results in the flow over the semi-infinite body  $ABC$ . This is a half-body that stretches to infinity in the downstream direction; i.e., the body is not closed. However, if we take a sink of equal strength as the source and add it to the flow downstream of point  $D$ , then the resulting body shape will be closed. Let us examine this flow in more detail.

Consider a polar coordinate system with a source and sink placed a distance  $b$  to the left and right of the origin, respectively, as sketched in Fig. 3.16. The strengths of the source and sink are  $\Lambda$  and  $-\Lambda$ , respectively (equal and opposite). In addition, superimpose a uniform stream with velocity  $V_\infty$ , as shown in Fig. 3.16. The stream function for the combined flow at any point  $P$  with coordinates  $(r, \theta)$  is obtained from Eqs. (3.57) and (3.72):

$$\psi = V_\infty r \sin \theta + \frac{\Lambda}{2\pi} \theta_1 - \frac{\Lambda}{2\pi} \theta_2 \quad (3.80)$$

$$\text{or} \quad \psi = V_\infty r \sin \theta + \frac{\Lambda}{2\pi} (\theta_1 - \theta_2) \quad (3.80)$$

The velocity field is obtained by differentiating Eq. (3.80) according to Eq. (2.142a and b). Note from the geometry of Fig. 3.16 that  $\theta_1$  and  $\theta_2$  in Eq. (3.80) are functions of  $r$ ,  $\theta$ , and  $b$ . In turn, by setting  $V = 0$ , two stagnation points are found, namely, points  $A$  and  $B$  in Fig. 3.16. These stagnation points are located such that (see Prob. 3.13)

$$OA = OB = \sqrt{b^2 + \frac{\Lambda b}{\pi V_\infty}} \quad (3.81)$$

The equation of the streamlines is given by Eq. (3.80) as

$$\psi = V_\infty r \sin \theta + \frac{\Lambda}{2\pi} (\theta_1 - \theta_2) = \text{const} \quad (3.82)$$

The equation of the specific streamline going through the stagnation points is obtained from Eq. (3.82) by noting that  $\theta = \theta_1 = \theta_2 = \theta_1 = \theta_2 = 0$  at point  $A$  and  $\theta = \theta_1 = \theta_2 = \pi$  at point  $B$ . Hence, for the stagnation streamline, Eq. (3.82) yields a value of zero for the constant. Thus, the stagnation streamline is given by  $\psi = 0$ , i.e.,

$$V_\infty r \sin \theta + \frac{\Lambda}{2\pi} (\theta_1 - \theta_2) = 0 \quad (3.83)$$

the equation of an oval, as sketched in Fig. 3.16. Equation (3.83) is also the dividing streamline; all the flow from the source is consumed by the sink and is contained entirely inside the oval, whereas the flow outside the oval has originated with the uniform stream only. Therefore, in Fig. 3.16 the region inside the oval can be replaced by a solid body with the shape given by  $\psi = 0$ , and the region outside the oval can be interpreted as the inviscid, potential (irrotational), incompressible flow over the solid body. This problem was first solved in the nineteenth century by the famous Scottish engineer W. J. M. Rankine; hence, the shape given by Eq. (3.83) and sketched in Fig. 3.16 is called a *Rankine oval*.

### 3.12 DOUBLET FLOW: OUR THIRD ELEMENTARY FLOW

There is a special, degenerate case of a source-sink pair that leads to a singularity called a doublet. The doublet is frequently used in the theory of incompressible flow; the purpose of this section is to describe its properties.

Consider a source of strength  $\Lambda$  and a sink of equal (but opposite) strength  $-\Lambda$  separated by a distance  $l$ , as shown in Fig. 3.17a. At any point  $P$  in the flow, the stream function is

$$\psi = \frac{\Lambda}{2\pi} (\theta_1 - \theta_2) = -\frac{\Lambda}{2\pi} \Delta\theta \quad (3.84)$$

where  $\Delta\theta = \theta_2 - \theta_1$  as seen from Fig. 3.17a. Equation (3.84) is the stream function for a source-sink pair separated by the distance  $l$ .

Now, in Fig. 3.17a let the distance  $l$  approach zero while the absolute magnitude of the strengths of the source and sink increase in such a fashion that the product  $l/\Lambda$  remains constant. This limiting process is shown in Fig. 3.17b. In the limit, as  $l \rightarrow 0$  while  $l/\Lambda$  remains constant, we obtain a special flow pattern defined as a *doublet*. The strength of the doublet is denoted by  $\kappa$  and is defined as  $\kappa \equiv l/\Lambda$ . The stream function for a doublet is obtained from Eq. (3.84) as follows:

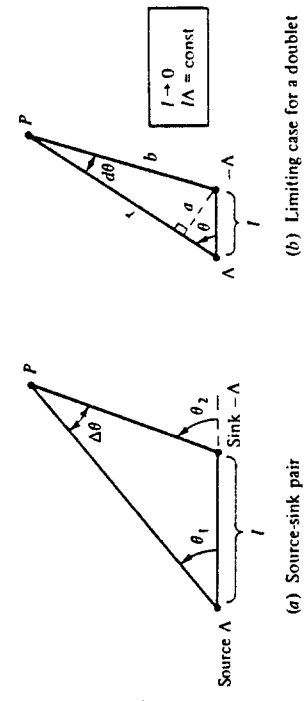


Figure 3.17 How a source-sink pair approaches a doublet in the limiting case.

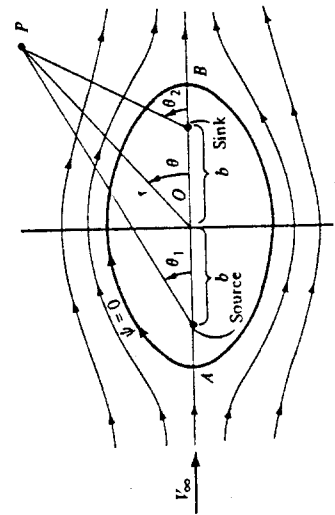


Figure 3.16 Superposition of a uniform flow and a source-sink pair; flow over a Rankine oval.

$$\psi = \lim_{\substack{l \rightarrow 0 \\ \kappa = \Lambda = \text{const}}} \left( -\frac{\Lambda}{2\pi} d\theta \right) \quad (3.85)$$

where in the limit  $\Delta\theta \rightarrow d\theta \rightarrow 0$ . (Note that the source strength  $\Lambda$  approaches an infinite value in the limit.) In Fig. 3.17b, let  $r$  and  $b$  denote the distances to point  $P$  from the source and sink, respectively. Draw a line from the sink perpendicular to  $r$ , and denote the length along this line by  $a$ . For an infinitesimal  $d\theta$ , the geometry of Fig. 3.17b yields

$$a = l \sin \theta$$

$$b = r - l \cos \theta$$

$$d\theta = \frac{a}{b} = \frac{l \sin \theta}{r - l \cos \theta} \quad (3.86)$$

Hence,

$$d\theta = \frac{a}{b} = \frac{l \sin \theta}{r - l \cos \theta}$$

Substituting Eq. (3.86) into (3.85), we have

$$\psi = \lim_{\substack{l \rightarrow 0 \\ \kappa = \text{const}}} \left( -\frac{\Lambda}{2\pi} \frac{l \sin \theta}{r - l \cos \theta} \right)$$

$$\psi = \lim_{\substack{l \rightarrow 0 \\ \kappa = \text{const}}} \left( -\frac{\kappa}{2\pi} \frac{\sin \theta}{r - l \cos \theta} \right)$$

$$\boxed{\psi = -\frac{\kappa \sin \theta}{2\pi r}} \quad (3.87)$$

or

$$\boxed{\phi = \frac{\kappa \cos \theta}{2\pi r}} \quad (3.88)$$

Equation (3.87) is the stream function for a doublet. In a similar fashion, the velocity potential for a doublet is given by (see Prob. 3.14)

$$\boxed{\phi = -\frac{\kappa \sin \theta}{2\pi r}} \quad (3.89)$$

or

The streamlines of a doublet flow are obtained from Eq. (3.87):

$$\begin{aligned} \psi &= -\frac{\kappa \sin \theta}{2\pi r} = \text{const} = c \\ r &= -\frac{\kappa}{2\pi} \sin \theta \end{aligned} \quad (3.90)$$

Equation (3.89) gives the equation for the streamlines in doublet flow. Recall from analytic geometry that the following equation in polar coordinates

$$r = d \sin \theta$$

is a circle with a diameter  $d$  on the vertical axis and with the center located  $d/2$  directly above the origin. Comparing Eqs. (3.89) and (3.90), we see that the streamlines for a doublet are a family of circles with diameter  $\kappa/2\pi$ , as sketched in Fig. 3.18. The different circles correspond to different values of the parameter  $c$ . Note that in Fig. 3.17 we placed the source to the left of the sink; hence, in Fig. 3.18 the direction of flow is out of the origin to the left and back into the origin from the right. In Fig. 3.17, we could just as well have placed the sink to the left of the source. In such a case, the signs in Eqs. (3.87) and (3.88) would be reversed, and the flow in Fig. 3.18 would be in the opposite direction. Therefore, a doublet has associated with it a sense of direction — the direction with which the flow moves around the circular streamlines. By convention, we designate the direction of the doublet by an arrow drawn from the sink to the source, as shown in Fig. 3.18. In Fig. 3.18, the arrow points to the left, which is consistent with the form of Eqs. (3.87) and (3.88). If the arrow would point to the right, the sense of rotation would be reversed, Eq. (3.87) would have a positive sign, and Eq. (3.88) would have a negative sign.

Returning to Fig. 3.17, note that in the limit as  $l \rightarrow 0$ , the source and sink fall on top of each other. However, they do not extinguish each other, because the absolute magnitude of their strengths becomes infinitely large in the limit, and we have a singularity of strength ( $\infty - \infty$ ); this is an indeterminate form which can have a finite value.

As in the case of a source or sink, it is useful to interpret the doublet flow shown in Fig. 3.18 as being *induced* by a discrete doublet of strength  $\kappa$  placed at the origin. Therefore, a doublet is a singularity that induces about it the double-lobe circular flow pattern shown in Fig. 3.18.

### 3.13 NONLIFTING FLOW OVER A CIRCULAR CYLINDER

Consulting our road map given in Fig. 3.4, we see that we are well into the third column, having already discussed uniform flow, sources and sinks, and doublets.

Along the way, we have seen how the flow over a semi-infinite body can be simulated by the combination of a uniform flow with a source, and the flow over an oval-shaped body can be constructed by superimposing a uniform flow and a source-sink pair. In

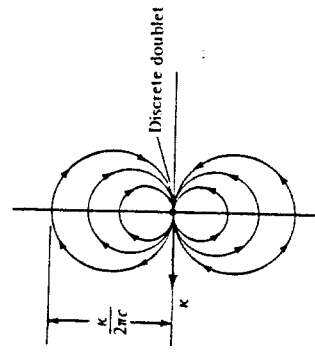


Figure 3.18 Doublet flow with strength  $\kappa$ .

this section, we demonstrate that the combination of a uniform flow and a doublet produces the flow over a circular cylinder. A circular cylinder is one of the most basic geometric shapes available, and the study of the flow around such a cylinder is a classic problem in aerodynamics.

Consider the addition of a uniform flow with velocity  $V_\infty$  and a doublet of strength  $\kappa$ , as shown in Fig. 3.19. The direction of the doublet is upstream, facing into the uniform flow. From Eqs. (3.57) and (3.87), the stream function for the combined flow is

$$\psi = V_\infty r \sin \theta - \frac{\kappa}{2\pi} \frac{\sin \theta}{r} \quad (3.91)$$

$$\text{or } \psi = V_\infty r \sin \theta \left( 1 - \frac{\kappa}{2\pi V_\infty r^2} \right) \quad (3.92)$$

Let  $R^2 \equiv \kappa/2\pi V_\infty$ . Then Eq. (3.91) can be written as

$$\boxed{\psi = (V_\infty r \sin \theta) \left( 1 - \frac{R^2}{r^2} \right)} \quad (3.92)$$

Equation (3.92) is the stream function for a uniform flow–doublet combination; it is also the stream function for the flow over a circular cylinder of radius  $R$  as shown in Fig. 3.19 and as demonstrated below.

The velocity field is obtained by differentiating Eq. (3.92), as follows:

$$V_r = \frac{1}{r} \frac{\partial \psi}{\partial \theta} = \frac{1}{r} (V_\infty r \cos \theta) \left( 1 - \frac{R^2}{r^2} \right) \quad (3.93)$$

$$V_r = \left( 1 - \frac{R^2}{r^2} \right) V_\infty \cos \theta \quad (3.94)$$

$$V_\theta = -\frac{\partial \psi}{\partial r} = -[(V_\infty r \sin \theta) \frac{2R^2}{r^3} + \left( 1 - \frac{R^2}{r^2} \right) (V_\infty \sin \theta)] \quad (3.95)$$

$$V_\theta = -\left( 1 + \frac{R^2}{r^2} \right) V_\infty \sin \theta \quad (3.96)$$

To locate the stagnation points, set Eqs. (3.93) and (3.94) equal to zero.

$$\left( 1 - \frac{R^2}{r^2} \right) V_\infty \cos \theta = 0 \quad (3.95)$$

$$\left( 1 + \frac{R^2}{r^2} \right) V_\infty \sin \theta = 0 \quad (3.96)$$

Simultaneously solving Eqs. (3.95) and (3.96) for  $r$  and  $\theta$ , we find that there are two stagnation points, located at  $(r, \theta) = (R, 0)$  and  $(R, \pi)$ . These points are denoted as  $A$  and  $B$ , respectively, in Fig. 3.19.

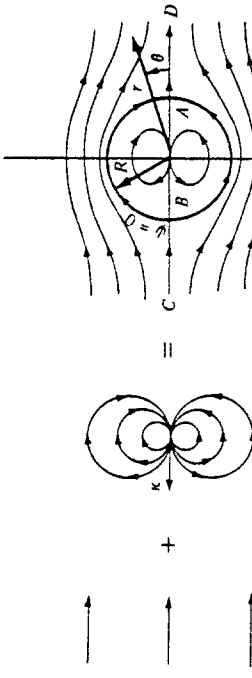


Figure 3.19 Superposition of a uniform flow and a doublet; nonlifting flow over a circular cylinder.

The equation of the streamline that passes through the stagnation point  $B$  is obtained by inserting the coordinates of  $B$  into Eq. (3.92). For  $r = R$  and  $\theta = \pi$ , Eq. (3.92) yields  $\psi = 0$ . Similarly, inserting the coordinates of point  $A$  into Eq. (3.92), we also find that  $\psi = 0$ . Hence, the same streamline goes through both stagnation points. Moreover, the equation of this streamline, from Eq. (3.92), is

$$\psi = (V_\infty r \sin \theta) \left( 1 - \frac{R^2}{r^2} \right) = 0 \quad (3.97)$$

Note that Eq. (3.97) is satisfied by  $r = R$  for all values of  $\theta$ . However, recall that  $R^2 \equiv \kappa / 2\pi V_\infty$ , which is a constant. Moreover, in polar coordinates,  $r = \text{constant} = R$  is the equation of a circle of radius  $R$  with its center at the origin. Therefore, Eq. (3.97) describes a circle with radius  $R$ , as shown in Fig. 3.19. Moreover, Eq. (3.97) is satisfied by  $\theta = \pi$  and  $\theta = 0$  for all values of  $r$ ; hence, the entire horizontal axis through points  $A$  and  $B$ , extending infinitely far upstream and downstream, is part of the stagnation streamline.

Note that the  $\psi = 0$  streamline, since it goes through the stagnation points, is the dividing streamline. That is, all the flow inside  $\psi = 0$  (inside the circle) comes from the doublet, and all the flow outside  $\psi = 0$  (outside the circle) comes from the uniform flow. Therefore, we can replace the flow inside the circle by a solid body, and the external flow will not know the difference. Consequently, *the inviscid irrotational, incompressible flow over a circular cylinder of radius R can be synthesized by adding a uniform flow with velocity V\_\infty and a doublet of strength \kappa, where R is related to V\_\infty and \kappa through*

$$R = \sqrt{\frac{\kappa}{2\pi V_\infty}} \quad (3.98)$$

Note from Eqs. (3.92) to (3.94) that the entire flow field is symmetrical about both the horizontal and vertical axes through the center of the cylinder, as clearly seen by

the streamline pattern sketched in Fig. 3.19. Hence, the pressure distribution is also symmetrical about both axes. As a result, the pressure distribution over the top of the cylinder is exactly balanced by the pressure distribution over the bottom of the cylinder, i.e., there is no net lift. Similarly, the pressure distribution over the front of the cylinder, i.e., over the back of the cylinder, is exactly balanced by the pressure distribution over the back of the cylinder, i.e., there is no net drag. In real life, the result of zero lift is easy to accept, but the result of zero drag makes no sense. We know that any aerodynamic body immersed in a real flow will experience a drag. This paradox between the theoretical result of zero drag, and the knowledge that in real life the drag is finite, was encountered in the year 1744 and has been known as d'Alembert's paradox ever since. For d'Alembert and other fluid dynamic researchers during the eighteenth and nineteenth centuries, this paradox was unexplained and perplexing. Of course, today we know that the drag is due to viscous effects which generate frictional shear stress at the body surface and which cause the flow to separate from the surface on the back of the body, thus creating a large wake downstream of the body and destroying the symmetry of the flow about the vertical axis through the cylinder. These viscous effects are discussed in detail in Chaps. 15 and 16. However, such viscous effects are not included in our present analysis of the inviscid flow over the cylinder. As a result, the inviscid theory predicts that the flow closes smoothly and completely behind the body, as sketched in Fig. 3.19. It predicts no wake, and no asymmetries, resulting in the theoretical result of zero drag.

Let us quantify the above discussion. The velocity distribution on the surface of the cylinder is given by Eqs. (3.93) and (3.94) with  $r = R$ , resulting in

$$V_r = 0 \quad (3.99)$$

$$V_\theta = -2V_\infty \sin \theta \quad (3.100)$$

Note that at the surface of the cylinder,  $V_r$  is geometrically normal to the surface; hence, Eq. (3.99) is consistent with the physical boundary condition that the component of velocity normal to a stationary solid surface must be zero. Equation (3.100) gives the tangential velocity, which is the full magnitude of velocity on the surface of the cylinder, i.e.,  $V = V_\theta = -2V_\infty \sin \theta$  on the surface. The minus sign in Eq. (3.100) is consistent with the sign convention in polar coordinates that  $V_\theta$  is positive in the direction of increasing  $\theta$ , i.e., in the counterclockwise direction as shown in Fig. 3.20. However, in Fig. 3.19, the surface velocity for  $0 \leq \theta \leq \pi$  is obviously in the opposite direction of increasing  $\theta$ ; hence, the minus sign in Eq. (3.100) is proper. For  $\pi \leq \theta \leq 2\pi$ , the surface flow is in the same direction as increasing  $\theta$ , but  $\sin \theta$  is itself negative; hence, once again the minus sign in Eq. (3.100) is proper. Note from Eq. (3.100) that the velocity at the surface reaches a maximum value of  $2V_\infty$  at the top

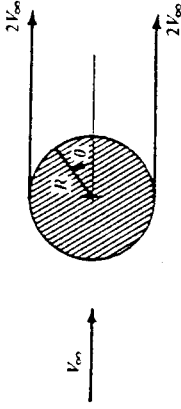


Figure 3.19 Maximum velocity in the flow over a circular cylinder.

and the bottom of the cylinder (where  $\theta = \pi/2$  and  $3\pi/2$ , respectively), as shown in Fig. 3.21. Indeed, these are the points of maximum velocity for the entire flow field around the cylinder, as can be seen from Eqs. (3.93) and (3.94).

The pressure coefficient is given by Eq. (3.38):

$$C_p = 1 - \left( \frac{V}{V_\infty} \right)^2 \quad (3.38)$$

Combining Eqs. (3.100) and (3.38), the surface pressure coefficient over a circular cylinder is

$$C_p = 1 - 4 \sin^2 \theta \quad (3.101)$$

Note that  $C_p$  varies from 1.0 at the stagnation points to  $-3.0$  at the points of maximum velocity. The pressure coefficient distribution over the surface is sketched in Fig. 3.22. The regions corresponding to the top and bottom halves of the cylinder are identified at the top of Fig. 3.22. Clearly the pressure distribution over the top half of the cylinder is equal to the pressure distribution over the bottom half, and hence, the lift must be zero, as discussed earlier. Moreover, the regions corresponding to the front and rear halves of the cylinder are identified at the bottom of Fig. 3.22. Clearly, the pressure distributions over the front and rear halves are the same, and hence, the drag is

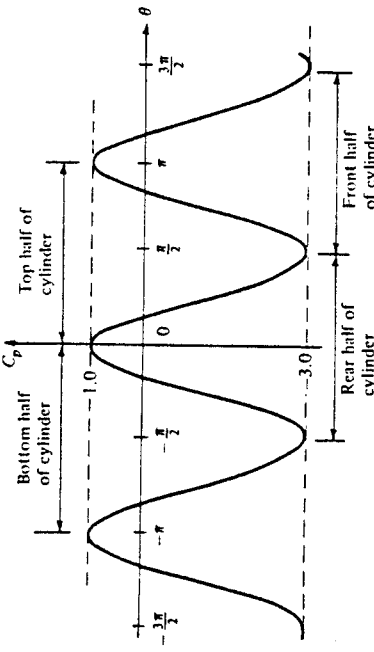


Figure 3.22 Pressure coefficient distribution over the surface of a circular cylinder; theoretical results for inviscid, incompressible flow.

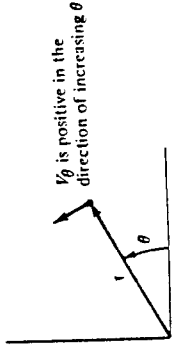


Figure 3.20 Sign convention for  $V_\theta$  in polar coordinates.

theoretically zero, as also discussed previously. These results are confirmed by Eqs. (1.15) and (1.16). Since  $c_f = 0$  (we are dealing with an inviscid flow), Eqs. (1.15) and (1.16) become, respectively,

$$c_n = \frac{1}{c} \int_0^c (C_{p,l} - C_{p,u}) dx \quad (3.102)$$

$$c_a = \frac{1}{c} \int_{1,E}^{r,E} (C_{p,u} - C_{p,l}) dy \quad (3.103)$$

For the circular cylinder, the chord  $c$  is the horizontal diameter. From Fig. 3.22,  $C_{p,l} = C_{p,u}$  for corresponding stations measured along the chord, and hence, the integrands in Eqs. (3.102) and (3.103) are identically zero, yielding  $c_n = c_a = 0$ . In turn, the lift and drag are zero, thus again confirming our previous conclusions.

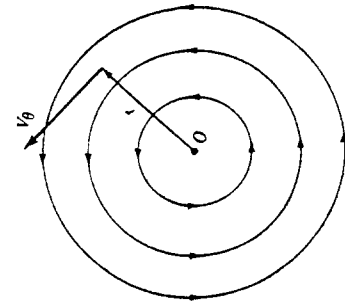
### 3.14 VORTEX FLOW: OUR FOURTH ELEMENTARY FLOW

Again, consulting our chapter road map in Fig. 3.4, we have discussed three elementary flows — uniform flow, source flow, and doublet flow — and have superimposed these elementary flows to obtain the nonlifting flow over several body shapes, such as ovals and circular cylinders. In this section, we introduce our fourth, and last, elementary flow: vortex flow. In turn, in Secs. 3.15 and 3.16, we see how the superposition of flows involving such vortices leads to cases with finite lift.

Consider a flow where all the streamlines are concentric circles about a given point, as sketched in Fig. 3.23. Moreover, let the velocity along any given circular streamline be constant, but let it vary from one streamline to another inversely with distance from the common center. Such a flow is called a *vortex flow*. Examine Fig. 3.23; the velocity components in the radial and tangential directions are  $V_r$  and  $V_\theta$ , respectively, where  $V_r = 0$  and  $V_\theta = \text{constant}/r$ . It is easily shown (try it yourself) that (1) vortex flow is a physically possible incompressible flow, i.e.,  $\nabla \cdot \mathbf{V} = 0$  at every point, and (2) vortex flow is irrotational, i.e.,  $\nabla \times \mathbf{V} = 0$ , at every point except the origin.

From the definition of vortex flow, we have

$$V_\theta = \frac{\text{const}}{r} = \frac{C}{r} \quad (3.104)$$



To evaluate the constant  $C$ , take the circulation around a given circular streamline of radius  $r$ .

$$\Gamma = - \oint_C \mathbf{V} \cdot d\mathbf{s} = -V_\theta(2\pi r) \quad (3.105)$$

$$V_\theta = -\frac{\Gamma}{2\pi r} \quad (3.106)$$

Comparing Eqs. (3.104) and (3.105), we see that

$$C = -\frac{\Gamma}{2\pi} \quad (3.107)$$

Therefore, for vortex flow, Eq. (3.106) demonstrates that the circulation taken about all streamlines is the same value, namely,  $\Gamma = -2\pi C$ . By convention,  $\Gamma$  is called the *strength* of the vortex flow, and Eq. (3.105) gives the velocity field for a vortex flow of strength  $\Gamma$ . Note from Eq. (3.105) that  $V_\theta$  is negative when  $\Gamma$  is positive, i.e., a vortex of positive strength rotates in the *clockwise* direction. (This is a consequence of our sign convention on circulation defined in Sec. 2.13, namely, that positive circulation is clockwise.)

We stated earlier that vortex flow is irrotational except at the origin. What happens at  $r = 0$ ? What is the value of  $\nabla \times \mathbf{V}$  at  $r = 0$ ? To answer these questions, recall Eq. (2.128) relating circulation to vorticity

$$\Gamma = - \iint_S (\nabla \times \mathbf{V}) \cdot d\mathbf{s} \quad (2.128)$$

Combining Eqs. (3.106) and (2.128),

$$2\pi C = \iint_S (\nabla \times \mathbf{V}) \cdot d\mathbf{s} \quad (3.107)$$

Since we are dealing with two-dimensional flow, the flow sketched in Fig. 3.23 takes place in the plane of the paper. Hence, in Eq. (3.107), both  $\nabla \times \mathbf{V}$  and  $d\mathbf{s}$  are in the same direction, both perpendicular to the plane of the flow. Thus, Eq. (3.107) can be written as

$$2\pi C = \iint_S (\nabla \times \mathbf{V}) \cdot d\mathbf{s} = \iint_S |\nabla \times \mathbf{V}| dS \quad (3.108)$$

In Eq. (3.108), the surface integral is taken over the circular area inside the streamline along which the circulation  $\Gamma = -2\pi C$  is evaluated. However,  $\Gamma$  is the same for all the circular streamlines. In particular, choose a circle as close to the origin as we wish; i.e., let  $r \rightarrow 0$ . The circulation will still remain  $\Gamma = -2\pi C$ . However, the area inside this small circle around the origin will become infinitesimally small, and

$$\iint_S |\nabla \times \mathbf{V}| dS \rightarrow |\nabla \times \mathbf{V}| dS \quad (3.109)$$

Figure 3.23 Vortex flow.

Combining Eqs. (3.108) and (3.109), in the limit as  $r \rightarrow 0$ , we have

$$2\pi C = |\nabla \times \mathbf{V}| dS$$

$$\text{or} \quad |\nabla \times \mathbf{V}| = \frac{2\pi C}{dS} \quad (3.110)$$

However, as  $r \rightarrow 0$ ,  $dS \rightarrow 0$ . Therefore, in the limit as  $r \rightarrow 0$ , from Eq. (3.110), we have

$$|\nabla \times \mathbf{V}| \rightarrow \infty$$

**Conclusion:** Vortex flow is irrotational everywhere except at the point  $r = 0$ , where the vorticity is infinite. Therefore, the origin,  $r = 0$ , is a singular point in the flow field. We see that, along with sources, sinks, and doublets, the vortex flow contains a singularity. Hence, we can interpret the singularity itself, i.e., point  $O$  in Fig. 3.23, to be a point vortex which induces about it the circular vortex flow shown in Fig. 3.23. The velocity potential for vortex flow can be obtained as follows:

$$\frac{\partial \phi}{\partial r} = V_r = 0 \quad (3.111a)$$

$$\frac{1}{r} \frac{\partial \phi}{\partial \theta} = V_\theta = -\frac{\Gamma}{2\pi r} \quad (3.111b)$$

Integrating Eqs. (3.111a and b), we find

$$\boxed{\phi = -\frac{\Gamma}{2\pi} \theta} \quad (3.112)$$

Equation (3.112) is the velocity potential for vortex flow.

The stream function is determined in a similar manner.

$$\frac{1}{r} \frac{\partial \psi}{\partial \theta} = V_r = 0 \quad (3.113a)$$

$$-\frac{\partial \psi}{\partial r} = V_\theta = -\frac{\Gamma}{2\pi r} \quad (3.113b)$$

Integrating Eqs. (3.113a and b), we have

$$\boxed{\psi = \frac{\Gamma}{2\pi} \ln r} \quad (3.114)$$

Equation (3.114) is the stream function for vortex flow. Note that since  $\psi = \text{constant}$  is the equation of a streamline, Eq. (3.114) states that the streamlines of vortex flow are given by  $r = \text{constant}$ ; i.e., the streamlines are circles. Thus, Eq. (3.114) is consistent with our definition of vortex flow. Also note from Eq. (3.112) that equipotential

lines are given by  $\theta = \text{constant}$ , i.e., straight radial lines from the origin. Once again we see that equipotential lines and streamlines are mutually perpendicular.

At this stage, we summarize the pertinent results for our four elementary flows in Table 3.1.

### 3.15 LIFTING FLOW OVER A CYLINDER

In Sec. 3.13, we superimposed a uniform flow and a doublet to synthesize the flow over a circular cylinder, as shown in Fig. 3.19. In addition, we proved that both the lift and drag were zero for such a flow. However, the streamline pattern shown at the right of Fig. 3.19 is not the only flow that is theoretically possible around a circular cylinder. It is the only flow that is consistent with zero lift. However, there are other possible flow patterns around a circular cylinder — different flow patterns which result in a nonzero lift on the cylinder. Such lifting flows are discussed in this section.

Now you might be hesitant at this moment, perplexed by the question as to how a lift could possibly be exerted on a circular cylinder. Is not the body perfectly symmetric, and would not this geometry always result in a symmetric flow field with a consequent zero lift, as we have already discussed? You might be so perplexed that you run down to the laboratory, place a stationary cylinder in a low-speed tunnel, and measure the lift. To your satisfaction, you measure no lift, and you walk away muttering that the subject of this section is ridiculous — there is no lift on the cylinder. However, go back to the wind tunnel, and this time run a test with the cylinder spinning about its axis at relatively high revolutions per minute. This time you measure a finite lift. Also, by this time you might be thinking about other situations: spin on a baseball causes it to curve, and spin on a golf ball causes it to hook or slice. Clearly, in real life there are nonsymmetric aerodynamic forces acting on these symmetric, spinning bodies. So maybe the subject matter of this section is not so ridiculous after all. Indeed, as you will soon appreciate, the concept of lifting flow over a cylinder will start us on

Table 3.1

Type of flow	Velocity	$\phi$	$\psi$
Uniform flow in $x$ direction	$u = V_\infty$	$V_{\infty x}$	$V_{\infty y}$
Source	$V_r = \frac{\Lambda}{2\pi r}$	$\frac{\Lambda}{2\pi} \ln r$	$\frac{\Lambda}{2\pi} \theta$
Vortex	$V_\theta = -\frac{\Gamma}{2\pi r}$	$-\frac{\Gamma}{2\pi} \theta$	$\frac{\Gamma}{2\pi} \ln r$
Doublet	$V_r = \frac{\kappa}{2\pi} \frac{\cos \theta}{r^2}$	$\frac{\kappa}{2\pi} \cos \theta$	$-\frac{\kappa}{2\pi} \frac{\sin \theta}{r}$
	$V_\theta = -\frac{\kappa}{2\pi} \frac{\sin \theta}{r^2}$		

a journey which leads directly to the theory of the lift generated by airfoils, as discussed in Chap. 4.

Consider the flow synthesized by the addition of the nonlifting flow over a cylinder and a vortex of strength  $\Gamma$ , as shown in Fig. 3.24. The stream function for nonlifting flow over a circular cylinder of radius  $R$  is given by Eq. (3.92):

$$\psi_1 = (V_\infty r \sin \theta) \left( 1 - \frac{R^2}{r^2} \right) \quad (3.92)$$

The stream function for a vortex of strength  $\Gamma$  is given by Eq. (3.114). Recall that the stream function is determined within an arbitrary constant; hence, Eq. (3.114) can be written as

$$\psi_2 = \frac{\Gamma}{2\pi} \ln r + \text{const} \quad (3.115)$$

Since the value of the constant is arbitrary, let

$$\text{Const} = -\frac{\Gamma}{2\pi} \ln R \quad (3.116)$$

Combining Eqs. (3.115) and (3.116), we obtain

$$\psi = \frac{\Gamma}{2\pi} \ln \frac{r}{R} \quad (3.117)$$

Equation (3.117) is the stream function for a vortex of strength  $\Gamma$  and is just as valid as Eq. (3.114) obtained earlier; the only difference between these two equations is a constant of the value given by Eq. (3.116).

The resulting stream function for the flow shown at the right of Fig. 3.24 is

$$\psi = \psi_1 + \psi_2$$

$$\boxed{\psi = (V_\infty r \sin \theta) \left( 1 - \frac{R^2}{r^2} \right) + \frac{\Gamma}{2\pi} \ln \frac{r}{R}} \quad (3.118)$$

From Eq. (3.118), if  $r = R$ , then  $\psi = 0$  for all values of  $\theta$ . Since  $\psi = \text{constant}$  is the equation of a streamline,  $r = R$  is therefore a streamline of the flow, but  $r = R$  is the equation of a circle of radius  $R$ . Hence, Eq. (3.118) is a valid stream function for the inviscid, incompressible flow over a circular cylinder of radius  $R$ , as shown at the right of Fig. 3.24. Indeed, our previous result given by Eq. (3.92) is simply a special case of Eq. (3.118) with  $\Gamma = 0$ .

The resulting streamline pattern given by Eq. (3.118) is sketched at the right of Fig. 3.24. Note that the streamlines are no longer symmetrical about the horizontal axis through point  $O$ , and you might suspect (correctly) that the cylinder will experience a resulting finite normal force. However, the streamlines are symmetrical about the vertical axis through  $O$ , and as a result the drag will be zero, as we prove shortly. Note also that, because a vortex of strength  $\Gamma$  has been added to the flow, the circulation about the cylinder is now finite and equal to  $\Gamma$ .

The velocity field can be obtained by differentiating Eq. (3.118). An equally direct method of obtaining the velocities is to add the velocity field of a vortex to the velocity field of the nonlifting cylinder. (Recall that because of the linearity of the flow, the velocity components of the superimposed elementary flows add directly.) Hence, from Eqs. (3.93) and (3.94) for nonlifting flow over a cylinder of radius  $R$ , and Eq. (3.11a and b) for vortex flow, we have, for the lifting flow over a cylinder of radius  $R$ ,

$$V_r = \left( 1 - \frac{R^2}{r^2} \right) V_\infty \cos \theta \quad (3.119)$$

$$V_\theta = -\left( 1 + \frac{R^2}{r^2} \right) V_\infty \sin \theta - \frac{\Gamma}{2\pi r} \quad (3.120)$$

To locate the stagnation points in the flow, set  $V_r = V_\theta = 0$  in Eqs. (3.119) and (3.120), and solve for the resulting coordinates  $(r, \theta)$ .

$$V_r = \left( 1 - \frac{R^2}{r^2} \right) V_\infty \cos \theta = 0 \quad (3.121)$$

$$V_\theta = -\left( 1 + \frac{R^2}{r^2} \right) V_\infty \sin \theta - \frac{\Gamma}{2\pi r} = 0 \quad (3.122)$$

From Eq. (3.121),  $r = R$ . Substituting this result into Eq. (3.122) and solving for  $\theta$ , we obtain

$$\theta = \arcsin \left( -\frac{\Gamma}{4\pi V_\infty R} \right) \quad (3.123)$$

Since  $\Gamma$  is a positive number, from Eq. (3.123)  $\theta$  must be in the third and fourth quadrants. That is, there can be two stagnation points on the bottom half of the circular cylinder, as shown by points 1 and 2 in Fig. 3.25a. These points are located at  $(R, \theta)$ , where  $\theta$  is given by Eq. (3.123). However, this result is valid only when  $\Gamma/4\pi V_\infty R < 1$ . If  $\Gamma/4\pi V_\infty R > 1$ , then Eq. (3.123) has no meaning. If  $\Gamma/4\pi V_\infty R = 1$ , there is only one stagnation point on the surface of the cylinder, namely, point  $(R, -\pi/2)$  labeled as point 3 in Fig. 3.25b. For the case of  $\Gamma/4\pi V_\infty R > 1$ , return to Eq. (3.121). We saw

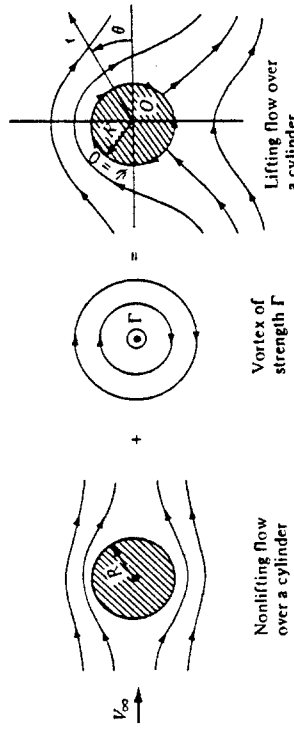


Figure 3.24 The synthesis of lifting flow over a circular cylinder.

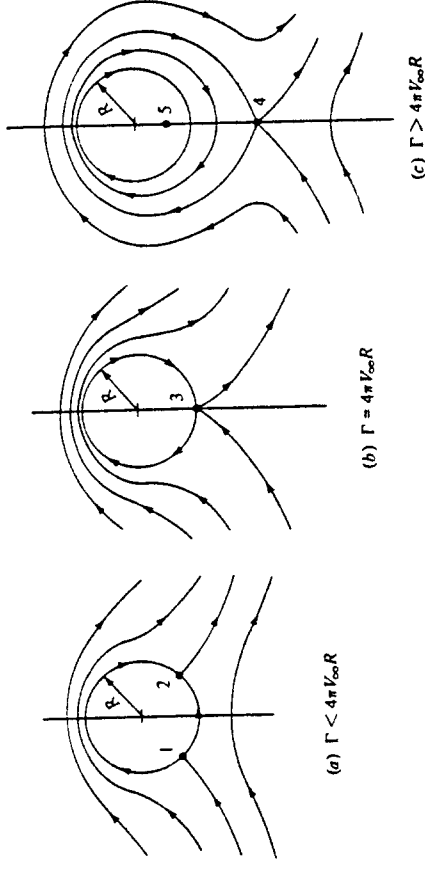


Figure 3.25 Stagnation points for the lifting flow over a circular cylinder.

earlier that it is satisfied by  $r = R$ ; however, it is also satisfied by  $\theta = \pi/2$  or  $-\pi/2$ . Substituting  $\theta = -\pi/2$  into Eq. (3.122), and solving for  $r$ , we have

$$r = \frac{\Gamma}{4\pi V_\infty} \pm \sqrt{\left(\frac{\Gamma}{4\pi V_\infty}\right)^2 - R^2} \quad (3.124)$$

Hence, for  $\Gamma/4\pi V_\infty R > 1$ , there are two stagnation points, one inside and the other outside the cylinder, and both on the vertical axis, as shown by points 4 and 5 in Fig. 3.25c. [How does one stagnation point fall *inside* the cylinder? Recall that  $r = R$ , or  $\psi = 0$ , is just one of the allowed streamlines of the flow. There is a theoretical flow inside the cylinder — flow that is issuing from the doublet at the origin superimposed with the vortex flow for  $r < R$ . The circular streamline  $r = R$  is the dividing streamline between this flow and the flow from the freestream. Therefore, as before, we can replace the dividing streamline by a solid body — our circular cylinder — and the *external* flow will not know the difference. Hence, although one stagnation point falls inside the body (point 5), we are not realistically concerned about it. Instead, from the point of view of flow over a solid cylinder of radius  $R$ , point 4 is the only meaningful stagnation point for the case  $\Gamma/4\pi V_\infty R > 1$ .]

The results shown in Fig. 3.25 can be visualized as follows. Consider the inviscid incompressible flow of given freestream velocity  $V_\infty$  over a cylinder of given radius  $R$ . If there is no circulation, i.e., if  $\Gamma = 0$ , the flow is given by the sketch at the right of Fig. 3.19, with horizontally opposed stagnation points A and B. Now assume that a circulation is imposed on the flow, such that  $\Gamma < 4\pi V_\infty R$ . The flow sketched in Fig. 3.25a will result; the two stagnation points will move to the lower surface of the cylinder as shown by points 1 and 2. Assume that  $\Gamma$  is further increased until  $\Gamma = 4\pi V_\infty R$ . The flow sketched in Fig. 3.25b will result, with only one stagnation point at the bottom of the cylinder, as shown by point 3. When  $\Gamma$  is increased still further such that  $\Gamma > 4\pi V_\infty R$ , the flow sketched in Fig. 3.25c will result. The stagnation point will lift from the cylinder's surface and will appear in the flow directly below the cylinder, as shown by point 4.

From the above discussion,  $\Gamma$  is clearly a parameter that can be chosen freely. There is no single value of  $\Gamma$  that "solves" the flow over a circular cylinder; rather, the circulation can be any value. Therefore, *for the incompressible flow over a circular cylinder, there are an infinite number of possible potential flow solutions, corresponding to the infinite choice for values of  $\Gamma$ .* This statement is not limited to flow over circular cylinders, but rather it is a general statement that holds for the incompressible potential flow over all smooth two-dimensional bodies. We return to these ideas in subsequent sections.

From the symmetry, or lack of it, in the flows sketched in Figs. 3.24 and 3.25, we intuitively concluded earlier that a finite normal force (lift) must exist on the body but that the drag is zero, i.e., d'Alembert's paradox still prevails. Let us quantify these statements by calculating expressions for lift and drag, as follows.

The velocity on the surface of the cylinder is given by Eq. (3.120) with  $r = R$ :

$$\mathbf{V} = \mathbf{V}_\theta = -2V_\infty \sin \theta - \frac{\Gamma}{2\pi R} \mathbf{e}_y \quad (3.125)$$

In turn, the pressure coefficient is obtained by substituting Eq. (3.125) into Eq. (3.38).

$$C_p = 1 - \left( \frac{V}{V_\infty} \right)^2 = 1 - \left( -2 \sin \theta - \frac{\Gamma}{2\pi RV_\infty} \right)^2$$

$$C_p = 1 - \left[ 4 \sin^2 \theta + \frac{2\Gamma \sin \theta}{\pi RV_\infty} + \left( \frac{\Gamma}{2\pi RV_\infty} \right)^2 \right] \quad (3.126)$$

In Sec. 1.5, we discussed in detail how the aerodynamic force coefficients can be obtained by integrating the pressure coefficient and skin friction coefficient over the surface. For inviscid flow,  $c_f = 0$ . Hence, the drag coefficient  $c_d$  is given by Eq. (1.16) as

$$c_d = c_a = \frac{1}{c} \int_{LE}^{TE} (C_{p,u} - C_{p,l}) dy$$

$$c_d = \frac{1}{c} \int_{LE}^{TE} C_{p,u} dy - \frac{1}{c} \int_{LE}^{TE} C_{p,l} dy \quad (3.127)$$

Converting Eq. (3.127) to polar coordinates, we note that

$$y = R \sin \theta \quad dy = R \cos \theta d\theta \quad (3.128)$$

Substituting Eq. (3.128) into (3.127), and noting that  $c = 2R$ , we have

$$c_d = \frac{1}{2} \int_{\pi}^{0} C_{p,u} dy - \frac{1}{2} \int_{\pi}^{2\pi} C_{p,l} dy \quad (3.129)$$

The limits of integration in Eq. (3.129) are explained as follows. In the first integral, we are integrating from the leading edge (the front point of the cylinder), moving over the top surface of the cylinder. Hence,  $\theta$  is equal to  $\pi$  at the leading edge and, moving over the top surface, decreases to 0 at the trailing edge. In the second integral, we are integrating from the leading edge to the trailing edge while moving over the bottom surface of the cylinder. Hence,  $\theta$  is equal to  $2\pi$  at the leading edge and, moving over

the bottom surface, increases to  $2\pi$  at the trailing edge. In Eq. (3.129), both  $C_{p,u}$  and  $C_{p,l}$  are given by the same analytic expression for  $C_p$ , namely, Eq. (3.126). Hence, Eq. (3.129) can be written as

$$c_d = -\frac{1}{2} \int_0^{\pi} C_p \cos \theta d\theta - \frac{1}{2} \int_{-\pi}^{2\pi} C_p \cos \theta d\theta \quad (3.130)$$

$$\text{or} \quad c_d = -\frac{1}{2} \int_0^{2\pi} C_p \cos \theta d\theta \quad (3.130)$$

Substituting Eq. (3.126) into (3.130), and noting that

$$\int_0^{2\pi} \cos \theta d\theta = 0 \quad (3.131a)$$

$$\int_0^{2\pi} \sin^2 \theta \cos \theta d\theta = 0 \quad (3.131b)$$

$$\int_0^{2\pi} \sin \theta \cos \theta d\theta = 0 \quad (3.131c)$$

we immediately obtain

$$c_d = 0 \quad (3.132)$$

Equation (3.132) confirms our intuitive statements made earlier. The drag on a cylinder in an inviscid, incompressible flow is zero, regardless of whether or not the flow has circulation about the cylinder.

The lift on the cylinder can be evaluated in a similar manner as follows. From Eq. (1.15) with  $c_f = 0$ ,

$$c_l = c_n = -\frac{1}{c} \int_0^c C_{p,l} dx - \frac{1}{c} \int_0^c C_{p,u} dx \quad (3.133)$$

Converting to polar coordinates,

$$x = R \cos \theta \quad dx = -R \sin \theta d\theta \quad (3.134)$$

Substituting Eq. (3.134) into (3.133), we have

$$c_l = -\frac{1}{2} \int_{-\pi}^{2\pi} C_{p,l} \sin \theta d\theta + \frac{1}{2} \int_{-\pi}^0 C_{p,u} \sin \theta d\theta \quad (3.135)$$

Again, noting that  $C_{p,l}$  and  $C_{p,u}$  are both given by the same analytic expression, namely, Eq. (3.126), Eq. (3.135) becomes

$$c_l = -\frac{1}{2} \int_0^{2\pi} C_p \sin \theta d\theta \quad (3.136)$$

Substituting Eq. (3.126) into (3.136), and noting that

$$\int_0^{2\pi} \sin \theta d\theta = 0 \quad (3.137a)$$

$$\int_0^{2\pi} \sin^3 \theta d\theta = 0 \quad (3.137b)$$

$$\int_0^{2\pi} \sin^2 \theta d\theta = \pi \quad (3.137c)$$

we immediately obtain

$$c_l = \frac{\Gamma}{RV_s} \quad (3.138)$$

From the definition of  $c_l$  (see Sec. 1.5), the lift per unit span  $L'$  can be obtained from

$$L' = q_\infty S c_l = \frac{1}{2} \rho_\infty V_\infty^2 S c_l \quad (3.139)$$

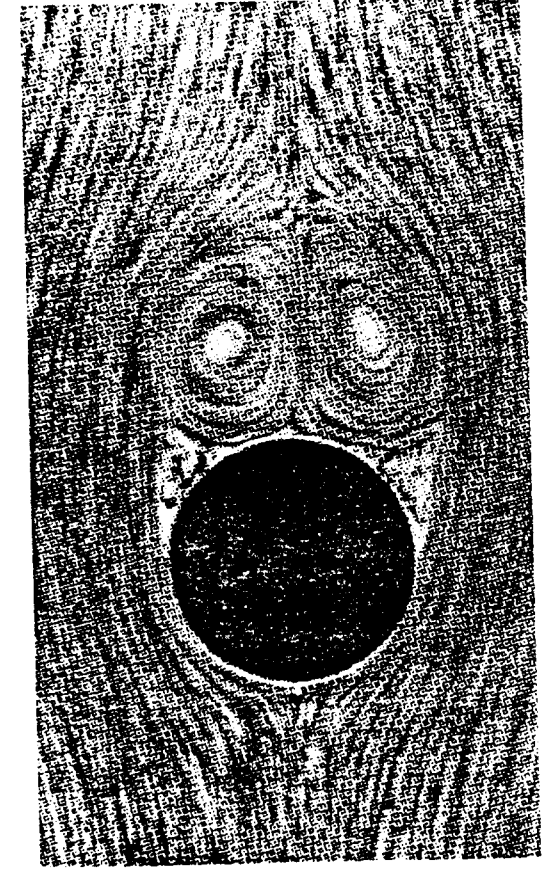
Here, the planform area  $S = 2R(1)$ . Therefore, combining Eqs. (3.138) and (3.139), we have

$$L' = \frac{1}{2} \rho_\infty V_\infty^2 2R \frac{\Gamma}{RV_s} \quad (3.140)$$

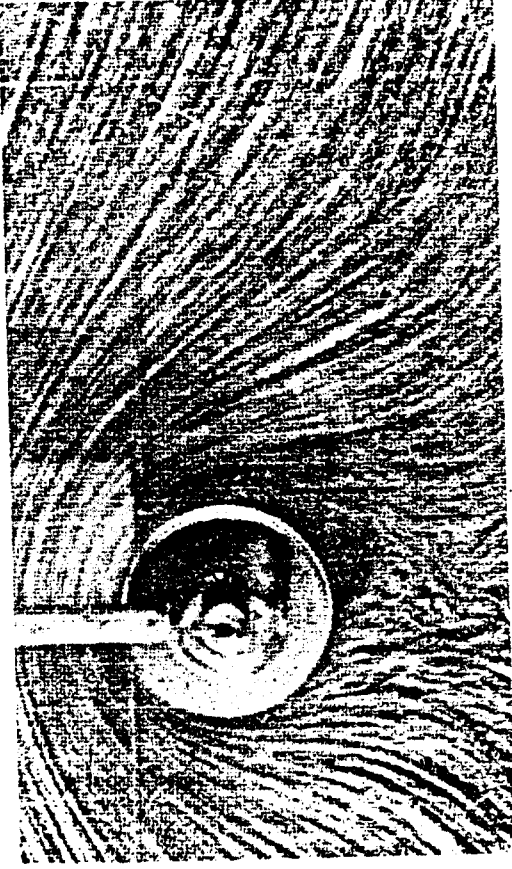
or

Equation (3.140) gives the lift per unit span for a circular cylinder with circulation  $\Gamma$ . It is a remarkably simple result, and it states that *the lift per unit span is directly proportional to circulation*. Equation (3.140) is a powerful relation in theoretical aerodynamics. It is called the *Kutta-Joukowski theorem*, named after the German mathematician M. Wilhelm Kutta (1867–1944) and the Russian physicist Nikolai E. Joukowski (1847–1921) who independently obtained it during the first decade of this century. We will have more to say about the Kutta-Joukowski theorem in Sec. 3.16.

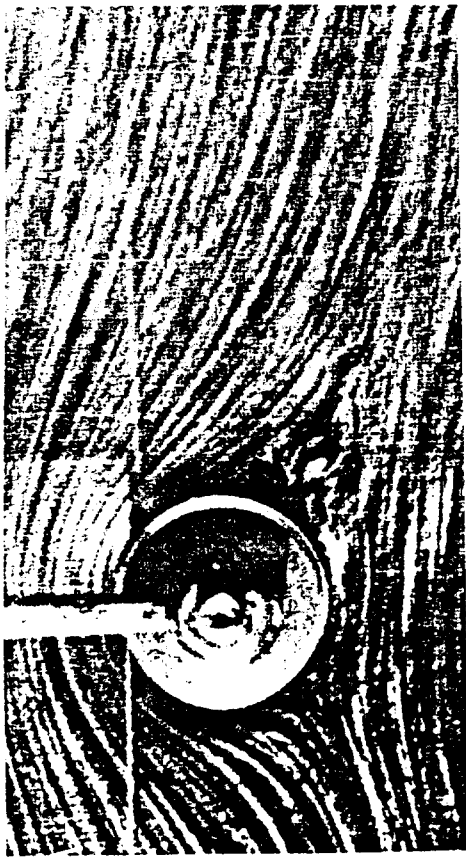
What are the connections between the above theoretical results and real life? As stated earlier, the prediction of zero drag is totally erroneous—viscous effects cause skin friction and flow separation which always produce a finite drag, as will be discussed in Chaps. 15 and 16. The inviscid flow treated in this chapter simply does not model the proper physics for drag calculations. On the other hand, the prediction of lift via Eq. (3.140) is quite realistic. Let us return to the wind-tunnel experiments mentioned at the beginning of this chapter. If a stationary, nonspinning cylinder is placed in a low-speed wind tunnel, the flow field will appear as shown in Fig. 3.26a. The streamlines over the front of the cylinder are similar to theoretical predictions, as sketched at the right of Fig. 3.19. However, because of viscous effects, the flow separates over the rear of the cylinder, creating a recirculating flow in the wake downstream of the body. This separated flow greatly contributes to the finite drag measured for the cylinder. On the other hand, Fig. 3.26a shows a reasonably symmetric flow about the horizontal axis, and the measurement of lift is essentially zero. Now, let us *spin* the



(a)



(b)

Figure 3.26 (c) Spinning cylinder: peripheral velocity of the surface =  $6V_\infty$ .

important, a *finite lift* is measured for the spinning cylinder in the wind tunnel. What is happening here? Why does spinning the cylinder produce lift? In actuality, the friction between the fluid and the surface of the cylinder tends to drag the fluid near the surface in the same direction as the rotational motion. Superimposed on top of the usual nonspinning flow, this "extra" velocity contribution creates a higher-than-usual velocity at the top of the cylinder and a lower-than-usual velocity at the bottom, as sketched in Fig. 3.27. These velocities are assumed to be just outside the viscous boundary layer on the surface. Recall from Bernoulli's equation that as the velocity increases, the pressure decreases. Hence, from Fig. 3.27, the pressure on the top of the cylinder is lower than on the bottom. This pressure imbalance creates a net upward force, i.e., a finite lift. Therefore, the theoretical prediction embodied in Eq. (3.140) that the flow over a circular cylinder can produce a finite lift is verified by experimental observation.

The general ideas discussed above concerning the generation of lift on a spinning circular cylinder in a wind tunnel also apply to a spinning sphere. This explains why a baseball pitcher can throw a curve and how a golfer can hit a hook or slice—all of which are due to nonsymmetric flows about the spinning bodies and, hence, the generation of an aerodynamic force perpendicular to the body's angular velocity vector. This

Figure 3.26 These flow-field pictures were obtained in water, where aluminum filings were scattered on the surface to show the direction of the streamlines. (From Ref. 8.) (a) Shown above is the case for the nonspinning cylinder. (b) Spinning cylinder; peripheral velocity of the surface =  $3V_\infty$ .

cylinder in a clockwise direction about its axis. The resulting flow fields are shown in Fig. 3.26b and c. For a moderate amount of spin (Fig. 3.26b), the stagnation points move to the lower part of the cylinder, similar to the theoretical flow sketched in Fig. 3.25a. If the spin is sufficiently increased (Fig. 3.26c), the stagnation point lifts off the surface, similar to the theoretical flow sketched in Fig. 3.25c. And what is most

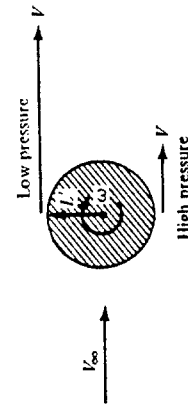


Figure 3.27 Creation of lift on a spinning cylinder.

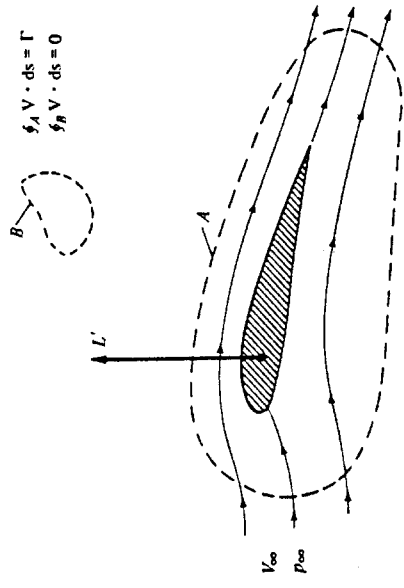
phenomenon is called the *Magnus effect*, named after the German engineer who first observed and explained it in Berlin in 1852.

It is interesting to note that a rapidly spinning cylinder can produce a much higher lift than an airplane wing of the same planform area; however, the drag on the cylinder is also much higher than a well-designed wing. As a result, the Magnus effect is not employed for powered flight. On the other hand, in the 1920s, the German engineer Anton Flettner replaced the sail on a boat with a rotating circular cylinder with its axis vertical to the deck. In combination with the wind, this spinning cylinder provided propulsion for the boat. Moreover, by the action of two cylinders in tandem and rotating in opposite directions, Flettner was able to turn the boat around. Flettner's device was a technical success, but an economic failure because the maintenance on the machinery to spin the cylinders at the necessary high rotational speeds was too costly. Today, the Magnus effect has an important influence on the performance of spinning missiles; indeed, a certain amount of modern high-speed aerodynamic research has focused on the Magnus forces on spinning bodies for missile applications.

### 3.16 THE KUTTA-JOUKOWSKI THEOREM AND THE GENERATION OF LIFT

Although the result given by Eq. (3.140) was derived for a circular cylinder, it applies in general to cylindrical bodies of arbitrary cross section. For example, consider the incompressible flow over an airfoil section, as sketched in Fig. 3.28. Let curve  $A$  be any curve in the flow *enclosing* the airfoil. If the airfoil is producing lift, the velocity field around the airfoil will be such that the line integral of velocity around  $A$  will be finite, i.e., the circulation

$$\Gamma = \oint_A \mathbf{v} \cdot d\mathbf{s}$$



is finite. In turn, the lift per unit span  $L'$  on the airfoil will be given by the *Kutta-Joukowski theorem*, as embodied in Eq. (3.140):

$$L' = \rho_v V_\infty \Gamma \quad (3.140)$$

This result underscores the importance of the concept of circulation, defined in Sec. 2.13. The Kutta-Joukowski theorem states that lift per unit span on a two-dimensional body is directly proportional to the circulation around the body. Indeed, the concept of circulation is so important at this stage of our discussion that you should reread Sec. 2.13 before proceeding further.

The general derivation of Eq. (3.140) for bodies of arbitrary cross section can be carried out using the method of complex variables. Such mathematics is beyond the scope of this book. (It can be shown that arbitrary functions of complex variables are general solutions of Laplace's equation, which in turn governs incompressible potential flow. Hence, more advanced treatments of such flows utilize the mathematics of complex variables as an important tool. See Ref. 9 for a particularly lucid treatment of inviscid, incompressible flow at a more advanced level.)

In Sec. 3.15, the lifting flow over a circular cylinder was synthesized by superimposing a uniform flow, a doublet, and a vortex. Recall that all three elementary flows are irrotational at all points, except for the vortex, which has infinite vorticity at the origin. Therefore, the lifting flow over a cylinder as shown in Fig. 3.25 is irrotational at every point except at the origin. If we take the circulation around any curve *not* enclosing the origin, we obtain from Eq. (2.128) the result that  $\Gamma = 0$ . It is only when we choose a curve that encloses the origin, where  $\nabla \times \mathbf{V}$  is infinite, that Eq. (2.128) yields a finite  $\Gamma$ , equal to the strength of the vortex. The same can be said about the flow over the airfoil in Fig. 3.28. As we show in Chap. 4, the flow *outside* the airfoil is irrotational, and the circulation around any closed curve *not* enclosing the airfoil (such as curve  $B$  in Fig. 3.28) is consequently zero. On the other hand, we also show in Chap. 4 that the flow over an airfoil is synthesized by distributing vortices either on the surface or inside the airfoil. These vortices have the usual singularities in  $\nabla \times \mathbf{V}$ , and therefore, if we choose a curve that encloses the airfoil (such as curve  $A$  in Fig. 3.28), Eq. (2.128) yields a finite value of  $\Gamma$ , equal to the *sum* of the vortex strengths distributed on or inside the airfoil. The important point here is that, in the Kutta-Joukowski theorem, the value of  $\Gamma$  used in Eq. (3.140) must be evaluated around a closed curve that *encloses the body*; the curve can be otherwise arbitrary, but it must have the body inside it.

At this stage, let us pause and assess our thoughts. The approach we have discussed above—the definition of circulation and the use of Eq. (3.140) to obtain the lift—is the essence of the *circulation theory of lift* in aerodynamics. Its development at the turn of the twentieth century created a breakthrough in aerodynamics. However, let us keep things in perspective. The circulation theory of lift is an *alternative* way of thinking about the generation of lift on an aerodynamic body. Keep in mind that the true physical sources of the aerodynamic force on a body are the pressure and shear stress distributions exerted on the surface of the body, as explained in Sec. 1.5. The Kutta-Joukowski theorem is simply an alternate way of expressing the *consequences* of the surface

Figure 3.28 Circulation around a lifting airfoil.

pressure distribution; it is a mathematical expression that is consistent with the special tools we have developed for the analysis of inviscid, incompressible flow. Indeed, recall that Eq. (3.140) was derived in Sec. 3.15 by integrating the pressure distribution over the surface. Therefore, it is not quite proper to say that circulation "causes" lift. Rather, lift is "caused" by the net imbalance of the surface pressure distribution, and circulation is simply a defined quantity determined from the same pressures. The relation between the surface pressure distribution (which produces lift  $L$ ) and circulation is given by Eq. (3.140). However, in the theory of incompressible, potential flow, it is generally much easier to determine the circulation around the body rather than calculate the detailed surface pressure distribution. Therein lies the power of the circulation theory of lift.

Consequently, the theoretical analysis of lift on two-dimensional bodies in incompressible, inviscid flow focuses on the calculation of the circulation about the body. Once  $\Gamma$  is obtained, then the lift per unit span follows directly from the Kutta-Joukowski theorem. As a result, in subsequent sections we constantly address the question: How can we calculate the circulation for a given body in a given incompressible, inviscid flow?

### 3.17 NONLIFTING FLOWS OVER ARBITRARY BODIES: THE NUMERICAL SOURCE PANEL METHOD

In this section, we return to the consideration of nonlifting flows. Recall that we have already dealt with the nonlifting flows over a semi-infinite body and a Rankine oval and both the nonlifting and the lifting flows over a circular cylinder. For those cases, we added our elementary flows in certain ways and discovered that the dividing streamlines turned out to fit the shapes of such special bodies. However, this indirect method of starting with a given combination of elementary flows and seeing what body shape comes out of it can hardly be used in a practical sense for bodies of arbitrary shape. For example, consider the airfoil in Fig. 3.28. Do we know in advance the correct combination of elementary flows to synthesize the flow over this specific body? The answer is no. Rather, what we want is a direct method; i.e., let us specify the shape of an arbitrary body and solve for the distribution of singularities which, in combination with a uniform stream, produce the flow over the given body. The purpose of this section is to present such a direct method, limited for the present to nonlifting flows. We consider a numerical method appropriate for solution on a high-speed digital computer. The technique is called the *source panel method*, which, since the late 1960s, has become a standard aerodynamic tool in industry and most research laboratories. In fact, the numerical solution of potential flows by both source and vortex panel techniques has revolutionized the analysis of low-speed flows. We return to various numerical panel techniques in Chaps. 4 through 6. As a modern student of aerodynamics, it is necessary for you to become familiar with the fundamentals of such panel methods. The purpose of the present section is to introduce the basic ideas of the source panel method, which is a technique for the numerical solution of nonlifting flows over arbitrary bodies.

First, let us extend the concept of a source or sink introduced in Sec. 3.10. In that section, we dealt with a single line source, as sketched in Fig. 3.14. Now imagine that we have an infinite number of such line sources side-by-side, where the strength of each line source is infinitesimally small. Those side-by-side line sources form a *source sheet*, as shown in perspective in the upper left of Fig. 3.29. If we look along the series of line sources (looking along the  $z$  axis in Fig. 3.29), the source sheet will appear as sketched at the lower right of Fig. 3.29. Here, we are looking at an edge view of the sheet; the line sources are all perpendicular to the page. Let  $s$  be the distance measured along the source sheet in the edge view. Define  $\lambda = \lambda(s)$  to be the *source strength per unit length along  $s$* . [To keep things in perspective, recall from Sec. 3.10 that the strength of a single line source  $\Lambda$  was defined as the volume flow rate per unit depth, i.e., per unit length in the  $z$  direction. Typical units for  $\Lambda$  are square meters per second or square feet per second. In turn, the strength of a source sheet  $\lambda(s)$  is the volume flow rate per unit depth (in the  $z$  direction) and per unit length (in the  $s$  direction). Typical units for  $\lambda$  are meters per second or feet per second.] Therefore, the strength of an infinitesimal portion  $ds$  of the sheet, as shown in Fig. 3.29, is  $\lambda ds$ . This small section of the source sheet can be treated as a distinct source of strength  $\lambda ds$ . Now consider point  $P$  in the flow, located a distance  $r$  from  $ds$ ; the cartesian coordinates of  $P$  are  $(x, y)$ . The small section of the source sheet of strength  $\lambda ds$  induces an infinitesimally small potential,  $d\phi$ , at point  $P$ . From Eq. (3.67),  $d\phi$  is given by

$$d\phi = \frac{\lambda ds}{2\pi} \ln r \quad (3.141)$$

The complete velocity potential at point  $P$ , induced by the entire source sheet from  $a$  to  $b$ , is obtained by integrating Eq. (3.141):

$$\phi(x, y) = \int_a^b \frac{\lambda ds}{2\pi} \ln r \quad (3.142)$$

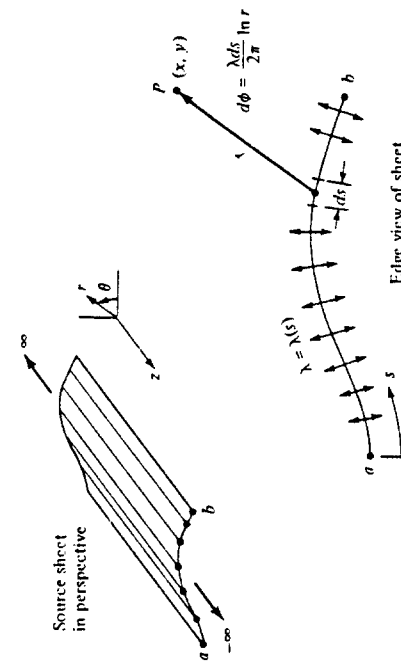


Figure 3.29 Source sheet.

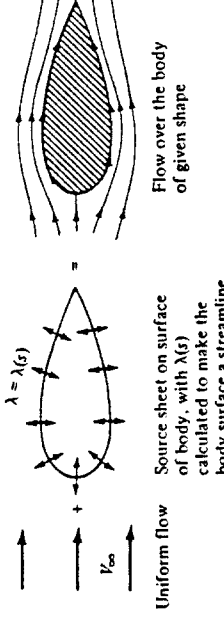


Figure 3.30 Superposition of a uniform flow and a source sheet on a body of given shape, to produce the flow over the body.

Note that, in general,  $\lambda(s)$  can change from positive to negative along the sheet; i.e., the "source" sheet is really a combination of line sources and line sinks.

Next, consider a given body of arbitrary shape in a flow with freestream velocity  $V_\infty$ , as shown in Fig. 3.30. Let us cover the surface of the prescribed body with a source sheet, where the strength  $\lambda(s)$  varies in such a fashion that the combined action of the uniform flow and the source sheet makes the airfoil surface a streamline. Our problem now becomes one of finding the appropriate  $\lambda(s)$ . The solution of this problem is carried out numerically, as follows.

Let us approximate the source sheet by a series of straight panels, as shown in Fig. 3.31. Moreover, let the source strength  $\lambda$  per unit length be constant over a given panel, but allow it to vary from one panel to the next. That is, if there are a total of  $n$  panels, the source panel strengths per unit length are  $\lambda_1, \lambda_2, \dots, \lambda_j, \dots, \lambda_n$ . These panel strengths are unknown; the main thrust of the panel technique is to solve for  $\lambda_i, j = 1$  to  $n$ , such that the body surface becomes a streamline of the flow. This boundary condition is imposed numerically by defining the midpoint of each panel to be a *control point* and by determining the  $\lambda_j$ 's such that the normal component of the flow velocity is zero at each control point. Let us now quantify this strategy.

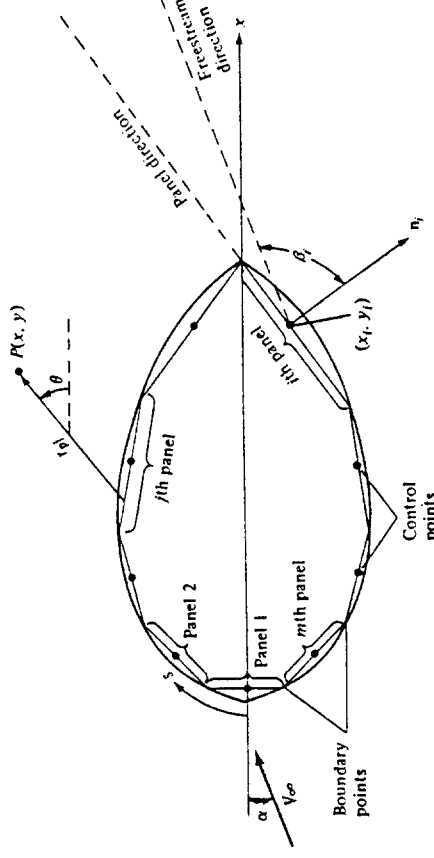


Figure 3.31 Source panel distribution over the surface of a body of arbitrary shape.

Let  $P$  be a point located at  $(x, y)$  in the flow, and let  $r_{ij}$  be the distance from any point on the  $j$ th panel to  $P$ , as shown in Fig. 3.31. The velocity potential induced at  $P$  due to the  $j$ th panel  $\Delta\phi_j$  is, from Eq. (3.142),

$$\Delta\phi_j = \frac{\lambda_j}{2\pi} \int_j \ln r_{ij} ds_j \quad (3.143)$$

In Eq. (3.143),  $\lambda_j$  is constant over the  $j$ th panel, and the integral is taken over the  $j$ th panel only. In turn, the potential at  $P$  due to all the panels is Eq. (3.143) summed over all the panels.

$$\phi(P) = \sum_j \Delta\phi_j = \sum_{j=1}^n \frac{\lambda_j}{2\pi} \int_j \ln r_{ij} ds_j \quad (3.144)$$

In Eq. (3.144), the distance  $r_{ij}$  is given by

$$r_{ij} = \sqrt{(x_i - x_j)^2 + (y_i - y_j)^2} \quad (3.145)$$

where  $(x_j, y_j)$  are coordinates along the surface of the  $j$ th panel. Since point  $P$  is just an arbitrary point in the flow, let us put  $P$  at the control point of the  $j$ th panel. Let the coordinates of this control point be given by  $(x_i, y_i)$  as shown in Fig. 3.31. Then Eqs. (3.144) and (3.145) become

$$\phi(x_i, y_i) = \sum_{j=1}^n \frac{\lambda_j}{2\pi} \int_j \ln r_{ij} ds_j \quad (3.146)$$

and

$$r_{ij} = \sqrt{(x_i - x_j)^2 + (y_i - y_j)^2} \quad (3.147)$$

Equation (3.146) is physically the contribution of *all* the panels to the potential at the control point of the  $j$ th panel.

Recall that the boundary condition is applied at the control points, i.e., the normal component of the flow velocity is zero at the control points. To evaluate this component, first consider the component of freestream velocity perpendicular to the panel. Let  $\mathbf{n}_i$  be the unit vector normal to the  $i$ th panel, directed out of the body as shown in Fig. 3.31. Also, note that the slope of the  $i$ th panel is  $(dy/dx)$ . In general, the freestream velocity will be at some incidence angle  $\alpha$  to the  $x$  axis, as shown in Fig. 3.31. Therefore, inspection of the geometry of Fig. 3.31 reveals that the component of  $V_\infty$  normal to the  $i$ th panel is

$$V_{\infty,n} = \mathbf{V}_\infty \cdot \mathbf{n}_i = V_\infty \cos \beta_i \quad (3.148)$$

where  $\beta_i$  is the angle between  $\mathbf{V}_\infty$  and  $\mathbf{n}_i$ . Note that  $V_{\infty,n}$  is positive when directed away from the body, and negative when directed toward the body.

The normal component of velocity induced at  $(x_i, y_i)$  by the source panels is, from Eq. (3.146),

$$V_n = -\frac{\partial}{\partial n_i} [\phi(x_i, y_i)] \quad (3.149)$$

where the derivative is taken in the direction of the outward unit normal vector, and hence again,  $V_n$  is positive when directed away from the body. When the derivative in

Eq. (3.149) is carried out,  $r_{ij}$  appears in the denominator. Consequently, a singular point arises on the  $i$ th panel because when  $j = i$ , at the control point itself  $r_{ii} = 0$ . It can be shown that when  $j = i$ , the contribution to the derivative is simply  $\lambda_i/2$ . Hence, Eq. (3.149) combined with Eq. (3.146) becomes

$$V_n = \frac{\lambda_i}{2} + \sum_{\substack{j=1 \\ (j \neq i)}}^n \frac{\lambda_j}{2\pi} \int_{\partial n_i} \frac{\partial}{\partial n_i} (\ln r_{ij}) ds_j \quad (3.150)$$

In Eq. (3.150), the first term  $\lambda_i/2$  is the normal velocity induced at the  $i$ th control point by the  $i$ th panel itself, and the summation is the normal velocity induced at the  $i$ th control point by all the other panels.

The normal component of the flow velocity at the  $i$ th control point is the sum of that due to the freestream (Eq. (3.148)) and that due to the source panels [Eq. (3.150)]. The boundary condition states that this sum must be zero.

$$V_{\infty,n} + V_n = 0 \quad (3.151)$$

Substituting Eqs. (3.148) and (3.150) into (3.151), we obtain

$$\frac{\lambda_i}{2} + \sum_{\substack{j=1 \\ (j \neq i)}}^n \frac{\lambda_j}{2\pi} \int_{\partial n_i} \frac{\partial}{\partial n_i} (\ln r_{ij}) ds_j + V_\infty \cos \beta_i = 0 \quad (3.152)$$

Equation (3.152) is the crux of the source panel method. The values of the integrals in Eq. (3.152) depend simply on the panel geometry; they are not properties of the flow. Let  $I_{i,j}$  be the value of this integral when the control point is on the  $i$ th panel and the integral is over the  $j$ th panel. Then, Eq. (3.152) can be written as

$$\frac{\lambda_i}{2} + \sum_{\substack{j=1 \\ (j \neq i)}}^n \frac{\lambda_j}{2\pi} I_{i,j} + V_\infty \cos \beta_i = 0 \quad (3.153)$$

Equation (3.153) is a linear *algebraic* equation with  $n$  unknowns  $\lambda_1, \lambda_2, \dots, \lambda_n$ . It represents the flow boundary condition evaluated at the control point of the  $i$ th panel. Now apply the boundary condition to the control points of *all* the panels, i.e., in Eq. (3.153), let  $i = 1, 2, \dots, n$ . The results will be a system of  $n$  linear algebraic equations with  $n$  unknowns ( $\lambda_1, \lambda_2, \dots, \lambda_n$ ), which can be solved simultaneously by conventional numerical methods.

Look what has happened! After solving the system of equations represented by Eq. (3.153) with  $i = 1, 2, \dots, n$ , we now have the distribution of source panel strengths which, in an approximate fashion, cause the body surface in Fig. 3.31 to be a streamline of the flow. This approximation can be made more accurate by increasing the number of panels, hence more closely representing the source sheet of continuously varying strength  $\lambda(s)$  shown in Fig. 3.30. Indeed, the accuracy of the source panel method is amazingly good; a circular cylinder can be accurately represented by as few as eight panels, and most airfoil shapes, by 50 to 100 panels. (For an airfoil, it is desirable to cover the leading-edge region with a number of small panels to accurately represent the rapid surface curvature and to use larger panels over the relatively flat portions of the body. Note that in general, all the panels in Fig. 3.31 can be different lengths.)

Once the  $\lambda_i$ 's ( $i = 1, 2, \dots, n$ ) are obtained, the velocity *tangent* to the surface at each control point can be calculated as follows. Let  $s$  be the distance along the body surface, measured positive from front to rear, as shown in Fig. 3.31. The component of freestream velocity tangent to the surface is

$$V_{\infty,s} = V_\infty \sin \beta_i \quad (3.154)$$

The tangential velocity  $V_s$  at the control point of the  $i$ th panel induced by all the panels is obtained by differentiating Eq. (3.146) with respect to  $s$ .

$$V_s = \frac{\partial \phi}{\partial s} = \sum_{j=1}^n \frac{\lambda_j}{2\pi} \int_{\partial S} \frac{\partial}{\partial s} (\ln r_{ij}) ds_j \quad (3.155)$$

[The tangential velocity on a flat source panel induced by the panel itself is zero; hence, in Eq. (3.155), the term corresponding to  $j = i$  is zero. This is easily seen by intuition, because the panel can only emit volume flow from its surface in a direction perpendicular to the panel itself.] The total surface velocity at the  $i$ th control point  $V_i$  is the sum of the contribution from the freestream [Eq. (3.154)] and from the source panels [Eq. (3.155)].

$$V_i = V_{\infty,s} + V_s = V_\infty \sin \beta_i + \sum_{j=1}^n \frac{\lambda_j}{2\pi} \int_{\partial S} \frac{\partial}{\partial s} (\ln r_{ij}) ds_j \quad (3.156)$$

In turn, the pressure coefficient at the  $i$ th control point is obtained from Eq. (3.38).

$$C_{p,i} = 1 - \left( \frac{V_i}{V_\infty} \right)^2$$

In this fashion, the source panel method gives the pressure distribution over the surface of a nonlifting body of arbitrary shape.

When you carry out a source panel solution as described above, the accuracy of your results can be tested as follows. Let  $S_j$  be the length of the  $j$ th panel. Recall that  $\lambda_j$  is the strength of the  $j$ th panel *per unit length*. Hence, the strength of the  $j$ th panel itself is  $\lambda_j S_j$ . For a closed body, such as in Fig. 3.31, the sum of all the source and sink strengths must be zero, or else the body itself would be adding or absorbing mass from the flow — an impossible situation for the case we are considering here. Hence, the values of the  $\lambda_j$ 's obtained above should obey the relation

$$\sum_{j=1}^n \lambda_j S_j = 0 \quad (3.157)$$

Equation (3.157) provides an independent check on the accuracy of the numerical results.

**Example 3.6** Calculate the pressure coefficient distribution around a circular cylinder using the source panel technique.

**SOLUTION** We choose to cover the body with eight panels of equal length, as shown in Fig. 3.32. This choice is arbitrary; however, experience has shown that, for the

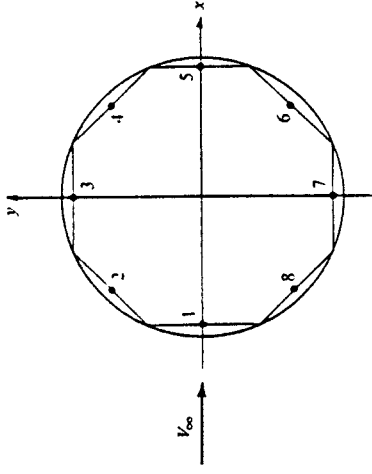


Figure 3.32 Source panel distribution around a circular cylinder.

case of a circular cylinder, the arrangement shown in Fig. 3.32 provides sufficient accuracy. The panels are numbered from 1 to 8, and the control points are shown by the dots in the center of each panel.

Let us evaluate the integrals  $I_{i,j}$ , which appear in Eq. (3.153). Consider Fig. 3.33, which illustrates two arbitrarily chosen panels. In Fig. 3.33,  $(x_i, y_i)$  are the coordinates of the control point of the  $i$ th panel, and  $(x_j, y_j)$  are the running coordinates over the entire  $j$ th panel. The coordinates of the boundary points for the  $i$ th panel are  $(X_i, Y_i)$  and  $(X_{i+1}, Y_{i+1})$ ; similarly, the coordinates of the boundary points for the  $j$ th panel are  $(X_j, Y_j)$  and  $(X_{j+1}, Y_{j+1})$ . In this problem,  $\mathbf{V}_\infty$  is in the  $x$  direction; hence, the angles between the  $x$  axis and the unit vectors  $\mathbf{n}_i$  and  $\mathbf{n}_j$  are  $\beta_i$  and  $\beta_j$ , respectively. Note that in general both  $\beta_i$  and  $\beta_j$  vary from 0 to  $2\pi$ . Recall that the integral  $I_{i,j}$  is evaluated at the  $i$ th control point and the integral is taken over the complete  $j$ th panel.

$$I_{i,j} = \int_J \frac{\partial}{\partial n_i} (\ln r_{ij}) dy_j \quad (3.158)$$

Since

$$r_{ij} = \sqrt{(x_i - x_j)^2 + (y_i - y_j)^2}$$

then

$$\begin{aligned} \frac{\partial}{\partial n_i} (\ln r_{ij}) &= \frac{1}{r_{ij}} \frac{\partial r_{ij}}{\partial n_i} \\ &= \frac{1}{r_{ij}} \frac{1}{2} [(x_i - x_j)^2 + (y_i - y_j)^2]^{-1/2} \\ &\cdot \left[ 2(x_i - x_j) \frac{dx_i}{dn_i} + 2(y_i - y_j) \frac{dy_i}{dn_i} \right] \end{aligned}$$

$$\text{or} \quad \frac{\partial}{\partial n_i} (\ln r_{ij}) = \frac{(x_i - x_j) \cos \beta_i + (y_i - y_j) \sin \beta_i}{(x_i - x_j)^2 + (y_i - y_j)^2} \quad (3.159)$$

Note in Fig. 3.33 that  $\Phi_i$  and  $\Phi_j$  are angles measured in the counterclockwise direction from the  $x$  axis to the bottom of each panel. From this geometry,

$$\beta_i = \Phi_i + \frac{\pi}{2} \quad (3.160a)$$

$$\sin \beta_i = \cos \Phi_i \quad (3.160b)$$

$$\cos \beta_i = -\sin \Phi_i \quad (3.160c)$$

Also from the geometry of Fig. 3.33, we have

$$x_j = X_j + s_j \cos \Phi_j \quad (3.161a)$$

$$y_j = Y_j + s_j \sin \Phi_j \quad (3.161b)$$

Substituting Eqs. (3.159) to (3.161) into (3.158), we obtain

$$I_{i,j} = \int_0^{s_j} \frac{C s_j + D}{s_j^2 + 2A s_j + B} ds_j \quad (3.162)$$

where

$$A = -(x_i - X_j) \cos \Phi_j - (y_i - Y_j) \sin \Phi_j$$

$$B = (x_i - X_j)^2 + (y_i - Y_j)^2$$

$$C = \sin(\Phi_i - \Phi_j)$$

$$D = (y_i - Y_j) \cos \Phi_i - (x_i - X_j) \sin \Phi_i$$

$$S_j = \sqrt{(X_{j+1} - X_j)^2 + (Y_{j+1} - Y_j)^2}$$

Letting

$$E = \sqrt{B - A^2} = (x_i - X_j) \sin \Phi_j - (y_i - Y_j) \cos \Phi_j$$

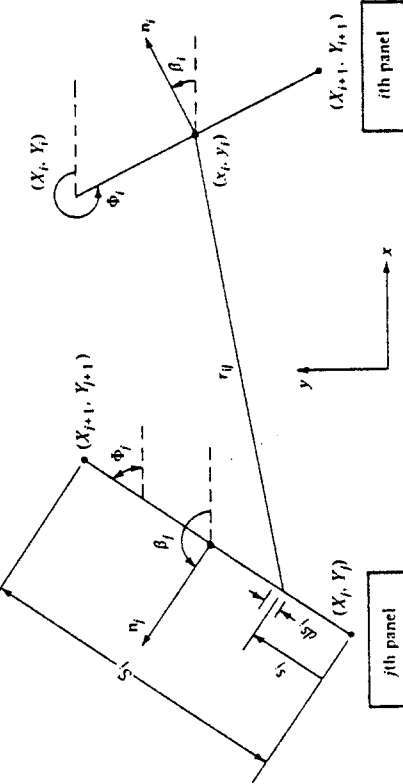


Figure 3.33 Geometry required for the evaluation of  $I_{i,j}$ .

we obtain an expression for Eq. (3.162) from any standard table of integrals,

$$I_{ij} = \frac{C}{2} \ln \left( \frac{S_j^2 + 2AS_j + B}{B} \right) + \frac{D - AC}{E} \left( \tan^{-1} \frac{S_j + A}{E} - \tan^{-1} \frac{A}{E} \right) \quad (3.163)$$

Equation (3.163) is a general expression for two arbitrarily oriented panels; it is not restricted to the case of a circular cylinder.

We now apply Eq. (3.163) to the circular cylinder shown in Fig. 3.32. For purposes of illustration, let us choose panel 4 as the *i*th panel and panel 2 as the *j*th panel; i.e., let us calculate  $I_{4,2}$ . From the geometry of Fig. 3.32, assuming a unit radius for the cylinder, we see that

$$\begin{aligned} X_j &= -0.9239 & X_{j+1} &= -0.3827 & Y_j &= 0.3827 \\ Y_{j+1} &= 0.9239 & \Phi_j &= 315^\circ & \Phi_{j+1} &= 45^\circ \\ x_i &= 0.6533 & y_i &= 0.6533 \end{aligned}$$

Hence, substituting these numbers into the above formulas, we obtain

$$\begin{aligned} A &= -1.3065 & B &= 2.5607 & C &= -1 & D &= 1.3065 \\ S_j &= 0.7654 & E &= 0.9239 \end{aligned}$$

Inserting the above values into Eq. (3.163), we obtain

$$I_{4,2} = 0.4018$$

Return to Figs. 3.32 and 3.33. If we now choose panel 1 as the *j*th panel, keeping panel 4 as the *i*th panel, we obtain, by means of a similar calculation,  $I_{4,1} = 0.4074$ . Similarly,  $I_{4,3} = 0.3528$ ,  $I_{4,5} = 0.3528$ ,  $I_{4,6} = 0.4018$ ,  $I_{4,7} = 0.4074$ , and  $I_{4,8} = 0.4084$ .

Return to Eq. (3.153), which is evaluated for the *i*th panel. Written for panel 4, Eq. (3.153) becomes (after multiplying each term by 2 and noting that  $\beta_i = 45^\circ$  for panel 4)

$$0.4074\lambda_1 + 0.4018\lambda_2 + 0.3528\lambda_3 + \pi\lambda_4 + 0.3528\lambda_5 + 0.4018\lambda_6 + 0.4074\lambda_7 + 0.4084\lambda_8 = -0.7071 2\pi V_x \quad (3.164)$$

Equation (3.164) is a linear algebraic equation in terms of the eight unknowns,  $\lambda_1, \lambda_2, \dots, \lambda_8$ . If we now evaluate Eq. (3.153) for each of the seven other panels, we obtain a total of eight equations, including Eq. (3.164), which can be solved simultaneously for the eight unknown  $\lambda$ 's. The results are

$$\begin{aligned} \lambda_1/2\pi V_x &= 0.3765 & \lambda_2/2\pi V_x &= 0.2662 & \lambda_3/2\pi V_x &= 0 \\ \lambda_4/2\pi V_x &= -0.2662 & \lambda_5/2\pi V_x &= -0.3765 & \lambda_6/2\pi V_x &= -0.2662 \\ \lambda_7/2\pi V_x &= 0 & \lambda_8/2\pi V_x &= 0.2662 \end{aligned}$$

Note the symmetrical distribution of the  $\lambda$ 's, which is to be expected for the nonlifting circular cylinder. Also, as a check on the above solution, return to Eq. (3.157). Since each panel in Fig. 3.32 has the same length, Eq. (3.157) can be written simply as

$$\sum_{j=1}^n \lambda_j = 0$$

Substituting the values for the  $\lambda$ 's obtained above into Eq. (3.157), we see that the equation is identically satisfied.

The velocity at the control point of the *i*th panel can be obtained from Eq. (3.156). In that equation, the integral over the *j*th panel is a geometric quantity which is evaluated in a similar manner as before. The result is

$$\int \frac{\partial}{\partial s} (\ln r_\eta) ds_j = \frac{D - AC}{2E} \ln \frac{S_j^2 + 2AS_j + B}{B} - C \left( \tan^{-1} \frac{S_j + A}{E} - \tan^{-1} \frac{A}{E} \right) \quad (3.165)$$

With the integrals in Eq. (3.156) evaluated by Eq. (3.165), and with the values for  $\lambda_1, \lambda_2, \dots, \lambda_8$  obtained above inserted into Eq. (3.156), we obtain the velocities  $V_1, V_2, \dots, V_8$ . In turn, the pressure coefficients  $C_{p,1}, C_{p,2}, \dots, C_{p,8}$  are obtained directly from

$$C_{p,i} = 1 - \left( \frac{V_i}{V_\infty} \right)^2$$

Results for the pressure coefficients obtained from this calculation are compared with the exact analytical result Eq. (3.101) in Fig. 3.34. Amazingly enough, in spite of the relatively crude paneling shown in Fig. 3.32, the numerical pressure coefficient results are excellent.

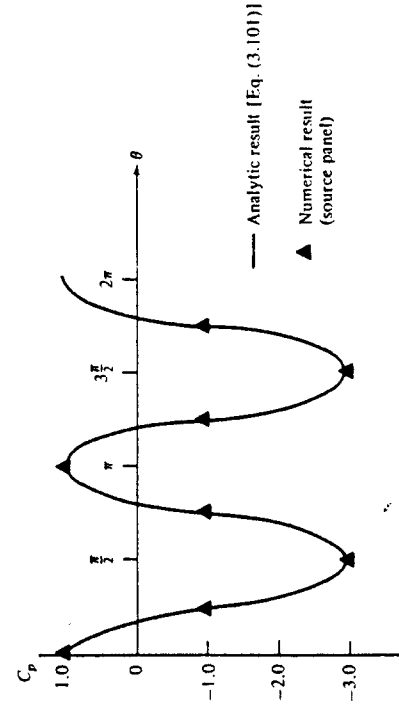


Figure 3.34 Pressure distribution over a circular cylinder; comparison of the source panel results and theory.

### 3.18 HISTORICAL NOTE: BERNOULLI AND EULER— THE ORIGINS OF THEORETICAL FLUID DYNAMICS

Bernoulli's equation, expressed by Eqs. (3.14) and (3.15), is historically the most famous equation in fluid dynamics. Moreover, we derived Bernoulli's equation from the general momentum equation in partial differential equation form. The momentum equation is just one of the three fundamental equations of fluid dynamics—the others being continuity and energy. These equations are derived and discussed in Chap. 2 and applied to an incompressible flow in Chap. 3. Where did these equations first originate? How old are they, and who is responsible for them? Considering the fact that all of fluid dynamics in general, and aerodynamics in particular, is built on these fundamental equations, it is important to pause for a moment and examine their historical roots.

As discussed in Sec. 1.1, Isaac Newton, in his *Principia* of 1687, was the first to establish on a rational basis the relationships between force, momentum, and acceleration. Although he tried, he was unable to apply these concepts properly to a moving fluid. The real foundations of theoretical fluid dynamics were not laid until the next century—developed by a triumvirate consisting of David Bernoulli, Leonhard Euler, and Jean Le Rond d'Alembert.

First, consider Bernoulli. Actually, we must consider the whole family of Bernoulli's because Daniel Bernoulli was a member of a prestigious family that dominated European mathematics and physics during the early part of the eighteenth century. Figure 3.35 is a portion of the Bernoulli family tree. It starts with Niklaus Bernoulli, who was a successful merchant and druggist in Basel, Switzerland, during the seventeenth century. With one eye on this family tree, let us simply list some of the subsequent members of this highly accomplished family:

1. Jakob—Daniel's uncle. Mathematician and physicist, he was professor of mathematics at the University of Basel. He made major contributions to the development of calculus and coined the term "integral."
2. Johann—Daniel's father. He was a professor of mathematics at Groningen, Netherlands, and later at the University of Basel. He taught the famous French and Jean Le Rond d'Alembert.

Niklaus Bernoulli

mathematician L'Hospital the elements of calculus, and after the death of Newton in 1727 he was considered Europe's leading mathematician at that time.

3. Niklaus—Daniel's cousin. He studied mathematics under his uncles and held a master's degree in mathematics and a doctor of jurisprudence.
4. Niklaus—Daniel's brother. He was Johann's favorite son. He held a master of arts degree, and assisted with much of Johann's correspondence to Newton and Liebniz concerning the development of calculus.
5. Daniel himself—to be discussed below.
6. Johann—Daniel's other brother. He succeeded his father in the Chair of Mathematics at Basel and won the Prize of the Paris Academy four times for his work.
7. Johann—Daniel's nephew. A gifted child, he earned the master of jurisprudence at the age of 14. When he was 20, he was invited by Frederick II to reorganize the astronomical observatory at the Berlin Academy.
8. Jakob—Daniel's other nephew. He graduated in jurisprudence but worked in mathematics and physics. He was appointed to the Academy in St. Petersburg, Russia, but he had a promising career prematurely ended with he drowned in the river Neva at the age of 30.

With such a family pedigree, Daniel Bernoulli was destined for success.

Daniel Bernoulli was born in Groningen, Netherlands, on February 8, 1700. His father, Johann, was a professor at Groningen but returned to Basel, Switzerland, in 1705 to occupy the Chair of Mathematics which had been vacated by the death of Jacob Bernoulli. At the University of Basel, Daniel obtained a master's degree in 1716 in philosophy and logic. He went on to study medicine in Basel, Heidelberg, and Strasbourg, obtaining his Ph. D. in anatomy and botany in 1721. During these studies, he maintained an active interest in mathematics. He followed this interest by moving briefly to Venice, where he published an important work entitled *Exercitationes Mathematicae* in 1724. This earned him much attention and resulted in his winning the prize awarded by the Paris Academy—the first of 10 he was eventually to receive. In 1725, Daniel moved to St. Petersburg, Russia, to join the academy. The St. Petersburg Academy had gained a substantial reputation for scholarship and intellectual accomplishment at that time. During the next 8 years, Bernoulli experienced his most creative period. While at St. Petersburg, he wrote his famous book *Hydrodynamica*, completed in 1734, but not published until 1738. In 1733, Daniel returned to Basel to occupy the Chair of Anatomy and Botany, and in 1750 moved to the Chair of Physics created exclusively for him. He continued to write, give very popular and well-attended lectures in physics, and make contributions to mathematics and physics until his death in Basel on March 17, 1782.

Daniel Bernoulli was famous in his own time. He was a member of virtually all the existing learned societies and academies, such as Bologna, St. Petersburg, Berlin, Paris, London, Bern, Turin, Zurich, and Mannheim. His importance to fluid dynamics is centered on his book *Hydrodynamica* (1738). (With this book, Daniel introduced the term "hydrodynamics" to the literature.) In this book, he ranged over such topics as jet propulsion, manometers, and flow in pipes. Of most importance, he attempted to obtain a relationship between pressure and velocity. Unfortunately, his derivation was somewhat obscure, and Bernoulli's equation, ascribed by history to Daniel via his

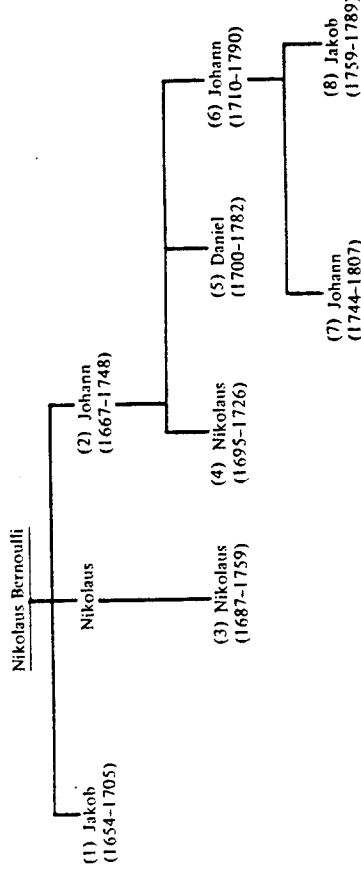


Figure 3.35 Bernoulli's family tree.

*Hydrodynamica*, is not to be found in this book, at least not in the form we see it today [such as Eqs. (3.14) and (3.15)]. The propriety of Eqs. (3.14) and (3.15) is further complicated by his father, Johann, who also published a book in 1743 entitled *Hydraulica*. It is clear from this latter book that the father understood Bernoulli's theorem better than his son; Daniel thought of pressure strictly in terms of the height of a manometer column, whereas Johann had the more fundamental understanding that pressure was a force acting on the fluid. (It is interesting to note that Johann Bernoulli was a person of some sensitivity and irritability, with an overpowering drive for recognition. He tried to undercut the impact of Daniel's *Hydrodynamica* by predating the publication date of *Hydraulica* to 1728, to make it appear to have been the first of the two. There was little love lost between son and father.)

During Daniel Bernoulli's most productive years, partial differential equations had not yet been introduced into mathematics and physics; hence, he could not approach the derivation of Bernoulli's equation in the same fashion as we have in Sec. 3.2. The introduction of partial differential equations to mathematical physics was due to d'Alembert in 1747. d'Alembert's role in fluid mechanics is detailed in Sec. 3.20. Suffice it to say here that his contributions were equally if not more important than Bernoulli's, and d'Alembert represents the second member of the triumvirate which molded the foundations of theoretical fluid dynamics in the eighteenth century.

The third and probably pivotal member of this triumvirate was Leonhard Euler. He was a giant among eighteenth-century mathematicians and scientists. As a result of his contributions, his name is associated with numerous equations and techniques, e.g., the Euler numerical solution of ordinary differential equations, eulerian angles in geometry, and the momentum equations for inviscid fluid flow [see Eq. (3.12)].

Leonhard Euler was born on April 15, 1707, in Basel, Switzerland. His father was a Protestant minister who enjoyed mathematics as a pastime. Therefore, Euler grew up in a family atmosphere that encouraged intellectual activity. At the age of 13, Euler entered the University of Basel which at that time had about 100 students and 19 professors. One of those professors was Johann Bernoulli, who tutored Euler in mathematics. Three years later, Euler received his master's degree in philosophy.

It is interesting that three of the people most responsible for the early development of theoretical fluid dynamics — Johann and Daniel Bernoulli and Euler — lived in the same town of Basel, were associated with the same university, and were contemporaries. Indeed, Euler and the Bernoulli's were close and respected friends — so much that, when Daniel Bernoulli moved to teach and study at the St. Petersburg Academy in 1725, he was able to convince the academy to hire Euler as well. At this invitation, Euler left Basel for Russia; he never returned to Switzerland, although he remained a Swiss citizen throughout his life.

Euler's interaction with Daniel Bernoulli in the development of fluid mechanics grew strong during these years at St. Petersburg. It was here that Euler conceived of pressure as a point property that can vary from point to point throughout a fluid and obtained a differential equation relating pressure and velocity, i.e., *Euler's equation* given by Eq. (3.12). In turn, Euler integrated the differential equation to obtain, for the first time in history, Bernoulli's equation in the form of Eq. (3.14) and (3.15). Hence, we see that Bernoulli's equation is really a misnomer; credit for it is legitimately shared by Euler.

When Daniel Bernoulli returned to Basel in 1733, Euler succeeded him at St. Petersburg as a professor of physics. Euler was a dynamic and prolific man; by 1741 he had prepared 90 papers for publication and written the two-volume book *Mechanica*. The atmosphere surrounding St. Petersburg was conducive to such achievement. Euler wrote in 1749: "I and all others who had the good fortune to be for some time with the Russian Imperial Academy cannot but acknowledge that we owe everything which we are and possess to the favorable conditions which we had there."

However, in 1740, political unrest in St. Petersburg caused Euler to leave for the Berlin Society of Sciences, at that time just formed by Frederick the Great. Euler lived in Berlin for the next 25 years, where he transformed the society into a major academy. In Berlin, Euler continued his dynamic mode of working, preparing at least 380 papers for publication. Here, as a competitor with d'Alembert (see Sec. 3.20), Euler formulated the basis for mathematical physics.

In 1766, after a major disagreement with Frederick the Great over some financial aspects of the academy, Euler moved back to St. Petersburg. His second period of his life in Russia became one of physical suffering. In that same year, he became blind in one eye after a short illness. An operation in 1771 resulted in restoration of his sight, but only for a few days. He did not take proper precautions after the operation, and within a few days, he was completely blind. However, with the help of others, he continued his work. His mind was as sharp as ever, and his spirit did not diminish. His literary output even increased — about half of his total papers were written after 1765!

On September 18, 1783, Euler conducted business as usual — giving a mathematics lesson, making calculations of the motion of balloons, and discussing with friends the planet of Uranus, which had recently been discovered. At about 5 p.m., he suffered a brain hemorrhage. His only words before losing consciousness were "I am dying." By 11 p.m., one of the greatest minds in history had ceased to exist.

With the lives of Bernoulli, Euler, and d'Alembert (see Sec. 3.20) as background, let us now trace the genealogy of the basic equations of fluid dynamics. For example, d'Alembert gave a paper in Paris, entitled "Essai d'une nouvelle theorie de la resistance des fluides," in which he formulated differential equations for the conservation of mass in special applications to plane and axisymmetric flows. Euler took d'Alembert's results and, 8 years later, generalized them in a series of three basic papers on fluid mechanics. In these papers, Euler published, for the first time in history, the continuity equation in the form of Eq. (2.43) and the momentum equations in the form of Eqs. (2.104a to c), without the viscous terms. Hence, two of the three basic conservation equations used today in modern fluid dynamics were well established long before the American Revolutionary War — such equations were contemporary with the time of George Washington and Thomas Jefferson!

The origin of the energy equation in the form of Eq. (2.87) without viscous terms has its roots in the development of thermodynamics in the nineteenth century. Its precise first use is obscure and is buried somewhere in the rapid development of physical science in the nineteenth century.

The purpose of this section has been to give you some feeling for the historical development of the fundamental equations of fluid dynamics. Maybe we can appreciate these equations more when we recognize that they have been with us for quite some time and that they are the product of much thought from some of the greatest minds of the eighteenth century.

### 3.19 HISTORICAL NOTE: d'ALEMBERT AND HIS PARADOX

You can well imagine the frustration that Jean le Rond d'Alembert felt in 1744 when, in a paper, entitled "Traité de l'équilibre et des mouvements de fluids pour servir de suite au traité de dynamique," he obtained the result of zero drag for the inviscid, incompressible flow over a closed two-dimensional body. Using different approaches, d'Alembert encountered this result again in 1752 in his paper entitled "Essai sur la resistance" and again in 1768 in his "Opuscules mathématiques." In this last paper can be found the quote given at the beginning of Chap. 15; in essence, he had given up trying to explain the cause of this paradox. Even though the prediction of fluid-dynamic drag was a very important problem in d'Alembert's time, and in spite of the number of great minds that addressed it, the fact that viscosity is responsible for drag was not appreciated. Instead, d'Alembert's analyses used momentum principles in a frictionless flow, and quite naturally he found that the flow field closed smoothly around the downstream portion of the bodies, resulting in zero drag. Who was this man, d'Alembert? Considering the role his paradox played in the development of fluid dynamics, it is worth our time to take a closer look at the man himself.

d'Alembert was born illegitimately in Paris on November 17, 1717. His mother was Madame De Tenun, a famous salon hostess of that time, and his father was Chevalier Destouches-Canon, a cavalry officer. d'Alembert was immediately abandoned by his mother (she was an ex-nun who was afraid of being forceably returned to the convent). However, his father quickly arranged for a home for d'Alembert — with a family of modest means named Rousseau. d'Alembert lived with this family for the next 47 years. Under the support of his father, d'Alembert was educated at the Collège de Quatre-Nations, where he studied law and medicine, and later turned to mathematics. For the remainder of his life, d'Alembert would consider himself a mathematician. By a program of self-study, d'Alembert learned the works of Newton and the Bernoulli's. His early mathematics caught the attention of the Paris Academy of Sciences, of which he became a member in 1741. d'Alembert published frequently and sometimes rather hastily, in order to be in print before his competition. However, he made substantial contributions to the science of his time. For example, he was (1) the first to formulate the wave equation of classical physics, (2) the first to express the concept of a partial differential equation — he used separation of variables — and (4) the first to express the differential equations of fluid dynamics in terms of a field. His contemporary Leonhard Euler (see Secs. 1.1 and 3.18) later expanded greatly on these equations and was responsible for developing them into a truly rational approach for fluid-dynamic analysis.

During the course of his life, d'Alembert became interested in many scientific and mathematical subjects, including vibrations, wave motion, and celestial mechanics. In

the 1750s he had the honored position of science editor for the *Encyclopédia* — a major French intellectual endeavor of the eighteenth century which attempted to compile all existing knowledge into a large series of books. As he grew older, he also wrote papers on nonscientific subjects, mainly musical structure, law, and religion.

In 1765, d'Alembert became very ill. He was helped to recover by the nursing of Mlle. Julie de Lespinasse, the woman who was d'Alembert's only love throughout his life. Although he never married, d'Alembert lived with Julie de Lespinasse until she died in 1776. d'Alembert had always been a charming gentleman, renowned for his intelligence, gaiety, and considerable conversational ability. However, after Mlle. de Lespinasse's death, he became frustrated and morose — living a life of despair. He died in this condition on October 29, 1783, in Paris.

d'Alembert was one of the great mathematicians and physicists of the eighteenth century. He maintained active communications and dialogue with both Bernoulli and Euler and ranks with them as one of the founders of modern fluid dynamics. This, then, is the man behind the paradox, which has existed as an integral part of fluid dynamics for the past two centuries.

### 3.20 SUMMARY

Return to the road map given in Fig. 3.4. Examine each block of the road map to remind yourself of the route we have taken in this discussion of the fundamentals of inviscid, incompressible flow. Before proceeding further, make certain that you feel comfortable with the detailed material represented by each block, and how each block is related to the overall flow of ideas and concepts.

For your convenience, some of the highlights of this chapter are summarized below.

*Bernoulli's equation:*

$$p + \frac{1}{2} \rho V^2 = \text{const}$$

- (a) Applies to inviscid, incompressible flows only.
- (b) Holds along a streamline for a rotational flow.
- (c) Holds at every point throughout an irrotational flow.
- (d) In the form given above, body forces (such as gravity) are neglected, and steady flow is assumed.

*Quasi-one-dimensional continuity equation:*

$\rho AV = \text{const}$	(for compressible flow)
$AV = \text{const}$	(for incompressible flow)

From a measurement of the Pitot pressure  $p_0$  and static pressure  $p_1$ , the velocity of an incompressible flow is given by

$$V_1 = \sqrt{\frac{2(p_0 - p_1)}{\rho}} \quad (3.34)$$

#### Pressure coefficient:

$$\text{Definition: } C_p = \frac{p - p_\infty}{q_\infty} \quad (3.36)$$

where dynamic pressure is  $q_\infty \equiv \frac{1}{2}\rho_\infty V_\infty^2$ .

$$\text{For incompressible steady flow with no friction: } C_p = 1 - \left(\frac{V}{V_\infty}\right)^2 \quad (3.38)$$

#### Governing equations:

$$\nabla \cdot \mathbf{V} = 0 \quad (\text{condition of incompressibility}) \quad (3.39)$$

$$\nabla^2 \phi = 0 \quad (\text{Laplace's equation; holds for irrotational, incompressible flow}) \quad (3.40)$$

$$\nabla^2 \psi = 0$$

#### Boundary conditions:

$$u = \frac{\partial \phi}{\partial x} = \frac{\partial \psi}{\partial y} = V_\infty \quad \text{at infinity}$$

$$v = \frac{\partial \phi}{\partial y} = -\frac{\partial \psi}{\partial x} = 0$$

$$\mathbf{V} \cdot \mathbf{n} = 0 \quad \text{at body (flow tangency condition)}$$

$$\psi = \frac{\Lambda}{2\pi} \theta \quad (3.72)$$

$$V_r = \frac{\Lambda}{2\pi r} \quad V_\theta = 0 \quad (3.62)$$

$$(c) \text{ Doublet flow: } \phi = \frac{\kappa}{2\pi} \frac{\cos \theta}{r} \quad (3.88)$$

$$\psi = -\frac{\kappa}{2\pi} \frac{\sin \theta}{r} \quad (3.87)$$

$$(d) \text{ Vortex flow: } \phi = -\frac{\Gamma}{2\pi} \theta \quad (3.112)$$

$$\psi = \frac{\Gamma}{2\pi} \ln r \quad (3.114)$$

$$V_\theta = -\frac{\Gamma}{2\pi r} \quad V_r = 0 \quad (3.105)$$

#### Inviscid flow over a cylinder:

##### (a) Nonlifting (uniform flow and doublet)

$$\psi = (V_\infty r \sin \theta) \left( 1 - \frac{R^2}{r^2} \right) \quad (3.92)$$

where  $R$  = radius of cylinder =  $\kappa/2\pi V_\infty$ .

Surface velocity:  $V_\theta = -2V_\infty \sin \theta$

Surface pressure coefficient:  $C_p = 1 - 4 \sin^2 \theta$

$$L = D = 0$$

##### (b) Lifting (uniform flow + doublet + vortex)

$$\psi = (V_\infty r \sin \theta) \left( 1 - \frac{R^2}{r^2} \right) + \frac{\Gamma}{2\pi} \ln \frac{r}{R} \quad (3.118)$$

$$\text{Surface velocity: } V_\theta = -2V_\infty \sin \theta - \frac{\Gamma}{2\pi R} \quad (3.125)$$

$$L' = \rho_s V_\infty \Gamma \quad (\text{lift per unit span})$$

$$D = 0$$

$$(b) \text{ Source flow: } \phi = \frac{\Lambda}{2\pi} \ln r \quad (3.67)$$

#### Elementary flows:

$$(a) \text{ Uniform flow: } \phi = V_\infty x = V_\infty r \cos \theta \quad (3.53)$$

$$\psi = V_\infty y = V_\infty r \sin \theta \quad (3.55)$$

$$(b) \text{ Source flow: } \phi = \frac{\Lambda}{2\pi} \ln r$$

**Kutta-Joukowski theorem:** For a closed two-dimensional body of arbitrary shape, the lift per unit span is  $L' = \rho_x V_x \Gamma$ .

**Source panel method:** This is a numerical method for calculating the nonlifting flow over bodies of arbitrary shape. Governing equations:

$$\frac{\lambda_i}{2} + \sum_{j=1}^n \frac{\lambda_j}{2\pi} \int_j \frac{\partial}{\partial n_j} (\ln r_{ij}) d\delta_j + V_x \cos \beta_i = 0 \quad (i = 1, 2, \dots, n) \quad (3.152)$$

## PROBLEMS

**Note:** All the following problems assume an inviscid, incompressible flow. Also, standard sea level density and pressure are  $1.23 \text{ kg/m}^3$  ( $0.002377 \text{ slug/ft}^3$ ) and  $1.01 \times 10^5 \text{ N/m}^2$  ( $2116 \text{ lb/ft}^2$ ), respectively.

3.1 For an irrotational flow, show that Bernoulli's equation holds between any points in the flow, not just along a streamline.

3.2 Consider a venturi with a throat-to-inlet area ratio of 0.8, mounted on the side of an airplane fuselage. The airplane is in flight at standard sea level. If the static pressure at the throat is  $2100 \text{ lb/in}^2$ , calculate the velocity of the airplane.

3.3 Consider a venturi with a small hole drilled in the side of the throat. This hole is connected via a tube to a closed reservoir. The purpose of the venturi is to create a vacuum in the reservoir when the venturi is placed in an airstream. (The *vacuum* is defined as the pressure difference *below* the outside ambient pressure.) The venturi has a throat-to-inlet area ratio of 0.85. Calculate the maximum vacuum obtainable in the reservoir when the venturi is placed in an airstream of  $90 \text{ m/s}$  at standard sea level conditions.

3.4 Consider a low-speed open-circuit subsonic wind tunnel with an inlet-to-throat area ratio of 12. The tunnel is turned on, and the pressure difference between the inlet (the settling chamber) and the test section is read as a height difference of 10 cm on a U-tube mercury manometer. (The density of liquid mercury is  $1.36 \times 10^4 \text{ kg/m}^3$ .) Calculate the velocity of the air in the test section.

3.5 Assume that a Pitot tube is inserted into the test-section flow of the wind tunnel in Prob. 3.4. The tunnel test section is completely sealed from the outside ambient pressure. Calculate the pressure measured by the Pitot tube, assuming the static pressure at the tunnel inlet is atmospheric.

3.6 A Pitot tube on an airplane flying at standard sea level reads  $1.07 \times 10^5 \text{ N/m}^2$ . What is the velocity of the airplane?

3.7 At a given point on the surface of the wing of the airplane in Prob. 3.6, the flow velocity is  $130 \text{ m/s}$ . Calculate the pressure coefficient at this point.

3.8 Consider a uniform flow with velocity  $V_x$ . Show that this flow is a physically possible incompressible flow and that it is irrotational everywhere.

3.9 Show that a source flow is a physically possible incompressible flow everywhere except at the origin. Also show that it is irrotational everywhere.

3.10 Prove that the velocity potential and the stream function for a uniform flow, Eqs. (3.53) and (3.55), respectively, satisfy Laplace's equation.

3.11 Prove that the velocity potential and the stream function for a source flow, Eqs. (3.67) and (3.72), respectively, satisfy Laplace's equation.

3.12 Consider the flow over a semi-infinite body as discussed in Sec. 3.11. If  $V_x$  is the velocity of the uniform stream, and the stagnation point is 1 ft upstream of the source:

- (a) Draw the resulting semi-infinite body to scale on graph paper.

(b) Plot the pressure coefficient distribution over the body; i.e., plot  $C_p$  versus distance along the centerline of the body.

3.13 Derive Eq. (3.81). *Hint:* Make use of the symmetry of the flow field shown in Fig. 3.16; i.e., start with the knowledge that the stagnation points must lie on the axis aligned with the direction of  $V_x$ .

3.14 Derive the velocity potential for a doublet; i.e., derive Eq. (3.88). *Hint:* The easiest method is to start with Eq. (3.87) for the stream function and extract the velocity potential.

3.15 Consider the nonlifting flow over a circular cylinder. Derive an expression for the pressure coefficient at an arbitrary point  $(r, \theta)$  in this flow, and show that it reduces to Eq. (3.101) on the surface of the cylinder.

3.16 Consider the nonlifting flow over a circular cylinder of a given radius, where  $V_x = 20 \text{ ft/s}$ . If  $V_x$  is doubled, that is,  $V_x = 40 \text{ ft/s}$ , does the shape of the streamlines change? Explain.

3.17 Consider the lifting flow over a circular cylinder of a given radius and with a given circulation. If  $V_x$  is doubled, keeping the circulation the same, does the shape of the streamlines change? Explain.

3.18 The lift on a spinning circular cylinder in a free stream with a velocity of  $30 \text{ m/s}$  and at standard sea level conditions is  $6 \text{ N/m}$  of span. Calculate the circulation around the cylinder.

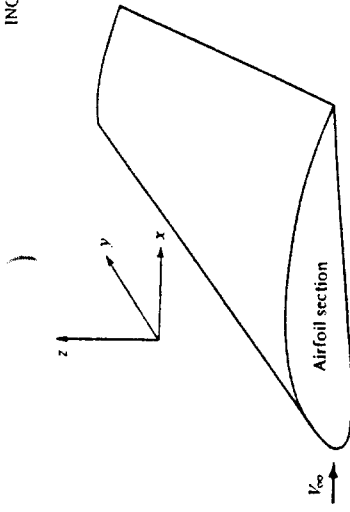


Figure 4.1 Definition of an airfoil section.

*Of the many problems now engaging attention, the following are considered of immediate importance and will be considered by the committee as rapidly as funds can be secured for the purpose. . . . The evolution of more efficient wing sections of practical form, embodying suitable dimensions for an economical structure, with moderate travel of the center-of-pressure and still affording a large range of angle-of-attack combined with efficient action.*

*From the First Annual Report of the NACA, 1915*

## 4.1 INTRODUCTION

With the advent of successful powered flight at the turn of the twentieth century, the importance of aerodynamics ballooned almost overnight. In turn, interest grew in the understanding of the aerodynamic action of such lifting surfaces as fixed wings on airplanes and, later, rotors on helicopters. In the period 1912–1918, the analysis of airplane wings took a giant step forward when Ludwig Prandtl and his colleagues at Göttingen, Germany, showed that the aerodynamic consideration of wings could be split into two parts: (1) the study of the *section* of a wing—an airfoil—and (2) the modification of such airfoil properties to account for the complete, finite wing. This approach is still used today; indeed, the theoretical calculation and experimental measurement of modern airfoil properties have been a major part of the aeronautics research carried out by the National Aeronautics and Space Administration (NASA) in the 1970s and 1980s. (See chapter 5 of Ref. 2 for a historical sketch on airfoil development and Ref. 10 for a description of modern airfoil research.) Following Prandtl's philosophy, the present chapter deals exclusively with airfoils, whereas Chap. 5 treats the case of a complete, finite wing. Therefore, in this chapter and Chap. 5, we make a major excursion into aerodynamics as applied to airplanes.

What is an airfoil? Consider a wing as drawn in perspective in Fig. 4.1. The wing extends in the *y* direction (the span direction). The freestream velocity  $V_\infty$  is parallel to the

*xz* plane. Any section of the wing cut by a plane parallel to the *xz* plane is called an *airfoil*. The purpose of this chapter is to present theoretical methods for the calculation of airfoil properties. Since we are dealing with inviscid flow, we are not able to predict airfoil drag; indeed, d'Alembert's paradox says that the drag on an airfoil is zero—clearly not a realistic answer. We will have to wait until Chap. 15 and a discussion of viscous flow before predictions of drag can be made. However, the lift and moments on the airfoil are due mainly to the pressure distribution, which (below the stall) is dictated by inviscid flow. Therefore, this chapter concentrates on the theoretical prediction of airfoil lift and moments.

The road map for this chapter is given in Fig. 4.2. After some initial discussion on airfoil nomenclature and characteristics, we present two approaches to low-speed airfoil theory. One is the classical thin airfoil theory developed during the period 1910–1920 (the right-hand branch of Fig. 4.2). The other is the modern numerical approach for arbitrary airfoils using vortex panels (the left-hand branch of Fig. 4.2). Please refer to this road map as you work your way through this chapter.

## 4.2 AIRFOIL NOMENCLATURE

The first patented airfoil shapes were developed by Horatio F. Phillips in 1884. Phillips was an Englishman who carried out the first serious wind-tunnel experiments on airfoils. In 1902, the Wright brothers conducted their own airfoil tests in a wind tunnel, developing relatively efficient shapes which contributed to their successful first flight on December 17, 1903 (see Sec. 1.1). Clearly, in the early days of powered flight, airfoil design was basically customized and personalized. However, in the early 1930s, the National Advisory Committee for Aeronautics (NACA)—the forerunner of NASA—embarked on a series of definitive airfoil experiments using airfoil shapes that were constructed rationally and systematically. Many of these NACA airfoils are in common use today. Therefore, in this chapter we follow the nomenclature established by the NACA; such nomenclature is now a well-known standard.

Consider the airfoil sketched in Fig. 4.3. The *mean camber line* is the locus of points halfway between the upper and lower surfaces as measured perpendicular to the mean camber line itself. The most forward and rearward points of the mean camber line

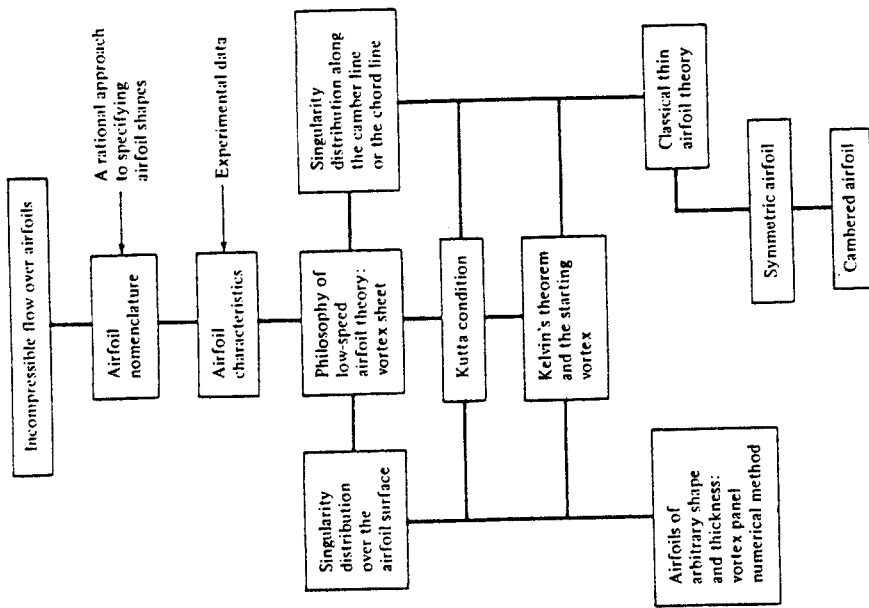


Figure 4.2 Road map for Chap. 4.

are the *leading* and *trailing edges*, respectively. The straight line connecting the leading and trailing edges is the *chord line* of the airfoil, and the precise distance from the leading to the trailing edge measured along the chord line is simply designated the *chord*  $c$  of the airfoil. The *camber* is the maximum distance between the mean camber line and the chord line, measured perpendicular to the chord line. The *thickness* is the

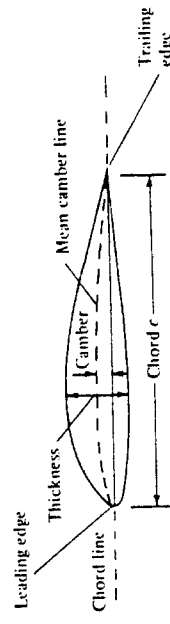


Figure 4.3 Airfoil nomenclature.

distance between the upper and lower surfaces, also measured perpendicular to the chord line. The shape of the airfoil at the leading edge is usually circular, with a leading edge radius of approximately  $0.02c$ . The shapes of all standard NACA airfoils are generated by specifying the shape of the mean camber line and then wrapping a specified symmetrical thickness distribution around the mean camber line.

The force-and-moment system on an airfoil was discussed in Sec. 1.5, and the relative wind, angle of attack, lift, and drag were defined in Fig. 1.10. You should review these considerations before proceeding further.

The NACA identified different airfoil shapes with a logical numbering system. For example, the first family of NACA airfoils, developed in the 1930s, was the "four-digit" series, such as the NACA 2412 airfoil. Here, the first digit is the maximum camber in hundredths of chord, the second digit is the location of maximum camber along the chord from the leading edge in tenths of chord, and the last two digits give the maximum thickness in hundredths of chord. For the NACA 2412 airfoil, the maximum camber is  $0.02c$  located at  $0.4c$  from the leading edge, and the maximum thickness is  $0.12c$ . It is common practice to state these numbers in percent of chord, i.e., 2 percent camber at 40 percent chord, with 12 percent thickness. An airfoil with no camber, i.e., with the camber line and chord line coincident, is called a *symmetric airfoil*. Clearly, the shape of a symmetric airfoil is the same above and below the chord line. For example, the NACA 0012 airfoil is a symmetric airfoil with a maximum thickness of 12 percent.

The second family of NACA airfoils was the "five-digit" series, such as the NACA 23012 airfoil. Here, the first digit when multiplied by  $\frac{1}{10}$  gives the design lift coefficient in tenths, the next two digits when divided by 2 give the location of maximum camber along the chord from the leading edge in hundredths of chord, and the final two digits give the maximum thickness in hundredths of chord. For the NACA 23012 airfoil, the design lift coefficient is 0.3, the location of maximum camber is at  $0.15c$ , and the airfoil has 12 percent maximum thickness.

One of the most widely used family of NACA airfoils is the "6-series" laminar flow airfoils, developed during World War II. An example is the NACA 65-218. Here, the first digit simply identifies the series, the second gives the location of minimum pressure in tenths of chord from the leading edge (for the basic symmetric thickness distribution at zero lift), the third digit is the design lift coefficient in tenths, and the last two digits give the maximum thickness in hundredths of chord. For the NACA 65-218 airfoil, the 6 is the series designation, the minimum pressure occurs at 0.5c for the basic symmetric thickness distribution at zero lift, the design lift coefficient is 0.2, and the airfoil is 18 percent thick.

The complete NACA airfoil numbering system is given in Ref. 11. Indeed, Ref. 11 is a definitive presentation of the classic NACA airfoil work up to 1949. It contains a discussion of airfoil theory, its application, coordinates for the shape of NACA airfoils, and a huge bulk of experimental data for these airfoils. This author strongly encourages you to read Ref. 11 for a thorough presentation of airfoil characteristics.

<sup>\*</sup> The design lift coefficient is the theoretical lift coefficient for the airfoil when the angle of attack is parallel to the freestream velocity.

As a matter of interest, the following is a short partial listing of airplanes in service in 1982 which use standard NACA airfoils.

Airplane	Airfoil
Beechcraft Sundowner	NACA 63A415
Beechcraft Bonanza	NACA 23016.5 (at root)
Cessna 150	NACA 23012 (at tip)
Fairchild A-10	NACA 2412
Gates Learjet 24D	NACA 6716 (at root)
General Dynamics F-16	NACA 6713 (at tip)
Lockheed C-5 Galaxy	NACA 6A109
	NACA 6A204
	NACA 0012 (modified)

In addition, many of the large aircraft companies today design their own special-purpose airfoils; e.g., the Boeing 727, 737, 747, 757, and 767 all have specially designed Boeing airfoils. Such capability is made possible by modern airfoil design computer programs utilizing either panel techniques or direct numerical finite-difference solutions of the governing partial differential equations for the flow field. (Such equations are developed in Chap. 2.)

### 4.3 AIRFOIL CHARACTERISTICS

Before discussing the theoretical calculation of airfoil properties, let us examine some typical results. During the 1930s and 1940s, the NACA carried out numerous measurements of the lift, drag, and moment coefficients on the standard NACA airfoils. These experiments were performed at low speeds in a wind tunnel where the constant-chord wing spanned the entire test section from one sidewall to the other. In this fashion, the flow "sees" a wing without wing tips—a so-called infinite wing, which theoretically stretches to infinity along the span (in the  $y$  direction in Fig. 4.1). Because the airfoil section is the same at any spanwise location along the infinite wing, the properties of the airfoil and the infinite wing are identical. Hence, airfoil data are frequently called infinite wing data. (In contrast, we see in Chap. 5 that the properties of a finite wing are somewhat different than its airfoil properties.)

The typical variation of lift coefficient with angle of attack for an airfoil is sketched in Fig. 4.4. At low-to-moderate angles of attack,  $c_l$  varies linearly with  $\alpha$ ; the slope of this straight line is denoted by  $a_0$  and is called the *lift slope*. In this region, the flow moves smoothly over the airfoil and is attached over most of the surface, as shown in the streamline picture at the left of Fig. 4.4. However, as  $\alpha$  becomes large, the flow tends to separate from the top surface of the airfoil, creating a large wake of relatively "dead air" behind the airfoil as shown at the right of Fig. 4.4. Inside this separated region, the flow is recirculating, and part of the flow is actually moving in a direction opposite to the freestream—so-called reversed flow. (Refer also to Fig. 1.25.) This

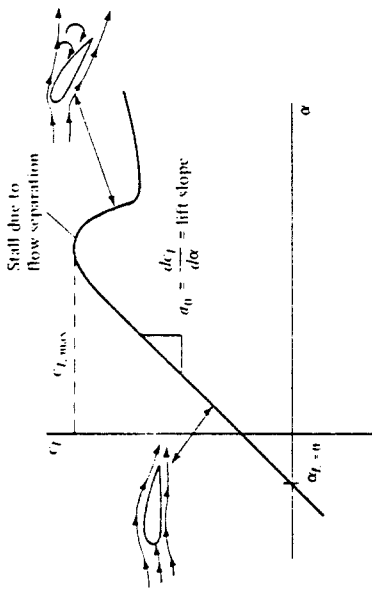


Figure 4.4 Schematic of lift-coefficient variation with angle of attack for an airfoil.

separated flow is due to viscous effects and is discussed in Chap. 15. The consequence of this separated flow at high  $\alpha$  is a precipitous decrease in lift and a large increase in drag; under such conditions the airfoil is said to be *stalled*. The maximum value of  $c_l$ , which occurs just prior to the stall, is denoted by  $c_{l,\max}$ ; it is one of the most important aspects of airfoil performance, because it determines the stalling speed of an airplane. The higher is  $c_{l,\max}$ , the lower is the stalling speed. A great deal of modern airfoil research has been directed toward increasing  $c_{l,\max}$ . Again examining Fig. 4.4, we see that  $c_l$  increases linearly with  $\alpha$  until flow separation begins to have an effect. Then the curve becomes nonlinear,  $c_l$  reaches a maximum value, and finally the airfoil stalls. At the other extreme of the curve, noting Fig. 4.4, the lift at  $\alpha = 0$  is finite; indeed, the lift goes to zero only when the airfoil is pitched to some negative angle of attack. The value of  $\alpha$  when lift equals zero is called the *zero-lift angle of attack* and is denoted by  $\alpha_{l=0}$ . For a symmetric airfoil,  $\alpha_{l=0} = 0$ , whereas for all airfoils with positive camber (camber above the chord line),  $\alpha_{l=0}$  is a negative value, usually on the order of  $-2$  or  $-3^\circ$ .

The inviscid flow airfoil theory discussed in this chapter allows us to predict the lift slope  $a_0$  and  $\alpha_{l=0}$  for a given airfoil. It does not allow us to calculate  $c_{l,\max}$ , which is a difficult viscous flow problem, to be discussed in Chaps. 15 and 16. Experimental results for lift and moment coefficients for the NACA 2412 airfoil are given in Fig. 4.5. Here, the moment coefficient is taken about the quarter-chord point. Recall from Sec. 1.6 that the force-and-moment system on an airfoil can be transferred to any convenient point; however, the quarter-chord point is commonly used. (Refresh your mind on this concept by reviewing Sec. 1.6, especially Fig. 1.17.) Also shown in Fig. 4.5 are theoretical results to be discussed later. Note that the experimental data are given for two different Reynolds numbers. The lift slope  $a_0$  is not influenced by  $Re$ ; however,  $c_{l,\max}$  is dependent upon  $Re$ . This makes sense, because  $c_{l,\max}$  is governed by viscous effects, and  $Re$  is a similarity parameter that governs the strength of inertia forces relative to viscous forces in the flow. [See Sec. 1.7 and Eq. (1.35).] The moment coefficient is also insensitive to  $Re$  except at large  $\alpha$ . The NACA 2412 airfoil is a commonly used airfoil, and the results given in Fig. 4.5 are

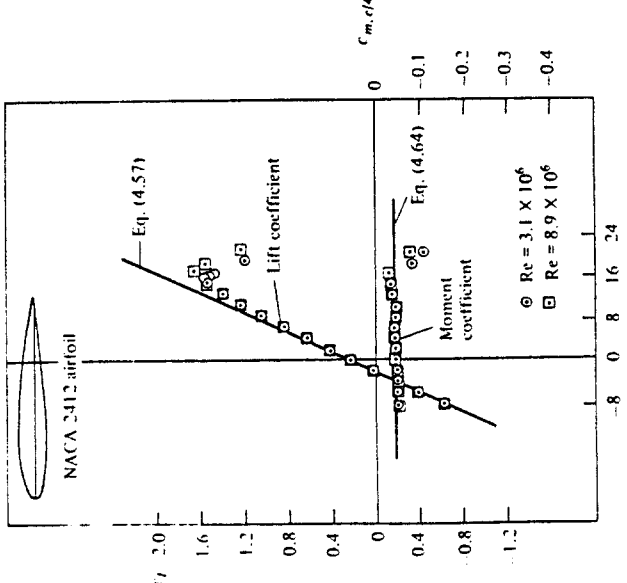


Figure 4.5 Experimental data for lift coefficient and moment coefficient about the quarter-chord point for an NACA 2412 airfoil. (Data obtained from Abbott and von Doenhoff, Ref. 11.) Also shown is a comparison with theory described in Sec. 4.8.

quite typical of airfoil characteristics. For example, note from Fig. 4.5 that  $c_{l,0} = -2.1^\circ$ ,  $c_{l,\max} \approx 1.6$ , and the stall occurs at  $\alpha \approx 16^\circ$ .

This chapter deals with airfoil theory for an inviscid, incompressible flow; such theory is incapable of predicting airfoil drag, as noted earlier. However, for the sake of completeness, experimental data for the drag coefficient  $c_d$  for the NACA 2412 airfoil are given in Fig. 4.6 as a function of the angle of attack  $\alpha$ . The physical source of this drag coefficient is both skin friction drag and pressure drag due to flow separation (so-called form drag). The sum of these two effects yields the profile drag coefficient  $c_d$  for the airfoil, which is plotted in Fig. 4.6. Note that  $c_d$  is sensitive to  $Re$ , which is to be expected since both skin friction and flow separation are viscous effects. Again, we must wait until Chaps. 15 and 16 to obtain some tools for theoretically predicting  $c_d$ .

Also plotted in Fig. 4.6 is the moment coefficient about the aerodynamic center  $c_{m,ac}$ . In general, moments on an airfoil are a function of  $\alpha$ . However, there is one point on the airfoil about which the moment is independent of angle of attack; such a point

<sup>†</sup>In many references, such as Ref. 11, it is common to plot  $c_d$  versus  $c_l$ , rather than  $c_l$ . A plot of  $c_d$  versus  $c_l$  is called a *drag polar*. For the sake of consistency with Fig. 4.5, we choose to plot  $c_d$  versus  $\alpha$  here.

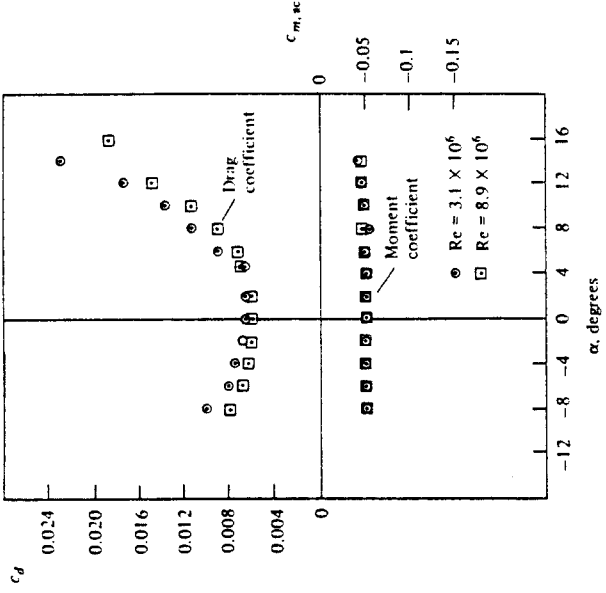


Figure 4.6 Experimental data for profile drag coefficient and moment coefficient about the aerodynamic center for the NACA 2412 airfoil. (Data from Abbott and von Doenhoff, Ref. 11.)

is defined as the *aerodynamic center*. Clearly, the data in Fig. 4.6 illustrate a constant value for  $c_{m,ac}$  over a wide range of  $\alpha$ .

For an elementary but extensive discussion of airfoil and wing properties, see chapter 5 of Ref. 2.

**SOLUTION** At standard sea level,  $\rho = 1.23 \text{ kg/m}^3$ .

$$q_s = \frac{1}{2} \rho V_s^2 = \frac{1}{2} (1.23) (70)^2 = 3013.5 \text{ N/m}^2$$

$$c_l = \frac{L'}{q_s S} = \frac{L'}{q_s C(1)} = \frac{1.254}{3013.5(0.64)} = 0.65$$

From Fig. 4.5, for  $c_l = 0.65$ , we obtain  $\alpha = 4^\circ$ .

To obtain the drag per unit span, we must use the data in Fig. 4.6. However, since  $c_d = f(Re)$ , let us calculate  $Re$ . At standard sea level,  $\mu = 1.789 \times 10^{-5} \text{ kg/(m} \cdot \text{s)}$ . Hence,

$$Re = \frac{\rho_s V_s C}{\mu_s} = \frac{1.23(70)(0.64)}{1.789 \times 10^{-5}} = 3.08 \times 10^6$$

Therefore, using the data for  $Re = 3.1 \times 10^6$  in Fig. 4.6, we find  $c_d = 0.0068$ . Thus,

$$\rho' - \rho, Sc_d - q_r c(1)c_d = 3013.5(0.64)(0.0068) = 13.1 \text{ N/m}$$

#### 4.4 PHILOSOPHY OF THEORETICAL SOLUTIONS FOR LOW-SPEED FLOW OVER AIRFOILS: THE VORTEX SHEET

In Sec. 3.14, the concept of vortex flow was introduced; refer to Fig. 3.23 for a schematic of the flow induced by a point vortex of strength  $\Gamma$  located at a given point  $O$ . (Recall that Fig. 3.23, with its counterclockwise flow, corresponds to a negative value of  $\Gamma$ . By convention, a positive  $\Gamma$  induces a clockwise flow.) Let us now expand our concept of a point vortex. Referring to Fig. 3.23, imagine a straight line perpendicular to the page, going through point  $O$ , and extending to infinity both out of and into the page. This line is a straight *vortex filament* of strength  $\Gamma$ . A straight vortex filament is drawn in perspective in Fig. 4.7. (Here we show a clockwise flow, which corresponds to a positive value of  $\Gamma$ .) The flow induced in any plane perpendicular to the straight vortex filament by the filament itself is identical to that induced by a point vortex of strength  $\Gamma$ ; i.e., in Fig. 4.7 the flows in the planes perpendicular to the vortex filament at  $O$  and  $O'$  are identical to each other and are identical to the flow induced by a point vortex of strength  $\Gamma$ . Indeed, the point vortex described in Sec. 3.14 is simply a section of a straight vortex filament.

In Sec. 3.17 we introduced the concept of a source sheet, which is an infinite number of line sources side by side, with the strength of each line source being in-

finitesimally small. For vortex flow, consider an analogous situation. Imagine an infinite number of straight vortex filaments side by side, where the strength of each filament is infinitesimally small. These side-by-side vortex filaments form a *vortex sheet*, as shown in perspective in the upper left of Fig. 4.8. If we look along the series of vortex filaments (looking along the  $y$  axis in Fig. 4.8), the vortex sheet will appear as sketched at the lower right of Fig. 4.8. Here, we are looking at an edge view of the sheet; the vortex filaments are all perpendicular to the page. Let  $s$  be the distance measured along the vortex sheet in the edge view. Define  $\gamma = \gamma(s)$  as the strength of the vortex sheet, per unit length along  $s$ . Thus, the strength of an infinitesimal portion  $ds$  of the sheet is  $\gamma ds$ . This small section of the vortex sheet can be treated as a distinct vortex of strength  $\gamma ds$ . Now consider point  $P$  in the flow, located a distance  $r$  from  $ds$ ; the cartesian coordinates of  $P$  are  $(x, z)$ . The small section of the vortex sheet of strength  $\gamma ds$  induces an infinitesimally small velocity,  $dV$ , at point  $P$ . From Eq. (3.105),  $dV$  is given by

$$(4.1) \quad dV = -\frac{\gamma ds}{2\pi r}$$

and is in a direction perpendicular to  $r$ , as shown in Fig. 4.8. The velocity at  $P$  induced by the entire vortex sheet is the summation of Eq. (4.1) from point  $a$  to point  $b$ . Note that  $dV$ , which is perpendicular to  $r$ , changes direction at point  $P$  as we sum from  $a$  to  $b$ ; hence, the incremental velocities induced at  $P$  by different sections of the vortex sheet must be added vectorially. Because of this, it is sometimes more convenient to deal with the velocity potential. Again referring to Fig. 4.8, the increment in velocity potential,  $d\phi$ , induced at point  $P$  by the elemental vortex  $\gamma ds$  is, from Eq. (3.112),

$$(4.2) \quad d\phi = -\frac{\gamma ds}{2\pi} \theta$$

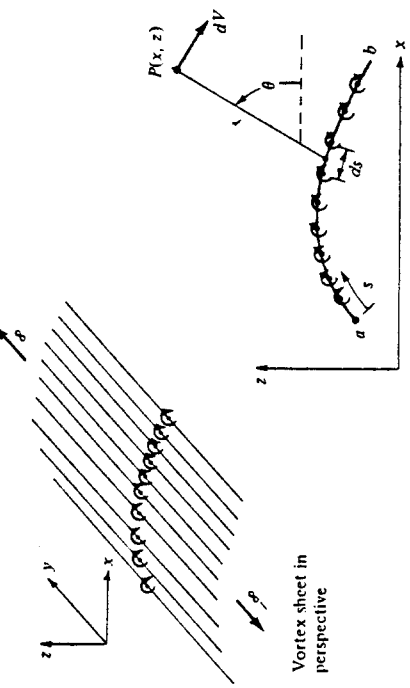


Figure 4.7 Vortex filament.

Edge view of sheet

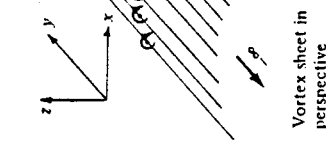


Figure 4.8 Vortex sheet.

In turn, the velocity potential at  $P$  due to the entire vortex sheet from  $a$  to  $b$  is

$$\phi(x, y) = -\frac{1}{2\pi} \int_a^b \theta \gamma ds \quad (4.3)$$

Equation (4.1) is particularly useful for our discussion of classical thin airfoil theory, whereas Eq. (4.3) is important for the numerical vortex panel method.

Recall from Sec. 3.14 that the circulation  $\Gamma$  around a point vortex is equal to the strength of the vortex. Similarly, the circulation around the vortex sheet in Fig. 4.8 is the sum of the strengths of the elemental vortices; i.e.,

$$\Gamma = \int_a^b \gamma ds \quad (4.4)$$

Recall that the source sheet introduced in Sec. 3.17 has a discontinuous change in the direction of the *normal* component of velocity across the sheet (from Fig. 3.29, note that the normal component of velocity changes direction by  $180^\circ$  in crossing the sheet), whereas the tangential component of velocity is the same immediately above and below the source sheet. In contrast, for a vortex sheet, there is a discontinuous change in the tangential component of velocity across the sheet, whereas the normal component of velocity is preserved across the sheet. This change in tangential velocity across the vortex sheet is related to the strength of the sheet as follows. Consider a vortex sheet as sketched in Fig. 4.9. Consider the rectangular dashed path enclosing a section of the sheet of length  $ds$ . The velocity components tangential to the top and bottom of this rectangular path are  $u_1$  and  $u_2$ , respectively, and the velocity components tangent to the left and right sides are  $v_1$  and  $v_2$ , respectively. The top and bottom of the path are separated by the distance  $dn$ . From the definition of circulation given by Eq. (2.127), the circulation around the dashed path is

$$\Gamma = -(v_2 dn - u_1 ds - v_1 dn + u_2 ds) \quad (4.5)$$

or

$$\Gamma = (u_1 - u_2) ds + (v_1 - v_2) dn \quad (4.5)$$

However, since the strength of the vortex sheet contained inside the dashed path is  $\gamma ds$ , we also have

$$\Gamma = \gamma ds \quad (4.6)$$

Therefore, from Eqs. (4.5) and (4.6),

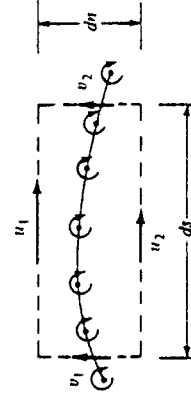


Figure 4.9 Tangential velocity jump across a vortex sheet.

$$\gamma ds = (u_1 - u_2) ds + (v_1 - v_2) dn \quad (4.7)$$

Let the top and bottom of the dashed line approach the vortex sheet; i.e., let  $dn \rightarrow 0$ . In the limit,  $u_1$  and  $u_2$  become the velocity components tangent to the vortex sheet immediately above and below the sheet, respectively, and Eq. (4.7) becomes

$$\gamma ds = (u_1 - u_2) ds$$

$$\gamma = u_1 - u_2 \quad (4.8)$$

Equation (4.8) is important; it states that *the local jump in tangential velocity across the vortex sheet is equal to the local sheet strength*.

We have now defined and discussed the properties of a vortex sheet. The concept of a vortex sheet is instrumental in the analysis of the low-speed characteristics of an airfoil. A philosophy of airfoil theory of inviscid, incompressible flow is as follows. Consider an airfoil of arbitrary shape and thickness in a freestream with velocity  $V_\infty$ , as sketched in Fig. 4.10. Replace the airfoil surface with a vortex sheet of variable strength  $\gamma(s)$ , as also shown in Fig. 4.10. Calculate the variation of  $\gamma$  as a function of  $s$  such that the induced velocity field from the vortex sheet when added to the uniform velocity of magnitude  $V_\infty$  will make the vortex sheet (hence the airfoil surface) a *streamline of the flow*. In turn, the circulation around the airfoil will be given by

$$\Gamma = \int \gamma ds$$

where the integral is taken around the complete surface of the airfoil. Finally, the resulting lift is given by the Kutta-Joukowski theorem:

$$L' = \rho_\infty V_\infty \Gamma$$

This philosophy is not new. It was first exposed by Ludwig Prandtl and his colleagues at Göttingen, Germany, during the period 1912–1922. However, no general analytical solution for  $\gamma = \gamma(s)$  exists for an airfoil of arbitrary shape and thickness. Rather, the strength of the vortex sheet must be found numerically, and the practical implementation of the above philosophy had to wait until the 1960s with the advent of large digital computers. Today, the above philosophy is the foundation of the modern vortex panel method, to be discussed in Sec. 4.9.

The concept of replacing the airfoil surface in Fig. 4.10 with a vortex sheet is more than just a mathematical device; it also has physical significance. In real life, there is a thin boundary layer on the surface, due to the action of friction between the surface and the airflow (see Fig. 1.24). This boundary layer is a highly viscous region in which



Figure 4.10 Simulation of an arbitrary airfoil by distributing a vortex sheet over the airfoil surface.

the large velocity gradients produce substantial vorticity; that is,  $\nabla \times \mathbf{V}$  is finite within the boundary layer. (Review Sec. 2.12 for a discussion of vorticity.) Hence, in real life there is a distribution of vorticity along the airfoil surface due to viscous effects, and our philosophy of replacing the airfoil surface with a vortex sheet (such as in Fig. 4.10) can be construed as a way of modeling this effect in an inviscid flow.<sup>f</sup>

Imagine that the airfoil in Fig. 4.10 is made very thin. If you were to stand back and look at such a thin airfoil from a distance, the portions of the vortex sheet on the top and bottom surface of the airfoil would almost coincide. This gives rise to a method of approximating a thin airfoil by replacing it with a single vortex sheet distributed over the camber line of the airfoil, as sketched in Fig. 4.11. The strength of this vortex sheet,  $\gamma(s)$ , is calculated such that, in combination with the freestream, the camber line becomes a streamline of the flow. Although the approach shown in Fig. 4.11 is approximate in comparison with the case shown in Fig. 4.10, it has the advantage of yielding a closed-form analytical solution. This philosophy of thin airfoil theory was first developed by Max Munk, a colleague of Prandtl, in 1922 (see Ref. 12). It is discussed in Secs. 4.7 and 4.8.

#### 4.5 THE KUTTA CONDITION

The lifting flow over a circular cylinder was discussed in Sec. 3.15, where we observed that an infinite number of potential flow solutions were possible, corresponding to the infinite choice of  $\Gamma$ . For example, Fig. 3.25 illustrates three different flows over the cylinder, corresponding to three different values of  $\Gamma$ . The same situation applies to the potential flow over an airfoil; for a given airfoil at a given angle of attack, there are an infinite number of valid theoretical solutions, corresponding to an infinite choice of  $\Gamma$ . For example, Fig. 4.12 illustrates two different flows over the same airfoil at the same angle of attack but with different values of  $\Gamma$ . At first, this may seem to pose a dilemma. We know from experience that a given airfoil at a given angle of attack produces a single value of lift (e.g., see Fig. 4.5). So although there are an

<sup>f</sup>It is interesting to note that some very recent research by NASA in 1982 is hinting that even as complex a problem as flow separation, heretofore thought to be a completely viscous-dominated phenomenon, may in reality be an inviscid-dominated flow which requires only a rotational flow. For example, some inviscid flow-field numerical solutions for flow over a circular cylinder, when vorticity is introduced either by means of a nonuniform freestream or a curved shock wave, are accurately predicting the separated flow on the rearward side of the cylinder. However, as exciting as these results may be, they are too preliminary to be emphasized in this book. We continue to talk about flow separation in Chaps. 15 and 16 as being a viscous-dominated effect, until definitely proved otherwise. This recent research is mentioned here only as another example of the physical connection between vorticity, vortex sheets, viscosity, and real life.

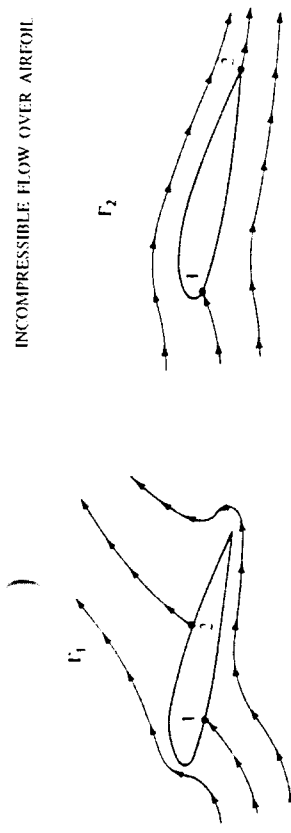


Figure 4.12 Effect of different values of circulation on the potential flow over a given airfoil at a given angle of attack. Points 1 and 2 are stagnation points.

infinite number of possible potential flow solutions, nature knows how to pick a particular solution. Clearly, the philosophy discussed in the previous section is not complete—we need an additional condition that fixes  $\Gamma$  for a given airfoil at a given  $\alpha$ .

To attempt to find this condition, let us examine some experimental results for the development of the flow field around an airfoil which is set into motion from an initial state of rest. Figure 4.13 shows a series of classic photographs of the flow over an airfoil, taken from Prandtl and Tietjens (Ref. 8). In Fig. 4.13a, the flow has just started, and the flow pattern is just beginning to develop around the airfoil. In these early moments of development, the flow tries to curl around the sharp trailing edge from the bottom surface to the top surface, similar to the sketch shown at the left of Fig. 4.12. However, more advanced considerations of inviscid, incompressible flow (see, for example, Ref. 9) show the theoretical result that the velocity becomes infinitely large at a sharp corner. Hence, the type of flow sketched at the left of Fig. 4.12, and shown in Fig. 4.13a, is not tolerated very long by nature. Rather, as the real flow develops over the airfoil, the stagnation point on the upper surface (point 2 in Fig. 4.12) moves toward the trailing edge. Figure 4.13b shows this intermediate stage. Finally, after the initial transient process dies out, the steady flow shown in Fig. 4.13c is reached. This photograph demonstrates that the flow is smoothly leaving the top and the bottom surfaces of the airfoil at the trailing edge. This flow pattern is sketched at the right of Fig. 4.12 and represents the type of pattern to be expected for the steady flow over an airfoil.

Reflecting on Figs. 4.12 and 4.13, we emphasize again that in establishing the steady flow over a given airfoil at a given angle of attack, nature adopts that particular value of circulation ( $\Gamma_2$  in Fig. 4.12) which results in the flow leaving smoothly at the trailing edge. This observation was first made and used in a theoretical analysis by the German mathematician M. Wilhelm Kutta in 1902. Therefore, it has become known as the *Kutta condition*.

In order to apply the Kutta condition in a theoretical analysis, we need to be more precise about the nature of the flow at the trailing edge. The trailing edge can have a finite angle, as shown in Figs. 4.12 and 4.13 and as sketched at the left of Fig. 4.14, or it can be cusped, as shown at the right of Fig. 4.14. First, consider the trailing edge with a finite angle, as shown at the left of Fig. 4.14. Denote the velocities along the top surface and the bottom surface as  $V_1$  and  $V_2$ , respectively.  $V_1$  is parallel to the top

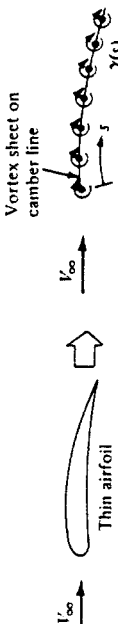


Figure 4.11 Thin airfoil approximation.

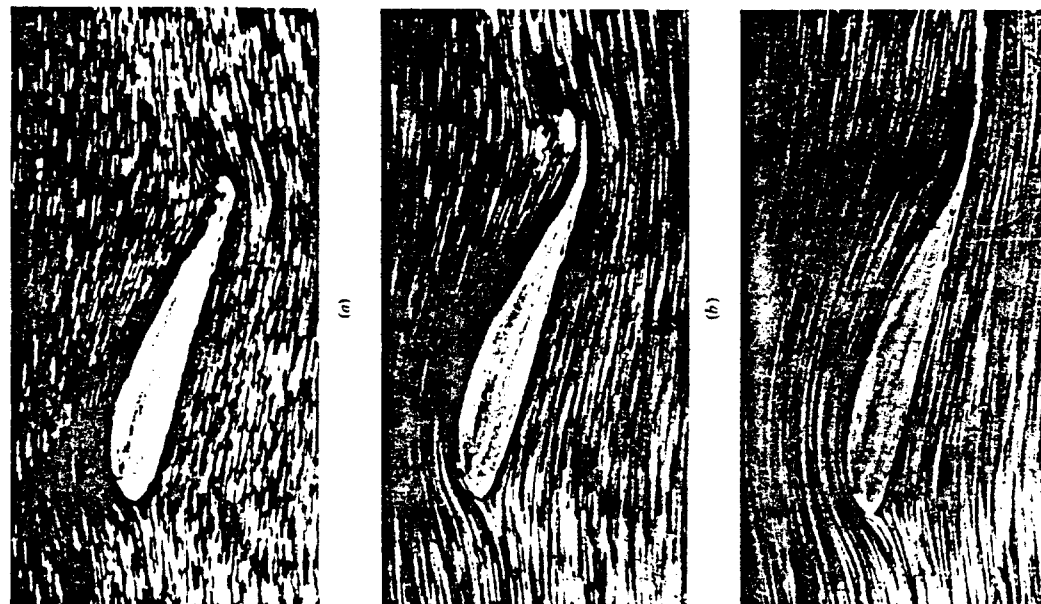


Figure 4.13 The development of steady flow over an airfoil: the airfoil is impulsively started from rest and attains a steady velocity through the fluid. (a) A moment just after starting. (b) An intermediate time. (c) The final steady flow. (From Prandtl and Tietjens, Ref. 8.)

surface at point  $a$ , and  $V_2$  is parallel to the bottom surface at point  $a$ . For the finite-angle trailing edge, if these velocities were finite at point  $a$ , then we would have two velocities in two different directions at the same point, as shown at the left of Fig. 4.14. However, this is not physically possible, and the only recourse is for both  $V_1$  and  $V_2$  to

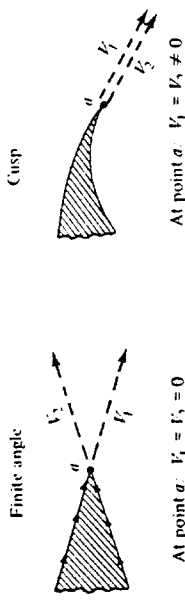


Figure 4.14 Different possible shapes of the trailing edge and their relation to the Kutta condition.

be zero at point  $a$ . That is, for the finite trailing edge, point  $a$  is a stagnation point, where  $V_1 = V_2 = 0$ . In contrast, for the cusped trailing edge shown at the right of Fig. 4.14,  $V_1$  and  $V_2$  are in the same direction at point  $a$ , and hence both  $V_1$  and  $V_2$  can be finite. However, the pressure at point  $a$ ,  $p_a$ , is a single, unique value, and Bernoulli's equation applied at both the top and bottom surfaces immediately adjacent to point  $a$  yields

$$p_a + \frac{1}{2}\rho V_1^2 = p_a + \frac{1}{2}\rho V_2^2$$

or

$$V_1 = V_2$$

Hence, for the cusped trailing edge, we see that the velocities leaving the top and bottom surfaces of the airfoil at the trailing edge are finite and equal in magnitude and direction.

We can summarize the statement of the Kutta condition as follows:

1. For a given airfoil at a given angle of attack, the value of  $\Gamma$  around the airfoil is such that the flow leaves the trailing edge smoothly.
2. If the trailing-edge angle is finite, then the trailing edge is a stagnation point.
3. If the trailing edge is cusped, then the velocities leaving the top and bottom surfaces at the trailing edge are finite and equal in magnitude and direction.

Consider again the philosophy of simulating the airfoil with vortex sheets placed either on the surface or on the camber line, as discussed in Sec. 4.4. The strength of such a vortex sheet is variable along the sheet and is denoted by  $\gamma(s)$ . The statement of the Kutta condition in terms of the vortex sheet is as follows. At the trailing edge (TE), from Eq. (4.8), we have

$$\gamma(\text{TE}) = \gamma(a) = V_1 - V_2 \quad (4.9)$$

However, for the finite-angle trailing edge,  $V_1 = V_2 = 0$ ; hence from Eq. (4.9),  $\gamma(\text{TE}) = 0$ . For the cusped trailing edge,  $V_1 = V_2 \neq 0$ ; hence from Eq. (4.9), we again obtain the result that  $\gamma(\text{TE}) = 0$ . Therefore, the Kutta condition expressed in terms of the strength of the vortex sheet is

$$\gamma(\text{TE}) = 0 \quad (4.10)$$

## 4.6 KELVIN'S CIRCULATION THEOREM AND THE STARTING VORTEX

In this section we put the finishing touch to the overall philosophy of airfoil theory before developing the quantitative aspects of the theory itself in subsequent sections. This section also ties up a loose end introduced by the Kutta condition described in the previous section. Specifically, the Kutta condition states that the circulation around an airfoil is just the right value to ensure that the flow smoothly leaves the trailing edge.

**Question:** How does nature generate this circulation? Does it come from nowhere, or

is circulation somehow conserved over the whole flow field? Let us examine these

matters more closely.

Consider an arbitrary inviscid, incompressible flow as sketched in Fig. 4.15. Assume that all body forces  $\mathbf{f}$  are zero. Choose an arbitrary curve,  $C_1$ , and identify the fluid elements that are on this curve at a given instant in time  $t_1$ . Also, by definition the circulation around curve  $C_1$  is  $\Gamma_1 = -\int_{C_1} \mathbf{V} \cdot d\mathbf{s}$ . Now let these specific fluid elements move downstream. At some later time,  $t_2$ , these same fluid elements will form another curve  $C_2$ , around which the circulation is  $\Gamma_2 = -\int_{C_2} \mathbf{V} \cdot d\mathbf{s}$ . For the conditions stated above, we can readily show that  $\Gamma_1 = \Gamma_2$ . In fact, since we are following a set of specific fluid elements, we can state that circulation around a closed curve formed by a set of contiguous fluid elements remains constant as the fluid elements move throughout the flow. Recall from Sec. 2.9 that the substantial derivative gives the time rate of change following a given fluid element. Hence, a mathematical statement of the above discussion is simply

$$\boxed{\frac{D\Gamma}{Dt} = 0} \quad (4.11)$$

which says that the time rate of change of circulation around a closed curve consisting of the same fluid elements is zero. Equation (4.11) along with its supporting discussion is called *Kelvin's circulation theorem*.† Its derivation from first principles is left as Prob. 4.3.

Kelvin's theorem helps to explain the generation of circulation around an airfoil, as follows. Consider an airfoil in a fluid at rest, as shown in Fig. 4.16a. Because  $\mathbf{V} = 0$  everywhere, the circulation around curve  $C_1$  is zero. Now start the flow in motion over the airfoil. Initially, the flow will tend to curl around the trailing edge, as explained in Sec. 4.5 and illustrated at the left of Fig. 4.12. In so doing, the velocity at the trailing edge theoretically becomes infinite. In real life, the velocity tends toward a very large finite number. Consequently, during the very first moments after the flow is started, a thin region of very large velocity gradients (and therefore high vorticity) is formed at the trailing edge. This high-vorticity region is fixed to the same fluid elements, and consequently it is flushed downstream as the fluid elements begin to move downstream from the trailing edge. As it moves downstream, this thin sheet of intense vorticity is unstable, and it tends to roll up and form a picture similar to a point vortex. This vortex is called the *starting vortex* and is sketched in Fig. 4.16b. After the flow around the airfoil has come to a steady state where the flow leaves the trailing edge smoothly (the Kutta condition), the high velocity gradients at the trailing edge disappear, and vorticity is no longer produced at that point. However, the starting vortex has already been formed during the starting process, and it moves steadily downstream with the flow forever after. Figure 4.16b shows the flow field sometime after steady flow has been

†Kelvin's theorem also holds for an inviscid compressible flow in the special case where  $\rho = \rho(p)$ ; i.e., the density is some single-valued function of pressure. Such is the case for isentropic flow, to be treated in later chapters.

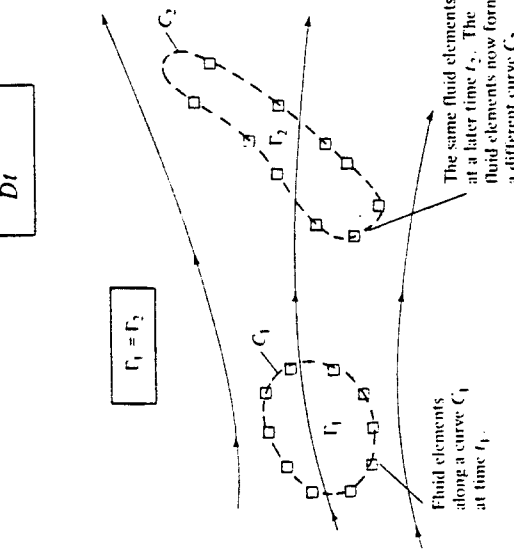


Figure 4.15 Kelvin's theorem.

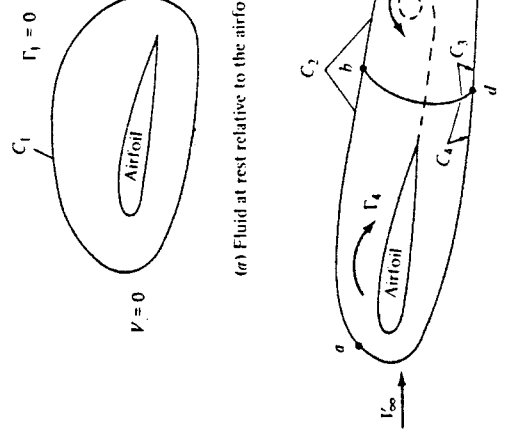


Figure 4.16 The creation of the starting vortex and the resulting generation of circulation around the airfoil.

achieved over the airfoil, with the starting vortex somewhere downstream. The fluid elements that initially made up curve  $C_1$  in Fig. 4.16a have moved downstream and now make up curve  $C_2$ , which is the complete circuit  $abcta$  shown in Fig. 4.16b. Thus, from Kelvin's theorem, the circulation  $\Gamma_2$  around curve  $C_2$  (which encloses both the airfoil and the starting vortex) is the same as that around curve  $C_1$ , namely zero.  $\Gamma_2 = \Gamma_1 = 0$ . Now let us subdivide  $C_2$  into two loops by making the cut  $bd$ , thus forming curves  $C_3$  (circuit  $bcdh$ ) and  $C_4$  (circuit  $dhda$ ). Curve  $C_3$  encloses the starting vortex, and curve  $C_4$  encloses the airfoil. The circulation  $\Gamma_3$  around curve  $C_3$  is due to the starting vortex; by inspecting of Fig. 4.16b, we see that  $\Gamma_3$  is in the counterclockwise direction, i.e., a negative value. The circulation around curve  $C_4$  enclosing the airfoil is  $\Gamma_4$ . Since the cut  $bd$  is common to both  $C_3$  and  $C_4$ , the sum of the circulations around  $C_3$  and  $C_4$  is simply equal to the circulation around  $C_2$ .

$$\Gamma_3 + \Gamma_4 = \Gamma_2$$

However, we have already established that  $\Gamma_2 = 0$ . Hence,

$$\Gamma_4 = -\Gamma_3$$

that is, *the circulation around the airfoil is equal and opposite to the circulation around the starting vortex.*

This brings us to the crux of this section. As the flow over an airfoil is started, the large velocity gradients at the sharp trailing edge result in the formation of a region of intense vorticity which rolls up downstream of the trailing edge, forming the starting vortex. This starting vortex has associated with it a counterclockwise circulation. Therefore, as an equal-and-opposite reaction, a clockwise circulation around the airfoil is generated. As the starting process continues, vorticity from the trailing edge is constantly fed into the starting vortex, making it stronger with a consequent larger counterclockwise circulation. In turn, the clockwise circulation around the airfoil becomes stronger, making the flow at the trailing edge more closely approach the Kutta condition, thus weakening the vorticity shed from the trailing edge. Finally, the starting vortex builds up to just the right strength such that the equal-and-opposite clockwise circulation around the airfoil leads to smooth flow from the trailing edge (the Kutta condition is exactly satisfied). When this happens, the vorticity shed from the leading edge becomes zero, the starting vortex no longer grows in strength, and a steady circulation exists around the airfoil.

## 4.7 CLASSICAL THIN AIRFOIL THEORY: THE SYMMETRIC AIRFOIL

Some experimentally observed characteristics of airfoils and a philosophy for the theoretical prediction of these characteristics have been discussed in the preceding sections. Referring to our chapter road map in Fig. 4.2, we have now completed the central branch. In this section, we move to the right-hand branch of Fig. 4.2, namely a quantitative development of thin airfoil theory. The basic equations necessary for the calculation of airfoil lift and moments are established in this section, with an application to symmetric airfoils. The case of cambered airfoils will be treated in Sec. 4.8.

For the time being, we deal with *thin* airfoils; for such a case, the airfoil can be simulated by a vortex sheet placed along the camber line, as discussed in Sec. 4.4. Our purpose is to calculate the variation of  $\gamma(s)$  such that the camber line becomes a streamline of the flow and such that the Kutta condition is satisfied at the trailing edge, i.e.,  $\gamma(\text{TE}) = 0$  [see Eq. (4.10)]. Once we have found the particular  $\gamma(s)$  which satisfies these conditions, then the total circulation  $\Gamma$  around the airfoil is found by integrating  $\gamma(s)$  from the leading edge to the trailing edge. In turn, the lift is calculated from  $\Gamma$  via the Kutta-Joukowski theorem.

Consider a vortex sheet placed on the camber line of an airfoil, as sketched in Fig. 4.17a. The freestream velocity is  $V_\infty$ , and the airfoil is at the angle of attack  $\alpha$ . The  $x$  axis is oriented along the chord line, and the  $z$  axis is perpendicular to the chord. The distance measured along the camber line is denoted by  $s$ . The shape of the camber line is given by  $z = z(x)$ . The chord length is  $c$ . In Fig. 4.17a,  $w'$  is the component of velocity normal to the camber line induced by the vortex sheet;  $w' = w'(s)$ . For a thin airfoil, we rationalized in Sec. 4.4 that the distribution of a vortex sheet over the surface of the airfoil, when viewed from a distance, looks almost the same as a vortex sheet placed on the camber line. Let us stand back once again and view Fig. 4.17a from a distance. If the airfoil is thin, the camber line is close to the chord line, and viewed from a distance, the vortex sheet appears to fall approximately on the chord line. Therefore, once again let us reorient our thinking and place the vortex sheet on the chord line, as sketched in Fig. 4.17b. Here,  $y = \gamma(x)$ . We still wish the camber line to be a streamline of the flow, and  $\gamma = \gamma(x)$  is calculated to satisfy this condition as well as the Kutta condition  $\gamma(c) = 0$ . That is, the strength of the vortex sheet on the chord line is determined such that the camber line (not the chord line) is a streamline.

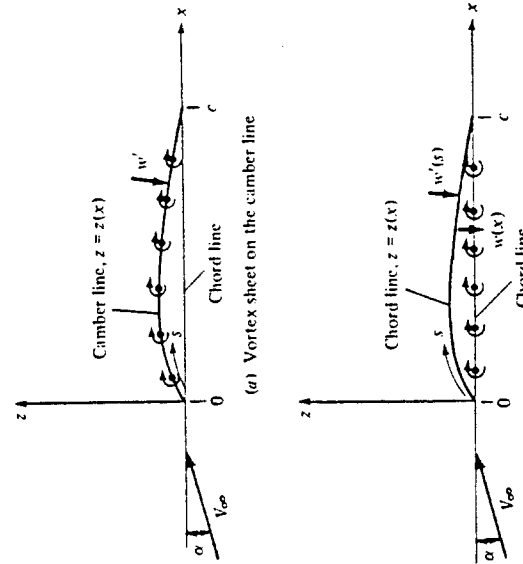


Figure 4.17 Placement of the vortex sheet for thin airfoil analysis.

For the camber line to be a streamline, the component of velocity normal to the camber line must be zero at all points along the camber line. The velocity at any point in the flow is the sum of the uniform freestream velocity and the velocity induced by the vortex sheet. Let  $V_{x,n}$  be the component of the freestream velocity normal to the camber line. Thus, for the camber line to be a streamline,

$$V_{x,n} + w'(s) = 0 \quad (4.12)$$

at every point along the camber line.

An expression for  $V_{x,n}$  in Eq. (4.12) is obtained by the inspection of Fig. 4.18. At any point  $P$  on the camber line, where the slope of the camber line is  $dz/dx$ , the geometry of Fig. 4.18 yields

$$V_{x,n} = V_x \sin \left[ \alpha + \tan^{-1} \left( -\frac{dz}{dx} \right) \right] \quad (4.13)$$

For a thin airfoil at small angle of attack, both  $\alpha$  and  $\tan^{-1}(-dz/dx)$  are small values. Using the approximation that  $\sin \theta \approx \tan \theta \approx \theta$  for small  $\theta$ , where  $\theta$  is in radians, Eq. (4.13) reduces to

$$V_{x,n} = V_x \left( \alpha - \frac{dz}{dx} \right) \quad (4.14)$$

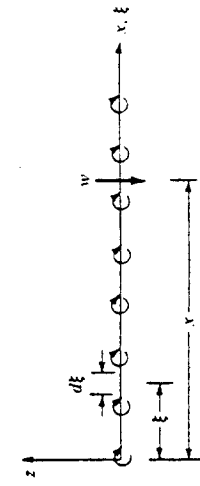
Equation (4.14) gives the expression for  $V_{x,n}$  to be used in Eq. (4.12). Keep in mind that, in Eq. (4.14),  $\alpha$  is in radians.

Returning to Eq. (4.12), let us develop an expression for  $w'(s)$  in terms of the strength of the vortex sheet. Refer again to Fig. 4.17b. Here, the vortex sheet is along the chord line, and  $w'(s)$  is the component of velocity normal to the camber line induced by the vortex sheet. Let  $w(x)$  denote the component of velocity normal to the *chord line* induced by the vortex sheet, as also shown in Fig. 4.17b. If the airfoil is thin, the camber line is close to the chord line, and it is consistent with thin airfoil theory to make the approximation that

$$s \approx x$$

the fundamental equation of thin airfoil theory; it is simply a statement that the camber line is a streamline of the flow.

Note that Eq. (4.18) is written at a given point  $x$  on the chord line, and that  $dz/dx$  is evaluated at that point  $x$ . The variable  $\xi$  is simply a dummy variable of integration which varies from 0 to  $c$  along the chord line, as shown in Fig. 4.19. The vortex strength  $\gamma = \gamma(\xi)$  is a variable along the chord line. For a given airfoil at a given angle of attack, both  $\alpha$  and  $dz/dx$  are known values in Eq. (4.18). Indeed, the only unknown in Eq. (4.18) is the vortex strength  $\gamma(\xi)$ . Hence, Eq. (4.18) is an integral equation, the solution of which yields the variation of  $\gamma(\xi)$  such that the camber line is a streamline



and

$$w'(s) \approx w(x) \quad (4.15)$$

An expression for  $w(x)$  in terms of the strength of the vortex sheet is easily obtained from Eq. (4.1), as follows. Consider Fig. 4.19, which shows the vortex sheet along the chord line. We wish to calculate the value of  $w(x)$  at the location  $x$ . Consider an elemental vortex of strength  $\gamma d\xi$  located at a distance  $\gamma d\xi$  from the origin along the chord line, as shown in Fig. 4.19. The strength of the vortex sheet,  $\gamma$ , varies with the distance along the chord; that is,  $\gamma = \gamma(\xi)$ . The velocity  $dw$  at point  $x$  induced by the elemental vortex at point  $\xi$  is given by Eq. (4.1) as

$$dw = -\frac{\gamma(\xi) d\xi}{2\pi(x - \xi)} \quad (4.16)$$

In turn, the velocity  $w(x)$  induced at point  $x$  by *all* the elemental vortices along the chord line is obtained by integrating Eq. (4.16) from the leading edge ( $\xi = 0$ ) to the trailing edge ( $\xi = c$ ).

$$w(x) = - \int_0^c \frac{\gamma(\xi) d\xi}{2\pi(x - \xi)} \quad (4.17)$$

Combined with the approximation stated by Eq. (4.15), Eq. (4.17) gives the expression for  $w'(s)$  to be used in Eq. (4.12).

Recall that Eq. (4.12) is the boundary condition necessary for the camber line to be a streamline. Substituting Eqs. (4.14), (4.15), and (4.17) into (4.12), we obtain

$$V_x \left( \alpha - \frac{dz}{dx} \right) - \int_0^c \frac{\gamma(\xi) d\xi}{2\pi(x - \xi)} = 0$$

$$\frac{1}{2\pi} \int_0^c \frac{\gamma(\xi) d\xi}{x - \xi} = V_x \left( \alpha - \frac{dz}{dx} \right) \quad (4.18)$$

or

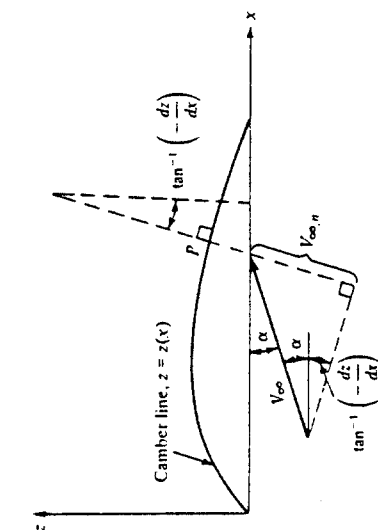


Figure 4.18 Determination of the component of freestream velocity normal to the camber line.

Figure 4.19 Calculation of the induced velocity at the chord line.

of the flow. The central problem of thin airfoil theory is to solve Eq. (4.18) for  $\gamma(\xi)$ , subject to the Kutta condition, namely, that  $\gamma(c) = 0$ .

In this section, we treat the case of a symmetric airfoil. As stated in Sec. 4.2, a symmetric airfoil has no camber; the camber line is coincident with the chord line. Hence, for this case,  $dz/dx = 0$ , and Eq. (4.18) becomes

$$\frac{1}{2\pi} \int_0^{\xi} \frac{\gamma(\xi) d\xi}{x - \xi} = V_x \alpha \quad (4.19)$$

In essence, within the framework of thin airfoil theory, a symmetric airfoil is treated the same as a flat plate; note that our theoretical development does not account for the airfoil thickness distribution. Equation (4.19) is an *exact* expression for the inviscid, incompressible flow over a flat plate at angle of attack.

To help deal with the integral in Eqs. (4.18) and (4.19), let us transform  $\xi$  into  $\theta$  via the following transformation:

$$\xi = \frac{c}{2} (1 - \cos \theta) \quad (4.20)$$

Since  $x$  is a fixed point in Eqs. (4.18) and (4.19), it corresponds to a particular value of  $\theta$ , namely  $\theta_0$ , such that

$$x = \frac{c}{2} (1 - \cos \theta_0) \quad (4.21)$$

Also, from Eq. (4.20),

$$d\xi = \frac{c}{2} \sin \theta d\theta \quad (4.22)$$

Substituting Eqs. (4.20) to (4.22) into (4.19), and noting that the limits of integration become  $\theta = 0$  at the leading edge (where  $\xi = 0$ ) and  $\theta = \pi$  at the trailing edge (where  $\xi = c$ ), we obtain

$$\frac{1}{2\pi} \int_0^{\pi} \frac{\gamma(\theta) \sin \theta d\theta}{\cos \theta - \cos \theta_0} = V_x \alpha \quad (4.23)$$

A rigorous solution of Eq. (4.23) for  $\gamma(\theta)$  can be obtained from the mathematical theory of integral equations, which is beyond the scope of this book. Instead, we simply state that the solution is

$$\boxed{\gamma(\theta) = 2\alpha V_x \frac{(1 + \cos \theta)}{\sin \theta}} \quad (4.24)$$

We can verify this solution by substituting Eq. (4.24) into (4.23), yielding

$$\frac{1}{2\pi} \int_0^{\pi} \frac{\gamma(\theta) \sin \theta d\theta}{\cos \theta - \cos \theta_0} = \frac{V_x \alpha}{\pi} \int_0^{\pi} \frac{(1 + \cos \theta) d\theta}{\cos \theta - \cos \theta_0} \quad (4.25)$$

The following standard integral appears frequently in airfoil theory and is derived in appendix E of Ref. 9.

$$\int_0^{\pi} \frac{\cos n\theta d\theta}{\cos \theta - \cos \theta_0} = \frac{\pi \sin n\theta_0}{\sin \theta_0} \quad (4.26)$$

Using Eq. (4.26) in the right-hand side of Eq. (4.25), we find that

$$\begin{aligned} \frac{V_x \alpha}{\pi} \int_0^{\pi} \frac{(1 + \cos \theta) d\theta}{\cos \theta - \cos \theta_0} &= \frac{V_x \alpha}{\pi} \left( \int_0^{\pi} \frac{\cos \theta d\theta}{\cos \theta - \cos \theta_0} + \int_0^{\pi} \frac{\cos \theta d\theta}{\cos \theta - \cos \theta_0} \right) \\ &= \frac{V_x \alpha}{\pi} (0 + \pi) = V_x \alpha \end{aligned} \quad (4.27)$$

Substituting Eq. (4.27) into (4.25), we have

$$\frac{1}{2\pi} \int_0^{\pi} \frac{\gamma(\theta) \sin \theta d\theta}{\cos \theta - \cos \theta_0} = V_x \alpha$$

which is identical to Eq. (4.23). Hence, we have shown that Eq. (4.24) is indeed the solution to Eq. (4.23). Also note that at the trailing edge, where  $\theta = \pi$ , Eq. (4.24) yields

$$\gamma(\pi) = 2\alpha V_x \frac{0}{0}$$

which is an indeterminant form. However, using L'Hospital's rule on Eq. (4.24),

$$\gamma(\pi) = 2\alpha V_x \frac{-\sin \pi}{-\cos \pi} = 0$$

Thus, Eq. (4.24) also satisfies the Kutta condition.

We are now in a position to calculate the lift coefficient for a thin, symmetric airfoil. The total circulation around the airfoil is

$$\Gamma = \int_0^{\pi} \gamma(\xi) d\xi \quad (4.28)$$

Using Eqs. (4.20) and (4.22), Eq. (4.28) transforms to

$$\Gamma = \frac{c}{2} \int_0^{\pi} \gamma(\theta) \sin \theta d\theta \quad (4.29)$$

Substituting Eq. (4.24) into (4.29),

$$\Gamma = \alpha c V_x \int_0^{\pi} (1 + \cos \theta) d\theta = \pi \alpha c V_x \quad (4.30)$$

Substituting Eq. (4.30) into the Kutta-Joukowski theorem, the lift per unit span is

$$L' = \rho_x V_x \Gamma = \pi \alpha c \rho_x V_x^2 \quad (4.31)$$

The lift coefficient is

$$c_l = \frac{L'}{q_x S} \quad (4.32)$$

where

$$S = c(1)$$

Substituting Eq. (4.31) into (4.32), we have

$$c_l = \frac{\pi \alpha \rho_x V_x^2}{\frac{1}{2} \rho_x V_x^2 c(1)}$$

$$\boxed{c_l = 2\pi\alpha}$$

and

$$\boxed{\text{Lift slope} = \frac{dc_l}{d\alpha} = 2\pi} \quad (4.34)$$

Equations (4.33) and (4.34) are important results; they state the theoretical result that the lift coefficient is *linearly proportional to angle of attack*, which is supported by the experimental results discussed in Sec. 4.3. They also state that the theoretical lift slope is equal to  $2\pi \text{ rad}^{-1}$ , which is 0.11 degree $^{-1}$ . The experimental lift coefficient data for an NACA 0012 symmetric airfoil are given in Fig. 4.20; note that Eq. (4.33) accurately predicts  $c_l$  over a large range of angle of attack. (The NACA 0012 airfoil section is commonly used on airplane tails and helicopter blades.)

The moment about the leading edge can be calculated as follows. Consider the elemental vortex of strength  $\gamma(\xi) d\xi$  located a distance  $\xi$  from the leading edge, as sketched in Fig. 4.21. The circulation associated with this elemental vortex is  $d\Gamma = \gamma(\xi) d\xi$ . In turn, the increment of lift,  $dL$ , contributed by the elemental vortex is  $dL = \rho_x V_x d\Gamma$ . This increment of lift creates a moment about the leading edge  $dM = -\xi(dL)$ . The total moment about the leading edge (LE) (per unit span) due to the entire vortex sheet is therefore

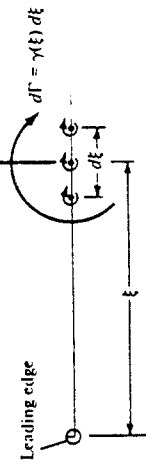


Figure 4.21 Calculation of moments about the leading edge.

$$\boxed{M'_{LE} = - \int_0^c \xi(dL) = -\rho_x V_x \int_0^c \xi\gamma(\xi) d\xi} \quad (4.35)$$

Transforming Eq. (4.35) via Eqs. (4.20) and (4.22), and performing the integration, we obtain (the details are left for Prob. 4.4):

$$\boxed{M'_{LE} = -q_x c^2 \frac{\pi\alpha}{2}} \quad (4.36)$$

The moment coefficient is

$$\boxed{c_{m,LE} = \frac{M'_{LE}}{q_x S c}}$$

where  $S = c(1)$ . Hence,

$$\boxed{c_{m,LE} = \frac{M'_{LE}}{q_x c^2} = -\frac{\pi\alpha}{2}} \quad (4.37)$$

However, from Eq. (4.33),

$$\boxed{\pi\alpha = \frac{c_l}{2}} \quad (4.38)$$

Combining Eqs. (4.37) and (4.38),

$$\boxed{c_{m,LE} = -\frac{c_l}{4}} \quad (4.39)$$

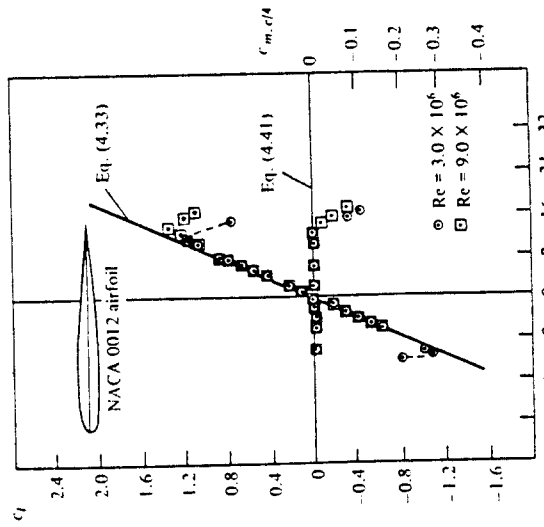
From Eq. (1.22), the moment coefficient about the quarter-chord point is

$$\boxed{c_{m,c/4} = c_{m,LE} + \frac{c_l}{4}} \quad (4.40)$$

Combining Eqs. (4.39) and (4.40), we have

$$\boxed{c_{m,c/4} = 0} \quad (4.41)$$

Figure 4.20 Comparison between theory and experiment for the lift and moment coefficients for an NACA 0012 airfoil. (Experimental data are from Abbott and von Doenhoff, Ref. 11.)



In Sec. 1.6, a definition is given for the center of pressure as that point about which the moments are zero. Clearly, Eq. (4.41) demonstrates the theoretical result that the center of pressure is at the quarter-chord point for a symmetric airfoil.

By the definition given in Sec. 4.3, that point on an airfoil where moments are independent of angle of attack is called the aerodynamic center. From Eq. (4.41), the moment about the quarter-chord is zero for all values of  $\alpha$ . Hence, for a symmetric airfoil, we have the theoretical result that the *quarter-chord point is both the center of pressure and the aerodynamic center*.

The above theoretical result for  $c_{m,c/4} = 0$  is supported by the experimental data given in Fig. 4.20. Also note that the experimental value of  $c_{m,c/4}$  is constant over a wide range of  $\alpha$ , thus demonstrating that the real aerodynamic center is essentially at the quarter chord.

Let us summarize the above results. The essence of thin airfoil theory is to find a distribution of vortex sheet strength along the chord line that will make the camber line a streamline of the flow while satisfying the Kutta condition  $\gamma(\text{TE}) = 0$ . Such a vortex distribution is obtained by solving Eq. (4.18) for  $\gamma(\xi)$ , or in terms of the transformed independent variable  $\theta$ , solving Eq. (4.23) for  $\gamma(\theta)$  [recall that Eq. (4.23) is written for a symmetric airfoil]. The resulting vortex distribution  $\gamma(\theta)$  for a symmetric airfoil is given by Eq. (4.24). In turn, this vortex distribution, when inserted into the Kutta-Joukowski theorem, gives the following important theoretical results for a symmetric airfoil:

1.  $C_l = 2\pi\alpha$ .
2. Lift slope =  $2\pi$ .
3. The center of pressure and the aerodynamic center are both located at the quarter-chord point.

## 4.8 THE CAMBERED AIRFOIL

Thin airfoil theory for a cambered airfoil is a generalization of the method for a symmetric airfoil discussed in Sec. 4.7. To treat the cambered airfoil, return to Eq. (4.18):

$$\frac{1}{2\pi} \int_0^x \frac{\gamma(\xi) d\xi}{x - \xi} = V_x \left( \alpha - \frac{dz}{dx} \right) \quad (4.18)$$

For a cambered airfoil,  $dz/dx$  is finite, and this makes the analysis more elaborate than in the case of a symmetric airfoil, where  $dz/dx = 0$ . Once again, let us transform Eq. (4.18) via Eqs. (4.20) to (4.22), obtaining

$$\frac{1}{2\pi} \int_0^\pi \frac{\gamma(\theta) \sin \theta d\theta}{\cos \theta - \cos \theta_0} = V_x \left( \alpha - \frac{dz}{dx} \right) \quad (4.42)$$

We wish to obtain a solution for  $\gamma(\theta)$  from Eq. (4.42), subject to the Kutta condition  $\gamma(\pi) = 0$ . Such a solution for  $\gamma(\theta)$  will make the camber line a streamline of the flow. However, as before, a rigorous solution of Eq. (4.42) for  $\gamma(\theta)$  is beyond the scope of this book. Rather, the result is stated below:

$$\gamma(\theta) = 2V_x \left( A_0 \frac{1 + \cos \theta}{\sin \theta} + \sum_{n=1}^{\infty} A_n \sin n\theta \right) \quad (4.43)$$

Note that the above expression for  $\gamma(\theta)$  consists of a leading term very similar to Eq. (4.24) for a symmetric airfoil, plus a Fourier sine series with coefficients  $A_n$ . The values of  $A_n$  depend on the shape of the camber line,  $dz/dx$ , and  $A_0$  depends on both  $dz/dx$  and  $\alpha$ , as shown below.

The coefficients  $A_0$  and  $A_n$  ( $n = 1, 2, 3, \dots$ ) in Eq. (4.43) must be specific values in order that the camber line be a streamline of the flow. To find these specific values, substitute Eq. (4.43) into Eq. (4.42).

$$\frac{1}{\pi} \int_0^\pi A_0 \left( 1 + \cos \theta \right) d\theta + \frac{1}{\pi} \sum_{n=1}^{\infty} \int_0^\pi A_n \frac{\sin n\theta \sin \theta d\theta}{\cos \theta - \cos \theta_0} = \alpha - \frac{dz}{dx} \quad (4.44)$$

The first integral can be evaluated from the standard form given in Eq. (4.26). The remaining integrals can be obtained from another standard form, which is derived in appendix E of Ref. 9, and which is given below:

$$\int_0^\pi \frac{\sin n\theta \sin \theta d\theta}{\cos \theta - \cos \theta_0} = -\pi \cos n\theta_0 \quad (4.45)$$

Hence, using Eqs. (4.26) and (4.45), we can reduce Eq. (4.44) to

$$\begin{aligned} A_0 - \sum_{n=1}^{\infty} A_n \frac{\sin \theta_0}{\cos \theta - \cos \theta_0} &= \alpha - \frac{dz}{dx} \\ \frac{dz}{dx} &= (\alpha - A_0) + \sum_{n=1}^{\infty} A_n \cos n\theta_0 \quad (4.46) \end{aligned}$$

or

Recall that Eq. (4.46) was obtained directly from Eq. (4.42), which is the transformed version of the fundamental equation of thin airfoil theory, Eq. (4.18). Furthermore, recall that Eq. (4.18) is evaluated at a given point  $x$  along the chord line, as sketched in Fig. 4.19. Hence, Eq. (4.46) is also evaluated at the given point  $x$ ; here,  $dz/dx$  and  $\theta_0$  correspond to the same point  $x$  on the chord line. Also, recall that  $dz/dx$  is a function of  $\theta_0$ , where  $x = (c/2)(1 - \cos \theta_0)$  from Eq. (4.21).

Examine Eq. (4.46) closely. It is in the form of a Fourier cosine series expansion for the function of  $dz/dx$ . In general, the Fourier cosine series representation of a function  $f(\theta)$  over an interval  $0 \leq \theta \leq \pi$  is given by

$$f(\theta) = B_0 + \sum_{n=1}^{\infty} B_n \cos n\theta \quad (4.47)$$

where, from Fourier analysis, the coefficients  $B_0$  and  $B_n$  are given by

$$B_0 = \frac{1}{\pi} \int_0^\pi f(\theta) d\theta \quad (4.48)$$

$$B_n = \frac{2}{\pi} \int_0^\pi f(\theta) \cos n\theta d\theta \quad (4.49)$$

(See, for example, page 217 of Ref. 6.) In Eq. (4.46), the function  $dz/dx$  is analogous to  $f(\theta)$  in the general form given in Eq. (4.47). Thus, from Eqs. (4.48) and (4.49), the coefficients in Eq. (4.46) are given by

$$\alpha - A_0 = \frac{1}{\pi} \int_0^\pi \frac{dz}{dx} d\theta_0 \quad (4.50)$$

or

$$A_0 = \alpha - \frac{1}{\pi} \int_0^\pi \frac{dz}{dx} d\theta_0$$

and

$$A_n = \frac{2}{\pi} \int_0^\pi \frac{dz}{dx} \cos n\theta_0 d\theta_0 \quad (4.51)$$

Keep in mind that in the above,  $dz/dx$  is a function of  $\theta_0$ . Note from Eq. (4.50) that  $A_0$  depends on both  $\alpha$  and the shape of the camber line (through  $dz/dx$ ), whereas from Eq. (4.51) the values of  $A_n$  depend only on the shape of the camber line.

Pause for a moment and think about what we have done. We are considering the flow over a cambered airfoil of given shape,  $dz/dx$ , at a given angle of attack  $\alpha$ . In order to make the camber line a streamline of the flow, the strength of the vortex sheet along the chord line must have the distribution  $\gamma(\theta)$  given by Eq. (4.43), where the coefficients  $A_0$  and  $A_n$  are given by Eqs. (4.50) and (4.51), respectively. Also note that Eq. (4.43) satisfies the Kutta condition  $\gamma(\pi) = 0$ . Actual numbers for  $A_0$  and  $A_n$  can be obtained for a given shape airfoil at a given angle of attack simply by carrying out the integrations indicated in Eqs. (4.50) and (4.51). For an example of such calculations applied to an NACA 2412 airfoil, see pages 120–125 of Ref. 13. Also note that, when  $dz/dt = 0$ , Eqs. (4.43) reduces to Eq. (4.24) for a symmetric airfoil. Hence, the symmetric airfoil is a special case of Eq. (4.43).

Let us now obtain expressions for the aerodynamic coefficients for a cambered airfoil. The total circulation due to the entire vortex sheet from the leading edge to the trailing edge is

$$\Gamma = \int_0^\pi \gamma(\xi) d\xi = \frac{c}{2} \int_0^\pi \gamma(\theta) \sin \theta d\theta \quad (4.52)$$

Substituting Eq. (4.43) for  $\gamma(\theta)$  into Eq. (4.52), we obtain

$$\Gamma = cV_x \left[ A_0 \int_0^\pi (1 + \cos \theta) d\theta + \sum_{n=1}^{\infty} A_n \int_0^\pi \sin n\theta \sin \theta d\theta \right] \quad (4.53)$$

From any standard table of integrals,

$$\int_0^\pi (1 + \cos \theta) d\theta = \pi$$

$$\int_0^\pi \sin n\theta \sin \theta d\theta = \begin{cases} \frac{\pi}{2} & \text{for } n = 1 \\ 0 & \text{for } n \neq 1 \end{cases}$$

and

Hence, Eq. (4.53) becomes

$$\Gamma = cV_x \left( \pi A_0 + \frac{\pi}{2} A_1 \right) \quad (4.54)$$

From Eq. (4.54), the lift per unit span is

$$L' = \rho_x V_x \Gamma = \rho_x V_x^2 c \left( \pi A_0 + \frac{\pi}{2} A_1 \right) \quad (4.55)$$

In turn, Eq. (4.55) leads to the lift coefficient in the form

$$c_l = \frac{L'}{\frac{1}{2} \rho_x V_x^2 c (1)} = \pi (2A_0 + A_1) \quad (4.56)$$

Recall that the coefficients  $A_0$  and  $A_1$  in Eq. (4.56) are given by Eqs. (4.50) and (4.51), respectively. Hence, Eq. (4.56) becomes

$$c_l = 2\pi \left[ \alpha + \frac{1}{\pi} \int_0^\pi \frac{dz}{dx} (\cos \theta_0 - 1) d\theta_0 \right]$$

$$\text{Lift slope} = \frac{dc_l}{d\alpha} = 2\pi \quad (4.58)$$

Equations (4.57) and (4.58) are important results. Note that, as in the case of the symmetric airfoil, the theoretical lift slope for a cambered airfoil is  $2\pi$ . It is a general result from thin airfoil theory that  $dc_l/d\alpha = 2\pi$  for any shape airfoil. However, the expression for  $c_l$  itself differs between a symmetric and a cambered airfoil, the difference being the integral term in Eq. (4.57). This integral term has physical significance, as follows. Return to Fig. 4-4, which illustrates the lift curve for an airfoil. The angle of zero lift is denoted by  $\alpha_{l=0}$  and is a negative value. From the geometry shown in Fig. 4-4, clearly

$$c_l = \frac{dc_l}{d\alpha} (\alpha - \alpha_{l=0}) \quad (4.59)$$

Substituting Eq. (4.58) into (4.59), we have

$$c_l = 2\pi(\alpha - \alpha_{l=0}) \quad (4.60)$$

Comparing Eqs. (4.60) and (4.57), we see that the integral term in Eq. (4.57) is simply the negative of the zero-lift angle; that is,

$$\alpha_{l=0} = -\frac{1}{\pi} \int_0^\pi \frac{dz}{dx} (\cos \theta_0 - 1) d\theta_0 \quad (4.61)$$

Hence, from Eq. (4.61), thin airfoil theory provides a means to predict the angle of zero lift. Note that Eq. (4.61) yields  $\alpha_{l=0} = 0$  for a symmetric airfoil, which is consistent with the results shown in Fig. 4-20. Also note that the more highly cambered the airfoil, the larger the absolute magnitude of  $\alpha_{l=0}$ .

Returning to Fig. 4.21, the moment about the leading edge can be obtained by substituting  $\gamma(\theta)$  from Eq. (4.43) into the transformed version of Eq. (4.35). The details are left for Prob. 4.9. The result for the moment coefficient is

$$c_{m,k} = -\frac{\pi}{2} \left( A_0 + A_1 - \frac{A_2}{2} \right) \quad (4.62)$$

Substituting Eq. (4.56) into (4.62), we have

$$c_{m,k} = -\left[ \frac{c_l}{4} + \frac{\pi}{4} (A_1 - A_2) \right] \quad (4.63)$$

Note that, for  $dz/dx = 0$ ,  $A_1 = A_2 = 0$ , and Eq. (4.63) reduces to Eq. (4.39) for a symmetric airfoil.

The moment coefficient about the quarter chord can be obtained by substituting Eq. (4.63) into (4.40), yielding

$$c_{m,c/4} = \frac{\pi}{4} (A_2 - A_1) \quad (4.64)$$

Unlike the symmetric airfoil, where  $c_{m,c/4} = 0$ , Eq. (4.64) demonstrates that  $c_{m,c/4}$  is finite for a cambered airfoil. Therefore, the quarter chord is *not* the center of pressure for a cambered airfoil. However, note that  $A_1$  and  $A_2$  depend only on the shape of the camber line and do not involve the angle of attack. Hence, from Eq. (4.64),  $c_{m,c/4}$  is *independent* of  $\alpha$ . Thus, the quarter-chord point is the *theoretical location* of the aerodynamic center for a cambered airfoil.

The location of the center of pressure can be obtained from Eq. (1.21):

$$x_{cp} = -\frac{M'_{lift}}{L'} = -\frac{c_{m,k} c}{c_l} \quad (4.65)$$

Substituting Eq. (4.63) into (4.65), we obtain

$$x_{cp} = \frac{c}{4} \left[ 1 + \frac{\pi}{c_l} (A_1 - A_2) \right] \quad (4.66)$$

Equation (4.66) demonstrates that the center of pressure for a cambered airfoil varies with the lift coefficient. Hence, as the angle of attack changes, the center of pressure also changes. Indeed, as the lift approaches zero,  $x_{cp}$  moves toward infinity; i.e., it leaves the airfoil! For this reason, the center of pressure is not always a convenient point at which to draw the force system on an airfoil. Rather, the force-and-moment system on an airfoil is more conveniently considered at the aerodynamic center. (Return to Fig. 1.17 and the discussion at the end of Sec. 1.6 for the referencing of the force-and-moment system on an airfoil.)

In Ref. 13, the numerical values of  $A_0$ ,  $A_1$ , and  $A_2$  are obtained for an NACA 2412 airfoil by integrating Eqs. (4.50) and (4.51). The results are  $A_0 = \alpha - 0.004517$ ,  $A_1 = 0.08146$ , and  $A_2 = 0.01387$ . When substituted into Eqs. (4.57), (4.61), and (4.64), these numbers yield the following values for the theoretical aerodynamic properties of the NACA 2412 airfoil:  $c_l = 2\pi\alpha + 0.2297$ ,  $\alpha_{l=0} = -2.095^\circ$ , and  $c_{m,c/4} = -0.05309$ . These theoretical results are compared with experimental data in Fig. 4.5. Reflecting on this comparison, we conclude that thin airfoil theory does a reasonable job in predicting the actual airfoil lift and moment properties.

This brings to an end our introduction to classical thin airfoil theory. Returning to our road map in Fig. 4.2, we have now completed the right-hand branch.

## 4.9 LIFTING FLOWS OVER ARBITRARY BODIES: THE VORTEX PANEL NUMERICAL METHOD

The thin airfoil theory described in Sec. 4.7 and 4.8 is just what it says — it applies only to thin airfoils at small angles of attack. (Make certain that you understand exactly where in the development of thin airfoil theory these assumptions are made and the reasons for making them.) The advantage of thin airfoil theory is that closed-form expressions are obtained for the aerodynamic coefficients. Moreover, the results compare favorably with experimental data for airfoils of about 1/2 percent thickness or less. However, the airfoils on many low-speed airplanes are thicker than 1/2 percent. Moreover, we are frequently interested in high angles of attack, such as occur during takeoff and landing. Finally, we are sometimes concerned with the generation of aerodynamic lift on other body shapes, such as automobiles or submarines. Hence, thin airfoil theory is quite restrictive when we consider the whole spectrum of aerodynamic applications. We need a method that allows us to calculate the aerodynamic characteristics of bodies of arbitrary shape, thickness, and orientation. Such a method is described in this section. Specifically, we treat the vortex panel method, which is a numerical technique that has come into widespread use since the early 1970s. In reference to our road map in Fig. 4.2, we now move to the left-hand branch. Also, since this chapter deals with airfoils, we limit our attention to two-dimensional bodies.

The vortex panel method is directly analogous to the source panel method described in Sec. 3.17. However, because a source has zero circulation, source panels are useful only for nonlifting cases. In contrast, vortices have circulation, and hence vortex panels can be used for lifting cases. (Because of the similarities between source and vortex panel methods, return to Sec. 3.17 and review the basic philosophy of the source panel method before proceeding further.)

The philosophy of covering a body *surface* with a vortex sheet of such a strength to make the surface a streamline of the flow was discussed in Sec. 4.4. We then went on to simplify this idea by placing the vortex sheet on the camber line of the airfoil as shown in Fig. 4.11, thus establishing the basis for thin airfoil theory. We now return to the original idea of wrapping the vortex sheet over the complete surface of the body, as shown in Fig. 4.10. We wish to find  $\gamma(s)$  such that the body surface becomes a streamline of the flow. There exists no closed-form analytical solution for  $\gamma(s)$ ;

rather, the solution must be obtained numerically. This is the purpose of the vortex panel method.

Let us approximate the vortex sheet shown in Fig. 4.10 by a series of straight panels, as shown earlier in Fig. 3.31. (In Chap. 3, Fig. 3.31 was used to discuss source panels; here, we use the same sketch for our discussion of vortex panels.) Let the vortex strength  $\gamma(s)$  per unit length be constant over a given panel, but allow it to vary from one panel to the next. That is, for the  $n$  panels shown in Fig. 3.31, the vortex panel strengths per unit length are  $\gamma_1, \gamma_2, \dots, \gamma_j, \dots, \gamma_n$ . These panel strengths are unknowns; the main thrust of the panel technique is to solve for  $\gamma_i, j = 1 \text{ to } n$ , such that the body surface becomes a streamline of the flow and such that the Kutta condition is satisfied. As explained in Sec. 3.17, the midpoint of each panel is a control point at which the boundary condition is applied; i.e., at each control point, the normal component of the flow velocity is zero.

Let  $P$  be a point located at  $(x, y)$  in the flow, and let  $r_{ij}$  be the distance from any point on the  $j$ th panel to  $P$ , as shown in Fig. 3.31. The radius  $r_{ij}$  makes the angle  $\theta_{ij}$  with respect to the  $x$  axis. The velocity potential induced at  $P$  due to the  $j$ th panel,  $\Delta\phi_j$ , is, from Eq. (4.3),

$$\Delta\phi_j = -\frac{1}{2\pi} \int_j \theta_{ij} \gamma_j ds_j \quad (4.67)$$

In Eq. (4.67),  $\gamma_j$  is constant over the  $j$ th panel, and the integral is taken over the  $j$ th panel only. The angle  $\theta_{ij}$  is given by

$$\theta_{ij} = \tan^{-1} \frac{y - y_j}{x - x_j} \quad (4.68)$$

In turn, the potential at  $P$  due to *all* the panels is Eq. (4.67) summed over all the panels:

$$\phi(P) = \sum_{j=1}^n \phi_j = -\sum_{j=1}^n \frac{\gamma_j}{2\pi} \int_j \theta_{ij} ds_j \quad (4.69)$$

Since point  $P$  is just an arbitrary point in the flow, let us put  $P$  at the control point of the  $i$ th panel shown in Fig. 3.31. The coordinates of this control point are  $(x_i, y_i)$ . Then Eqs. (4.68) and (4.69) become

$$\theta_{ij} = \tan^{-1} \frac{y_i - y_j}{x_i - x_j} \quad (4.70)$$

and

$$\phi(x_i, y_i) = -\sum_{j=1}^n \frac{\gamma_j}{2\pi} \int_j \theta_{ij} ds_j$$

Equation (4.70) is physically the contribution of *all* the panels to the potential at the control point of the  $i$ th panel.

At the control points, the normal component of the velocity is zero; this velocity is the superposition of the uniform flow velocity and the velocity induced by all the vortex panels. The component of  $V_x$  normal to the  $i$ th panel is given by Eq. (3.148):

$$V_{x,n} = V_x \cos \beta_i \quad (3.148)$$

The normal component of velocity induced at  $(x_i, y_i)$  by the vortex panels is

$$V_n = \frac{\partial}{\partial n_i} [\phi(x_i, y_i)] \quad (4.71)$$

Combining Eqs. (4.70) and (4.71), we have

$$V_n = -\sum_{j=1}^n \frac{\gamma_j}{2\pi} \int_j \frac{\partial \theta_{ij}}{\partial n_i} ds_j \quad (4.72)$$

where the summation is over all the panels. The normal component of the flow velocity at  $i$ th control point is the sum of that due to the freestream [Eq. (3.148)] and that due to the vortex panels [Eq. (4.72)]. The boundary condition states that this sum must be zero:

$$V_{x,n} + V_n = 0 \quad (4.73)$$

Substituting Eqs. (3.148) and (4.72) into (4.73), we obtain

$$V_x \cos \beta_i - \sum_{j=1}^n \frac{\gamma_j}{2\pi} \int_j \frac{\partial \theta_{ij}}{\partial n_i} ds_j = 0 \quad (4.74)$$

Equation (4.74) is the crux of the vortex panel method. The values of the integrals in Eq. (4.74) depend simply on the panel geometry; they are not properties of the flow. Let  $J_{i,j}$  be the value of this integral when the control point is on the  $i$ th panel. Then Eq. (4.74) can be written as

$$V_x \cos \beta_i - \sum_{j=1}^n \frac{\gamma_j}{2\pi} J_{i,j} = 0 \quad (4.75)$$

Equation (4.75) is a linear algebraic equation with  $n$  unknowns,  $\gamma_1, \gamma_2, \dots, \gamma_n$ . It represents the flow boundary condition evaluated at the control point of the  $i$ th panel. If Eq. (4.75) is applied to the control points of *all* the panels, we obtain a system of  $n$  linear equations with  $n$  unknowns.

To this point, we have been deliberately paralleling the discussion of the source panel method given in Sec. 3.17; however, the similarity stops here. For the source panel method, the  $n$  equations for the  $n$  unknown source strengths are routinely solved, giving the flow over a nonlifting body. In contrast, for the lifting case with vortex panels, in addition to the  $n$  equations given by Eq. (4.75) applied at all the panels, we must also satisfy the Kutta condition. This can be done in several ways. For example, consider Fig. 4.22, which illustrates a detail of the vortex panel distribution at the

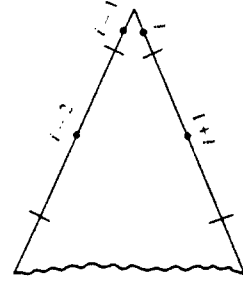


Figure 4.22 Vortex panels at the trailing edge.

trailing edge. Note that the length of each panel can be different; their length and distribution over the body is up to your discretion. Let the two panels at the trailing edge (panels  $i$  and  $i - 1$  in Fig. 4.22) be very small. The Kutta condition is applied precisely at the trailing edge and is given by  $\gamma(\text{TE}) = 0$ . To approximate this numerically, if points  $i$  and  $i - 1$  are close enough to the trailing edge, we can write

$$\gamma_i = -\gamma_{i-1} \quad (4.76)$$

such that the strengths of the two vortex panels  $i$  and  $i - 1$  exactly cancel at the point where they touch at the trailing edge. Thus, in order to impose the Kutta condition on the solution of the flow, Eq. (4.76) (or an equivalent expression) must be included. Note that Eq. (4.75) evaluated at all the panels and Eq. (4.76) constitute an *over-determined* system of  $n$  unknowns with  $n + 1$  equations. Therefore, to obtain a determined system, Eq. (4.75) is not evaluated at one of the control points on the body. That is, we choose to ignore one of the control points, and we evaluate Eq. (4.75) at the other  $n - 1$  control points. This, in combination with Eq. (4.76), now gives a system of  $n$  linear algebraic equations with  $n$  unknowns, which can be solved by standard techniques.

At this stage, we have conceptually obtained the values of  $\gamma_1, \gamma_2, \dots, \gamma_n$  which make the body surface a streamline of the flow and which also satisfy the Kutta condition. In turn, the flow velocity tangent to the surface can be obtained directly from  $\gamma$ . To see this more clearly, consider the airfoil shown in Fig. 4.23. We are concerned only with the flow outside the airfoil and on its surface. Therefore, let the velocity be zero at every point *inside* the body, as shown in Fig. 4.23. In particular, the velocity just inside the vortex sheet on the surface is zero. This corresponds to  $u_2 = 0$  in Eq. (4.8). Hence the velocity just outside the vortex sheet is, from Eq. (4.8),

$$\gamma = u_1 - u_2 = u_1 - 0 = u_1$$

In Eq. (4.8),  $u$  denotes the velocity tangential to the vortex sheet. In terms of the picture shown in Fig. 4.23, we obtain  $V_a = \gamma_a$  at point  $a$ ,  $V_b = \gamma_b$  at point  $b$ , etc. Therefore, the local velocities tangential to the airfoil surface are equal to the local values of  $\gamma$ .

In turn, the local pressure distribution can be obtained from Bernoulli's equation. The total circulation and the resulting lift are obtained as follows. Let  $s_j$  be the length of the  $j$ th panel. Then the circulation due to the  $j$ th panel is  $\gamma_j s_j$ . In turn, the total circulation due to all the panels is

$$\Gamma = \sum_{j=1}^n \gamma_j s_j \quad (4.77)$$

Hence, the lift per unit span is obtained from

$$L' = \rho_\infty V_\infty \sum_{j=1}^n \gamma_j s_j \quad (4.78)$$

The presentation in this section is intended to give only the general flavor of the vortex panel method. There are many variations of the method in use today, and you are encouraged to read the modern literature, especially as it appears in the *AIAA Journal* and the *Journal of Aircraft* since 1970. The vortex panel method as described

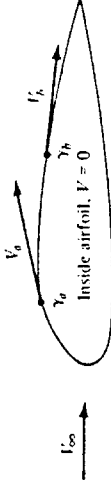


Figure 4.23 Airfoil as a solid body, with zero velocity inside the profile.

in this section is termed a "first-order" method because it assumes a constant value of  $\gamma$  over a given panel. Although the method may appear to be straightforward, its numerical implementation can sometimes be frustrating. For example, the results for a given body are sensitive to the number of panels used, their various sizes, and the way they are distributed over the body surface (i.e., it is usually advantageous to place a large number of small panels near the leading and trailing edges of an airfoil and a smaller number of larger panels in the middle). The need to ignore one of the control points in order to have a determined system in  $n$  equations for  $n$  unknowns also introduces some arbitrariness in the numerical solution. Which control point do you ignore? Different choices sometimes yield different numerical answers for the distribution of  $\gamma$  over the surface. Moreover, the resulting numerical distributions for  $\gamma$  are not always smooth, but rather they have oscillations from one panel to the next as a result of numerical inaccuracies. The problems mentioned above are usually overcome in different ways by different groups who have developed relatively sophisticated panel programs for practical use. Again, you are encouraged to consult the literature for more information.

Such accuracy problems have encouraged the development of higher-order panel techniques. For example, a "second-order" panel method assumes a *linear* variation of  $\gamma$  over a given panel, as sketched in Fig. 4.24. Here, the value of  $\gamma$  at the edges of each panel is matched to its neighbors, and the values  $\gamma_1, \gamma_2, \gamma_3$ , etc., at the *boundary points* become the unknowns to be solved. The flow-tangency boundary condition is still applied at the *control point* of each panel, as before. Some results using a second-order vortex panel technique are given in Fig. 4.25, which shows the distribution of pressure coefficients over the upper and lower surfaces of an NACA 0012 airfoil at a 9° angle of attack. The circles and squares are numerical results from a second-order vortex panel technique developed at the University of Maryland, and the solid lines are from NACA results given in Ref. 11. Excellent agreement is obtained.

Finally, many groups developing and using panel techniques use a combination of source panels and vortex panels for lifting bodies — source panels to accurately represent-

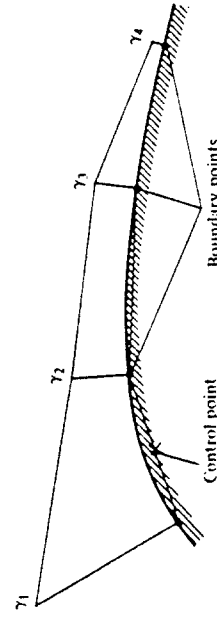


Figure 4.24 Linear distribution of  $\gamma$  over each panel — a second-order panel method.

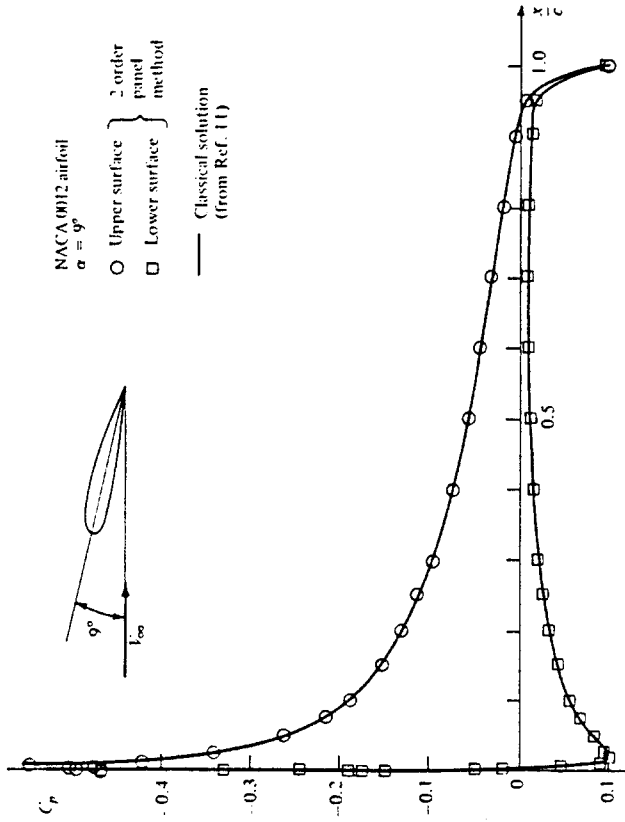


Figure 4.25 Pressure coefficient distribution over an NACA 0012 airfoil: comparison between second-order vortex panel method and NACA theoretical results from Ref. 11. The numerical panel results were obtained by one of the author's graduate students, Mr. Tae-Hwan Cho.

sent the thickness of the body and vortex panels to provide circulation. Again, you are encouraged to consult the literature. For example, Ref. 14 is a classic paper on panel methods, and Ref. 15 highlights many of the basic concepts of panel methods along with actual computer program statement listings for simple applications.

#### 4.10 MODERN LOW-SPEED AIRFOILS

The nomenclature and aerodynamic characteristics of standard NACA airfoils are discussed in Sec. 4.2 and 4.3; before progressing further, you should review these sections in order to reinforce your knowledge of airfoil behavior, especially in light of our discussions on airfoil theory. Indeed, the purpose of this section is to provide a modern sequel to the airfoils discussed in Sec. 4.2 and 4.3.

During the 1970s, NASA designed a series of low-speed airfoils that have performance superior to the earlier NACA airfoils. The standard NACA airfoils were based almost exclusively on experimental data obtained during the 1930s and 1940s. In contrast, the new NASA airfoils were designed on a computer using a numerical technique similar to the source and vortex panel methods discussed earlier, along with numerical predictions of the viscous flow behavior (skin friction and flow separation).

Wind-tunnel tests were then conducted to verify the computer-designed profiles and to obtain the definitive airfoil properties. Out of this work first came the general aviation-Whitcomb [GA(W)-1] airfoil, which has since been redesignated the LS(1)-0417 airfoil. The shape of this airfoil is given in Fig. 4.26, obtained from Ref. 16. Note that it has a large leading-edge radius ( $0.08c$  in comparison to the standard  $0.02c$ ) in order to flatten the usual peak in pressure coefficient near the nose. Also, note that the bottom surface near the trailing edge is canted in order to increase the camber and hence the aerodynamic loading in that region. Both design features tend to discourage flow separation over the top surface at high angle of attack, hence yielding higher values of the maximum lift coefficient. The experimentally measured lift and moment properties (from Ref. 16) are given in Fig. 4.27, where they are compared with the properties for an NACA 2412 airfoil, obtained from Ref. 11. Note that  $C_{l,\max}$  for the NASA LS(1)-0417 is considerably higher than for the NACA 2412.

The NASA LS(1)-0417 airfoil has a maximum thickness of 17 percent and a design lift coefficient of 0.4. Using the same camber line, NASA has extended this airfoil into a family of low-speed airfoils of different thicknesses, e.g., the NASA LS(1)-0409 and the LS(1)-0413. (See Ref. 17 for more details.) In comparison with the standard NACA airfoils having the same thicknesses, these new LS(1)-04xx airfoils all have

1. Approximately 30 percent higher  $C_{l,\max}$ .
2. Approximately a 50 percent increase in the ratio of lift to drag ( $L/D$ ) at a lift coefficient of 1.0. This value of  $c_l = 1.0$  is typical of the climb lift coefficient for general aviation aircraft, and a high value of  $L/D$  greatly improves the climb performance. (See Ref. 2 for a general introduction to airplane performance and the importance of a high  $L/D$  ratio to airplane efficiency.)

It is interesting to note that the shape of the airfoil in Fig. 4.26 is very similar to the supercritical airfoils to be discussed in Chap. 11. The development of the supercritical airfoil by NASA aerodynamicist Richard Whitcomb in 1965 resulted in a major improvement in airfoil drag behavior at high subsonic speeds, near Mach 1. The supercritical airfoil was a major breakthrough in high-speed aerodynamics. The LS(1)-0417 low-speed airfoil shown in Fig. 4.26, first introduced as the GA(W)-1 airfoil, was a later spin-off from supercritical airfoil research. It is also interesting to note that the first production aircraft to use the NASA LS(1)-0417 airfoil was the Piper PA-38 Tomahawk, introduced in the late 1970s.

In summary, new airfoil development is alive and well in the aeronautics of the late twentieth century. Moreover, in contrast to the purely experimental development of the earlier airfoils, we now enjoy the benefit of powerful computer programs using panel



Figure 4.26 Profile for the NASA LS(1)-0417 airfoil. When first introduced, this airfoil was labeled the GA(W)-1 airfoil, a nomenclature which has now been superseded. (From Ref. 16.)

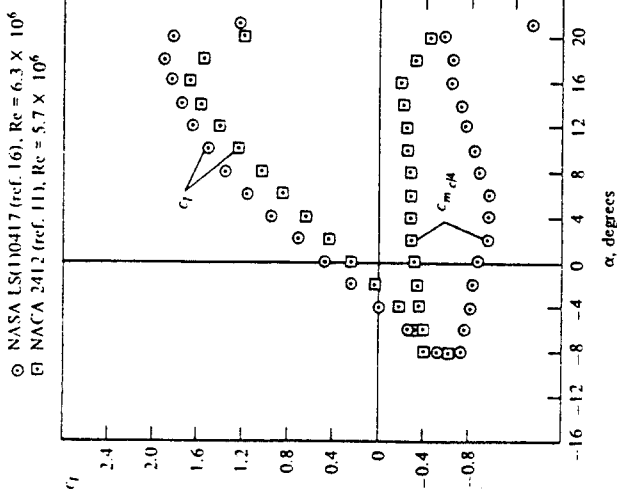


Figure 4.27 Comparison of the modern NASA LS(1)-0417 airfoil with the standard NACA 2412 airfoil.

methods and advanced viscous flow solutions for the design of new airfoils. Indeed, NASA has established an official Airfoil Design Center at The Ohio State University, which services the entire general aviation industry with over 30 different computer programs for airfoil design and analysis. For additional information on such new low-speed airfoil development, you are urged to read Ref. 16, which is the classic first publication dealing with these airfoils, as well as the concise review given in Ref. 17.

#### 4.11 HISTORICAL NOTE: KUTTA, JOUKOWSKI, AND THE CIRCULATION THEORY OF LIFT

Frederick W. Lanchester (1868–1946), an English engineer, automobile manufacturer, and self-styled aerodynamicist, was the first to connect the idea of circulation with lift. His thoughts were originally set forth in a presentation given before the Birmingham Natural History and Philosophical Society in 1894 and later contained in a paper submitted to the Physical Society, which turned it down. Finally, in 1907 and 1908, he published two books, entitled *Aerodynamics* and *Aerodonetics*, where his thoughts on circulation and lift were described in detail. His books were later translated into German in 1909 and French in 1914. Unfortunately, Lanchester's style of writing was difficult to read and understand; this is partly responsible for the general lack of interest shown by British scientists in Lanchester's work. Consequently, little positive benefit was

derived from Lanchester's writings. (See Sec. 5.6 for a more detailed portrait of Lanchester and his work.)

Quite independently, and with total lack of knowledge of Lanchester's thinking, M. Wilhelm Kutta (1867–1944) developed the idea that lift and circulation are related. Kutta was born in Pitschen, Germany, in 1867 and obtained a Ph.D. in mathematics from the University of Munich in 1902. After serving as professor of mathematics at several German technical schools and universities, he finally settled at the Technische Hochschule in Stuttgart in 1911 until his retirement in 1935. Kutta's interest in aerodynamics was initiated by the successful glider flights of Otto Lilienthal in Berlin during the period 1890–1896 (see chapter 1 of Ref. 2). Kutta attempted to theoretically calculate the lift on the curved wing surfaces used by Lilienthal. In the process, he surmised from experimental data that the flow left the trailing edge of a sharp-edged body smoothly and that this condition fixed the circulation around the body (the Kutta condition, described in Sec. 4.5). At the same time, he was convinced that circulation and lift were connected. Kutta was reluctant to publish these ideas, but after the strong insistence of his teacher, S. Finsterwalder, he wrote a paper entitled "Auftriebskräfte in Stromenden Flüssigkeiten" (Lift in Flowing Fluids). This was actually a short note abstracted from his longer graduation paper in 1902, but it represents the first time in history where the concepts of the Kutta condition as well as the connection of circulation with lift were officially published. Finsterwalder clearly repeated the ideas of his student in a lecture given on September 6, 1909, in which he stated:

On the upper surface the circulatory motion increases the translatory one, therefore there is high velocity and consequently low pressure, while on the lower surface the two movements are opposite, therefore there is low velocity with high pressure, with the result of a thrust upward.

However, in his 1902 note, Kutta did not give the precise quantitative relation between circulation and lift. This was left to Nikolai Y. Joukowski (Zhukowski). Joukowski was born in Orehkovo in central Russia on January 5, 1847. The son of an engineer, he became an excellent student of mathematics and physics, graduating with a Ph.D. in applied mathematics from Moscow University in 1882. He subsequently held a joint appointment as a professor of mechanics at Moscow University and the Moscow Higher Technical School. It was at this latter institution that Joukowski built in 1902 the first wind tunnel in Russia. Joukowski was deeply interested in aeronautics, and he combined a rare gift for both experimental and theoretical work in the field. He expanded his wind tunnel into a major aerodynamics laboratory in Moscow. Indeed, during World War I, his laboratory was used as a school to train military pilots in the principles of aerodynamics and flight. When he died in 1921, Joukowski was by far the most noted aerodynamicist in Russia.

Much of Joukowski's fame was derived from a paper published in 1906, wherein he gives, for the first time in history, the relation  $L' = \rho_s V_x \Gamma$  — the Kutta-Joukowski theorem. In Joukowski's own words:

If an irrotational two-dimensional fluid current, having at infinity the velocity  $V_x$ , surrounds any closed contour on which the circulation of velocity is  $\Gamma$ , the force of the aerodynamic pressure acts on this contour in a direction perpendicular to the velocity and has the value

$L' = p, \mathbf{V}, \Gamma$

The direction of this force is found by causing to rotate through a right angle the vector  $V$ , around its origin in an inverse direction to that of the circulation.

Joukowski was unaware of Kutta's 1902 note, and developed his ideas on circulation and lift independently. However, in recognition of Kutta's contribution, the equation given above has propagated through the twentieth century as the "Kutta-Joukowski theorem."

Hence, by 1906—just 3 years after the first successful flight of the Wright brothers—the circulation theory of lift was in place, ready to aid aerodynamics in the design and understanding of lifting surfaces. In particular, this principle formed the cornerstone of the thin airfoil theory described in Secs. 4.7 and 4.8. Thin airfoil theory was developed by Max Munk, a colleague of Prandtl in Germany, during the first few years after World War I. However, the very existence of thin airfoil theory, as well as its amazingly good results, rests upon the foundation laid by Lanchester, Kutta, and Joukowski a decade earlier.

## 4.12 SUMMARY

Return to the road map given in Fig. 4.2. Make certain that you feel comfortable with the material represented by each box on the road map and that you understand the flow of ideas from one box to another. If you are uncertain about one or more aspects, review the pertinent sections before progressing further.

Some important results from this chapter are itemized below.

A vortex sheet can be used to synthesize the inviscid, incompressible flow over an airfoil. If the distance along the sheet is given by  $s$  and the strength of the sheet per unit length is  $\gamma(s)$ , then the velocity potential induced at point  $(x, y)$  by a vortex sheet that extends from point  $a$  to point  $b$  is

$$\phi(x, y) = -\frac{1}{2\pi} \int_a^b \theta \gamma(s) ds \quad (4.3)$$

The circulation associated with this vortex sheet is

$$\Gamma = \int_a^b \gamma(s) ds \quad (4.4)$$

Across the vortex sheet, there is a tangential velocity discontinuity, where

$$\gamma = u_1 - u_2 \quad (4.8)$$

The Kutta condition is an observation that for a lifting airfoil of given shape at a given angle of attack, nature adopts that particular value of circulation around the

airfoil which results in the flow leaving smoothly at the trailing edge. If the trailing-edge angle is finite, then the trailing edge is a stagnation point. If the trailing edge is cusped, then the velocities leaving the top and bottom surfaces at the trailing edge are finite and equal in magnitude and direction. In either case,

$$\gamma(\text{TE}) = 0 \quad (4.10)$$

Thin airfoil theory is predicated on the replacement of the airfoil by the mean camber line. A vortex sheet is placed along the chord line, and its strength adjusted such that, in conjunction with the uniform freestream, the camber line becomes a streamline of the flow while at the same time satisfying the Kutta condition. The strength of such a vortex sheet is obtained from the fundamental equation of thin airfoil theory,

$$\frac{1}{2\pi} \int_0^c \frac{\gamma(\xi) d\xi}{x - \xi} = V_x \left( \alpha - \frac{d\alpha}{dx} \right) \quad (4.18)$$

Results of thin airfoil theory:

Symmetric airfoil

1.  $c_l = 2\pi\alpha$ .
  2. Lift slope  $= dc_l/d\alpha = 2\pi$ .
  3. The center of pressure and the aerodynamic center are both at the quarter-chord point.
  4.  $C_{m,c/4} = C_{m,\infty} = 0$ .
- Cambered airfoil
1.  $c_l = 2\pi[\alpha + (1/\pi) \int_0^c (dz/dx)(\cos \theta_0 - 1) d\theta_0]$ .
  2. Lift slope  $= dc_l/d\alpha = 2\pi$ .
  3. The aerodynamic center is at the quarter-chord point.
  4. The center of pressure varies with the lift coefficient.

The vortex panel method is an important numerical technique for the solution of the inviscid, incompressible flow over bodies of arbitrary shape, thickness, and angle of attack. For panels of constant strength, the governing equations are

$$V_x \cos \beta_i - \sum_{j=1}^n \frac{\gamma_j}{2\pi} \int_j \frac{\partial \theta_{ij}}{\partial n_i} ds_j = 0 \quad (i = 1, 2, \dots, n)$$

$$\gamma_i = -\gamma_{i-1}$$

which is one way of expressing the Kutta condition for the panels immediately above and below the trailing edge.

## PROBLEMS

4.1 Consider the data for the NACA 2412 airfoil given in Fig. 4.5. Calculate the lift and moment about the quarter-chord (per unit span) for this airfoil when the angle of attack is  $4^\circ$  and the freestream is at standard sea level conditions with a velocity of 50 ft/s. The chord of the airfoil is 2 ft.

4.2 Consider an NACA 2412 airfoil with a 2-m chord in an airstream with a velocity of 50 m/s at standard sea level conditions. If the lift per unit span is 1353 N, what is the angle of attack?

4.3 Starting with the definition of circulation, derive Kelvin's circulation theorem, Eq. (4.11).

4.4 Starting with Eq. (4.35), derive Eq. (4.36).

4.5 Consider a thin, symmetric airfoil at  $1.5^\circ$  angle of attack. From the results of thin airfoil theory, calculate the lift coefficient and the moment coefficient about the leading edge.

4.6 The NACA 4412 airfoil has a mean camber line given by

$$\frac{z}{c} = \begin{cases} 0.25 \left[ 0.8 \frac{x}{c} - \left( \frac{x}{c} \right)^2 \right] & \text{for } 0 \leq \frac{x}{c} \leq 0.4 \\ 0.11 \left[ 0.2 + 0.8 \frac{x}{c} - \left( \frac{x}{c} \right)^2 \right] & \text{for } 0.4 \leq \frac{x}{c} \leq 1 \end{cases}$$

Using thin airfoil theory, calculate

(a)  $\alpha_{L,0}$     (b)  $c_L$  when  $\alpha = 3^\circ$

4.7 For the airfoil given in Prob. 4.6, calculate  $c_{m,0}/c$  and  $x_{cp}/c$  when  $\alpha = 3^\circ$ .

4.8 Compare the results of Probs. 4.6 and 4.7 with experimental data for the NACA 4412 airfoil, and note the percentage difference between theory and experiment. (*Hin:* A good source of experimental airfoil data is Ref. 11.)

4.9 Starting with Eqs. (4.35) and (4.43), derive Eq. (4.62).

## INCOMPRESSIBLE FLOW OVER FINITE WINGS

*The one who has most carefully watched the soaring birds of prey sees man with wings and the faculty of using them.*

*James Means, Editor of the Aeronautical Annual, 1895*

### 5.1 INTRODUCTION: DOWNWASH AND INDUCED DRAG

In Chap. 4 we discussed the properties of airfoils, which are the same as the properties of a wing of infinite span; indeed, airfoil data are frequently denoted as "infinite wing" data. However, all real airplanes have wings of finite span, and the purpose of the present chapter is to apply our knowledge of airfoil properties to the analysis of such finite wings. This is the second step in Prandtl's philosophy of wing theory, as described in Sec. 4.1. You should review Sec. 4.1 before proceeding further.

*Question:* Why are the aerodynamic characteristics of a finite wing any different than the properties of its airfoil sections? Indeed, an airfoil is simply a section of a wing, and at first thought, you might expect the wing to behave exactly the same as the airfoil. However, as studied in Chap. 4, the flow over an airfoil is two-dimensional. In contrast, a finite wing is a three-dimensional body, and consequently the flow over the finite wing is three-dimensional; i.e., there is a component of flow in the spanwise direction. To see this more clearly, examine Fig. 5.1, which gives the top and front views of a finite wing. The physical mechanism for generating lift on the wing is the existence of a high pressure on the bottom surface and a low pressure on the top surface. The net imbalance of the pressure distribution creates the lift, as discussed in Sec. 1.5. However, as a by-product of this pressure imbalance, the flow near the wing tips tends to curl around the tips, being forced from the high-pressure region just underneath the tips to the low-pressure region on top. This flow around the wing tips is shown in the front view of the wing in Fig. 5.1. As a result, on the top surface of the wing, there is generally a spanwise component of flow from the tip toward the wing root, causing the streamlines over the top surface to bend toward the root, as sketched on the top view shown in Fig. 5.1. Similarly, on the bottom surface of the wing, there is generally a

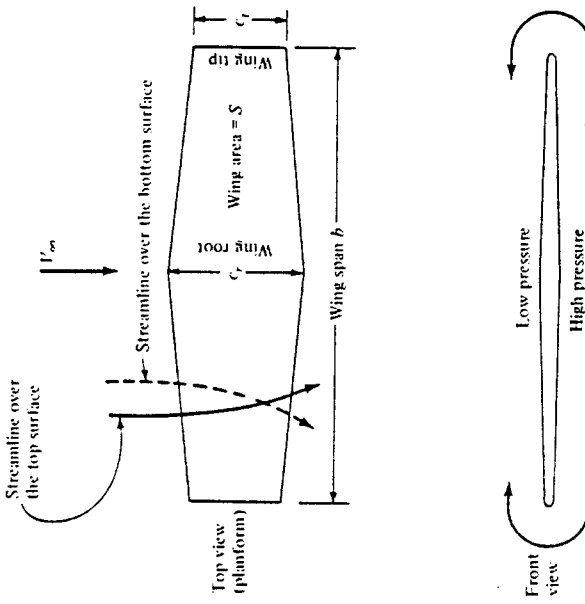


Figure 5.2 Finite wing. In this figure, the curvature of the streamlines over the top and bottom of the wing is exaggerated for clarity.

spanwise component of flow from the root toward the tip, causing the streamlines over the bottom surface to bend toward the tip. Clearly, the flow over the finite wing is three-dimensional, and therefore you would expect the overall aerodynamic properties of such a wing to differ from those of its airfoil sections.

The tendency for the flow to "leak" around the wing tips has another important effect on the aerodynamics of the wing. This flow establishes a circulatory motion which trails downstream of the wing; i.e., a trailing vortex is created at each wing tip. These wing-tip vortices are sketched in Fig. 5.2 and are illustrated in Fig. 5.3. The tip vortices are essentially weak "tornadoes" that trail downstream of the finite wing. (For

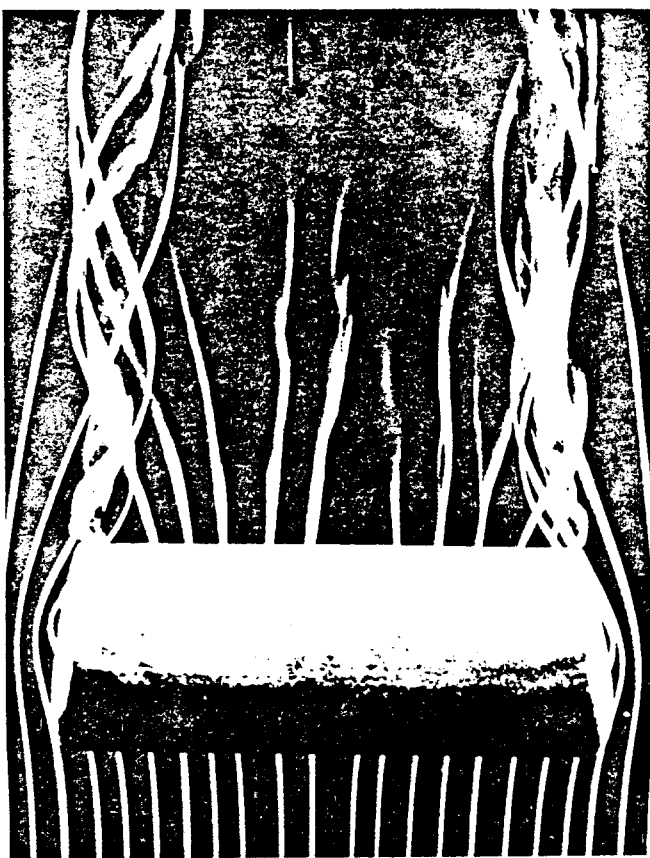


Figure 5.3 Wing-tip vortices from a rectangular wing. The wing is in a smoke tunnel, where individual streamtubes are made visible by means of smoke filaments. [From H. Head, M. R. in "Flow Visualization II," W. Merzkirch (ed.), Hemisphere Publishing Co., 1982, pp. 399-403. Also available in Van Dyke, M., "An Album of Fluid Motion," Parabolic Press, 1982.]

large airplanes such as a Boeing 747, these tip vortices can be powerful enough to cause light airplanes following too closely to go out of control. Such accidents have occurred, and this is one reason for large spacings between aircraft landing or taking off consecutively at airports.) These wing-tip vortices downstream of the wing induce a small downward component of air velocity in the neighborhood of the wing itself. This can be seen by inspecting Fig. 5.3; the two vortices tend to drag the surrounding air around with them, and this secondary movement induces a small velocity component in the downward direction at the wing. This downward component is called *downwash*, denoted by the symbol  $w$ . In turn, the downwash combines with the freestream velocity  $V_\infty$  to produce a *local relative wind* which is carried downward in the vicinity of each airfoil section of the wing, as sketched in Fig. 5.4.

Examine Fig. 5.4 closely. The angle between the chord line and the direction of  $V_r$  is the angle of attack  $\alpha$ , as defined in Sec. 1.5 and as used throughout our discussion of airfoil theory in Chap. 4. We now more precisely define  $\alpha$  as the *geometric angle of attack*. In Fig. 5.4, the local relative wind is inclined below the direction of  $V_r$  by the angle  $\alpha_r$ , called the *induced angle of attack*. The presence of downwash, and its effect on inclining the local relative wind in the downward direction, has two important effects on the local airfoil section, as follows:

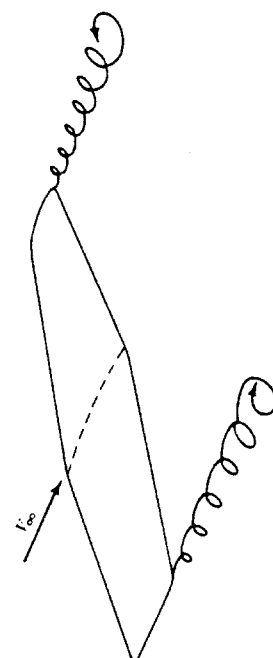


Figure 5.4 Schematic of wing-tip vortices.

by the aircraft engine, which is the only source of power associated with the airplane. Since the energy of the vortices serves no useful purpose, this power is essentially lost. In effect, the extra power provided by the engine that goes into the vortices is the extra power required from the engine to overcome the induced drag.

Clearly, from the discussion in this section, the characteristics of a finite wing are *not* identical to the characteristics of its airfoil sections. Therefore, let us proceed to develop a theory that will enable us to analyze the aerodynamic properties of finite wings. In the process, we follow the road map given in Fig. 5.5 — keep in touch with this road map as we progress through the present chapter.

In this chapter, we note a difference in nomenclature. For the two-dimensional bodies considered in the previous chapters, the lift, drag, and moments per unit span have been denoted with primes, for example,  $L'$ ,  $D'$ , and  $M'$ , and the corresponding lift, drag, and moment coefficients have been denoted by lowercase letters, for example,  $c_l$ ,  $c_d$ , and  $c_m$ . In contrast, the lift, drag, and moments on a complete three-dimensional body such as a finite wing are given without primes, for example  $L$ ,  $D$ , and  $M$ , and the corresponding lift, drag, and moment coefficients are given by capital letters, for example,  $C_l$ ,  $C_d$ , and  $C_M$ . This distinction has already been mentioned in Sec. 1.5.

Finally, we note that the total drag on a subsonic finite wing in real life is the sum of the induced drag  $D_i$ , the skin friction drag  $D_f$ , and the pressure drag  $D_p$  due to flow separation. The latter two contributions are due to viscous effects, which are discussed in Chaps. 15 and 16. The sum of these two viscous-dominated drag contributions is called profile drag, as discussed in Sec. 4.3. The profile drag coefficient  $C_d$  for an NACA 2412 airfoil was given in Fig. 4.6. At a moderate angle of attack, the profile drag

$$\alpha_{\text{eff}} = \alpha - \alpha_i \quad (5.1)$$

1. The angle of attack actually seen by the local airfoil section is the angle between the chord line and the local relative wind. This angle is given by  $\alpha_{\text{eff}}$  in Fig. 5.4 and is defined as the *effective angle of attack*. Hence, although the wing is at a geometric angle of attack  $\alpha$ , the local airfoil section is seeing a smaller angle, namely, the effective angle of attack  $\alpha_{\text{eff}}$ . From Fig. 5.4,

$$\alpha_{\text{eff}} = \alpha - \alpha_i$$

2. The local lift vector is aligned perpendicular to the local relative wind and hence is inclined behind the vertical by the angle  $\alpha_i$ , as shown in Fig. 5.4. Consequently, there is a component of the local lift vector in the direction of  $V_x$ ; that is, there is a *drag* created by the presence of downwash. This drag is defined as *induced drag*, denoted by  $D_i$  in Fig. 5.4.

Hence, we see that the presence of downwash over a finite wing reduces the angle of attack that each section effectively sees, and moreover, it creates a component of drag — the induced drag  $D_i$ . Keep in mind that we are still dealing with an inviscid, incompressible flow, where there is no skin friction or flow separation. For such a flow, there is a *finite* drag — the induced drag — on a finite wing. D'Alembert's paradox does *not* occur for a finite wing.

The tilting backward of the lift vector shown in Fig. 5.4 is one way of visualizing the physical generation of induced drag. Two alternate ways are as follows:

1. The three-dimensional flow induced by the wing-tip vortices shown in Figs. 5.2 and 5.3 simply alters the pressure distribution on the finite wing in such a fashion that a net pressure imbalance exists in the direction of  $V_x$ ; that is, drag is created. In this sense, induced drag is a type of "pressure drag."
2. The wing-tip vortices contain a large amount of translational and rotational kinetic energy. This energy has to come from somewhere; indeed, it is ultimately provided

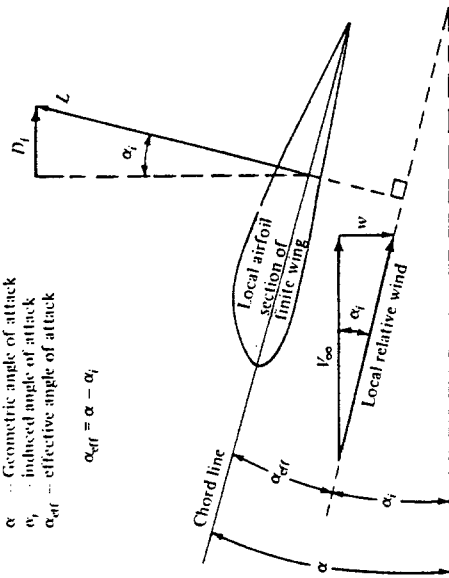


Figure 5.4 Effect of downwash on the local flow over a local airfoil section of a finite wing.

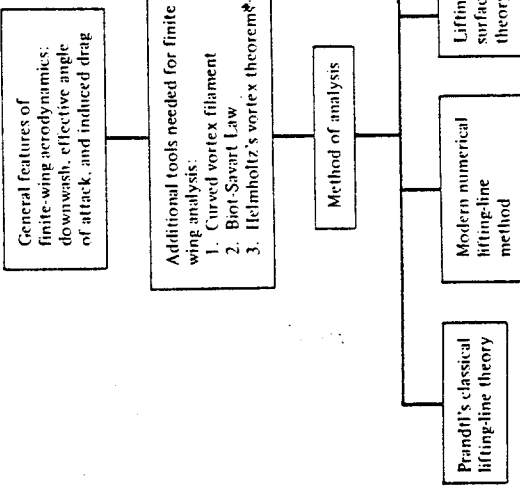


Figure 5.5 Roadmap for Chap. 5.

coefficient for a finite wing is essentially the same as for its airfoil sections. Hence, defining the profile drag coefficient as

$$(5.2) \quad c_d = \frac{D_f + D_p}{q_\infty S}$$

and the induced drag coefficient as

$$(5.3) \quad C_{D,i} = \frac{D_i}{q_\infty S}$$

the total drag coefficient for the finite wing,  $C_D$ , is given by

$$(5.4) \quad C_D = c_d + C_{D,i}$$

In Eq. (5.4), the value of  $c_d$  is usually obtained from airfoil data, such as given in Fig. 4.6. The value of  $C_{D,i}$  can be obtained from finite-wing theory as presented in this chapter. Indeed, one of the central objectives of the present chapter is to obtain an expression for induced drag and to study its variation with certain design characteristics of the finite wing. (See chapter 5 of Ref. 2 for an additional discussion of the characteristics of finite wings.)

## 5.2 THE VORTEX FILAMENT, THE BIOT-SAVART LAW, AND HELMHOLTZ'S THEOREMS

To establish a rational aerodynamic theory for a finite wing, we need to introduce a few additional aerodynamic tools. To begin with, we expand the concept of a vortex filament first introduced in Sec. 4.4. In Sec. 4.4, we discussed a *straight* vortex filament extending to  $\pm\infty$ . (Review the first paragraph of Sec. 4.4 before proceeding further.)

In general, a vortex filament can be *curved*, as shown in Fig. 5.6. Here, only a portion of the filament is illustrated. The filament induces a flow field in the surrounding space. If the circulation is taken about any path enclosing the filament, a constant value,  $\Gamma$ , is obtained. Hence, the strength of the vortex filament is defined as  $\Gamma$ . Consider a directed segment of the filament  $d\mathbf{l}$ , as shown in Fig. 5.6. The radius vector from  $d\mathbf{l}$  to an arbitrary point  $P$  in space is  $\mathbf{r}$ . The segment  $d\mathbf{l}$  induces a velocity at  $P$  equal to

$$(5.5) \quad d\mathbf{V} = \frac{\Gamma}{4\pi} \frac{d\mathbf{l} \times \mathbf{r}}{|\mathbf{r}|^3}$$

Equation (5.5) is called the *Biot-Savart law* and is one of the most fundamental relations in the theory of inviscid, incompressible flow. Its derivation is given in more advanced books (see, e.g., Ref. 9). Here, we must accept it without proof. However, you might feel more comfortable if we draw an analogy with electromagnetic theory. If the vortex filament in Fig. 5.6 were instead visualized as a wire carrying an electrical current  $I$ , then the magnetic field strength  $d\mathbf{B}$  induced at point  $P$  by a segment of the wire  $d\mathbf{l}$  with the current moving in the direction of  $d\mathbf{l}$  is

$$(5.6) \quad d\mathbf{B} = \frac{\mu I}{4\pi} \frac{d\mathbf{l} \times \mathbf{r}}{|\mathbf{r}|^3}$$

where  $\mu$  is the permeability of the medium surrounding the wire. Equation (5.6) is identical in form to Eq. (5.5). Indeed, the Biot-Savart law is a general result of potential theory, and potential theory describes electromagnetic fields as well as inviscid, incompressible flows. In fact, our use of the word "induced" in describing velocities generated by the presence of vortices, sources, etc., is a carry-over from the study of electromagnetic fields induced by electrical currents. When developing their finite-wing theory during the period 1911–1918, Prandtl and his colleagues even carried the electrical terminology over to the generation of drag, hence the term "induced" drag.

Return again to our picture of the vortex filament in Fig. 5.6. Keep in mind that this single vortex filament and the associated Biot-Savart law [Eq. (5.5)] are simply conceptual aerodynamic tools to be used for synthesizing more complex flows of an inviscid, incompressible fluid. They are, for all practical purposes, a solution of the governing equation for inviscid, incompressible flow — Laplace's equation (see Sec. 3.7) — and, by themselves, are not of particular value. However, when a number of vortex filaments are used in conjunction with a uniform freestream, it is possible to synthesize a flow which has a practical application. The flow over a finite wing is one such example, as we will soon see.

Let us apply the Biot-Savart law to a straight vortex filament of infinite length, as sketched in Fig. 5.7. The strength of the filament is  $\Gamma$ . The velocity induced at point  $P$  by the directed segment of the vortex filament,  $d\mathbf{l}$ , is given by Eq. (5.5). Hence, the velocity induced at  $P$  by the entire vortex filament is

$$(5.7) \quad \mathbf{V} = \int_{-\infty}^{\infty} \frac{\Gamma}{4\pi} \frac{d\mathbf{l} \times \mathbf{r}}{|\mathbf{r}|^3}$$

From the definition of the vector cross product (see Sec. 2.2), the direction of  $\mathbf{V}$  is downward in Fig. 5.7. The magnitude of the velocity,  $V = |\mathbf{V}|$ , is given by

$$(5.8) \quad V = \frac{\Gamma}{4\pi} \int_{-\infty}^{\infty} \frac{\sin \theta}{r^2} dt$$

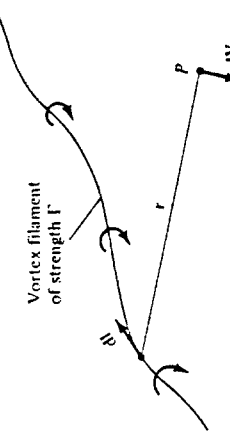


Figure 5.6 Vortex filament and illustration of the Biot-Savart law.

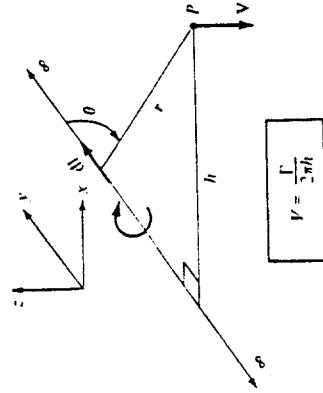


Figure 5.7 Velocity induced at point  $P$  by the vortex filament.

In Fig. 5.7, let  $h$  be the perpendicular distance from point  $P$  to the vortex filament. Then, from the geometry shown in Fig. 5.7,

$$(5.9a) \quad r = \frac{h}{\sin \theta}$$

$$(5.9b) \quad l = \frac{h}{\tan \theta}$$

$$(5.9c) \quad dl = -\frac{h}{\sin^2 \theta} d\theta$$

Substituting Eqs. (5.9a to c) in Eq. (5.8), we have

$$(5.10) \quad V = \frac{\Gamma}{4\pi} \int_{-\pi}^{\pi} \frac{\sin \theta}{r^2} dl = -\frac{\Gamma}{4\pi h} \int_{-\pi}^{\pi} \sin \theta d\theta$$

$$\text{or} \quad V = \frac{\Gamma}{2\pi h}$$

Thus, the velocity induced at a given point  $P$  by an infinite, straight vortex filament at a perpendicular distance  $h$  from  $P$  is simply  $\Gamma/2\pi h$ , which is precisely the result given by Eq. (3.105) for a point vortex in two-dimensional flow. [Note that the minus sign in Eq. (3.105) does not appear in Eq. (5.10); this is because  $V$  in Eq. (5.10) is simply the absolute magnitude of  $V$ , and hence it is positive by definition.]

Consider the semi-infinite vortex filament shown in Fig. 5.8. The filament extends from point  $A$  to  $\infty$ . Point  $P$  can be considered a boundary of the flow. Let  $P$  be a point in the plane through  $A$  perpendicular to the filament. Then, by an integration similar to that above (try it yourself), the velocity induced at  $P$  by the semi-infinite vortex filament is

$$(5.11) \quad V = \frac{\Gamma}{4\pi h}$$

We use Eq. (5.11) in the next section.

The great German mathematician, physicist, and physician Hermann von Helmholtz (1821–1894) was the first to make use of the vortex filament concept in

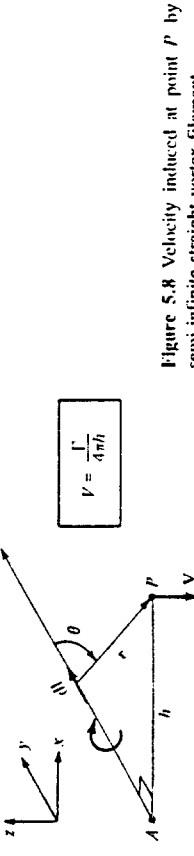


Figure 5.8 Velocity induced at point  $P$  by a semi-infinite straight vortex filament.

the analysis of inviscid, incompressible flow. In the process, he established several basic principles of vortex behavior which have become known as Helmholtz' vortex theorems:

1. The strength of a vortex filament is constant along its length.
2. A vortex filament cannot end in a fluid; it must extend to the boundaries of the fluid (which can be  $\pm\infty$ ) or form a closed path.

We make use of these theorems in the following sections.

Finally, let us introduce the concept of *lift distribution* along the span of a finite wing. Consider a given spanwise location  $y$ , where the local chord is  $c$ , the local geometric angle of attack is  $\alpha$ , and the airfoil section is a given shape. The lift per unit span at this location is  $L'(y)$ . Now consider another location  $y_2$  along the span, where  $c$ ,  $\alpha$ , and the airfoil shape may be different. (Most finite wings have a variable chord, with the exception of a simple rectangular wing. Also, many wings are geometrically twisted so that  $\alpha$  is different at different spanwise locations — so-called geometric twist. If the tip is at a lower  $\alpha$  than the root, the wing is said to have *washout*; if the tip is at a higher  $\alpha$  than the root, the wing has *washin*. In addition, the wings on a number of modern airplanes have different airfoil sections along the span, with different values of  $\alpha_{l=6}$ ; this is called *aerodynamic twist*.) Consequently, the lift per unit span at this different location,  $L'(y_2)$ , will in general be different from  $L'(y)$ . Therefore, there is a distribution of lift per unit span along the wing, that is  $L' = L'(y)$ , as sketched in Fig. 5.9. In turn, the circulation is also a function of  $y$ ,  $\Gamma(y) = L'(y)/\rho_x V_r$ . Note from Fig. 5.9 that the lift distribution goes to zero at the tips; this is because there is a pressure equalization from the bottom to the top of the wing precisely at  $y = -b/2$  and  $b/2$ , and hence no lift is created at these points. The calculation of the lift distribution  $L(y)$  [or the circulation distribution  $\Gamma(y)$ ] is one of the central problems of finite-wing theory. It is addressed in the following sections.

In summary, we wish to calculate the induced drag, the total lift, and the lift distribution for a finite wing. This is the purpose of the remainder of this chapter.

### 5.3 PRANDTL'S CLASSICAL LIFTING-LINE THEORY

The first practical theory for predicting the aerodynamic properties of a finite wing was developed by Ludwig Prandtl and his colleagues at Göttingen, Germany, during the period 1911–1918, spanning World War I. The utility of Prandtl's theory is so great that it is still in use today for preliminary calculations of finite-wing characteristics. The

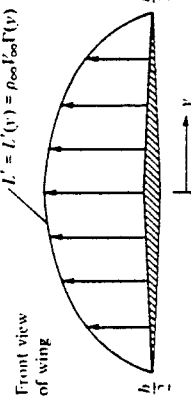


Figure 5.9 Sketch of the lift distribution along the span of a wing.

purpose of this section is to describe Prandtl's theory and to lay the groundwork for the modern numerical methods described in subsequent sections.

Prandtl reasoned as follows. A vortex filament of strength  $\Gamma$  which is somehow bound to a fixed location in a flow — a so-called bound vortex — will experience a force  $L = \rho_s V_x \Gamma$  from the Kutta-Joukowski theorem. This bound vortex is in contrast to a free vortex, which moves with the same fluid elements throughout a flow. Therefore, let us replace a finite wing of span  $b$  with a bound vortex, extending from  $y = -b/2$  to  $y = b/2$ , as sketched in Fig. 5.10. However, due to Helmholtz' theorem, a vortex filament cannot end in the fluid. Therefore, assume the vortex filament continues as two free vortices trailing downstream from the wing tips to infinity, as also shown in Fig. 5.10. This vortex (the bound plus the two free) is in the shape of a horseshoe and therefore is called a *horseshoe vortex*.

A single horseshoe vortex is shown in Fig. 5.11. Consider the downwash  $w$  induced along the bound vortex from  $-b/2$  to  $b/2$  by the horseshoe vortex. Examining Fig. 5.11, the bound vortex induces no velocity along itself; however, the two trailing vortices both contribute to the induced velocity along the bound vortex, and both contributions are in the downward direction. Consistent with the  $xyz$  coordinate system in Fig. 5.11, such a downward velocity is negative; that is,  $w$  (which is in the  $z$ -direction) is a negative value when directed downward and a positive value when directed upward. If the origin is taken at the center of the bound vortex, then the velocity at any point  $y$  along the bound vortex induced by the trailing semi-infinite vortices is, from Eq. (5.11),

$$w(y) = -\frac{\Gamma}{4\pi(b/2 + y)} - \frac{\Gamma}{4\pi(b/2 - y)} \quad (5.12)$$

In Eq. (5.12), the first term on the right-hand side is the contribution from the left trailing vortex (trailing from  $-b/2$ ), and the second term is the contribution from the right trailing vortex (trailing from  $b/2$ ). Equation (5.12) reduces to

$$w(y) = -\frac{\Gamma}{4\pi} \frac{b}{(b/2)^2 - y^2} \quad (5.13)$$

This variation of  $w(y)$  is sketched in Fig. 5.11. Note that  $w$  approaches  $-\infty$  as  $y$  approaches  $-b/2$  or  $b/2$ .

The downwash distribution due to the single horseshoe vortex shown in Fig. 5.11 does not realistically simulate that of a finite wing; the downwash approaching an infinite value at the tips is especially disconcerting. During the early evolution of finite-wing theory, this problem perplexed Prandtl and his colleagues. After several years of effort, a resolution of this problem was obtained which, in hindsight, was simple and straightforward. Instead of representing the wing by a single horseshoe vortex, let us superimpose a large number of horseshoe vortices, each with a different length of the bound vortex, but with all the bound vortices coincident along a single line, called the *lifting line*. This concept is illustrated in Fig. 5.12, where only three horseshoe vortices are shown for the sake of clarity. In Fig. 5.12, a horseshoe vortex of strength  $d\Gamma_1$  is shown, where the bound vortex spans the entire wing from  $-b/2$  to  $b/2$  (from point  $A$  to point  $F$ ). Superimposed on this is a second horseshoe vortex of strength  $d\Gamma_2$ , where its bound vortex spans only part of the wing, from point  $B$  to point  $E$ . Finally, superimposed on this is a third horseshoe vortex of strength  $d\Gamma_3$ , where its bound vortex spans only the part of the wing from point  $C$  to point  $D$ . As a result, the circulation varies along the line of bound vortices — the lifting line defined above.

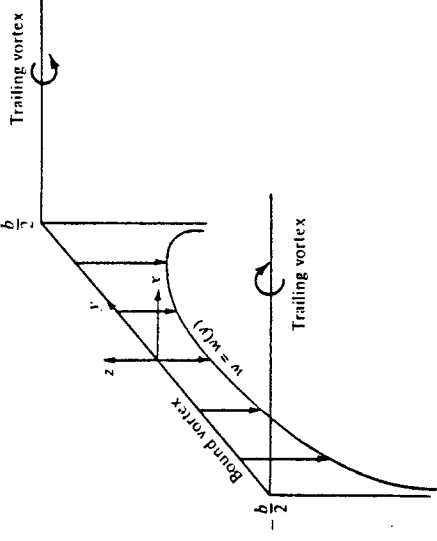


Figure 5.11 Downwash distribution along the  $y$  axis for a single horseshoe vortex.

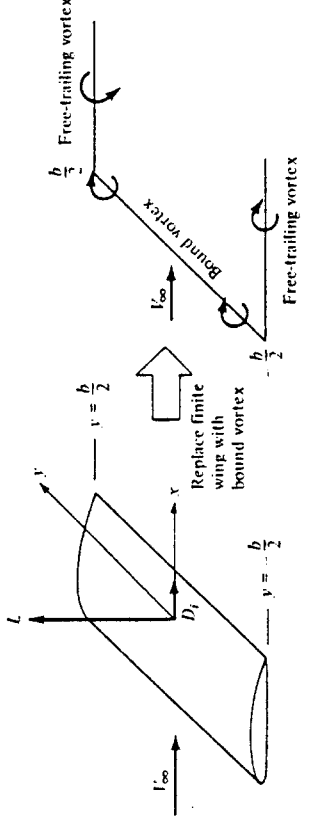


Figure 5.10 Replacement of the finite wing with a bound vortex.

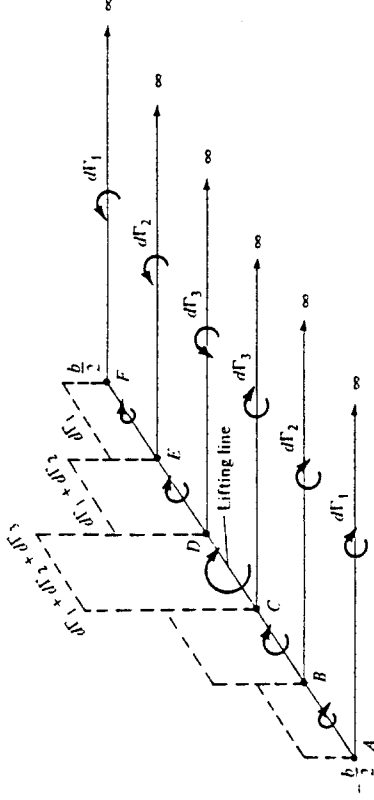


Figure 5.12 Superposition of a finite number of horseshoe vortices along the lifting line.

Along  $AB$  and  $EF$ , where only one vortex is present, the circulation is  $d\Gamma_1$ . However, along  $BC$  and  $DE$ , where two vortices are superimposed, the circulation is the sum of their strengths,  $d\Gamma_1 + d\Gamma_2$ . Along  $CD$ , three vortices are superimposed, and hence the circulation is  $d\Gamma_1 + d\Gamma_2 + d\Gamma_3$ . This variation of  $\Gamma$  along the lifting line is denoted by the vertical bars in Fig. 5.12. Also note from Fig. 5.12 that we now have a series of trailing vortices distributed over the span, rather than just two vortices trailing downstream of the tips as shown in Fig. 5.11. The series of trailing vortices in Fig. 5.12 represent pairs of vortices, each pair associated with a given horseshoe vortex. Note that the strength of each trailing vortex is equal to the *change in circulation* along the lifting line.

Let us extrapolate Fig. 5.12 to the case where an *infinite number* of horseshoe vortices are superimposed along the lifting line, each with a vanishingly small strength,  $d\Gamma$ . This case is illustrated in Fig. 5.13. Note that the vertical bars in Fig. 5.12 have

now become a continuous distribution of  $\Gamma(y)$  along the lifting line in Fig. 5.13. The value of the circulation at the origin is  $\Gamma_0$ . Also note that the finite number of trailing vortices in Fig. 5.12 have become a *continuous vortex sheet* trailing downstream of the lifting line in Fig. 5.13. This vortex sheet is parallel to the direction of  $V_\infty$ . The total strength of the sheet integrated across the span of the wing is zero, because it consists of pairs of trailing vortices of equal strength but in opposite directions.

Let us single out an infinitesimally small segment of the lifting line,  $dy$ , located at the coordinate  $y$  as shown in Fig. 5.13. The circulation at  $y$  is  $\Gamma(y)$ , and the change in circulation over the segment  $dy$  is  $d\Gamma = (d\Gamma/dy) dy$ . In turn, the strength of the trailing vortex at  $y$  must equal the change in circulation  $d\Gamma$  along the lifting line; this is simply an extrapolation of our result obtained for the strength of the finite trailing vortices in Fig. 5.12. Consider more closely the trailing vortex of strength  $d\Gamma$  which intersects the lifting line at coordinate  $y$ , as shown in Fig. 5.13. Also consider the arbitrary location  $y_0$  along the lifting line. Any segment of the trailing vortex,  $dx$ , will induce a velocity at  $y_0$  with a magnitude and direction given by the Biot-Savart law, Eq. (5.5). In turn, the velocity  $dw$  at  $y_0$  induced by the entire semi-infinite trailing vortex located at  $y$  is given by Eq. (5.11), which in terms of the picture given in Fig. 5.13 yields

$$dw = - \frac{(d\Gamma/dy) dy}{4\pi(y_0 - y)} \quad (5.14)$$

The minus sign in Eq. (5.14) is needed for consistency with the picture shown in Fig. 5.13; for the trailing vortex shown, the direction of  $dw$  at  $y_0$  is upward and hence is a positive value, whereas  $\Gamma$  is decreasing in the  $y$  direction, making  $d\Gamma/dy$  a negative quantity. The minus sign in Eq. (5.14) makes the positive  $dw$  consistent with the negative  $d\Gamma/dy$ .

The total velocity  $w$  induced at  $y_0$  by the entire trailing vortex sheet is the summation of Eq. (5.14) over all the vortex filaments, i.e., the integral of Eq. (5.14) from  $-b/2$  to  $b/2$ .

$$w(y_0) = - \frac{1}{4\pi} \int_{-b/2}^{b/2} \frac{(d\Gamma/dy) dy}{y_0 - y} \quad (5.15)$$

Equation (5.15) is important in that it gives the value of the downwash at  $y_0$  due to all the trailing vortices. (Keep in mind that, although we label  $w$  as downwash,  $w$  is treated as positive in the upward direction in order to be consistent with the normal convention in an  $xyz$  rectangular coordinate system.)

Pause for a moment, and assess the status of our discussion so far. We have replaced the finite wing with the model of a lifting line along which the circulation  $\Gamma(y)$  varies continuously, as shown in Fig. 5.13. In turn, we have obtained an expression for the downwash along the lifting line, given by Eq. (5.15). However, our central problem still remains to be solved; i.e., we want to *calculate*  $\Gamma(y)$  for a given finite wing, along with its corresponding total lift and induced drag. Therefore, we must press on.

Return to Fig. 5.4, which shows the local airfoil section of a finite wing. Assume this section is located at the arbitrary spanwise station  $y_0$ . From Fig. 5.4, the induced angle of attack  $\alpha_i$  is given by

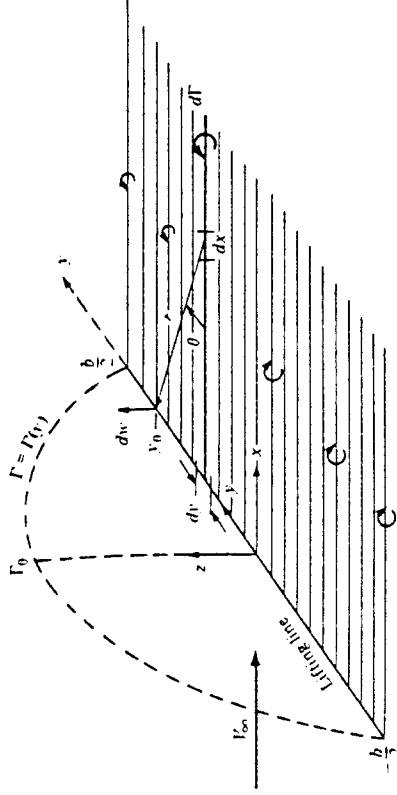


Figure 5.13 Superposition of an infinite number of horseshoe vortices along the lifting line.

$$\alpha_t(y_0) = \tan^{-1} \left( \frac{-w(y_0)}{V_s} \right) \quad (5.16)$$

[Note in Fig. 5.4 that  $w$  is downward and hence is a negative quantity. Since  $\alpha_t$  in Fig. 5.4 is positive, the negative sign in Eq. (5.16) is necessary for consistency.] Generally,  $w$  is much smaller than  $V_s$ , and hence  $\alpha_t$  is a small angle, on the order of a few degrees at most. For small angles, Eq. (5.16) yields

$$\alpha_t(y_0) = -\frac{w(y_0)}{V_s} \quad (5.17)$$

Substituting Eq. (5.15) into (5.17), we obtain

$$\alpha_t(y_0) = \frac{1}{4\pi V_s} \int_{-b/2}^{b/2} \frac{(d\Gamma/dy) dy}{y_0 - y} \quad (5.18)$$

i.e., an expression for the induced angle of attack in terms of the circulation distribution  $\Gamma(y)$  along the wing.

Consider again the effective angle of attack  $\alpha_{\text{eff}}$ , shown in Fig. 5.4. As explained in Sec. 5.1,  $\alpha_{\text{eff}}$  is the angle of attack actually seen by the local airfoil section. Since the downwash varies across the span, then  $\alpha_{\text{eff}}$  is also variable;  $\alpha_{\text{eff}} = \alpha_{\text{eff}}(y_0)$ . The lift coefficient for the airfoil section located at  $y = y_0$  is

$$c_l = a_0[\alpha_{\text{eff}}(y_0) - \alpha_{t=0}] = 2\pi[\alpha_{\text{eff}}(y_0) - \alpha_{t=0}] \quad (5.19)$$

In Eq. (5.19), the local section lift slope  $a_0$  has been replaced by the thin airfoil theoretical value of  $2\pi$  (rad $^{-1}$ ). Also, for a wing with aerodynamic twist, the angle of zero lift,  $\alpha_{t=0}$ , in Eq. (5.19) varies with  $y_0$ . If there is no aerodynamic twist,  $\alpha_{t=0}$  is constant across the span. In any event,  $\alpha_{t=0}$  is a known property of the local airfoil sections. From the definition of lift coefficient and from the Kutta-Joukowski theorem, we have, for the local airfoil section located at  $y_0$ ,

$$L' = \frac{1}{2} \rho_s V_s^2 c(y_0) c_l = \rho_s V_s \Gamma(y_0) \quad (5.20)$$

From Eq. (5.20), we obtain

$$c_l = \frac{2\Gamma(y_0)}{V_s c(y_0)} \quad (5.21)$$

Substituting Eq. (5.21) into (5.19) and solving for  $\alpha_{\text{eff}}$ ,

$$\alpha_{\text{eff}} = \frac{\Gamma(y_0)}{\pi V_s c(y_0)} + \alpha_{t=0} \quad (5.22)$$

The above results come into focus if we refer to Eq. (5.1):

$$\alpha_{\text{eff}} = \alpha - \alpha_t \quad (5.1)$$

Substituting Eqs. (5.18) and (5.22) into (5.22) into (5.1), we obtain

$$\boxed{\alpha(y_0) = \frac{\Gamma(y_0)}{\pi V_s c(y_0)} + \alpha_{t=0}(y_0) + \frac{1}{4\pi V_s} \int_{-b/2}^{b/2} \frac{(d\Gamma/dy) dy}{y - y_0} \quad (5.23)}$$

the fundamental equation of Prandtl's lifting-line theory; it simply states that the geometric angle of attack is equal to the sum of the effective angle plus the induced angle of attack. In Eq. (5.23),  $\alpha_{\text{eff}}$  is expressed in terms of  $\Gamma$ , and  $\alpha_t$  is expressed in terms of an integral containing  $d\Gamma/dy$ . Hence, Eq. (5.23) is an integro-differential equation, in which the only unknown is  $\Gamma$ ; all the other quantities,  $\alpha$ ,  $c$ ,  $V_s$ , and  $\alpha_{t=0}$ , are known for a finite wing of given design at a given geometric angle of attack in a freestream with given velocity. Thus, a solution of Eq. (5.23) yields  $\Gamma = \Gamma(y_0)$ , where  $y_0$  ranges along the span from  $-b/2$  to  $b/2$ .

The solution  $\Gamma = \Gamma(y_0)$  obtained from Eq. (5.23) gives us the three main aerodynamic characteristics of a finite wing, as follows:

$$\Gamma'(y_0) = \rho_s V_s \Gamma(y_0) \quad (5.24)$$

1. The lift distribution is obtained from the Kutta-Joukowski theorem.

$$L = \int_{-b/2}^{b/2} L'(y) dy \quad (5.25)$$

or

$$L = \rho_s V_s \int_{-b/2}^{b/2} \Gamma(y) dy \quad (5.26)$$

(Note that we have dropped the subscript on  $y$ , for simplicity.) The lift coefficient follows immediately from Eq. (5.25).

$$C_L = \frac{L}{q_s S} = \frac{2}{V_s S} \int_{-b/2}^{b/2} \Gamma(y) dy \quad (5.26)$$

3. The induced drag is obtained by inspection of Fig. 5.4. The induced drag per unit span is

$$D'_i = L'_i \sin \alpha_t$$

Since  $\alpha_t$  is small, this relation becomes

$$D'_i = L'_i \alpha_t \quad (5.27)$$

The total induced drag is obtained by integrating Eq. (5.27) over the span.

$$D_i = \int_{-b/2}^{b/2} L'(y) \alpha_t(y) dy \quad (5.28)$$

$$D_i = \rho_s V_s \int_{-b/2}^{b/2} \Gamma(y) \alpha_t(y) dy \quad (5.29)$$

In turn, the induced drag coefficient is

$$C_{D,i} = \frac{D_i}{q_r S} = \frac{2}{V_x S} \int_{-b/2}^{b/2} \Gamma(y) \alpha_i(y) dy \quad (5.30)$$

In Eqs. (5.27), to (5.30)  $\alpha_i(y)$  is obtained from Eq. (5.18).

Therefore, in Prandtl's lifting-line theory the solution of Eq. (5.23) for  $\Gamma(y)$  is clearly the key to obtaining the aerodynamic characteristics of a finite wing. Before discussing the general solution of this equation, let us consider a special case, as outlined below.

### Elliptical Lift Distribution

Consider a circulation distribution given by

$$\Gamma(y) = \Gamma_0 \sqrt{1 - \left(\frac{2y}{b}\right)^2} \quad (5.31)$$

In Eq. (5.31), note the following:

1.  $\Gamma_0$  is the circulation at the origin, as shown in Fig. 5.13.
2. The circulation varies elliptically with distance  $y$  along the span; hence, it is designated as an *elliptical circulation distribution*. Since  $L'(y) = \rho_s V_x \Gamma(y)$ , we also have

$$L'(y) = \rho_s V_x \Gamma_0 \sqrt{1 - \left(\frac{2y}{b}\right)^2}$$

Hence, we are dealing with an *elliptical lift distribution*.

3.  $\Gamma(b/2) = \Gamma(-b/2) = 0$ . Thus, the circulation, hence lift, properly goes to zero at the wing tips, as shown in Fig. 5.13. We have not obtained Eq. (5.31) as a direct solution of Eq. (5.23); rather, we are simply stipulating a lift distribution that is elliptic. We now ask the question, What are the aerodynamic properties of a finite wing with such an elliptic lift distribution?

First, let us calculate the downwash. Differentiating Eq. (5.31), we obtain

$$\frac{d\Gamma}{dy} = -\frac{4\Gamma_0}{b^2} \frac{y}{(1 - 4y^2/b^2)^{1/2}} \quad (5.32)$$

Substituting Eq. (5.32) into (5.15), we have

$$w(y_0) = \frac{\Gamma_0}{\pi b^2} \int_{-b/2}^{b/2} \frac{y}{(1 - 4y^2/b^2)^{1/2}} (y_0 - y) dy \quad (5.33)$$

The integral can be evaluated easily by making the substitution

$$y = \frac{b}{2} \cos \theta \quad dy = -\frac{b}{2} \sin \theta d\theta$$

Hence, Eq. (5.33) becomes

$$w(\theta_0) = -\frac{\Gamma_0}{2\pi b} \int_{-\pi}^0 \frac{\cos \theta}{\cos \theta_0 - \cos \theta} d\theta \quad (5.34)$$

or

$$w(\theta_0) = -\frac{\Gamma_0}{2\pi b} \int_0^\pi \frac{\cos \theta}{\cos \theta - \cos \theta_0} d\theta \quad (5.34)$$

The integral in Eq. (5.34) is the standard form given by Eq. (4.26) for  $n = 1$ . Hence, Eq. (5.34) becomes

$$w(\theta_0) = -\frac{\Gamma_0}{2b} \quad (5.35)$$

which states the interesting and important result that the *downwash is constant over the span for an elliptical lift distribution*. In turn, from Eq. (5.17), we obtain, for the induced angle of attack,

$$\alpha_i = -\frac{w}{V_x} = \frac{\Gamma_0}{2bV_x} \quad (5.36)$$

For an elliptic lift distribution, the induced angle of attack is also constant along the span. Note from Eqs. (5.35) and (5.36) that both the downwash and induced angle of attack go to zero as the wing span becomes infinite—which is consistent with our previous discussions on airfoil theory.

A more useful expression for  $\alpha_i$  can be obtained as follows. Substituting Eq. (5.31) into (5.25), we have

$$L = \rho_s V_x \Gamma_0 \int_{-b/2}^{b/2} \left(1 - \frac{4y^2}{b^2}\right)^{1/2} dy \quad (5.37)$$

Again using the transformation  $y = (b/2) \cos \theta$ , Eq. (5.37) readily integrates to

$$L = \rho_s V_x \Gamma_0 \frac{b}{2} \int_0^\pi \sin^2 \theta d\theta = \rho_s V_x \Gamma_0 \frac{b}{4} \pi \quad (5.38)$$

Solving Eq. (5.38) for  $\Gamma_0$ , we have

$$\Gamma_0 = \frac{4L}{\rho_s V_x b \pi} \quad (5.39)$$

However,  $L = \frac{1}{4} \rho_s V_x^2 S C_L$ . Hence, Eq. (5.39) becomes

$$\Gamma_0 = \frac{2V_x S C_L}{b \pi} \quad (5.40)$$

Substituting Eq. (5.40) into (5.36), we obtain

$$\alpha_i = \frac{2V_x S C_L}{b \pi} \frac{1}{2bV_x}$$

$$\text{or} \quad \alpha_i = \frac{SC_L}{\pi b^2} \quad (5.41)$$

An important geometric property of a finite wing is the *aspect ratio*, denoted by AR and defined as

$$AR = \frac{b^2}{S}$$

Hence, Eq. (5.41) becomes

$$\alpha_i = \frac{C_L}{\pi AR} \quad (5.42)$$

Equation (5.42) is a useful expression for the induced angle of attack, as shown below. The induced drag coefficient is obtained from Eq. (5.30), noting that  $\alpha_i$  is constant.

$$C_{D,i} = \frac{2\alpha_i}{V_\infty S} \int_{-\theta/2}^{\theta/2} \Gamma(y) dy = \frac{2\alpha_i \Gamma_0 b}{V_\infty S} \frac{b}{2} \int_0^\pi \sin^2 \theta d\theta = \frac{\pi \alpha_i \Gamma_0 b}{2 V_\infty S} \quad (5.42a)$$

Substituting Eqs. (5.40) and (5.42) into (5.42a), we obtain

$$C_{D,i} = \frac{\pi b}{2 V_\infty S} \left( \frac{C_L}{\pi AR} \right) \frac{2 V_\infty S C_L}{b \pi} \quad (5.43)$$

$$\text{or} \quad C_{D,i} = \frac{C_L^2}{\pi AR} \quad (5.43)$$

Equation (5.43) is an important result. It states that the induced drag coefficient is directly proportional to the square of the lift coefficient. The dependence of induced drag on the lift is not surprising, for the following reason. In Sec. 5.1 we saw that induced drag is a consequence of the presence of the wing-tip vortices, which in turn are produced by the difference in pressure between the lower and upper wing surfaces. The lift is produced by this same pressure difference. Hence, induced drag is intimately related to the production of lift on a finite wing; indeed, induced drag is frequently called the *drag due to lift*. Equation (5.43) dramatically illustrates this point. Clearly, an airplane cannot generate lift for free; the induced drag is the price for the generation of lift. The power required from an aircraft engine to overcome the induced drag is simply the power required to generate the lift of the aircraft. Also note that, because  $C_{D,i} \propto C_L^2$ , the induced drag coefficient increases rapidly as  $C_L$  increases, and becomes a substantial part of the total drag coefficient when  $C_L$  is high, e.g., when the airplane is flying slowly such as on takeoff or landing. Even at relatively high cruising speeds, induced drag is typically 25 percent of the total drag.

Another important aspect of induced drag is evident in Eq. (5.43); that is,  $C_{D,i}$  is *inversely proportional to aspect ratio*. Hence, to reduce the induced drag, we want a finite wing with the highest possible aspect ratio. Wings with high and low aspect ratios

$$AR = b^2/S$$



Figure 5.14 Schematic of high- and low-aspect-ratio wings.

are sketched in Fig. 5.14. Unfortunately, the design of very high aspect ratio wings with sufficient structural strength is difficult. Therefore, the aspect ratio of a conventional aircraft is a compromise between conflicting aerodynamic and structural requirements. It is interesting to note that the aspect ratio of the 1903 Wright Flyer was 6 and that today the aspect ratios of conventional subsonic aircraft range typically from 6 to 8. (Exceptions are the Lockheed U-2 high-altitude reconnaissance aircraft with  $AR = 14.3$  and sailplanes with aspect ratios in the 10 to 22 range.)

Another property of the elliptical lift distribution is as follows. Consider a wing with no geometric twist (that is,  $\alpha$  is constant along the span) and no aerodynamic twist (that is,  $\alpha_{t=0}$  is constant along the span). From Eq. (5.42), we have seen that  $\alpha_i$  is constant along the span. Hence,  $\alpha_{eff} = \alpha - \alpha_i$  is also constant along the span. Since the local section lift coefficient  $c_l$  is given by

$$c_l = a_0(\alpha_{eff} - \alpha_{t=0})$$

then assuming that  $a_0$  is the same for each section ( $a_0 = 2\pi$  from thin airfoil theory),  $c_l$  must be constant along the span. The lift per unit span is given by

$$L'(y) = q_\infty c_l c_i \quad (5.44)$$

Solving Eq. (5.44) for the chord, we have

$$c(y) = \frac{L'(y)}{q_\infty c_i} \quad (5.45)$$

In Eq. (5.45),  $q_\infty$  and  $c_i$  are constant along the span. However,  $L'(y)$  varies elliptically along the span. Thus, Eq. (5.45) dictates that for such an elliptic lift distribution, the chord must vary elliptically along the span; i.e., for the conditions given above, the wing planform is elliptical.

The related characteristics—the elliptic lift distribution, the elliptic planform, and the constant downwash—are sketched in Fig. 5.15. Although an elliptical lift distribution may appear to be a restricted, isolated case, in reality it gives a reasonable approximation for the induced drag coefficient for an arbitrary finite wing. The form of  $C_{D,i}$  given by Eq. (5.43) is only slightly modified for the general case. Let us now consider the case of a finite wing with a general lift distribution.

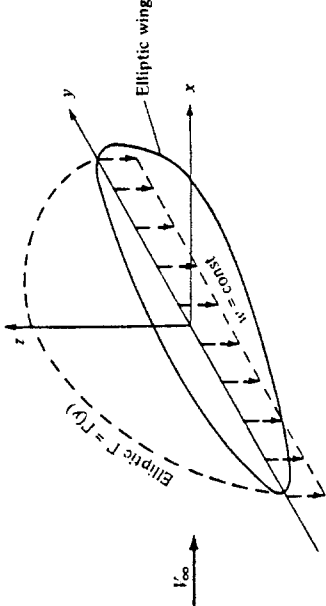


Figure 5.15 Illustration of the related quantities: an elliptic lift distribution, elliptic planform, and constant downwash.

### General Lift Distribution

Consider the transformation

$$y = -\frac{b}{2} \cos \theta \quad (5.46)$$

where the coordinate in the spanwise direction is now given by  $\theta$ , with  $0 \leq \theta \leq \pi$ . In terms of  $\theta$ , the elliptic lift distribution given by Eq. (5.31) is written as

$$\Gamma(\theta) = \Gamma_0 \sin \theta \quad (5.47)$$

Equation (5.47) hints that a Fourier sine series would be an appropriate expression for the general circulation distribution along an arbitrary finite wing. Hence, assume for the general case that

$$\Gamma(\theta) = 2bV_\infty \sum_{n=1}^N A_n \sin n\theta \quad (5.48)$$

where as many terms,  $N$ , in the series can be taken as we desire for accuracy. The coefficients  $A_n$  (where  $n = 1, 2, \dots, N$ ) in Eq. (5.48) are unknowns; however, they must satisfy the fundamental equation of Prandtl's lifting-line theory; i.e., the  $A_n$ 's must satisfy Eq. (5.23). Differentiating Eq. (5.48), we obtain

$$\frac{d\Gamma}{dy} = \frac{d\Gamma}{d\theta} \frac{d\theta}{dy} = 2bV_\infty \sum_{n=1}^N nA_n \cos n\theta \frac{d\theta}{dy} \quad (5.49)$$

Substituting Eqs. (5.48) and (5.49) into (5.23), we obtain

$$\begin{aligned} \alpha(\theta_0) &= \frac{2b}{\pi c(\theta_0)} \sum_{n=1}^N A_n \sin n\theta_0 + \alpha_{L=0}(\theta_0) \\ &+ \frac{1}{\pi} \int_0^\pi \frac{\sum_{n=1}^N nA_n \cos n\theta}{\cos \theta - \cos \theta_0} d\theta \end{aligned} \quad (5.50)$$

The integral in Eq. (5.50) is the standard form given by Eq. (4.26). Hence, Eq. (5.50) becomes

$$\boxed{\alpha(\theta_0) = \frac{2b}{\pi c(\theta_0)} \sum_{n=1}^N A_n \sin n\theta_0 + \alpha_{L=0}(\theta_0) + \sum_{n=1}^N nA_n \frac{\sin n\theta_0}{\sin \theta_0}} \quad (5.51)$$

Examine Eq. (5.51) closely. It is evaluated at a given spanwise location; hence,  $\theta_0$  is specified. In turn,  $b$ ,  $c(\theta_0)$ , and  $\alpha_{L=0}$  ( $\theta_0$ ) are known quantities from the geometry and airfoil section of the finite wing. The only unknowns in Eq. (5.51) are the  $A_n$ 's. Hence, written at a given spanwise location (a specified  $\theta_0$ ), Eq. (5.51) is one algebraic equation with  $N$  unknowns,  $A_1, A_2, \dots, A_N$ . However, let us choose  $N$  different spanwise stations, and let us evaluate Eq. (5.51) at each of these  $N$  stations. We then obtain a system of  $N$  independent algebraic equations with  $N$  unknowns, namely,  $A_1, A_2, \dots, A_N$ . In this fashion, actual numerical values are obtained for the  $A_n$ 's—numerical values which ensure that the general circulation distribution given by Eq. (5.48) satisfies the fundamental equation of finite-wing theory, Eq. (5.23).

Now that  $\Gamma(\theta)$  is known via Eq. (5.48), the lift coefficient for the finite wing follows immediately from the substitution of Eq. (5.48) into (5.26).

$$C_L = \frac{2}{V_\infty S} \int_{-b/2}^{b/2} \Gamma(y) dy = \frac{2b^2}{S} \sum_{n=1}^N A_n \int_0^\pi \sin n\theta \sin \theta d\theta \quad (5.52)$$

In Eq. (5.52), the integral is

$$\int_0^\pi \sin n\theta \sin \theta d\theta = \begin{cases} \frac{\pi}{2} & \text{for } n = 1 \\ 0 & \text{for } n \neq 1 \end{cases} \quad (5.53)$$

Hence, Eq. (5.52) becomes

$$C_L = A_1 \frac{\pi b^2}{S} = A_1 \pi AR \quad (5.54)$$

Note that  $C_L$  depends only on the leading coefficient of the Fourier series expansion. (However, although  $C_L$  depends on  $A_1$  only, we must solve for all the  $A_n$ 's simultaneously in order to obtain  $A_1$ .)

The induced drag coefficient is obtained from the substitution of Eq. (5.48) into Eq. (5.30) as follows:

$$\begin{aligned} C_{D,i} &= \frac{2}{V_\infty S} \int_{-b/2}^{b/2} \Gamma(y) \alpha_i(y) dy \\ &= \frac{2b^2}{S} \int_0^\pi \left( \sum_{n=1}^N A_n \sin n\theta \right) \alpha_i(\theta) \sin \theta d\theta \end{aligned} \quad (5.54)$$

The induced angle of attack  $\alpha_i(\theta)$  in Eq. (5.54) is obtained from the substitution of Eqs. (5.46) and (5.49) into (5.18), which yields

$$\begin{aligned}\alpha_i(y_0) &= \frac{1}{4\pi V_\infty} \int_{-\delta/2}^{\delta/2} \frac{(d\Gamma/dy) dy}{y_0 - y} \\ &= \frac{1}{\pi} \sum_1^N nA_n \int_0^\pi \frac{\cos n\theta}{\cos \theta - \cos \theta_0} d\theta\end{aligned}\quad (5.55)$$

The integral in Eq. (5.55) is the standard form given by eq. (4.26). Hence, Eq. (5.55) becomes

$$\alpha_i(\theta_0) = \sum_1^N nA_n \frac{\sin n\theta_0}{\sin \theta_0} \quad (5.56)$$

In Eq. (5.56),  $\theta_0$  is simply a dummy variable which ranges from 0 to  $\pi$  across the span of the wing; it can therefore be replaced by  $\theta$ , and Eq. (5.56) can be written as

$$\alpha_i(\theta) = \sum_1^N nA_n \frac{\sin n\theta}{\sin \theta} \quad (5.57)$$

Substituting Eq. (5.57) into (5.54), we have

$$C_{D,i} = \frac{2b^2}{S} \int_0^\pi \left( \sum_1^N A_n \sin n\theta \right) \left( \sum_1^N nA_n \sin n\theta \right) d\theta \quad (5.58)$$

Examine Eq. (5.58) closely; it involves the product of two summations. Also, note that from the standard integral,

$$\int_0^\pi \sin m\theta \sin k\theta = \begin{cases} 0 & \text{for } m \neq k \\ \frac{\pi}{2} & \text{for } m = k \end{cases} \quad (5.59)$$

Hence, in Eq. (5.58), the mixed product terms involving unequal subscripts (such as  $A_1 A_2$ ,  $A_2 A_4$ ) are, from Eq. (5.59), equal to zero. Hence, Eq. (5.58) becomes

$$\begin{aligned}C_{D,i} &= \frac{2b^2}{S} \left( \sum_1^N nA_n^2 \right) \frac{\pi}{2} = \pi AR \sum_1^N nA_n^2 \\ &= \pi AR A_i^2 \left( 1 + \sum_2^N n \left( \frac{A_n}{A_i} \right)^2 \right)\end{aligned}\quad (5.60)$$

Substituting Eq. (5.53) for  $C_L$  into Eq. (5.60), we obtain

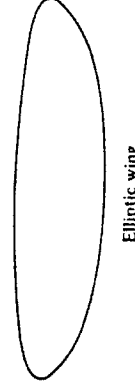
$$C_{D,i} = \frac{C_L^2}{\pi AR} (1 + \delta) \quad (5.61)$$

where  $\delta = \sum_2^N n(A_n/A_i)^2$ . Note that  $\delta \geq 0$ ; hence, the factor  $1 + \delta$  in Eq. (5.61) is either greater than 1 or at least equal to 1. Let us define a span efficiency factor,  $e$ , as  $e = (1 + \delta)^{-1}$ . Then, Eq. (5.61) can be written as

$$C_{D,i} = \frac{C_L^2}{\pi e AR} \quad (5.62)$$

where  $e \leq 1$ . Comparing Eqs. (5.61) and (5.62) for the general lift distribution with Eq. (5.43) for the elliptical lift distribution, note that  $\delta = 0$  and  $e = 1$  for the elliptical lift distribution. Hence, the lift distribution which yields minimum induced drag is the *elliptical lift distribution*. This is why we have a practical interest in the elliptical lift distribution.

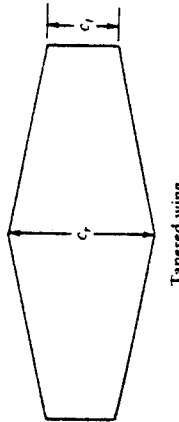
Recall that for a wing with no aerodynamic twist and no geometric twist, an elliptical lift distribution is generated by a wing with an elliptical planform, as sketched at the top of Fig. 5.16. Several aircraft have been designed in the past with elliptical wings; the most famous, perhaps, being the British Spitfire from World War II, shown in Fig. 5.17. However, elliptic planforms are more expensive to manufacture than, say, a simple rectangular wing as sketched in the middle of Fig. 5.16. On the other hand, a rectangular wing generates a lift distribution far from optimum. A compromise is the tapered wing shown at the bottom of Fig. 5.16. The tapered wing can be designed with a taper ratio, i.e., tip chord/root chord  $= c_r/c_t$ , such that the lift distribution closely approximates the elliptic case. The variation of  $\delta$  as a function of taper ratio for wings



Elliptic wing



Rectangular wing



Tapered wing

Figure 5.16 Various planforms for straight wings.

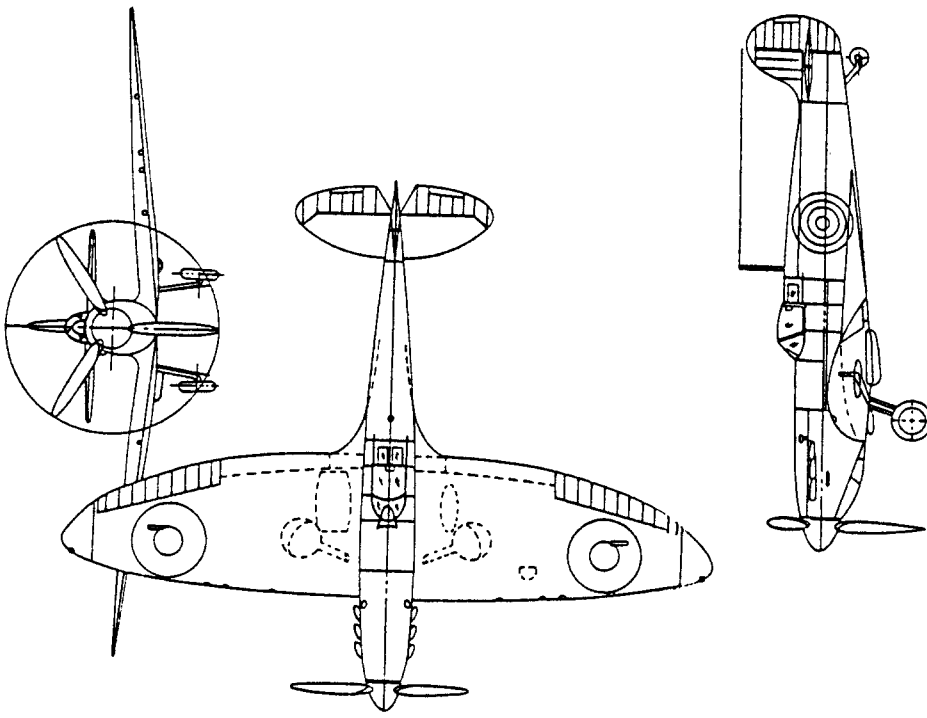


Figure 5.17 Three views of the Supermarine Spitfire, a famous British World War II fighter.

of different aspect ratio is illustrated in Fig. 5.18. Such calculations of  $\delta$  were first performed by the famous English aerodynamicist, Hermann Glauert and published in Ref. 18 in the year 1926. Note from Fig. 5.18 that a tapered wing can be designed with an induced drag coefficient reasonably close to the minimum value. In addition, tapered wings with straight leading and trailing edges are considerably easier to manufacture than elliptic planforms. Therefore, most conventional aircraft employ tapered rather than elliptic wing planforms.

#### Effect of Aspect Ratio

Returning to Eqs. (5.61) and (5.62), note that the induced drag coefficient for a finite wing with a general lift distribution is inversely proportional to the aspect ratio, as was

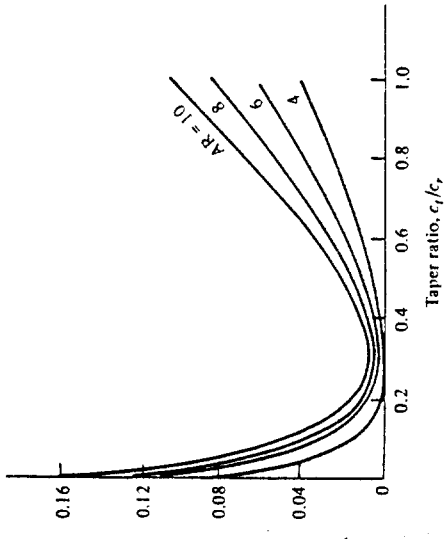


Figure 5.18 Induced drag factor  $\delta$  as a function of taper ratio. (From McCormick, B. W., "Aerodynamics, Aeronautics, and Flight Mechanics," John Wiley & Sons, New York, 1979.)

discussed earlier in conjunction with the case of the elliptic lift distribution. Note that AR, which typically varies from 6 to 22 for standard subsonic airplanes and sailplanes, has a much stronger effect on  $C_D$ , than the value of  $\delta$ , which from Fig. 5.18 varies only by about 10 percent over the practical range of taper ratio. Hence, the primary design factor for minimizing induced drag is not the closeness to an elliptical lift distribution but rather the ability to make the aspect ratio as large as possible. The determination that  $C_{D,i}$  is inversely proportional to AR was one of the great victories of Prandtl's lifting-line theory. In 1915, Prandtl verified this result with a series of classic experiments wherein the lift and drag of seven rectangular wings with different aspect ratios were measured. The data are given in Fig. 5.19. Recall from Eq. (5.4) that the total drag of a finite wing is given by

$$C_D = c_d + \frac{C_l^2}{\pi e AR} \quad (5.63)$$

The parabolic variation of  $C_D$  with  $C_l$  as expressed in Eq. (5.63) is reflected in the data of Fig. 5.19. If we consider two wings with different aspect ratios  $AR_1$  and  $AR_2$ , Eq. (5.63) gives the drag coefficients  $C_{D,1}$  and  $C_{D,2}$  for the two wings as

$$C_{D,1} = c_d + \frac{C_l^2}{\pi e AR_1} \quad (5.64a)$$

$$C_{D,2} = c_d + \frac{C_l^2}{\pi e AR_2} \quad (5.64b)$$

Assume that the wings are at the same  $C_l$ . Also, since the airfoil section is the same for both wings,  $c_d$  is essentially the same. Moreover, the variation of  $e$  between the wings is only a few percent and can be ignored. Hence, subtracting Eq. (5.64b) from (5.64a), we obtain

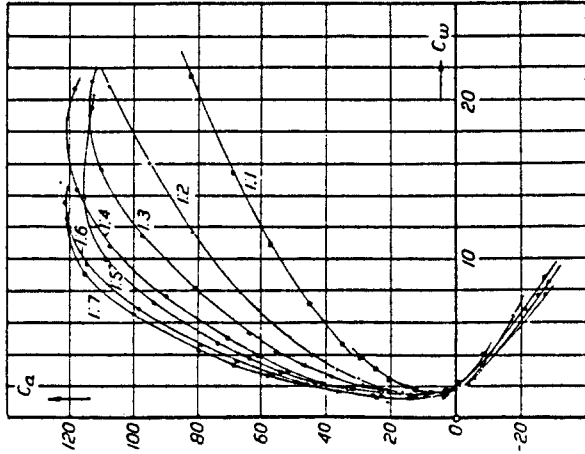


Figure 5.19 Prandtl's classic rectangular wing data for seven different aspect ratios from 1 to 7; variation of lift coefficient versus drag coefficient. For historical interest, we reproduce here Prandtl's actual graphs. Note that, in his nomenclature,  $C_a$  = lift coefficient and  $C_w$  = drag coefficient. Also, the numbers on both the ordinate and abscissa are 100 times the actual values of the coefficients. (Taken from L. Prandtl, "Applications of Modern Hydrodynamics to Aeronautics," NACA Report No. 116, 1921.)

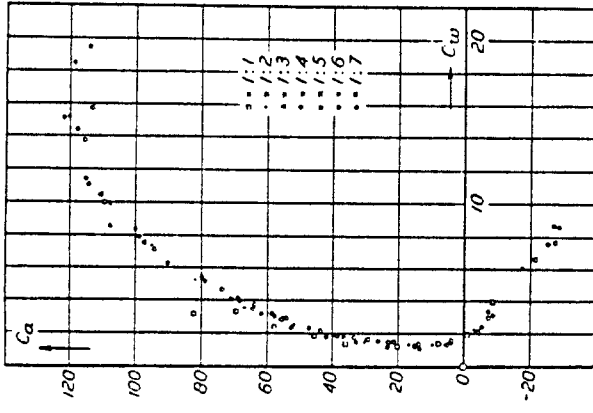


Figure 5.19 Data of Fig. 5.19 scaled by Prandtl to an aspect ratio of 5.

$$C_{D,1} = C_{D,2} + \frac{C_l^2}{\pi e} \left( \frac{1}{AR_1} - \frac{1}{AR_2} \right) \quad (5.65)$$

Equation (5.65) can be used to scale the data of a wing with aspect ratio  $AR_1$  to correspond to the case of another aspect ratio  $AR_2$ . For example, Prandtl scaled the data of Fig. 5.19 to correspond to a wing with an aspect ratio of 5. For this case, Eq. (5.65) becomes

$$C_{D,1} = C_{D,2} + \frac{C_l^2}{\pi e} \left( \frac{1}{5} - \frac{1}{AR_2} \right) \quad (5.66)$$

Inserting the respective values of  $C_{D,2}$  and  $AR_2$  from Fig. 5.19 into Eq. (5.66), Prandtl found that the resulting data for  $C_{D,1}$  versus  $C_l$  collapsed to essentially the same curve, as shown in Fig. 5.20. Hence, the inverse dependence of  $C_{D,1}$  on  $AR$  was substantially verified as early as 1915.

There are two primary differences between airfoil and finite-wing properties. We have discussed one difference, namely, that a finite wing generates induced drag. However, a second major difference appears in the lift slope. In Fig. 4.4, the lift slope for an airfoil was defined as  $a_0 \equiv dc_l/d\alpha$ . Let us denote the lift slope for a finite wing as  $a \equiv dC_l/d\alpha$ . When the lift slope of a finite wing is compared with that of its airfoil section, we find that  $a < a_0$ . To see this more clearly, return to Fig. 5.4, which illustrates the influence of downwash on the flow over a local airfoil section of a finite wing. Note that although the geometric angle of attack of the finite wing is  $\alpha$ , the airfoil section effectively senses a smaller angle of attack, namely  $\alpha_{eff} = \alpha - \alpha_i$ . For the time being, consider an elliptic wing with no twist; hence,  $\alpha_i$  and  $\alpha_{eff}$  are both

constant along the span. Moreover,  $c_l$  is also constant along the span, and therefore,  $C_l = c_l$ . Assume that we plot  $C_l$  for the finite wing versus  $\alpha_{eff}$ , as shown at the top of Fig. 5.21. Because we are using  $\alpha_{eff}$  the lift slope corresponds to that for an infinite wing,  $a_0$ . However, in real life our naked eyes cannot see  $\alpha_{eff}$ ; instead, what we actually observe is a finite wing with a certain angle between the chord line and the relative wind, i.e., in practice we always observe the geometric angle of attack  $\alpha$ . Hence,  $C_l$  for a finite wing is generally given as a function of  $\alpha$ , as sketched at the bottom of Fig. 5.21. Since  $\alpha > \alpha_{eff}$ , the bottom abscissa is stretched, and hence the bottom lift curve is less inclined; it has a slope equal to  $a$ , and Fig. 5.21 clearly shows that  $a < a_0$ . The effect of a finite wing is to reduce the lift slope. Also, recall that at zero lift, there are no induced effects; i.e.,  $\alpha_i = C_{D,i} = 0$ . Thus, when  $C_l = 0$ ,  $\alpha = \alpha_{eff}$ . As a result,  $\alpha_{l=0}$  is the same for the finite and the infinite wings, as shown in Fig. 5.21.

The values of  $a_0$  and  $a$  are related as follows. From the top of Fig. 5.21,

$$\frac{dC_l}{d(\alpha - \alpha_i)} = a_0$$

Integrating, we find

$$C_l = a_0(\alpha - \alpha_i) + \text{const} \quad (5.67)$$

Substituting Eq. (5.42) into (5.67), we obtain

$$C_l = a_0 \left( \alpha - \frac{C_l}{\pi AR} \right) + \text{const} \quad (5.68)$$

Differentiating Eq. (5.68) with respect to  $\alpha$ , and solving for  $dC_l/d\alpha$ , we obtain

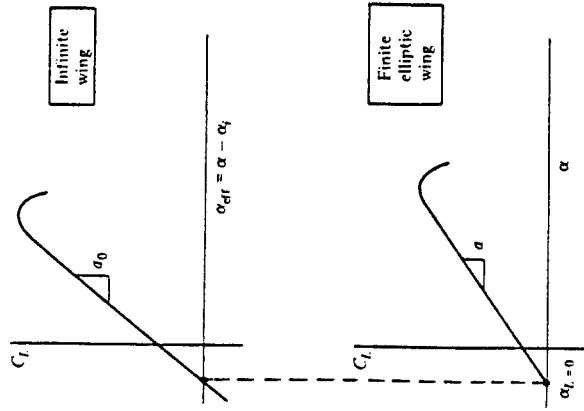


Figure 5.21 Lift curves for an infinite wing versus a finite elliptic wing.

$$\frac{dC_L}{d\alpha} = a = \frac{a_0}{1 + a_0/\pi AR} \quad (5.69)$$

Equation (5.69) gives the desired relation between  $a_0$  and  $a$  for an elliptic finite wing. For a finite wing of general planform, Eq. (5.69) is slightly modified, as given below:

$$a = \frac{a_0}{1 + (a_0/\pi AR)(1 + \tau)} \quad (5.70)$$

In Eq. (5.70),  $\tau$  is a function of the Fourier coefficients  $A_n$ . Values of  $\tau$  were first calculated by Glauert in the early 1920s and were published in Ref. 18, which should be consulted for more details. Values of  $\tau$  typically range between 0.05 and 0.25.

Of most importance in Eqs. (5.69) and (5.70) is the aspect-ratio variation. Note that for low-AR wings, a substantial difference can exist between  $a_0$  and  $a$ . However, as  $AR \rightarrow \infty$ ,  $a \rightarrow a_0$ . The effect of aspect ratio on the lift curve is dramatically shown in Fig. 5.22, which gives classic data obtained on rectangular wings by Prandtl in 1915. Note the reduction in  $dC_L/d\alpha$  as AR is reduced. Moreover, using the equations obtained above, Prandtl scaled the data in Fig. 5.22 to correspond to an aspect ratio of 5; his results collapsed to essentially the same curve, as shown in Fig. 5.23. In this manner, the aspect-ratio variation given in Eqs. (5.69) and (5.70) was confirmed as early as the year 1915.

### Physical Significance

Consider again the basic model underlying Prandtl's lifting-line theory. Return to Fig. 5.13 and study it carefully. An infinite number of infinitesimally weak horseshoe vortices are superimposed in such a fashion to generate a lifting line which spans the

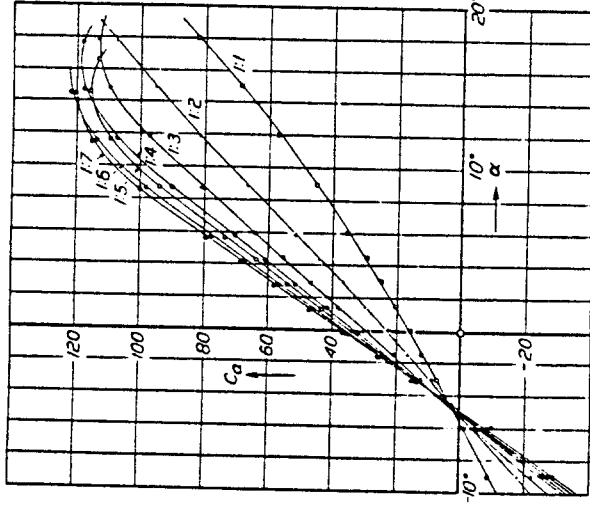


Figure 5.22 Prandtl's classic rectangular wing data. Variation of lift coefficient with angle of attack for seven different aspect ratios from 1 to 7. Nomenclature and scale are the same as given in Fig. 5.19.

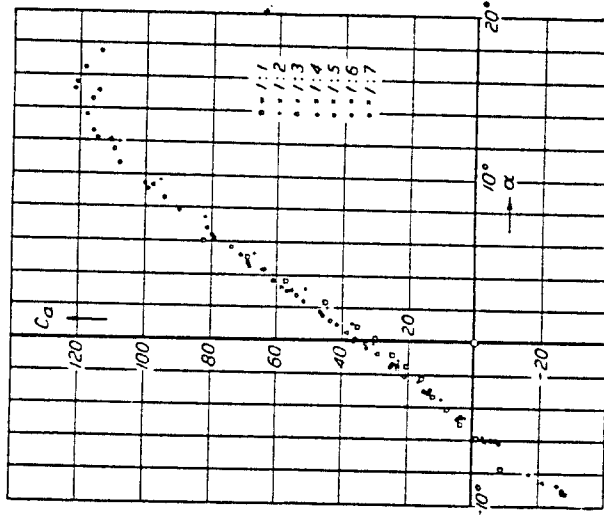


Figure 5.23 Data of Fig. 5.22 scaled by Prandtl to an aspect ratio of 5.

shown in Fig. 5.13 has real physical significance. To see this more clearly, return to Fig. 5.1. Note that in the three-dimensional flow over a finite wing, the streamlines leaving the trailing edge from the top and bottom surfaces are in different directions; i.e., there is a discontinuity in the tangential velocity at the trailing edge. We know from Chap. 4 that a discontinuous change in tangential velocity is theoretically allowed across a vortex sheet. In real life such discontinuities do not exist; rather the different velocities at the trailing edge generate a thin region of large velocity gradients — a thin region of shear flow with very large vorticity. Hence, a sheet of vorticity actually trails downstream from the trailing edge of a finite wing in real life. This sheet tends to roll up at the edges and helps to form the wing-tip vortices sketched in Fig. 5.2. Thus, Prandtl's lifting-line model with its trailing vortex sheet is physically consistent with the actual flow downstream of a finite wing.

**Example 5.1** Consider a finite wing with an aspect ratio of 8 and a taper ratio of 0.8. The airfoil section is thin and symmetric. Calculate the lift and induced drag coefficients for the wing when it is at an angle of attack of  $5^\circ$ . Assume that  $\delta = \tau$ .

**Solution** From Fig. 5.18,  $\delta = 0.055$ . Hence, from the stated assumption,  $\tau$  also equals 0.055. From Eq. (5.70), assuming  $a_0 = 2\pi$  from thin airfoil theory,

$$\begin{aligned} a &= \frac{a_0}{1 + a_0/\pi AR(1 + \tau)} = \frac{2\pi}{1 + 2\pi(1.055)/8\pi} = 4.97 \text{ rad}^{-1} \\ &= 0.0867 \text{ degree}^{-1} \end{aligned}$$

Since the airfoil is symmetric,  $\alpha_{L=0} = 0^\circ$ . Thus,

$$C_L = \alpha a = (0.0867 \text{ degree}^{-1})(5^\circ) = \boxed{0.4335}$$

From Eq. (5.61)

$$C_D = \frac{C_L^2}{\pi AR}(1 + \delta) = \frac{(0.4335)^2(1 + 0.055)}{8\pi} = \boxed{0.00789}$$

#### 5.4. A NUMERICAL NONLINEAR LIFTING-LINE METHOD

The classical Prandtl lifting-line theory described in Sec. 5.3 assumes a linear variation of  $C_L$  versus  $\alpha_{eff}$ . This is clearly seen in Eq. (5.19). However, as the angle of attack approaches and exceeds the stall angle, the lift curve becomes nonlinear, as shown in Fig. 4.4. This high-angle-of-attack regime is of interest to modern aerodynamicists. For example, when an airplane is in a spin, the angle of attack can range from 40 to  $90^\circ$ ; an understanding of high-angle-of-attack aerodynamics is essential to the prevention of such spins. In addition, modern fighter airplanes achieve optimum maneuverability by pulling high angles of attack at subsonic speeds. Therefore, there are practical reasons for extending Prandtl's classical theory to account for a nonlinear lift curve. One simple extension is described in this section.

The classical theory developed in Sec. 5.4 is essentially closed form; i.e., the results are analytical equations as opposed to a purely numerical solution. Of course,

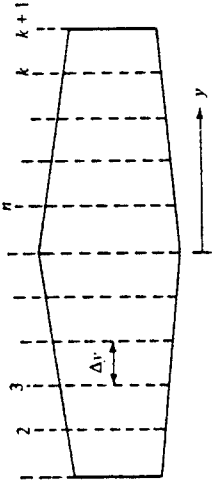


Figure 5.24 Stations along the span for a numerical solution.

4. Using  $\alpha_e$  from step 3, obtain the effective angle of attack  $\alpha_{eff}$  at each station from

$$\alpha_{eff}(y_n) = \alpha - \alpha_i(y_n)$$

5. With the distribution of  $\alpha_{eff}$  calculated from step 4, obtain the section lift coefficient ( $c_l$ )<sub>n</sub> at each station. These values are read from the known lift curve for the airfoil.
6. From  $(c_l)_n$  obtained in step 5, a new circulation distribution is calculated from the Kutta-Joukowski theorem and the definition of lift coefficient.

$$L'(y_n) = \rho_s V_s^2 \Gamma(y_n) = \frac{1}{2} \rho_s V_s^2 c_s(c_l)_n$$

Hence

$$\Gamma(y_n) = \frac{1}{2} \rho_s c_s(c_l)_n$$

where  $c_s$  is the local section chord. Keep in mind that in all the above steps,  $n$  ranges from 1 to  $k + 1$ .

7. The new distribution of  $\Gamma$  obtained in step 6 is compared with the values that were initially fed into step 3. If the results from step 6 do not agree with the input to step 3, then a new input is generated. If the previous input to step 3 is designated as  $\Gamma_{old}$  and the result of step 6 is designated as  $\Gamma_{new}$ , then the new input to step 3 is determined from

$$\Gamma_{input} = \Gamma_{old} + D(\Gamma_{new} - \Gamma_{old})$$

where  $D$  is a damping factor for the iterations. Experience has found that the iterative procedure requires heavy damping, with typical values of  $D$  on the order of 0.05.

8. Steps 3 to 7 are repeated a sufficient number of cycles until  $\Gamma_{new}$  and  $\Gamma_{old}$  agree at each spanwise station to within acceptable accuracy. If this accuracy is stipulated to be within 0.01 percent for a stretch of five previous iterations, then a minimum of 50 and sometimes as many as 150 iterations may be required for convergence.

9. From the converged  $\Gamma(y)$ , the lift and induced drag coefficients are obtained from Eqs. (5.26) and (5.30), respectively. The integrations in these equations can again be carried out by Simpson's rule.

The procedure outlined above generally works smoothly and quickly on a high-speed digital computer. Typical results are shown in Fig. 5.25, which shows the circulation distributions for rectangular wings with three different aspect ratios. The solid lines are from the classical calculations of Prandtl (Sec. 5.3), and the symbols are from the numerical method described above. Excellent agreement is obtained, thus verifying the integrity and accuracy of the numerical method. Also, Fig. 5.25 should be studied as an example of typical circulation distributions over general finite wings, with  $\Gamma$  reasonably high over the center section of the wing but rapidly dropping to zero at the tips.

An example of the use of the numerical method for the nonlinear regime is shown in Fig. 5.26. Here,  $C_L$  versus  $\alpha$  is given for a rectangular wing up to an angle of attack of  $50^\circ$  — well beyond stall. The numerical results are compared with existing experimental data obtained at the University of Maryland (Ref. 19). The numerical lifting-line solution at high angle of attack agrees with experiment to within 20 percent, and much closer for many cases. Therefore, such solutions give reasonable preliminary

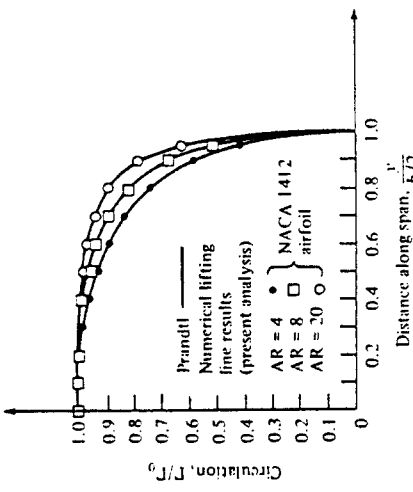


Figure 5.25 Lift distribution for a rectangular wing: comparison between Prandtl's classical theory and the numerical lifting-line method of Ref. 20.

engineering results for the high-angle-of-attack poststall region. However, it is wise not to stretch the applicability of lifting-line theory too far. At high angles of attack, the flow is highly three dimensional. This is clearly seen in the surface oil pattern on a rectangular wing at high angle of attack shown in Fig. 5.27. At high  $\alpha$ , there is a strong spanwise flow, in combination with mushroom-shaped flow separation regions. Clearly, the basic assumptions of lifting-line theory, classical or numerical, cannot properly account for such three-dimensional flows.

For more details and results on the numerical lifting-line method, please see Ref. 20.

## 5.5 LIFTING-SURFACE THEORY; VORTEX LATTICE NUMERICAL METHOD

Prandtl's classical lifting-line theory (Sec. 5.3) gives reasonable results for straight wings at moderate to high aspect ratio. However, for low-aspect-ratio straight wings,

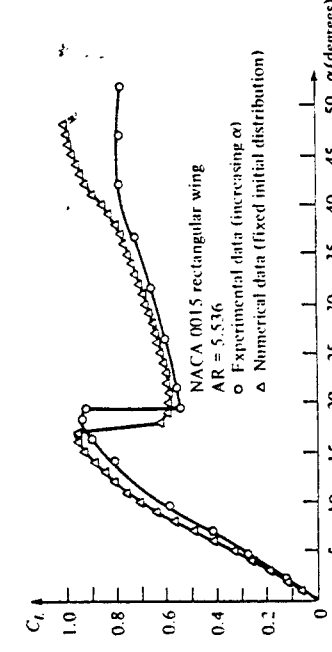


Figure 5.26 Lift coefficient versus angle of attack; comparison between experimental and numerical results.

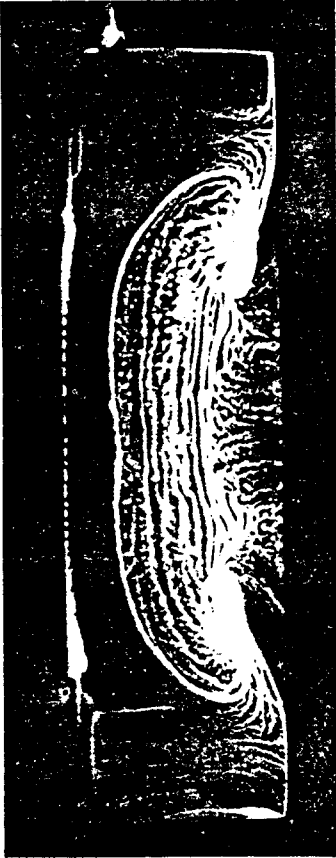


Figure 5.27 Surface oil flow pattern on a stalled, finite rectangular wing with a Clark Y-14 airfoil section.  $AR = 3.5$ ,  $\alpha = 22.8^\circ$ ,  $Re = 245,000$  (based on chord length). This pattern was established by coating the wing surface with pigmented mineral oil and inserting the model in a low-speed subsonic wind tunnel. In the photograph shown, flow is from top to bottom. Note the highly three-dimensional flow pattern. (Courtesy of Allen E. Winkelmann, University of Maryland.)

swept wings, and delta wings, classical lifting-line theory is inappropriate. For such planforms, sketched in Fig. 5.28, a more sophisticated model must be used. The purpose of this section is to introduce such a model and to discuss its numerical implementation. However, it is beyond the scope of this book to elaborate on the details of such higher-order models; rather, only the flavor is given here. You are encouraged to pursue this subject by reading the literature and by taking more advanced studies in aerodynamics.

Return to Fig. 5.13. Here, a simple lifting line spans the wing, with its associated trailing vortices. The circulation  $\Gamma$  varies with  $y$  along the lifting line. Let us extend this model by placing a series of lifting lines on the plane of the wing, at different chordwise stations; i.e., consider a large number of lifting lines all parallel to the  $y$  axis, located at different values of  $x$ , as shown in Fig. 5.29. In the limit of an infinite number of lines of infinitesimal strength, we obtain a vortex sheet, where the vortex lines run parallel to the  $y$  axis. The strength of this sheet (per unit length in the  $x$  direction) is denoted by  $\gamma$ , where  $\gamma$  varies in the  $y$  direction, analogous to the variation of  $\Gamma$  for the single lifting line in Fig. 5.13. Moreover, each lifting line will have, in general, a different overall strength, so that  $\gamma$  varies with  $x$  also. Hence,  $\gamma = \gamma(x, y)$  as

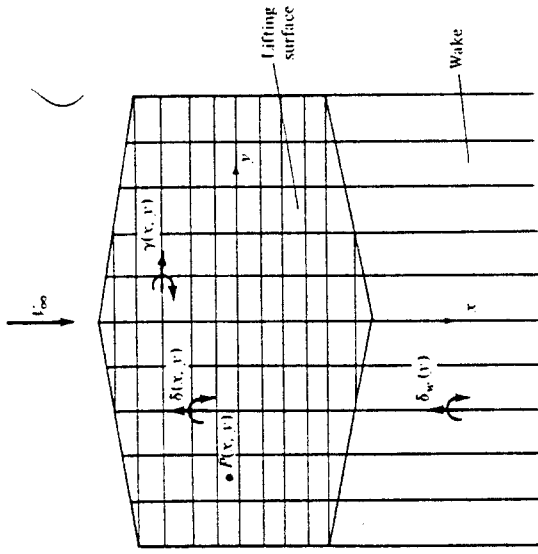


Figure 5.29 Schematic of a lifting surface.

shown in Fig. 5.29. In addition, recall that each lifting line has a system of trailing vortices; hence, the series of lifting lines are crossed by a series of superimposed trailing vortices parallel to the  $x$  axis. In the limit of an infinite number of infinitesimally weak vortices, these trailing vortices form another vortex sheet of strength  $\delta$  (per unit length in the  $y$  direction). [Note that this  $\delta$  is different than the  $\delta$  used in Eq. (5.61); the use of the same symbol in both cases is standard, and there should be no confusion since the meanings and context are completely different.] To see this more clearly, consider a single line parallel to the  $x$  axis. As we move along this line from the leading edge to the trailing edge, we pick up an additional superimposed trailing vortex each time we cross a lifting line. Hence,  $\delta$  must vary with  $x$ . Moreover, the trailing vortices are simply parts of the horseshoe vortex systems, the leading edges of which make up the various lifting lines. Since the circulation about each lifting line varies in the  $y$  direction, the strengths of different trailing vortices will in general be different. Hence,  $\delta$  also varies in the  $y$  direction; i.e.,  $\delta = \delta(x, y)$ , as shown in Fig. 5.29. The two vortex sheets — the one with vortex lines running parallel to  $y$  with strength  $\gamma$  (per unit length in the  $x$  direction) and the other with vortex lines running parallel to  $x$  with strength  $\delta$  (per unit length in the  $y$  direction) — results in a *lifting surface* distributed over the entire planform of the wing, as shown in Fig. 5.29. At any given point on the surface, the strength of the lifting surface is given by both  $\gamma$  and  $\delta$ , which are functions of  $x$  and  $y$ . We denote  $\gamma = \gamma(x, y)$  as the spanwise vortex strength distribution and  $\delta = \delta(x, y)$  as the chordwise vortex strength distribution.

Note that downstream of the trailing edge we have no spanwise vortex lines, only trailing vortices. Hence, the wake consists of only chordwise vortices. The strength of this wake vortex sheet is given by  $\delta_w$  (per unit length in the  $y$  direction). Since in the

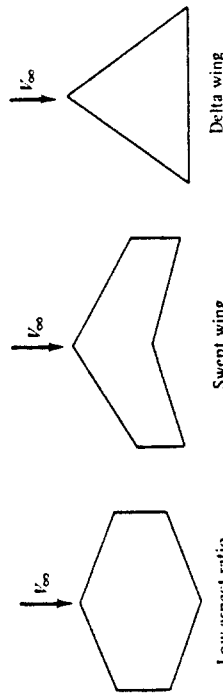


Figure 5.28 Types of wing planforms for which classical lifting-line theory is not appropriate.

wake the trailing vortices do not cross any vortex lines, the strength of any given trailing vortex is constant with  $x$ . Hence  $\delta_w$  depends only on  $y$  and, throughout the wake,  $\delta_w(y)$  is equal to its value at the trailing edge.

Now that we have defined the lifting surface, of what use is it? Consider point  $P$  located at  $(x, y)$  on the wing, as shown in Fig. 5.29. The lifting surface and the wake vortex sheet both induce a normal component of velocity at point  $P$ . Denote this normal velocity by  $w(x, y)$ . We want the wing planform to be a stream surface of the freestream — we want the sum of the induced  $w(x, y)$  and the normal component of the freestream velocity to be zero at point  $P$ , and for all points on the wing — this is the flow-tangency condition on the wing surface. (Keep in mind that we are treating the wing as a flat surface in this discussion.) The central theme of lifting-surface theory is to find  $\gamma(x, y)$  and  $\delta(x, y)$  such that the flow-tangency condition is satisfied at all points on the wing. [Recall that in the wake,  $\delta_w(y)$  is fixed by the trailing edge values of  $\delta(x, y)$ ; hence,  $\delta_w(y)$  is not, strictly speaking, one of the unknown dependent variables.]

Let us obtain an expression for the induced normal velocity  $w(x, y)$  in terms of  $\gamma$ ,  $\delta$ , and  $\delta_w$ . Consider the sketch given in Fig. 5.30, which shows a portion of the planform of a finite wing. Consider the point given by the coordinates  $(\xi, \eta)$ . At this point, the spanwise vortex strength is  $\gamma(\xi, \eta)$ . Consider a thin ribbon, or filament, of the spanwise vortex sheet of incremental length  $d\xi$  in the  $x$  direction. Hence, the strength of this filament is  $\gamma d\xi$ , and the filament stretches in the  $y$  (or  $\eta$ ) direction. Also consider point  $P$  located at  $(x, y)$  and removed a distance  $r$  from the point  $(\xi, \eta)$ . From the Biot-Savart law, Eq. (5.5), the incremental velocity induced at  $P$  by a segment  $d\eta$  of this vortex filament of strength  $\gamma d\xi$  is

$$|\mathbf{d}V| = \left| \frac{\Gamma}{4\pi} \frac{\mathbf{dl} \times \mathbf{r}}{|\mathbf{r}|^3} \right| = \frac{\gamma d\xi (d\eta) r \sin \theta}{4\pi r^3} \quad (5.73)$$

Examining Fig. 5.30, and following the right-hand rule for the strength  $\gamma$ , note that  $|\mathbf{d}V|$  is induced downward, into the plane of the wing, i.e., in the negative  $z$  direction. Following the usual sign convention that  $w$  is positive in the upward direction, i.e., in the positive  $z$  direction, we denote the contribution of Eq. (5.73) to the induced velocity  $w$  as  $(dw)_r = -|\mathbf{d}V|$ . Also, note that  $\sin \theta = (x - \xi)/r$ . Hence, Eq. (5.73) becomes

$$(dw)_r = -\frac{\gamma}{4\pi} \frac{(x - \xi)d\xi d\eta}{r^3} \quad (5.74)$$

Considering the contribution of the elemental chordwise vortex of strength  $\delta d\eta$  to the induced velocity at  $P$ , we find by an analogous argument that

$$(dw)_\delta = -\frac{\delta}{4\pi} \frac{(y - \eta)d\xi d\eta}{r^3} \quad (5.75)$$

To obtain the velocity induced at  $P$  by the entire lifting surface, Eqs. (5.74) and (5.75) must be integrated over the wing planform, designated as region  $S$  in Fig. 5.30. Moreover, the velocity induced at  $P$  by the complete wake is given by an equation analogous to Eq. (5.75), but with  $\delta_w$  instead of  $\delta$ , and integrated over the wake, designated as region  $W$  in Fig. 5.30. Noting that

$$r = \sqrt{(x - \xi)^2 + (y - \eta)^2}$$

the normal velocity induced at  $P$  by both the lifting surface and the wake is

$$w(x, y) = -\frac{1}{4\pi} \iint_S \frac{(x - \xi)\gamma(\xi, \eta) + (y - \eta)\delta(\xi, \eta)}{[(x - \xi)^2 + (y - \eta)^2]^{1/2}} d\xi d\eta$$

$$-\frac{1}{4\pi} \iint_W \frac{(y - \eta)\delta_w(\xi, \eta)}{[(x - \xi)^2 + (y - \eta)^2]^{1/2}} d\xi d\eta \quad (5.76)$$

The central problem of lifting-surface theory is to solve Eq. (5.76) for  $\gamma(\xi, \eta)$  and  $\delta(\xi, \eta)$  such that the sum of  $w(x, y)$  and the normal component of the freestream is zero, i.e., such that the flow is tangent to the planform surface  $S$ . The details of various lifting-surface solutions are beyond the scope of this book; rather, our purpose here simply was to present the flavor of the basic model.

The advent of the high-speed digital computer has made possible the implementation of numerical solutions based on the lifting-surface concept. These solutions are similar to the panel solutions for two-dimensional flow discussed in Chaps. 3 and 4 in that the wing planform is divided into a number of panels, or elements. On each panel, either constant or prescribed variations of both  $\gamma$  and  $\delta$  can be made. Control points on the panels can be chosen, where the net normal flow velocity is zero. The evaluation of equations like Eq. (5.76) at these control points results in a system of

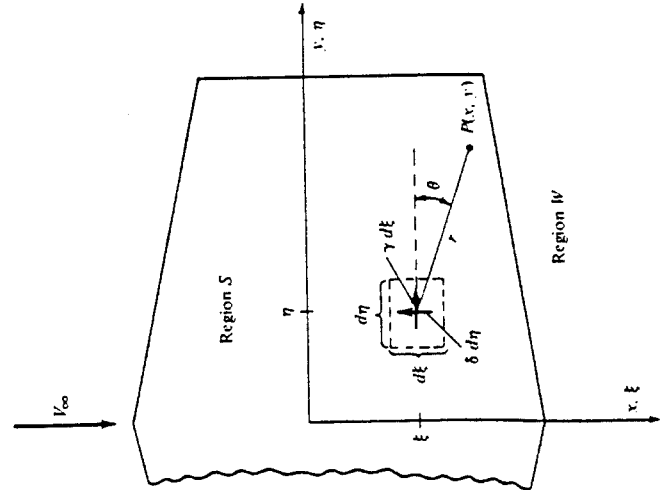


Figure 5.30 Velocity induced at point  $P$  by an infinitesimal segment of the lifting surface. The velocity is perpendicular to the plane of the paper.

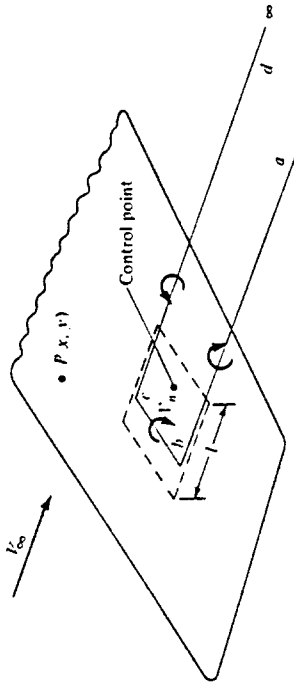


Figure 5.31 Schematic of a single horseshoe vortex, which is part of a vortex system on the wing.

simultaneous algebraic equations which can be solved for the values of the  $\gamma$ 's and  $\delta$ 's on all the panels.

A related but somewhat simpler approach is to superimpose a finite number of horseshoe vortices of different strengths  $\Gamma_r$  on the wing surface. For example, consider Fig. 5.31, which shows part of a finite wing. The dashed lines define a panel on the wing planform, where  $l$  is the length of the panel in the flow direction. The panel is a trapezoid; it does not have to be a square, or even a rectangle. A horseshoe vortex,  $abcd$ , of strength  $\Gamma_r$  is placed on the panel such that the segment  $bc$  is a distance  $l/4$  from the front of the panel. A control point is placed on the center line of the panel at a distance  $l/4$  from the front. The velocity induced at an arbitrary point  $P$  only by the single horseshoe vortex can be calculated from the Biot-Savart law by treating each of the vortex filaments  $ab$ ,  $bc$ , and  $cd$  separately. Now consider the entire wing covered by a finite number of panels, as sketched in Fig. 5.32. A series of horseshoe vortices are now superimposed. For example, on one panel at the leading edge, we have the horseshoe vortex  $abcd$ . On the panel behind it, we have the horseshoe vortex  $ae'fd$ . On the next panel, we have  $agh'd$ , and on the next,  $ajid$ , and so on. The entire wing is covered by this lattice of horseshoe vortices, each of different unknown strength  $\Gamma_r$ . At

## 5.6 HISTORICAL NOTE: LANCHESTER AND PRANDTL—THE EARLY DEVELOPMENT OF FINITE-WING THEORY

On June 27, 1866, in a paper entitled "Aerial Locomotion" given to the Aeronautical Society of Great Britain, the Englishman Francis Wenham expressed for the first time in history the effect of aspect ratio on finite-wing aerodynamics. He theorized (correctly) that most of the lift of a wing occurs from the portion near the leading edge, and hence a long, narrow wing would be most efficient. He suggested stacking a number of long thin wings above each other to generate the required lift, and he built two full-size gliders in 1858, both with five wings each, to demonstrate (successfully) his ideas. (Wenham is also known for designing and building the first wind tunnel in history, at Greenwich, England, in 1871.)

However, the true understanding of finite-wing aerodynamics, as well as ideas for the theoretical analysis of finite wings, did not come until 1907. In that year, Frederick W. Lanchester published his now famous book entitled *Aerodynamics*. We have met Lanchester before—in Sec. 4.11 concerning his role in the development of the circulation theory of lift. Here, we examine his contributions to finite-wing theory.

In Lanchester's *Aerodynamics*, we find the first mention of vortices that trail downstream of the wing tips. Figure 5.33 is one of Lanchester's own drawings from his 1907 book, showing the "vortex trunk" which forms at the wing tip. Moreover, he knew that a vortex filament could not end in space (see Sec. 5.2), and he theorized that the vortex filaments which constituted the two wing-tip vortices must cross the wing along its span—the first concept of bound vortices in the spanwise direction. Hence, the essence of the horseshoe vortex concept originated with Lanchester. In his own words,

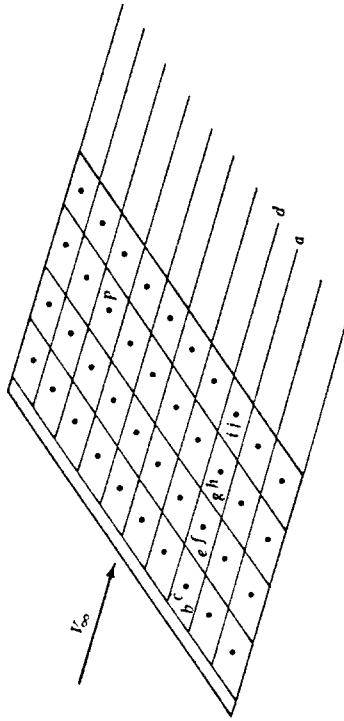


Figure 5.32 Vortex lattice system on a finite wing.

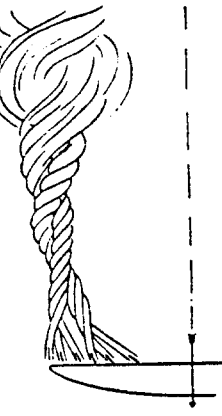


Figure 5.33 A figure from Lanchester's *Aerodynamics*, 1907; this is his own drawing of the wing-tip vortex on a finite wing.

Thus the author regards the two trailing vortices as a definite proof of the existence of a cyclic component of equal strength in the motion surrounding the airfoil itself.

Considering the foresight and originality of Lanchester's thinking, let us pause for a moment and look at the man himself. Lanchester was born on October 23, 1868, in Lewisham, England. The son of an architect, Lanchester became interested in engineering at an early age. (He was told by his family that his mind was made up at the age of 4.) He studied engineering and mining during the years 1886–1889 at the Royal College of Science in South Kensington, London, but never officially graduated. He was a quick-minded and innovative thinker and became a designer at the Forward Gas Engine Company in 1889, specializing in internal combustion engines. He rose to the post of assistant works manager. In the early 1890s, Lanchester became very interested in aeronautics, and along with his development of high-speed engines, he also carried out numerous aerodynamic experiments. It was during this period that he formulated his ideas on both the circulation theory of lift and the finite-wing vortex concept. A serious paper written by Lanchester first for the Royal Society, and then for the Physical Society, was turned down for publication—something Lanchester never forgot. Finally, his aeronautical concepts were published in his two books *Aerodynamics* and *Aerodrometics* in 1907 and 1908, respectively. To his detriment, Lanchester had a style of writing and a means of explanation which were not easy to follow, and his works were not immediately seized upon by other researchers. Lanchester's bitter feelings about the public's receipt of his papers and books are graphically seen in his letter to the Daniel Guggenheim Medal Fund decades later. In a letter dated June 6, 1931, Lanchester writes:

So far as aeronautical science is concerned, I cannot say that I experienced anything but discouragement; in the early days my theoretical work (backed by a certain amount of experimental verification), mainly concerning the vortex theory of sustentation and the screw propeller, was refused by the two leading scientific societies in this country, and I was seriously warned that my profession as an engineer would suffer if I dabbled in a subject that was merely a dream of madmen! When I published my two volumes in 1907 and 1908 they were well received on the whole, but this was mainly due to the success of the brothers Wright, and the general interest aroused on the subject.

In 1899, he formed the Lanchester Motor Company, Limited, and sold automobiles of his own design. He married in 1919, but had no children. Lanchester maintained his interest in automobiles and related mechanical devices until his death on March 8, 1946, at the age of 77.

In 1908, Lanchester visited Göttingen, Germany, and fully discussed his wing theory with Ludwig Prandtl and his student Theodore von Karman. Prandtl spoke no English, Lanchester spoke no German, and in light of Lanchester's unclear way of explaining his ideas, there appeared to be little chance of understanding between the two parties. However, shortly after, Prandtl began to develop his own wing theory, using a bound vortex along the span and assuming that the vortex trails downstream from both wing tips. The first mention of Prandtl's work on finite-wing theory was made in a paper by O. Föppl in 1911, discussing some of Föppl's experimental work on finite wings. Commenting on his results, Föppl says:

They agree very closely with the theoretical investigation by Professor Prandtl on the current around an airplane with a finite span wing. Already Lanchester in his work, "Aerodynamics" (translated into German by C. and A. Runge) indicated that to the two extremities of an airplane wing are attached two vortex ropes (Wirbelzopfe) which make possible the transition from the flow around the airplane, which occurs nearly according to Kutta's theory, to the flow of the undisturbed fluid at both sides. These two vortex ropes continue the vortex which, according to Kutta's theory, takes place on the lamina. We are led to admit this owing to the Helmholtz theorem that vortices cannot end in the fluid. At any rate these two vortex ropes have been made visible in the Göttingen Institute by emitting an ammonia cloud into the air. Prandtl's theory is constructed on the consideration of this current in reality existing.

In the same year, Prandtl expressed his own first published words on the subject. In a paper given at a meeting of the Representatives of Aeronautical Science in Göttingen in November, 1911, entitled "Results and Purposes of the Model Experimental Institute of Göttingen," Prandtl states:

Another theoretical research relates to the conditions of the current which is formed by the air behind an airplane. The lift generated by the airplane is, on account of the principle of action and reaction, necessarily connected with a descending current behind the airplane. Now it seemed very useful to investigate this descending current in all its details. It appears that the descending current is formed by a pair of vortices, the vortex filaments of which start from the airplane wing tips. The distance of the two vortices is equal to the span of the airplane, their strength is equal to the circulation of the current around the airplane and the current in the vicinity of the airplane is fully given by the superposition of the uniform current with that of a vortex consisting of three rectilinear sections.

In discussing the results of his theory, Prandtl goes on to state in the same paper:

The same theory supplies, taking into account the variations of the current on the airplane which came from the lateral vortices, a relationship showing the dependence of the airplane lift on the aspect ratio; in particular it gives the possibility of extrapolating the results thus obtained experimentally to the airplane of infinite span wing. From the maximum aspect ratios measured by us (1.9 to that of 1:∞) the lifts increase further in marked degree—by some 30 or 40 percent. I would add here a remarkable result of this extrapolation, which is, that the results of Kutta's theory of the infinite wing, at least so far as we are dealing with small cambers and small angles of incidence, have been confirmed by these experimental results.

Starting from this line of thought we can attack the problem of calculating the surface of an airplane so that lift is distributed along its span in a determined manner, previously fixed. The experimental trial of these calculations has not yet been made, but it will be in the near future.

It is clear from the above comments that Prandtl<sup>\*</sup> was definitely following the model proposed earlier by Lanchester. Moreover, the major concern of the finite-wing theory was first in the calculation of lift—no mention is made of induced drag. It is interesting to note that Prandtl's theory first began with a single horseshoe vortex, such as sketched in Fig. 5.11. The results were not entirely satisfactory. During the period 1911–1918, Prandtl and his colleagues expanded and refined his finite-wing theory, which evolved to the concept of a lifting line consisting of an infinite number of horseshoe vortices, as sketched in Fig. 5.13. In 1918, the term "induced drag" was coined by Max Munk, a colleague of Prandtl at Göttingen. Much of Prandtl's development of finite-wing theory was classified secret by the German government during World War I. Finally,

his lifting-line theory was released to the outside world, and his ideas were published in English in a special NACA report written by Prandtl and published in 1922, entitled "Applications of Modern Hydrodynamics to Aerodynamics" (NACA TR 116). Hence, the theory we have outlined in Sec. 5.3 was well-established more than 60 years ago. One of Prandtl's strengths was the ability to base his thinking on sound ideas, and to apply intuition that resulted in relatively straightforward theories that most engineers could understand and appreciate. This is in contrast to the difficult writings of Lanchester. As a result, the lifting theory for finite wings has come down through the years identified as *Prandtl's lifting-line theory*, although we have seen that Lanchester was the first to propose the basic model on which lifting-line theory is built.

In light of Lanchester's 1908 visit with Prandtl and Prandtl's subsequent development of the lifting-line theory, there has been some discussion over the years that Prandtl basically stole Lanchester's ideas. However, this is clearly not the case. We have seen in the above quotes that Prandtl's group at Göttingen was giving full credit to Lanchester as early as 1911. Moreover, Lanchester never gave the world a clear and practical theory with which results could be readily obtained — Prandtl did. Therefore, in this book we have continued the tradition of identifying the lifting-line theory with Prandtl's name. On the other hand, for very good reasons, in England and various places in western Europe, the theory is labeled the *Lanchester-Prandtl theory*.

To help put the propriety in perspective, Lanchester was awarded the Daniel Guggenheim Medal in 1936 (Prandtl had received this award some years earlier). In the medal citation, we find the following words:

Lanchester was the foremost person to propound the now famous theory of flight based on the Vortex theory, so brilliantly followed up by Prandtl and others. He first put forward his theory in a paper read before the Birmingham Natural History and Philosophical Society on 19th June, 1894. In a second paper in 1897, in his two books published in 1907 and 1908, and in his paper read before the Institution of Automobile Engineers in 1916, he further developed this doctrine.

Perhaps the best final words on Lanchester are contained in this excerpt from his obituary found in the British periodical *Flight* in March 1946:

And now Lanchester has passed from our ken but not from our thoughts. It is to be hoped that the nation which neglected him during much of his lifetime will at any rate perpetuate his work by a memorial worthy of the "Grand Old Man" of aerodynamics.

## 5.7 HISTORICAL NOTE: PRANDTL — THE MAN

The modern science of aerodynamics rests on a strong fundamental foundation, a large percentage of which was established in one place by one man — at the University of Göttingen by Ludwig Prandtl. Prandtl never received a Noble Prize, although his contributions to aerodynamics and fluid mechanics are felt by many to be of that caliber. Throughout this book, you will encounter his name in conjunction with major advances in aerodynamics: thin airfoil theory in Chap. 4, finite-wing theory in Chap. 5, supersonic shock- and expansion-wave theory in Chap. 9, compressibility corrections in

Chap. 11, and what may be his most important contribution, namely the boundary layer concept in Chap. 16. Who was this man who has had such a major impact on fluid dynamics? Let us take a closer look.

Ludwig Prandtl was born on February 4, 1874, in Freising, Bavaria. His father was Alexander Prandtl, a professor of surveying and engineering at the agricultural college at Weihenstephan, near Freising. Although three children were born into the Prandtl family, two died at birth, and Ludwig grew up as an only child. His mother, the former Magdalene Ostermann, had a protracted illness, and partly as a result of this, Prandtl became very close to his father. At an early age, Prandtl became interested in his father's books on physics, machinery, and instruments. Much of Prandtl's remarkable ability to intuitively go to the heart of a physical problem can be traced to his environment at home as a child, where his father, a great lover of nature, induced Ludwig to observe natural phenomena and to reflect on them.

In 1894, Prandtl began his formal scientific studies at the Technische Hochschule in Munich, where his principal teacher was the well-known mechanics professor, August Föppl. Six years later, he graduated from the University of Munich with a Ph.D., with Föppl as his advisor. However, by this time Prandtl was alone, his father having died in 1896 and his mother in 1898.

By 1900, Prandtl had not done any work or shown any interest in fluid mechanics. Indeed, his Ph.D. thesis at Munich was in solid mechanics, dealing with unstable elastic equilibrium in which bending and distortion acted together. (It is not generally recognized by people in fluid dynamics that Prandtl continued his interest and research in solid mechanics through most of his life — this work is eclipsed, however, by his major contributions to the study of fluid flow.) However, soon after graduation from Munich, Prandtl had his first major encounter with fluid mechanics. Joining the Nuremberg works of the Maschinenfabrik Augsburg as an engineer, Prandtl worked in an office designing mechanical equipment for the new factory. He was made responsible for redesigning an apparatus for removing machine shavings by suction. Finding no reliable information in the scientific literature about the fluid mechanics of suction, Prandtl arranged his own experiments to answer a few fundamental questions about the flow. The result of this work was his new design for shavings' cleaners. The apparatus was modified with pipes of improved shape and size, and carried out satisfactory operation at one-third its original power consumption. Prandtl's contributions in fluid mechanics had begun.

One year later, in 1901, he became Professor of Mechanics in the Mathematical Engineering Department at the Technische Hochschule in Hanover. (Please note that in Germany a "technical high school" is equivalent to a technical university in the United States.) It was at Hanover that Prandtl enhanced and continued his new found interest in fluid mechanics. It was here that Prandtl developed his boundary-layer theory and became interested in supersonic flow through nozzles. In 1904, Prandtl delivered his famous paper on the concept of the boundary layer to the Third Congress on Mathematicians at Heidelberg. Entitled "Über Flüssigkeitsbewegung bei sehr kleiner Reibung," Prandtl's Heidelberg paper established the basis for most modern calculations of skin friction, heat transfer, and flow separation (see Chaps. 15 and 16). From that time on, the star of Prandtl was to rise meteorically. Later than year, he moved to

the prestigious University of Göttingen to become Director of the Institute for Technical Physics, later to be renamed Applied Mechanics. Prandtl spent the remainder of his life at Göttingen, building his laboratory into the world's greatest aerodynamic research center of the 1904–1930 time period.

At Göttingen, during 1905–1908 Prandtl carried out numerous experiments on supersonic flow through nozzles and developed oblique shock- and expansion-wave theory (see Chap. 9). He took the first photographs of the supersonic flow through nozzles, using a special schlieren optical system (see chapter 4 of Ref. 21). From 1910 to 1920, he devoted most of his efforts to low-speed aerodynamics, principally airfoil and wing theory, developing the famous lifting-line theory for finite wings (see Sec. 5.3). Prandtl returned to high-speed flows in the 1920s, during which he contributed to the evolution of the famous Prandtl-Glauert compressibility correction (see Secs. 11.4 and 11.11).

By the 1930s, Prandtl was recognized worldwide as the "elder statesman" of fluid dynamics. Although he continued to do research in various areas, including structural mechanics and meteorology, his "Nobel Prize-level" contributions to fluid dynamics had all been made. Prandtl remained at Göttingen throughout the turmoil of World War II, engrossed in his work and seemingly insulated from the intense political and physical disruptions brought about by Nazi Germany. In fact, the German Air Ministry provided Prandtl's laboratory with new equipment and financial support. Prandtl's attitude at the end of the war is reflected in his comments to a U.S. Army interrogation team which swept through Göttingen in 1945; he complained about bomb damage to the roof of his house, and he asked how the Americans planned to support his current and future research. Prandtl was 70 at the time and was still going strong. However, the fate of Prandtl's laboratory at this time is summed up in the words of Irmgard Flugge-Lotz and Wilhelm Flugge, colleagues of Prandtl, who wrote 28 years later in the *Annual Review of Fluid Mechanics* (Vol. 5, 1973):

World War II swept over all of us. At its end some of the research equipment was dismantled, and most of the research staff was scattered with the winds. Many are now in this country (the United States) and in England, some have returned. The seeds sown by Prandtl have sprouted in many places, and there are now many "second growth" Göttingers who do not even know that they are.

What type of person was Prandtl? By all accounts he was a gracious man, studious, likeable, friendly, and totally focused on those things that interested him. He enjoyed music and was an accomplished pianist. Figure 5.34 shows a rather introspective man busily at work. One of Prandtl's most famous students, Theodore von Karman, wrote in his autobiography *The Wind and Beyond* (Little, Brown and Company, Boston, 1967) that Prandtl bordered on being naive. A favorite story along these lines is that, in 1909, Prandtl decided that he should be married, but he did not know quite what to do. He finally wrote to Mrs. Föppl, the wife of his respected teacher, asking permission to marry one of her two daughters. Prandtl and Föppl's daughters were acquainted, but nothing more than that. Moreover, Prandtl did not stipulate which daughter. The Föppl's made a family decision that Prandtl should marry the oldest daughter, Gertrude. The marriage took place, leading to a happy relationship. The Prandtl's had two daughters, born in 1914 and 1917.



Figure 5.34 Ludwig Prandtl (1875–1953).

Prandtl was considered a tedious lecturer because he could hardly make a statement without qualifying it. However, he attracted excellent students who later went on to distinguish themselves in fluid mechanics — such as Jakob Ackeret in Zurich, Switzerland, Adolf Busemann in Germany, and Theodore von Karman at Aachen, Germany, and later at Cal Tech in the United States. Prandtl died in 1953. He was clearly the father of modern aerodynamics — a monumental figure in fluid dynamics. His impact will be felt for centuries to come.

## 5.8 SUMMARY

Return to the chapter road map in Fig. 5.5, and review the straightforward path we have taken during the development of finite-wing theory. Make certain that you feel comfortable with the flow of ideas before proceeding further.

A brief summary of the important results of this chapter follows.

The wing-tip vortices from a finite wing induce a downwash which reduces the angle of attack effectively seen by a local airfoil section.

$$\alpha_{\text{eff}} = \alpha - \alpha_t$$

In turn, the presence of downwash results in a component of drag defined as induced drag,  $D_d$ .

$$a = \frac{a_0}{1 + (a_0/\pi AR)(1 + \tau)} \quad (5.70)$$

For low-aspect-ratio wings, swept wings, and delta wings, lifting-surface theory is more often used. In modern aerodynamics, such lifting-surface theory is implemented by the vortex panel or the vortex lattice techniques.

Vortex sheets and vortex filaments are useful in modeling the aerodynamics of finite wings. The velocity induced by a directed segment  $d\mathbf{l}$  of a vortex filament is given by the Biot-Savart law:

$$dV = \frac{\Gamma}{4\pi} \frac{dl \times r}{|r|^3} \quad (5.2)$$

In Prandtl's classical lifting-line theory, the finite wing is replaced by a single spanwise lifting line along which the circulation  $\Gamma(y)$  varies. A system of vortices trail downstream from the lifting line, which induces a downwash at the lifting line. The circulation distribution is determined from the fundamental equation

$$\alpha(y_0) = \frac{\Gamma(y_0)}{\pi V_\infty c(y_0)} + \alpha_{t=0}(y_0) + \frac{1}{4\pi V_\infty} \int_{-b/2}^{b/2} \frac{(d\Gamma/dy) dy}{y_0 - y} \quad (5.23)$$

Results from classical lifting-line theory:  
Elliptic wing  
Downwash is constant:

$$w = -\frac{\Gamma_0}{2b} \quad (5.35)$$

$$\alpha_i = \frac{C_L}{\pi AR} \quad (5.42)$$

$$C_{D,i} = \frac{C_L^2}{\pi AR} \quad (5.43)$$

$$a = \frac{a_0}{1 + a_0/\pi AR} \quad (5.69)$$

General wing:

$$C_{D,i} = \frac{C_L^2}{\pi AR} (1 + \delta) = \frac{C_L^2}{\pi e AR} \quad (5.61) \text{ and } (5.62)$$

## THREE-DIMENSIONAL INCOMPRESSIBLE FLOW

*Treat nature in terms of the cylinder, the sphere, the cone, all in perspective.*

Paul Cézanne, 1890

### 6.1 INTRODUCTION

To this point in our aerodynamic discussions, we have been working mainly in a two-dimensional world; the flows over the bodies treated in Chap. 3 and the airfoils in Chap. 4 involved only two dimensions in a single plane — so-called planar flows. In Chap. 5, the analyses of a finite wing were carried out in the plane of the wing, in spite of the fact that the detailed flow over a finite wing is truly three-dimensional. The relative simplicity of dealing with two dimensions, i.e., having only two independent variables, is self-evident and is the reason why a large bulk of aerodynamic theory deals with two-dimensional flows. Fortunately, the two-dimensional analyses go a long way toward understanding many practical flows, but they also have distinct limitations.

The real world of aerodynamic applications is three-dimensional. However, because of the addition of one more independent variable, the analyses generally become more complex. The accurate calculation of three-dimensional flow fields has been, and still is, one of the most active areas of aerodynamic research.

The purpose of this book is to present the fundamentals of aerodynamics. Therefore, it is important to recognize the predominance of three-dimensional flows, although it is beyond our scope to go into detail. Therefore, the purpose of this chapter is to introduce some very basic considerations of three-dimensional incompressible flow. This chapter is short; we do not even need a road map to guide us through it. Its function is simply to open the door to the analysis of three-dimensional flow.

The governing fluid flow equations have already been developed in three dimensions in Chaps. 2 and 3. In particular, if the flow is irrotational, Eq. (2.145) states that

$$\mathbf{V} = \nabla \phi \quad (2.145)$$

where, if the flow is also incompressible, the velocity potential is given by Laplace's equation,

$$\nabla^2 \phi = 0 \quad (3.40)$$

Solutions of Eq. (3.40) for flow over a body must satisfy the flow-tangency boundary condition on the body, i.e.,

$$\mathbf{V} \cdot \mathbf{n} = 0 \quad (3.48a)$$

where  $\mathbf{n}$  is a unit vector normal to the body surface. In all of the above equations,  $\phi$  is in general a function of three-dimensional space; e.g., in spherical coordinates,  $\phi = \phi(r, \theta, \Phi)$ . Let us use these equations to treat some elementary three-dimensional incompressible flows.

### 6.2 THREE-DIMENSIONAL SOURCE

Return to Laplace's equation written in spherical coordinates, as given by Eq. (3.43). Consider the velocity potential given by

$$\phi = -\frac{C}{r} \quad (6.1)$$

where  $C$  is a constant and  $r$  is the radial coordinate from the origin. Equation (6.1) satisfies Eq. (3.43), and hence it describes a physically possible incompressible, irrotational three-dimensional flow. Combining Eq. (6.1) with the definition of the gradient in spherical coordinates, Eq. (2.18), we obtain

$$\mathbf{V} = \nabla \phi = \frac{C}{r^2} \mathbf{e}_r \quad (6.2)$$

In terms of the velocity components, we have

$$V_r = \frac{C}{r^2} \quad (6.3a)$$

$$V_\theta = 0 \quad (6.3b)$$

$$V_\phi = 0 \quad (6.3c)$$

Clearly, Eq. (6.2), or Eqs. (6.3a to c), describe a flow with straight streamlines emanating from the origin, as sketched in Fig. 6.1. Moreover, from Eq. (6.2) or (6.3a), the velocity varies inversely as the square of the distance from the origin. Such a flow is defined as a *three-dimensional source*. Sometimes it is called simply a *point source*, in contrast to the two-dimensional line source discussed in Sec. 3.10.

To evaluate the constant  $C$  in Eq. (6.3a), consider a sphere of radius  $r$  and surface  $S$  centered at the origin. From Eq. (2.37), the mass flow across the surface of this sphere is

$$\text{Mass flow} = \oint_S \rho \mathbf{V} \cdot d\mathbf{S}$$

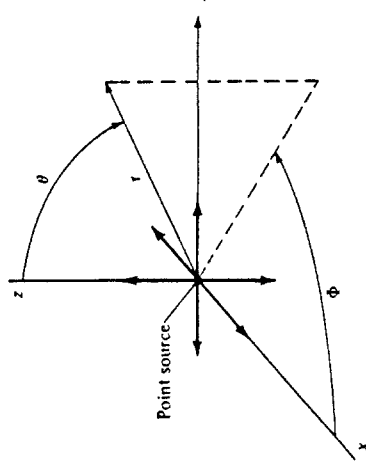


Figure 6.1 Three-dimensional (point) source.

Hence, the *volume* flow, denoted by  $\lambda$ , is

$$\lambda = \oint_S \mathbf{v} \cdot d\mathbf{s} \quad (6.4)$$

On the surface of the sphere, the velocity is a constant value equal to  $V_r = C/r^2$  and is normal to the surface. Hence, Eq. (6.4) becomes

$$\lambda = \frac{C}{r^2} 4\pi r^2 = 4\pi C$$

Hence

$$C = \frac{\lambda}{4\pi}$$

Substituting Eq. (6.5) into (6.3a), we find

$$V_r = \frac{\lambda}{4\pi r^2} \quad (6.6)$$

Compare Eq. (6.6) with its counterpart for a two-dimensional source given by Eq. (3.62). Note that the three-dimensional effect is to cause an inverse  $r$ -squared variation and that the quantity  $4\pi$  appears rather than  $2\pi$ . Also, substituting Eq. (6.5) into (6.1), we obtain, for a point source,

$$\phi = -\frac{\lambda}{4\pi r} \quad (6.7)$$

In the above equations,  $\lambda$  is defined as the *strength* of the source. When  $\lambda$  is a negative quantity, we have a point sink.

### 6.3 THREE-DIMENSIONAL DOUBLET

Consider a sink and source of equal but opposite strength located at points  $O$  and  $A$ , as sketched in Fig. 6.2. The distance between the source and sink is  $l$ . Consider an arbitrary point  $P$  located a distance  $r$  from the sink and a distance  $r_1$  from the source. From Eq. (6.7), the velocity potential at  $P$  is

$$\phi = -\frac{\lambda}{4\pi} \left( \frac{1}{r_1} - \frac{1}{r} \right)$$

$$\phi = -\frac{\lambda}{4\pi} \frac{r - r_1}{rr_1} \quad (6.8)$$

Let the source approach the sink as their strengths become infinite; i.e., let

$$l \rightarrow 0 \quad \text{as} \quad \lambda \rightarrow \infty$$

In the limit, as  $l \rightarrow 0$ ,  $r - r_1 \rightarrow OB = l \cos \theta$ , and  $rr_1 \rightarrow r^2$ . Thus, in the limit, Eq. (6.8) becomes

$$\phi = -\lim_{l \rightarrow 0} \frac{\lambda}{4\pi} \frac{r - r_1}{rr_1} = -\frac{\lambda}{4\pi} \frac{l \cos \theta}{r^2}$$

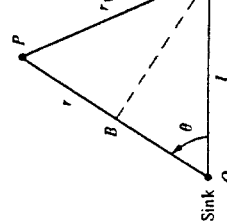
$$\phi = -\frac{\mu \cos \theta}{4\pi r^2} \quad (6.9)$$

where  $\mu = \lambda l$ . The flow field produced by Eq. (6.9) is a *three-dimensional doublet*;  $\mu$  is defined as the strength of the doublet. Compare Eq. (6.9) with its two-dimensional counterpart given in Eq. (3.88). Note that the three-dimensional effects lead to an inverse  $r$ -squared variation and introduce a factor  $4\pi$ , versus  $2\pi$  for the two-dimensional case.

From Eqs. (2.18) and (6.9), we find

$$\mathbf{V} = \nabla \phi = \frac{\mu}{2\pi r^3} \mathbf{e}_r + \frac{\mu}{4\pi r^3} \frac{\sin \theta}{r} \mathbf{e}_\theta + 0 \mathbf{e}_\phi \quad (6.10)$$

The streamlines of this velocity field are sketched in Fig. 6.3. Shown are the streamlines in the  $zr$  plane; they are the same in all the  $zr$  planes, i.e., for all values of  $\Phi$ .

Figure 6.2 Source-sink pair. In the limit as  $l \rightarrow 0$ , a three-dimensional doublet is obtained.

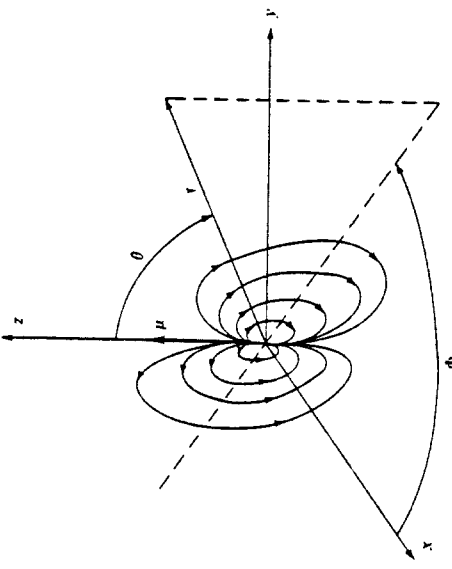


Figure 6.3 Sketch of streamlines in the  $xz$  plane ( $\Phi = \text{constant}$ ) for a three-dimensional doublet.

Hence, the flow induced by the three-dimensional doublet is a series of stream surfaces generated by revolving the streamlines in Fig. 6.3 about the  $z$  axis. Compare these streamlines with the two-dimensional case illustrated in Fig. 3.18; they are qualitatively similar but quantitatively different.

Note that the flow in Fig. 6.3 is independent of  $\Phi$ ; indeed, Eq. (6.10) clearly shows that the velocity field depends only on  $r$  and  $\theta$ . Such a flow is defined as **axisymmetric flow**. Once again we have a flow with two independent variables. For this reason, axisymmetric flow is sometimes labelled “two-dimensional” flow. However, it is quite different than the two-dimensional planar flows discussed earlier. In reality, axisymmetric flow is a degenerate three-dimensional flow, and it is somewhat misleading to refer to it as “two-dimensional.” Mathematically, it has only two independent variables, but it exhibits some of the same physical characteristics as general three-dimensional flows, such as the three-dimensional relieving effect to be discussed later.

#### 6.4 FLOW OVER A SPHERE

Consider again the flow induced by the three-dimensional doublet illustrated in Fig. 6.3. Superimpose on this flow a uniform velocity field of magnitude  $V_\infty$  in the negative  $z$  direction. Since we are more comfortable visualizing a free stream which moves horizontally, say from left to right, let us flip the coordinate system in Fig. 6.3 on its side. The picture shown in Fig. 6.4 results.

Examining Fig. 6.4, the spherical coordinates of the free stream are

$$V_r = -V_\infty \cos \theta \quad (6.11a)$$

$$V_\theta = V_\infty \sin \theta \quad (6.11b)$$

$$V_\phi = 0 \quad (6.11c)$$

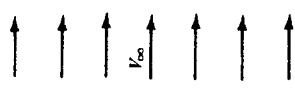


Figure 6.4 The superposition of a uniform flow and a three-dimensional doublet.

Adding  $V_r$ ,  $V_\theta$ , and  $V_\phi$  for the free stream, Eqs. (6.11a to c), to the representative components for the doublet given in Eq. (6.10), we obtain, for the combined flow,

$$V_r = -V_\infty \cos \theta + \frac{\mu}{2\pi} \frac{\cos \theta}{r^3} = -\left(V_\infty - \frac{\mu}{2\pi r^3}\right) \cos \theta \quad (6.12)$$

$$V_\theta = V_\infty \sin \theta + \frac{\mu}{4\pi} \frac{\sin \theta}{r^3} = \left(V_\infty + \frac{\mu}{4\pi r^3}\right) \sin \theta \quad (6.13)$$

$$V_\phi = 0 \quad (6.14)$$

To find the stagnation points in the flow, set  $V_r = V_\theta = 0$  in Eqs. (6.12) and (6.13). From Eq. (6.13),  $V_\theta = 0$  gives  $\sin \theta = 0$ ; hence, the stagnation points are located at  $\theta = 0$  and  $\pi$ . From Eq. (6.12), with  $V_r = 0$  we obtain

$$V_\infty - \frac{\mu}{2\pi R^3} = 0 \quad (6.15)$$

where  $r = R$  is the radial coordinate of the stagnation points. Solving Eq. (6.15) for  $R$ , we obtain

$$R = \left(\frac{\mu}{2\pi V_\infty}\right)^{1/3} \quad (6.16)$$

Hence, there are two stagnation points, both on the  $z$  axis, with  $(r, \theta)$  coordinates  $\left[\left(\frac{\mu}{2\pi V_\infty}\right)^{1/3}, 0\right]$  and  $\left[\left(\frac{\mu}{2\pi V_\infty}\right)^{1/3}, \pi\right]$

Insert the value of  $r = R$  from Eq. (6.16) into the expression for  $V_r$  given by Eq. (6.12). We obtain

$$V_r = -\left(V_\infty - \frac{\mu}{2\pi R^3}\right) \cos \theta = -\left[V_\infty - \frac{\mu}{2\pi} \left(\frac{2\pi V_\infty}{\mu}\right)\right] \cos \theta$$

$$= -(V_\infty - V_\infty) \cos \theta = 0$$

Thus,  $V_r = 0$  when  $r = R$  for all values of  $\theta$  and  $\Phi$ . This is precisely the flow-tangency condition for flow over a sphere of radius  $R$ . Hence, the velocity field given by Eqs. (6.12) to (6.14) is the incompressible flow over a sphere of radius  $R$ . This flow is shown in Fig. 6.5; it is qualitatively similar to the flow over the cylinder shown in Fig. 3.19, but quantitatively the two flows are different.

On the surface of the sphere, where  $r = R$ , the tangential velocity is obtained from Eq. (6.13) as follows:

$$V_\theta = \left( V_\infty + \frac{\mu}{4\pi R^3} \right) \sin \theta \quad (6.17)$$

From Eq. (6.16),

$$\mu = 2\pi R^3 V_\infty \quad (6.18)$$

Substituting Eq. (6.18) into (6.17), we have

$$V_\theta = \left( V_\infty + \frac{1}{4\pi} \frac{2\pi R^3 V_\infty}{R^3} \right) \sin \theta$$

$$V_\theta = \frac{1}{2} V_\infty \sin \theta \quad (6.19)$$

The maximum velocity occurs at the top and bottom points of the sphere, and its magnitude is  $\frac{1}{2} V_\infty$ . Compare these results with the two-dimensional circular cylinder case given by Eq. (3.100). For the two-dimensional flow, the maximum velocity is  $2V_\infty$ . Hence, for the same  $V_\infty$ , the maximum surface velocity on a sphere is less than that for a cylinder. The flow over a sphere is somewhat "relieved" in comparison with the flow over a cylinder. The flow over a sphere has an extra dimension in which to move out of the way of the solid body; the flow can move sideways as well as up and down. In contrast, the flow over a cylinder is more constrained; it can only move up and down. Hence, the maximum velocity on a sphere is less than that on a cylinder. This is an example of the three-dimensional relieving effect, which is a general phenomenon for all types of three-dimensional flows.

The pressure distribution on the surface of the sphere is given by Eqs. (3.38) and (6.19) as follows:

$$C_p = 1 - \left( \frac{V}{V_\infty} \right)^2 = 1 - \left( \frac{3}{2} \sin \theta \right)^2$$

$$C_p = 1 - \frac{9}{4} \sin^2 \theta \quad (6.20)$$

or

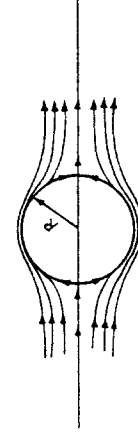


Figure 6.5 Schematic of the incompressible flow over a sphere.

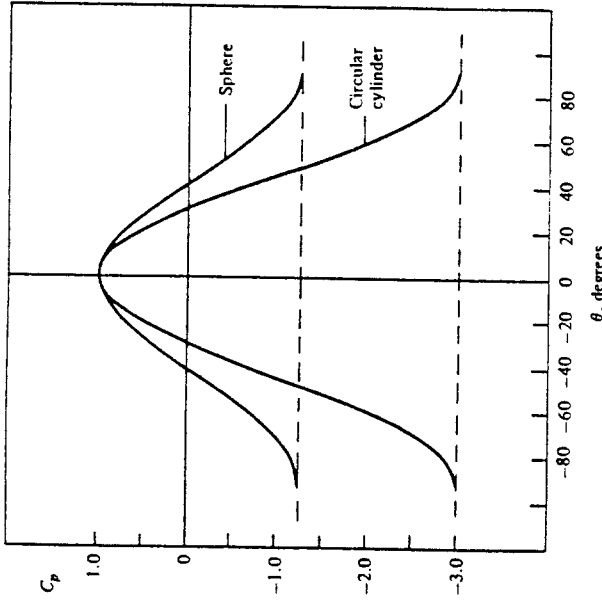


Figure 6.6 The pressure distribution over the surface of a sphere and a cylinder. Illustration of the three-dimensional relieving effect.

Compare Eq. (6.20) with the analogous result for a circular cylinder given by Eq. (3.101). Note that the absolute magnitude of the pressure coefficient on a sphere is less than that for a cylinder — again an example of the three-dimensional relieving effect. The pressure distributions over a sphere and a cylinder are compared in Fig. 6.6, which dramatically illustrates the three-dimensional relieving effect.

## 6.5 GENERAL THREE-DIMENSIONAL FLOWS: PANEL TECHNIQUES

In modern aerodynamic applications, three-dimensional, inviscid, incompressible flows are almost always calculated by means of numerical panel techniques. The philosophy of the two-dimensional panel methods discussed in previous chapters is readily extended to three dimensions. The details are beyond the scope of this book — indeed, there are dozens of different variations, and the resulting computer programs are frequently long and sophisticated. However, the general idea behind all such panel programs is to cover the three-dimensional body with panels over which there is an unknown distribution of singularities (such as point sources, doublets, or vortices). Such paneling is illustrated in Fig. 6.7. These unknowns are solved through a system of simultaneous linear algebraic equations generated by calculating the induced velocity at control points on the panels and applying the flow-tangency condition. For a non-

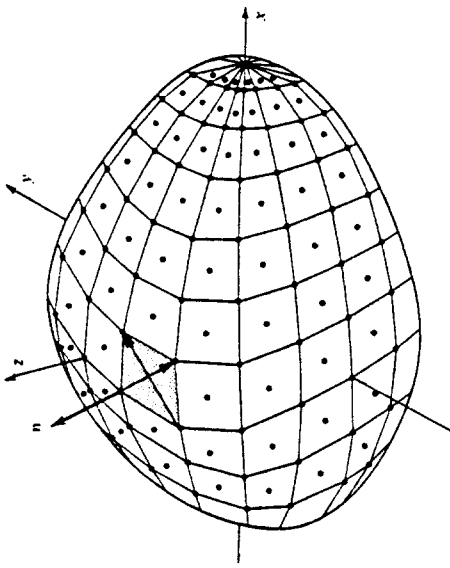


Figure 6.7 Distribution of three-dimensional source panels over a general nonlifting body (Ref. 14).  
(Courtesy of the McDonnell Douglas Corp.)

lifting body such as illustrated in Fig. 6.7, a distribution of source panels is sufficient. However, for a lifting body, both source and vortex panels (or their equivalent) are necessary. A striking example of the extent to which panel methods are now used for three-dimensional lifting bodies is shown in Fig. 6.8, which illustrates the paneling used for calculations made by the Boeing Company of the potential flow over a Boeing 747-space shuttle piggyback combination. Such applications are very impressive; moreover, they have become an industry standard and are today used routinely as part of the airplane design process by the major aircraft companies.

Examining Figs. 6.7 and 6.8, one aspect stands out, namely, the geometric complexity of distributing panels over the three-dimensional bodies. How do you get the computer to "see" the precise shape of the body? How do you distribute the panels over the body, i.e., do you put more at the wing leading edges and less on the fuselage, etc.? How many panels do you use? These are all nontrivial questions. It is not unusual for an aerodynamicist to spend weeks or even a few months determining the best geometric distribution of panels over a complex body.

We end this chapter on the following note. From the time they were introduced in the 1960s, panel techniques have revolutionized the calculation of three-dimensional potential flows. However, no matter how complex the application of these methods may be, the techniques are still based on the fundamentals we have discussed in this and all the preceding chapters. You are encouraged to pursue these matters further by reading the literature, particularly as it appears in such journals as the *Journal of Aircraft* and the *AAIA Journal*.

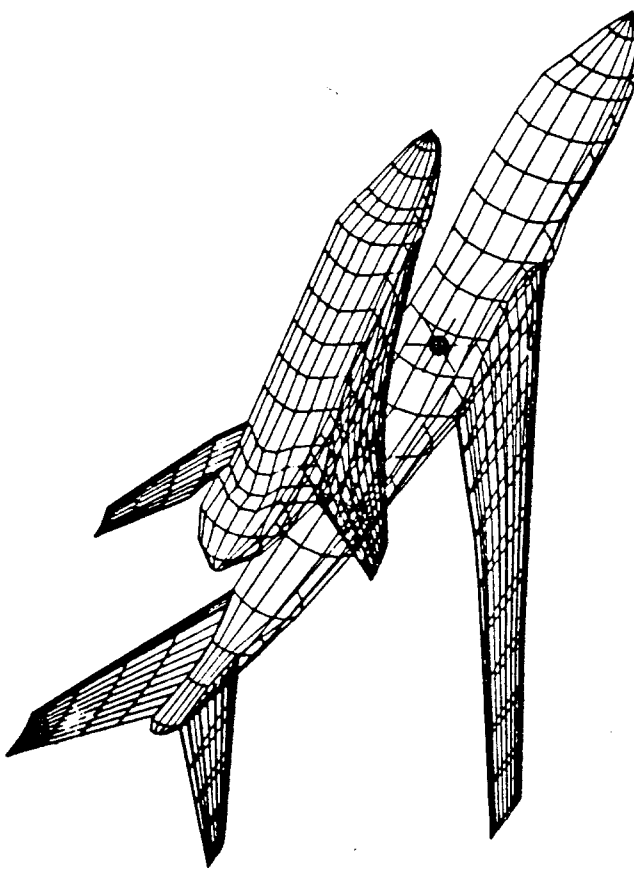


Figure 6.8 Panel distribution for the analysis of the Boeing 747 carrying the space shuttle orbiter (Courtesy of the Boeing Airplane Company.)

## 6.6 SUMMARY

For a three-dimensional (point) source,

$$V_r = \frac{\lambda}{4\pi r^2} \quad (6.6)$$

$$\phi = -\frac{\lambda}{4\pi r} \quad \text{and} \quad (6.7)$$

For a three-dimensional doublet,

$$\phi = -\frac{\mu}{4\pi} \frac{\cos \theta}{r^2} \quad (6.9)$$

$$\mathbf{V} = \frac{\mu}{2\pi} \frac{\cos \theta}{r^3} \mathbf{e}_r + \frac{\mu}{4\pi} \frac{\sin \theta}{r^3} \mathbf{e}_\theta \quad (6.10)$$

The flow over a sphere is generated by superimposing a three-dimensional doublet and a uniform flow. The resulting surface velocity and pressure distributions are given by

$$V_\theta = \frac{1}{2} V_\infty \sin \theta \quad (6.19)$$

$$C_p = 1 - \frac{1}{4} \sin^2 \theta \quad (6.20)$$

In comparison with flow over a cylinder, the surface velocity and magnitude of the pressure coefficient are smaller for the sphere—an example of the three-dimensional relieving effect.

In modern aerodynamic applications, inviscid, incompressible flows over complex three-dimensional bodies are usually computed via three-dimensional panel techniques.

### PROBLEMS

- 6.1 Prove that three-dimensional source flow is irrotational.
- 6.2 Prove that three-dimensional source flow is a physically possible incompressible flow.
- 6.3 A sphere and a circular cylinder (with its axis perpendicular to the flow) are mounted in the same freestream. A pressure tap exists at the top of the sphere, and this is connected via a tube to one side of a manometer. The other side of the manometer is connected to a pressure tap on the surface of the cylinder. This tap is located on the cylindrical surface such that no deflection of the manometer fluid takes place. Calculate the location of this tap.

*With the realization of aeroplane and missile speeds equal to or even surpassing many times the speed of sound, thermodynamics has entered the scene and will never again leave our considerations.*

*Jakob Ackeret, 1962*

### 7.1 INTRODUCTION

On September 30, 1935, the leading aerodynamicists from all corners of the world converged on Rome, Italy. Some of them arrived in airplanes which, in those days, lumbered along at speeds of 130 mi/h. Ironically, these people were gathering to discuss airplane aerodynamics not at 130 mi/h but rather at the unbelievable speeds of 500 mi/h and faster. By invitation only, such aerodynamic giants as Theodore von Kármán and Eastman Jacobs from the United States, Ludwig Prandtl and Adolf Busemann from Germany, Jakob Ackeret from Switzerland, G. I. Taylor from England, Arturo Crocco and Enrico Pistoletti from Italy, and others assembled for the fifth Volta Conference, which had as its topic "High Velocities in Aviation." Although the jet engine had not yet been developed, these men were convinced that the future of aviation was "faster and higher." At that time, some aeronautical engineers felt that airplanes would never fly faster than the speed of sound—the myth of the "sound barrier" was propagating through the ranks of aviation. However, the people who attended the fifth Volta Conference knew better. For 6 days, inside an impressive Renaissance building that served as the city hall during the Holy Roman Empire, these individuals presented papers that discussed flight at high subsonic, supersonic, and even hypersonic speeds. Among these presentations was the first public revelation of the concept of a swept wing for high-speed flight. Adolf Busemann, who originated the concept, discussed the technical reasons why swept wings would have less drag at high speeds than conventional straight wings. (One year later, the swept wing concept was

classified by the German Luftwaffe as a military secret. The Germans went on to produce a large bulk of swept-wing research during World War II, resulting in the design of the first operational jet airplane—the Me 262—which had a moderate degree of sweep.) Many of the discussions at the Volta Conference centered on the effects of “compressibility” at high subsonic speeds, i.e., the effects of variable density, because this was clearly going to be the first problem to be encountered by future high-speed airplanes. For example, Eastman Jacobs presented wind-tunnel test results for compressibility effects on standard NACA four- and five-digit airfoils at high subsonic speeds and noted extraordinarily large increases in drag beyond certain freestream Mach numbers. In regard to supersonic flows, Ludwig Prandtl presented a series of photographs showing shock waves inside nozzles and on various bodies—with some of the photographs dating as far back as 1907, when Prandtl started serious work in supersonic aerodynamics. (Clearly, Ludwig Prandtl was busy with much more than just the development of his incompressible airfoil and finite-wing theory discussed in Chaps. 4 and 5.) Jakob Ackeret gave a paper on the design of supersonic wind tunnels, which, under his direction, were being established in Italy, Switzerland, and Germany. There were also presentations on propulsion techniques for high-speed flight, including rockets and ramjets. The atmosphere surrounding the participants in the Volta Conference was exciting and heady; the conference launched the world aerodynamic community into the area of high-speed subsonic and supersonic flight—an area which today is as commonplace as the 130-mi/h flight speeds of 1935. Indeed, the purpose of the next eight chapters of this book is to present the fundamentals of such high-speed flight.

In contrast to the low-speed, incompressible flows discussed in Chaps. 3 to 6, the pivotal aspect of high-speed flow is that the density is a variable. Such flows are called *compressible flows* and are the subject of Chaps. 7 to 14. Return to Fig. 1.27, which gives a block diagram categorizing types of aerodynamic flows. In Chaps. 7 to 14, we discuss flows which fall into blocks *D* and *F*; i.e., we will deal with *inviscid compressible flow*. In the process we touch all the flow regimes itemized in blocks *G* through *J*. These flow regimes are illustrated in Fig. 1.26; study Figs. 1.26 and 1.27 carefully, and review the surrounding discussion in Sec. 1.10 before proceeding further.

In addition to variable density, another pivotal aspect of high-speed compressible flow is *energy*. A high-speed flow is a high-energy flow. For example, consider the flow of air at standard sea level conditions moving at twice the speed of sound. The internal energy of 1 kg of this air is  $2.07 \times 10^5 \text{ J}$ , whereas the kinetic energy is larger, namely  $2.31 \times 10^5 \text{ J}$ . When the flow velocity is decreased, some of this kinetic energy is lost and reappears as an increase in internal energy, hence increasing the temperature of the gas. Therefore, in a high-speed flow, energy transformations and temperature changes are important considerations. Such considerations come under the science of *thermodynamics*. For this reason, thermodynamics is a vital ingredient in the study of compressible flow. One purpose of the present chapter is to briefly review the particular aspects of thermodynamics which are essential to our subsequent discussions of compressible flow.

The road map for this chapter is given in Fig. 7.1. As our discussion proceeds, refer to this road map in order to provide an orientation for our ideas.

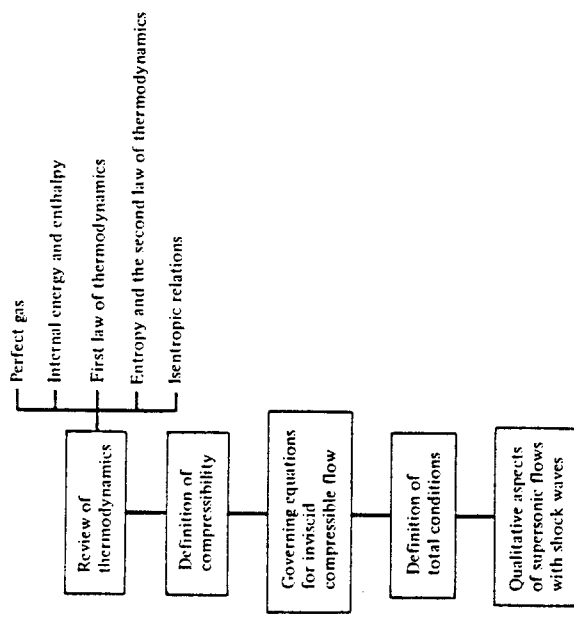


Figure 7.1 Road map for Chap. 7.

## 7.2 A BRIEF REVIEW OF THERMODYNAMICS

The importance of thermodynamics in the analysis and understanding of compressible flow was underscored in Sec. 7.1. Hence, the purpose of the present section is to review those aspects of thermodynamics which are important to compressible flows. This is in no way intended to be an exhaustive discussion of thermodynamics; rather, it is a review of only those fundamental ideas and equations which will be of direct use in subsequent chapters. If you have studied thermodynamics, this review should serve as a ready reminder of some important relations. If you are not familiar with thermodynamics, this section is somewhat self-contained so as to give you a feeling for the fundamental ideas and equations which we use frequently in subsequent chapters.

### Perfect Gas

As described in Sec. 1.2, a gas is a collection of particles (molecules, atoms, ions, electrons, etc.) which are in more or less random motion. Due to the electronic structure of these particles, a force field pervades the space around them. The force field due to one particle reaches out and interacts with neighboring particles, and vice versa. Hence, these fields are called *intermolecular forces*. However, if the particles of the gas are far enough apart, the influence of the intermolecular forces is small and can be neglected. A gas in which the intermolecular forces are neglected is defined as a *perfect gas*. For a perfect gas,  $p$ ,  $\rho$ , and  $T$  are related through the following *equation of state*.

$$p = \rho RT \quad (7.1)$$

where  $R$  is the specific gas constant, which is a different value for different gases. For air at standard conditions,  $R = 287 \text{ J/(kg} \cdot \text{K)} = 1716 \text{ (ft} \cdot \text{lb})/\text{slug} \cdot ^\circ\text{R}$ .

At the temperatures and pressures characteristic of many compressible flow applications, the gas particles are, on the average, more than 10 molecular diameters apart; this is far enough to justify the assumption of a perfect gas. Therefore, throughout the remainder of this book, we use the equation of state in the form of Eq. (7.1), or its counterpart,

$$pv = RT \quad (7.2)$$

where  $v$  is the specific volume, i.e., the volume per unit mass;  $v = 1/\rho$ . (*Please note:* Starting with this chapter, we use the symbol  $v$  to denote both specific volume and the  $y$  component of velocity. This usage is standard, and in all cases it should be obvious and cause no confusion.)

### Internal Energy and Enthalpy

Consider an individual molecule of a gas, say an  $\text{O}_2$  molecule in air. This molecule is moving through space in a random fashion, occasionally colliding with a neighboring molecule. Because of its velocity through space, the molecule has translational kinetic energy. In addition, the molecule is made up of individual atoms which we can visualize as connected to each other along various axes; for example, we can visualize the  $\text{O}_2$  molecule as a "dumbbell" shape, with an O atom at each end of a connecting axis. In addition to its translational motion, such a molecule can execute a rotational motion in space; the kinetic energy of this rotation contributes to the net energy of the molecule.

Also, the atoms of a given molecule can vibrate back and forth along and across the molecular axis, thus contributing a potential and kinetic energy of vibration to the molecule. Finally, the motion of the electrons around each of the nuclei of the molecule contributes an "electronic" energy to the molecule. Hence, the energy of a given molecule is the sum of its translational, rotational, vibrational, and electronic energies.

Now consider a finite volume of gas consisting of a large number of molecules. The sum of the energies of all the molecules in this volume is defined as the *internal energy* of the gas. The internal energy per unit mass of gas is defined as the specific internal energy, denoted by  $e$ . A related quantity is the specific enthalpy, denoted by  $h$  and defined as

$$h = e + pv \quad (7.3)$$

For a perfect gas, both  $e$  and  $h$  are functions of temperature only.

$$e = e(T) \quad (7.4a)$$

$$h = h(T) \quad (7.4b)$$

Let  $de$  and  $dh$  represent differentials of  $e$  and  $h$ , respectively. Then, for a perfect gas,

$$de = c_v dT \quad (7.5a)$$

$$dh = c_p dT \quad (7.5b)$$

where  $c_v$  and  $c_p$  are the specific heats at constant volume and constant pressure, respectively. In Eqs. (7.5a and b)  $c_v$  and  $c_p$  can themselves be functions of  $T$ . However, for moderate temperatures (for air, for  $T < 1000 \text{ K}$ ), the specific heats are reasonably constant. A perfect gas where  $c_v$  and  $c_p$  are constants is defined as a *calorically perfect gas*, for which Eqs. (7.5a and b) become

$$e = c_v T \quad (7.6a)$$

$$h = c_p T \quad (7.6b)$$

For a large number of practical compressible flow problems, the temperatures are moderate; for this reason, in this book we always treat the gas as calorically perfect; i.e., we assume that the specific heats are constant. For a discussion of compressible flow problems where the specific heats are not constant (such as the high-temperature chemically reacting flow over a high-speed atmospheric entry vehicle, i.e., the space shuttle), see Ref. 21.

Note that  $e$  and  $h$  in Eqs. (7.3) through (7.6) are thermodynamic state variables— they depend only on the state of the gas and are independent of any process. Although  $c_v$  and  $c_p$  appear in these equations, there is no restriction to just a constant volume or a constant pressure process. Rather, Eqs. (7.5a and b) and (7.6a and b) are relations for thermodynamic state variables, namely,  $e$  and  $h$  as functions of  $T$ , and have nothing to do with the process that may be taking place.

For a specific gas,  $c_p$  and  $c_v$  are related through the equation

$$c_p - c_v = R \quad (7.7)$$

Dividing Eq. (7.7) by  $c_p$ , we obtain

$$1 - \frac{c_v}{c_p} = \frac{R}{c_p} \quad (7.8)$$

Define  $\gamma \equiv c_p/c_v$ . For air at standard conditions,  $\gamma = 1.4$ . Then Eq. (7.8) becomes

$$1 - \frac{1}{\gamma} = \frac{R}{c_p} \quad (7.9)$$

or

$$c_p = \frac{\gamma R}{\gamma - 1} \quad (7.3)$$

Similarly, dividing Eq. (7.7) by  $c_v$ , we obtain

$$c_v = \frac{R}{\gamma - 1} \quad (7.10)$$

Equations (7.9) and (7.10) are particularly useful in our subsequent discussion of compressible flow.

### First Law of Thermodynamics

Consider a fixed mass of gas, which we define as the *system*. (For simplicity, assume a unit mass, e.g., 1 kg or 1 slug.) The region outside the system is called the *surroundings*. The interface between the system and its surroundings is called the *boundary*, as shown in Fig. 7.2. Assume that the system is stationary. Let  $\delta q$  be an incremental amount of heat added to the system across the boundary, as sketched in Fig. 7.2. Examples of the source of  $\delta q$  are radiation from the surroundings which is absorbed by the mass in the system and thermal conduction due to temperature gradients across the boundary. Also, let  $\delta w$  denote the work done on the system by the surroundings (say, by a displacement of the boundary, squeezing the volume of the system to a smaller value). As discussed earlier, due to the molecular motion of the gas, the system has an internal energy  $e$ . The heat added and work done on the system cause a change in energy, and since the system is stationary, this change in energy is simply  $de$ :

$$\boxed{\delta q + \delta w = de} \quad (7.11)$$

This is the *first law of thermodynamics*: it is an empirical result confirmed by experience. In Eq. (7.11),  $e$  is a state variable. Hence,  $de$  is an exact differential, and its value depends only on the initial and final states of the system. In contrast,  $\delta q$  and  $\delta w$  depend on the process in going from the initial to the final states.

For a given  $de$ , there are in general an infinite number of different ways (processes) by which heat can be added and work done on the system. We are primarily concerned with three types of processes:

1. *Adiabatic process*. One in which no heat is added to or taken away from the system
2. *Reversible process*. One in which no dissipative phenomena occur, i.e., where the effects of viscosity, thermal conductivity, and mass diffusion are absent
3. *Isentropic process*. One which is both adiabatic and reversible

For a reversible process, it can be easily shown that  $\delta w = -p dv$ , where  $dv$  is an incremental change in the volume due to a displacement of the boundary of the system. Thus, Eq. (7.11) becomes

$$\delta q - p dv = de \quad (7.12)$$

### Entropy and the Second Law of Thermodynamics

Consider a block of ice in contact with a red-hot plate of steel. Experience tells us that the ice will warm up (and probably melt) and the steel plate will cool down. However, Eq. (7.11) does not necessarily say this will happen. Indeed, the first law allows that the ice may get cooler and the steel plate hotter — just as long as energy is conserved during the process. Obviously, in real life this does not happen; instead nature imposes another condition on the process, a condition which tells us *which direction* a process will take. To ascertain the proper direction of a process, let us define a new state variable, the entropy, as follows:

$$ds = \frac{\delta q_{rev}}{T} \quad (7.13)$$

where  $s$  is the entropy of the system,  $\delta q_{rev}$  is an incremental amount of heat added reversibly to the system, and  $T$  is the system temperature. Do not be confused by the above definition. It defines a change in entropy in terms of a reversible addition of heat,  $\delta q_{rev}$ . However, entropy is a state variable, and it can be used in conjunction with any type of process, reversible or irreversible. The quantity  $\delta q_{rev}$  in Eq. (7.13) is just an artifice; an effective value of  $\delta q_{rev}$  can always be assigned to relate the initial and end points of an irreversible process, where the actual amount of heat added is  $\delta q$ . Indeed an alternative and probably more lucid relation is

$$\boxed{ds = \frac{\delta q}{T} + ds_{irrev}} \quad (7.14)$$

In Eq. (7.14),  $\delta q$  is the actual amount of heat added to the system during an actual irreversible process, and  $ds_{irrev}$  is the generation of entropy due to the irreversible, dissipative phenomena of viscosity, thermal conductivity, and mass diffusion occurring *within* the system. These dissipative phenomena always increase the entropy:

$$\boxed{ds_{irrev} \geq 0} \quad (7.15)$$

In Eq. (7.15), the equals sign denotes a reversible process, where by definition no dissipative phenomena occur within the system. Combining Eqs. (7.14) and (7.15), we have

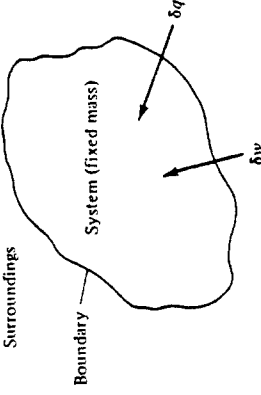


Figure 7.2 Thermodynamic system.

$$ds \geq \frac{\delta q}{T} \quad (7.16)$$

Furthermore, if the process is adiabatic,  $\delta q = 0$ , and Eq. (7.16) becomes

$$ds \geq 0 \quad (7.17)$$

Equations (7.16) and (7.17) are forms of the *second law of thermodynamics*. The second law tells us in what direction a process will take place. A process will proceed in a direction such that the entropy of the system plus that of its surroundings always increases or, at best, stays the same. In our example of the ice in contact with hot steel, consider the system to be both the ice and steel plate combined. The simultaneous heating of the ice and cooling of the plate yield a net increase in entropy for the system. On the other hand, the impossible situation of the ice getting cooler and the plate hotter would yield a net decrease in entropy, a situation forbidden by the second law. In summary, the concept of entropy in combination with the second law allows us to predict the *direction* that nature takes.

The practical calculation of entropy is carried out as follows. In Eq. (7.12), assume that heat is added reversibly, then the definition of entropy, Eq. (7.13), substituted in Eq. (7.12) yields

$$Td\sigma - p dv = de \quad (7.18)$$

or

$$Td\sigma = de + p dv \quad (7.19)$$

From the definition of enthalpy, Eq. (7.3), we have

$$dh = de + p dv + v dp \quad (7.20)$$

Combining Eqs. (7.18) and (7.19), we obtain

$$Td\sigma = dh - v dp \quad (7.21)$$

Equations (7.18) and (7.20) are important; they are essentially alternate forms of the first law expressed in terms of entropy. For a perfect gas, recall Eqs. (7.5a and b), namely,  $de = c_p dT$  and  $dh = c_p dT$ . Substituting these relations into Eqs. (7.18) and (7.20), we obtain

$$ds = c_p \frac{dT}{T} + \frac{p dv}{T} \quad (7.22)$$

and

$$ds = c_p \frac{dT}{T} - \frac{v dp}{T} \quad (7.23)$$

Working with Eq. (7.22), substitute the equation of state  $p v = RT$ , or  $v/T = R/p$ , into the last term.

$$ds = c_p \frac{dT}{T} - R \frac{dp}{p} \quad (7.24)$$

Consider a thermodynamic process with initial and end states denoted by 1 and 2, respectively. Equation (7.23), integrated between states 1 and 2, becomes

$$s_2 - s_1 = \int_{T_1}^{T_2} c_p \frac{dT}{T} - R \int_{p_1}^{p_2} \frac{dp}{p} \quad (7.25)$$

For a calorically perfect gas, both  $R$  and  $c_p$  are constants; hence, Eq. (7.24) becomes

$$s_2 - s_1 = c_p \ln \frac{T_2}{T_1} - R \ln \frac{p_2}{p_1} \quad (7.26)$$

In a similar fashion, Eq. (7.21) leads to

$$s_2 - s_1 = c_v \ln \frac{T_2}{T_1} + R \ln \frac{v_2}{v_1} \quad (7.27)$$

Equations (7.25) and (7.26) are practical expressions for the calculation of the entropy change of a calorically perfect gas between two states. Note from these equations that  $s$  is a function of two thermodynamic variables, for example  $s = s(p, T)$ ,  $s = s(v, T)$ .

### Isentropic Relations

We have defined an isentropic process as one which is both adiabatic and reversible. Consider Eq. (7.14). For an adiabatic process,  $\delta q = 0$ . Also, for a reversible process,  $ds_{rev} = 0$ . Thus, for an adiabatic, reversible process, Eq. (7.14) yields  $ds = 0$ , or entropy is constant; hence the word "isentropic." For such an isentropic process, Eq. (7.25) is written as

$$\begin{aligned} 0 &= c_p \ln \frac{T_2}{T_1} - R \ln \frac{p_2}{p_1} \\ \ln \frac{p_2}{p_1} &= \frac{c_p}{R} \ln \frac{T_2}{T_1} \\ \frac{p_2}{p_1} &= \left( \frac{T_2}{T_1} \right)^{c_p/R} \end{aligned} \quad (7.28)$$

However, from Eq. (7.9),

$$\frac{c_p}{R} = \frac{\gamma}{\gamma - 1}$$

and hence Eq. (7.27) is written as

$$\frac{p_2}{p_1} = \left( \frac{T_2}{T_1} \right)^{\gamma(\gamma-1)} \quad (7.28)$$

In a similar fashion, Eq. (7.26) written for an isentropic process gives

$$\begin{aligned} 0 &= c_v \ln \frac{T_2}{T_1} + R \ln \frac{v_2}{v_1} \\ \ln \frac{v_2}{v_1} &= -\frac{c_v}{R} \ln \frac{T_2}{T_1} \\ \frac{v_2}{v_1} &= \left( \frac{T_2}{T_1} \right)^{-c_v/R} \end{aligned} \quad (7.29)$$

From Eq. (7.10),

$$\frac{c_v}{R} = \frac{1}{\gamma - 1} \quad (7.30)$$

and hence Eq. (7.29) is written as

$$\frac{v_2}{v_1} = \left( \frac{T_2}{T_1} \right)^{-1/(\gamma-1)} \quad (7.31)$$

Since  $\rho_2/\rho_1 = v_1/v_2$ , Eq. (7.30) becomes

$$\frac{\rho_2}{\rho_1} = \left( \frac{T_2}{T_1} \right)^{1/(\gamma-1)} \quad (7.32)$$

Combining Eqs. (7.28) and (7.32), we can summarize the isentropic relations as

$$\boxed{\frac{p_2}{p_1} = \left( \frac{\rho_2}{\rho_1} \right)^\gamma = \left( \frac{T_2}{T_1} \right)^{\gamma(\gamma-1)}} \quad (7.33)$$

Equation (7.32) is very important; it relates pressure, density, and temperature for an isentropic process. We use this equation frequently, so make certain to brand it on your mind. Also, keep in mind the source of Eq. (7.32); it stems from the first law and the definition of entropy. Therefore, Eq. (7.32) is basically an energy relation for an isentropic process.

Why is Eq. (7.32) so important? Why is it frequently used? Why are we so interested in an isentropic process when it seems so restrictive — requiring both adiabatic and reversible conditions? The answers rest on the fact that a large number of practical compressible flow problems can be assumed to be isentropic — contrary to what you might initially think. For example, consider the flow over an airfoil or through a rocket engine. In the regions adjacent to the airfoil surface and the rocket nozzle walls, a boundary layer is formed wherein the dissipative mechanisms of viscosity, thermal conduction, and diffusion are strong. Hence, the entropy increases within these boundary layers. However, consider the fluid elements moving outside the boundary layer. Here, the dissipative effects of viscosity, etc., are very small and can be neglected.

Moreover, no heat is being transferred to or from the fluid element (i.e., we are not heating the fluid element with a Bunsen burner or cooling it in a refrigerator); thus, the flow outside the boundary layer is adiabatic. Consequently, the fluid elements outside the boundary layer are experiencing an adiabatic reversible process — namely, isentropic flow. In the vast majority of practical applications, the viscous boundary layer adjacent to the surface is thin compared with the entire flow field, and hence large regions of the flow can be assumed isentropic. This is why a study of isentropic flow is directly applicable to many types of practical compressible flow problems. In turn, Eq. (7.32) is a powerful relation for such flows, valid for a calorically perfect gas. This ends our brief review of thermodynamics. Its purpose has been to give a quick summary of ideas and equations which will be employed throughout our subsequent discussions of compressible flow. For a more thorough discussion of the power and beauty of thermodynamics, see any good thermodynamics text, such as Refs. 22 to 24.

**Example 7.1** Consider a Boeing 747 flying at a standard altitude of 36,000 ft. The pressure at a point on the wing is 400 lb/ft<sup>2</sup>. Assuming isentropic flow over the wing, calculate the temperature at this point.

**SOLUTION** At a standard altitude of 36,000 ft,  $p_\infty = 476 \text{ lb/ft}^2$  and  $T_\infty = 391^\circ\text{R}$ . From Eq. (7.32),

$$\begin{aligned} \frac{p}{p_\infty} &= \left( \frac{T}{T_\infty} \right)^{\gamma(\gamma-1)} \\ T &= T_\infty \left( \frac{p}{p_\infty} \right)^{(r-1)/r} = 391 \left( \frac{400}{476} \right)^{0.4114} = \boxed{372^\circ\text{R}} \end{aligned}$$

### 7.3 DEFINITION OF COMPRESSIBILITY

All real substances are compressible to some greater or lesser extent; i.e., when you squeeze or press on them, their density will change. This is particularly true of gases, much less so for liquids, and virtually unnoticeable for solids. The amount by which a substance can be compressed is given by a specific property of the substance called the **compressibility**, defined below.

Consider a small element of fluid of volume  $\mathbf{v}$ , as sketched in Fig. 7.3. The pressure exerted on the sides of the element is  $p$ . Assume the pressure is now increased by an infinitesimal amount,  $dp$ . The volume of the element will change by a corresponding amount,  $d\mathbf{v}$ ; here, the volume will decrease; hence,  $d\mathbf{v}$  shown in Fig. 7.3 is a negative quantity. By definition, the compressibility  $\tau$  of the fluid is

$$\tau = -\frac{1}{v} \frac{dv}{dp} \quad (7.33)$$

Physically, the compressibility is the fractional change in volume of the fluid element per unit change in pressure. However, Eq. (7.33) is not precise enough. We know from experience that when a gas is compressed (say, in a bicycle pump), its temperature

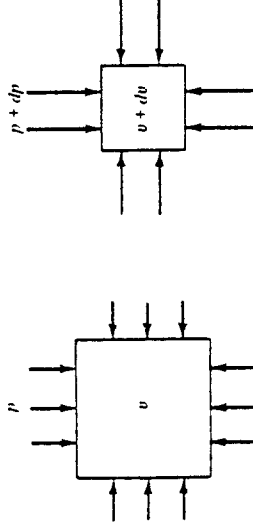


Figure 7.3 Definition of compressibility.

tends to increase, depending on the amount of heat transferred into or out of the gas through the boundaries of the system. If the temperature of the fluid element in Fig. 7.3 is held constant (due to some heat transfer mechanism), then  $\tau$  is identified as the *isothermal compressibility*  $\tau_T$ , defined from Eq. (7.33) as

$$\tau_T = -\frac{1}{v} \left( \frac{\partial v}{\partial p} \right)_T \quad (7.34)$$

On the other hand, if no heat is added to or taken away from the fluid element, and if friction is ignored, the compression of the fluid element takes place isentropically, and  $\tau$  is identified as the *isentropic compressibility*  $\tau_s$ , defined from Eq. (7.33) as

$$\tau_s = -\frac{1}{v} \left( \frac{\partial v}{\partial p} \right)_s, \quad (7.35)$$

where the subscript  $s$  denotes that the partial derivative is taken at constant entropy. Both  $\tau_T$  and  $\tau_s$  are precise thermodynamic properties of the fluid; their values for different gases and liquids can be obtained from various handbooks of physical properties. In general, the compressibility of gases is several orders of magnitude larger than that of liquids.

The role of the compressibility  $\tau$  in determining the properties of a fluid in motion is seen as follows. Define  $v$  as the specific volume, i.e., the volume per unit mass. Hence,  $v = 1/\rho$ . Substituting this definition into Eq. (7.33), we obtain

$$\tau = \frac{1}{\rho} \frac{dp}{dp} \quad (7.36)$$

Thus, whenever the fluid experiences a change in pressure,  $dp$ , the corresponding change in density,  $d\rho$ , from Eq. (7.36) is

$$d\rho = \rho \tau dp \quad (7.37)$$

Consider a fluid flow, say, for example, the flow over an airfoil. If the fluid is a liquid, where the compressibility  $\tau$  is very small, then for a given pressure change  $dp$  from one point to another in the flow, Eq. (7.37) states that  $d\rho$  will be negligibly small. In turn, we can reasonably assume that  $\rho$  is constant and that the flow of a liquid is incompressible. On the other hand, if the fluid is a gas, where the compressibility  $\tau$  is large, then for a given pressure change  $dp$  from one point to another in the flow, Eq. (7.37) indicates that  $d\rho$  can be large. Thus,  $\rho$  is *not* constant, and in general, the flow of a gas

is a *compressible flow*. The exception to this is the *low-speed flow* of a gas; in such flows, the actual magnitude of the pressure changes throughout the flow field is small compared with the pressure itself. Thus, for a low-speed flow,  $dp$  in Eq. (7.37) is small, and even though  $\tau$  is large, the value of  $dp$  can be dominated by the small  $d\rho$ . In such cases,  $\rho$  can be assumed to be constant, hence allowing us to analyze low-speed gas flows as incompressible flows (such as discussed in Chaps. 3 to 6).

Later, we demonstrate that the most convenient index to gauge whether a gas flow can be considered incompressible, or whether it must be treated as compressible, is the Mach number  $M$ , defined in Chap. 1 as the ratio of local flow velocity  $V$  to the local speed of sound,  $a$ .

$$M \equiv \frac{V}{a} \quad (7.38)$$

We show that, when  $M > 0.3$ , the flow should be considered compressible. Also, we show that the speed of sound in a gas is related to the isentropic compressibility  $\tau_s$ , given by Eq. (7.35).

## 7.4 GOVERNING EQUATIONS FOR INVISCID, COMPRESSIBLE FLOW

In Chaps. 3 to 6, we studied inviscid, incompressible flow; recall that the primary dependent variables for such flows are  $p$  and  $\mathbf{V}$ , and hence we need only two basic equations, namely, the continuity and momentum equations, to solve for these two unknowns. Indeed, the basic equations are combined to obtain Laplace's equation and Bernoulli's equation, which are the primary tools used for the applications discussed in Chaps. 3 to 6. Note that both  $\rho$  and  $T$  are assumed to be constant throughout such inviscid, incompressible flows. As a result, no additional governing equations are required; in particular, there is no need for the energy equation or energy concepts in general. Basically, incompressible flow obeys purely mechanical laws and does not require thermodynamic considerations.

In contrast, for compressible flow,  $\rho$  is variable and becomes an unknown. Hence we need an additional governing equation—the energy equation—which in turn introduces internal energy  $e$  as an unknown. Since  $e$  is related to temperature, then  $T$  also becomes an important variable. Therefore, the primary dependent variables for the study of compressible flow are  $p$ ,  $\mathbf{V}$ ,  $\rho$ ,  $e$ , and  $T$ ; to solve for these five variables, we need five governing equations. Let us examine this situation further.

To begin with, the flow of a compressible fluid is governed by the basic equations derived in Chap. 2. At this point in our discussion, it is most important for you to be familiar with these equations as well as their derivation. Therefore, before proceeding further, return to Chap. 2 and carefully review the basic ideas and relations contained therein. This is a serious study tip, and if you follow it, the material in our next seven chapters will flow much easier for you. In particular, review the integral and differential forms of the continuity equation (Sec. 2.4), the momentum equation (Sec. 2.5), and the energy equation (Sec. 2.7); indeed, pay particular attention to the energy equation

because this is an important aspect which sets compressible flow apart from incompressible flow.

For convenience, some of the more important forms of the governing equations for an inviscid, compressible flow from Chap. 2 are repeated below:

*Continuity:* From Eq. (2.39),

$$\frac{\partial}{\partial t} \iiint_V \rho dV + \iint_S \rho \mathbf{V} \cdot d\mathbf{S} = 0 \quad (7.39)$$

From Eq. (2.43),

$$\frac{\partial \rho}{\partial t} + \nabla \cdot \rho \mathbf{V} = 0 \quad (7.40)$$

*Momentum:* From Eq. (2.55),

$$\frac{\partial}{\partial t} \iiint_V \rho \mathbf{V} dV + \iint_S (\rho \mathbf{V} \cdot d\mathbf{S}) \mathbf{V} = - \iint_S p d\mathbf{S} + \iint_V \rho \mathbf{f} dV \quad (7.41)$$

From Eqs. (2.104a to c),

$$\rho \frac{Du}{Dt} = - \frac{\partial p}{\partial x} + \rho f_x \quad (7.42a)$$

$$\rho \frac{Dv}{Dt} = - \frac{\partial p}{\partial y} + \rho f_y \quad (7.42b)$$

$$\rho \frac{Dw}{Dt} = - \frac{\partial p}{\partial z} + \rho f_z \quad (7.42c)$$

*Energy:* From Eq. (2.86),

$$\begin{aligned} \frac{\partial}{\partial t} \iiint_V \rho \left( e + \frac{V^2}{2} \right) dV + \iint_S \rho \left( e + \frac{V^2}{2} \right) \mathbf{V} \cdot d\mathbf{S} \\ = \iint_V \dot{q} \rho dV - \iint_S p \mathbf{V} \cdot d\mathbf{S} + \iint_V \rho (\mathbf{f} \cdot \mathbf{V}) dV \end{aligned} \quad (7.43)$$

From Eq. (2.105),

$$\rho \frac{D(e + V^2/2)}{Dt} = \rho \dot{q} - \nabla \cdot p \mathbf{V} + \rho (\mathbf{f} \cdot \mathbf{V}) \quad (7.44)$$

The above continuity, momentum, and energy equations are three equations in terms of the five unknowns  $p$ ,  $\mathbf{V}$ ,  $\rho$ ,  $T$ , and  $e$ . Assuming a calorically perfect gas, the additional two equations needed to complete the system are obtained from Sec. 7.2:

*Equation of state:*

$$\begin{aligned} p &= \rho R T \\ e &= c_v T \end{aligned} \quad (7.6a)$$

*Internal energy:*

$$\frac{D(e + V^2/2)}{Dt} = - \nabla \cdot p \mathbf{V} \quad (7.45)$$

In regard to the basic equations for compressible flow, please note that Bernoulli's equation as derived in Sec. 3.2 and given by Eq. (3.13) does *not* hold for compressible flow; it clearly contains the assumption of constant density and, hence, is invalid for compressible flow. This warning is necessary because experience shows that a certain number of students of aerodynamics, apparently attracted by the simplicity of Bernoulli's equation, attempt to use it for all situations, compressible as well as incompressible. Do not do it! Always remember that Bernoulli's equation in the form of Eq. (3.13) holds for incompressible flow only, and we must dismiss it from our thinking when dealing with compressible flow.

As a final note, we use both the integral and differential forms of the above equations in our subsequent discussions. Make certain that you feel comfortable with these equations before proceeding further.

## 7.5 DEFINITION OF TOTAL (STAGNATION) CONDITIONS

At the beginning of Sec. 3.4, the concept of static pressure  $p$  was discussed in some detail. Static pressure is a measure of the purely random motion of molecules in a gas; it is the pressure you feel when you ride along with the gas at the local flow velocity. In contrast, the total (or stagnation) pressure was defined in Sec. 3.4 as the pressure existing at a point (or points) in the flow where  $\mathbf{V} = 0$ . Let us now define the concept of total conditions more precisely.

Consider a fluid element passing through a given point in a flow where the local pressure, temperature, density, Mach number, and velocity are  $p$ ,  $T$ ,  $\rho$ ,  $M$ , and  $\mathbf{V}$ , respectively. Here,  $p$ ,  $T$ , and  $\rho$  are static quantities, i.e., static pressure, static temperature, and static density, respectively; they are the pressure, temperature, and density you feel when you ride along with the gas at the local flow velocity. Now imagine that you grab hold of the fluid element and *adiabatically* slow it down to zero velocity. Clearly, you would expect (correctly) that the values of  $p$ ,  $T$ , and  $\rho$  would change as the fluid element is brought to rest. In particular, the value of the temperature of the fluid element after it has been brought to rest adiabatically is defined as the *total temperature*, denoted by  $T_0$ . The corresponding value of enthalpy is defined as the *total enthalpy*  $h_0$ , where  $h_0 = c_p T_0$  for a calorically perfect gas. Keep in mind that we do not have to *actually* bring the flow to rest in real life in order to talk about the total temperature or total enthalpy; rather, they are *defined quantities* that would exist at a point in a flow if (in our imagination) the fluid element passing through that point were brought to rest adiabatically. Therefore, at a given point in a flow, where the static temperature and enthalpy are  $T$  and  $h$ , respectively, we can also assign a value of total temperature  $T_0$  and a value of total enthalpy  $h_0$  defined as above.

The energy equation, Eq. (7.44), provides some important information about total enthalpy and hence total temperature, as follows. Assume that the flow is adiabatic ( $\dot{q} = 0$ ), and that body forces are negligible ( $\mathbf{f} = 0$ ). For such a flow, Eq. (7.44) becomes

$$\rho \frac{D(e + V^2/2)}{Dt} = \rho \dot{q} - \nabla \cdot p \mathbf{V} + \rho (\mathbf{f} \cdot \mathbf{V}) \quad (7.44)$$

Expand the right-hand side of Eq. (7.45) using the following vector identity:

$$\nabla \cdot p \mathbf{V} \equiv p \nabla \cdot \mathbf{V} + \mathbf{V} \cdot \nabla p \quad (7.46)$$

Also, note that the substantial derivative defined in Sec. 2.9 follows the normal laws of differentiation; for example,

$$\rho \frac{D(p/\rho)}{Dt} = \rho \frac{p Dp/Dt - p D\rho/Dt}{\rho^2} = \frac{Dp}{Dt} - \frac{p}{\rho} \frac{D\rho}{Dt} \quad (7.47)$$

Recall the form of the continuity equation given by Eq. (2.99):

$$\frac{D\rho}{Dt} + \rho \nabla \cdot \mathbf{V} = 0 \quad (2.99)$$

Substituting Eq. (2.99) into (7.47), we obtain

$$\rho \frac{D(p/\rho)}{Dt} = \frac{Dp}{Dt} + p \nabla \cdot \mathbf{V} = \frac{\partial p}{\partial t} + \mathbf{V} \cdot \nabla p + p \nabla \cdot \mathbf{V} \quad (7.48)$$

Substituting Eq. (7.46) into (7.45), and adding Eq. (7.48) to the result, we obtain

$$\frac{D}{Dt} \left( e + \frac{p}{\rho} + \frac{V^2}{2} \right) = -p \nabla \cdot \mathbf{V} - \mathbf{V} \cdot \nabla p + \frac{\partial p}{\partial t} + \mathbf{V} \cdot \nabla p + p \nabla \cdot \mathbf{V} \quad (7.49)$$

Note that

$$e + \frac{p}{\rho} = e + p \mathbf{v} \equiv h \quad (7.50)$$

Substituting Eq. (7.50) into (7.49), and noting that some of the terms on the right-hand side of Eq. (7.49) cancel each other, we have

$$\frac{D(h + V^2/2)}{Dt} = \frac{\partial p}{\partial t} \quad (7.51)$$

If the flow is steady,  $\partial p/\partial t = 0$ , and Eq. (7.51) becomes

$$\rho \frac{D(h + V^2/2)}{Dt} = 0 \quad (7.52)$$

From the definition of the substantial derivative given in Sec. 2.9, Eq. (7.52) states that the time rate of change of  $h + V^2/2$  following a moving fluid element is zero; that is,

$$h + \frac{V^2}{2} = \text{const} \quad (7.53)$$

along a streamline. Recall that the assumptions which led to Eq. (7.53) are that the flow is steady, adiabatic, and inviscid. In particular, since Eq. (7.53) holds for an adiabatic flow, it can be used to elaborate on our previous definition of total enthalpy. Since  $h_0$

)

is defined as that enthalpy which would exist at a point if the fluid element were brought to rest adiabatically, we find from Eq. (7.53) with  $V = 0$  and hence  $h = h_0$  that the value of the constant in Eq. (7.53) is  $h_0$ . Hence, Eq. (7.53) can be written as

$$h + \frac{V^2}{2} = h_0 \quad (7.54)$$

Equation (7.54) is important; it states that at any point in a flow, the total enthalpy is given by the sum of the static enthalpy plus the kinetic energy, all per unit mass. Whenever we have the combination  $h + V^2/2$  in any subsequent equations, it can be identically replaced by  $h_0$ . For example, Eq. (7.52), which was derived for a steady, adiabatic, inviscid flow, states that

$$\rho \frac{Dh_0}{Dt} = 0$$

i.e., the total enthalpy is constant along a streamline. Moreover, if all the streamlines of the flow originate from a common uniform freestream (as is usually the case), then  $h_0$  is the same for each streamline. Consequently, we have for such a steady, adiabatic flow that

$$h_0 = \text{const} \quad (7.55)$$

throughout the *entire* flow, and  $h_0$  is equal to its freestream value. Equation (7.55), although simple in form, is a powerful tool. For steady, inviscid, adiabatic flow, Eq. (7.55) is a statement of the energy equation, and hence it can be used in place of the more complex partial differential equation given by Eq. (7.52). This is a great simplification, as we will see in subsequent discussions.

For a calorically perfect gas,  $h_0 = c_p T_0$ . Thus, the above results also state that the total temperature is constant throughout the steady, inviscid, adiabatic flow of a calorically perfect gas, i.e.,

$$T_0 = \text{const} \quad (7.56)$$

For such a flow, Eq. (7.56) can be used as a form of the governing energy equation.

Keep in mind that the above discussion marbled two trains of thought: on the one hand we dealt with the general concept of an adiabatic flow field [which led to Eqs. (7.51) to (7.53)], and on the other hand we dealt with the definition of total enthalpy [which led to Eq. (7.54)]. These two trains of thought are really separate and should not be confused. Consider, for example, a general *nonadiabatic* flow, such as a viscous boundary layer with heat transfer. Clearly, Eqs. (7.51) to (7.53) do not hold for such a flow. However, Eq. (7.54) holds locally at each point in the flow, because the assumption of an adiabatic flow contained in Eq. (7.54) is made through the *definition* of  $h_0$ .

and has nothing to do with the general overall flow field. For example, consider two different points, 1 and 2, in the general flow. At point 1, the local static enthalpy and velocity are  $h_1$  and  $V_1$ , respectively. Hence, the local total enthalpy at point 1 is  $h_{0,1} = h_1 + V_1^2/2$ . At point 2, the local static enthalpy and velocity are  $h_2$  and  $V_2$ , respectively. Hence, the local total enthalpy at point 2 is  $h_{0,2} = h_2 + V_2^2/2$ . If the flow between points 1 and 2 is nonadiabatic, then  $h_{0,1} \neq h_{0,2}$ . Only for the special case where the flow is adiabatic between the two points would  $h_{0,1} = h_{0,2}$ . Of course, this is the special case treated by Eqs. (7.55) and (7.56).

Return to the beginning of this section, where we considered a fluid element passing through a point in a flow where the local properties are  $p$ ,  $T$ ,  $\rho$ ,  $M$ , and  $V$ . Once again, imagine that you grab hold of the fluid element and slow it down to zero velocity, but this time, let us slow it down both adiabatically and reversibly. That is, let us slow the fluid element down to zero velocity *isentropically*. When the fluid element is brought to rest isentropically, the resulting pressure and density are defined as the *total pressure*  $p_0$  and *total density*  $\rho_0$ . (Since an isentropic process is also adiabatic, the resulting temperature is the same total temperature  $T_0$  as discussed earlier.) As before, keep in mind that we do not have to actually bring the flow to rest in real life in order to talk about total pressure and total density; rather, they are *defined* quantities that would exist at a point in a flow (if (in our imagination) the fluid element passing through that point were brought to rest isentropically). Therefore, at a given point in a flow, where the static pressure and static density are  $p$  and  $\rho$ , respectively, we can also assign a value of total pressure  $p_0$ , and total density  $\rho_0$  defined as above.

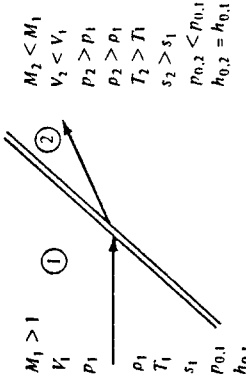
The definition of  $p_0$  and  $\rho_0$  deals with an isentropic compression to zero velocity. Keep in mind that the isentropic assumption is involved with the definition only. The concept of total pressure and density can be applied throughout any general *non-isentropic* flow. For example, consider two different points, 1 and 2, in a general flow field. At point 1, the local static pressure and static density are  $p_1$  and  $\rho_1$ , respectively; also the local total pressure and total density are  $p_{0,1}$  and  $\rho_{0,1}$ , respectively, defined as above. Similarly, at point 2, the local static pressure and static density are  $p_2$  and  $\rho_2$ , respectively, and the local total pressure and total density are  $p_{0,2}$  and  $\rho_{0,2}$ , respectively. If the flow is nonisentropic between points 1 and 2, then  $p_{0,1} \neq p_{0,2}$  and  $\rho_{0,1} \neq \rho_{0,2}$ . Indeed, if the general flow field is isentropic throughout, then both  $p_0$  and  $\rho_0$  are constant values throughout the flow.

As a corollary to the above considerations, we need another defined temperature, denoted by  $T^*$ , and defined as follows. Consider a point in a subsonic flow where the local static temperature is  $T$ . At this point, imagine that the fluid element is speeded up to sonic velocity, *adiabatically*. The temperature it would have at such sonic conditions is denoted as  $T^*$ . Similarly, consider a point in a supersonic flow, where the local static temperature is  $T$ . At this point, imagine that the fluid element is slowed down to sonic velocity, *adiabatically*. Again, the temperature it would have at such sonic conditions is denoted as  $T^*$ . The quantity  $T^*$  is simply a defined quantity at a given point in a flow, in exactly the same vein as  $T_0$ ,  $p_0$ , and  $\rho_0$  are defined quantities.

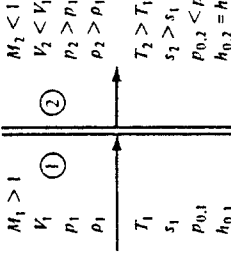
## 7.6 SOME ASPECTS OF SUPERSONIC FLOW: SHOCK WAVES

Return to the different regimes of flow sketched in Fig. 1.26. Note that subsonic compressible flow is qualitatively (but not quantitatively) the same as incompressible flow; Fig. 1.26a shows a subsonic flow with a smoothly varying streamline pattern, where the flow far ahead of the body is forewarned about the presence of the body and begins to adjust accordingly. In contrast, supersonic flow is quite different, as sketched in Fig. 1.26d and e. Here, the flow is dominated by shock waves, and the flow upstream of the body does not know about the presence of the body until it encounters the leading-edge shock wave. In fact, any flow with a supersonic region, such as those sketched in Fig. 1.26b to e, is subject to shock waves. Thus, an essential ingredient of a study of supersonic flow is the calculation of the shape and strength of shock waves. This is the main thrust of Chaps. 8 and 9.

A shock wave is an extremely thin region, typically on the order of  $10^{-5}$  cm, across which the flow properties can change drastically. The shock wave is usually at an oblique angle to the flow, such as sketched in Fig. 7.4a; however, there are many cases where we are interested in a shock wave normal to the flow, as sketched in Fig. 7.4b. Normal shock waves are discussed at length in Chap. 8, whereas oblique shocks are considered in Chap. 9. In both cases, the shock wave is an almost explosive compression process, where the pressure increases almost discontinuously across the wave.



(a) Oblique shock wave



(b) Normal shock wave

Figure 7.4 Qualitative pictures of flow through oblique and normal shock waves.

Examine Fig. 7.4 closely. In region 1 ahead of the shock, the Mach number, flow velocity, pressure, density, temperature, entropy, total pressure, and total enthalpy are denoted by  $M_1$ ,  $V_1$ ,  $p_1$ ,  $\rho_1$ ,  $T_1$ ,  $s_1$ ,  $p_{0,1}$ , and  $h_{0,1}$ , respectively. The analogous quantities in region 2 behind the shock are  $M_2$ ,  $V_2$ ,  $p_2$ ,  $\rho_2$ ,  $T_2$ ,  $s_2$ ,  $p_{0,2}$ , and  $h_{0,2}$ , respectively. The qualitative changes across the wave are noted in Fig. 7.4. The pressure, density, temperature, and entropy increase across the shock, whereas the total pressure, Mach number, and velocity decrease. Physically, the flow across a shock wave is adiabatic (we are not heating the gas with a laser beam or cooling it in a refrigerator, for example). Therefore, recalling the discussion in Sec. 7.5, the total enthalpy is constant across the wave. In both the oblique shock and normal shock cases, the flow ahead of the shock wave must be supersonic, that is,  $M_1 > 1$ . Behind the oblique shock, the flow usually remains supersonic, that is,  $M_2 > 1$ , but at a reduced Mach number, that is,  $M_2 < M_1$ . However, as discussed in Chap. 9, there are special cases where the oblique shock is strong enough to decelerate the downstream flow to a subsonic Mach number; hence,  $M_2 < 1$  can occur behind an oblique shock. For the normal shock, as sketched in Fig. 7.4b, the downstream flow is always subsonic, that is,  $M_2 < 1$ . Study the qualitative variations illustrated in Fig. 7.4 closely. They are important, and you should have them in mind for our subsequent discussions. One of the primary purposes of Chaps. 8 and 9 is to develop a shock wave theory which allows the quantitative evaluation of these variations. We prove that pressure increases across the shock, that the upstream Mach number must be supersonic, etc. Moreover, we obtain equations that allow the direct calculation of changes across the shock.

Several photographs of shock waves are shown in Fig. 7.5. Since air is transparent, we cannot usually see shock waves with the naked eye. However, because the density



Figure 7.5 (Continued) Schlieren photographs illustrating shock waves on various bodies. (Courtesy of the NASA Langley Research Center.)

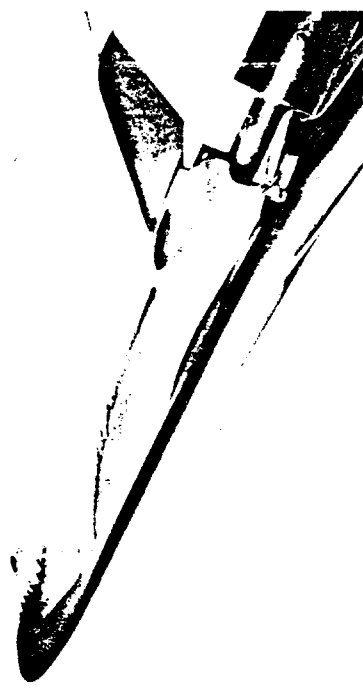


Figure 7.5 (Continued) "Tension shell" body once proposed for a Martian entry vehicle at Mach 8. (Courtesy of the NASA Langley Research Center.)

changes across the shock wave, light rays propagating through the flow will be refracted across the shock. Special optical systems, such as shadowgraphs, schlieren, and interferometers, take advantage of this refraction and allow the visual imaging of shock waves on a screen or a photographic negative. For details of the design and

Figure 7.5 Schlieren photographs illustrating shock waves on various bodies. Apollo Command Module wind-tunnel model at Mach 8. (Courtesy of the NASA Langley Research Center.)

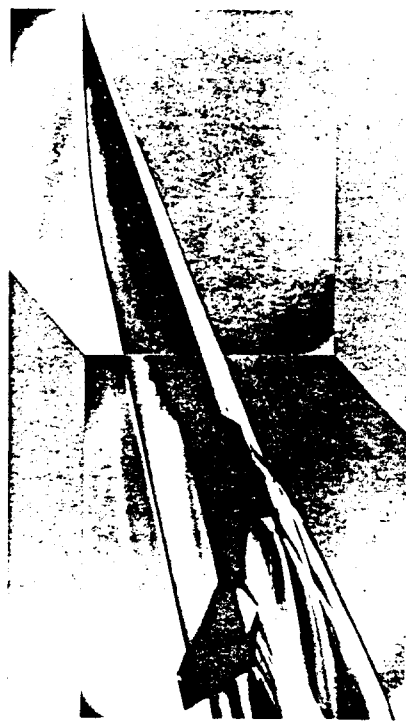


Figure 7.5 (Continued) A conceptual hypersonic aircraft at Mach 6. (Courtesy of the NASA Langley Research Center.)

characteristics of these optical systems, see Refs. 25 and 26. (Under certain conditions, you can see the refracted light from a shock wave with your naked eye. Recall from Fig. 1.26b that a shock wave can form in the locally supersonic region on the top surface of an airfoil if the freestream subsonic Mach number is high enough. The next time you are flying in a jet transport, and the sun is directly overhead, look out the window along the span of the wing. If you are lucky, you will see the shock wave dancing back and forth over the top of the wing.)

In summary, compressible flows introduce some very exciting physical phenomena into our aerodynamic studies. Moreover, as the flow changes from subsonic to supersonic, the complete nature of the flow changes, not the least of which is the occurrence of shock waves. The purpose of the next seven chapters is to describe and analyze these flows.

## 7.7 SUMMARY

As usual, examine the road map for this chapter (Fig. 7.1), and make certain that you feel comfortable with the material represented by this road map before continuing further. Some of the highlights of this chapter are summarized below.

### *Thermodynamic relations*

Equation of state:

For a calorically perfect gas,

$$(7.1)$$

### General definition of compressibility:

$$(7.33)$$

$$\epsilon = c_v T \quad \text{and} \quad h = c_p T \quad (7.6a \text{ and } b)$$

$$c_p = \frac{\gamma R}{\gamma - 1} \quad (7.9)$$

$$c_v = \frac{R}{\gamma - 1} \quad (7.10)$$

Forms of the first law:

$$\delta q + \delta w = de \quad (7.11)$$

$$T ds = de + p dv \quad (7.18)$$

$$T ds = dh - v dp \quad (7.20)$$

Definition of entropy:

$$ds = \frac{\delta q_{rev}}{T} \quad (7.13)$$

$$ds = \frac{\delta q}{T} + ds_{inrev} \quad (7.14)$$

The second law:

$$ds \geq \frac{\delta q}{T} \quad (7.16)$$

or, for an adiabatic process,

$$ds \geq 0 \quad (7.17)$$

Entropy changes can be calculated from (for a calorically perfect gas)

$$s_2 - s_1 = c_p \ln \frac{T_2}{T_1} - R \ln \frac{p_2}{p_1} \quad (7.25)$$

$$\text{and} \quad s_2 - s_1 = c_v \ln \frac{T_2}{T_1} - R \ln \frac{v_2}{v_1} \quad (7.26)$$

For an isentropic flow,

$$\frac{p_2}{p_1} = \left( \frac{\rho_2}{\rho_1} \right)^{\gamma} = \left( \frac{T_2}{T_1} \right)^{\gamma(\gamma-1)} \quad (7.32)$$

$$\text{For an isothermal process, } \tau_I = -\frac{1}{v} \left( \frac{\partial v}{\partial p} \right)_T \quad (7.34)$$

$$\text{For an isentropic process, } \tau_s = -\frac{1}{v} \left( \frac{\partial v}{\partial p} \right)_s \quad (7.35)$$

The governing equations for inviscid, compressible flow are

$$\begin{aligned} \text{Continuity:} \quad & \frac{\partial}{\partial t} \iiint_V \rho dV + \oint_S \rho \mathbf{V} \cdot d\mathbf{S} = 0 \quad (7.39) \\ \text{Momentum:} \quad & \frac{\partial \rho}{\partial t} + \nabla \cdot \rho \mathbf{V} = 0 \quad (7.40) \end{aligned}$$

*Momentum:*

$$\frac{\partial}{\partial t} \iiint_V \rho \mathbf{V} dV + \oint_S (\rho \mathbf{V} \cdot d\mathbf{S}) \mathbf{V} = - \oint_S \rho \mathbf{V} \cdot d\mathbf{S} + \iiint_V \rho f dV \quad (7.41)$$

$$\rho \frac{D\mathbf{u}}{Dt} = - \frac{\partial \mathbf{p}}{\partial x} + \rho \mathbf{f}, \quad (7.42a)$$

$$\rho \frac{D\mathbf{v}}{Dt} = - \frac{\partial \mathbf{p}}{\partial y} + \rho \mathbf{f}_y, \quad (7.42b)$$

$$\rho \frac{D\mathbf{w}}{Dt} = - \frac{\partial \mathbf{p}}{\partial z} + \rho \mathbf{f}_z, \quad (7.42c)$$

*Energy:*

$$\begin{aligned} \frac{\partial}{\partial t} \iiint_V \rho \left( e + \frac{V^2}{2} \right) dV + \oint_S \rho \left( e + \frac{V^2}{2} \right) \mathbf{V} \cdot d\mathbf{S} \\ = \iiint_V \dot{q} p dV - \oint_S \rho \mathbf{V} \cdot d\mathbf{S} + \iiint_V \rho (\mathbf{f} \cdot \mathbf{V}) dV \quad (7.43) \end{aligned}$$

$$\rho \frac{D(e + V^2/2)}{Dt} = \rho \dot{q} - \nabla \cdot \rho \mathbf{V} + \rho (\mathbf{f} \cdot \mathbf{V}) \quad (7.44)$$

If the flow is steady and adiabatic, Eqs. (7.43) and (7.44) can be replaced by

$$h_0 = h + \frac{V^2}{2} = \text{const}$$

*Equation of state (perfect gas):*

$$p = \rho R T \quad (7.1)$$

$$e = c_v T \quad (7.6a)$$

*Internal energy (calorically perfect gas):*

Total temperature  $T_0$  and total enthalpy  $h_0$  are defined as the properties that would exist if (in our imagination) we slowed the fluid element at a point in the flow to zero velocity adiabatically. Similarly, total pressure  $p_0$  and total density  $\rho_0$  are defined as the properties that would exist if (in our imagination) we slowed the fluid element at a point in the flow to zero velocity isentropically. If a general flow field is adiabatic,  $h_0$  is constant throughout the flow; in contrast, if the flow field is nonadiabatic,  $h_0$  varies from one point to another. Similarly, if a general flow field is isentropic,  $p_0$  and  $\rho_0$  are constant throughout the flow; in contrast, if the flow field is nonisentropic,  $p_0$  and  $\rho_0$  vary from one point to another.

Shock waves are very thin regions in a supersonic flow across which the pressure, density, temperature, and entropy increase; the Mach number, flow velocity, and total pressure decrease; and the total enthalpy stays the same.

## PROBLEMS

**Note:** In the following problems, you will deal with both the International System of Units (SI) (N, kg, m, s, K) and the English Engineering System (lb, slug, ft, s, °R). Which system to use will be self-evident in each problem. All problems deal with calorically perfect air as the gas, unless otherwise noted. Also, recall that 1 atm = 2116 lb/ft<sup>2</sup> = 1.01 × 10<sup>5</sup> N/m<sup>2</sup>.

**7.1** The temperature and pressure at the stagnation point of a high-speed missile are 934°R and 7.8 atm, respectively. Calculate the density at this point.

**7.2** Calculate  $c_p$ ,  $c_v$ ,  $e$ , and  $h$  for

- (a) The stagnation point conditions given in Problem 7.1
- (b) Air at standard sea level conditions

(if you do not remember what standard sea level conditions are, find them in an appropriate reference, such as Ref. 2.)

**7.3** Just upstream of a shock wave, the air temperature and pressure are 288 K and 1 atm, respectively; just downstream of the wave, the air temperature and pressure are 690 K and 8.656 atm, respectively. Calculate the changes in enthalpy, internal energy, and entropy across the wave.

**7.4** Consider the isentropic flow over an airfoil. The freestream conditions are  $T_\infty = 245$  K and  $p_\infty = 4.35 \times 10^5$  N/m<sup>2</sup>. At a point on the airfoil, the pressure is  $3.6 \times 10^5$  N/m<sup>2</sup>. Calculate the density at this point.

**7.5** Consider the isentropic flow through a supersonic wind-tunnel nozzle. The reservoir properties are  $T_0 = 500$  K and  $p_0 = 10$  atm. If  $p = 1$  atm at the nozzle exit, calculate the exit temperature and density.

- 7.6 Consider air at a pressure of 0.2 atm. Calculate the values of  $\tau_f$  and  $\tau_i$ . Express your answer in SI units.
- 7.7 Consider a point in a flow where the velocity and temperature are 1300 ft/s and 480°R, respectively. Calculate the total enthalpy at this point.
- 7.8 In the reservoir of a supersonic wind tunnel, the velocity is negligible, and the temperature is 1000 K. The temperature at the nozzle exit is 600 K. Assuming adiabatic flow through the nozzle, calculate the velocity at the exit.
- 7.9 An airfoil is in a freestream where  $p_\infty = 0.61$  atm,  $\rho_\infty = 0.819$  kg/m<sup>3</sup>, and  $V_\infty = 300$  m/s. At a point on the airfoil surface, the pressure is 0.5 atm. Assuming isentropic flow, calculate the velocity at that point.
- 7.10 Calculate the percentage error obtained if Prob. 7.9 is solved using (incorrectly) the incompressible Bernoulli equation.
- 7.11 Repeat Prob. 7.9, considering a point on the airfoil surface where the pressure is 0.3 atm.
- 7.12 Repeat Prob. 7.10, considering the flow of Prob. 7.11.

## CHAPTER EIGHT

### NORMAL SHOCK WAVES AND RELATED TOPICS

*Shock wave: A large-amplitude compression wave, such as that produced by an explosion, caused by supersonic motion of a body in a medium.*

*From the American Heritage Dictionary of the English Language, 1969.*

#### 8.1 INTRODUCTION

The purpose of this chapter and Chap. 9 is to develop shock-wave theory, thus giving us the means to calculate the changes in the flow properties across a wave. These changes were discussed qualitatively in Sec. 7.6; make certain that you are familiar with these changes before continuing.

The focus of this chapter is on normal shock waves, as sketched in Fig. 7.4b. At first thought, a shock wave which is normal to the upstream flow may seem to be a very special case — and therefore a case of little practical interest — but nothing could be further from the truth. Normal shocks occur frequently in nature. Two such examples are sketched in Fig. 8.1; there are many more. The supersonic flow over a blunt body is shown at the left of Fig. 8.1. Here, a strong bow shock wave exists in front of the body. (We study such bow shocks in Chap. 9.) Although this wave is curved, the region of the shock closest to the nose is essentially normal to the flow. Moreover, the streamline that passes through this normal portion of the bow shock later impinges on the nose of the body and controls the values of stagnation (total) pressure and temperature at the nose. Since the nose region of high-speed blunt bodies is of practical interest in the calculation of drag and aerodynamic heating, the properties of the flow behind the normal portion of the shock wave take on some importance. In another example, shown at the right of Fig. 8.1, supersonic flow is established inside a nozzle (which can be a supersonic wind tunnel, a rocket engine, etc.) where the back pressure is high enough to cause a normal shock wave to stand inside the nozzle. (We discuss such "overexpanded" nozzle flows in Chap. 10.) The conditions under which this shock wave will occur and the determination of flow properties at the nozzle exit downstream of the normal shock are both important questions to be answered. In summary, for these and many other applications, the study of normal shock waves is important.

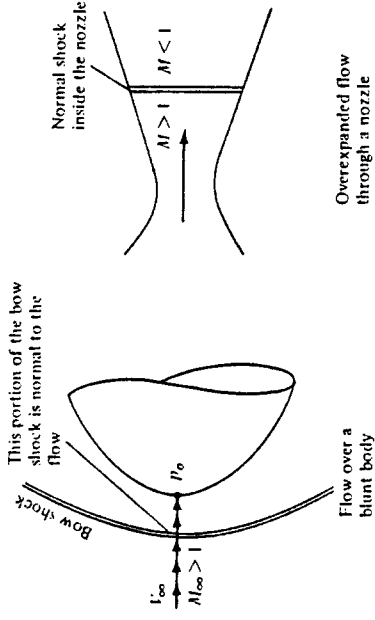


Figure 8.1 Two examples where normal shock waves are of interest.

Finally, we will find that many of the normal shock relations derived in this chapter carry over directly to the analysis of oblique shock waves, as discussed in Chap. 9. So once again, time spent on normal shock waves is time well spent.

The road map for this chapter is given in Fig. 8.2. As you can see, our objectives are fairly short and straightforward. We start with a derivation of the basic continuity, momentum, and energy equations for normal shock waves, and then we employ these basic relations to obtain detailed equations for the calculation of flow properties across the shock wave. In addition, we emphasize the physical trends indicated by the equations. On the way toward this objective, we take three side streets having to do with (1) the speed of sound, (2) special forms of the energy equation, and (3) a further discussion of the criteria used to judge when a flow must be treated as compressible.

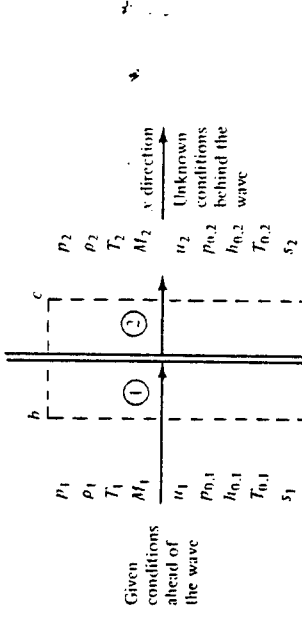
1. The flow is steady, that is,  $\partial/\partial t = 0$ .
2. The flow is adiabatic, that is,  $\dot{q} = 0$ . We are not adding or taking away heat from the control volume (we are not heating the shock wave with a Bunsen burner, for example). The temperature increases across the shock wave, not because heat is

## 8.2 THE BASIC NORMAL SHOCK EQUATIONS

Consider the normal shock wave sketched in Fig. 8.3. Region 1 is a uniform flow upstream of the shock, and region 2 is a different uniform flow downstream of the shock. The pressure, density, temperature, Mach number, velocity, total pressure, total enthalpy, total temperature, and entropy in region 1 are  $p_1, \rho_1, T_1, M_1, u_1, p_{0,1}, h_{0,1}, T_{0,1}$ , and  $s_1$ , respectively. The corresponding variables in region 2 are denoted by  $p_2, \rho_2, T_2, M_2, u_2, p_{0,2}, h_{0,2}, T_{0,2}$ , and  $s_2$ . (Note that we are denoting the magnitude of the flow velocity by  $u$  rather than  $V$ ; reasons for this will become obvious as we progress.) The problem of the normal shock wave is simply stated as follows: given the flow properties upstream of the wave ( $p_1, T_1, M_1$ , etc.), calculate the flow properties ( $p_2, T_2, M_2$ , etc.) downstream of the wave. Let us proceed.

Consider the rectangular control volume  $abcd$  given by the dashed line in Fig. 8.3. The shock wave is inside the control volume, as shown. Side  $ab$  is the edge view of the left face of the control volume; this left face is perpendicular to the flow, and its area is  $A$ . Side  $cd$  is the edge view of the right face of the control volume; this right face is also perpendicular to the flow, and its area is  $A$ . We apply the integral form of conservation equations to this control volume. In the process, we observe three important physical facts about the flow given in Fig. 8.3:

1. The flow is steady, that is,  $\partial/\partial t = 0$ .
2. The flow is adiabatic, that is,  $\dot{q} = 0$ . We are not adding or taking away heat from the control volume (we are not heating the shock wave with a Bunsen burner, for example). The temperature increases across the shock wave, not because heat is



The shock wave is a thin region of highly viscous flow. The flow through the shock is adiabatic but nonisentropic

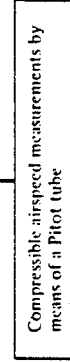


Figure 8.2 Road map for Chap. 8.

Figure 8.3 Sketch of a normal wave.

being added, but rather because kinetic energy is converted to internal energy across the shock wave.

3. There are no viscous effects on the sides of the control volume. The shock wave itself is a thin region of extremely high velocity and temperature gradients; hence, friction and thermal conduction play an important role on the flow structure inside the wave. However, the wave itself is buried inside the control volume, and with the integral form of the conservation equations, we are not concerned about the details of what goes on inside the control volume.
4. There are no body forces;  $\mathbf{f} = 0$ .

Consider the continuity equation in the form of Eq. (7.39). For the conditions described above, Eq. (7.39) becomes

$$\oint_S \rho \mathbf{V} \cdot d\mathbf{S} = 0 \quad (8.1)$$

To evaluate Eq. (8.1) over the face  $ab$ , note that  $\mathbf{V}$  is pointing into the control volume whereas  $d\mathbf{S}$  by definition is pointing out of the control volume, in the opposite direction of  $\mathbf{V}$ ; hence,  $\mathbf{V} \cdot d\mathbf{S}$  is negative. Moreover,  $\rho$  and  $|\mathbf{V}|$  are uniform over the face  $ab$  and equal to  $\rho_1$  and  $u_1$ , respectively. Hence, the contribution of face  $ab$  to the surface integral in Eq. (8.1) is simply  $-\rho_1 u_1 A$ . Over the right face,  $cd$ , both  $\mathbf{V}$  and  $d\mathbf{S}$  are in the same direction, and hence  $\mathbf{V} \cdot d\mathbf{S}$  is positive. Moreover,  $\rho$  and  $|\mathbf{V}|$  are uniform over the face  $cd$  and equal to  $\rho_2$  and  $u_2$ , respectively. Thus, the contribution of face  $cd$  to the surface integral is  $\rho_2 u_2 A$ . On sides  $bc$  and  $ad$ ,  $\mathbf{V}$  and  $d\mathbf{S}$  are always perpendicular; hence,  $\mathbf{V} \cdot d\mathbf{S} = 0$ , and these sides make no contribution to the surface integral. Hence, for the control volume shown in Fig. 8.3, Eq. (8.1) becomes

$$\begin{aligned} -\rho_1 u_1 A + \rho_2 u_2 A &= 0 \\ \boxed{\rho_1 u_1 = \rho_2 u_2} \end{aligned} \quad (8.2)$$

Equation (8.2) is the continuity equation for normal shock waves.

Consider the momentum equation in the form of Eq. (7.41). For the flow we are treating here, Eq. (7.41) becomes

$$\oint_S (\rho \mathbf{V} \cdot d\mathbf{S}) \mathbf{V} = -\oint_S \rho d\mathbf{S} \quad (8.3)$$

Equation (8.3) is a vector equation. Note that in Fig. 8.3, the flow is moving only in one direction, i.e., in the  $x$  direction. Hence, we need to consider only the scalar  $x$  component of Eq. (8.3), which is

$$\oint_S (\rho \mathbf{V} \cdot d\mathbf{S}) u = -\oint_S (\rho dS) \quad (8.4)$$

In Eq. (8.4),  $(\rho dS)_x$  is the  $x$  component of the vector  $(\rho dS)$ . Note that over the face  $ab$ ,  $d\mathbf{S}$  points to the left, i.e., in the negative  $x$  direction. Hence  $(\rho dS)_x$  is negative over

face  $ab$ . By similar reasoning,  $(\rho dS)_x$  is positive over the face  $cd$ . Again noting that all the flow variables are uniform over the faces  $ab$  and  $cd$ , the surface integrals in Eq. (8.4) become

$$\rho_1 (-u_1 A) u_1 + \rho_2 (u_2 A) u_2 = -(p_1 A + p_2 A) \quad (8.5)$$

or

$$\boxed{p_1 + \rho_1 u_1^2 = p_2 + \rho_2 u_2^2} \quad (8.6)$$

Equation (8.6) is the momentum equation for normal shock waves.

Consider the energy equation in the form of Eq. (7.43). For steady, adiabatic, inviscid flow with no body forces, this equation becomes

$$\oint_S \rho \left( e + \frac{V^2}{2} \right) \mathbf{V} \cdot d\mathbf{S} = -\oint_S \rho \mathbf{V} \cdot d\mathbf{S} \quad (8.7)$$

Evaluating Eq. (8.7) for the control surface shown in Fig. 8.3, we have

$$-\rho_1 \left( e_1 + \frac{u_1^2}{2} \right) u_1 A + \rho_2 \left( e_2 + \frac{u_2^2}{2} \right) u_2 A = -(-p_1 u_1 A + p_2 u_2 A)$$

Rearranging,

$$\rho_1 u_1 + \rho_1 \left( e_1 + \frac{u_1^2}{2} \right) u_1 = p_2 u_2 + \rho_2 \left( e_2 + \frac{u_2^2}{2} \right) u_2 \quad (8.8)$$

Dividing by Eq. (8.2), i.e., dividing the left-hand side of Eq. (8.8) by  $\rho_1 u_1$  and the right-hand side by  $\rho_2 u_2$ ,

$$\frac{p_1}{\rho_1} + e_1 + \frac{u_1^2}{2} = \frac{p_2}{\rho_2} + e_2 + \frac{u_2^2}{2} \quad (8.9)$$

From the definition of enthalpy,  $h \equiv e + pv = e + p/\rho$ . Hence, Eq. (8.9) becomes

$$\boxed{h_1 + \frac{u_1^2}{2} = h_2 + \frac{u_2^2}{2}} \quad (8.10)$$

Equation (8.10) is the energy equation for normal shock waves. Equation (8.10) should come as no surprise; the flow through a shock wave is adiabatic, and we derived in Sec. 7.5 the fact that for a steady, adiabatic flow,  $h_0 = h + V^2/2 = \text{const}$ . Equation (8.10) simply states that  $h_0$  (hence, for a calorically perfect gas,  $T_0$ ) is constant across the shock wave. Therefore, Eq. (8.10) is consistent with the general results obtained in Sec. 7.5.

Repeating the above results for clarity, the basic normal shock equations are

$$\boxed{\rho_1 u_1 = \rho_2 u_2} \quad (8.2)$$

$$\boxed{p_1 + \rho_1 u_1^2 = p_2 + \rho_2 u_2^2} \quad (8.6)$$

$$\boxed{h_1 + \frac{u_1^2}{2} = h_2 + \frac{u_2^2}{2}} \quad (8.10)$$

*Continuity:*

*Momentum:*

*Energy:*

Examine these equations closely. Recall from Fig. 8.3 that all conditions upstream of the wave,  $\rho_1$ ,  $u_1$ ,  $p_1$ , etc., are known. Thus, the above equations are a system of three algebraic equations in four unknowns,  $\rho_2$ ,  $u_2$ ,  $p_2$ , and  $h_2$ . However, if we add the following thermodynamic relations

$$h_2 = c_p T_2$$

$$p_2 = \rho_2 R T_2$$

we have five equations for five unknowns, namely,  $\rho_2$ ,  $u_2$ ,  $p_2$ ,  $h_2$ , and  $T_2$ . In Sec. 8.6, we explicitly solve these equations for the unknown quantities behind the shock. However, rather than going directly to that solution, we first take three side trips as shown in the road map in Fig. 8.2. These side trips involve discussions of the speed of sound (Sec. 8.3), alternate forms of the energy equation (Sec. 8.4), and compressibility (Sec. 8.5) — all of which are necessary for a viable discussion of shock-wave properties in Sec. 8.6.

Finally, we note that Eqs. (8.2), (8.6), and (8.10) are not limited to normal shock waves; they describe the changes that take place in any steady, adiabatic, inviscid flow where only one direction is involved. That is, in Fig. 8.3, the flow is in the  $x$  direction only. This type of flow, where the flow-field variables are functions of  $x$  only [ $p = p(x)$ ,  $u = u(x)$ , etc.], is defined as *one-dimensional flow*. Thus, Eqs. (8.2), (8.6), and (8.10) are governing equations for one-dimensional, steady, adiabatic, inviscid flow.

### 8.3 SPEED OF SOUND

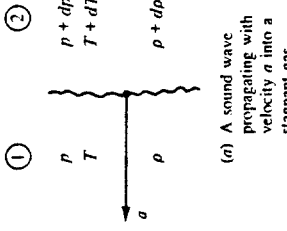
Common experience tells us that sound travels through air at some finite velocity. For example, you see a flash of lightning in the distance, but you hear the corresponding thunder at some later moment. What is the physical mechanism of the propagation of sound waves? How can we calculate the speed of sound? What properties of the gas does it depend on? The speed of sound is an extremely important quantity which dominates the physical properties of compressible flow, and hence the answers to the above questions are vital to our subsequent discussions. The purpose of this section is to address these questions.

The physical mechanism of sound propagation in a gas is based on molecular motion. For example, imagine that you are sitting in a room, and suppose that a firecracker goes off in one corner. When the firecracker detonates, chemical energy (basically a form of heat release) is transferred to the air molecules adjacent to the firecracker. These energized molecules are moving about in a random fashion. They eventually collide with some of their neighboring molecules and transfer their high energy to these neighbors. In turn, these neighboring molecules eventually collide with their neighbors and transfer energy in the process. By means of this "domino" effect, the energy released by the firecracker is propagated through the air by molecular collisions. Moreover, because  $T$ ,  $p$ , and  $\rho$  for a gas are macroscopic averages of the detailed microscopic molecular motion, the regions of energized molecules are also regions of slight variations in the local temperature, pressure, and density. Hence, as

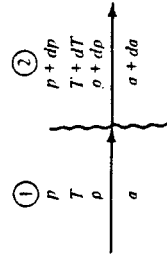
this energy wave from the firecracker passes over our eardrums, we "hear" the slight pressure changes in the wave. This is *sound*, and the propagation of the energy wave is simply the propagation of a *sound wave* through the gas.

Because a sound wave is propagated by molecular collisions, and because the molecules of a gas are moving with an average velocity of  $\sqrt{8RT/\pi}$  given by kinetic theory, then we would expect the velocity of propagation of a sound wave to be approximately the average molecular velocity. Indeed, the speed of sound is about three-quarters of the average molecular velocity. In turn, because the kinetic theory expression given above for the average molecular velocity depends only on the *temperature* of the gas, we might expect the speed of sound to also depend on temperature only. Let us explore this matter further; indeed, let us now derive an equation for the speed of sound in a gas. Although the propagation of sound is due to molecular collisions, we do not use such a microscopic picture for our derivation. Rather, we take advantage of the fact that the macroscopic properties  $p$ ,  $T$ ,  $\rho$ , etc., change across the wave, and we use our macroscopic equations of continuity, momentum, and energy to analyze these changes.

Consider a sound wave propagating through a gas with velocity  $a$ , as sketched in Fig. 8.4a. Here, the sound wave is moving from right to left into a stagnant gas (region 1), where the local pressure, temperature, and density are  $p$ ,  $T$ , and  $\rho$ , respectively. Behind the sound wave (region 2), the gas properties are slightly different and are given by  $p + dp$ ,  $T + dT$ , and  $\rho + d\rho$ , respectively. Now imagine that you hop on the wave and ride with it. When you look upstream, into region 1, you see the gas moving toward you with a relative velocity  $a$ , as sketched in Fig. 8.4b. When you look downstream, into region 2, you see the gas receding away from you with a relative velocity  $a + da$ ,



(a) A sound wave propagating with velocity  $a$  into a stagnant gas



(b) A stationary sound wave in a moving gas; the upstream velocity relative to the wave is  $a$

Figure 8.4 Moving and stationary sound waves; two analogous pictures, only the perspective is different.

as also shown in Fig. 8.4. (We have enough fluid-dynamic intuition by now to realize that because the pressure changes across the wave by the amount  $dp$ , then the relative flow velocity must also change across the wave by some amount  $da$ . Hence, the relative flow velocity behind the wave is  $a + da$ .) Consequently, in Fig. 8.4b, we have a picture of a stationary sound wave, with the flow ahead of it moving left to right with velocity  $a$ . The pictures in Fig. 8.4a and b are analogous; only the perspective is different. For purposes of analysis, we use Fig. 8.4b.

(Note that Fig. 8.4b is similar to the picture of a normal shock wave shown in Fig. 8.3. In Fig. 8.3, the normal shock wave is stationary, and the upstream flow is moving left to right at a velocity  $u_1$ . If the upstream flow were to be suddenly shut off, then the normal shock wave in Fig. 8.3 would suddenly propagate to the left with a wave velocity of  $u_1$ , similar to the moving sound wave shown in Fig. 8.4a. The analysis of moving waves is slightly more subtle than the analysis of stationary waves; hence, it is simpler to begin a study of shock waves and sound waves with the pictures of stationary waves as shown in Figs. 8.3 and 8.4b. Also, please note that the sound wave in Fig. 8.4b is nothing more than an infinitely weak normal shock wave.)

Examine closely the flow through the sound wave sketched in Fig. 8.4b. The flow is one-dimensional. Moreover, it is adiabatic, because we have no source of heat transfer into or out of the wave (e.g., we are not "zapping" the wave with a laser beam or heating it with a torch). Finally, the gradients within the wave are very small—the changes  $dp$ ,  $dT$ ,  $d\rho$ , and  $da$  are infinitesimal. Therefore, the influence of dissipative phenomena (viscosity and thermal conduction) is negligible. As a result, the flow through the sound wave is both adiabatic and reversible—the flow is *isentropic*. Since we have now established that the flow is one-dimensional and isentropic, let us apply the appropriate governing equations to the picture shown in Fig. 8.4b.

Applying the continuity equation, Eq. (8.2), to Fig. 8.4b, we have

$$\begin{aligned} \rho a &= (\rho + dp)(a + da) \\ \rho a &= \rho a + a dp + \rho da + dp da \end{aligned} \quad (8.11)$$

The product of two differentials,  $dp da$ , can be neglected in comparison with the other terms in Eq. (8.11). Hence solving Eq. (8.11) for  $a$ , we obtain

$$a = -\rho \frac{da}{dp} \quad (8.12)$$

Now consider the one-dimensional momentum equation, Eq. (8.6), applied to Fig. 8.4b.

$$p + \rho a^2 = (p + dp) + (\rho + dp)(a + da)^2 \quad (8.13)$$

Again ignoring products of differentials, Eq. (8.13) becomes

$$dp = -2a\rho da - a^2 dp \quad (8.14)$$

Solving Eq. (8.14) for  $da$ , we have

$$da = \frac{dp + a^2 dp}{-2a\rho} \quad (8.15)$$

Substituting Eq. (8.15) into (8.12),

$$a = -\rho \frac{dp/dp + a^2}{-2a\rho} \quad (8.16)$$

Solving Eq. (8.16) for  $a^2$ ,

$$a^2 = \frac{dp}{d\rho} \quad (8.17)$$

As discussed above, the flow through a sound wave is isentropic; hence, in Eq. (8.17), the rate of change of pressure with respect to density,  $dp/d\rho$ , is an isentropic change. Hence, we can rewrite Eq. (8.17) as

$$a = \sqrt{\left(\frac{\partial p}{\partial \rho}\right)} \quad (8.18)$$

Equation (8.18) is a fundamental expression for the speed of sound in a gas.

Assume that the gas is calorically perfect. For such a case, the isentropic relation given by Eq. (7.32) holds, namely,

$$\frac{p_1}{p_2} = \left(\frac{\rho_1}{\rho_2}\right)^\gamma \quad (8.19)$$

From Eq. (8.19), we have

$$\frac{p}{\rho^\gamma} = \text{const} = c \quad (8.20)$$

or

$$p = c\rho^\gamma \quad (8.20)$$

Differentiating Eq. (8.20) with respect to  $\rho$ , we obtain

$$\left(\frac{\partial p}{\partial \rho}\right)_s = c\gamma\rho^{\gamma-1} \quad (8.21)$$

Substituting Eq. (8.20) for the constant  $c$  in Eq. (8.21), we have

$$\left(\frac{\partial p}{\partial \rho}\right)_s = \left(\frac{p}{\rho^\gamma}\right)\gamma\rho^{\gamma-1} = \frac{\gamma p}{\rho} \quad (8.22)$$

Substituting Eq. (8.22) into (8.18), we obtain

$$a = \sqrt{\frac{\gamma p}{\rho}} \quad (8.23)$$

Equation (8.23) is an expression for the speed of sound in a calorically perfect gas. At first glance, Eq. (8.23) seems to imply that the speed of sound would depend on both  $p$  and  $\rho$ . However, pressure and density are related through the perfect gas equation of state,

$$\frac{P}{\rho} = RT \quad (8.24)$$

Hence, substituting Eq. (8.24) into (8.23), we have

$$a = \sqrt{\gamma RT} \quad (8.25)$$

which is our final expression for the speed of sound; it clearly states that the *speed of sound in a calorically perfect gas is a function of temperature only*. This is consistent with our earlier discussion of the speed of sound being a molecular phenomenon, and therefore it is related to the average molecular velocity  $\sqrt{8RT/\pi}$ .

The speed of sound at standard sea level is a useful value to remember; it is

$$a_s = 340.9 \text{ m/s} = 1117 \text{ ft/s}$$

Recall the definition of compressibility given in Sec. 7.3. In particular, from Eq. (7.35) for the isentropic compressibility, repeated below,

$$\tau_s = -\frac{1}{v} \left( \frac{\partial v}{\partial p} \right), \quad (8.26)$$

and recalling that  $v = 1/p$  (hence,  $dv = -dp/p^2$ ), we have

$$\tau_s = -\rho \left[ -\frac{1}{\rho^2} \left( \frac{\partial p}{\partial \rho} \right)_s \right] = \frac{1}{\rho(\partial p / \partial \rho)_s}, \quad (8.26)$$

However, recall from Eq. (8.18) that  $(\partial p / \partial \rho)_s = a^2$ . Hence, Eq. (8.26) becomes

$$\begin{aligned} \tau_s &= \frac{1}{\rho a^2}, \\ a &= \sqrt{\frac{1}{\rho \tau_s}}, \end{aligned} \quad (8.27)$$

or

$$\boxed{\frac{a^2}{\gamma - 1} + \frac{u^2}{2} = \frac{a_0^2}{\gamma - 1} + \frac{u_0^2}{2}} \quad (8.32)$$

Since  $a = \sqrt{\gamma RT}$ , Eq. (8.31) can be written as

$$\boxed{\frac{\gamma RT_1}{\gamma - 1} + \frac{u_1^2}{2} = \frac{a_0^2}{\gamma - 1} + \frac{u_0^2}{2}} \quad (8.32)$$

If we consider point 2 in Eq. (8.32) to be a stagnation point, where the stagnation speed of sound is denoted by  $a_0$ , then, with  $u_2 = 0$ , Eq. (8.32) yields (dropping the subscript 1)

$$\boxed{\frac{a^2}{\gamma - 1} + \frac{u^2}{2} = \frac{a_0^2}{\gamma - 1}} \quad (8.33)$$

Hence, we see that the square of the Mach number is proportional to the ratio of kinetic energy to internal energy of a gas flow. In other words, the Mach number is a

measure of the directed motion of the gas compared with the random thermal motion of the molecules.

## 8.4 SPECIAL FORMS OF THE ENERGY EQUATION

In this section, we elaborate upon the energy equation for adiabatic flow, as originally given by Eq. (7.44). In Sec. 7.5, we obtained for a steady, adiabatic, inviscid flow the result that

$$h_1 + \frac{V_1^2}{2} = h_2 + \frac{V_2^2}{} \quad (8.28)$$

where  $V_1$  and  $V_2$  are velocities at any two points along a three-dimensional streamline. For the sake of consistency in our current discussion of one-dimensional flow, let us use  $u_1$  and  $u_2$  in Eq. (8.28):

$$h_1 + \frac{u_1^2}{2} = h_2 + \frac{u_2^2}{} \quad (8.29)$$

However, keep in mind that all the subsequent results in this section hold in general along a streamline and are by no means limited to just one-dimensional flows. Specializing Eq. (8.29) to a calorically perfect gas, where  $h = c_p T$ , we have

$$\boxed{c_p T_1 + \frac{u_1^2}{2} = c_p T_2 + \frac{u_2^2}{2}} \quad (8.30)$$

From Eq. (7.9), Eq. (8.30) becomes

$$\boxed{\frac{\gamma RT_1}{\gamma - 1} + \frac{u_1^2}{2} = \frac{\gamma RT_2}{\gamma - 1} + \frac{u_2^2}{2}} \quad (8.31)$$

Equation (8.27) relates the speed of sound to the compressibility of a gas. The lower the compressibility, the higher the speed of sound. Recall that for the limiting case of an incompressible fluid,  $\tau_s = 0$ . Hence, Eq. (8.27) states that the speed of sound in a theoretically incompressible fluid is infinite. In turn, for an incompressible flow with finite velocity  $V$ , the Mach number,  $M = V/a$ , is zero. Hence, the incompressible flows treated in Chaps. 3 to 6 are theoretically zero-Mach-number flows.

Finally, in regard to additional physical meaning of the Mach number, consider a fluid element moving along a streamline. The kinetic and internal energies per unit mass are  $V^2/2$  and  $e$ , respectively. Their ratio is [recalling Eqs. (7.6a), (7.10), and (8.25)]

$$\boxed{\frac{V^2/2}{e} = \frac{V^2/2}{c_v T} = \frac{V^2/2}{RT/(\gamma - 1)} = \frac{(\gamma/2)V^2}{a^2/(\gamma - 1)} = \frac{\gamma(\gamma - 1)}{2} M^2} \quad (8.33)$$

In Eq. (8.33),  $a$  and  $u$  are the speed of sound and flow velocity, respectively, at any given point in the flow, and  $a_0$  is the stagnation (or total) speed of sound associated with

that same point. Equivalently, if we have any two points along a streamline, Eq. (8.33) states that

$$\frac{a_1^2}{\gamma - 1} + \frac{u_1^2}{2} = \frac{a_2^2}{\gamma - 1} + \frac{u_2^2}{2} = \frac{a_0^2}{\gamma - 1} = \text{const} \quad (8.34)$$

Recalling the definition of  $a^*$  given at the end of Sec. 7.5, let point 2 in Eq. (8.32) represent sonic flow, where  $u = a^*$ . Then,

$$\frac{a^2}{\gamma - 1} + \frac{u^2}{2} = \frac{a^{*2}}{\gamma - 1} + \frac{a^{*2}}{2} \quad (8.35)$$

or

$$\frac{a^2}{\gamma - 1} + \frac{u^2}{2} = \frac{\gamma + 1}{2(\gamma - 1)} a^{*2} \quad (8.35)$$

In Eq. (8.35),  $a$  and  $u$  are the speed of sound and flow velocity, respectively, at any given point in the flow, and  $a^*$  is a characteristic value associated with that same point. Equivalently, if we have any two points along a streamline, Eq. (8.35) states that

$$\frac{a_1^2}{\gamma - 1} + \frac{u_1^2}{2} = \frac{a_2^2}{\gamma - 1} + \frac{u_2^2}{2} = \frac{\gamma + 1}{2(\gamma - 1)} a^{*2} = \text{const} \quad (8.36)$$

Comparing the right-hand sides of Eqs. (8.34) and (8.36), the two properties  $a_0$  and  $a^*$  associated with the flow are related by

$$\frac{\gamma + 1}{2(\gamma - 1)} a^{*2} = \frac{a_0^2}{\gamma - 1} = \text{const} \quad (8.37)$$

Clearly, these defined quantities,  $a_0$  and  $a^*$ , are both constants along a given streamline in a steady, adiabatic, inviscid flow. If all the streamlines emanate from the same uniform freestream conditions, then  $a_0$  and  $a^*$  are constants throughout the entire flow field.

Recall the definition of total temperature  $T_0$ , as discussed in Sec. 7.5. In Eq. (8.30), let  $u_2 = 0$ ; hence  $T_2 = T_0$ . Dropping the subscript 1, we have

$$c_p T + \frac{u^2}{2} = c_p T_0 \quad (8.38)$$

Equation (8.38) provides a formula from which the defined total temperature  $T_0$  can be calculated from the given actual conditions of  $T$  and  $u$  at any given point in a general flow field. Equivalently, if we have any two points along a streamline in a steady, adiabatic, inviscid flow, Eq. (8.38) states that

$$c_p T_1 + \frac{u_1^2}{2} = c_p T_2 + \frac{u_2^2}{2} = c_p T_0 = \text{const} \quad (8.39)$$

If all the streamlines emanate from the same uniform freestream, then Eq. (8.39) holds throughout the entire flow, not just along a streamline.

For a calorically perfect gas, the ratio of total temperature to static temperature,  $T_0/T$ , is a function of Mach number only, as follows. From Eqs. (8.38) and (7.9), we have

$$\begin{aligned} \frac{T_0}{T} &= 1 + \frac{u^2}{2c_p T} = \frac{u^2}{1 + 2\gamma RT/(\gamma - 1)} = 1 + \frac{u^2}{2a^2/(\gamma - 1)} \\ &= 1 + \frac{\gamma - 1}{2} \left( \frac{u}{a} \right)^2 \end{aligned}$$

$$\boxed{\frac{T_0}{T} = 1 + \frac{\gamma - 1}{2} M^2} \quad (8.40)$$

Hence

$$\boxed{\frac{T_0}{T} = 1 + \frac{\gamma - 1}{2} M^2} \quad (8.40)$$

Equation (8.40) is very important; it states that only  $M$  (and, of course, the value of  $\gamma$ ) dictates the ratio of total temperature to static temperature.

Recall the definition of total pressure  $p_0$  and total density  $\rho_0$ , as discussed in Sec. 7.5. These definitions involve an *isentropic* compression of the flow to zero velocity. From Eq. (7.32), we have

$$\frac{p_0}{p} = \left( \frac{\rho_0}{\rho} \right)^\gamma = \left( \frac{T_0}{T} \right)^{\gamma/(\gamma-1)} \quad (8.41)$$

Combining Eqs. (8.40) and (8.41), we obtain

$$\begin{aligned} \frac{p_0}{p} &= \left( 1 + \frac{\gamma - 1}{2} M^2 \right)^{\gamma/(\gamma-1)} \\ &= \left( 1 + \frac{\gamma - 1}{2} M^2 \right)^{1/(\gamma-1)} \end{aligned}$$

Similar to the case of  $T_0/T$ , we see from Eqs. (8.42) and (8.43) that the total-to-static ratios  $p_0/p$  and  $\rho_0/\rho$  are determined by  $M$  and  $\gamma$  only. Hence, for a given gas (i.e., given  $\gamma$ ), the ratios  $T_0/T$ ,  $p_0/p$ , and  $\rho_0/\rho$  depend only on Mach number.

Equations (8.40), (8.42), and (8.43) are very important; they should be branded on your mind. They provide formulas from which the defined quantities  $T_0$ ,  $p_0$ , and  $\rho_0$  can be calculated from the actual conditions of  $M$ ,  $T$ ,  $p$ , and  $\rho$  at a given point in a general flow field (assuming a calorically perfect gas). They are so important that values of  $T_0/T$ ,  $p_0/p$ , and  $\rho_0/\rho$  obtained from Eqs. (8.40), (8.42), and (8.43), respectively, are tabulated as functions of  $M$  in App. A for  $\gamma = 1.4$  (which corresponds to air at standard conditions).

Consider a point in a general flow where the velocity is exactly sonic, i.e., where  $M = 1$ . Denote the static temperature, pressure, and density at this sonic condition as  $T^*$ ,  $p^*$ , and  $\rho^*$ , respectively. Inserting  $M = 1$  into Eqs. (8.40), (8.42), and (8.43), we obtain

$$\frac{T^*}{T_0} = \frac{2}{\gamma + 1}$$

$$\frac{P^*}{P_0} = \left( \frac{2}{\gamma + 1} \right)^{\gamma/(r-1)}$$

$$\frac{\rho^*}{\rho_0} = \left( \frac{2}{\gamma + 1} \right)^{1/(r-1)}$$
(8.44)

For  $\gamma = 1.4$ , these ratios are

$$\frac{T^*}{T_0} = 0.833 \quad \frac{P^*}{P_0} = 0.528 \quad \frac{\rho^*}{\rho_0} = 0.634$$

which are useful numbers to keep in mind for subsequent discussions.

We have one final item of business in this section. In Chap. 1 we defined the Mach number as  $M = V/a$  (or, following the one-dimensional notation in this chapter,  $M = u/a$ ). In turn, this allowed us to define several regimes of flow, among them being

- $M < 1$  (subsonic flow)
- $M = 1$  (sonic flow)
- $M > 1$  (supersonic flow)

In the definition of  $M$ ,  $a$  is the local speed of sound,  $a = \sqrt{\gamma RT}$ . In the theory of supersonic flow, it is sometimes convenient to introduce a "characteristic" Mach number,  $M^*$ , defined as

$$M^* \equiv \frac{u}{a^*}$$

where  $a^*$  is the value of the speed of sound at sonic conditions, *not* the actual local value. This is the same  $a^*$  introduced at the end of Sec. 7.5 and used in Eq. (8.35). The value of  $a^*$  is given by  $a^* = \sqrt{\gamma RT^*}$ . Let us now obtain a relation between the actual Mach number  $M$  and this defined characteristic Mach number  $M^*$ . Dividing Eq. (8.35) by  $u^2$ , we have

$$\frac{(a/u)^2}{\gamma - 1} + \frac{1}{2} = \frac{\gamma + 1}{2(\gamma - 1)} \left( \frac{a^*}{u} \right)^2$$

$$\frac{(1/M)^2}{\gamma - 1} = \frac{\gamma + 1}{2(\gamma - 1)} \left( \frac{1}{M^*} \right)^2 - \frac{1}{2}$$

$$M^2 = \frac{2}{(\gamma + 1)/M^* - (\gamma - 1)}$$
(8.47)

Equation (8.47) gives  $M$  as a function of  $M^*$ . Solving Eq. (8.47) for  $M^{*2}$ , we have

$$M^{*2} = \frac{(\gamma + 1)M^2}{2 + (\gamma - 1)M^2}$$
(8.48)

which gives  $M^*$  as a function of  $M$ . As can be shown by inserting numbers into Eq. (8.48) (try some yourself),

$$M^* = 1 \quad \text{if } M = 1$$

$$M^* < 1 \quad \text{if } M < 1$$

$$M^* > 1 \quad \text{if } M > 1$$

$$M^* \rightarrow \sqrt{\frac{\gamma + 1}{\gamma - 1}} \quad \text{if } M \rightarrow \infty$$

Therefore,  $M^*$  acts qualitatively in the same fashion as  $M$  except that  $M^*$  approaches a finite value when the actual Mach number approaches infinity.

In summary, a number of equations have been derived in this section, all of which stem in one fashion or another from the basic energy equation for steady, inviscid, adiabatic flow. Make certain that you understand these equations and become very familiar with them before progressing further. These equations are pivotal in the analysis of shock waves and in the study of compressible flow in general.

**Example 8.1** Consider a point in an airflow where the local Mach number, static pressure, and static temperature are 3.5, 0.3 atm, and 180 K, respectively. Calculate the local values of  $P_0$ ,  $T_0$ ,  $T^*$ ,  $a^*$ , and  $M^*$  at this point.

**SOLUTION** From App. A, for  $M = 3.5$ ,  $P_0/p = 76.27$  and  $T_0/T = 3.45$ . Hence,

$$P_0 = \left( \frac{P_0}{P} \right) P = 76.27(0.3 \text{ atm}) = 22.9 \text{ atm}$$

$$T_0 = \frac{T_0}{T} T = 3.45(180) = 621 \text{ K}$$

For  $M = 1$ ,  $T_0/T^* = 1.2$ . Hence,

$$T^* = \frac{T_0}{1.2} = \frac{621}{1.2} = 517.5 \text{ K}$$

$$a^* = \sqrt{\gamma R T^*} = \sqrt{1.4(287)(517.5)} = 456 \text{ m/s}$$

$$a = \sqrt{\gamma R T} = \sqrt{1.4(287)(180)} = 268.9 \text{ m/s}$$

$$V = Ma = 3.5(268.9) = 941 \text{ m/s}$$

$$M^* = \frac{V}{a^*} = \frac{941}{456} = 2.06$$

The above result for  $M^*$  can also be obtained directly from Eq. (8.48):

$$M^{*2} = \frac{(\gamma + 1)M^2}{2 + (\gamma - 1)M^2} = \frac{2.4(3.5)^2}{2 + 0.4(3.5)^2} = 4.26$$

Hence,  $M^* = \sqrt{4.26} = 2.06$ , as obtained above.

## 8.5 WHEN IS A FLOW COMPRESSIBLE?

As a corollary to Sec. 8.4, we are now in a position to examine the question, When does a flow have to be considered compressible, i.e., when do we have to use analyses based on Chaps. 7 to 14 rather than the incompressible techniques discussed in Chaps. 3 to 6? There is no specific answer to this question; for subsonic flows, it is a matter of the degree of accuracy desired whether we treat  $\rho$  as a constant or as a variable, whereas for supersonic flow the qualitative aspects of the flow are so different that the density *must* be treated as variable. We have stated several times in the preceding chapters the rule of thumb that a flow can be reasonably assumed to be incompressible when  $M < 0.3$ , whereas it should be considered compressible when  $M > 0.3$ . There is nothing magic about the value 0.3, but it is a convenient dividing line. We are now in a position to add substance to this rule of thumb.

Consider a fluid element initially at rest, say, an element of the air around you. The density of this gas at rest is  $\rho_0$ . Let us now accelerate this fluid element isentropically to some velocity  $V$  and Mach number  $M$ , say, by expanding the air through a nozzle. As the velocity of the fluid element increases, the other flow properties will change according to the basic governing equations derived in Chap. 7 and in this chapter. In particular, the density  $\rho$  of the fluid element will change according to Eq. (8.43):

$$\frac{\rho_0}{\rho} = \left(1 + \frac{\gamma - 1}{2} M^2\right)^{1/(\gamma - 1)} \quad (8.43)$$

For  $\gamma = 1.4$ , this variation is illustrated in Fig. 8.5, where  $\rho/\rho_0$  is plotted as a function of  $M$  from zero to sonic flow. Note that at low subsonic Mach numbers, the variation of  $\rho/\rho_0$  is relatively flat. Indeed, for  $M < 0.32$ , the value of  $\rho$  deviates from  $\rho_0$  by less than 5 percent, and for all practical purposes the flow can be treated as incompressible. However, for  $M > 0.32$ , the variation in  $\rho$  is larger than 5 percent, and its change becomes even more pronounced as  $M$  increases. As a result, many aerodynamicists have adopted the rule of thumb that the density variation should be accounted for at Mach numbers above 0.3; i.e., the flow should be treated as compressible. Of course, keep in mind that all flows, even at the lowest Mach numbers, are, strictly speaking, compressible. Incompressible flow is really a myth. However, as shown in Fig. 8.5, the *assumption* of incompressible flow is very reasonable at low Mach numbers. For this reason, the analyses in Chaps. 3 to 6 and the vast bulk of existing literature for incompressible flow are quite practical for many aerodynamic applications.

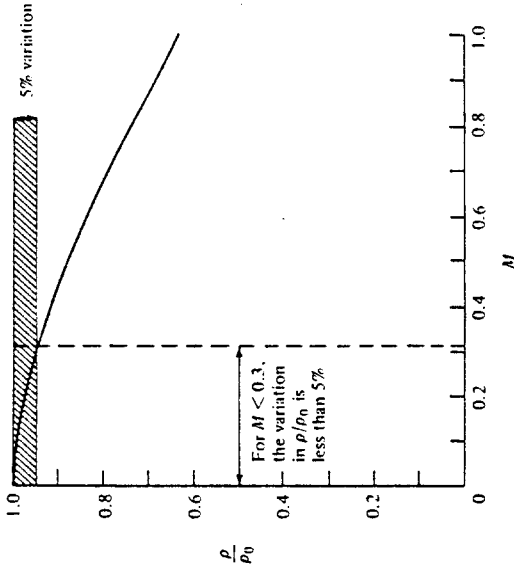


Figure 8.5 Isentropic variation of density with Mach number.

## 8.6 CALCULATION OF NORMAL SHOCK-WAVE PROPERTIES

Consider again the road map given in Fig. 8.2. We have finished our three side trips (Secs. 8.3 to 8.5) and are now ready to get back on the main road toward the calculation of changes of flow properties across a normal shock wave. Return again to Sec. 8.2, and recall the basic normal shock equations given by Eqs. (8.2), (8.6), and (8.10):

*Continuity:*  $\rho_1 u_1 = \rho_2 u_2 \quad (8.2)$

*Momentum:*  $p_1 + \rho_1 u_1^2 = p_2 + \rho_2 u_2^2 \quad (8.6)$

*Energy:*  $h_1 + \frac{u_1^2}{2} = h_2 + \frac{u_2^2}{2} \quad (8.10)$

In addition, for a calorically perfect gas, we have  

$$h_2 = c_p T_2 \quad (8.49)$$

$$p_2 = \rho_2 R T_2 \quad (8.50)$$

Return again to Fig. 8.3, and recall the basic normal shock-wave problem: given the conditions in region 1 ahead of the shock, calculate the conditions in region 2 behind the shock. Examining the five equations given above, we see that they involve five unknowns, namely,  $\rho_2$ ,  $u_2$ ,  $p_2$ ,  $h_2$ , and  $T_2$ . Hence, Eqs. (8.2), (8.6), (8.10), (8.49), and (8.50) are sufficient for determining the properties behind a normal shock wave in a calorically perfect gas. Let us proceed.

First, dividing Eq. (8.6) by (8.2),

$$\frac{p_1}{\rho_1 u_1} + u_1 = \frac{p_2}{\rho_2 u_2} + u_2 \quad (8.51)$$

$$\frac{p_1}{\rho_1 u_1} - \frac{p_2}{\rho_2 u_2} = u_2 - u_1$$

Recalling from Eq. (8.23) that  $a = \sqrt{\gamma p / \rho}$ , Eq. (8.51) becomes

$$\frac{a_1^2}{\gamma u_1} - \frac{a_2^2}{\gamma u_2} = u_2 - u_1 \quad (8.52)$$

Equation (8.52) is a combination of the continuity and momentum equations. The energy equation, Eq. (8.10), can be used in one of its alternate forms, namely, Eq. (8.35), rearranged below, and applied first in region 1 and then in region 2.

$$a_1^2 = \frac{\gamma + 1}{2} a^{*2} - \frac{\gamma - 1}{2} u_1^2 \quad (8.53)$$

$$a_2^2 = \frac{\gamma + 1}{2} a^{*2} - \frac{\gamma - 1}{2} u_2^2 \quad (8.54)$$

In Eqs. (8.53) and (8.54),  $a^*$  is the same constant value because the flow across the shock wave is adiabatic (see Secs. 7.5 and 8.4). Substituting Eqs. (8.53) and (8.54) into Eq. (8.52), we have

$$\frac{\gamma + 1}{2} \frac{a^{*2}}{\gamma u_1} - \frac{\gamma - 1}{2 \gamma} u_1 - \frac{\gamma + 1}{2} \frac{a^{*2}}{\gamma u_2} + \frac{\gamma - 1}{2 \gamma} u_2 = u_2 - u_1$$

$$\text{or } \frac{\gamma + 1}{2 \gamma u_1 u_2} (u_2 - u_1) a^{*2} + \frac{\gamma - 1}{2 \gamma} (u_2 - u_1) = u_2 - u_1$$

Dividing by  $u_2 - u_1$ ,

$$\frac{\gamma + 1}{2 \gamma u_1 u_2} a^{*2} + \frac{\gamma - 1}{2 \gamma} = 1$$

Solving for  $a^*$ , we obtain

$$a^{*2} = u_1 u_2 \quad (8.55)$$

Equation (8.55) is called the *Prandtl relation* and is a useful intermediate relation for normal shock waves. For example, from Eq. (8.55),

$$1 = \frac{u_1 u_2}{a^* a^*} \quad (8.56)$$

Recall the definition of characteristic Mach number,  $M^* = u/a^*$ , given in Sec. 8.4. Hence, Eq. (8.56) becomes

$$1 = M_1^* M_2^* \quad (8.64)$$

$$\text{or } M_2^* = \frac{1}{M_1^*} \quad (8.57)$$

Substituting Eq. (8.48) into (8.57), we have

$$\frac{(\gamma + 1) M_2^2}{2 + (\gamma - 1) M_2^2} = \left[ \frac{(\gamma + 1) M_1^2}{2 + (\gamma - 1) M_1^2} \right]^{-1} \quad (8.58)$$

Solving Eq. (8.58) for  $M_2^2$ ,

$$M_2^2 = \frac{1 + [(\gamma - 1)/2] M_1^2}{\gamma M_1^2 - (\gamma - 1)/2} \quad (8.59)$$

Equation (8.59) is our first major result for a normal shock wave. Examine Eq. (8.59) closely; it states that *the Mach number behind the wave,  $M_2$ , is a function only of the Mach number ahead of wave,  $M_1$* . Moreover, if  $M_1 = 1$ , then  $M_2 = 1$ . This is the case of an infinitely weak normal shock wave, defined as a *Mach wave*. Furthermore, for  $M_1 > 1$ , then  $M_2 < 1$ ; that is, the Mach number behind the normal shock wave is *subsonic*. As  $M_1$  increases above 1, the normal shock wave becomes stronger, and  $M_2$  becomes progressively less than 1. However, in the limit as  $M_1 \rightarrow \infty$ ,  $M_2$  approaches a finite minimum value,  $M_2 \rightarrow \sqrt{(\gamma - 1)/2\gamma}$ , which for air is 0.378.

Let us now obtain the ratios of the thermodynamic properties  $\rho_2/\rho_1$ ,  $p_2/p_1$ , and  $T_2/T_1$  across a normal shock wave. Rearranging Eq. (8.2) and using Eq. (8.55), we have

$$\frac{\rho_2}{\rho_1} = \frac{u_1}{u_2} = \frac{u_1^2}{u_2^2} = \frac{a_1^2}{a_2^2} = M_1^{*2} \quad (8.60)$$

Substituting Eq. (8.48) into (8.60), we obtain

$$\frac{\rho_2}{\rho_1} = \frac{u_1}{u_2} = \frac{(\gamma + 1) M_1^2}{2 + (\gamma - 1) M_1^2} \quad (8.61)$$

To obtain the pressure ratio, return to the momentum equation, Eq. (8.6), combined with the continuity equation, Eq. (8.2).

$$p_2 - p_1 = \rho_1 u_1^2 - \rho_2 u_2^2 = \rho_1 u_1 (u_1 - u_2) = \rho_1 u_1^2 \left( 1 - \frac{u_2}{u_1} \right) \quad (8.62)$$

Dividing Eq. (8.62) by  $p_1$ , and recalling that  $a_1^2 = \gamma p_1 / \rho_1$ , we obtain

$$\frac{p_2 - p_1}{p_1} = \frac{\gamma \rho_1 u_1^2}{\gamma p_1} \left( 1 - \frac{u_2}{u_1} \right) = \frac{\gamma u_1^2}{a_1^2} \left( 1 - \frac{u_2}{u_1} \right) = \gamma M_1^2 \left( 1 - \frac{u_2}{u_1} \right) \quad (8.63)$$

For  $u_2/u_1$  in Eq. (8.63), substitute Eq. (8.61):

$$\frac{p_2 - p_1}{p_1} = \gamma M_1^2 \left[ 1 - \frac{2 + (\gamma - 1) M_1^2}{(\gamma + 1) M_1^2} \right] \quad (8.64)$$

Equation (8.64) simplifies to

$$\boxed{\frac{p_2}{p_1} = 1 + \frac{2\gamma}{\gamma + 1} (M_1^2 - 1)}$$

To obtain the temperature ratio, recall the equation of state  $p = \rho RT$ . Hence,

$$\boxed{\frac{T_2}{T_1} = \left( \frac{p_2}{p_1} \right) \left( \frac{\rho_1}{\rho_2} \right)} \quad (8.65)$$

Substituting Eqs. (8.61) and (8.65) into (8.66), and recalling that  $h = c_p T$ , we obtain

$$\boxed{\frac{T_2}{T_1} = \frac{h_2}{h_1} = \left[ 1 + \frac{2\gamma}{\gamma + 1} (M_1^2 - 1) \right] \frac{2 + (\gamma - 1)M_1^2}{(\gamma + 1)M_1^2}} \quad (8.67)$$

Equations (8.61), (8.65), and (8.67) are important. Examine them closely. Note that  $\rho_2/\rho_1$ ,  $p_2/p_1$ , and  $T_2/T_1$  are *functions of the upstream Mach number  $M_1$  only*. Therefore, in conjunction with Eq. (8.59) for  $M_2$ , we see that the upstream Mach number  $M_1$  is the determining parameter for changes across a normal shock wave in a calorically perfect gas. This is a dramatic example of the power of Mach number as a governing parameter in compressible flows. In the above equations, if  $M_1 = 1$ , then  $p_2/p_1 = \rho_2/\rho_1 = T_2/T_1 = 1$ ; that is, we have the case of a normal shock wave of vanishing strength — a Mach wave. As  $M_1$  increases above 1,  $p_2/p_1$ ,  $\rho_2/\rho_1$ , and  $T_2/T_1$  progressively increase above 1. In the limiting case of  $M_1 \rightarrow \infty$  in Eqs. (8.59), (8.61), (8.65), and (8.67), we find, for  $\gamma = 1.4$ ,

$$\lim_{M_1 \rightarrow \infty} M_2 = \sqrt{\frac{\gamma - 1}{2\gamma}} = 0.378 \quad (\text{as discussed previously})$$

$$\lim_{M_1 \rightarrow \infty} \frac{\rho_2}{\rho_1} = \frac{\gamma + 1}{\gamma - 1} = 6$$

$$\lim_{M_1 \rightarrow \infty} \frac{p_2}{p_1} = \infty \quad \lim_{M_1 \rightarrow \infty} \frac{T_2}{T_1} = \infty$$

Note that, as the upstream Mach number increases toward infinity, the pressure and temperature increase without bound, whereas the density approaches a rather moderate finite limit.

We have stated earlier that shock waves occur in supersonic flows; a stationary normal shock such as shown in Fig. 8.3 does not occur in subsonic flow. That is, in Eqs. (8.59), (8.61), (8.65), and (8.67), the upstream Mach number is supersonic,  $M_1 \geq 1$ . However, on a *mathematical basis*, these equations also allow solutions for  $M_1 \leq 1$ . These equations embody the continuity, momentum, and energy equations, which in principle do not care whether the value of  $M_1$  is subsonic or supersonic. Here is an ambiguity which can only be resolved by appealing to the second law of thermodynamics (see Sec. 7.2). Recall that the second law determines the *direction* which a

given process can take. Let us apply the second law to the flow across a normal shock wave, and examine what it tells us about allowable values of  $M_1$ .

First, consider the entropy change across the normal shock wave. From Eq. (7.25),

$$\boxed{s_2 - s_1 = c_p \ln \frac{T_2}{T_1} - R \ln \frac{p_2}{p_1}} \quad (7.25)$$

with Eqs. (8.65) and (8.67), we have

$$\begin{aligned} s_2 - s_1 &= c_p \ln \left\{ \left[ 1 + \frac{2\gamma}{\gamma + 1} (M_1^2 - 1) \right] \frac{2 + (\gamma - 1)M_1^2}{(\gamma + 1)M_1^2} \right\} \\ &\quad - R \ln \left[ 1 + \frac{2\gamma}{\gamma + 1} (M_1^2 - 1) \right] \end{aligned} \quad (8.68)$$

From Eq. (8.68), we see that the entropy change  $s_2 - s_1$  across the shock is a function of  $M_1$  only. The second law dictates that

$$s_2 - s_1 \geq 0$$

In Eq. (8.68), if  $M_1 = 1$ ,  $s_2 = s_1$ , and if  $M_1 > 1$ , then  $s_2 - s_1 > 0$ , both of which obey the second law. However, if  $M_1 < 1$ , then Eq. (8.68) gives  $s_2 - s_1 < 0$ , which is *not* allowed by the second law. Consequently, in nature, only cases involving  $M_1 \geq 1$  are valid; i.e., normal shock waves can occur only in supersonic flow.

Why does the entropy increase across the shock wave? The second law tells us that it must, but what mechanism does nature use to accomplish this increase? To answer these questions, recall that a shock wave is a very thin region (on the order of  $10^{-5}$  cm) across which some large changes occur almost discontinuously. Therefore, within the shock wave itself, large gradients in velocity and temperature occur; i.e., the mechanisms of friction and thermal conduction are strong. These are dissipative, irreversible mechanisms that always increase the entropy. Therefore, the precise entropy increase predicted by Eq. (8.68) for a given supersonic  $M_1$  is appropriately provided by nature in the form of friction and thermal conduction within the interior of the shock wave itself.

In Sec. 7.5, we defined the total temperature  $T_0$  and total pressure  $p_0$ . What happens to these total conditions across a shock wave? To help answer this question, consider Fig. 8.6, which illustrates the definition of total conditions ahead of and behind the shock. In region 1 ahead of the shock, a fluid element has the actual conditions of  $M_1$ ,  $p_1$ ,  $T_1$ , and  $s_1$ . Now imagine that we bring this fluid element to rest isentropically, creating the “imaginary” state 1a ahead of the shock. In state 1a, the fluid element at rest would have a pressure and temperature  $p_{01}$  and  $T_{01}$ , respectively, i.e., the total pressure and total temperature, respectively, in region 1. The entropy in state 1a would still be  $s_1$  because the fluid element is brought to rest isentropically;  $s_{1a} = s_1$ . Now consider region 2 behind the shock. Again consider a fluid element with the actual conditions of  $M_2$ ,  $p_2$ ,  $T_2$ , and  $s_2$ , as sketched in Fig. 8.6. And again let us imagine that we bring this fluid element to rest isentropically, creating the “imaginary” state 2a behind the shock. In state 2a, the fluid element at rest would have pressure and temperature  $p_{02}$  and  $T_{02}$ , respectively, i.e., the total pressure and total temperature,

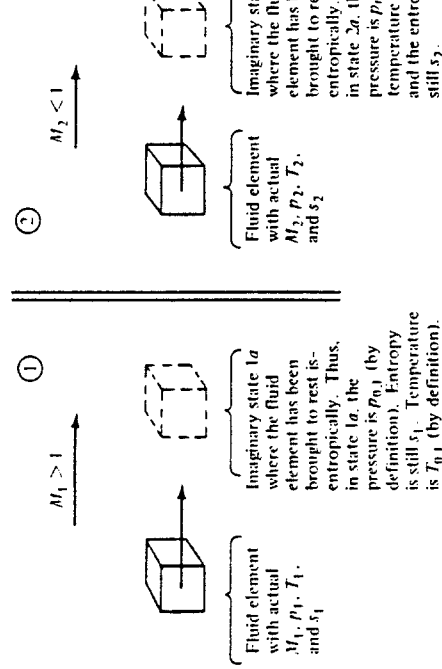


Figure 8.6 Total conditions ahead of and behind a normal shock wave.

respectively, in region 2. The entropy in state 2a would still be  $s_2$  because the fluid element is brought to rest isentropically;  $s_{2a} = s_2$ . The questions are now asked: How does  $T_{0,2}$  compare with  $T_{0,1}$ , and how does  $p_{0,2}$  compare with  $p_{0,1}$ ?

To answer the first of these questions, consider Eq. (8.30):

$$c_p T_1 + \frac{u_1^2}{2} = c_p T_2 + \frac{u_2^2}{2} \quad (8.30)$$

From Eq. (8.38), the total temperature is given by

$$c_p T_0 = c_p T + \frac{u^2}{2} \quad (8.38)$$

Combining Eqs. (8.30) and (8.38), we have

$$c_p T_{0,1} = c_p T_{0,2}$$

or

$$T_{0,1} = T_{0,2}$$

Equation (8.69) states that *total temperature is constant across a stationary normal shock wave*. This should come as no surprise; the flow across a shock wave is adiabatic, and in Sec. 7.5 we demonstrated that in a steady, adiabatic, inviscid flow of a calorically perfect gas, the total temperature is constant.

To examine the variation of total pressure across a normal shock wave, write Eq. (7.25) between the imaginary states 1a and 2a:

$$s_{2a} - s_{1a} = c_p \ln \frac{T_{2a}}{T_{1a}} - R \ln \frac{p_{2a}}{p_{1a}} \quad (8.70)$$

However, from the above discussion, as well as the sketch in Fig. 8.6, we have  $s_{2a} = s_2$ ,  $s_{1a} = s_1$ ,  $T_{2a} = T_{0,2}$ ,  $T_{1a} = T_{0,1}$ ,  $p_{2a} = p_{0,2}$ , and  $p_{1a} = p_{0,1}$ . Thus, Eq. (8.70) becomes

$$s_2 - s_1 = c_p \ln \frac{T_{0,2}}{T_{0,1}} - R \ln \frac{p_{0,2}}{p_{0,1}} \quad (8.71)$$

We have already shown that  $T_{0,2} = T_{0,1}$ ; hence, Eq. (8.71) yields

$$s_2 - s_1 = -R \ln \frac{p_{0,2}}{p_{0,1}} \quad (8.72)$$

$$\frac{p_{0,2}}{p_{0,1}} = e^{-(s_2 - s_1)/R} \quad (8.73)$$

From Eq. (8.68), we know that  $s_2 - s_1 > 0$  for a normal shock wave. Hence, Eq. (8.73) states that  $p_{0,2} < p_{0,1}$ . *The total pressure decreases across a shock wave*. Moreover, since  $s_2 - s_1$  is a function of  $M_1$  only [from Eq. (8.68)], then Eq. (8.73) clearly states that the total pressure ratio  $p_{0,2}/p_{0,1}$  across a normal shock wave is a function of  $M_1$  only.

In summary, we have now verified the qualitative changes across a normal shock wave as sketched in Fig. 7.4b and as originally discussed in Sec. 7.6. Moreover, we have obtained closed-form analytic expressions for these changes in the case of a calorically perfect gas. We have seen that  $p_2/p_1$ ,  $\rho_2/\rho_1$ ,  $T_2/T_1$ ,  $M_2$ , and  $p_{0,2}/p_{0,1}$  are functions of the upstream Mach number  $M_1$  only. To help you obtain a stronger physical feeling of normal shock-wave properties, these variables are plotted in Fig. 8.7 as a function of  $M_1$ . Note that (as stated earlier) these curves show how, as  $M_1$  becomes very large,  $T_2/T_1$  and  $p_2/p_1$  also become very large, whereas  $\rho_2/\rho_1$  and  $M_2$  approach finite limits. Examine Fig. 8.7 carefully, and become comfortable with the trends shown. The results given by Eqs. (8.59), (8.61), (8.65), (8.67), and (8.73) are so important that they are tabulated as a function of  $M_1$  in App. B for  $\gamma = 1.4$ .

**Example 8.2** Consider a normal shock wave in air where the upstream flow properties are  $u_1 = 680$  m/s,  $T_1 = 288$  K, and  $p_1 = 1$  atm. Calculate the velocity, temperature, and pressure downstream of the shock.

**SOLUTION**

$$a_1 = \sqrt{\gamma R T_1} = \sqrt{1.4(287)(288)} = 340 \text{ m/s}$$

$$M_1 = \frac{u_1}{a_1} = \frac{680}{340} = 2$$

From App. B, since  $p_2/p_1 = 4.5$ ,  $T_2/T_1 = 1.687$ ,  $M_2 = 0.5774$ , then

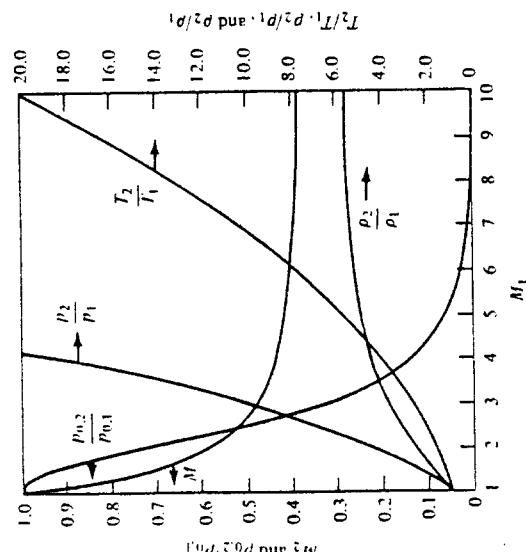


Figure 8.7 The variation of properties across a normal shock wave as a function of upstream Mach number:  
 $\gamma = 1.4$ .

$$\begin{aligned} p_2 &= \frac{p_2}{p_1} p_1 = 4.5(1 \text{ atm}) = [4.5 \text{ atm}] \\ T_2 &= \frac{T_2}{T_1} T_1 = 1.687(288) = [486 \text{ K}] \\ a_2 &= \sqrt{\gamma R T_2} = \sqrt{1.4(287)(486)} = 442 \text{ m/s} \\ u_2 &= M_1 a_1 = 0.5774(486) = [255 \text{ m/s}] \end{aligned}$$

## 8.7 MEASUREMENT OF VELOCITY IN A COMPRESSIBLE FLOW

The use of a Pitot tube for measuring the velocity of a low-speed, incompressible flow was discussed in Sec. 3.4. Before progressing further, return to Sec. 3.4, and review the principal aspects of a Pitot tube, as well as the formulas used to obtain the flow velocity from the Pitot pressure, assuming incompressible flow.

For low-speed, incompressible flow, we saw in Sec. 3.4 that the velocity can be obtained from a knowledge of both the total pressure and the static pressure at a point. The total pressure is measured by a Pitot tube, and the static pressure is obtained from a static pressure orifice or by some independent means. The important aspect of Sec. 3.4 is that the pressure sensed by a Pitot tube, along with the static pressure, is all that is necessary to extract the flow velocity for an incompressible flow. In the present section, we see that the same is true for a compressible flow, both subsonic and supersonic, if we consider the Mach number rather than the velocity. In both subsonic and supersonic compressible flows, a knowledge of the Pitot pressure and the static

pressure is sufficient to calculate Mach number, although the formulas are different for each Mach-number regime. Let us examine this matter further.

### Subsonic Compressible Flow

Consider a Pitot tube in a subsonic, compressible flow, as sketched in Fig. 8.8a. As usual, the mouth of the Pitot tube (point *b*) is a stagnation region. Hence, a fluid element moving along streamline *ab* is brought to rest isentropically at point *b*. In turn, the pressure sensed at point *b* is the total pressure of the freestream,  $p_{0,1}$ . This is the Pitot pressure read at the end of the tube. If, in addition, we know the freestream static pressure  $p_1$ , then the Mach number in region 1 can be obtained from Eq. (8.42),

$$\frac{p_{0,1}}{p_1} = \left(1 + \frac{\gamma - 1}{2} M_1^2\right)^{\gamma/(y-1)} \quad (8.42)$$

or solving for  $M_1^2$ ,

$$M_1^2 = \frac{2}{\gamma - 1} \left[ \left( \frac{p_{0,1}}{p_1} \right)^{(y-1)/y} - 1 \right] \quad (8.74)$$

Clearly, from Eq. (8.74), the Pitot pressure  $p_{0,1}$  and the static pressure  $p_1$  allow the direct calculation of Mach number.

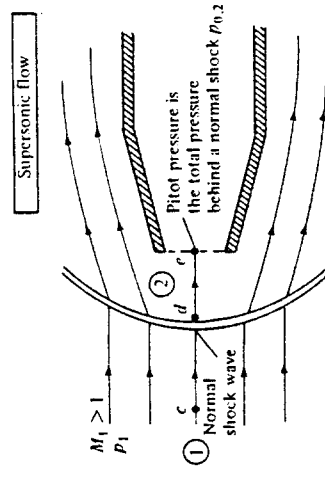
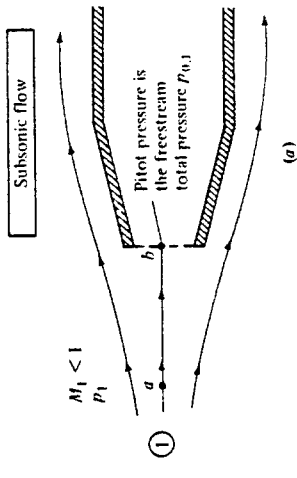


Figure 8.8 A Pitot tube in (a) subsonic flow and (b) supersonic flow.

(b)

The flow velocity can be obtained from Eq. (8.74) by recalling that  $M_1 = u_1/a_1$ . Hence,

$$u_1^2 = \frac{2a_1^2}{\gamma - 1} \left[ \left( \frac{p_{0,1}}{p_1} \right)^{\gamma/(1-\gamma)} - 1 \right] \quad (8.75)$$

From Eq. (8.75), we see that, unlike incompressible flow, a knowledge of  $p_{0,1}$  and  $p_1$  is not sufficient to obtain  $u_1$ ; we also need the freestream speed of sound,  $a_1$ .

### Supersonic Flow

Consider a Pitot tube in a supersonic freestream, as sketched in Fig. 8.8b. As usual, the mouth of the Pitot tube (point *e*) is a stagnation region. Hence, a fluid element moving along streamline *cde* is brought to rest at point *e*. However, because the freestream is supersonic and the Pitot tube presents an obstruction to the flow, there is a strong bow shock wave in front of the tube, much like the picture shown at the left of Fig. 8.1 for supersonic flow over a blunt body. Hence, streamline *cde* crosses the normal portion of the bow shock. A fluid element moving along streamline *cde* will first be decelerated *nonisentropically* to a subsonic velocity at point *d* just behind the shock. Then it is isentropically compressed to zero velocity at point *e*. As a result, the pressure at point *e* is *not* the total pressure of the freestream but rather the total pressure *behind a normal shock wave*,  $p_{0,2}$ . This is the Pitot pressure read at the end of the tube. Keep in mind that because of the entropy increase across the shock, there is a loss in total pressure across the shock,  $p_{0,2} < p_{0,1}$ . However, knowing  $p_{0,2}$  and the freestream static pressure  $p_1$  is still sufficient to calculate the freestream Mach number  $M_1$ , as follows:

$$\frac{p_{0,2}}{p_1} = \frac{p_{0,2}/p_2}{p_2/p_1} \quad (8.76)$$

Here,  $p_{0,2}/p_2$  is the ratio of total pressure to static pressure in region 2 immediately behind the normal shock, and  $p_2/p_1$  is the static pressure ratio across the shock. From Eq. (8.42),

$$\frac{p_{0,2}}{p_2} = \left( 1 + \frac{\gamma - 1}{2} M_1^2 \right)^{\gamma/(1-\gamma)} \quad (8.77)$$

where, from Eq. (8.59),

$$M_1^2 = \frac{1 + [(\gamma - 1)/2] M_1^2}{\gamma M_1^2 - (\gamma - 1)/2} \quad (8.78)$$

Also, from Eq. (8.65),

$$\frac{p_2}{p_1} = 1 + \frac{2}{\gamma + 1} (M_1^2 - 1) \quad (8.79)$$

Substituting Eq. (8.78) into (8.77), and substituting the result as well as Eq. (8.79) into Eq. (8.76), we obtain, after some algebraic simplification (see Prob. 8.14),

$$\boxed{\frac{p_{0,2}}{p_1} = \left( \frac{(\gamma + 1)^2 M_1^2}{4 \gamma M_1^2 - 2(\gamma - 1)} \right)^{\gamma/(1-\gamma)} \frac{1 - \gamma + 2\gamma M_1^2}{\gamma + 1}} \quad (8.80)$$

Equation (8.80) is called the *Rayleigh Pitot tube formula*. It relates the Pitot pressure  $p_{0,2}$  and the freestream static pressure  $p_1$  to the freestream Mach number  $M_1$ . Equation (8.80) gives  $M_1$  as an implicit function of  $p_{0,2}/p_1$  and allows the calculation of  $M_1$  from a known  $p_{0,2}/p_1$ . For convenience in making calculations, the ratio  $p_{0,2}/p_1$  is tabulated versus  $M_1$  in App. B.

**Example 8.3** A Pitot tube is inserted into an airflow where the static pressure is 1 atm. Calculate the flow Mach number when the Pitot tube measures (a) 1.276 atm, (b) 2.714 atm, (c) 12.06 atm.

**SOLUTION** First, we must assess whether the flow is subsonic or supersonic. At Mach 1, the Pitot tube would measure  $p_0 = p/0.528 = 1.893 p$ . Hence, when  $p_0 < 1.893$  atm, the flow is subsonic, and when  $p_0 > 1.893$  atm, the flow is supersonic.

(a) Pitot tube measurement = 1.276 atm. The flow is subsonic. Hence, the Pitot tube is directly sensing the total pressure of the flow. From App. A, for  $p_0/p = 1.276$ ,  $\boxed{M = 0.6}$ .

(b) Pitot tube measurement = 2.714 atm. The flow is supersonic. Hence, the Pitot tube is sensing the total pressure behind a normal shock wave. From App. B, for  $p_{0,2}/p_1 = 2.714$ ,  $\boxed{M_1 = 1.3}$ .

(c) Pitot tube measurement = 12.06 atm. The flow is supersonic. From App. B, for  $p_{0,2}/p_1 = 12.06$ ,  $\boxed{M_1 = 3.0}$ .

## 8.8 SUMMARY

Return to the road map given in Fig. 8.2, and make certain that you are comfortable with the areas we have covered in this chapter. A brief summary of the more important relations is given below.

$$\boxed{a = \sqrt{\left( \frac{\partial p}{\partial \rho} \right)_s}} \quad (8.18)$$

For a calorically perfect gas,

$$\boxed{a = \sqrt{\frac{\gamma p}{\rho}}} \quad (8.23)$$

or

$$\boxed{a = \sqrt{\gamma R T}} \quad (8.25)$$

The speed of sound depends only on the gas temperature.

For a steady, adiabatic, inviscid flow, the energy equation can be expressed as

$$h_1 + \frac{u_1^2}{2} = h_2 + \frac{u_2^2}{2} \quad (8.29)$$

$$c_p T_1 + \frac{u_1^2}{2} = c_p T_2 + \frac{u_2^2}{2} \quad (8.30)$$

$$\frac{a_1^2}{\gamma - 1} + \frac{u_1^2}{2} = \frac{a_2^2}{\gamma - 1} + \frac{u_2^2}{2} \quad (8.32)$$

$$\frac{a^2}{\gamma - 1} + \frac{u^2}{2} = \frac{a_0^2}{\gamma - 1} \quad (8.33)$$

$$\frac{a^2}{\gamma - 1} + \frac{u^2}{2} = \frac{\gamma + 1}{2(\gamma - 1)} a^{*2} \quad (8.35)$$

Total conditions in a flow are related to static conditions via

$$c_p T + \frac{u^2}{2} = c_p T_0 \quad (8.38)$$

$$\frac{T_0}{T} = 1 + \frac{\gamma - 1}{2} M^2 \quad (8.40)$$

$$\frac{p_0}{p} = \left(1 + \frac{\gamma - 1}{2} M^2\right)^{\gamma/(\gamma-1)} \quad (8.42)$$

$$\frac{\rho_0}{\rho} = \left(1 + \frac{\gamma - 1}{2} M^2\right)^{1/(\gamma-1)} \quad (8.43)$$

Note that the ratios of total to static properties are a function of local Mach number only. These functions are tabulated in App. A.

The basic normal shock equations are

**Continuity:**  $\rho_1 u_1 = \rho_2 u_2 \quad (8.2)$

**Momentum:**  $p_1 + \rho_1 u_1^2 = p_2 + \rho_2 u_2^2 \quad (8.6)$

**Energy:**  $h_1 + \frac{u_1^2}{2} = h_2 + \frac{u_2^2}{2} \quad (8.10)$

These equations lead to relations for changes across a normal shock as a function of upstream Mach number  $M_1$  only.

$$M_2^2 = \frac{1 + [(\gamma - 1)/2] M_1^2}{\gamma M_1^2 - (\gamma - 1)/2} \quad (8.59)$$

$$\frac{p_2}{p_1} = \frac{u_1}{u_2} = \frac{(\gamma + 1) M_1^2}{2 + (\gamma - 1) M_1^2} \quad (8.61)$$

$$\frac{p_2}{p_1} = 1 + \frac{2\gamma}{\gamma + 1} (M_1^2 - 1) \quad (8.65)$$

$$\frac{T_2}{T_1} = \frac{h_2}{h_1} = \left[1 + \frac{2\gamma}{\gamma + 1} (M_1^2 - 1)\right] \frac{2 + (\gamma - 1) M_1^2}{(\gamma + 1) M_1^2} \quad (8.67)$$

$$\begin{aligned} s_2 - s_1 &= c_p \ln \left\{ \left[1 + \frac{2\gamma}{\gamma + 1} (M_1^2 - 1)\right] \frac{2 + (\gamma - 1) M_1^2}{(\gamma + 1) M_1^2} \right\} \\ &\quad - R \ln \left[ 1 + \frac{2\gamma}{\gamma + 1} (M_1^2 - 1) \right] \end{aligned} \quad (8.68)$$

$$\frac{p_{0,2}}{p_{0,1}} = e^{-(s_2 - s_1)/R} \quad (8.73)$$

The normal shock properties are tabulated versus  $M_1$  in App. B.

For a calorically perfect gas, the total temperature is constant across a normal shock wave.

$$T_{0,2} = T_{0,1}$$

However, there is a loss in total pressure across the wave.

$$p_{0,2} < p_{0,1}$$

For subsonic and supersonic compressible flow, the freestream Mach number is determined by the ratio of Pitot pressure to freestream static pressure. However, the equations are different.

**Subsonic flow:**  $M_1^2 = \frac{2}{\gamma - 1} \left[ \left( \frac{p_{0,1}}{p_1} \right)^{(\gamma-1)/\gamma} - 1 \right] \quad (8.74)$

**Supersonic flow:**  $\frac{p_{0,2}}{p_1} = \left[ \frac{(\gamma + 1)^2 M_1^2}{4 \gamma M_1^2 - 2(\gamma - 1)} \right]^{\gamma/(\gamma-1)} \frac{1 - \gamma + 2\gamma M_1^2}{\gamma + 1} \quad (8.80)$

**PROBLEMS**

8.1 Consider air at a temperature of 230 K. Calculate the speed of sound.

8.2 The temperature in the reservoir of a supersonic wind tunnel is 519°R. In the test section, the flow velocity is 1385 ft/s. Calculate the test-section Mach number. Assume the tunnel flow is adiabatic.

8.3 At a given point in a flow,  $T = 300$  K,  $p = 1.2$  atm, and  $V = 250$  m/s. At this point, calculate the corresponding values of  $p_0$ ,  $T_0$ ,  $p^*$ ,  $T^*$ , and  $M^*$ .

8.4 At a given point in a flow,  $T = 700$  R,  $p = 1.6$  atm, and  $V = 2983$  ft/s. At this point, calculate the corresponding values of  $p_0$ ,  $T_0$ ,  $p^*$ ,  $T^*$ , and  $M^*$ .

8.5 Consider the isentropic flow through a supersonic nozzle. If the test-section conditions are given by  $p = 1$  atm,  $T = 230$  K, and  $M = 2$ , calculate the reservoir pressure and temperature.

8.6 Consider the isentropic flow over an airfoil. The freestream conditions correspond to a standard altitude of 10,000 ft and  $M_\infty = 0.82$ . At a given point on the airfoil,  $M = 1.0$ . Calculate  $p$  and  $T$  at this point. (Note: You will have to consult a standard atmosphere table for this problem, such as given in Ref. 2. If you do not have one, you can find such tables in any good technical library.)

8.7 The flow just upstream of a normal shock wave is given by  $p_1 = 1$  atm,  $T_1 = 288$  K, and  $M_1 = 2.6$ . Calculate the following properties just downstream of the shock:  $p_2$ ,  $T_2$ ,  $\rho_2$ ,  $M_2$ ,  $p_{02}$ ,  $T_{02}$ , and the change in entropy across the shock.

8.8 The pressure upstream of a normal shock wave is 1 atm. The pressure and temperature downstream of the wave are 10.33 atm and 1390°R, respectively. Calculate the Mach number and temperature upstream of the wave and the total temperature and total pressure downstream of the wave.

8.9 The entropy increase across a normal shock wave is  $199.5 \text{ J/(kg} \cdot \text{K)}$ . What is the upstream Mach number?

8.10 The flow just upstream of a normal shock wave is given by  $p_1 = 1800 \text{ lb/ft}^2$ ,  $T_1 = 480^\circ\text{R}$ , and  $M_1 = 3.1$ . Calculate the velocity and  $M^*$  behind the shock.

8.11 Consider a flow with a pressure and temperature of 1 atm and 288 K. A Pitot tube is inserted into this flow and measures a pressure of 1.555 atm. What is the velocity of the flow?

8.12 Consider a flow with a pressure and temperature of  $2116 \text{ lb/ft}^2$  and  $519^\circ\text{R}$ , respectively. A Pitot tube is inserted into this flow and measures a pressure of  $7712.8 \text{ lb/ft}^2$ . What is the velocity of this flow?

8.13 Repeat Probs. 8.11 and 8.12 using (incorrectly) Bernoulli's equation for incompressible flow. Calculate the percent error induced by using Bernoulli's equation.

8.14 Derive the Rayleigh Pitot tube formula, Eq. (8.80).

## OBLIQUE SHOCK AND EXPANSION WAVES

### CHAPTER NINE

*In the case of air (and the same is true for all gases) the shock wave is extremely thin so that calculations based on one-dimensional flow are still applicable for determining the changes in velocity and density on passing through it, even when the rest of the flow system is not limited to one dimension, provided that only the velocity component normal to the wave is considered.*

G. I. Taylor and J. W. MacColl, 1934

### 9.1 INTRODUCTION

In Chap. 8 we discussed normal shock waves, i.e., shock waves that make an angle of 90° with the upstream flow. The behavior of normal shock waves is important; moreover, the study of normal shock waves provides a relatively straightforward introduction to shock-wave phenomena. However, examining Fig. 7.4a and the photographs shown in Fig. 7.5, we see that, in general, a shock wave will make an oblique angle with respect to the upstream flow. These are called *oblique shock waves* and are the subject of part of this chapter. A normal shock wave is simply a special case of the general family of oblique shocks, namely, the case where the wave angle is 90°.

In addition to oblique shock waves, where the pressure increases discontinuously across the wave, supersonic flows are also characterized by oblique expansion waves, where the pressure *decreases continuously* across the wave. Let us examine these two types of waves further. Consider a supersonic flow over a wall with a corner at point A, as sketched in Fig. 9.1. In Fig. 9.1a, the wall is turned upward at the corner through the deflection angle  $\theta$ , i.e., the corner is concave. The flow at the wall must be tangent to the wall; hence, the streamline at the wall is also deflected upward through the angle  $\theta$ . The bulk of the gas is above the wall, and in Fig. 9.1a, the streamlines are turned upward, *into* the main bulk of the flow. Whenever a supersonic flow is "turned into itself" as shown in Fig. 9.1a, an oblique shock wave will occur. The originally horizontal streamlines ahead of the wave are uniformly deflected in crossing the wave, such that the streamlines behind the wave are parallel to each other and inclined upward at the deflection angle  $\theta$ . Across the wave, the Mach number discontinuously decreases, and the pressure, density, and temperature discontinuously increase. In contrast,

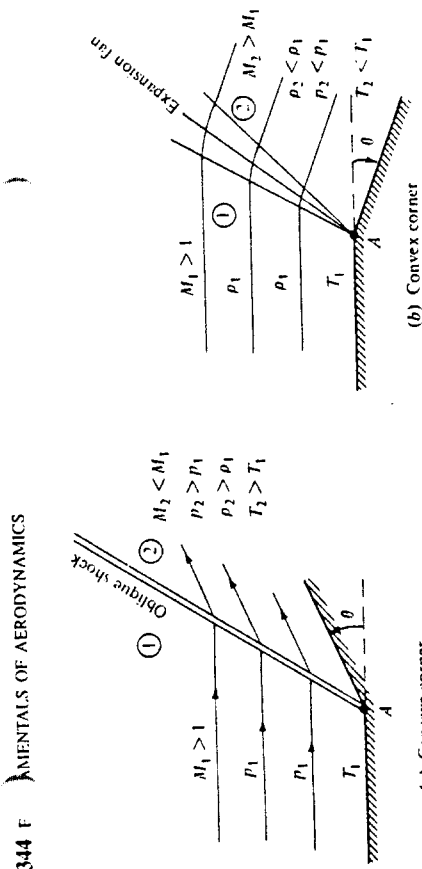


Figure 9.1 Supersonic flow over a corner.

Fig. 9.1b shows the case where the wall is turned downward at the corner through the deflection angle  $\theta$ , i.e., the corner is convex. Again, the flow at the wall must be tangent to the wall; hence, the streamline at the wall is deflected downward through the angle  $\theta$ . The bulk of the gas is above the wall, and in Fig. 9.1b, the streamlines are turned downward, away from the main bulk of the flow. Whenever a supersonic flow is "turned away from itself" as shown in Fig. 9.1b, an expansion wave will occur. This expansion wave is in the shape of a fan centered at the corner. The fan continuously opens in the direction away from the corner, as shown in Fig. 9.1b. The originally horizontal streamlines ahead of the expansion wave are deflected smoothly and continuously through the expansion fan such that the streamlines behind the wave are parallel to each other and inclined downward at the deflection angle  $\theta$ . Across the expansion wave, the Mach number increases, and the pressure, temperature, and density decrease. Hence, an expansion wave is the direct antithesis of a shock wave.

Oblique shock and expansion waves are prevalent in two- and three-dimensional supersonic flows. These waves are inherently two-dimensional in nature, in contrast to the one-dimensional normal shock waves discussed in Chap. 8. That is, in Fig. 9.1a and b, the flow-field properties are a function of  $x$  and  $y$ . The purpose of the present chapter is to determine and study the properties of these oblique waves.

What is the physical mechanism that creates waves in a supersonic flow? To address this question, recall our picture of the propagation of a sound wave via molecular collisions, as portrayed in Sec. 8.3. If a slight disturbance takes place at some point in a gas, information is transmitted to other points in the gas by sound waves which propagate in all directions away from the source of the disturbance. Now consider a body in a flow, as sketched in Fig. 9.2. The gas molecules which impact the body surface experience a change in momentum. In turn, this change is transmitted to neighboring molecules by random molecular collisions. In this fashion, information about the presence of the body attempts to be transmitted to the surrounding flow via molecular collisions; i.e., the information is propagated upstream at approximately the local speed of sound. If the upstream flow is subsonic, as shown in Fig. 9.2a, the disturbances have no problem working their way far upstream, thus giving the incoming

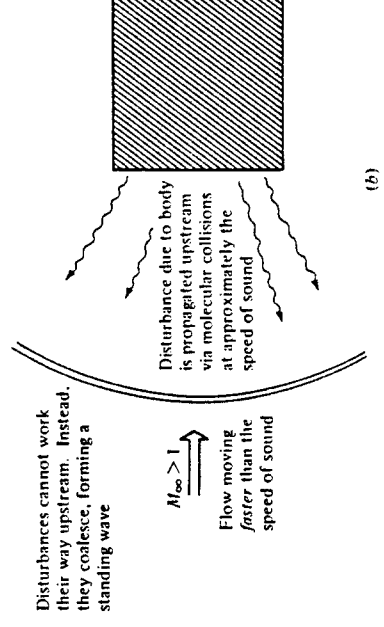


Figure 9.2 Propagation of disturbances. (a) Subsonic flow. (b) Supersonic flow.

flow plenty of time to move out of the way of the body. On the other hand, if the upstream flow is supersonic, as shown in Fig. 9.2b, the disturbances cannot work their way upstream; rather, at some finite distance from the body, the disturbance waves pile up and coalesce, forming a standing wave in front of the body. Hence, the physical generation of waves in a supersonic flow — both shock and expansion waves — is due to the propagation of information via molecular collisions and due to the fact that such propagation cannot work its way into certain regions of the supersonic flow.

Why are most waves oblique rather than normal to the upstream flow? To answer this question, consider a small source of disturbance moving through a stagnant gas. For lack of anything better, let us call this disturbance source a "beeper," which periodically emits sound. First, consider the beeper moving at subsonic speed through the gas, as shown in Fig. 9.3a. The speed of the beeper is  $V$ , where  $V < a$ . At time  $t = 0$ , the beeper is located at point A; at this point, it emits a sound wave which propagates in all directions at the speed of sound,  $a$ . At a later time,  $t$ , this sound wave has

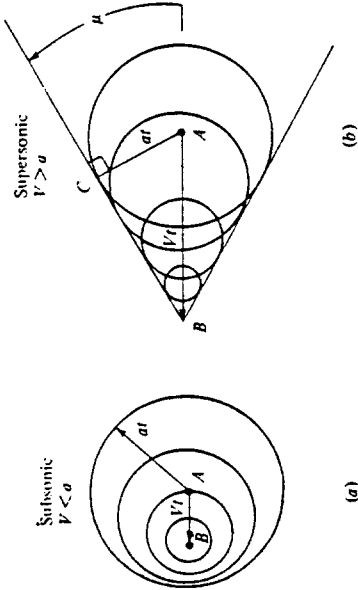


Figure 9.3 Another way of visualizing the propagation of disturbances in (a) subsonic and (b) supersonic flow.

propagated a distance  $at$  from point A and is represented by the circle of radius  $at$  shown in Fig. 9.3a. During the same time, the beeper has moved a distance  $Vt$  and is now at point B in Fig. 9.3a. Moreover, during its transit from A to B, the beeper has emitted several other sound waves, which at time  $t$  are represented by the smaller circles in Fig. 9.3a. Note that the beeper always stays *inside* the family of circular sound waves and that the waves continuously move ahead of the beeper. This is because the beeper is traveling at a subsonic speed,  $V < a$ . In contrast, consider the beeper moving at a supersonic speed,  $V > a$ , through the gas, as shown in Fig. 9.3b. At time  $t = 0$ , the beeper is located at point A, where it emits a sound wave. At a later time,  $t$ , this sound wave has propagated a distance  $at$  from point A and is represented by the circle of radius  $at$  shown in Fig. 9.3b. During the same time, the beeper has moved a distance  $Vt$  to point B. Moreover, during its transit from A to B, the beeper has emitted several other sound waves, which at time  $t$  are represented by the smaller circles in Fig. 9.3b. However, in contrast to the subsonic case, the beeper is now constantly outside the family of circular sound waves; i.e., it is moving ahead of the wave fronts because  $V > a$ . Moreover, something new is happening; these wave fronts form a disturbance envelope given by the straight line BC, which is tangent to the family of circles. This line of disturbances is defined as a *Mach wave*. In addition, the angle ABC which the Mach wave makes with respect to the direction of motion of the beeper is defined as the *Mach angle*  $\mu$ . From the geometry of Fig. 9.3b, we readily find that

$$\sin \mu = \frac{at}{Vt} = \frac{a}{V} = \frac{1}{M}$$

Thus, the Mach angle is simply determined by the local Mach number as

$$\mu = \sin^{-1} \frac{1}{M}$$

Examining Fig. 9.3b, the Mach wave, i.e., the envelope of disturbances in the supersonic flow, is clearly *oblique* to the direction of motion. If the disturbances are stronger

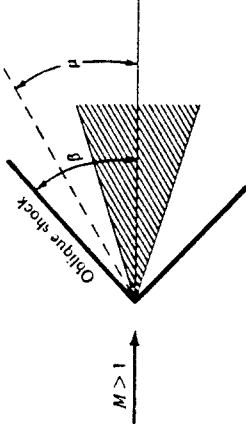


Figure 9.4 Relation between the oblique shock wave angle and the Mach angle.

than a simple sound wave, then the wave front becomes stronger than a Mach wave, creating an oblique shock wave at an angle  $\beta$  to the freestream, where  $\beta > \mu$ . This comparison is shown in Fig. 9.4. However, the physical mechanism creating the oblique shock is essentially the same as that described above for the Mach wave. Indeed, a Mach wave is a limiting case for oblique shock; i.e., it is an infinitely weak oblique shock.

This finishes our discussion of the physical source of oblique waves in a supersonic flow. Let us now proceed to develop the equations which allow us to calculate the change in properties across these oblique waves, first for oblique shock waves, and then for expansion waves. In the process, we follow the road map given in Fig. 9.5.

## 9.2 OBLIQUE SHOCK RELATIONS

Consider the oblique shock wave sketched in Fig. 9.6. The angle between the shock wave and the upstream flow direction is defined as the *wave angle*, denoted by  $\beta$ . The

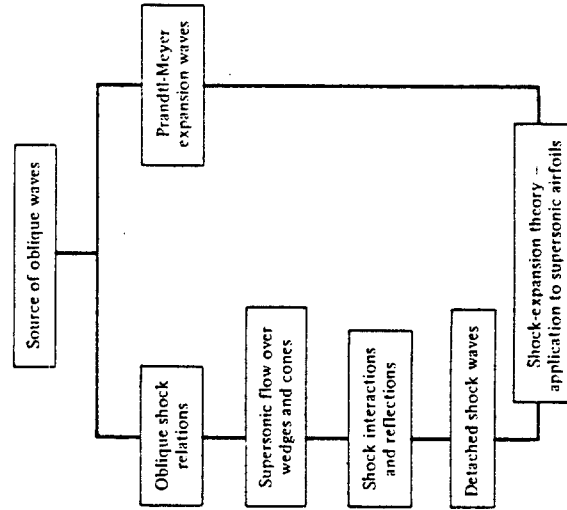


Figure 9.5 Road map for Chap. 9.

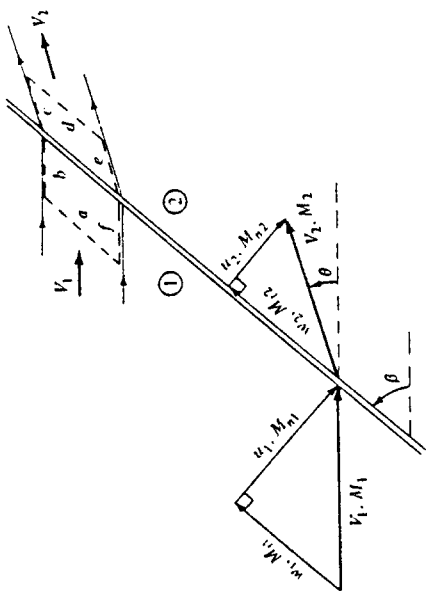


Figure 9.6 Oblique shock geometry.

upstream flow (region 1) is horizontal, with a velocity  $V_1$  and Mach number  $M_1$ . The downstream flow (region 2) is inclined upward through the deflection angle  $\theta$  and has velocity  $V_2$  and Mach number  $M_2$ . The upstream velocity  $V_1$  is split into components tangential and normal to the shock wave,  $w_1$  and  $u_1$ , respectively, with the associated tangential and normal Mach numbers  $M_{n,1}$  and  $M_{n,1}$ , respectively. Similarly, the downstream velocity is split into tangential and normal components  $w_2$  and  $u_2$ , respectively, with the associated Mach numbers  $M_{n,2}$  and  $M_{n,2}$ .

Consider the control volume shown by the dashed lines in the upper part of Fig. 9.6. Sides  $a$  and  $d$  are parallel to the shock wave. Segments  $b$  and  $c$  follow the upper streamline, and segments  $e$  and  $f$  follow the lower streamline. Let us apply the integral form of the conservation equations to this control volume, keeping in mind that we are dealing with a steady, inviscid, adiabatic flow with no body forces. For these assumptions, the continuity equation, Eq. (2.39), becomes

$$\oint \rho \mathbf{V} \cdot d\mathbf{S} = 0$$

This surface integral evaluated over faces  $a$  and  $d$  yields  $-\rho_1 u_1 A_1 + \rho_2 u_2 A_2$ , where  $A_1 = A_2 =$  area of faces  $a$  and  $d$ . The faces,  $b$ ,  $c$ ,  $e$ , and  $f$  are parallel to the velocity and, hence, contribute nothing to the surface integral (that is,  $\mathbf{V} \cdot d\mathbf{S} = 0$  for these faces). Thus, the continuity equation for an oblique shock wave is

$$-\rho_1 u_1 A_1 + \rho_2 u_2 A_2 = 0$$

$$\boxed{\rho_1 u_1 = \rho_2 u_2}$$

Keep in mind that  $u_1$  and  $u_2$  in Eq. (9.2) are **normal** to the shock wave.

The integral form of the momentum equation, Eq. (2.55), is a vector equation. Hence, it can be resolved into two components, tangential and normal to the shock

wave. First, consider the tangential component, keeping in mind the type of flow we are considering:

$$\iint_S (\rho \mathbf{V} \cdot d\mathbf{S}) w = - \iint_S (\rho dS)_{\text{tangential}} \quad (9.3)$$

In Eq. (9.3),  $w$  is the component of velocity tangential to the wave. Since  $d\mathbf{S}$  is perpendicular to the control surface, then  $(\rho dS)_{\text{tangential}}$  over faces  $a$  and  $d$  is zero. Also, since the vectors  $\rho d\mathbf{S}$  on faces  $b$  and  $f$  are equal and opposite, the pressure integral in Eq. (9.3) involves two tangential forces that cancel each other over faces  $b$  and  $f$ . The same is true for faces  $c$  and  $e$ . Hence, Eq. (9.3) becomes

$$-(\rho_1 u_1 A_1) w_1 + (\rho_2 u_2 A_2) w_2 = 0$$

Dividing Eq. (9.4) by Eq. (9.2), we have

$$\boxed{w_1 = w_2} \quad (9.5)$$

Equation (9.5) is an important result; it states that the **tangential component of the flow velocity is constant across an oblique shock**.

The normal component of the integral momentum equation is, from Eq. (2.55),

$$\iint_S (\rho \mathbf{V} \cdot d\mathbf{S}) u = - \iint_S (\rho dS)_{\text{normal}} \quad (9.6)$$

Here, the pressure integral evaluated over faces  $a$  and  $d$  yields the net sum  $-\rho_1 A_1 + \rho_2 A_2$ . Once again, the equal and opposite pressure forces on  $b$  and  $f$  cancel, as do those on  $c$  and  $e$ . Hence, Eq. (9.6) becomes, for the control volume shown in Fig. 9.6,

$$-(\rho_1 u_1 A_1) u_1 + (\rho_2 u_2 A_2) u_2 = -(-\rho_1 A_1 + \rho_2 A_2)$$

Since  $A_1 = A_2$ , this becomes

$$\boxed{\rho_1 + \rho_1 u_1^2 = \rho_2 + \rho_2 u_2^2} \quad (9.7)$$

Again, note that the only velocities appearing in Eq. (9.7) are the components **normal** to the shock.

Finally, consider the integral form of the energy equation, Eq. (2.86). For our present case, this can be written as

$$\iint_S \rho \left( e + \frac{V^2}{2} \right) \mathbf{V} \cdot d\mathbf{S} = - \iint_S \rho \mathbf{V} \cdot d\mathbf{S} \quad (9.8)$$

Again noting that the flow is tangent to faces  $b$ ,  $c$ ,  $f$ , and  $e$ , and hence  $\mathbf{V} \cdot d\mathbf{S} = 0$  on these faces, Eq. (9.8) becomes, for the control volume in Fig. 9.6,

$$-\rho_1 \left( e_1 + \frac{V_1^2}{2} \right) u_1 A_1 + \rho_2 \left( e_2 + \frac{V_2^2}{2} \right) u_2 A_2 = -(-\rho_1 u_1 A_1 + \rho_2 u_2 A_2) \quad (9.9)$$

Collecting terms in Eq. (9.9), we have

$$\begin{aligned} -\rho_1 u_1 \left( e_1 + \frac{p_1}{\rho_1} + \frac{V_1^2}{2} \right) + \rho_2 u_2 \left( e_2 + \frac{p_2}{\rho_2} + \frac{V_2^2}{2} \right) &= 0 \\ \text{or} \quad \rho_1 u_1 \left( h_1 + \frac{V_1^2}{2} \right) &= \rho_2 u_2 \left( h_2 + \frac{V_2^2}{2} \right) \end{aligned} \quad (9.10)$$

Dividing Eq. (9.10) by (9.2), we have

$$h_1 + \frac{V_1^2}{2} = h_2 + \frac{V_2^2}{2} \quad (9.11)$$

Since  $h_1 + V^2/2 = h_0$ , we have again the familiar result that the *total enthalpy is constant across the shock wave*. Moreover, for a calorically perfect gas,  $h_0 = c_p T_0$ ; hence, the *total temperature is constant across the shock wave*. Carrying Eq. (9.11) a bit further, note from Fig. 9.6 that  $V^2 = u^2 + w^2$ . Also, from Eq. (9.5), we know that  $w_1 = w_2$ . Hence,

$$V_1^2 - V_2^2 = (u_1^2 + w_1^2) - (u_2^2 + w_2^2) = u_1^2 - u_2^2$$

Thus, Eq. (9.11) becomes

$$h_1 + \frac{u_1^2}{2} = h_2 + \frac{u_2^2}{2} \quad (9.12)$$

Let us now gather our results. Look carefully at Eqs. (9.2), (9.7), and (9.12). They are the continuity, normal momentum, and energy equations, respectively, for an oblique shock wave. Note that they involve the *normal components only* of velocity,  $u_1$  and  $u_2$ ; the tangential component  $w$  does not appear in these equations. Hence, we deduce that *changes across an oblique shock wave are governed only by the component of velocity normal to the wave*.

Again, look hard at Eqs. (9.2), (9.7), and (9.12). *They are precisely the governing equations for a normal shock wave*, as given by Eqs. (8.2), (8.6), and (8.10). Hence, precisely the same algebra as applied to the normal shock equations in Sec. 8.6, when applied to Eqs. (9.2), (9.7), and (9.12), will lead to identical expressions for changes across an oblique shock in terms of the normal component of the upstream Mach number  $M_{n,1}$ . Note that

$$M_{n,1} = M_1 \sin \beta \quad (9.13)$$

Hence, for an oblique shock wave, with  $M_{n,1}$  given by Eq. (9.13), we have, from Eqs. (8.59), (8.61), and (8.65),

$$M_{n,2}^2 = \frac{1 + [(\gamma - 1)/2]M_{n,1}^2}{\gamma M_{n,1}^2 - (\gamma - 1)/2} \quad (9.14)$$

$$\frac{p_2}{\rho_1} = \frac{(\gamma + 1)M_{n,1}^2}{2 + (\gamma - 1)M_{n,1}^2} \quad (9.15)$$

$$\frac{p_2}{p_1} = 1 + \frac{2\gamma}{\gamma + 1} (M_{n,1}^2 - 1) \quad (9.16)$$

The temperature ratio  $T_2/T_1$  follows from the equation of state:

$$\frac{T_2}{T_1} = \frac{p_2}{p_1} \frac{\rho_1}{\rho_2} \quad (9.17)$$

Note that  $M_{n,2}$  is the *normal* Mach number behind the shock wave. The downstream Mach number itself,  $M_2$ , can be found from  $M_{n,2}$  and the geometry of Fig. 9.6 as

$$M_2 = \frac{M_{n,2}}{\sin(\beta - \theta)} \quad (9.18)$$

Examine Eqs. (9.14) to (9.17). They state that oblique shock-wave properties in a calorically perfect gas depend only on the normal component of the upstream Mach number  $M_{n,1}$ . However, note from Eq. (9.13) that  $M_{n,1}$  depends on both  $M_1$  and  $\beta$ . Recall from Sec. 8.6 that changes across a normal shock wave depend on one parameter only — the upstream Mach number  $M_1$ . In contrast, we now see that changes across an oblique shock wave depend on two parameters — say,  $M_1$  and  $\beta$ . However, this distinction is slightly moot because in reality a normal shock wave is a special case of oblique shocks where  $\beta = \pi/2$ .

Equation (9.18) introduces the deflection angle  $\theta$  into our oblique shock analysis; we need  $\theta$  to be able to calculate  $M_2$ . However,  $\theta$  is not an independent, third parameter; rather,  $\theta$  is a function of  $M_1$  and  $\beta$ , as derived below. From the geometry of Fig. 9.6,

$$\tan \beta = \frac{u_1}{w_1} \quad (9.19)$$

$$\tan(\beta - \theta) = \frac{u_2}{w_2} \quad (9.20)$$

Dividing Eq. (9.20) by (9.19), recalling that  $w_1 = w_2$ , and invoking the continuity equation, Eq. (9.2), we obtain

$$\frac{\tan(\beta - \theta)}{\tan \beta} = \frac{u_2}{u_1} = \frac{p_1}{p_2} \quad (9.21)$$

Combining Eq. (9.21) with Eqs. (9.13) and (9.15), we obtain

$$\frac{\tan(\beta - \theta)}{\tan \beta} = \frac{2 + (\gamma - 1)M_1^2 \sin^2 \beta}{(\gamma + 1)M_1^2 \sin^2 \beta} \quad (9.22)$$

which gives  $\theta$  as an implicit function of  $M_1$  and  $\beta$ . After some trigonometric substitutions and rearrangement, Eq. (9.22) can be cast explicitly for  $\theta$  as

$$\boxed{\tan \theta = 2 \cot \beta \frac{M_1^2 \sin^2 \beta - 1}{M_1^2(\gamma + \cos 2\beta) + 2} \quad (9.23)}$$

Equation (9.23) is an important equation. It is called the  $\theta$ - $\beta$ - $M$  relation, and it specifies  $\theta$  as a unique function of  $M_1$  and  $\beta$ . This relation is vital to the analysis of oblique shock waves, and results from it are plotted in Fig. 9.7 for  $\gamma = 1.4$ . Examine this figure closely. It is a plot of wave angle versus deflection angle, with the Mach number

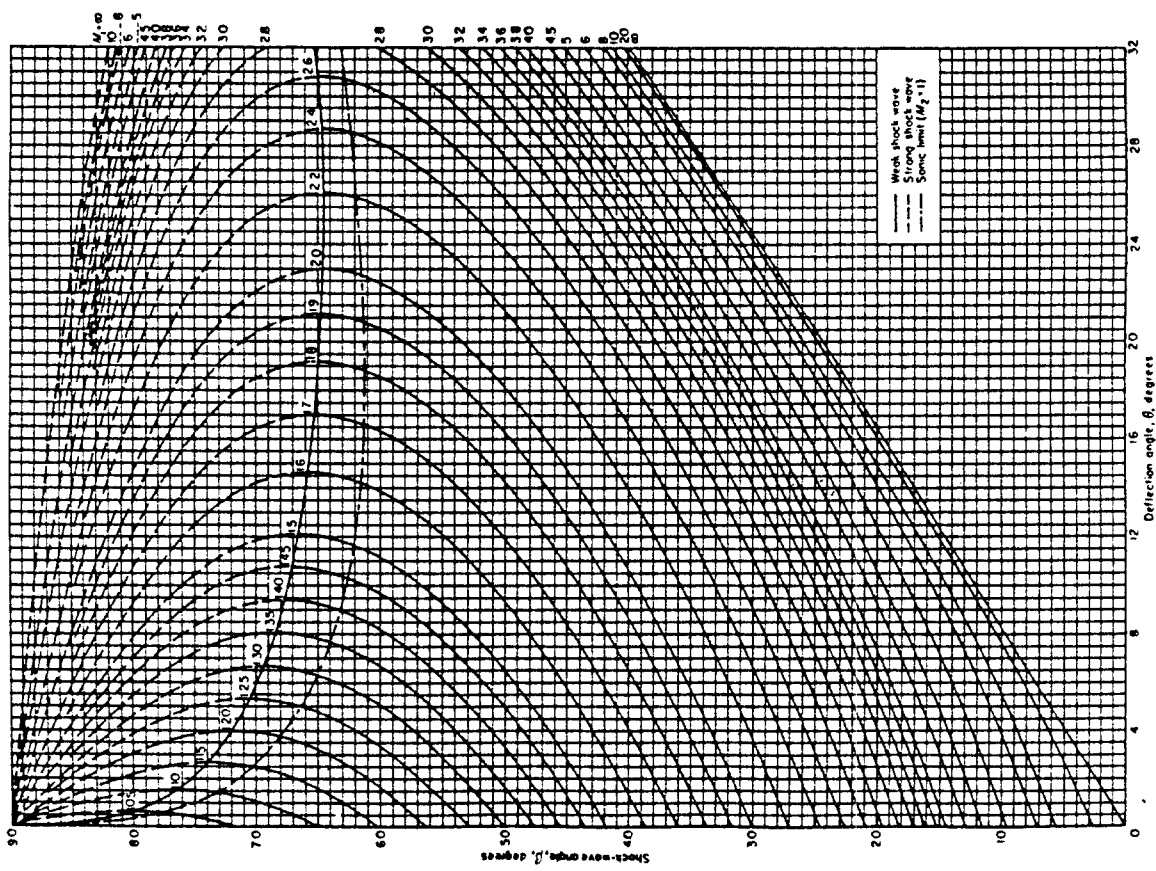
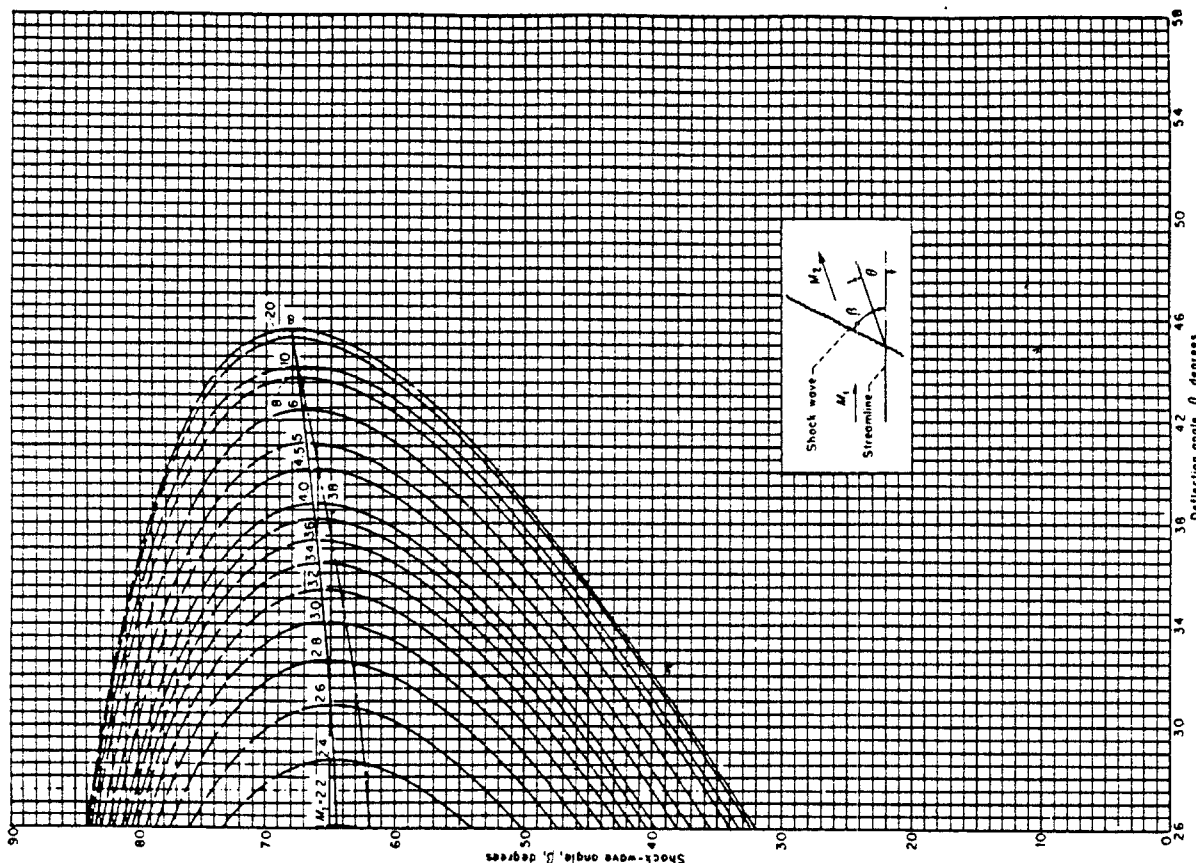


Figure 9.7 Oblique shock properties:  $\gamma = 1.4$ . The  $\theta$ - $M$  diagram. (From NACA Report 1135, Ames Research Staff, "Equations, Tables and Charts for Compressible Flow," 1953.)

as a parameter. The results given in Fig. 9.7 are plotted in some detail — this is a chart which you will need to use for solving oblique shock problems.

Figure 9.7 illustrates a wealth of physical phenomena associated with oblique shock waves. For example,



- For any given upstream Mach number  $M_1$ , there is a maximum deflection angle,  $\theta_{\max}$ . If the physical geometry is such that  $\theta > \theta_{\max}$ , then no solution exists for a straight oblique shock wave. Instead, nature establishes a curved shock wave, detached from the corner or the nose of a body. This is illustrated in Fig. 9.8. Here,

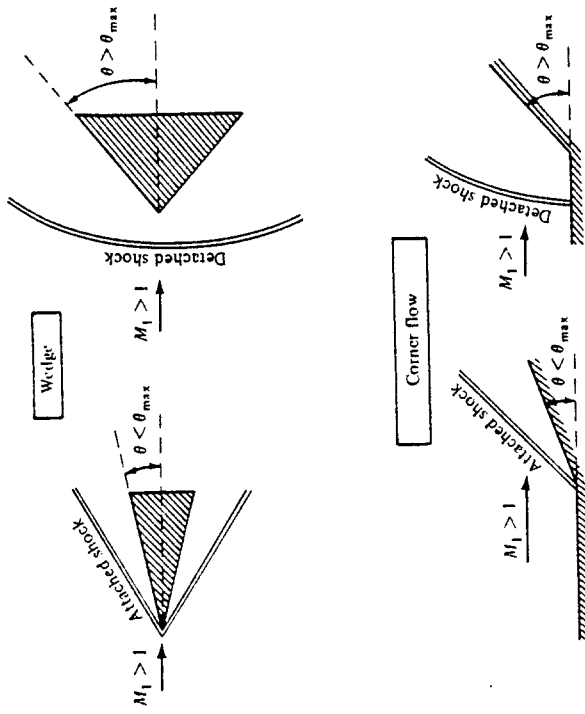


Figure 9.8 Attached and detached shocks.

the left side of the figure illustrates flow over a wedge and a concave corner where the deflection angle is less than  $\theta_{\max}$  for the given upstream Mach number. Therefore, we see a straight oblique shock wave attached to the nose of the wedge and to the corner. The right side of Fig. 9.8 gives the case where the deflection angle is greater than  $\theta_{\max}$ ; hence, there is no allowable straight oblique shock solution from the theory developed earlier in this section. Instead, we have a curved shock wave detached from the nose of the wedge or from the corner. Return to Fig. 9.7, and note that the value of  $\theta_{\max}$  increases with increasing  $M_1$ . Hence, at higher Mach numbers, the straight oblique shock solution can exist at higher deflection angles. However, there is a limit; as  $M_1$  approaches infinity,  $\theta_{\max}$  approaches  $45.5^\circ$  (for  $\gamma = 1.4$ ).

2. For any given  $\theta$  less than  $\theta_{\max}$ , there are two straight oblique shock solutions for a given upstream Mach number. For example, if  $M_1 = 2.0$  and  $\theta = 15^\circ$ , then from Fig. 9.7,  $\beta$  can equal either  $45.3$  or  $79.8^\circ$ . The smaller value of  $\beta$  is called the *weak* shock solution, and the larger value of  $\beta$  is the *strong* shock solution. These two cases are illustrated in Fig. 9.9. The classifications "weak" and "strong" derive from the fact that for a given  $M_1$ , the larger the wave angle, the larger the normal component of upstream Mach number,  $M_{n,1}$ , and from Eq. (9.16) the larger the pressure ratio  $p_2/p_1$ . Thus, in Fig. 9.9, the higher-angle shock wave will compress the gas more than the lower-angle shock wave, hence the terms "strong" and "weak" solutions. In nature, the weak shock solution usually prevails. Whenever you see straight, attached oblique shock waves, such as sketched at the left of

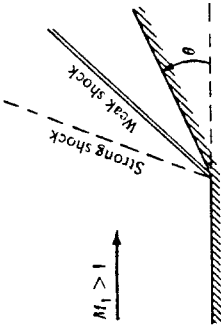


Figure 9.9 The weak and strong shock cases.

Fig. 9.8, they are almost always the weak shock solution. It is safe to make this assumption, unless you have specific information to the contrary. Note in Fig. 9.7 that the locus of points connecting all the values of  $\theta_{\max}$  (the curve that sweeps approximately horizontally across the middle of Fig. 9.7) divides the weak and strong shock solutions. Above this curve, the strong shock solution prevails (as further indicated by the  $\theta$ - $\beta$ - $M$  curves being dashed); below this curve, the weak shock solution prevails (where the  $\theta$ - $\beta$ - $M$  curves are shown as solid lines). Note that slightly below this curve is another curve which also sweeps approximately horizontally across Fig. 9.7. This curve is the dividing line above which  $M_2 < 1$  and below which  $M_2 > 1$ . For the strong shock solution, the downstream Mach number is always subsonic,  $M_2 < 1$ . For the weak shock solution very near  $\theta_{\max}$ , the downstream Mach number is also subsonic, but barely so. For the vast majority of cases involving the weak shock solution, the downstream Mach number is supersonic,  $M_2 > 1$ . Since the weak shock solution is almost always the case encountered in nature, we can readily state that the Mach number downstream of a straight, attached oblique shock is almost always supersonic.

3. If  $\theta = 0$ , then  $\beta$  equals either  $90^\circ$  or  $\mu$ . The case of  $\beta = 90^\circ$  corresponds to a normal shock wave (i.e., the normal shocks discussed in Chap. 8 belong to the family of strong shock solutions). The case of  $\beta = \mu$  corresponds to the Mach wave illustrated in Fig. 9.3b. In both cases, the flow streamlines experience no deflection across the wave.

4. (In all of the following discussions, we consider the weak shock solution exclusively, unless otherwise noted.) Consider an experiment where we have supersonic flow over a wedge of given semiangle  $\theta$ , as sketched in Fig. 9.10. Now assume that we increase the freestream Mach number  $M_1$ . As  $M_1$  increases, we observe that  $\beta$  decreases. For example, consider  $\theta = 20^\circ$  and  $M_1 = 2.0$ , as shown on the left of Fig. 9.10. From Fig. 9.7, we find that  $\beta = 53.3^\circ$ . Now assume  $M_1$  is increased to 5, keeping  $\theta$  constant at  $20^\circ$ , as sketched on the right of Fig. 9.10. Here, we find that  $\beta = 29.9^\circ$ . Interestingly enough, although this shock is at a lower wave angle, it is a stronger shock than the one on the left. This is because  $M_{n,1}$  is larger for the case on the right. Although  $\beta$  is smaller, which decreases  $M_{n,1}$ , the upstream Mach number  $M_1$  is larger, which increases  $M_{n,1}$  by an amount which more than compensates for the decreased  $\beta$ . For example, note the values of  $M_{n,1}$  and  $p_2/p_1$  given in Fig. 9.10. Clearly, the Mach 5 case on the right yields the stronger shock wave. Hence, in general for attached shocks with a fixed deflection angle, as the upstream Mach number  $M_1$  increases, the wave angle  $\beta$  decreases, and the shock

**Example 9.1** Consider a supersonic flow with  $M_1 = 2$ ,  $p = 1$  atm, and  $T = 288$  K. This flow is deflected at a compression corner through  $20^\circ$ . Calculate  $M$ ,  $p$ ,  $T$ ,  $p_0$ , and  $T_0$  behind the resulting oblique shock wave.

**SOLUTION** From Fig. 9.7, for  $M_1 = 2$  and  $\theta = 20^\circ$ ,  $\beta = 53.4^\circ$ . Hence,  $M_{n,1} = M_1 \sin \beta = 2 \sin 53.4^\circ = 1.606$ . From App. B, for  $M_{n,1} = 1.60$  (rounded to the nearest table entry),

$$M_{n,2} = 0.6684 \quad \frac{p_2}{p_1} = 2.82 \quad \frac{T_2}{T_1} = 1.388 \quad \frac{p_{0,2}}{p_{0,1}} = 0.8952$$

$$\text{Hence} \quad M_2 = \frac{M_{n,2}}{\sin(\beta - \theta)} = \frac{0.6684}{\sin(53.4^\circ - 20^\circ)} = \boxed{1.21}$$

$$p_2 = \frac{p_2}{p_1} p_1 = 2.82(1 \text{ atm}) = \boxed{2.82 \text{ atm}}$$

$$T_2 = \frac{T_2}{T_1} T_1 = 1.388(288) = \boxed{399.7 \text{ K}}$$

For  $M_1 = 2$ , from App. A,  $p_{0,1}/p_1 = 7.824$  and  $T_{0,1}/T_1 = 1.8$ ; thus,

$$p_{0,2} = \frac{p_{0,2}}{p_{0,1}} p_1 = 0.8952(7.824)(1 \text{ atm}) = \boxed{7.00 \text{ atm}}$$

The total temperature is constant across the shock. Hence,

$$T_{0,2} = T_{0,1} = \frac{T_{0,1}}{T_1} T_1 = 1.8(288) = \boxed{518.4 \text{ K}}$$

*Note:* For oblique shocks, the entry for  $p_{0,2}/p_1$  in App. B cannot be used to obtain  $p_{0,2}$ ; this entry in App. B is for normal shocks only and is obtained directly from Eq. (8.80). In turn, Eq. (8.80) is derived using (8.77), where  $M_2$  is the actual flow Mach number, not the normal component. Only in the case of a normal shock is this also the Mach number normal to the wave. Hence, Eq. (8.80) holds only for normal shocks; it cannot be used for oblique shocks with  $M_1$  replaced by  $M_{n,1}$ . For example, an incorrect calculation would be to use  $p_{0,2}/p_1 = 3.805$  for  $M_{n,1} = 1.60$ . This gives  $p_{0,2} = 3.805$  atm, a totally incorrect result compared with the correct value of 7.00 atm obtained above.

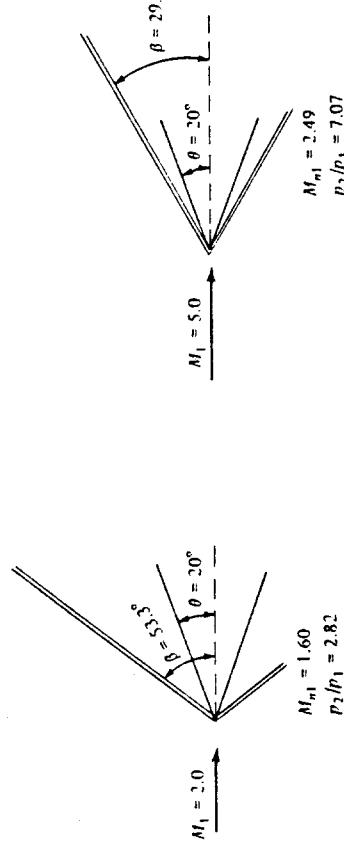


Figure 9.10 Effects of increasing the upstream Mach number.

wave becomes stronger. Going in the other direction, as  $M_1$  decreases, the wave angle increases, and the shock becomes weaker. Finally, if  $M_1$  is decreased enough, the shock wave will become detached. For the case of  $\theta = 20^\circ$  shown in Fig. 9.10, the shock will be detached for  $M_1 < 1.84$ .

5. Consider another experiment. Here, let us keep  $M_1$  fixed and increase the deflection angle. For example, consider the supersonic flow over a wedge shown in Fig. 9.11. Assume that we have  $M_1 = 2.0$  and  $\theta = 10^\circ$ , as sketched at the left of Fig. 9.11. The wave angle will be  $39.2^\circ$  (from Fig. 9.7). Now assume that the wedge is hinged so that we can increase its deflection angle, keeping  $M_1$  constant. In such a case, the wave angle will increase, as shown on the right of Fig. 9.11. Also,  $M_{n,1}$  will increase, and hence the shock will become stronger. Therefore, in general for attached shocks with a fixed upstream Mach number, as the deflection angle increases, the wave angle  $\beta$  increases, and the shock becomes stronger. However, once  $\theta$  exceeds  $\theta_{\max}$ , the shock wave will become detached. For the case of  $M_1 = 2.0$  in Fig. 9.11, this will occur when  $\theta > 23^\circ$ .

The physical properties of oblique shocks discussed above are very important. Before proceeding further, make certain to go over this discussion several times until you feel perfectly comfortable with these physical variations.

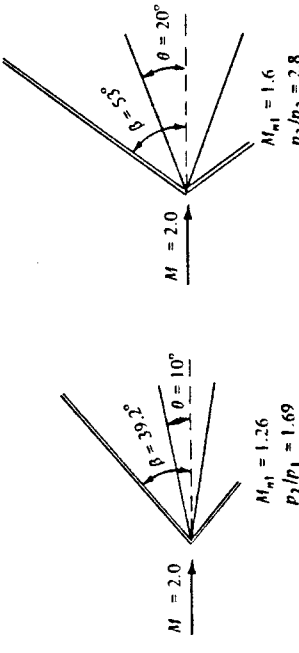


Figure 9.11 Effect of increasing the deflection angle.

### 9.3 SUPERSONIC FLOW OVER WEDGES AND CONES

For the supersonic flow over wedges, as shown in Figs. 9.10 and 9.11, the oblique shock theory developed in Sec. 9.2 is an exact solution of the flow field; no simplifying assumptions have been made. Supersonic flow over a wedge is characterized by an attached, straight oblique shock wave from the nose, a uniform flow downstream of the shock with streamlines parallel to the wedge surface, and a surface pressure equal to the static pressure behind the oblique shock,  $p_2$ . These properties are summarized in Fig. 9.12a. Note that the wedge is a two-dimensional profile; in Fig. 9.12a, it is a

ever, it is important for you to recognize that conical flows are inherently different from wedge flows and to recognize in what manner they differ. This has been the purpose of the present section.

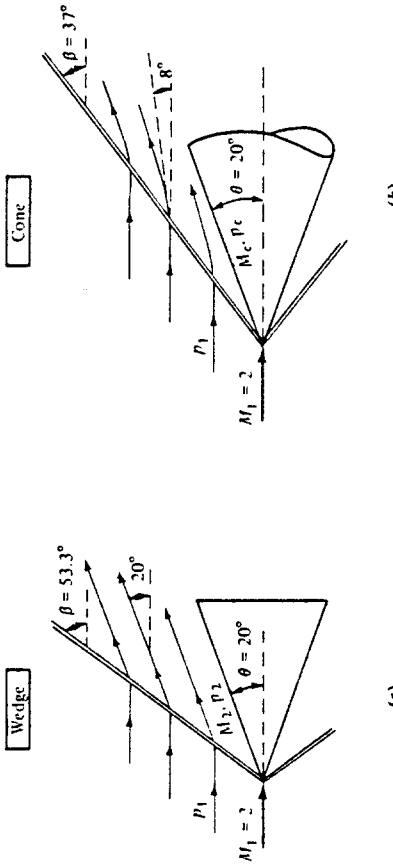


Figure 9.12 Relation between wedge and cone flow; illustration of the three-dimensional relieving effect.

section of a body that stretches to plus or minus infinity in the direction perpendicular to the page. Hence, wedge flow is, by definition, two-dimensional flow, and our two-dimensional oblique shock theory fits this case nicely.

In contrast, consider the supersonic flow over a cone, as sketched in Fig. 9.12b. There is a straight oblique shock which emanates from the tip, just as in the case of a wedge, but the similarity stops there. Recall from Chap. 6 that flow over a three-dimensional body experiences a "three-dimensional relieving effect." That is, in comparing the wedge and cone in Fig. 9.12, both with the same 20° angle, the flow over the cone has an extra dimension in which to move, and hence it more easily adjusts to the presence of the conical body in comparison to the two-dimensional wedge. One consequence of this three-dimensional relieving effect is that the shock wave on the cone is weaker than on the wedge; i.e., it has a smaller wave angle, as compared in Fig. 9.12. Specifically, the wave angles for the wedge and cone are 53.3 and 37°, respectively, for the same body angle of 20° and the same upstream Mach number of 2.0. In the case of the wedge (Fig. 9.12a), the streamlines are deflected by exactly 20° through the shock wave, and hence downstream of the shock the flow is exactly parallel to the wedge surface. In contrast, because of the weaker shock on the cone, the streamlines are deflected by only 8° through the shock, as shown in Fig. 9.12b. Therefore, between the shock wave and the cone surface, the streamlines must gradually curve upward in order to accommodate the 20° cone. Also, as a consequence of the three-dimensional relieving effect, the pressure on the surface of the cone,  $p_3$ , is less than the wedge surface pressure  $p_2$ , and the cone surface Mach number  $M_3$  is greater than that on the wedge surface,  $M_2$ . In short, the main differences between the supersonic flow over a cone and wedge, both with the same body angle, are that (1) the shock wave on the cone is weaker, (2) the cone surface pressure is less, and (3) the streamlines above the cone surface are curved rather than straight.

The analysis of the supersonic flow over a cone is more sophisticated than the oblique shock theory given in this chapter and is beyond the scope of this book. For details concerning supersonic conical flow analysis, see chapter 10 of Ref. 21. How-

## 9.4 SHOCK INTERACTIONS AND REFLECTIONS

Return to the oblique shock wave illustrated in Fig. 9.1a. In this picture, we can imagine the shock wave extending unchanged above the corner to infinity. However, in real life this does not happen. In reality, the oblique shock in Fig. 9.1a will impinge somewhere on another solid surface and/or will intersect other waves, either shock or expansion waves. Such wave intersections and interactions are important in the practical design and analysis of supersonic airplanes, missiles, wind tunnels, rocket engines, etc. A perfect historical example of this, as well as the consequences that can be caused by not paying suitable attention to wave interactions, is a ramjet flight-test program conducted in the early 1960s. During this period, a ramjet engine was mounted underneath the X-15 hypersonic airplane for a series of flight tests at high Mach numbers, in the range from 4 to 7. (The X-15, shown in Fig. 9.13, was an experimental, rocket-powered airplane designed to probe the lower end of hypersonic manned flight.) During the first high-speed tests, the shock wave from the engine cowling impinged on the bottom surface of the X-15, and because of locally high aerodynamic heating in the impingement region, a hole was burned in the X-15 fuselage. Although this problem was later fixed, it is a graphic example of what shock-wave interactions can do to a practical configuration.

The purpose of this section is to present a mainly qualitative discussion of shock-wave interactions. For more details, see chapter 4 of Ref. 21.

First, consider an oblique shock wave generated by a concave corner, as shown in Fig. 9.14. The deflection angle at the corner is  $\theta$ , thus generating an oblique shock at point A with a wave angle,  $\beta_1$ . Assume that a straight, horizontal wall is present above the corner, as also shown in Fig. 9.14. The shock wave generated at point A, called the *incident shock wave*, impinges on the upper wall at point B. *Question:* Does the shock wave simply disappear at point B? If not, what happens to it? To answer this question, we appeal to our knowledge of shock-wave properties. Examining Fig. 9.14, we see that the flow in region 2 behind the incident shock is inclined upward at the deflection angle  $\theta$ . However, the flow must be tangent everywhere along the upper wall; if the flow in region 2 were to continue unchanged, it would run into the wall and have no place to go. Hence, the flow in region 2 must eventually be bent downward through the angle  $\theta$  in order to maintain a flow tangent to the upper wall. Nature accomplishes this downward deflection via a second shock wave originating at the impingement point B in Fig. 9.14. This second shock is called the *reflected shock wave*. The purpose of the reflected shock is to deflect the flow in region 2 so that it is parallel to the upper wall in region 3, thus preserving the wall boundary condition.

The strength of the reflected shock wave is weaker than the incident shock. This is because  $M_2 < M_1$ , and  $M_2$  represents the upstream Mach number for the reflected shock wave. Since the deflection angles are the same, whereas the reflected shock sees

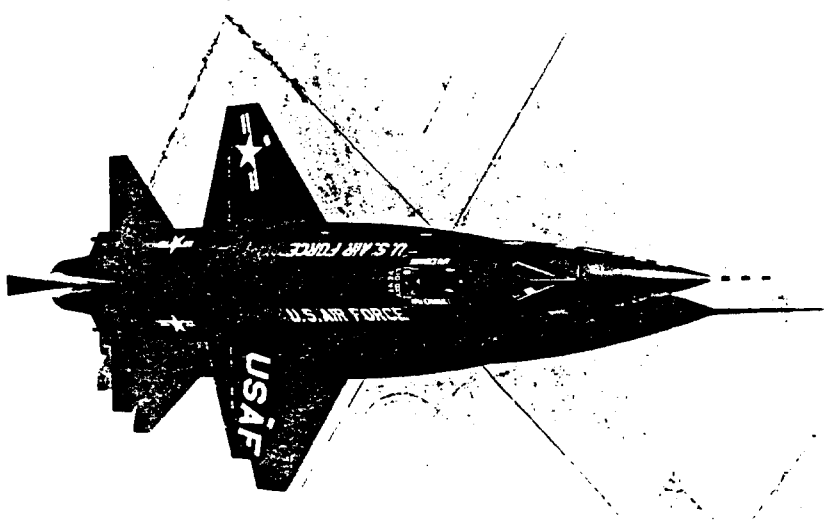


**Figure 9.13** The X-15 hypersonic research vehicle. Designed and built during the late 1950s, it served as a test vehicle for the U.S. Air Force and NASA. (*Courtesy of Rockville Int'l., North American.*)

a lower upstream Mach number, we know from Sec. 9.2 that the reflected wave must be weaker. For this reason, the angle the reflected shock makes with the upper wall,  $\Phi$ , is not equal to  $\beta_1$ ; that is, the wave reflection is not specular. The properties of the reflected shock are uniquely defined by  $M_2$  and  $\theta$ ; since  $M_2$  is in turn uniquely defined by  $M_1$  and  $\theta$ , then the properties in region 3 behind the reflected shock as well as the angle  $\Phi$  are easily determined from the given conditions of  $M_1$  and  $\theta$  by using the results of Sec. 9.2 as follows:

1. Calculate the properties in region 2 from the given  $M_1$  and  $\theta$ . In particular, this gives us  $M_2$ .
  2. Calculate the properties in region 3 from the value of  $M_2$  calculated above and the known deflection angle  $\theta$ .

An interesting situation can arise as follows. Assume that  $M_1$  is only slightly above the minimum Mach number necessary for a straight, attached shock wave at the given deflection angle  $\theta$ . For this case, the oblique shock theory from Sec. 9.2 allows a solution for a straight, attached incident shock. However, we know that the Mach number decreases across a shock, that is,  $M_2 < M_1$ . This decrease may be enough such that  $M_2$  is *not* above the minimum Mach number for the required deflection  $\theta$  through the reflected shock. In such a case, our oblique shock theory does not allow a solution for a straight reflected shock wave. The regular reflection as shown in Fig. 9.14 is not possible. Nature handles this situation by creating the wave pattern shown in Fig. 9.15. Here, the originally straight incident shock becomes curved as it nears the upper wall and becomes a normal shock wave at the upper wall. This allows the streamline at the wall to continue parallel to the wall behind the shock intersection. In addition, a curved reflected shock branches from the normal shock and propagates downstream. This wave pattern, shown in Fig. 9.15, is called a *Mach reflection*. The calculation of the wave pattern and general properties for a Mach reflection requires numerical techniques such as those to be discussed in Chap. [3].

Another type of shock interaction is shown in Fig. 9.16. Here, a shock wave is generated by the concave corner at point  $G$  and propagates upward. Denote this wave as shock  $A$ . Shock  $A$  is a *left-running wave*, so-called because if you stand on top of the wave and look downstream, you see the shock wave running in front of you toward the left. Another shock wave is generated by the concave corner at point  $H$ , and propagates downward. Denote this wave as shock  $B$ . Shock  $B$  is a *right-running wave*,

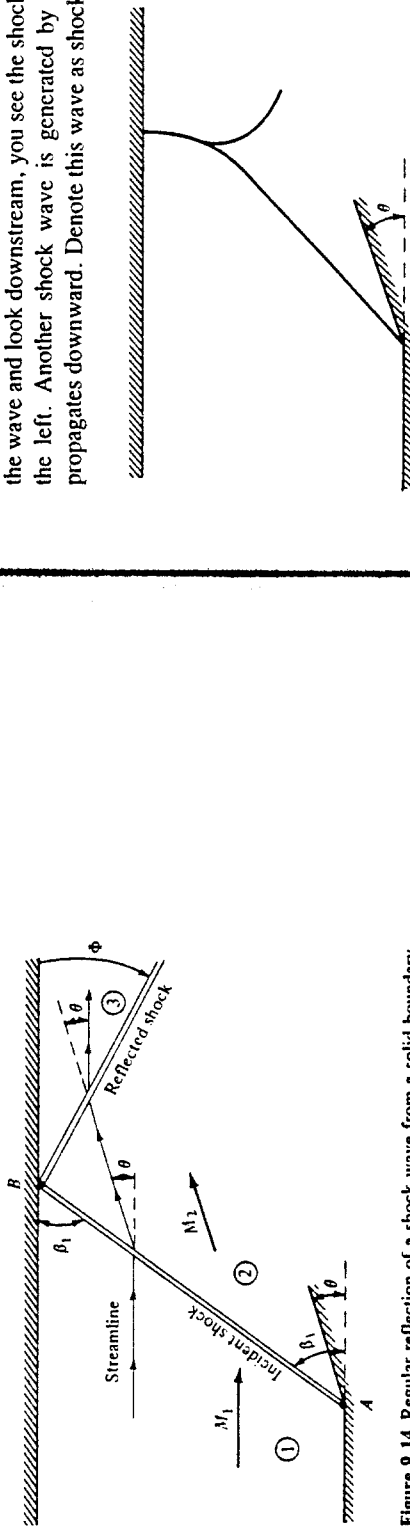


**Figure 9.14** Regular reflection of a shock wave from a solid boundary.

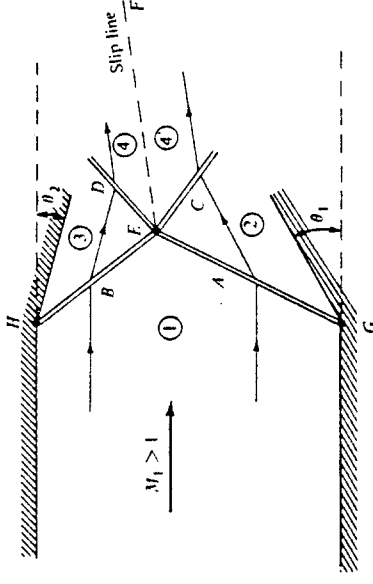


Figure 9.16 Intersection of right- and left-running shock waves.

so-called because if you stand on top of the wave and look downstream, you see the shock running in front of you toward the right. The picture shown in Fig. 9.16 is the intersection of right- and left-running shock waves. The intersection occurs at point *E*. At the intersection, wave *A* is refracted and continues as wave *D*. Similarly, wave *B* is refracted and continues as wave *C*. The flow behind the refracted shock *D* is denoted by region 4; the flow behind the refracted shock *C* is denoted by region 4'. These two regions are divided by a slip line, *EF*. Across the slip line, the pressures are constant, i.e.,  $p_4 = p_{4'}$ , and the direction (but not necessarily the magnitude) of velocity is the same, namely, parallel to the slip line. All other properties in regions 4 and 4' are different, most notably the entropy ( $s_4 \neq s_{4'}$ ). The conditions which must hold across the slip line, along with the known  $M_1$ ,  $\theta_1$ , and  $\theta_2$ , uniquely determine the shock wave interaction shown in Fig. 9.16. (See chapter 4 of Ref. 21 for details concerning the calculation of this interaction.)

Figure 9.17 illustrates the intersection of two left-running shocks generated at corners *A* and *B*. The intersection occurs at point *C*, at which the two shocks merge and propagate as the stronger shock *CD*, usually along with a weak reflected wave *CE*. This reflected wave is necessary to adjust the flow so that the velocities in regions 4 and 5 are in the same direction. Again, a slip line *CF* trails downstream of the intersection point.

The above cases are by no means all the possible wave interactions in a supersonic flow. However, they represent some of the more common situations encountered frequently in practice.

## 9.5 DETACHED SHOCK WAVE IN FRONT OF A BLUNT BODY

The curved bow shock which stands in front of a blunt body in a supersonic flow is sketched in Fig. 8.1. We are now in a position to better understand the properties of this bow shock, as follows.

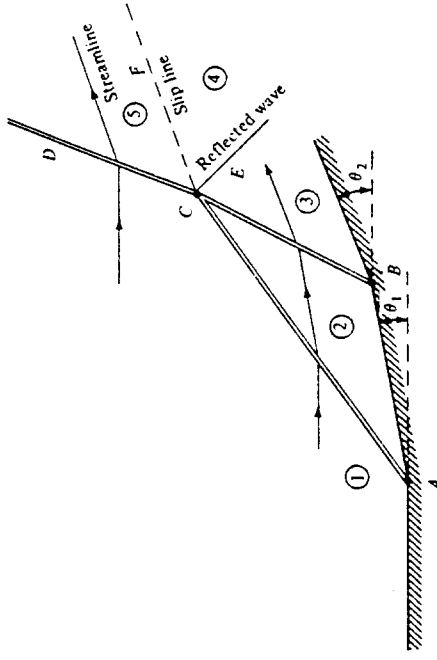


Figure 9.17 Intersection of two left-running shock waves.

The flow in Fig. 8.1 is sketched in more detail in Fig. 9.18. Here, the shock wave stands a distance  $\delta$  in front of the nose of the blunt body;  $\delta$  is defined as the *shock detachment distance*. At point *a*, the shock wave is normal to the upstream flow; hence, point *a* corresponds to a normal shock wave. Away from point *a*, the shock wave

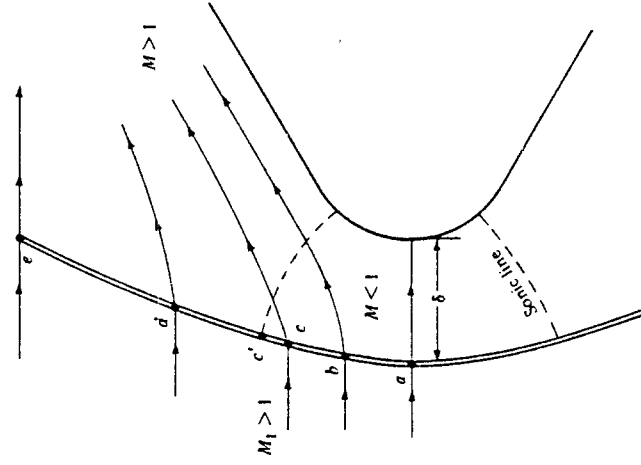


Figure 9.18 Flow over a supersonic blunt body.

gradually becomes curved and weaker, eventually evolving into a Mach wave at large distances from the body (illustrated by point  $c$  in Fig. 9.18).

A curved bow shock wave is one of the instances in nature when you can observe all possible oblique shock solutions at once for a given freestream Mach number,  $M_1$ . This takes place between points  $a$  and  $e$ . To see this more clearly, consider the  $\theta$ - $\beta$ - $M$  diagram sketched in Fig. 9.19 in conjunction with Fig. 9.18. In Fig. 9.19, point  $a$  corresponds to the normal shock, and point  $e$  corresponds to the Mach wave. Slightly above the centerline, at point  $b$  in Fig. 9.18, the shock is oblique but pertains to the strong shock wave solution in Fig. 9.19. The flow is deflected slightly upward behind the shock at point  $b$ . As we move further along the shock, the wave angle becomes more oblique, and the flow deflection increases until we encounter point  $c$ . Point  $c$  on the bow shock corresponds to the maximum deflection angle shown in Fig. 9.19. Above point  $c$ , from  $c$  to  $e$ , all points on the shock correspond to the weak shock solution. Slightly above point  $c$ , at point  $c'$ , the flow behind the shock becomes sonic. From  $a$  to  $c'$ , the flow is subsonic behind the bow shock; from  $c'$  to  $e$ , it is supersonic. Hence, the flow field between the curved bow shock and the blunt body is a mixed region of both subsonic and supersonic flow. The dividing line between the subsonic and supersonic regions is called the *sonic line*, shown as the dashed line in Fig. 9.18.

The shape of the detached shock wave, its detachment distance  $\delta$ , and the complete flow field between the shock and the body depend on  $M_1$  and the size and shape of the body. The solution of this flow field is not trivial. Indeed, the supersonic blunt-body problem was a major focus for supersonic aerodynamicists during the 1950s and 1960s, spurred by the need to understand the high-speed flow over blunt-nosed missiles and reentry bodies. Indeed, it was not until the late 1960s that truly sufficient numerical techniques became available for satisfactory engineering solutions of supersonic blunt-body flows. These modern techniques are discussed in Chap. 13.

## 9.6 PRANDTL-MEYER EXPANSION WAVES

Oblique shock waves, as discussed in Secs. 9.2 to 9.5, occur when a supersonic flow is turned into itself (see again Fig. 9.1a). In contrast, when a supersonic flow is turned away from itself, an expansion wave is formed, as sketched in Fig. 9.1b. Examine this figure carefully, and review the surrounding discussion in Sec. 9.1 before progressing further. The purpose of the present section is to develop a theory which allows us to calculate the changes in flow properties across such expansion waves. To this stage in our discussion of oblique waves, we have completed the left-hand branch of the road map in Fig. 9.5. In this section, we cover the right-hand branch.

The expansion fan in Fig. 9.1b is a *continuous* expansion region which can be visualized as an infinite number of Mach waves, each making the Mach angle  $\mu$  [see Eq. (9.1)] with the local flow direction. As sketched in Fig. 9.20, the expansion fan is bounded upstream by a Mach wave which makes the angle  $\mu_1$  with respect to the upstream flow, where  $\mu_1 = \arcsin(1/M_1)$ . The expansion fan is bounded downstream by another Mach wave which makes the angle  $\mu_2$  with respect to the downstream flow, where  $\mu_2 = \arcsin(1/M_2)$ . Since the expansion through the wave takes place across a

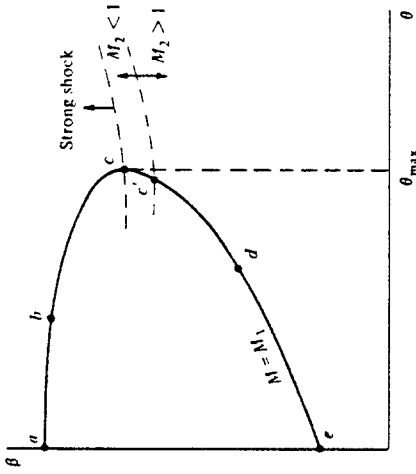


Figure 9.19  $\theta$ - $\beta$ - $M$  diagram for the sketch shown in Fig. 9.18.

continuous succession of Mach waves, and since  $d\sigma = 0$  for each Mach wave, the expansion is *isentropic*. This is in direct contrast to flow across an oblique shock, which always experiences an entropy increase. The fact that the flow through an expansion wave is isentropic is a greatly simplifying aspect, as we will soon appreciate.

An expansion wave emanating from a sharp convex corner as sketched in Figs. 9.1b and 9.20 is called a *centered* expansion wave. Ludwig Prandtl and his student Theodor Meyer first worked out a theory for centered expansion waves in 1907–1908, and hence such waves are commonly denoted as *Prandtl-Meyer expansion waves*.

The problem of an expansion wave is as follows: referring to Fig. 9.20, given the upstream flow (region 1) and the deflection angle  $\theta$ , calculate the downstream flow (region 2). Let us proceed.

Consider a very weak wave produced by an infinitesimally small flow deflection,  $d\theta$ , as sketched in Fig. 9.21. We consider the limit of this picture as  $d\theta \rightarrow 0$ ; hence, the wave is essentially a Mach wave at the angle  $\mu$  to the upstream flow. The velocity ahead of the wave is  $V$ . As the flow is deflected downward through the angle  $d\theta$ , the velocity is increased by the infinitesimal amount  $dV$ , and hence the flow velocity behind the wave is  $V + dV$  inclined at the angle  $d\theta$ . Recall from the treatment of the

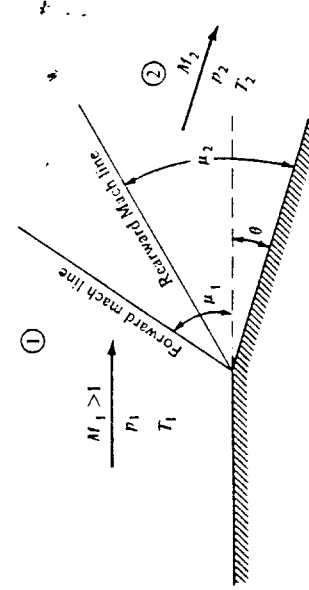


Figure 9.20 Prandtl-Meyer expansion.

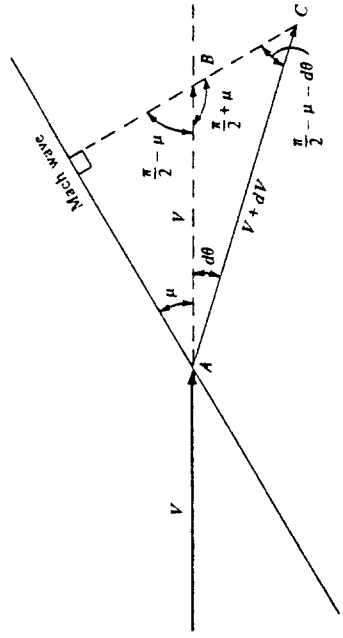


Figure 9.21 Geometrical construction for the infinitesimal changes across an infinitesimally weak wave (in the limit, a Mach wave).

momentum equation in Sec. 9.2 that any change in velocity across a wave takes place *normal* to the wave; the tangential component is unchanged across the wave. In Fig. 9.21, the horizontal line segment AB with length V is drawn behind the wave. Also, the line segment AC is drawn to represent the new velocity  $V + dV$  behind the wave. Then line BC is normal to the wave because it represents the line along which the change in velocity occurs. Examining the geometry in Fig. 9.21, from the law of sines applied to triangle ABC, we see that

$$\frac{V + dV}{V} = \frac{\sin(\pi/2 + \mu)}{\sin(\pi/2 - \mu - d\theta)} \quad (9.24)$$

However, from trigonometric identities,

$$\sin\left(\frac{\pi}{2} + \mu\right) = \cos\left(\frac{\pi}{2} - \mu\right) = \cos \mu \quad (9.25)$$

$$\sin\left(\frac{\pi}{2} - \mu - d\theta\right) = \cos(\mu + d\theta) = \cos \mu \cos d\theta - \sin \mu \sin d\theta \quad (9.26)$$

Substituting Eqs. (9.25) and (9.26) into (9.24), we have

$$1 + \frac{dV}{V} = \frac{\cos \mu}{\cos \mu \cos d\theta - \sin \mu \sin d\theta} \quad (9.27)$$

For small  $d\theta$ , we can make the small-angle assumptions  $\sin d\theta \approx d\theta$  and  $\cos d\theta \approx 1$ . Then, Eq. (9.27) becomes

$$1 + \frac{dV}{V} = \frac{\cos \mu}{\cos \mu - d\theta \sin \mu} = \frac{1}{1 - d\theta \tan \mu} \quad (9.28)$$

Note that the function  $1/(1 - x)$  can be expanded in a power series (for  $x < 1$ ) as

$$\frac{1}{1 - x} = 1 + x + x^2 + x^3 + \dots$$

Hence, Eq. (9.28) can be expanded as (ignoring terms of second order and higher)

$$1 + \frac{dV}{V} = 1 + d\theta \tan \mu + \dots \quad (9.29)$$

Thus, from Eq. (9.29),

$$d\theta = \frac{dV/V}{\tan \mu} \quad (9.30)$$

From Eq. (9.1), we know that  $\mu = \arcsin(1/M)$ . Hence, the right triangle in Fig. 9.22 demonstrates that

$$\tan \mu = \frac{1}{\sqrt{M^2 - 1}} \quad (9.31)$$

Substituting Eq. (9.31) into (9.30), we obtain

$$d\theta = \sqrt{M^2 - 1} \frac{dV}{V} \quad (9.32)$$

Equation (9.32) relates the infinitesimal change in velocity,  $dV$ , to the infinitesimal deflection  $d\theta$  across a wave of vanishing strength. In the precise limit of a Mach wave, of course  $dV$  and hence  $d\theta$  are zero. In this sense, Eq. (9.32) is an approximate equation for a finite  $d\theta$ , but it becomes a true equality as  $d\theta \rightarrow 0$ . Since the expansion fan illustrated in Figs. 9.1b and 9.20 is a region of an infinite number of Mach waves, Eq. (9.32) is a differential equation which precisely describes the flow inside the expansion wave.

Return to Fig. 9.20. Let us integrate Eq. (9.32) from region 1, where the deflection angle is zero and the Mach number is  $M_1$ , to region 2, where the deflection angle is  $\theta$  and the Mach number is  $M_2$ .

$$\int_0^\theta d\theta = \theta = \int_{M_1}^{M_2} \sqrt{M^2 - 1} \frac{dV}{V} \quad (9.33)$$

To carry out the integral on the right-hand side of Eq. (9.33),  $dV/V$  must be obtained in terms of  $M$ , as follows. From the definition of Mach number,  $M = V/a$ , we have  $V = Ma$ , or

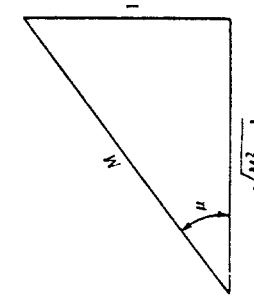


Figure 9.22 Right triangle associated with the Mach angle.

$$\ln V = \ln M + \ln a$$

Differentiating Eq. (9.34), we obtain

$$\frac{dV}{V} = \frac{dM}{M} + \frac{da}{a} \quad (9.35)$$

From Eqs. (8.25) and (8.40), we have

$$\left(\frac{a_0}{a}\right)^2 = \frac{T_0}{T} = 1 + \frac{\gamma - 1}{2} M^2 \quad (9.36)$$

Solving Eq. (9.36) for  $a$ ,

$$a = a_0 \left(1 + \frac{\gamma - 1}{2} M^2\right)^{-1} \quad (9.37)$$

Differentiating Eq. (9.37),

$$\frac{da}{a} = -\left(\frac{\gamma - 1}{2}\right) M \left(1 + \frac{\gamma - 1}{2} M^2\right)^{-1} dM \quad (9.38)$$

Substituting Eq. (9.38) into (9.35), we have

$$\frac{dV}{V} = \frac{1}{1 + [(\gamma - 1)/2] M^2} \frac{dM}{M} \quad (9.39)$$

Equation (9.39) is a relation for  $dV/V$  strictly in terms of  $M$  — this is precisely what is desired for the integral in Eq. (9.33). Hence, substituting Eq. (9.39) into (9.33), we have

$$\theta = \int_{M_1}^{M_2} \frac{\sqrt{M^2 - 1}}{1 + [(\gamma - 1)/2] M^2} \frac{dM}{M} \quad (9.40)$$

In Eq. (9.40), the integral

$$\nu(M) = \int \frac{\sqrt{M^2 - 1}}{1 + [(\gamma - 1)/2] M^2} \frac{dM}{M} \quad (9.41)$$

is called the *Prandtl-Meyer function*, denoted by  $\nu$ . Carrying out the integration, Eq. (9.41) becomes

$$\boxed{\nu(M) = \sqrt{\frac{\gamma + 1}{\gamma - 1}} \tan^{-1} \sqrt{\frac{\gamma - 1}{\gamma + 1} (M^2 - 1)} - \tan^{-1} \sqrt{M^2 - 1}} \quad (9.42)$$

The constant of integration that would ordinarily appear in Eq. (9.42) is not important, because it drops out when Eq. (9.42) is used for the definite integral in Eq. (9.40). For convenience, it is chosen as zero, such that  $\nu(M) = 0$  when  $M = 1$ . Finally, we can now write Eq. (9.40), combined with (9.41), as

$$\boxed{\theta = \nu(M_2) - \nu(M_1)} \quad (9.43)$$

$$(9.34)$$

where  $\nu(M)$  is given by Eq. (9.42) for a calorically perfect gas. The Prandtl-Meyer function  $\nu$  is very important; it is the key to the calculation of changes across an expansion wave. Because of its importance,  $\nu$  is tabulated as a function of  $M$  in App. C. For convenience, values of  $\mu$  are also tabulated in App. C.

How do the above results solve the problem stated in Fig. 9.20; i.e., how can we obtain the properties in region 2 from the known properties in region 1 and the known deflection angle  $\theta$ ? The answer is straightforward:

1. For the given  $M_1$ , obtain  $\nu(M_1)$  from App. C.
2. Calculate  $\nu(M_2)$  from Eq. (9.43), using the known  $\theta$  and the value of  $\nu(M_1)$  obtained in step 1.
3. Obtain  $M_2$  from App. C corresponding to the value of  $\nu(M_2)$  from step 2.
4. The expansion wave is isentropic; hence,  $p_0$  and  $T_0$  are constant through the wave. That is,  $T_{0,2} = T_{0,1}$  and  $p_{0,2} = p_{0,1}$ . From Eq. (8.40), we have

$$\frac{T_2}{T_1} = \frac{T_2/T_{0,2}}{T_1/T_{0,1}} = \frac{1 + [(\gamma - 1)/2] M_1^2}{1 + [(\gamma - 1)/2] M_2^2} \quad (9.44)$$

From Eq. (8.42), we have

$$\frac{p_2}{p_1} = \frac{p_2/p_0}{p_1/p_0} = \frac{\left(1 + [(\gamma - 1)/2] M_1^2\right)^{\gamma/(\gamma-1)}}{\left(1 + [(\gamma - 1)/2] M_2^2\right)^{\gamma/(\gamma-1)}} \quad (9.45)$$

Since we know both  $M_1$  and  $M_2$ , as well as  $T_1$  and  $p_1$ , Eqs. (9.44) and (9.45) allow the calculation of  $T_2$  and  $p_2$  downstream of the expansion wave.

**Example 9.2** A supersonic flow with  $M_1 = 1.5$ ,  $p_1 = 1$  atm, and  $T_1 = 288$  K is expanded around a sharp corner (see Fig. 9.20) through a deflection angle of  $15^\circ$ . Calculate  $M_2$ ,  $p_2$ ,  $T_2$ ,  $p_{0,2}$ ,  $T_{0,2}$ , and the angles that the forward and rearward Mach lines make with respect to the upstream flow direction.

**SOLUTION** From App. C, for  $M_1 = 1.5$ ,  $\nu_1 = 11.91^\circ$ . From Eq. (9.43),  $\nu_2 = \nu_1 + \theta = 11.91 + 15 = 26.91^\circ$ . Thus,  $\boxed{M_2 = 2.0}$  (rounding to the nearest entry in the table).

From App. A, for  $M_1 = 1.5$ ,  $p_{0,1}/p_1 = 3.671$  and  $T_{0,1}/T_1 = 1.45$ , and for  $M_2 = 2.0$ ,  $p_{0,2}/p_2 = 7.824$  and  $T_{0,2}/T_2 = 1.8$ . Since the flow is isentropic,  $T_{0,2} = T_{0,1}$  and  $p_{0,2}'' = p_{0,1}$ . Thus,

$$\boxed{p_2 = \frac{p_2}{p_{0,2}} \frac{p_{0,1}}{p_1} p_1 = \frac{1}{7.824} (1)(3.671)(1 \text{ atm}) = 0.469 \text{ atm}}$$

$$\boxed{T_2 = \frac{T_2}{T_{0,1}} \frac{T_{0,1}}{T_1} T_1 = \frac{1}{1.8} (1)(1.45)(288) = 232 \text{ K}}$$

$$\boxed{p_{0,2} = p_{0,1} = \frac{p_{0,1}}{p_1} p_1 = 3.671 (1 \text{ atm}) = 3.671 \text{ atm}}$$

$$\boxed{T_{0,2} = T_{0,1} = \frac{T_{0,1}}{T_1} T_1 = 1.45 (288) = 417.6 \text{ K}}$$

Returning to Fig. 9.20,

$$\text{Angle of forward Mach line} = \mu_1 = 41.81^\circ$$

$$\text{Angle of rearward Mach line} = 45^\circ - \theta = 30^\circ$$

## 9.7 SHOCK-EXPANSION THEORY: APPLICATIONS TO SUPERSONIC AIRFOILS

Consider a flat plate of length  $c$  at an angle of attack  $\alpha$  in a supersonic flow, as sketched in Fig. 9.23. On the top surface, the flow is turned away from itself; hence an expansion wave occurs at the leading edge, and the pressure on the top surface,  $p_2$ , is less than the freestream pressure,  $p_1 < p_2$ . At the trailing edge, the flow must return to approximately (but not precisely) the freestream direction. Here, the flow is turned back into itself, and consequently a shock wave occurs at the trailing edge. On the bottom surface, the flow is turned into itself; an oblique shock wave occurs at the leading edge, and the pressure on the bottom surface,  $p_3$ , is greater than the freestream pressure  $p_1 > p_3$ . At the trailing edge, the flow is turned into approximately (but not precisely) the freestream direction by means of an expansion wave. Examining Fig. 9.23, note that the top and bottom surfaces of the flat plate experience uniform pressure distribution of  $p_2$  and  $p_3$ , respectively, and that  $p_3 > p_2$ . This creates a net pressure imbalance which generates the resultant aerodynamic force  $R$ , shown in Fig. 9.23. Indeed, for a unit span, the resultant force and its components, lift and drag, per unit span are

$$R' = (n_1 - n_2)c \quad (9.46)$$

(0, 13)

$$D' \equiv (n_1 - n_2) c \sin \alpha$$

In Eqs. (9.47) and (9.48),  $p_3$  is calculated from oblique shock properties (Sec. 9.2), and  $p_2$  is calculated from expansion-wave properties (Sec. 9.6). Moreover, these are *exact* calculations; no approximations have been made. The inviscid, supersonic flow over a flat plate at angle of attack is exactly given by the combination of shock and expansion waves sketched in Fig. 9.23.

The flat-plate case given above is the simplest example of a general technique called *shock-expansion theory*. Whenever we have a body made up of straight line segments and the deflection angles are small enough so that no detached shock waves occur, the flow over the body goes through a series of distinct oblique shock and expansion waves, and the pressure distribution on the surface (hence the lift and drag) can be obtained *exactly* from both the shock- and expansion-wave theories discussed in this chapter.

As another example of the application of shock-expansion theory, consider the diamond-shape airfoil in Fig. 9.24. Assume the airfoil is at zero degrees angle of attack. The supersonic flow over the airfoil is first compressed and deflected through the angle  $\epsilon$  by the oblique shock wave at the leading edge. At midchord, the flow is expanded through an angle  $2\epsilon$ , creating an expansion wave. At the trailing edge, the flow is turned back to the freestream direction through another oblique shock. The pressure distributions on the front and back faces of the airfoil are sketched in Fig. 9.24; note that the pressures on faces  $a$  and  $c$  are uniform and equal to  $p_2$  and that the pressures on faces  $b$  and  $d$  are also uniform but equal to  $p_1$ , where  $p_1 < p_2$ . In the lift direction, perpendicular to the freestream, the pressure distributions on the top and bottom faces exactly cancel; that is,  $L' = 0$ . In contrast, in the drag direction, parallel to the freestream, the pressure on the front faces  $a$  and  $c$  is larger than on the back faces  $b$  and  $d$ , and this results in a finite drag. To calculate this drag (per unit span), consider the geometry of the diamond airfoil in Fig. 9.24, where  $l$  is the length of each face and  $t$  is the airfoil thickness. Then,

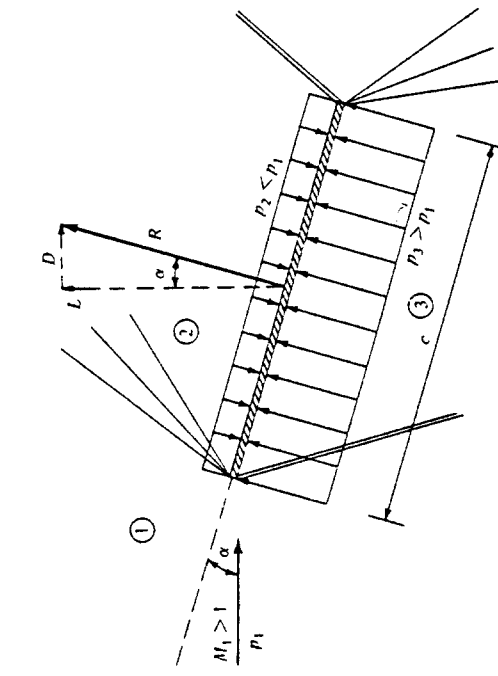


Figure 9.23 Flat plate at an angle of attack in a supersonic flow.

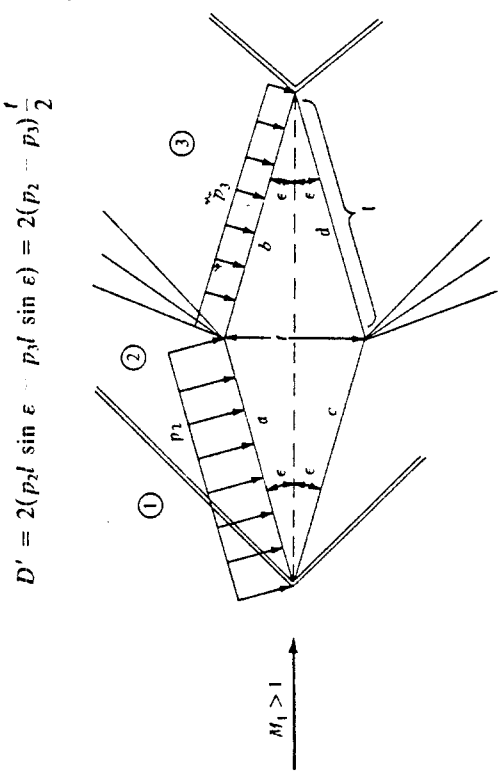


Figure 9.24 Diamond-wedge airfoil at  $0^\circ$  angle of attack in a supersonic flow.

$$\text{Hence } D' = (p_2 - p_1)t \quad (9.49)$$

In Eq. (9.49),  $p_2$  is calculated from oblique shock theory, and  $p_1$  is obtained from expansion-wave theory. Moreover, these pressures are the *exact* values for supersonic, inviscid flow over the diamond airfoil.

At this stage, it is worthwhile to recall our discussion in Sec. 1.5 concerning the source of aerodynamic force on a body. In particular, examine Eqs. (1.1), (1.2), (1.7), and (1.8). These equations give the means to calculate  $L'$  and  $D'$  from the pressure and shear stress distributions over the surface of a body of general shape. The results of the present section, namely, Eqs. (9.47) and (9.48) for a flat plate and Eq. (9.49) for the diamond airfoil, are simply specialized results from the more general formulas given in Sec. 1.5. However, rather than formally going through the integration indicated in Eqs. (1.7) and (1.8), we obtained our results for the simple bodies in Figs. 9.23 and 9.24 in a more direct fashion.

The results of this section illustrate a very important aspect of inviscid, supersonic flow. Note that Eq. (9.48) for the flat plate and Eq. (9.49) for the diamond airfoil predict a *finite drag* for these two-dimensional profiles. This is in direct contrast to our results for two-dimensional bodies in a low-speed, incompressible flow, as discussed in Chaps. 3 and 4, where the drag was theoretically zero. That is, in supersonic flow, d'Alembert's paradox does not occur. In a supersonic, inviscid flow, the drag per unit span on a two-dimensional body is finite. This new source of drag is called *wave drag*, and it represents a serious consideration in the design of all supersonic airfoils. The existence of wave drag is inherently related to the increase in entropy and consequently to the loss of total pressure across the oblique shock waves created by the airfoil.

Finally, the results of this section represent a merger of both the left- and right-hand branches of our road map shown in Fig. 9.5. As such, it brings us to a logical conclusion of our discussion of oblique waves in supersonic flows.

## 9.8 HISTORICAL NOTE: ERNST MACH — A BIOGRAPHICAL SKETCH

The Mach number is named in honor of Ernst Mach, an Austrian physicist and philosopher who was an illustrious and controversial figure in late nineteenth-century physics. Mach conducted the first meaningful experiments in supersonic flight, and his results triggered a similar interest in Ludwig Prandtl 20 years later. Who was Mach? What did he actually accomplish in supersonic aerodynamics? Let us look at this man further.

Mach was born at Turas, Moravia, in Austria, on February 18, 1838. His father, Johann, was a student of classical literature who settled with his family on a farm in 1840. An extreme individualist, Johann raised his family in an atmosphere of seclusion, working on various improved methods of farming, including silkworm cultivation. Ernst's mother, on the other hand, came from a family of lawyers and doctors and brought with her a love of poetry and music. Ernst seemed to thrive in this family atmosphere. Until the age of 14, his education came exclusively from instruction by his father, who read extensively in the Greek and Latin classics. In 1853, Mach

entered public school, where he became interested in the world of science. He went on to obtain a Ph.D. in physics in 1860 at the University of Vienna, writing his dissertation on electrical discharge and induction. In 1864, he became a full professor of mathematics at the University of Graz and was given the title of Professor of Physics in 1866. Mach's work during this period centered on optics — a subject which was to interest him for the rest of his life. The year 1867 was important for Mach — during that year he married, and he also became a professor of experimental physics at the University of Prague, a position he held for the next 28 years. While at Prague, Mach published over 100 technical papers — work which was to constitute the bulk of his technical contributions.

Mach's contribution to supersonic aerodynamics involves a series of experiments covering the period from 1873 to 1893. In collaboration with his son, Ludwig, Mach studied the flow over supersonic projectiles, as well as the propagation of second waves and shock waves. His work included the flow fields associated with meteorites, explosions, and gas jets. The main experimental data were photographic results. Mach combined his interest in optics and supersonic motion by designing several photographic techniques for making shock waves in air visible. He was the first to use the schlieren system in aerodynamics; this system senses density gradients and allows shock waves to appear on screens or photographic negatives. He also devised an interferometric technique which senses directly the change in density in a flow. A pattern of alternate dark and light bands are set up on a screen by the superposition of light rays passing through regions of different density. Shock waves are visible as a shift in this pattern along the shock. Mach's optical device still perpetuates today in the form of the Mach-Zehnder interferometer, an instrument present in many aerodynamic laboratories. Mach's major contributions in supersonic aerodynamics are contained in a paper given to the Academy of Sciences in Vienna in 1887. Here, for the first time in history, Mach shows a photograph of a weak wave on a slender cone moving at supersonic speed, and he demonstrates that the angle  $\mu$  between this wave and the direction of flight is given by  $\sin \mu = a/V$ . This angle was later denoted as the Mach angle by Prandtl and his colleagues after their work on shock and expansion waves in 1907 and 1908. Also, Mach was the first person to point out the discontinuous and marked changes in a flow field as the ratio  $V/a$  changes from below 1 to above 1.

It is interesting to note that the ratio  $V/a$  was not denoted as Mach number by Mach himself. Rather, the term "Mach number" was coined by the Swiss engineer Jacob Ackeret in his inaugural lecture in 1929 as Privatdozent at the Eidgenossische Technische Hochschule in Zurich. Hence, the term "Mach number" is of fairly recent usage, not being introduced into the English literature until the early 1930s.

In 1895, the University of Vienna established the Ernst Mach chair in the philosophy of inductive sciences. Mach moved to Vienna to occupy this chair. In 1897 he suffered a stroke which paralyzed the right side of his body. Although he eventually partially recovered, he officially retired in 1901. From that time until his death on February 19, 1916 near Munich, Mach continued to be an active thinker, lecturer, and writer.

In our time, Mach is most remembered for his early experiments on supersonic flow and, of course, through the Mach number itself. However, Mach's contempor-

ties, as well as Mach himself, viewed him more as a philosopher and historian of science. Coming at the end of the nineteenth century, when most physicists felt comfortable with Newtonian mechanics, and many believed that virtually all was known about physics, Mach's outlook on science is summarized by the following passage from his book *Die Mechanik*:

The most important result of our reflections is that precisely the apparently simplest mechanical theorems are of a very complicated nature; that they are founded on incomplete experiences, even on experiences that never can be fully completed; that in view of the tolerable stability of our environment they are, in fact, practically safeguarded to serve as the foundation of mathematical deduction; but that they by no means themselves can be regarded as mathematically established truths, but only as theorems that not only admit of constant control by experience but actually require it.

In other words, Mach was a staunch experimentalist who believed that the established laws of nature were simply theories and that only observations that are apparent to the senses are the fundamental truth. In particular, Mach could not accept the elementary ideas of atomic theory or the basis of relativity, both of which were beginning to surface during Mach's later years and, of course, were to form the basis of twentieth-century modern physics. As a result, Mach's philosophy did not earn him favor with most of the important physicists of his day. Indeed, at the time of his death, Mach was planning to write a book pointing out the flaws of Einstein's theory of relativity.

Although Mach's philosophy was controversial, he was respected for being a thinker. In fact, in spite of Mach's critical outlook on the theory of relativity, Albert Einstein had the following to say in the year of Mach's death: "I even believe that those who consider themselves to be adversaries of Mach scarcely know how much of Mach's outlook they have, so to speak, adsorbed with their mother's milk."

Hopefully, this section has given you a new dimension to think about whenever you encounter the term "Mach number." Maybe you will pause now and then to reflect on the man himself and to appreciate that the term "Mach number" is in honor of a man who devoted his life to experimental physics, but who at the same time was bold enough to view the physical world through the eyes of a self-styled philosopher.

## 9.9 SUMMARY

The road map given in Fig. 9.5 illustrates the flow of our discussion on oblique waves in supersonic flow. Review this road map, and make certain that you are familiar with all the ideas and results that are represented in Fig. 9.5.

Some of the more important results are summarized below.

An infinitesimal disturbance in a multidimensional supersonic flow creates a Mach wave which makes an angle  $\mu$  with respect to the upstream velocity. This angle is defined as the Mach angle and is given by

$$\mu = \sin^{-1} \frac{1}{M} \quad (9.1)$$

Changes across an oblique shock wave are determined by the normal component of velocity ahead of the wave. For a calorically perfect gas, the normal component of the upstream Mach number is the determining factor. Changes across an oblique shock can be determined from the normal shock relations derived in Chap. 8 by using  $M_{n,1}$  in these relations, where

$$M_{n,1} = M_1 \sin \beta \quad (9.13)$$

Changes across an oblique shock depend on two parameters, for example,  $M_1$  and  $\beta$ , or  $M_1$  and  $\theta$ . The relationship between  $M_1$ ,  $\beta$ , and  $\theta$  is given in Fig. 9.7, which should be studied closely.

Oblique shock waves incident on a solid surface reflect from that surface in such a fashion to maintain flow tangency on the surface. Oblique shocks also intersect each other, with the results of the intersection depending on the arrangement of the shocks.

The governing factor in the analysis of a centered expansion wave is the Prandtl-Meyer function  $\nu(M)$ . The key equation which relates the downstream Mach number  $M_1$ , the upstream Mach number  $M_2$ , and the deflection angle  $\theta$  is

$$\theta = \nu(M_2) - \nu(M_1) \quad (9.43)$$

The pressure distribution over a supersonic airfoil made up of straight line segments can usually be calculated exactly from a combination of oblique and expansion waves—i.e., from exact shock-expansion theory.

## PROBLEMS

9.1 A slender missile is flying at Mach 1.5 at low altitude. Assume the wave generated by the nose of the missile is a Mach wave. This wave intersects the ground 559 ft behind the nose. At what altitude is the missile flying?

9.2 Consider an oblique shock wave with a wave angle of  $30^\circ$  in a Mach 4 flow. The upstream pressure and temperature are  $2.65 \times 10^4 \text{ N/m}^2$  and  $223.3 \text{ K}$ , respectively (corresponding to a standard altitude of 10,000 m). Calculate the pressure, temperature, Mach number, total pressure, and total temperature behind the wave and the entropy increase across the wave.

9.3 Equation (8.80) does not hold for an oblique shock wave, and hence the column in App. B labeled  $p_{n,2}/p_n$ , can be used for an oblique shock wave. On the other hand, the column labeled  $M_{n,1}$  can be used for an oblique shock wave, using  $M_{n,1}$ . Explain why all this is so.

- 9.4 Consider an oblique shock wave with a wave angle of  $36.87^\circ$ . The upstream flow is given by  $M_1 = 3$  and  $p_1 = 1$  atm. Calculate the total pressure behind the shock using  
 (a)  $p_{n1}/p_0$ , from App. B (the correct way)  
 (b)  $p_{n1}/p_1$ , from App. B (the incorrect way)
- (Compare the results.)

9.5 Consider the flow over a  $22.2^\circ$  half-angle wedge. If  $M_1 = 2.5$ ,  $p_1 = 1$  atm, and  $T_1 = 300$  K, calculate the wave angle and  $p_2$ ,  $T_2$ , and  $M_2$ .

9.6 Consider a flat plate at an angle of attack  $\alpha$  to a Mach 2.4 airflow at 1 atm pressure. What is the maximum pressure that can occur on the plate surface and still have an attached shock wave at the leading edge? At what value of  $\alpha$  does this occur?

9.7 A  $30.2^\circ$  half-angle wedge is inserted into a freestream with  $M_\infty = 3.5$  and  $p_\infty = 0.5$  atm. A Pitot tube is located above the wedge surface and behind the shock wave. Calculate the magnitude of the pressure sensed by the Pitot tube.

9.8 Consider a Mach 4 airflow at a pressure of 1 atm. We wish to slow this flow to subsonic speed through a system of shock waves with as small a loss in total pressure as possible. Compare the loss in total pressure for the following three shock systems:

- A single normal shock wave
- An oblique shock with a deflection angle of  $25.3^\circ$ , followed by a normal shock
- An oblique shock with a deflection angle of  $25.3^\circ$ , followed by a second oblique shock of deflection angle of  $20^\circ$ , followed by a normal shock

From the results of (a), (b), and (c), what can you deduce about the efficiency of the various shock systems.

9.9 Consider an oblique shock generated at a compression corner with a deflection angle  $\theta = 18.2^\circ$ . A straight horizontal wall is present above the corner, as shown in Fig. 9.14. If the upstream flow has the properties  $M_1 = 3.2$ ,  $p_1 = 1$  atm and  $T_1 = 520^\circ\text{R}$ , calculate  $M_2$ ,  $p_2$ , and  $T_2$  behind the reflected shock from the upper wall. Also obtain the angle  $\Phi$  which the reflected shock makes with the upper wall.

9.10 Consider the supersonic flow over an expansion corner, such as given in Fig. 9.20. The deflection angle  $\theta = 23.38^\circ$ . If the flow upstream of the corner is given by  $M_1 = 2$ ,  $p_1 = 0.7$  atm,  $T_1 = 630^\circ\text{R}$ , calculate  $M_2$ ,  $p_2$ ,  $T_2$ ,  $p_{n2}$ ,  $p_{n3}$ , and  $T_{n2}$ , downstream of the corner. Also, obtain the angles the forward and rearward Mach lines make with respect to the upstream direction.

9.11 A supersonic flow at  $M_1 = 1.58$  and  $p_1 = 1$  atm expands around a sharp corner. If the pressure downstream of the corner is 0.1306 atm, calculate the deflection angle of the corner.

9.12 A supersonic flow at  $M_1 = 3$ ,  $T_1 = 285$  K, and  $p_1 = 1$  atm is deflected upward through a compression corner with  $\theta = 30.6^\circ$  and then is subsequently expanded around a corner of the same angle such that the flow direction is the same as its original direction. Calculate  $M_3$ ,  $p_3$ , and  $T_3$ , downstream of the expansion corner. Since the resulting flow is in the same direction as the original flow, would you expect  $M_3 = M_1$ ,  $p_3 = p_1$ , and  $T_3 = T_1$ ? Explain.

9.13 Consider an infinitely thin flat plate at an angle of attack  $\alpha$  in a Mach 2.6 flow. Calculate the lift and wave-drag coefficients for  
 (a)  $\alpha = 5^\circ$    (b)  $\alpha = 15^\circ$    (c)  $\alpha = 30^\circ$

(Note: Save the results of this problem for use in Chap. 12.)

9.14 Consider a diamond-wedge airfoil such as shown in Fig. 9.24, with a half-angle  $\epsilon = 10^\circ$ . The airfoil is at an angle of attack  $\alpha = 15^\circ$  to a Mach 3 freestream. Calculate the lift and wave-drag coefficients for the airfoil.

9.15 Consider sonic flow. Calculate the maximum deflection angle through which this flow can be expanded via a centered expansion wave.

## CHAPTER TEN

### COMPRESSIBLE FLOW THROUGH NOZZLES, DIFFUSERS, AND WIND TUNNELS

*Having wondered from what source there is so much difficulty in successfully applying the principles of dynamics to fluids than to solids, finally, turning the matter over more carefully in my mind, I found the true origin of the difficulty. I discovered it to consist of the fact that a certain part of the existing forces important in forming the throat (so called by me, not considered by others) was neglected, and moreover regarded as of no importance, for no other reason than the throat is composed of a very small, or even an infinitely small, quantity of fluid, such as occurs whenever fluid passes from a wider place to a narrower, or vice versa, from a narrower to a wider.*

*Johann Bernoulli, from his  
Hydraulics, 1743*

## 10.1 INTRODUCTION

Chapters 8 and 9 treated normal and oblique waves in supersonic flow. These waves are present on any aerodynamic vehicle in supersonic flight. Aeronautical engineers are concerned with observing the characteristics of such vehicles, especially the generation of lift and drag at supersonic speeds, as well as details of the flow field, including the shock- and expansion-wave patterns. To make such observations, we usually have two standard choices: (1) conduct flight tests using the actual vehicle, and (2) run wind-tunnel tests on a small-scale model of the vehicle. Flight tests, although providing the final answers in the full-scale environment, are costly and, not to say the least, dangerous if the vehicle is unproven. Hence, the vast bulk of supersonic aerodynamic data have been obtained in wind tunnels on the ground. What do such supersonic wind tunnels look like? How do we produce a uniform flow of supersonic gas in a laboratory environment? What are the characteristics of supersonic wind tunnels? The answers to these and other questions are addressed in this chapter.

The first practical supersonic wind tunnel was built and operated by Adolf Busemann in Germany in the mid-1930s, although Prandtl had a small supersonic facility operating as early as 1905 for the study of shock waves. A photograph of Busemann's tunnel is shown in Fig. 10.1. Such facilities proliferated quickly during and after World War II. Today, all modern aerodynamic laboratories have one or more supersonic wind

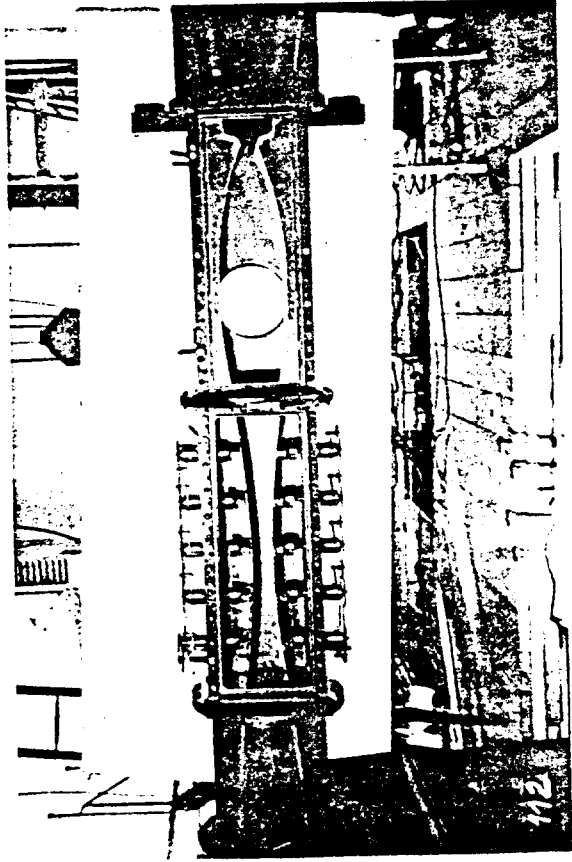


Figure 10.1 The first practical supersonic wind tunnel, built by A. Busemann in Germany in the mid 1930s.  
(Courtesy of A. Busemann.)

tunnels, and many are equipped with hypersonic tunnels as well. Such machines come in all sizes; an example of a moderately large hypersonic tunnel is shown in Fig. 10.2. In this chapter we discuss the aerodynamic fundamentals of compressible flow through ducts. Such fundamentals are vital to the proper design of high-speed wind tunnels, rocket engines, high-energy gas-dynamic and chemical lasers, and jet engines, to list just a few. Indeed, the material developed in this chapter is used almost daily by practicing aerodynamicists and is indispensable toward a full understanding of compressible flow.

The road map for this chapter is given in Fig. 10.3. After deriving the governing equations, we treat the cases of a nozzle and diffuser separately. Then we merge this information to examine the case of supersonic wind tunnels.



Figure 10.2 A large hypersonic wind tunnel at the U.S. Air Force Wright Aeronautical Laboratory, Dayton, Ohio. (Courtesy of the U.S. Air Force.)

by examining Fig. 10.4b. In particular, the velocity at the boundary of the streamtube must be tangent to the boundary, and hence it has components in the  $y$  and  $z$  directions as well as the axial  $x$  direction. However, if the area variation is moderate, the components in the  $y$  and  $z$  directions are small in comparison with the component in the  $x$  direction. In such a case, the flow-field variables can be assumed to vary with  $x$  only; i.e., the flow can be assumed to be uniform across any cross section at a given  $x$  station. Such a flow, where  $A = A(x)$ , but  $p = p(x)$ ,  $\rho = \rho(x)$ ,  $u = u(x)$ , etc., is defined as quasi-one-dimensional flow, as sketched in Fig. 10.4b. Such flow is the subject of this

## 10.2 GOVERNING EQUATIONS FOR QUASI-ONE-DIMENSIONAL FLOW

Recall the one-dimensional flow treated in Chap. 8. There, we considered the flow-field variables to be a function of  $x$  only, that is,  $p = p(x)$ ,  $\rho = \rho(x)$ , etc. Strictly speaking, a streamtube for such a flow must be of constant area; i.e., the one-dimensional flow discussed in Chap. 8 is constant-area flow, as sketched in Fig. 10.4a.

In contrast, assume that the area of the streamtube changes as a function of  $x$ , that is,  $A = A(x)$ , as sketched in Fig. 10.4b. Strictly speaking, this flow is three-dimensional; the flow-field variables are function of  $x$ ,  $y$ , and  $z$ , as can be seen simply

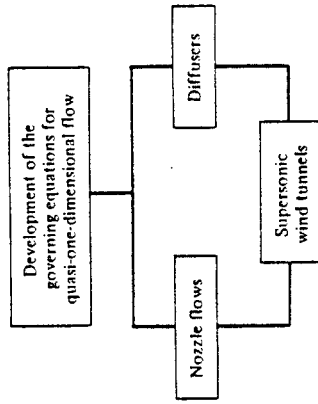
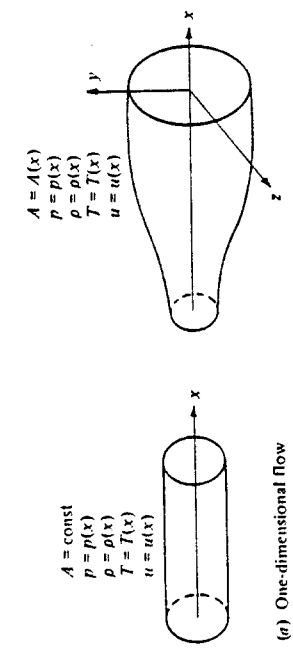


Figure 10.3 Road map for Chap. 10.



**Figure 10.4** One-dimensional and quasi-one-dimensional flows.

chapter. We have encountered quasi-one-dimensional flow earlier, in our discussion of incompressible flow through a duct in Sec. 3.3. Return to Sec. 3.3, and review the concepts presented there before progressing further.

Although the assumption of quasi-one-dimensional flow is an approximation to the actual flow in a variable-area duct, the integral forms of the conservation equations, namely, continuity [Eq. (2.39)], momentum [Eq. (2.55)], and energy [Eq. (2.86)], can be used to obtain governing equations for quasi-one-dimensional flow which are physically consistent, as follows. Consider the control volume given in Fig. 10.5. At station 1, the flow across area  $A_1$  is assumed to be uniform with properties  $p_1$ ,  $\rho_1$ ,  $u_1$ , etc. Similarly, at station 2, the flow across area  $A_2$  is assumed to be uniform with properties  $p_2$ ,  $\rho_2$ ,  $u_2$ , etc. The application of the integral form of the continuity equation was made to such a variable-area control volume in Sec. 3.3. The resulting continuity equation for steady, quasi-one-dimensional flow was obtained as Eq. (3.21), which in terms of the nomenclature in Fig. 10.5 yields

$$\rho_1 u_1 A_1 = \rho_2 u_2 A_2 \quad (10.1)$$

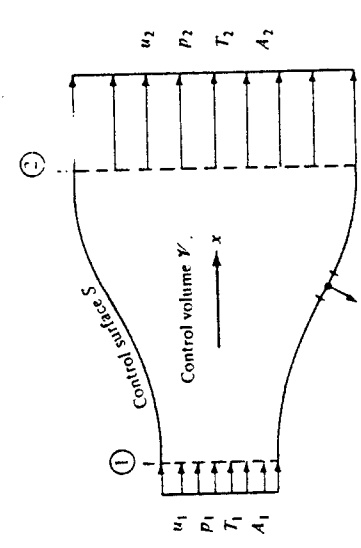


**Figure 10.5** Finite control volume for quasi-one-dimensional flow.

Consider the integral form of the momentum equation, Eq. (2.55). For a steady, inviscid flow with no body forces, this equation becomes

$$\oint_S (\rho V \cdot dS) V = - \oint_S p dS \quad (10.2)$$

Since Eq. (10.2) is a vector equation, let us examine its  $x$  component, given below:

$$\oint_S (\rho V \cdot dS) u = - \oint_S (p dS), \quad (10.3)$$

where  $(p dS)$  denotes the  $x$  component of the pressure force. Since Eq. (10.3) is a scalar equation, we must be careful about the sign of the  $x$  components when evaluating the surface integrals. All components pointing to the right in Fig. 10.5 are positive, and those pointing to the left are negative. The upper and lower surfaces of the control volume in Fig. 10.5 are streamlines; hence,  $V \cdot dS = 0$  along these surfaces. Also, recall that across  $A_1$ ,  $V$  and  $dS$  are in opposite directions; hence,  $V \cdot dS$  is negative. Therefore, the integral on the left of Eq. (10.3) becomes  $-\rho_1 u_1^2 A_1 + \rho_2 u_2^2 A_2$ . The pressure integral on the right of Eq. (10.2), evaluated over the faces  $A_1$  and  $A_2$  of the control volume, becomes  $-(p_1 A_1 + p_2 A_2)$ . (The negative sign in front of  $p_1 A_1$  is because  $dS$  over  $A_1$  points to the left, which is the negative direction for the  $x$  components.) Evaluated over the upper and lower surface of the control volume, the pressure integral can be expressed as

$$-\int_{A_1}^{A_2} -p dA = \int_{A_1}^{A_2} p dA \quad (10.4)$$

where  $dA$  is simply the  $x$  component of the vector  $dS$ , that is, the area  $dS$  projected on a plane perpendicular to the  $x$  axis. The negative sign inside the integral on the left of Eq. (10.4) is due to the direction of  $dS$  along the upper and lower surfaces; note that  $dS$  points in the backward direction along these surfaces, as shown in Fig. 10.5. Hence, the  $x$  component of  $p dS$  is to the left and, therefore, appears in our equations as a negative component. [Recall from Sec. 2.5 that the negative sign *outside* the pressure integral, i.e., outside the integral on the left of Eq. (10.4), is always present to account for the physical fact that the pressure force  $p dS$  exerted on a control surface always acts in the opposite direction of  $dS$ . If you are unsure about this, review the derivation of the momentum equation in Sec. 2.5. Also, do not let the signs in the above results confuse you; they are all quite logical if you keep track of the direction of the  $x$  components.] With the above results, Eq. (10.3) becomes

$$-\rho_1 u_1^2 A_1 + \rho_2 u_2^2 A_2 = -(p_1 A_1 + p_2 A_2) + \int_{A_1}^{A_2} p dA \quad (10.5)$$

$$p_1 A_1 + \rho_1 u_1^2 A_1 + \int_{A_1}^{A_2} p dA = p_2 A_2 + \rho_2 u_2^2 A_2$$

Equation (10.5) is the momentum equation for steady, quasi-one-dimensional flow.

Consider the energy equation given by Eq. (2.86). For inviscid, adiabatic, steady flow with no body forces, this equation becomes

$$\oint \oint \rho \left( e + \frac{V^2}{2} \right) V \cdot dS = - \oint \oint p V \cdot dS \quad (10.6)$$

Applied to the control volume in Fig. 10.5, Eq. (10.6) yields

$$\rho_1 \left( e_1 + \frac{u_1^2}{2} \right) (-u_1 A_1) + \rho_2 \left( e_2 + \frac{u_2^2}{2} \right) (u_2 A_2) = -(-p_1 u_1 A_1 + p_2 u_2 A_2)$$

1 : 21

$$i_1 A_{11} \left( e_1 + \frac{u_1}{2} \right) = p_1 u_2 A_2 + \rho_2 u_2 A_2 \left( e_2 + \frac{u_2}{2} \right) \quad (10.8)$$

. (10.1), we have

$$\frac{p_1}{\rho_1} + e_1 + \frac{u_1^2}{2} = \frac{p_2}{\rho_2} + e_2 + \frac{u_2^2}{2} \quad (10.8')$$

Recall that  $h = e + pv = e + p/\rho$ . Hence, Eq. (10.8) becomes

$$h_1 + \frac{u_1^2}{2} = h_2 + \frac{u_2^2}{2} \quad (10.9)$$

which is the energy equation for steady, adiabatic, inviscid quasi-one-dimensional flow. Examine Eq. (10.9) closely; it is a statement that the total enthalpy,  $h_0 = h + u^2/2$ , is a constant throughout the flow. Once again, this should come as no surprise; Eq. (10.9) is simply another example of the general result for steady, inviscid adiabatic flow discussed in Sec. 7.5. Hence, we can replace Eq. (10.9) by

$b_0 = \text{const}$

Pause for a moment and examine our results given above. We have applied the integral forms of the conservation equations to the control volume in Fig. 10.5. We have obtained, as a result, Eqs. (10.1), (10.5), and (10.9) or (10.10) as the governing continuity, momentum, and energy equations, respectively, for quasi-one-dimensional flow. Examine these equations — they are *algebraic* equations (with the exception of the single integral term in the momentum equation). In Fig. 10.5, assume that the inflow conditions  $p_1$ ,  $u_1$ ,  $p_1$ ,  $T_1$ , and  $h_1$  are given and that the area distribution  $A = A(x)$  is presented. Also, assume a calorically perfect gas, where

(10.11) (10.12)

and

Equations (10.1), (10.5), (10.9) or (10.10), (10.11), and (10.12) constitute five equations for the five unknowns  $\rho_2$ ,  $u_2$ ,  $p_2$ ,  $T_2$ , and  $h_2$ . We could, in principle, solve these equations directly for the unknown flow quantities at station 2 in Fig. 10.5. However,

such a direct solution would involve substantial algebraic manipulations. Instead, we take a simpler fact, as described in Sec. 10.3,

卷之三

Before moving on to a solution of the governing equations, let us examine some physical characteristics of a quasi-one-dimensional flow. To help this examination, we first obtain some *differential* expressions for the governing equations, in contrast to the algebraic equations obtained above. For example, consider Eq. (10.1), which states that

$$\partial u A = \text{const} \quad (10.13)$$

through a variable area dust Differentiating Eq. (10-13) we have

(10.14)

which is the differential form of the continuity equation for quasi-one-dimensional

To obtain a differential form of the momentum equation, apply Eq. (10.5) to the infinitesimal control volume sketched in Fig. 10.6. The flow going into the volume at station 1, where the area is  $A$ , has properties  $p$ ,  $u$ , and  $\rho$ . In traversing the length  $dx$ , where the area changes by  $dA$ , the flow properties change by the corresponding amounts  $dp$ ,  $d\rho$ , and  $du$ . Hence, the flow leaving at station 2 has the properties  $p + dp$ ,  $u + du$ , and  $\rho + d\rho$ , as shown in Fig. 10.6. For this case, Eq. (10.5) becomes [recognizing that the integral in Eq. (10.5) can be replaced by its integrand for the differential volume in Fig. 10.6]

*Differential volume in Fig. 10-3j*

$$pA + \rho u^2 A + p dA = (p + dp)(A + dA) + (\rho + d\rho)(u + du)^2(A + dA) \quad (10.15)$$

In Eq. (10.15), all products of differentials, such as  $d\rho dA$ ,  $d\rho (du)^2$ , are very small and can be ignored. Hence, Eq. (10.15) becomes

$$\Delta d\eta + \Delta u^2 d\theta + \alpha u^2 dA + 2\alpha u A du = 0 \quad (10.16)$$

Expanding the continuity equation, Eq. (10.14), and multiplying by  $u$ , we have

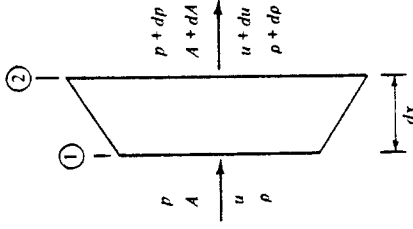


**Figure 10.6** Incremental control volume.

$$\rho u^2 dA + \rho u A du + A u^2 d\rho = 0 \quad (10.17)$$

Subtracting Eq. (10.17) from (10.16), we obtain

$$dp = -\rho u du \quad (10.18)$$

which is the differential form of the momentum equation for steady, inviscid, quasi-one-dimensional flow. Equation (10.18) is called *Euler's equation*. We have seen it before—as Eq. 3.12. In Sec. 3.2, it was derived from the differential form of the general momentum equation in three dimensions. (Make certain to review that derivation before progressing further.) In Sec. 3.2, we demonstrated that Eq. (3.12) holds along a streamline in a general three-dimensional flow. Now we see Euler's equation again, in Eq. (10.18), which was derived from the governing equations for quasi-one-dimensional flow. A differential form of the energy equation follows directly from Eq. (10.9), which states that

$$dh + \frac{u^2}{2} = \text{const}$$

Differentiating this equation, we have

$$du + u du = 0 \quad (10.19)$$

In summary, Eqs. (10.14), (10.18), and (10.19) are differential forms of the continuity, momentum, and energy equations, respectively, for a steady, inviscid, adiabatic, quasi-one-dimensional flow. We have obtained them from the algebraic forms of the equations derived earlier, applied essentially to the picture shown in Fig. 10.6. Now you might ask the question, Since we spent some effort obtaining partial differential equations for continuity, momentum, and energy in Chap. 2, applicable to a general three-dimensional flow, why would we not simply set  $\partial/\partial y = 0$  and  $\partial/\partial z = 0$  in those equations and obtain differential equations applicable to the one-dimensional flow treated in the present chapter? The answer is that we certainly could perform such a reduction, and we would obtain Eqs. (10.18) and (10.19) directly. [Return to the differential equations Eqs. (2.104a) and (2.105) and prove this to yourself.] However, if we take the general continuity equation, Eq. (2.43), and reduce it to one-dimensional flow, we obtain  $d(\rho u) = 0$ . Comparing this result with Eq. (10.14) for quasi-one-dimensional flow, we see an inconsistency. This is another example of the physical inconsistency between the *assumption* of quasi-one-dimensional flow in a variable-area duct and the three-dimensional flow which actually occurs in such a duct. The result obtained from Eq. (2.43), namely,  $d(\rho u) = 0$ , is a *truly* one-dimensional result, which applies to *constant-area* flows such as considered in Chap. 8. [Recall in Chap. 8 that the continuity equation was used in the form  $\rho u = \text{constant}$ , which is compatible with Eq. (2.43).] However, once we make the quasi-one-dimensional assumption, i.e., that uniform properties hold across a given cross section in a variable-area duct, then Eq. (10.14) is the *only* differential form of the continuity equation which insures mass conservation for such an assumed flow.

Let us now use the differential forms of the governing equations, obtained above, to study some physical characteristics of quasi-one-dimensional flow. Such physical information can be obtained from a particular combination of these equations, as follows. From Eq. (10.14),

$$\frac{dp}{\rho} + \frac{du}{u} + \frac{dA}{A} = 0 \quad (10.20)$$

We wish to obtain an equation which relates the change in velocity,  $du$ , to the change in area,  $dA$ . Hence, to eliminate  $d\rho/\rho$  in Eq. (10.20), consider Eq. (10.18) written as

$$\frac{dp}{\rho} = \frac{dp}{dp} \frac{dp}{\rho} = -u du \quad (10.21)$$

Keep in mind that we are dealing with inviscid, adiabatic flow. Moreover, for the time being, we are assuming no shock waves in the flow. Hence, the flow is *isentropic*. In particular, any change in density,  $d\rho$ , with respect to a change in pressure,  $dp$ , takes place isentropically; that is,

$$\frac{dp}{d\rho} = \left( \frac{\partial p}{\partial \rho} \right)_s \quad (10.22)$$

From Eq. (8.18) for the speed of sound, Eq. (10.22) becomes

$$\frac{dp}{dp} = \frac{1}{a^2} \quad (10.23)$$

Substituting Eq. (10.23) into (10.21), we have

$$\begin{aligned} a^2 \frac{dp}{\rho} &= -u du \\ \text{or} \quad \frac{dp}{\rho} &= -\frac{u du}{a^2} = -\frac{u^2 du}{a^2 u} = -M^2 \frac{du}{u} \end{aligned} \quad (10.24)$$

Substituting Eq. (10.24) into (10.21), we have

$$\begin{aligned} -M^2 \frac{du}{u} + \frac{du}{u} + \frac{dA}{A} &= 0 \\ \frac{dA}{A} &= (M^2 - 1) \frac{du}{u} \end{aligned} \quad (10.25)$$

Equation (10.25) is the desired equation which relates  $dA$  to  $du$ ; it is called the *area-velocity relation*.

Equation (10.25) is very important; study it closely. In the process, recall the standard convention for differentials; e.g., a positive value of  $du$  connotes an *increase* in velocity, a negative value of  $du$  connotes a *decrease* in velocity, etc. With this in mind, Eq. (10.25) tells us the following information:

- For  $0 \leq M < 1$  (subsonic flow), the quantity in parentheses in Eq. (10.25) is negative. Hence, an increase in velocity (positive  $du$ ) is associated with a decrease in area (negative  $dA$ ). Likewise, a decrease in velocity (negative  $du$ ) is associated with an increase in area (positive  $dA$ ). Clearly, for a subsonic compressible flow, to increase the velocity, we must have a convergent duct, and to decrease the velocity, we must have a divergent duct. These results are illustrated at the top of Fig. 10.7. Also, these results are similar to the familiar trends for incompressible flow studied in Sec. 3.3. Once again we see that subsonic compressible flow is qualitatively (but not quantitatively) similar to incompressible flow.
- For  $M > 1$  (supersonic flow), the quantity in parentheses in Eq. (10.25) is positive. Hence, an increase in velocity (positive  $du$ ) is associated with an increase in area (positive  $dA$ ). Likewise, a decrease in velocity (negative  $du$ ) is associated with a decrease in area (negative  $dA$ ). For a supersonic flow, to increase the velocity, we must have a divergent duct, and to decrease the velocity, we must have a convergent duct. These results are illustrated at the bottom of Fig. 10.7; they are the direct opposite of the trends for subsonic flow.
- For  $M = 1$  (sonic flow), Eq. (10.25) shows that  $dA = 0$  even though a finite  $du$  exists. Mathematically, this corresponds to a local maximum or minimum in the area distribution. Physically, it corresponds to a minimum area, as discussed below.

Imagine that we want to take a gas at rest and isentropically expand it to supersonic speeds. The above results show that we must first accelerate the gas subsonically in a convergent duct. However, as soon as sonic conditions are achieved, we must further expand the gas to supersonic speeds by diverging the duct. Hence, a nozzle designed to achieve supersonic flow at its exit is a *convergent-divergent* duct, as sketched at the top of Fig. 10.8. The minimum area of the duct is called the *throat*. Whenever an

*direct opposite* of the trends for subsonic flow.

Imagine that we want to take a gas at rest and isentropically expand it to supersonic speeds. The above results show that we must first accelerate the gas subsonically in a convergent duct. However, as soon as sonic conditions are achieved, we must further expand the gas to supersonic speeds by diverging the duct. Hence, a nozzle designed to achieve supersonic flow at its exit is a *convergent-divergent* duct, as sketched at the top of Fig. 10.8. The minimum area of the duct is called the *throat*. Whenever an

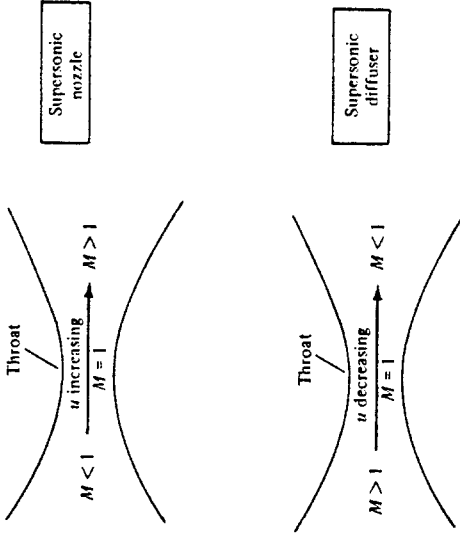


Figure 10.7 Compressible flow in converging and diverging ducts.

isentropic flow expands from subsonic to supersonic speeds, the flow must pass through a throat; moreover, in such a case,  $M = 1$  at the throat. The converse is also true; i.e., if we wish to take a supersonic flow and slow it down isentropically to subsonic speeds, we must first decelerate the gas in a convergent duct, and then as soon as sonic flow is obtained, we must further decelerate it to subsonic speeds in a divergent duct. Here, the convergent-divergent duct at the bottom of Fig. 10.8 is operating as a diffuser. Note that whenever an isentropic flow is slowed from supersonic to subsonic speeds, the flow must pass through a throat; moreover, in such a case,  $M = 0$ . Then we have  $dA/A = -du/u$ , which integrates to  $Au = \text{constant}$ . This is the familiar continuity equation for incompressible flow in ducts as derived in Sec. 3.3 and as given by Eq. (3.22).

As a final note on Eq. (10.25), consider the case when  $M = 0$ . Then we have  $dA/A = -du/u$ , which integrates to  $Au = \text{constant}$ . This is the familiar continuity equation for incompressible flow in ducts as derived in Sec. 3.3 and as given by Eq. (3.22).

### 10.3 NOZZLE FLOWS

In this section, we move to the left-hand branch of the road map given in Fig. 10.3; i.e., we study in detail the compressible flow through nozzles. To expedite this study, we first derive an important equation which relates Mach number to the ratio of duct area to sonic throat area.

Consider the duct shown in Fig. 10.9. Assume that sonic flow exists at the throat, where the area is  $A^*$ . The Mach number and the velocity at the throat are denoted by  $M^*$  and  $u^*$ , respectively. Since the flow is sonic at the throat,  $M^* = 1$  and  $u^* = a^*$ . (Note that the use of an asterisk to denote sonic conditions was introduced in Sec. 7.5; we continue this convention in our present discussion.) At any other section of this duct, the area, the Mach number, and the velocity are denoted by  $A$ ,  $M$ , and  $u$ , respectively, as shown in Fig. 10.9. Writing Eq. (10.1) between  $A$  and  $A^*$ , we have

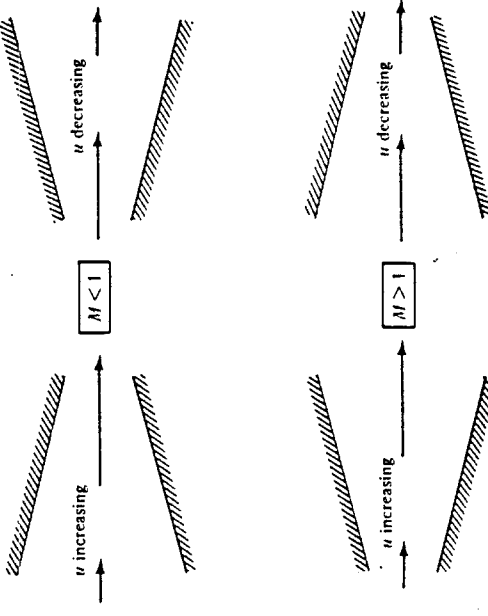


Figure 10.8 Illustration and comparison of a supersonic nozzle and a supersonic diffuser.

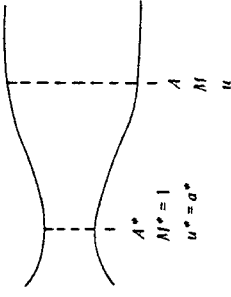


Figure 10.9 Geometry for the derivation of the area-Mach number relation.

Since  $u^* = a^*$ , Eq. (10.26) becomes

$$\frac{A}{A^*} = \frac{\rho^* a^*}{\rho u} = \frac{\rho^*}{\rho} \frac{\rho_0 a^*}{u} \quad (10.27)$$

where  $\rho_0$  is the stagnation density defined in Sec. 7.5 and is constant throughout an isentropic flow. From Eq. (8.46), we have

$$\frac{\rho^*}{\rho_0} = \left( \frac{2}{\gamma + 1} \right)^{1/(\gamma - 1)} \quad (10.28)$$

Also, from Eq. (8.43), we have

$$\frac{\rho_0}{\rho} = \left( 1 + \frac{\gamma - 1}{2} M^2 \right)^{1/(\gamma - 1)} \quad (10.29)$$

Also, recalling the definition of  $M^*$  in Sec. 8.4, as well as Eq. (8.48), we have

$$\frac{u}{a^*} = M^{*2} = \frac{[(\gamma + 1)/2]M^2}{1 + [(\gamma - 1)/2]M^2} \quad (10.30)$$

Squaring Eq. (10.27) and substituting Eqs. (10.28) to (10.30), we obtain

$$\begin{aligned} \left( \frac{A}{A^*} \right)^2 &= \left( \frac{\rho^*}{\rho_0} \right)^2 \left( \frac{\rho_0}{\rho} \right)^2 \left( \frac{a^*}{u} \right)^2 \\ \text{or } \left( \frac{A}{A^*} \right)^2 &= \left( \frac{2}{\gamma + 1} \right)^{2/(\gamma - 1)} \left( 1 + \frac{\gamma - 1}{2} M^2 \right)^{2/(\gamma - 1)} \frac{1 + [(\gamma - 1)/2]M^2}{[(\gamma + 2)/2]M^2} \end{aligned} \quad (10.31)$$

Algebraically simplifying Eq. (10.31), we have

$$\boxed{\left( \frac{A}{A^*} \right)^2 = \frac{1}{M^2} \left[ \frac{2}{\gamma + 1} \left( 1 + \frac{\gamma - 1}{2} M^2 \right) \right]^{1/(\gamma - 1)}} \quad (10.32)$$

Equation (10.32) is very important; it is called the *area-Mach number relation*, and it contains a striking result. "Turned inside out," Eq. (10.32) tells us that  $M = f(A/A^*)$ ; that is, *the Mach number at any location in the duct is a function of the ratio of the local duct area to the sonic throat area*. Recall from our discussion of Eq. (10.25) that  $A$  must be greater than or at least equal to  $A^*$ ; the case where  $A < A^*$  is physically not

possible in an isentropic flow. Thus, in Eq. (10.32),  $A/A^* \geq 1$ . Also, Eq. (10.32) yields two solutions for  $M$  at a given  $A/A^*$  — a subsonic value and a supersonic value. Which value of  $M$  that actually holds in a given case depends on the pressures at the inlet and exit of the duct, as explained later. The results for  $A/A^*$  as a function of  $M$ , obtained from Eq. (10.32), are tabulated in App. A. Examining App. A, we note that for subsonic values of  $M$ , as  $M$  increases,  $A/A^*$  decreases; i.e., the duct converges. At  $M = 1$ ,  $A/A^* = 1$  in App. A. Finally, for supersonic values of  $M$ , as  $M$  increases,  $A/A^*$  increases; i.e., the duct diverges. These trends in App. A are consistent with our physical discussion of convergent-divergent ducts at the end of Sec. 10.2. Moreover, App. A shows the double-valued nature of  $M$  as a function of  $A/A^*$ . For example, for  $A/A^* = 2$ , we have either  $M = 0.31$  or  $M = 2.0$ .

Consider a given convergent-divergent nozzle, as sketched in Fig. 10.10a. Assume that the area ratio at the inlet,  $A_1/A_0$ , is very large and that the flow at the inlet is fed

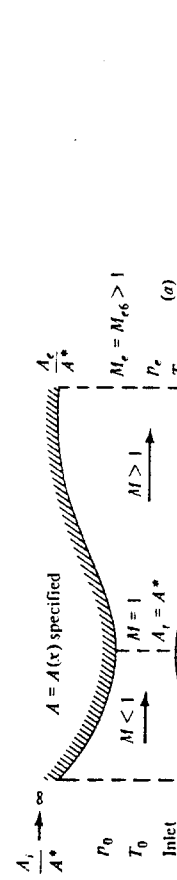


Figure 10.10 Isentropic supersonic nozzle flow.

from a large gas reservoir where the gas is essentially stationary. The reservoir pressure and temperature are  $p_0$  and  $T_0$ , respectively. Since  $A_0/A^*$  is very large, the subsonic Mach number at the inlet is very small,  $M \approx 0$ . Thus, the pressure and temperature at the inlet are essentially  $p_0$  and  $T_0$ , respectively. The area distribution of the nozzle,  $A = A(x)$ , is specified, so that  $A/A^*$  is known at every station along the nozzle. The area of the throat is denoted by  $A_t$ , and the exit area is denoted by  $A_e$ . The Mach number and static pressure at the exit are denoted by  $M_e$  and  $p_{e,0}$ , respectively. Assume that we have an isentropic expansion of the gas through this nozzle to a supersonic Mach number  $M_e = M_{e,6}$  at the exit (the reason for the subscript 6 will be apparent later). The corresponding exit pressure is  $p_{e,6}$ . For this expansion, the flow is sonic at the throat; hence,  $M = 1$  and  $A_t = A^*$  at the throat. The flow properties through the nozzle are a function of the local area ratio  $A/A^*$  and are obtained as follows:

1. The local Mach number as a function of  $x$  is obtained from Eq. (10.32), or more directly from the tabulated values in App. A. For the specified  $A = A(x)$ , we know the corresponding  $A/A^* = f(x)$ . Then read the related subsonic Mach numbers in the convergent portion of the nozzle from the first part of App. A (for  $M < 1$ ) and the related supersonic Mach numbers in the divergent portion of the nozzle from the second part of App. A (for  $M > 1$ ). The Mach number distribution through the complete nozzle is thus obtained and is sketched in Fig. 10.10b.
2. Once the Mach number distribution is known, then the corresponding variation of temperature, pressure, and density can be found from Eqs. (8.40), (8.42), and (8.43), respectively, or more directly from App. A. The distributions of  $p/p_0$  and  $T/T_0$  are sketched in Fig. 10.10c and d, respectively.

Examine the variations shown in Fig. 10.10. For the isentropic expansion of a gas through a convergent-divergent nozzle, the Mach number monotonically increases from near 0 at the inlet to  $M = 1$  at the throat, and to the supersonic value  $M_{e,6}$  at the exit. The pressure monotonically decreases from  $p_0$  at the inlet to  $0.528p_0$  at the throat and to the lower value  $p_{e,6}$  at the exit. Similarly, the temperature monotonically decreases from  $T_0$  at the inlet to  $0.833T_0$  at the throat and to the lower value  $T_{e,6}$  at the exit. Again, for the isentropic flow shown in Fig. 10.10, we emphasize that the distribution of  $M$ , and hence the resulting distributions of  $p$  and  $T$ , through the nozzle depends only on the local area ratio  $A/A^*$ . This is the key to the analysis of isentropic, supersonic, quasi-one-dimensional nozzle flows.

Imagine that you take a convergent-divergent nozzle, and simply place it on a table in front of you. What is going to happen? Is the air going to suddenly start flowing through the nozzle of its own accord? The answer is, Of course not! Rather, by this stage in your study of aerodynamics, your intuition should tell you that we have to impose a force on the gas in order to produce any acceleration. Indeed, this is the essence of the momentum equation derived in Sec. 2.5. For the inviscid flows considered here, the only mechanism to produce an accelerating force on a gas is a pressure gradient. Thus, returning to the nozzle on the table, a pressure difference must be created between the inlet and exit; only then will the gas start to flow through the nozzle. The exit pressure must be less than the inlet pressure, that is,  $p_e < p_0$ . More-

over, if we wish to produce the isentropic supersonic flow sketched in Fig. 10.10, the pressure  $p_e/p_0$  must be *precisely* the value stipulated by App. A for the known exit Mach number  $M_{e,6}$ ; that is,  $p_e/p_0 = p_{e,6}/p_0$ . If the pressure ratio is different from the above isentropic value, the flow either inside or outside the nozzle will be different from that shown in Fig. 10.10.

Let us examine the type of nozzle flows that occur when  $p_e/p_0$  is not equal to the precise isentropic value for  $M_{e,6}$ , that is, when  $p_e/p_0 \neq p_{e,6}/p_0$ . To begin with, consider the convergent-divergent nozzle sketched in Fig. 10.11a. If  $p_e = p_0$ , no pressure difference exists, and no flow occurs inside the nozzle. Now assume that  $p_e$  is minutely reduced below  $p_0$ , say  $p_e = 0.999p_0$ . This small pressure difference will produce a very low-speed subsonic flow inside the nozzle—essentially a gentle wind. The local Mach number will increase slightly through the convergent portion, reaching a maximum value at the throat, as shown by curve 1 in Fig. 10.11b. This Mach number at the throat will *not* be sonic; rather it will be some small subsonic value. Downstream of the throat, the local Mach number will decrease in the divergent section, reaching a very small but

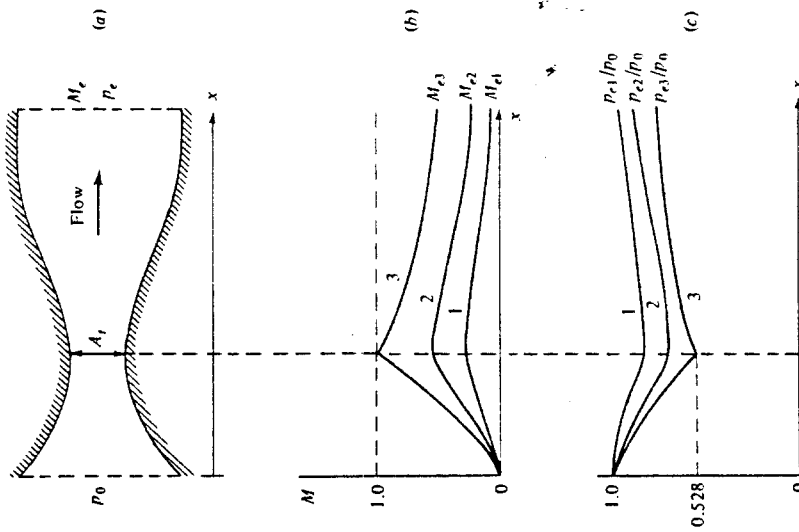


Figure 10.11 Isentropic subsonic nozzle flow.

finite value  $M_{r,1}$  at the exit. Correspondingly, the pressure in the convergent section will gradually decrease from  $p_0$  at the inlet to a minimum value at the throat, and then will gradually increase to the value  $p_{r,1}$  at the exit. This variation is shown as curve 1 in Fig. 10.11c. Please note that because the flow is not sonic at the throat in this case,  $A_r$  is not equal to  $A^*$ . Recall that  $A^*$ , which appears in Eq. (10.32), is the sonic throat area. In the case of purely subsonic flow through a convergent-divergent nozzle,  $A^*$  takes on the character of a reference area; it is not the same as the actual geometric area of the nozzle throat,  $A_r$ . Rather,  $A^*$  is the area the flow in Fig. 10.11 would have if it were somehow accelerated to sonic velocity. If this did happen, the flow area would have to be decreased further than shown in Fig. 10.11a. Hence, for a purely subsonic flow,  $A_r > A^*$ .

Assume that we further decrease the exit pressure in Fig. 10.11, say, to the value  $p_r = p_{r,2}$ . The flow is now illustrated by the curves labeled 2 in Fig. 10.11. The flow moves faster through the nozzle, and the maximum Mach number at the throat increases but remains less than 1. Now, let us reduce  $p_r$  to the value  $p_r = p_{r,3}$ , such that the flow just reaches sonic conditions at the throat. This is shown by curve 3 in Fig. 10.11. The throat Mach number is 1, and the throat pressure is  $0.528p_0$ . The flow downstream of the throat is subsonic.

Upon comparing Figs. 10.10 and 10.11, we are struck by an important physical difference. For a given nozzle shape, there is only one allowable isentropic flow solution for the supersonic case shown in Fig. 10.10. In contrast, there are an infinite number of possible isentropic subsonic solutions, each one corresponding to some value of  $p_r$ , where  $p_0 \geq p_r \geq p_{r,3}$ . Only three solutions of this infinite set of solutions are sketched in Fig. 10.11. Hence, the key factors for the analysis of purely subsonic flow in a convergent-divergent nozzle are both  $A/A^*$  and  $p_r/p_0$ .

Consider the mass flow through the convergent-divergent nozzle in Fig. 10.11. As the exit pressure is decreased, the flow velocity in the throat increases; hence, the mass flow increases. The mass flow can be calculated by evaluating Eq. (10.1) at the throat; that is,  $\dot{m} = \rho_r u_r A_r$ . As  $p_r$  decreases,  $u_r$  increases and  $\rho_r$  decreases. However, the percentage increase in  $u_r$  is much greater than the decrease in  $\rho_r$ . As a result,  $\dot{m}$  increases, as sketched in Fig. 10.12. When  $p_r = p_{r,3}$ , sonic flow is achieved at the throat, and  $\dot{m} = \rho^* u^* A^* = \rho^* u^* A_r$ . Now, if  $p_r$  is further reduced below  $p_{r,3}$ , the conditions at the throat take on a new behavior; they remain unchanged. From our discussion in Sec. 10.2, the Mach number at the throat cannot exceed 1; hence, as  $p_r$  is further reduced,  $M_r$  will remain equal to 1 at the throat. Consequently, the mass flow will remain constant as  $p_r$  is reduced below  $p_{r,3}$ , as shown in Fig. 10.12. In a sense, the flow at the throat, as well as upstream of the throat, becomes "frozen." Once the flow becomes sonic at the throat, disturbances cannot work their way upstream of the throat. Hence, the flow in the convergent section of the nozzle no longer communicates with the exit pressure and has no way of knowing that the exit pressure is continuing to decrease. This situation — when the flow goes sonic at the throat, and the mass flow remains constant no matter how low  $p_r$  is reduced — is called *choked flow*. It is a vital aspect of the compressible flow through ducts, and we consider it further in our subsequent discussions.

Return to the subsonic nozzle flows sketched in Fig. 10.11. Question: What happens in the duct when  $p_r$  is reduced below  $p_{r,3}$ ? In the convergent portion, as described

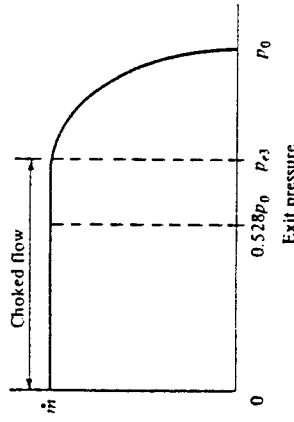


Figure 10.12 Variation of mass flow with exit pressure; illustration of choked flow.

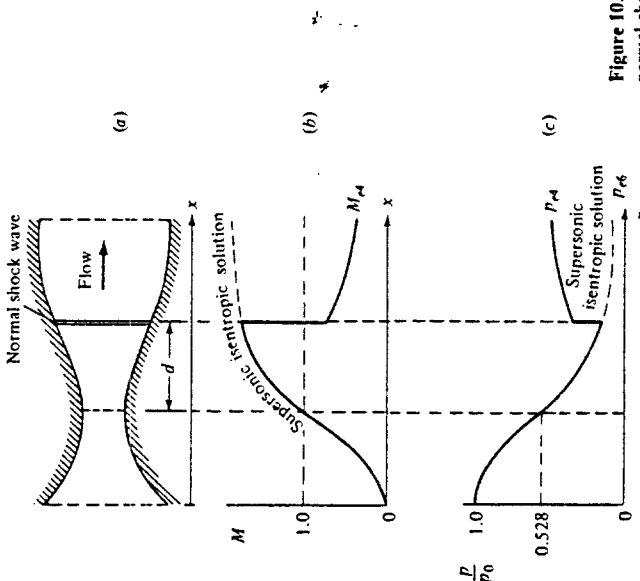


Figure 10.13 Supersonic nozzle flow with a normal shock inside the nozzle.

shown in Fig. 10.13b and c. Behind the shock wave, the flow is subsonic. This subsonic flow sees the divergent duct and isentropically slows down further as it moves to the exit. Correspondingly, the pressure experiences a discontinuous increase across the shock wave and then is further increased as the flow slows down toward the exit. The flow on both the left and right sides of the shock wave is isentropic; however, the entropy increases across the shock wave. Hence, the flow on the left side of the shock wave is isentropic with one value of entropy,  $s_1$ , and the flow on the right side of the shock wave is isentropic with another value of entropy,  $s_2$ , where  $s_2 > s_1$ . The location of the shock wave inside the nozzle, given by  $d$  in Fig. 10.13a, is determined by the requirement that the increase in static pressure across the wave plus that in the divergent portion of the subsonic flow behind the shock be just right to achieve  $p_{e,4}$  at the exit. As  $p_e$  is further reduced, the normal shock wave moves downstream, closer to the nozzle exit. At a certain value of exit pressure,  $p_e = p_{e,5}$ , the normal shock stands precisely at the exit. This is sketched in Fig. 10.14a to c. At this stage, when  $p_e = p_{e,5}$ , the flow through the entire nozzle, except precisely at the exit, is isentropic.

To this stage in our discussion, we have dealt with  $p_e$ , which is the pressure right at the nozzle exit. In Figs. 10.10, 10.11, 10.13, and 10.14a to c, we have not been concerned with the flow downstream of the nozzle exit. Now imagine that the nozzle exit. To this stage in our discussion, we have dealt with  $p_e$ , which is the pressure right at the nozzle exit. In Figs. 10.10, 10.11, 10.13, and 10.14a to c, we have not been concerned with the flow downstream of the nozzle exit. Now imagine that the nozzle

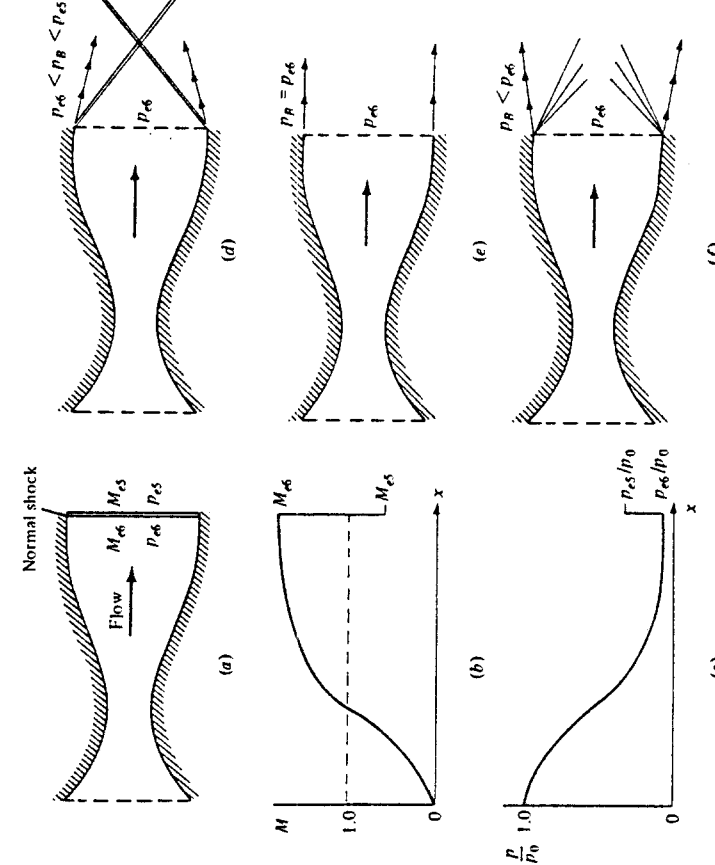


Figure 10.14 Supersonic nozzle flows with waves at the nozzle exit: (a), (b), and (c) pertain to a normal shock at the exit, (d) overexpanded nozzle, (e) isentropic expansion to the back pressure equal to the exit pressure, (f) underexpanded nozzle.

in Fig. 10.14a exhausts directly into a region of surrounding gas downstream of the exit. These surroundings could be, for example, the atmosphere. In any case, the pressure of the surroundings downstream of the exit is defined as the *back pressure*, denoted by  $p_b$ . When the flow at the nozzle exit is subsonic, the exit pressure must equal the back pressure,  $p_e = p_b$ , because a pressure discontinuity cannot be maintained in a steady subsonic flow. That is, when the exit flow is subsonic, the surrounding back pressure is impressed on the exit flow. Hence, in Fig. 10.11,  $p_b = p_{e,1}$  for curve 1,  $p_b = p_{e,2}$  for curve 2, and  $p_b = p_{e,3}$  for curve 3. For the same reason,  $p_b = p_{e,4}$  in Fig. 10.13, and  $p_b = p_{e,5}$  in Fig. 10.14. Hence, in discussing these figures, instead of stating that we reduced the exit pressure  $p_e$  and observed the consequences, we could just as well have stated that we reduced the back pressure  $p_b$ . It would have amounted to the same thing.

For the remainder of our discussion in this section, let us now imagine that we have control over  $p_b$  and that we are going to continue to decrease  $p_b$ . Consider the case when the back pressure is reduced below  $p_{e,5}$ . When  $p_{e,6} < p_b < p_{e,5}$ , the back pressure is still above the isentropic pressure at the nozzle exit. Hence, in flowing out to the surroundings, the jet of gas from the nozzle must somehow be compressed such that its pressure is compatible with  $p_b$ . This compression takes place across oblique shock waves attached to the exit, as shown in Fig. 10.14d. When  $p_b$  is reduced to the value such that  $p_b = p_{e,6}$ , there is no mismatch of the exit pressure and the back pressure; the nozzle jet exhausts smoothly into the surroundings without passing through any waves. This is shown in Fig. 10.14e. Finally, as  $p_b$  is reduced below  $p_{e,6}$  the jet of gas from the nozzle must expand further in order to match the lower back pressure. This expansion takes place across centered expansion waves attached to the exit, as shown in Fig. 10.14f.

When the situation in Fig. 10.14d exists, the nozzle is said to be *overexpanded*, because the pressure at the exit has expanded below the back pressure,  $p_{e,6} < p_b$ . That is, the nozzle expansion has gone too far, and the jet must pass through oblique shocks in order to come back up to the higher back pressure. Conversely, when the situation in Fig. 10.14f exists, the nozzle is said to be *underexpanded*, because the exit pressure is higher than the back pressure,  $p_{e,6} > p_b$ , and hence the flow is capable of additional expansion after leaving the nozzle.

Surveying Figs. 10.10 through 10.14, note that the purely isentropic supersonic flow originally illustrated in Fig. 10.10 exists throughout the nozzle for all cases when  $p_b \leq p_{e,5}$ . For example, in Fig. 10.14a, the isentropic supersonic flow solution holds throughout the nozzle except right at the exit, where a normal shock exists. In Fig. 10.14d to f, the flow through the entire nozzle, including at the exit plane, is given by the isentropic supersonic flow solution.

Keep in mind that our entire discussion of nozzle flows in this section is predicated on having a duct of *given shape*. We assume that  $A = A(x)$  is prescribed. When this

is the case, the quasi-one-dimensional theory of this chapter gives a reasonable prediction of the flow inside the duct, where the results are interpreted as mean properties averaged over each cross section. This theory does *not* tell us how to design the *contour* of the nozzle. In reality, if the walls of the nozzle are not curved just right, then oblique shocks occur inside the nozzle. To obtain the proper contour for a supersonic nozzle so that it produces isentropic shock-free flow inside the nozzle, we must account for the

three-dimensionality of the actual flow. This is one purpose of the method of characteristics, a technique for analyzing two- and three-dimensional supersonic flow. A brief introduction to the method of characteristics is given in Chap. 13.

**Example 10.1** Consider the isentropic supersonic flow through a convergent-divergent nozzle with an exit-to-throat area ratio of 10.25. The reservoir pressure and temperature are 5 atm and 600 K, respectively. Calculate  $M$ ,  $p$ , and  $T$  at the nozzle exit.

**SOLUTION** From the supersonic portion of App. A, for  $A_e/A^* = 10.25$ ,

$$M_e = \boxed{3.95}$$

$$\text{Also } \frac{p_e}{p_0} = \frac{1}{142} \quad \text{and} \quad \frac{T_e}{T_0} = \frac{1}{4.12}$$

$$\text{Thus } p_e = 0.007p_0 = 0.007(5) = \boxed{0.0352 \text{ atm}}$$

$$T_e = 0.2427T_0 = 0.2427(600) = \boxed{145.6^\circ\text{R}}$$

**Example 10.2** Consider the isentropic flow through a convergent-divergent nozzle with an exit-to-throat area ratio of 2. The reservoir pressure and temperature are 1 atm and 288 K, respectively. Calculate the Mach number, pressure, and temperature at both the throat and the exit for the cases where (a) the flow is supersonic at the exit and (b) the flow is subsonic throughout the entire nozzle except at the throat, where  $M = 1$ .

**SOLUTION (a)** At the throat, the flow is sonic. Hence,

$$M_t = \boxed{1.0}$$

$$p_t = p^* = \frac{p_e^*}{p_0} p_0 = 0.528(1 \text{ atm}) = \boxed{0.528 \text{ atm}}$$

$$T_t = T^* = \frac{T_e^*}{T_0} T_0 = 0.833(288) = \boxed{240 \text{ K}}$$

At the exit, the flow is supersonic. Hence, from the supersonic portion of App. A, for  $A_e/A^* = 2$ ,

$$M_e = \boxed{2.2}$$

$$p_e = \frac{p_e}{p_0} p_0 = \frac{1}{10.69}(1 \text{ atm}) = \boxed{0.0935 \text{ atm}}$$

$$T_e = \frac{T_e}{T_0} T_0 = \frac{1}{1.968}(288) = \boxed{146 \text{ K}}$$

(b) At the throat, the flow is still sonic. Hence, from above,  $M_t = 1.0$ ,  $p_t = 0.528$  atm, and  $T_t = 240$  K. However, at all other locations in the nozzle, the

flow is subsonic. At the exit, where  $A_e/A^* = 2$ , from the subsonic portion of App. A,

$$M_e = \boxed{0.3} \quad (\text{rounded to the nearest entry in App. A})$$

$$p_e = \frac{p_e}{p_0} p_0 = \frac{1}{1.064}(1 \text{ atm}) = \boxed{0.94 \text{ atm}}$$

$$T_e = \frac{T_e}{T_0} T_0 = \frac{1}{1.018}(288) = \boxed{282.9 \text{ K}}$$

**Example 10.3** For the nozzle in Example 10.2, assume the exit pressure is 0.973 atm. Calculate the Mach numbers at the throat and the exit.

**SOLUTION** In Example 10.2, we saw that if  $p_e = 0.94$  atm, the flow is sonic at the throat, but subsonic elsewhere. Hence,  $p_e = 0.94$  atm corresponds to  $p_{e,3}$  in Fig. 10.11. In the present problem,  $p_e = 0.973$  atm, which is higher than  $p_{e,3}$ . Hence, in this case, the flow is subsonic throughout the nozzle, including at the throat. For this case,  $A^*$  takes on a reference value, and the actual geometric throat area is denoted by  $A_r$ . At the exit,

$$\frac{p_0}{p_e} = \frac{1}{0.973} = 1.028$$

From the subsonic portion of App. A, for  $p_0/p_e = 1.028$ , we have

$$M_e = \boxed{0.2} \quad \text{and} \quad \frac{A_r}{A^*} = 2.964$$

$$\frac{A_t}{A^*} = \frac{A_r}{A_r} \frac{A_r}{A^*} = 0.5(2.964) = 1.482$$

From the subsonic portion of App. A, for  $A_t/A^* = 1.482$ , we have

$$M_t = \boxed{0.44} \quad (\text{nearest entry})$$

## 10.4 DIFFUSERS

The role of a diffuser was first introduced in Sec. 3.3 in the context of a low-speed subsonic wind tunnel. There, a diffuser was a divergent duct downstream of the test section whose role was to slow the higher-velocity air from the test section down to a very low velocity at the diffuser exit (see Fig. 3.8). Indeed, in general we can define a diffuser as any duct designed to slow an incoming gas flow to lower velocity at the exit of the diffuser. The incoming flow can be subsonic, as discussed in Fig. 3.8, or it can be supersonic, as discussed in the present section. However, the shape of the diffuser is drastically different, depending on whether the incoming flow is subsonic or supersonic.

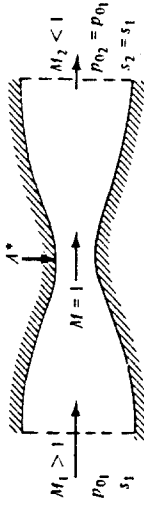
Before pursuing this matter further, let us elaborate on the concept of total pressure,  $p_0$ , as discussed in Sec. 7.5. In a semiqualitative sense, the total pressure of a flowing gas is a measure of the capacity of the flow to perform useful work. Let us consider two examples:

1. A pressure vessel containing stagnant air at 10 atm
2. A supersonic flow at  $M = 2.16$  and  $p = 1$  atm

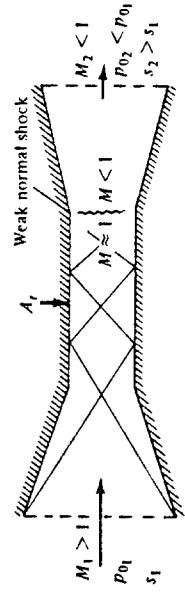
In case 1, the air velocity is zero; hence,  $p_0 = p = 10$  atm. Now, imagine that we want to use air to drive a piston in a piston-cylinder arrangement, where useful work is performed by the piston being displaced through a distance. The air is ducted into the cylinder from a large manifold, in the same vein as the reciprocating internal combustion engine in our automobile. In case 1, the pressure vessel can act as the manifold; hence the pressure on the piston is 10 atm, and a certain amount of useful work is performed, say  $W_1$ . However, in case 2, the supersonic flow must be slowed to a low velocity before we can readily feed it into the manifold. If this slowing process can be achieved without loss of total pressure, then the pressure in the manifold in this case is also 10 atm (assuming  $V \approx 0$ ), and the same amount of useful work,  $W_1$ , is performed. On the other hand, assume that in slowing down the supersonic stream, a loss of 3 atm takes place in the total pressure. Then the pressure in the manifold is only 7 atm, with the consequent generation of useful work,  $W_2$ , which is less than in the first case, that is,  $W_2 < W_1$ . The purpose of this simple example is to indicate that the total pressure of a flowing gas is indeed a measure of its capability to perform useful work. On this basis, a loss of total pressure is always an inefficiency — a loss of the capability to do a certain amount of useful work.

In light of the above, let us expand our definition of a diffuser. A diffuser is a duct designed to slow an incoming gas flow to lower velocity at the exit of the diffuser *with as small a loss in total pressure as possible*. Consequently, an ideal diffuser would be characterized by an *isentropic* compression to lower velocities; this is sketched in Fig. 10.15a, where a supersonic flow enters the diffuser at  $M_1$ , is isentropically compressed in a convergent duct to Mach 1 at the throat, where the area is  $A^*$ , and then is further isentropically compressed in a divergent duct to a low subsonic Mach number at the exit. Because the flow is isentropic,  $s_2 = s_1$ , and from Eq. (8.73),  $p_{02} = p_{01}$ . Indeed,  $p_0$  is constant throughout the entire diffuser — a characteristic of isentropic flow. However, common sense should tell you that the ideal diffuser in Fig. 10.15a can never be achieved. It is extremely difficult to slow a supersonic flow without generating shock waves in the process. For example, examine the convergent portion of the diffuser in Fig. 10.15a. Note that the supersonic flow is turned into itself; hence, the converging flow will inherently generate oblique shock waves, which will destroy the isentropic nature of the flow. Moreover, in real life, the flow is viscous; there will be an entropy increase within the boundary layers on the walls of the diffuser. For these reasons, an ideal isentropic diffuser can never be constructed; an ideal diffuser is of the nature of a "perpetual motion machine" — only a utopian wish in the minds of engineers.

An actual supersonic diffuser is sketched in Fig. 10.15b. Here, the incoming flow is slowed by a series of reflected oblique shocks, first in a convergent section usually



(a) Ideal (isentropic) supersonic diffuser



(b) Actual supersonic diffuser

Figure 10.15. The ideal (isentropic) diffuser compared with the actual situation.

consisting of straight walls, and then in a constant area throat. Due to the interaction of the shock waves with the viscous flow near the wall, the reflected shock pattern eventually weakens and becomes quite diffuse, sometimes ending in a weak normal shock wave at the end of the constant-area throat. Finally, the subsonic flow downstream of the constant-area throat is further slowed by moving through a divergent section. At the exit, clearly  $s_2 > s_1$ ; hence  $p_{02} < p_{01}$ . The art of diffuser design is to obtain as small a total pressure loss as possible, i.e., to design the convergent, divergent, and constant-area throat sections so that  $p_{02}/p_{01}$  is as close to unity as possible. Unfortunately, in most cases, we fall far short of that goal. For more details on supersonic diffusers, see chapter 5 of Ref. 21 and chapter 12 of Ref. 1.

Please note that due to the entropy increase across the shock waves and in the boundary layers, the real diffuser throat area  $A_t$  is larger than  $A^*$ , i.e., in Fig. 10.15,

$$A_t > A^*.$$

## 10.5 SUPERSONIC WIND TUNNELS

Return to the road map given in Fig. 10.3. The material for the left and right branches is covered in Sec. 10.3 and 10.4, respectively. In turn, a mating of these two branches gives birth to the fundamental aspects of supersonic wind tunnels, to be discussed in this section.

Imagine that you want to create a Mach 2.5 uniform flow in a laboratory for the purpose of testing a model of a supersonic vehicle, say a cone. How do you do it? Clearly, we need a convergent-divergent nozzle with an area ratio  $A_t/A^* = 2.637$  (see App. A). Moreover, we need to establish a pressure ratio,  $p_0/p_r = 17.09$ , across the nozzle in order to obtain a shock-free expansion to  $M_r = 2.5$  at the exit. Your first

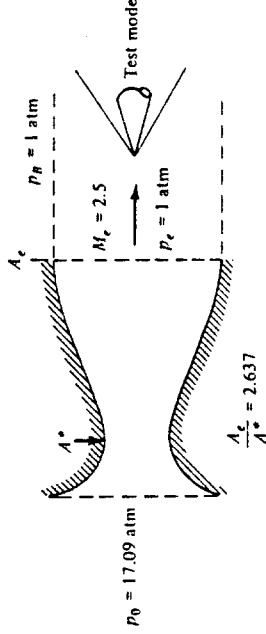


Figure 10.16 Nozzle exhausting directly to the atmosphere.

thought might be to exhaust the nozzle directly into the laboratory, as sketched in Fig. 10.16. Here, the Mach 2.5 flow passes into the surroundings as a "free jet." The test model is placed in the flow downstream of the nozzle exit. In order to make certain that the free jet does not have shock or expansion waves, the nozzle exit pressure  $p_e$  must equal the back pressure  $p_h$ , as originally sketched in Fig. 10.14e. Since the back pressure is simply that of the atmosphere surrounding the free jet,  $p_h = p_e = 1$  atm. Consequently, to establish the proper isentropic expansion through the nozzle, you need a high-pressure reservoir with  $p_0 = 17.09$  atm at the inlet to the nozzle. In this manner, you would be able to accomplish your objective, namely, to produce a uniform stream of air at Mach 2.5 in order to test a supersonic model, as sketched in Fig. 10.16.

In the above example, you may have a problem obtaining the high-pressure air supply at 17.09 atm. You need an air compressor or a bank of high-pressure air bottles — both of which can be expensive. It requires work, hence money, to create reservoirs of high-pressure air — the higher the pressure, the more the cost. So, can you accomplish your objective in a more efficient way, at less cost? The answer is yes, as follows. Instead of the free jet as sketched in Fig. 10.16, imagine that you have a long constant-area section downstream of the nozzle exit, with a normal shock wave standing at the end of the constant-area section; this is shown in Fig. 10.17. The pressure downstream of the normal shock wave is  $p_2 = p_h = 1$  atm. At  $M = 2.5$ , the static pressure ratio across the normal shock is  $p_2/p_e = 7.125$ . Hence, the pressure upstream of the normal shock is 0.14 atm. Since the flow is uniform in the constant-area section, this pressure is also equal to the nozzle exit pressure; that is,  $p_e = 0.14$  atm. Thus, in order to obtain the proper isentropic flow through the nozzle, which requires a pressure ratio of  $p_0/p_e = 17.09$ , we need a reservoir with a pressure of only 2.4 atm. This is considerably more efficient than the 17.09 atm required in Fig. 10.16. Hence, we have created a uniform Mach 2.5 flow (in the constant-area duct) at a considerable reduction in cost compared with the scheme in Fig. 10.16.

In Fig. 10.17, the normal shock wave is acting as a diffuser, slowing the air originally at Mach 2.5 to the subsonic value of Mach 0.513 immediately behind the shock. Hence, by the addition of this "diffuser," we can more efficiently produce our uniform Mach 2.5 flow. This illustrates one of the functions of a diffuser. However, the "normal shock diffuser" sketched in Fig. 10.17 has several problems:

1. A normal shock is the strongest possible shock, hence creating the largest total pressure loss. If we could replace the normal shock in Fig. 10.17 with a weaker

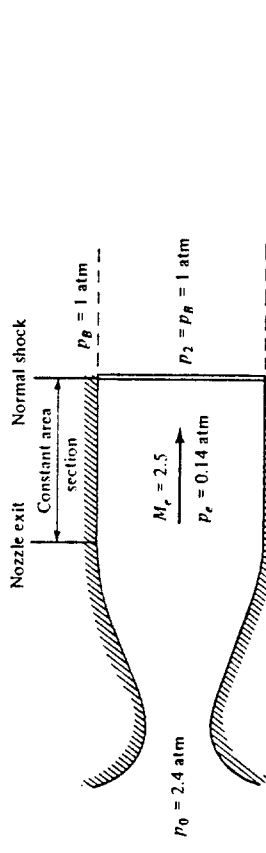


Figure 10.17 Nozzle exhausting into a constant-area duct, where a normal shock stands at the exit of the duct.

shock, the total pressure loss would be less, and the required reservoir pressure  $p_0$  would be less than 2.4 atm.

2. It is extremely difficult to hold a normal shock wave stationary at the duct exit; in real life, flow unsteadiness and instabilities would cause the shock to move somewhere else and to constantly fluctuate in position. Thus, we could never be certain about the quality of the flow in the constant-area duct.
3. As soon as a test model is introduced into the constant-area section, the oblique waves from the model would propagate downstream, causing the flow to become two- or three-dimensional. The normal shock sketched in Fig. 10.17 could not exist in such a flow.

Hence, let us replace the normal shock in Fig. 10.17 with the oblique shock diffuser shown in Fig. 10.15b. The resulting duct would appear as sketched in Fig. 10.18. Examine this figure closely. We have a convergent-divergent nozzle feeding a uniform supersonic flow into the constant-area duct, which is called the *test section*. This flow is subsequently slowed to a low subsonic speed by means of a diffuser. This arrangement — namely, a convergent-divergent nozzle, a test section, and a convergent-divergent diffuser — is a *supersonic wind tunnel*. A test model, the cone in Fig. 10.18, is placed in the test section, where aerodynamic measurements such as lift, drag, and pressure distribution, are made. The wave system from the model propagates downstream and interacts with the multireflected shocks in the diffuser. The pressure ratio required to run the supersonic tunnel is  $p_0/p_h$ . This can be obtained by

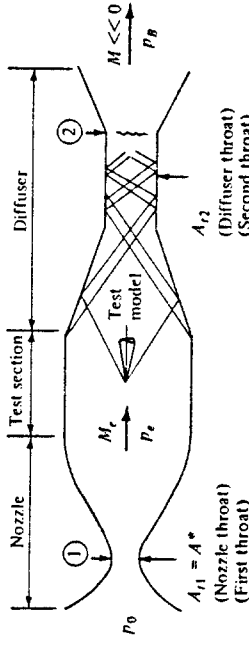


Figure 10.18 Sketch of a supersonic wind tunnel.

making  $p_0$  large via a high-pressure reservoir at the inlet to the nozzle or by making  $p_B$  small via a vacuum source at the exit of the diffuser, or a combination of both.

The main source of total pressure loss in a supersonic wind tunnel is the diffuser. How does the oblique shock diffuser in Fig. 10.18 compare with the hypothetical normal shock diffuser in Fig. 10.17? Is the total pressure loss across all the reflected oblique shocks in Fig. 10.18 greater or less than across the single normal shock wave in Fig. 10.17? This is an important question, since the smaller the total pressure loss in the diffuser, the smaller is the pressure ratio  $p_0/p_B$  required to run the supersonic tunnel. There is no pat answer to this question. However, it is usually true that progressively reducing the velocity of a supersonic flow through a series of oblique shocks to a low supersonic value, and then further reducing the flow to subsonic speeds across a weak normal shock, results in a *smaller* total pressure loss than simply reducing the flow to subsonic speeds across a single, strong normal shock wave at the initially high supersonic Mach number. This trend is illustrated by Prob. 9.8. Therefore, the oblique shock diffuser shown in Figs. 10.15b and 10.18 is usually more efficient than the simple normal shock diffuser shown in Fig. 10.17. This is not always true, however, because in an actual real-life oblique shock diffuser, the shock waves interact with the boundary layers on the walls, causing local thickening and even possible separation of the boundary layers. This creates an additional total pressure loss. Moreover, the simple aspect of skin friction exerted on the surface generates a total pressure loss. Hence, actual oblique shock diffusers may have efficiencies greater or less than a hypothetical normal shock diffuser. Nevertheless, virtually all supersonic wind tunnels use oblique shock diffusers qualitatively similar to that shown in Fig. 10.18.

Notice that the supersonic wind tunnel shown in Fig. 10.18 has two throats: the nozzle throat with area  $A_{r,1}$  is called the *first throat*, and the diffuser throat with area  $A_{r,2}$  is called the *second throat*. The mass flow through the nozzle can be expressed as  $\dot{m} = \rho u A$  evaluated at the first throat. This station is denoted as station 1 in Fig. 10.18, and hence the mass flow through the nozzle is  $\dot{m}_1 = \rho_1 u_1 A_{r,1} = \rho_1^* a_1^* A_{r,1}$ . In turn the mass flow through the diffuser can be expressed as  $\dot{m}_2 = \rho u A$  evaluated at station 2, namely,  $\dot{m}_2 = \rho_2 u_2 A_{r,2}$ . For steady flow through the wind tunnel,  $\dot{m}_1 = \dot{m}_2$ . Hence,

$$\rho_1^* a_1^* A_{r,1} = \rho_2 u_2 A_{r,2} \quad (10.33)$$

Since the thermodynamic state of the gas is irreversibly changed in going through the shock waves created by the test model and generated in the diffuser, clearly  $\rho_2$  and possibly  $u_2$  are different from  $\rho_1^*$  and  $a_1^*$ , respectively. Hence, from Eq. (10.33), the *second throat must have a different area from the first throat*; that is,  $A_{r,2} \neq A_{r,1}$ .

*Question:* How does  $A_{r,2}$  differ from  $A_{r,1}$ ? Let us assume that sonic flow occurs at both stations 1 and 2 in Fig. 10.18. Thus Eq. (10.33) can be written as

$$\frac{A_{r,2}}{A_{r,1}} = \frac{\rho_1^* a_1^*}{\rho_2^* a_2^*} \quad (10.34)$$

Recall from Sec. 8.4 that  $a^*$  is constant for an adiabatic flow. Also recall that the flow across shock waves is adiabatic (but not isentropic). Hence, the flow throughout the wind tunnel sketched in Fig. 10.18 is adiabatic, and therefore  $a_1^* = a_2^*$ . In turn, Eq. (10.34) becomes

$$\frac{A_{r,2}}{A_{r,1}} = \frac{\rho_1^*}{\rho_2^*} = \frac{p_1^*}{p_2^*} \quad (10.35)$$

Recall from Sec. 8.4 that  $T^*$  is also constant throughout the adiabatic flow of a calorically perfect gas. Hence, from the equation of state,

$$\frac{\rho_1^*}{p_2^*} = \frac{p_1^*/RT_1^*}{p_2^*/RT_2^*} = \frac{p_1^*}{p_2^*} \quad (10.36)$$

Substituting Eq. (10.36) into (10.35), we have

$$\frac{A_{r,2}}{A_{r,1}} = \frac{p_1^*}{p_2^*} \quad (10.37)$$

From Eq. (8.45), we have

$$p_1^* = p_{0,1} \left( \frac{2}{\gamma + 1} \right)^{\gamma/(\gamma-1)}$$

and

$$p_2^* = p_{0,2} \left( \frac{2}{\gamma + 1} \right)^{\gamma/(\gamma-1)}$$

Substituting the above into Eq. (10.37), we obtain

$$\boxed{\frac{A_{r,2}}{A_{r,1}} = \frac{p_{0,1}}{p_{0,2}}} \quad (10.38)$$

Examining Fig. 10.18, the total pressure always decreases across shock waves; therefore,  $p_{0,2} < p_{0,1}$ . In turn, from Eq. (10.38),  $A_{r,2} > A_{r,1}$ . Thus, the second throat must always be *larger* than the first throat. Only in the case of an ideal isentropic diffuser, where  $p_0 = \text{constant}$ , would  $A_{r,2} = A_{r,1}$ , and we have already discussed the impossibility of such an ideal diffuser.

Equation (10.38) is a useful relation to size the second throat relative to the first throat if we know the total pressure ratio across the tunnel. In the absence of such information, for the preliminary design of supersonic wind tunnels, the total pressure ratio across a normal shock is assumed.

For a given wind tunnel, if  $A_{r,2}$  is less than the value given by Eq. (10.38), the diffuser will "choke"; i.e., the diffuser cannot pass the mass flow coming from the isentropic, supersonic expansion through the nozzle. In this case, nature adjusts the flow through the wind tunnel by creating shock waves in the nozzle, which in turn reduce the Mach number in the test section, producing weaker shocks in the diffuser with an attendant overall reduction in the total pressure loss; i.e., nature adjusts the total pressure loss such that  $p_{0,1}/p_{0,2} = p_{0,1}/p_B$  satisfies Eq. (10.38). Sometimes this adjustment is so severe that a normal shock stands inside the nozzle, and the flow through the test section and diffuser is totally subsonic. Obviously, this choked situation is not desirable because we no longer have uniform flow at the desired Mach number in the test section. In such a case, the supersonic wind tunnel is said to be *unstarted*. The only way to rectify this situation is to make  $A_{r,2}/A_{r,1}$  large enough so that the diffuser can pass

the mass flow from the isentropic expansion in the nozzle, i.e., so that Eq. (10.38) is satisfied along with a shock-free isentropic nozzle expansion.

As a general concluding comment, the basic concepts and relations discussed in this chapter are not limited to nozzles, diffusers, and supersonic wind tunnels. Rather, we have been discussing quasi-one-dimensional flow, which can be applied in many applications involving flow in a duct. For example, inlets on jet engines, which diffuse the flow to lower speeds before entering the engine compressor, obey the same principles. Also, a rocket engine is basically a supersonic nozzle designed to optimize the thrust from the expanded jet. The applications of the ideas presented in this chapter are numerous, and you should make certain that you understand these ideas before progressing further.

In Sec. 1.2, we subdivided aerodynamics into external and internal flows. You are reminded that the material in this chapter deals exclusively with internal flows.

**Example 10.4** For the preliminary design of a Mach 2 supersonic wind tunnel, calculate the ratio of the diffuser throat area to the nozzle throat area.

**SOLUTION** Assuming a normal shock wave at the entrance of the diffuser (for starting), from App. B,  $p_{n,2}/p_{n,1} = 0.7209$  for  $M = 2.0$ . Hence, from Eq. (10.38)

$$\frac{A_{t,2}}{A_{t,1}} = \frac{p_{n,1}}{p_{n,2}} = \frac{1}{0.7209} = \boxed{1.387}$$

## 10.6 SUMMARY

The results of this chapter are highlighted below.

Quasi-one-dimensional flow is an approximation to the actual three-dimensional flow in a variable-area duct; this approximation assumes that  $p = p(x)$ ,  $u = u(x)$ ,  $T = T(x)$ , etc., although the area varies as  $A = A(x)$ . Thus, we can visualize the quasi-one-dimensional results as giving the mean properties at a given station, averaged over the cross section. The quasi-one-dimensional flow assumption gives reasonable results for many internal flow problems; it is a "workhorse" in the everyday application of compressible flow. The governing equations for this are:

$$\text{Continuity: } \rho_1 u_1 A_1 = \rho_2 u_2 A_2, \quad (10.1)$$

$$\text{Momentum: } p_1 A_1 + \rho_1 u_1^2 A_1 + \int_{A_1}^{A_2} p dA = p_2 A_2 + \rho_2 u_2^2 A_2 \quad (10.5)$$

$$\text{Energy: } h_1 + \frac{u_1^2}{2} = h_2 + \frac{u_2^2}{2} \quad (10.9)$$

The area velocity relation

$$\frac{dA}{A} = (M^2 - 1) \frac{du}{u} \quad (10.25)$$

tells us that:

1. To accelerate (decelerate) a subsonic flow, the area must decrease (increase).
2. To accelerate (decelerate) a supersonic flow, the area must increase (decrease).
3. Sonic flow can only occur at a throat or minimum area of the flow.

The isentropic flow of a calorically perfect gas through a nozzle is governed by the relation

$$\left(\frac{A}{A^*}\right)^2 = \frac{1}{M^2} \left[ \frac{2}{\gamma + 1} \left( 1 + \frac{\gamma - 1}{2} M^2 \right) \right]^{(\gamma+1)/(\gamma-1)} \quad (10.32)$$

This tells us that the Mach number in a duct is governed by the ratio of local duct area to the sonic throat area; moreover, for a given area ratio, there are two values of Mach number that satisfy Eq. (10.32) — a subsonic value and a supersonic value.

For a given convergent-divergent duct, there is only one possible isentropic flow solution for supersonic flow; in contrast, there are an infinite number of subsonic isentropic solutions, each one associated with a different pressure ratio across the nozzle,  $p_0/p_r = p_0/p_B$ .

In a supersonic wind tunnel, the ratio of second throat area to first throat area should be approximately

$$\frac{A_{t,2}}{A_{t,1}} = \frac{p_{0,1}}{p_{0,2}} \quad (10.38)$$

If  $A_{t,2}$  is reduced much below this value, the diffuser will choke and the tunnel will unstart.

## PROBLEMS

- 10.1 The reservoir pressure and temperature for a convergent-divergent nozzle are 5 atm and 520°R, respectively. The flow is expanded isentropically to supersonic speed at the nozzle exit. If the exit-to-throat area ratio is 2.193, calculate the following properties at the exit:  $M_r$ ,  $p_r$ ,  $T_r$ ,  $\rho_r$ ,  $u_r$ ,  $T_{0,r}$ .

**10.2** A flow is isentropically expanded to supersonic speeds in a convergent-divergent nozzle. The reservoir and exit pressures are 1 and 0.3143 atm, respectively. What is the value of  $A_*/A^*$ ?

**10.3** A Pitot tube inserted at the exit of a supersonic nozzle reads  $8.92 \times 10^4$  N/m<sup>2</sup>. If the reservoir pressure is  $2.02 \times 10^4$  N/m<sup>2</sup>, calculate the area ratio  $A_*/A^*$  of the nozzle.

**10.4** For the nozzle flow given in Prob. 10.1, the throat area is 4 in<sup>2</sup>. Calculate the mass flow through the nozzle.

**10.5** A closed-form expression for the mass flow through a choked nozzle is

$$\dot{m} = \frac{\rho_0 A^*}{\sqrt{\gamma}} \sqrt{\frac{\gamma}{R} \left( \frac{2}{\gamma + 1} \right)^{(r+1)/(r-1)}}$$

Derive this expression.

**10.6** Repeat Prob. 10.4, using the formula derived in Prob. 10.5, and check your answer from Prob. 10.4.

**10.7** A convergent-divergent nozzle with an exit-to-throat area ratio of 1.616 has exit and reservoir pressures equal to 0.947 and 1.0 atm, respectively. Assuming isentropic flow through the nozzle, calculate the Mach number and pressure at the throat.

**10.8** For the flow in Prob. 10.7, calculate the mass flow through the nozzle, assuming that the reservoir temperature is 288 K and the throat area is 0.3 m<sup>2</sup>.

**10.9** Consider a convergent-divergent nozzle with an exit-to-throat area ratio of 1.53. The reservoir pressure is 1 atm. Assuming isentropic flow, except for the possibility of a normal shock wave inside the nozzle, calculate the exit Mach number when the exit pressure  $p_2$  is

- (a) 0.94 atm
- (b) 0.886 atm
- (c) 0.75 atm
- (d) 0.154 atm

**10.10** A 20° half-angle wedge is mounted at 0° angle of attack in the test section of a supersonic wind tunnel. When the tunnel is operating, the wave angle from wedge leading edge is measured to be 41.8°. What is the exit-to-throat area ratio of the tunnel nozzle?

**10.11** The nozzle of a supersonic wind tunnel has an exit-to-throat area ratio of 6.79. When the tunnel is running, a Pitot tube mounted in the test section measures 1.448 atm. What is the reservoir pressure for the tunnel?

**10.12** We wish to design a supersonic wind tunnel which produces a Mach 2.8 flow at standard sea level conditions in the test section and has a mass flow of air equal to 1 slug/s. Calculate the necessary reservoir pressure and temperature, the nozzle throat and exit areas, and the diffuser throat area.

*During the war a British engineer named Frank Whittle invented the jet engine, and de Havilland built the first production-type model. He produced a jet plane named Vampire, the first to exceed 500 mph. Then he built the experimental DH 108, and released it to young Geoffrey for test. In the first cautious trials the new plane behaved beautifully; but as Geoffrey stepped up the speed he unexpectedly drew closer to an invisible wall in the sky then unknown to anyone, later named the sound barrier, which can destroy a plane not designed to pierce it. One evening he hit the speed of sound, and the plane disintegrated. Young Geoffrey's body was not found for ten days.*

*From the Royal Air Force Flying Review, as digested in Reader's Digest, 1959*

## 11.1 INTRODUCTION

The above quotation refers to an accident which took place on September 27, 1946, when Geoffrey de Havilland, son of the famed British airplane designer Sir Geoffrey de Havilland, took the D. H. 108 Swallow up for an attack on the world's speed record. At that time, no airplane had flown at or beyond the speed of sound. The Swallow was an experimental jet-propelled aircraft with swept wings and no tail. During its first high-speed, low-level run, the Swallow encountered major compressibility problems and broke up in the air. De Havilland was killed instantly. This accident strengthened the opinion of many that Mach 1 stood as a barrier to manned flight and that no airplane would ever fly faster than the speed of sound. This myth of the "sound barrier" originated in the early 1930s. It was in full force by the time of the Volta Conference in 1935 (see Sec. 7.1). In light of the above quotation, the idea of a sound barrier was still being discussed in the popular literature as late as 1959, 12 years after the first successful supersonic flight by Captain Charles Yeager on October 14, 1947.

Of course, we know today that the sound barrier is indeed a myth; the supersonic transport Concorde flies at Mach 2, and some military aircraft are capable of Mach 3 and slightly beyond. The X-15 hypersonic research airplane has flown at Mach 7, and

the Apollo lunar return capsule successfully reentered the earth's atmosphere at Mach 3.6. Supersonic flight is now an everyday occurrence. So, what caused the early concern about a sound barrier? In the present chapter, we develop a theory applicable to high-speed subsonic flight, and we see how the theory predicts a monotonically increasing drag going to infinity as  $M_\infty \rightarrow 1$ . It was this type of result which led some people in the early 1930s to believe that flight beyond the speed of sound was impossible. However, we also show in this chapter that the approximations made in the theory break down near Mach 1 and that in reality, although the drag coefficient at Mach 1 is large, it is still a manageable finite number.

Specifically, the purpose of this chapter is to examine the properties of two-dimensional airfoils at Mach numbers above 0.3, where we can no longer assume incompressible flow, but below Mach 1. That is, this chapter is an extension of the airfoil discussions in Chap. 4 (which applied to incompressible flow) to the high-speed subsonic regime.

In the process, we climb to a new tier in our study of compressible flow. If you survey our discussions so far of compressible flow, you will observe that they treat one-dimensional cases such as normal shock waves and flows in ducts. Even oblique shock waves, which are two- and three-dimensional in nature, depend only on the component of Mach number normal to the wave. Therefore, we have not been explicitly concerned with a multidimensional flow. As a consequence, note that the types of equations which allow an analysis of these flows are *algebraic equations* and hence are relatively easy to solve in comparison with partial differential equations. In Chaps. 8 to 10, we have dealt primarily with such algebraic equations. These algebraic equations were obtained by applying the integral forms of the conservation equations [Eqs. (2.39), (2.55), and (2.86)] to appropriate control volumes where the flow properties were uniform over the inflow and outflow faces of the control volume. However, for general two- and three-dimensional flows, we are usually not afforded such a luxury. Instead, we must deal directly with the governing equations in their partial differential equation form (see Chap. 2). Such is the nature of the present chapter. Indeed, for the remainder of our aerodynamic discussions in this book, we appeal mainly to the differential forms of the continuity, momentum, and energy equations (such as Eqs. (2.43), (2.104a to c), and (2.105)).

The road map for this chapter is given in Fig. 11.1. We are going to return to the concept of a velocity potential, first introduced in Sec. 2.15. We are going to combine our governing equations so as to obtain a single equation simply in terms of the velocity potential; i.e., we are going to obtain for compressible flow an equation analogous to Laplace's equation derived for incompressible flow in Sec. 3.7 [see Eq. (3.40)]. However, unlike Laplace's equation, which is linear, the exact velocity potential equation for compressible flow is nonlinear. By making suitable approximations, we are able to linearize this equation and apply it to thin airfoils at small angles of attack. The results enable us to correct incompressible airfoil data for the effects of compressibility — so-called *compressibility corrections*. Finally, we conclude this chapter by discussing several practical aspects of airfoil and general wing-body aerodynamics at speeds near Mach 1.

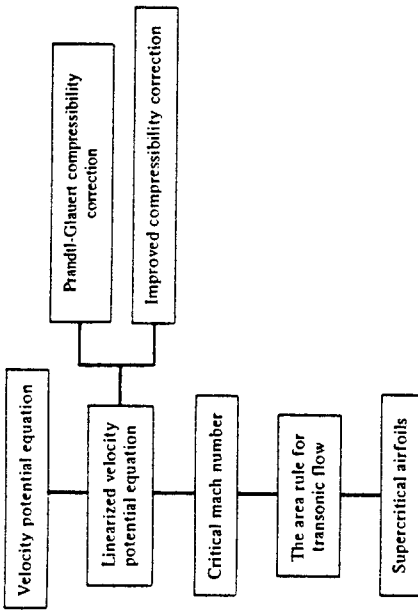


Figure 11.1 Road map for Chap. 11.

## 11.2 THE VELOCITY POTENTIAL EQUATION

The inviscid, compressible, subsonic flow over a body immersed in a uniform stream is *irrotational*, there is no mechanism in such a flow to start rotating the fluid elements (see Sec. 2.12). Thus, a velocity potential (see Sec. 2.15) can be defined. Since we are dealing with irrotational flow and the velocity potential, review Secs. 2.12 and 2.15 before progressing further.

Consider two-dimensional, steady, irrotational, isentropic flow. A velocity potential,  $\phi = \phi(x, y)$ , can be defined such that [from Eq. (2.145)]

$$\mathbf{V} = \nabla \phi \quad (11.1)$$

or in terms of the cartesian velocity components,

$$u = \frac{\partial \phi}{\partial x} \quad (11.2a)$$

$$v = \frac{\partial \phi}{\partial y} \quad (11.2b)$$

Let us proceed to obtain an equation for  $\phi$  which represents a combination of the continuity, momentum, and energy equations. Such an equation would be very useful, because it would be simply one governing equation in terms of one unknown, namely  $\phi$ .

The continuity equation for steady, two-dimensional flow is obtained from Eq. (2.43) as

$$\frac{\partial(\rho u)}{\partial x} + \frac{\partial(\rho v)}{\partial y} = 0 \quad (11.3)$$

$$\text{or } \frac{\partial u}{\partial x} + u \frac{\partial p}{\partial x} + v \frac{\partial p}{\partial y} + p \frac{\partial v}{\partial y} = 0 \quad (11.4)$$

Substituting Eqs. (11.2a and b) into (11.4), we have

$$\begin{aligned} \text{or } & \rho \left( \frac{\partial^2 \phi}{\partial x^2} + \frac{\partial \phi}{\partial x} \frac{\partial p}{\partial x} + \frac{\partial \phi}{\partial y} \frac{\partial p}{\partial y} + p \frac{\partial^2 \phi}{\partial y^2} \right) = 0 \\ & \rho \left( \frac{\partial^2 \phi}{\partial x^2} + \frac{\partial^2 \phi}{\partial y^2} \right) + \frac{\partial \phi}{\partial x} \frac{\partial p}{\partial x} + \frac{\partial \phi}{\partial y} \frac{\partial p}{\partial y} = 0 \end{aligned} \quad (11.5)$$

We are attempting to obtain an equation completely in terms of  $\phi$ ; hence, we need to eliminate  $p$  from Eq. (11.5). To do this, consider the momentum equation in terms of Euler's equation:

$$dp = -\rho V dV \quad (3.12)$$

This equation holds for a steady, compressible, inviscid flow and relates  $p$  and  $V$  along a streamline. It can readily be shown that Eq. (3.12) holds in any direction throughout an irrotational flow, not just along a streamline (try it yourself). Therefore, from Eqs. (3.12) and (11.2a and b), we have

$$dp = -\rho V dV = -\frac{\rho}{2} d(V^2) = -\frac{\rho}{2} d(u^2 + v^2) \quad (11.6)$$

$$dp = -\frac{\rho}{2} d \left[ \left( \frac{\partial \phi}{\partial x} \right)^2 + \left( \frac{\partial \phi}{\partial y} \right)^2 \right] \quad (11.6)$$

Recall that we are also considering the flow to be isentropic. Hence, any change in pressure,  $dp$ , in the flow is automatically accompanied by a corresponding isentropic change in density,  $d\rho$ . Thus, by definition

$$\frac{dp}{d\rho} = \left( \frac{\partial p}{\partial \rho} \right)_s \quad (11.7)$$

The right-hand side of Eq. (11.7) is simply the square of the speed of sound. Thus, Eq. (11.7) yields

$$dp = a^2 d\rho \quad (11.8)$$

Substituting Eq. (11.8) for the left side of Eq. (11.6), we have

$$dp = -\frac{\rho}{2a^2} d \left[ \left( \frac{\partial \phi}{\partial x} \right)^2 + \left( \frac{\partial \phi}{\partial y} \right)^2 \right] \quad (11.9)$$

Considering changes in the  $x$  direction, Eq. (11.9) directly yields

$$\begin{aligned} \frac{\partial \rho}{\partial x} &= -\frac{\rho}{2a^2} \frac{\partial}{\partial x} \left[ \left( \frac{\partial \phi}{\partial x} \right)^2 + \left( \frac{\partial \phi}{\partial y} \right)^2 \right] \\ \text{or } \frac{\partial \rho}{\partial x} &= -\frac{\rho}{a^2} \left( \frac{\partial \phi}{\partial x} \frac{\partial^2 \phi}{\partial x^2} + \frac{\partial \phi}{\partial y} \frac{\partial^2 \phi}{\partial x \partial y} \right) \end{aligned} \quad (11.10)$$

Similarly, for changes in the  $y$  direction, Eq. (11.9) gives

$$\frac{\partial \rho}{\partial y} = -\frac{\rho}{a^2} \left( \frac{\partial \phi}{\partial x} \frac{\partial^2 \phi}{\partial y \partial x} + \frac{\partial \phi}{\partial y} \frac{\partial^2 \phi}{\partial y^2} \right) \quad (11.11)$$

Substituting Eqs. (11.10) and (11.11) into (11.5), canceling the  $\rho$  which appears in each term, and factoring out the second derivatives of  $\phi$ , we obtain

$$\boxed{\left[ 1 - \frac{1}{a^2} \left( \frac{\partial \phi}{\partial x} \right)^2 \right] \frac{\partial^2 \phi}{\partial x^2} + \left[ 1 - \frac{1}{a^2} \left( \frac{\partial \phi}{\partial y} \right)^2 \right] \frac{\partial^2 \phi}{\partial y^2} - \frac{2}{a^2} \left( \frac{\partial \phi}{\partial x} \right) \left( \frac{\partial \phi}{\partial y} \right) \frac{\partial^2 \phi}{\partial x \partial y} = 0} \quad (11.12)$$

which is called the *velocity potential equation*. It is almost completely in terms of  $\phi$ ; only the speed of sound appears in addition to  $\phi$ . However,  $a$  can be readily expressed in terms of  $\phi$  as follows. From Eq. (8.33), we have

$$\begin{aligned} a^2 &= a_0^2 + \frac{\gamma - 1}{2} V^2 = a_0^2 + \frac{\gamma - 1}{2} (u^2 + v^2) \\ &= a_0^2 + \frac{\gamma - 1}{2} \left[ \left( \frac{\partial \phi}{\partial x} \right)^2 + \left( \frac{\partial \phi}{\partial y} \right)^2 \right] \end{aligned} \quad (11.13)$$

Since  $a_0$  is a known constant of the flow, Eq. (11.13) gives the speed of sound,  $a$ , as a function of  $\phi$ . Hence, substitution of Eq. (11.13) into (11.12) yields a single partial differential equation in terms of the unknown  $\phi$ . This equation represents a combination of the continuity, momentum, and energy equations. In principle, it can be solved to obtain  $\phi$  for the flow field around any two-dimensional shape, subject of course to the usual boundary conditions at infinity and along the body surface. These boundary conditions on  $\phi$  are detailed in Sec. 3.7, and are given by Eqs. (3.47a and b) and (3.48b).

Because Eq. (11.12) [along with Eq. (11.13)] is a single equation in terms of one dependent variable,  $\phi$ , the analysis of isentropic, irrotational, steady, compressible flow is greatly simplified—we only have to solve one equation instead of three or more. Once  $\phi$  is known, all the other flow variables are directly obtained as follows:

1. Calculate  $u$  and  $v$  from Eqs. (11.2a and b).
2. Calculate  $a$  from Eq. (11.13).
3. Calculate  $M = V/a = \sqrt{u^2 + v^2}/a$ .
4. Calculate  $T$ ,  $p$ , and  $\rho$  from Eqs. (8.40), (8.42), and (8.43), respectively. In these equations, the total conditions  $T_0$ ,  $P_0$ , and  $\rho_0$  are known quantities; they are constant throughout the flow field and hence are obtained from the given freestream conditions.

Although Eq. (11.12) has the advantage of being one equation with one unknown, it also has the distinct disadvantage of being a *nonlinear* partial differential equation. Such nonlinear equations are very difficult to solve analytically, and in modern aero-

dynamics, solutions of Eq. (11.12) are usually sought by means of sophisticated finite-difference numerical techniques. Indeed, no general analytical solution of Eq. (11.12) has been found to this day. Contrast this situation with that for incompressible flow, which is governed by Laplace's equation — a *linear* partial differential equation for which numerous analytical solutions are well-known.

Given this situation, aerodynamicists over the years have made assumptions regarding the physical nature of the flow field which are designed to simplify Eq. (11.12). These assumptions limit our considerations to the flow over slender bodies at small angles of attack. For subsonic and supersonic flows, these assumptions lead to an *approximate* form of Eq. (11.12) which is linear and hence can be solved analytically. These matters are the subject of the next section.

Keep in mind that, within the framework of steady, irrotational, isentropic flow, Eq. (11.12) is exact and holds for all Mach numbers, from subsonic to hypersonic, and for all two-dimensional body shapes, thin and thick.

### 11.3 THE LINEARIZED VELOCITY POTENTIAL EQUATION

Consider the two-dimensional, irrotational, isentropic flow over the body shown in Fig. 11.2. The body is immersed in a uniform flow with velocity  $V_x$  oriented in the  $x$  direction. At an arbitrary point  $P$  in the flow field, the velocity is  $\mathbf{V}$  with  $x$  and  $y$  components given by  $u$  and  $v$ , respectively. Let us now visualize the velocity  $\mathbf{V}$  as the sum of the uniform flow velocity plus some extra increments in velocity. For example, the  $x$  component of velocity,  $u$ , in Fig. 11.2 can be visualized as  $V_x$  plus an increment in velocity (positive or negative). Similarly, the  $y$  component of velocity,  $v$ , can be visualized as a simple increment itself, because the uniform flow has a zero component in the  $y$  direction. These increments are called *perturbations*, and

$$u = V_x + \hat{u} \quad v = \hat{v}$$

where  $\hat{u}$  and  $\hat{v}$  are called the *perturbation velocities*. These perturbation velocities are not necessarily small; indeed, they can be quite large in the stagnation region in front of the blunt nose of the body shown in Fig. 11.2. In the same vein, because  $\mathbf{V} = \nabla\phi$ , we can define a perturbation velocity potential,  $\hat{\phi}$ , such that

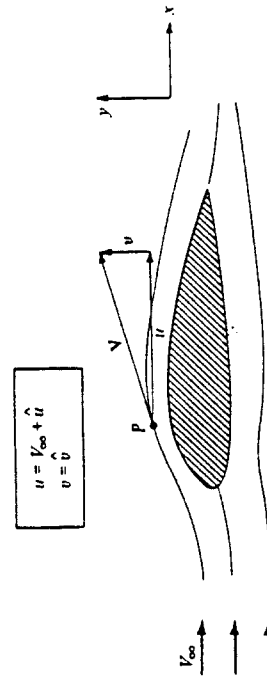


Figure 11.2 Uniform flow and perturbed flow.

$$\begin{aligned}\phi &= V_x x + \hat{\phi} \\ \frac{\partial \phi}{\partial x} &= \hat{u} \\ \frac{\partial \phi}{\partial y} &= \hat{v}\end{aligned}$$

where

$$\begin{aligned}\text{Hence } \frac{\partial \phi}{\partial x} &= V_x + \frac{\partial \hat{\phi}}{\partial x} \quad \frac{\partial \phi}{\partial y} = \frac{\partial \hat{\phi}}{\partial y} \\ \frac{\partial^2 \phi}{\partial x^2} &= \frac{\partial^2 \hat{\phi}}{\partial x^2} \quad \frac{\partial^2 \phi}{\partial y^2} = \frac{\partial^2 \hat{\phi}}{\partial y^2} \\ \frac{\partial^2 \phi}{\partial x \partial y} &= \frac{\partial^2 \hat{\phi}}{\partial x \partial y} = \frac{\partial^2 \phi}{\partial x \partial y} = \frac{\partial^2 \hat{\phi}}{\partial x \partial y}\end{aligned}$$

Substituting the above definitions into Eq. (11.12), and multiplying by  $a^2$ , we obtain

$$\left[ a^2 - \left( V_x + \frac{\partial \phi}{\partial x} \right)^2 \right] \frac{\partial^2 \phi}{\partial x^2} + \left[ a^2 - \left( \frac{\partial \phi}{\partial y} \right)^2 \right] \frac{\partial^2 \phi}{\partial y^2} - 2 \left( V_x + \frac{\partial \phi}{\partial x} \right) \left( \frac{\partial \phi}{\partial y} \right) \frac{\partial^2 \phi}{\partial x \partial y} = 0 \quad (11.14)$$

Equation (11.14) is called the *perturbation velocity potential equation*. It is precisely the same equation as Eq. (11.12) except that it is expressed in terms of  $\hat{\phi}$  instead of  $\phi$ . It is still a nonlinear equation.

To obtain better physical insight in some of our subsequent discussion, let us recast Eq. (11.14) in terms of the perturbation velocities. From the definition of  $\hat{\phi}$  given earlier, Eq. (11.14) can be written as

$$\left[ a^2 - (V_x + \hat{u})^2 \right] \frac{\partial \hat{u}}{\partial x} + (a^2 - \hat{v}^2) \frac{\partial \hat{v}}{\partial y} - 2(V_x + \hat{u})\hat{v} \frac{\partial \hat{u}}{\partial y} = 0 \quad (11.14a)$$

From the energy equation in the form of Eq. (8.32), we have

$$\frac{a^2}{\gamma - 1} + \frac{V_x^2}{2} = \frac{a^2}{\gamma - 1} + \frac{(V_x + \hat{u})^2 + \hat{v}^2}{2} \quad (11.15)$$

Substituting Eq. (11.15) into (11.14a), and algebraically rearranging, we obtain

$$\begin{aligned}(1 - M_x^2) \frac{\partial \hat{u}}{\partial x} + \frac{\partial \hat{v}}{\partial y} &= M_x^2 \left[ (\gamma + 1) \frac{\hat{u}}{V_x} + \frac{\gamma + 1}{2} \frac{\hat{u}^2}{V_x^2} + \frac{\gamma - 1}{2} \frac{\hat{v}^2}{V_x^2} \right] \frac{\partial \hat{u}}{\partial x} \\ &+ M_x^2 \left[ (\gamma - 1) \frac{\hat{u}}{V_x} + \frac{\gamma + 1}{2} \frac{\hat{v}^2}{V_x^2} + \frac{\gamma - 1}{2} \frac{\hat{u}^2}{V_x^2} \right] \frac{\partial \hat{v}}{\partial y} \\ &+ M_x^2 \left[ \frac{\hat{v}}{V_x} \left( 1 + \frac{\hat{u}}{V_x} \right) \left( \frac{\partial \hat{u}}{\partial y} + \frac{\partial \hat{v}}{\partial x} \right) \right]\end{aligned} \quad (11.16)$$

Equation (11.16) is still exact for irrotational, isentropic flow. Note that the left-hand side of Eq. (11.16) is linear but the right-hand side is nonlinear. Also, keep in mind that the size of the perturbations  $\hat{u}$  and  $\hat{v}$  can be large or small; Eq. (11.16) holds for both cases.

Let us now limit our considerations to *small* perturbations; i.e., assume that the body in Fig. 11.2 is a *slender* body at *small* angle of attack. In such a case,  $\hat{u}$  and  $\hat{v}$  will be small in comparison with  $V_\infty$ . Therefore, we have

$$\frac{\hat{u}}{V_\infty}, \frac{\hat{v}}{V_\infty} \ll 1 \quad \frac{\hat{u}^2}{V_\infty^2}, \frac{\hat{v}^2}{V_\infty^2} \ll 1$$

Keep in mind that products of  $\hat{u}$  and  $\hat{v}$  with their derivatives are also very small. With this in mind, examine Eq. (11.16). Compare like terms (coefficients of like derivatives) on the left- and right-hand sides of Eq. (11.16). We find

1. For  $0 \leq M_\infty \leq 0.8$  or  $M_\infty \geq 1.2$ , the magnitude of

$$M_\infty^2 \left[ (\gamma + 1) \frac{\hat{u}}{V_\infty} + \dots \right] \frac{\partial \hat{u}}{\partial x}$$

is small in comparison with the magnitude of

$$(1 - M_\infty^2) \frac{\partial \hat{u}}{\partial x}$$

Thus, ignore the former term.

2. For  $M_\infty < 5$  (approximately),

$$M_\infty^2 \left[ (\gamma - 1) \frac{\hat{u}}{V_\infty} + \dots \right] \frac{\partial \hat{v}}{\partial y}$$

is small in comparison with  $\partial \hat{v} / \partial y$ . So ignore the former term. Also,

$$M_\infty^2 \left[ \frac{\hat{v}}{V_\infty} \left( 1 + \frac{\hat{u}}{V_\infty} \right) \left( \frac{\partial \hat{u}}{\partial y} + \frac{\partial \hat{v}}{\partial x} \right) \right] \approx 0$$

With the above order-of-magnitude comparisons, Eq. (11.16) reduces to

$$(1 - M_\infty^2) \frac{\partial \hat{u}}{\partial x} + \frac{\partial \hat{v}}{\partial y} = 0 \quad (11.17)$$

or in terms of the perturbation velocity potential,

$$(1 - M_\infty^2) \frac{\partial^2 \hat{\phi}}{\partial x^2} + \frac{\partial^2 \hat{\phi}}{\partial y^2} = 0 \quad (11.18)$$

Examine Eq. (11.18). It is a *linear* partial differential equation and therefore is inherently simpler to solve than its parent equation, Eq. (11.16). However, we have paid a price for this simplicity. Equation (11.18) is no longer exact. It is only an approximation to the physics of the flow. Due to the assumptions made in obtaining Eq. (11.18), it is reasonably valid (but not exact) for the following combined situations:

1. *Small* perturbation, i.e., thin bodies at small angles of attack
2. *Subsonic* and *supersonic* Mach numbers

In contrast, Eq. (11.18) is not valid for thick bodies and for large angles of attack. Moreover, it cannot be used for transonic flow, where  $0.8 < M_\infty < 1.2$ , or for hypersonic flow, where  $M_\infty > 5$ .

We are interested in solving Eq. (11.18) in order to obtain the pressure distribution along the surface of a slender body. Since we are now dealing with approximate equations, it is consistent to obtain a linearized expression for the pressure coefficient—an expression which is approximate to the same degree as Eq. (11.18), but which is extremely simple and convenient to use. The linearized pressure coefficient can be derived as follows.

First recall the definition of the pressure coefficient  $C_p$  given in Sec. 1.5.

$$C_p \equiv \frac{p - p_\infty}{q_\infty} \quad (11.19)$$

where  $q_\infty = \frac{1}{2} \rho_\infty V_\infty^2$  = dynamic pressure. The dynamic pressure can be expressed in terms of  $M_\infty$  as follows:

$$q_\infty = \frac{1}{2} \rho_\infty V_\infty^2 = \frac{1}{2} \frac{\gamma T_\infty}{\gamma - 1} \rho_\infty V_\infty^2 = \frac{\gamma}{2} \frac{p_\infty}{\gamma p_\infty} V_\infty^2 \quad (11.20)$$

From Eq. (8.23), we have  $a_\infty^2 = \gamma T_\infty / \rho_\infty$ . Hence, Eq. (11.20) becomes

$$q_\infty = \frac{\gamma}{2} p_\infty \frac{V_\infty^2}{a_\infty^2} = \frac{\gamma}{2} p_\infty M_\infty^2 \quad (11.21)$$

Substituting Eq. (11.21) into (11.19), we have

$$C_p = \frac{2}{\gamma M_\infty^2} \left( \frac{p}{p_\infty} - 1 \right) \quad (11.22)$$

Equation (11.22) is simply an alternate form of the pressure coefficient expressed in terms of  $M_\infty$ . It is still an exact representation of the definition of  $C_p$ .

To obtain a linearized form of the pressure coefficient, recall that we are dealing with an adiabatic flow of a calorically perfect gas; hence, from Eq. (8.39),

$$T + \frac{V^2}{2c_p} = T_\infty + \frac{V_\infty^2}{2c_p} \quad (11.23)$$

Recalling from Eq. (7.9) that  $c_p = \gamma R / (\gamma - 1)$ , Eq. (11.23) can be written as

$$T - T_\infty = \frac{V_\infty^2 - V^2}{2\gamma R / (\gamma - 1)} \quad (11.24)$$

Also recalling that  $a_\infty^2 = \sqrt{\gamma R T_\infty}$ , Eq. (11.24) becomes

$$\frac{T}{T_\infty} - 1 = \frac{\gamma - 1}{2} \frac{V_\infty^2 - V^2}{\gamma R T_\infty} = \frac{\gamma - 1}{2} \frac{V_\infty^2 - V^2}{a_\infty^2} \quad (11.25)$$

In terms of the perturbation velocities

$$V^2 = (V_\infty + \hat{u})^2 + \hat{v}^2$$

Eq. (11.25) can be written as

$$\frac{T}{T_s} = 1 - \frac{\gamma - 1}{2\hat{u}^2} (2\hat{u}V_s + \hat{u}^2 + \hat{v}^2) \quad (11.26)$$

Since the flow is isentropic,  $p/p_s = (T/T_s)^{\gamma/(\gamma-1)}$ , and Eq. (11.26) becomes

$$\frac{p}{p_s} = \left[ 1 - \frac{\gamma - 1}{2\hat{u}^2} (2\hat{u}V_s + \hat{u}^2 + \hat{v}^2) \right]^{\gamma/(\gamma-1)} \quad (11.27)$$

or

$$\frac{p}{p_s} = \left[ 1 - \frac{\gamma - 1}{2} M_s^2 \left( \frac{2\hat{u}}{V_s} + \frac{\hat{u}^2 + \hat{v}^2}{V_s^2} \right) \right]^{\gamma/(\gamma-1)} \quad (11.27)$$

Equation (11.27) is still an exact expression. However, let us now make the assumption that the perturbations are small, i.e.,  $\hat{u}/V_s \ll 1$ ,  $\hat{u}^2/V_s^2 \ll 1$ , and  $\hat{v}^2/V_s^2 \ll 1$ . In this case, Eq. (11.27) is of the form

$$\frac{p}{p_s} = (1 - \epsilon)^{\gamma/(\gamma-1)} \quad (11.28)$$

where  $\epsilon$  is small. From the binomial expansion, neglecting higher-order terms, Eq. (11.28) becomes

$$\frac{p}{p_s} = 1 - \frac{\gamma}{\gamma - 1} \epsilon + \dots \quad (11.29)$$

Comparing Eqs. (11.27) to (11.29), we can express Eq. (11.27) as

$$\frac{p}{p_s} = 1 - \frac{\gamma}{2} M_s^2 \left( \frac{2\hat{u}}{V_s} + \frac{\hat{u}^2 + \hat{v}^2}{V_s^2} \right) + \dots \quad (11.30)$$

Substituting Eq. (11.30) into the expression for the pressure coefficient, Eq. (11.22), we obtain

$$C_p = \frac{2}{\gamma M_s^2} \left[ 1 - \frac{\gamma}{2} M_s^2 \left( \frac{2\hat{u}}{V_s} + \frac{\hat{u}^2 + \hat{v}^2}{V_s^2} \right) + \dots - 1 \right] \quad (11.31)$$

or

$$C_p = -\frac{2\hat{u}}{V_s} + \frac{\hat{u}^2 + \hat{v}^2}{V_s^2}$$

Since  $\hat{u}^2/V_s^2$  and  $\hat{v}^2/V_s^2 \ll 1$ , Eq. (11.31) becomes

$$C_p = -\frac{2\hat{u}}{V_s} \quad (11.32)$$

Equation (11.32) is the linearized form for the pressure coefficient; it is valid only for *small* perturbations. Equation (11.32) is consistent with the linearized perturbation velocity potential equation, Eq. (11.18). Note the simplicity of Eq. (11.32); it depends only on the  $x$  component of the velocity perturbation, namely,  $\hat{u}$ .

To round out our discussion on the basics of the linearized equations, we note that any solution to Eq. (11.18) must satisfy the usual boundary conditions at infinity and at the body surface. At infinity, clearly  $\hat{\phi} = \text{constant}$ ; that is,  $\hat{u} = \hat{v} = 0$ . At the body,

the flow-tangency condition holds. Let  $\theta$  be the angle between the tangent to the surface and the freestream. Then, at the surface, the boundary condition is obtained from Eq. (3.48c):

$$\tan \theta = \frac{u}{v} = \frac{\hat{v}}{V_x + \hat{u}} \quad (11.33)$$

which is an exact expression for the flow-tangency condition at the body surface. A simpler, approximate expression for Eq. (11.33), consistent with linearized theory, can be obtained by noting that for small perturbations,  $\hat{u} \ll V_x$ . Hence, Eq. (11.33) becomes

$$\boxed{\frac{\partial \hat{\phi}}{\partial y} = V_x \tan \theta} \quad (11.34)$$

Equation (11.34) is an *approximate* expression for the flow-tangency condition at the body surface, with accuracy of the same order as Eqs. (11.18) and (11.32).

## 11.4 PRANDTL-GLAUERT COMPRESSIBILITY CORRECTION

The aerodynamic theory for incompressible flow over thin airfoils at small angles of attack was presented in Chap. 4. For aircraft of the period 1933–1940, such theory was adequate for predicting airfoil properties. However, with the rapid evolution of high-power reciprocating engines spurred by World War II, the velocities of military fighter planes began to push close to 450 mi/h. Then, with the advent of the first operational jet-propelled airplanes in 1944 (the German Me 262), flight velocities took a sudden spurt into the 550 mi/h range and faster. As a result, the incompressible flow theory of Chap. 4 was no longer applicable to such aircraft; rather, high-speed airfoil theory had to deal with compressible flow. Because a vast bulk of data and experience had been collected over the years in low-speed aerodynamics, and because there was no desire to totally discard such data, the natural approach to high-speed subsonic aerodynamics was to search for methods that would allow relatively simple *corrections* to existing incompressible flow results which would approximately take into account the effects of compressibility. Such methods are called *compressibility corrections*. The first, and most widely known of these corrections is the Prandtl-Glauert compressibility correction, to be derived in this section. The Prandtl-Glauert method is based on the linearized perturbation velocity potential equation given by Eq. (11.18). Therefore, it is limited to thin airfoils at small angles of attack. Moreover, it is purely a subsonic theory and begins to give inappropriate results at values of  $M_\infty = 0.7$  and above.

Consider the subsonic, compressible, inviscid flow over the airfoil sketched in Fig. 11.3. The shape of the airfoil is given by  $y = f(x)$ . Assume that the airfoil is thin and that the angle of attack is small; in such a case, the flow is reasonably approximated by Eq. (11.18). Define

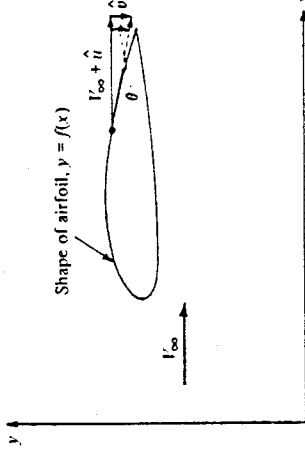


Figure 11.3 Airfoil in physical space.

so that Eq. (11.18) can be written as

$$\beta^2 \frac{\partial^2 \hat{\phi}}{\partial x^2} + \frac{\partial^2 \hat{\phi}}{\partial y^2} = 0 \quad (11.35)$$

Let us transform the independent variables  $x$  and  $y$  into a new space,  $\xi$  and  $\eta$ , such that

$$\xi = x \quad (11.36a)$$

$$\eta = \beta y \quad (11.36b)$$

Moreover, in this transformed space, consider a new velocity potential,  $\bar{\phi}$ , such that

$$\bar{\phi}(\xi, \eta) = \beta \hat{\phi}(x, y) \quad (11.36c)$$

To recast Eq. (11.35) in terms of the transformed variables, recall the chain rule of partial differentiation, that is,

$$\frac{\partial \hat{\phi}}{\partial x} = \frac{\partial \hat{\phi}}{\partial \xi} \frac{\partial \xi}{\partial x} + \frac{\partial \hat{\phi}}{\partial \eta} \frac{\partial \eta}{\partial x} \quad (11.37)$$

$$\frac{\partial \hat{\phi}}{\partial y} = \frac{\partial \hat{\phi}}{\partial \xi} \frac{\partial \xi}{\partial y} + \frac{\partial \hat{\phi}}{\partial \eta} \frac{\partial \eta}{\partial y} \quad (11.38)$$

From Eqs. (11.36a and b), we have

$$\frac{\partial \xi}{\partial x} = 1 \quad \frac{\partial \xi}{\partial y} = 0 \quad \frac{\partial \eta}{\partial x} = 0 \quad \frac{\partial \eta}{\partial y} = \beta$$

Hence, Eqs. (11.37) and (11.38) become

$$\frac{\partial \hat{\phi}}{\partial x} = \frac{\partial \hat{\phi}}{\partial \xi} \quad (11.39)$$

$$\frac{\partial \hat{\phi}}{\partial y} = \beta \frac{\partial \hat{\phi}}{\partial \eta} \quad (11.40)$$

Recalling Eq. (11.36c), Eqs. (11.39) and (11.40) become

$$\frac{\partial \hat{\phi}}{\partial x} = \frac{1}{\beta} \frac{\partial \bar{\phi}}{\partial \xi} \quad (11.41)$$

$$\frac{\partial \hat{\phi}}{\partial y} = \frac{\partial \bar{\phi}}{\partial \eta} \quad (11.42)$$

Differentiating Eq. (11.41) with respect to  $x$  (again using the chain rule), we obtain

$$\frac{\partial^2 \hat{\phi}}{\partial x^2} = \frac{1}{\beta} \frac{\partial^2 \bar{\phi}}{\partial \xi^2} \quad (11.43)$$

Differentiating Eq. (11.42) with respect to  $y$ , the result is

$$\frac{\partial^2 \hat{\phi}}{\partial y^2} = \beta \frac{\partial^2 \bar{\phi}}{\partial \eta^2} \quad (11.44)$$

Substitute Eqs. (11.43) and (11.44) into (11.35),

$$\begin{aligned} \beta^2 \frac{1}{\beta} \frac{\partial^2 \bar{\phi}}{\partial \xi^2} + \beta \frac{\partial^2 \bar{\phi}}{\partial \eta^2} &= 0 \\ \frac{\partial^2 \bar{\phi}}{\partial \xi^2} + \frac{\partial^2 \bar{\phi}}{\partial \eta^2} &= 0 \end{aligned} \quad (11.45)$$

or

Examine Eq. (11.45)—it should look familiar. Indeed, Eq. (11.45) is Laplace's equation. Recall from Chap. 3 that Laplace's equation is the governing relation for *incompressible flow*. Hence, starting with a subsonic compressible flow in physical  $(x, y)$  space where the flow is represented by  $\hat{\phi}(x, y)$  obtained from Eq. (11.35), we have related this flow to an incompressible flow in transformed  $(\xi, \eta)$  space, where the flow is represented by  $\bar{\phi}(\xi, \eta)$  obtained from Eq. (11.45). The relation between  $\bar{\phi}$  and  $\hat{\phi}$  is given by Eq. (11.36c).

Consider again the shape of the airfoil given in physical space by  $y = f(x)$ . The shape of the airfoil in the transformed space is expressed as  $\eta = q(\xi)$ . Let us compare the two shapes. First, apply the approximate boundary condition, Eq. (11.34), in physical space, noting that  $df/dx = \tan \theta$ . We obtain

$$V_x \frac{df}{dx} = \frac{\partial \hat{\phi}}{\partial y} = \frac{1}{\beta} \frac{\partial \bar{\phi}}{\partial y} = \frac{\partial \bar{\phi}}{\partial \eta} \quad (11.46)$$

Similarly, apply the flow-tangency condition in transformed space, which from Eq. (11.34) is

$$V_x \frac{dq}{d\xi} = \frac{\partial \bar{\phi}}{\partial \eta} \quad (11.47)$$

Examine Eqs. (11.46) and (11.47) closely. Note that the right-hand sides of these two equations are identical. Thus, from the left-hand sides, we obtain

$$\frac{df}{dx} = \frac{dq}{d\xi} \quad (11.48)$$

Equation (11.48) implies that the shape of the airfoil in the transformed space is the same as in the physical space. Hence, the above transformation relates the compressible flow over an airfoil in  $(x, y)$  space to the incompressible flow in  $(\xi, \eta)$  space over the *same* airfoil.

The above theory leads to an immensely practical result, as follows. Recall Eq. (11.32) for the linearized pressure coefficient. Inserting the above transformation into Eq. (11.32), we obtain

$$C_p = -\frac{2\bar{u}}{V_s} = -\frac{2}{V_s} \frac{\partial \bar{\phi}}{\partial x} = -\frac{2}{V_s} \beta \frac{1}{\partial x} \frac{\partial \bar{\phi}}{\partial \xi} = -\frac{2}{V_s} \beta \frac{1}{\partial \xi} \frac{\partial \bar{\phi}}{\partial \xi} \quad (11.49)$$

**Question:** What is the significance of  $\partial \bar{\phi} / \partial \xi$  in Eq. (11.49)? Recall that  $\bar{\phi}$  is the perturbation velocity potential for an incompressible flow in transformed space. Hence, from the definition of velocity potential,  $\partial \bar{\phi} / \partial \xi = \bar{u}$ , where  $\bar{u}$  is a perturbation velocity for the incompressible flow. Hence, Eq. (11.49) can be written as

$$C_p = \frac{1}{\beta} \left( -\frac{2\bar{u}}{V_s} \right) \quad (11.50)$$

From Eq. (11.32), the expression  $(-2\bar{u}/V_s)$  is simply the linearized pressure coefficient for the incompressible flow. Denote this incompressible pressure coefficient by  $C_{p,0}$ . Hence Eq. (11.50) gives

$$C_p = \frac{C_{p,0}}{\beta} \quad (11.51)$$

or recalling that  $\beta = \sqrt{1 - M_s^2}$

$$C_p = \frac{C_{p,0}}{\sqrt{1 - M_s^2}} \quad (11.52)$$

Equation (11.51) is called the *Prandtl-Glauert rule*; it states that, if we know the incompressible pressure distribution over an airfoil, then the compressible pressure distribution over the same airfoil can be obtained from Eq. (11.51). Therefore, Eq. (11.51) is truly a *compressibility correction* to incompressible data.

Consider the lift and moment coefficients for the airfoil. For an inviscid flow, the aerodynamic lift and moment on a body are simply integrals of the pressure distribution over the body, as described in Sec. 1.5. (If this is somewhat foggy in your mind, review Sec. 1.5 before progressing further.) In turn, the lift and moment coefficients are obtained from the integral of the pressure coefficient via Eqs. (1.15) to (1.19). Since Eq. (11.51) relates the compressible and incompressible pressure coefficients, the same relation must therefore hold for lift and moment coefficients:

$$c_l = \frac{c_{l,0}}{\sqrt{1 - M_s^2}} \quad (11.53)$$

$$c_m = \frac{c_{m,0}}{\sqrt{1 - M_s^2}} \quad (11.53)$$

The Prandtl-Glauert rule, embodied in Eqs. (11.51) to (11.53), was historically the first compressibility correction to be obtained. As early as 1922, Prandtl was using this result in his lectures at Göttingen, although without written proof. The derivation of Eqs. (11.51) to (11.53) was first formally published by the British aerodynamicist, Hermann Glauert, in 1928. Hence, the rule is named after both men. The Prandtl-Glauert rule was used exclusively until 1939, when an improved compressibility correction was developed. Because of their simplicity, Eqs. (11.51) to (11.53) are still used today for initial estimates of compressibility effects.

Recall that the results of Chaps. 3 and 4 proved that inviscid, incompressible flow over a closed, two-dimensional body theoretically produces zero drag—the well-known d'Alembert's paradox. Does the same paradox hold for inviscid, subsonic, compressible flow? The answer can be obtained by again noting that the only source of drag is the integral of the pressure distribution. If this integral is zero for an incompressible flow, and since the compressible pressure coefficient differs from the incompressible pressure coefficient by only a constant scale factor,  $\beta$ , then the integral must also be zero for a compressible flow. Hence, d'Alembert's paradox also prevails for inviscid, subsonic, compressible flow. However, as soon as the freestream Mach number is high enough to produce locally supersonic flow on the body surface with attendant shock waves, as shown in Fig. 1.26b, then a positive wave drag is produced, and d'Alembert's paradox no longer prevails.

**Example 11.1** At a given point on the surface of an airfoil, the pressure coefficient is  $-0.3$  at very low speeds. If the freestream Mach number is  $0.6$ , calculate  $C_p$  at this point.

SOLUTION From Eq. 11.51,

$$C_p = \frac{C_{p,0}}{\sqrt{1 - M^2}} = \frac{-0.3}{\sqrt{1 - (0.6)^2}} = [-0.375]$$

**Example 11.2** From Chap. 4, the theoretical lift coefficient for a thin, symmetric airfoil in an incompressible flow is  $c_l = 2\pi\alpha$ . Calculate the lift coefficient for  $M_s = 0.7$ .

SOLUTION From Eq. 11.52,

$$c_l = \frac{c_{l,0}}{\sqrt{1 - M_s^2}} = \frac{2\pi\alpha}{\sqrt{1 - (0.7)^2}} = [8.8\alpha]$$

*Note:* The effect of compressibility at Mach 0.7 is to increase the lift slope by the ratio  $8.8/2\pi = 1.4$ , or by 40 percent.

## 11.5 IMPROVED COMPRESSIBILITY CORRECTIONS

The importance of accurate compressibility corrections reached new highs during the rapid increase in airplane speeds spurred by World War II. Efforts were made to im-

prove upon the Prandtl-Glauert rule discussed in Sec. 11.4. Several of the more popular formulas are given below.

The Karaman-Tsien rule states

$$C_p = \frac{C_{p,0}}{\sqrt{1 - M_x^2} + [M_x^2/(1 + \sqrt{1 - M_x^2})] C_{p,0}/2} \quad (11.54)$$

This formula, derived in Refs. 27 and 28, has been widely adopted by the aeronautical industry since World War II.

הוּא וְעַמְקָם

$$C_r = \frac{C_{r,0}}{\sqrt{1 - M_r^2} + (M_r^2)^{1/2}[(\gamma - 1/2)M_r^2/(2\sqrt{1 - M_r^2})]C_s} \quad (11.55)$$

This formula is more recent than either the Prandtl-Glauert or the Karman-Tsien rules; it is derived in Ref. 29.

These compressibility corrections are compared in Fig. 11.4, which also shows experimental data for the  $C_p$  variation with  $M_\infty$  at the 0.3-chord location on an NACA 4412 airfoil. Note that the Prandtl-Glauert rule, although the simplest to apply, under-predicts the experimental data, whereas the improved compressibility corrections are clearly more accurate. Recall that the Prandtl-Glauert rule is based on linear theory. In

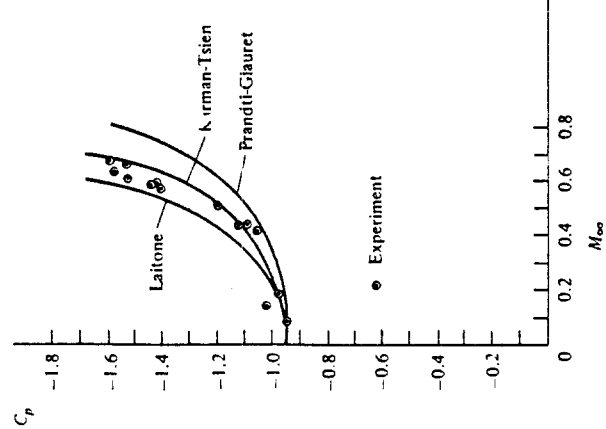


**Figure 11.4** Several compressibility corrections compared with experimental results for an NACA 4412 airfoil at an angle of attack  $\alpha = 1^\circ 53'$ . The experimental data are chosen for their historical significance; they are from NACA report no. 646, published in 1938 (Ref. 30). This was the first major NACA publication to address the compressibility problem in a systematic fashion; it covered work performed in the 2-ft high-speed tunnel at the Langley Aeronautical Laboratory and was carried out during 1935–1936.

contrast, both the Laitone and Karman-Tsien rules attempt to account for some of the nonlinear aspects of the flow.

1116 CRITICAL MACH NUMBER

Return to the road map given in Fig. 11.1. We have now finished our discussion of linearized flow and the associated compressibility corrections. Keep in mind that such linearized theory does *not* apply to the transonic flow regime,  $0.8 \leq M_\infty \leq 1.2$ . Transonic flow is highly nonlinear, and theoretical transonic aerodynamics is a challenging and sophisticated subject. For the remainder of this chapter, we deal with several aspects of transonic flow from a qualitative point of view. The theory of transonic aerodynamics is beyond the scope of this book.

Consider an airfoil in a low-speed flow, say with  $M_\infty = 0.3$ , as sketched in Fig. 11.5a. In the expansion over the top surface of the airfoil, the local flow Mach number  $M$  increases. Let point A represent the location on the airfoil surface where the pressure is a minimum, hence where  $M$  is a maximum. [In Fig. 11.5a, let us say this

/ Local  $M_A = 0.435$

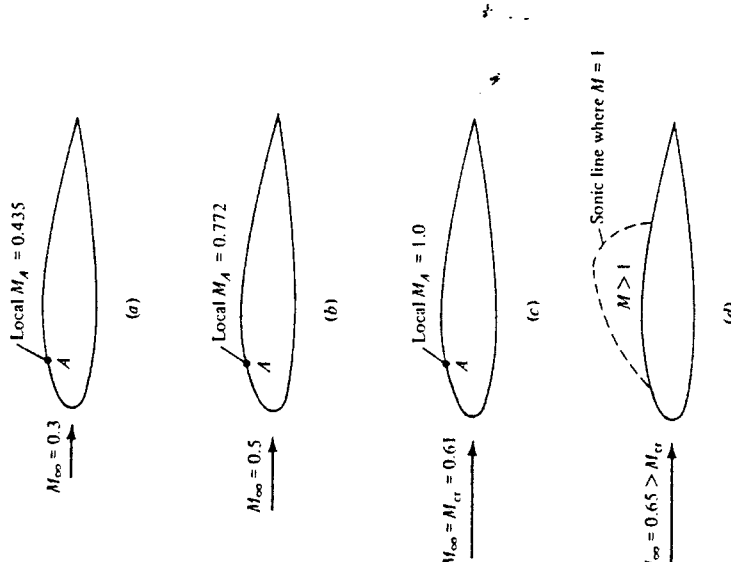


**Figure 11.5** Definition of critical Mach number. Point A is the location of minimum pressure on the top surface of the airfoil.

maximum is  $M_A = 0.435$ . Now assume that we gradually increase the freestream Mach number. As  $M_x$  increases,  $M_A$  also increases. For example, if  $M_x$  is increased to  $M = 0.5$ , the maximum local value of  $M$  will be 0.772, as shown in Fig. 11.5b. Let us continue to increase  $M_x$  until we achieve just the right value such that the local Mach number at the minimum pressure point equals 1, i.e., such that  $M_A = 1.0$ , as shown in Fig. 11.5c. When this happens, the freestream Mach number  $M_x$  is called the *critical Mach number*, denoted by  $M_{cr}$ . By definition, the critical Mach number is that *freestream Mach number at which sonic flow is first achieved on the airfoil surface*. In Fig. 11.5c,  $M_{cr} = 0.61$ .

One of the most important problems in high-speed aerodynamics is the determination of the critical Mach number of a given airfoil, because at values of  $M_x$  slightly above  $M_{cr}$ , the airfoil experiences a dramatic increase in drag coefficient (discussed in Sec. 11.7). The purpose of the present section is to give a method for estimating  $M_{cr}$ . Let  $p_s$  and  $p_A$  represent the static pressures in the freestream and at point A, respectively, in Fig. 11.5. For isentropic flow, where the total pressure  $p_0$  is constant, these static pressures are related through Eq. (8.42) as follows:

$$\frac{p_A}{p_s} = \frac{p_A/p_0}{p_s/p_0} = \left( \frac{1 + [(\gamma - 1)/2]M_x^2}{1 + [(\gamma - 1)/2]M_A^2} \right)^{\gamma/(\gamma-1)} \quad (11.56)$$

The pressure coefficient at point A is given by Eq. (11.22) as

$$C_{p,A} = \frac{2}{\gamma M_x^2} \left( \frac{p_A}{p_s} - 1 \right) \quad (11.57)$$

Combining Eqs. (11.56) and (11.57), we have

$$C_{p,A} = \frac{2}{\gamma M_x^2} \left[ \left( \frac{1 + [(\gamma - 1)/2]M_x^2}{1 + [(\gamma - 1)/2]M_A^2} \right)^{\gamma/(\gamma-1)} - 1 \right] \quad (11.58)$$

Equation (11.58) is useful in its own right; for a given freestream Mach number, it relates the local value of  $C_p$  to the local Mach number. However, for our purposes here, we ask the question, What is the value of the local  $C_p$  when the local Mach number is unity? By definition, this value of the pressure coefficient is called the *critical pressure coefficient*, denoted by  $C_{p,cr}$ . For a given freestream Mach number  $M_x$ , the value of  $C_{p,cr}$  can be obtained by inserting  $M_A = 1$  into Eq. (11.58):

$$C_{p,cr} = \frac{2}{\gamma M_x^2} \left[ \left( \frac{1 + [(\gamma - 1)/2]M_x^2}{1 + (\gamma - 1)/2} \right)^{\gamma/(\gamma-1)} - 1 \right] \quad (11.59)$$

Equation (11.59) allows us to calculate the pressure coefficient at any point in the flow where the local Mach number is 1, for a given freestream Mach number  $M_x$ . For example, if  $M_x$  is slightly greater than  $M_{cr}$ , say  $M_x = 0.65$  as shown in Fig. 11.5d, then a finite region of supersonic flow will exist above the airfoil. Eq. (11.59) allows us to calculate the pressure coefficient at only those points where  $M = 1$ , i.e., at only those points that fall on the sonic line in Fig. 11.5c. Now, returning to Fig. 11.5c, when the freestream Mach number is precisely equal to the critical Mach number, there is only one point where  $M = 1$ , namely, point A. The pressure coefficient at point A will be

$C_{p,cr}$ , which is obtained from Eq. (11.59). In this case,  $M_x$  in Eq. (11.59) is precisely  $M_{cr}$ . Hence,

$$C_{p,cr} = \frac{2}{\gamma M_{cr}^2} \left[ \left( \frac{1 + [(\gamma - 1)/2]M_{cr}^2}{1 + (\gamma - 1)/2} \right)^{\gamma/(\gamma-1)} - 1 \right] \quad (11.60)$$

Equation (11.60) shows that  $C_{p,cr}$  is a unique function of  $M_{cr}$ ; this variation is plotted as curve C in Fig. 11.6. Note that Eq. (11.60) is simply an aerodynamic relation for isentropic flow — it has no connection with the shape of a given airfoil. In this sense, Eq. (11.60), and hence curve C in Fig. 11.6, is a type of “universal relation” which can be used for all airfoils.

Equation (11.60), in conjunction with any one of the compressibility corrections given by Eqs. (11.51), (11.54), or (11.55), allows us to estimate the critical Mach number for a given airfoil as follows:

1. By some means, either experimental or theoretical, obtain the low-speed incompressible value of the pressure coefficient  $C_{p,0}$  at the minimum pressure point on the given airfoil.
2. Using any of the compressibility corrections Eq. (11.51), (11.54), or (11.55), plot the variation of  $C_p$  with  $M_x$ . This is represented by curve B in Fig. 11.6.
3. Somewhere on curve B, there will be a single point where the pressure coefficient corresponds to locally sonic flow. Indeed, this point must coincide with Eq. (11.60), represented by curve C in Fig. 11.6. Hence, the intersection of curves B and C represent the point corresponding to sonic flow at the minimum pressure location on the airfoil. In turn, the value of  $M_x$  at this intersection is, by definition, the critical Mach number, as shown in Fig. 11.6.

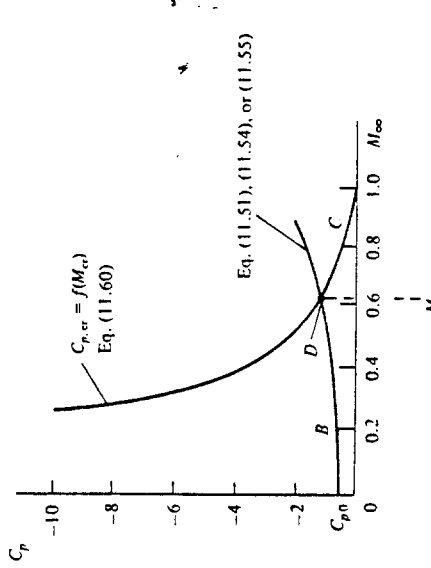


Figure 11.6 Estimation of critical Mach number.

The graphical construction in Fig. 11.6 is not an exact determination of  $M_{cr}$ . Although curve C is exact, curve B is approximate because it represents the approximate compressibility correction. Hence, Fig. 11.6 gives only an estimation of  $M_{cr}$ . However, such an estimation is quite useful for preliminary design, and the results from Fig. 11.6 are accurate enough for most applications.

Consider two airfoils, one thin and the other thick, as sketched in Fig. 11.7. First consider the low-speed incompressible flow over these airfoils. The flow over the thin airfoil is only slightly perturbed from the freestream. Hence, the expansion over the top surface is mild, and  $C_{p,0}$  at the minimum pressure point is a negative number of only small absolute magnitude, as shown in Fig. 11.7. [Recall from Eq. (11.32) that  $C_p \propto \hat{u}$ ; hence, the smaller the perturbation, the smaller is the absolute magnitude of  $C_p$ .] In contrast, the flow over the thick airfoil experiences a large perturbation from the freestream. The expansion over the top surface is strong, and  $C_{p,0}$  at the minimum pressure point is a negative number of large magnitude, as shown in Fig. 11.7. If we now perform the same construction for each airfoil as given in Fig. 11.6, we see that the thick airfoil will have a lower critical Mach number than the thin airfoil. This is clearly illustrated in Fig. 11.7. For high-speed airplanes, it is desirable to have  $M_{cr}$  as high as possible. Hence, modern high-speed subsonic airplanes are usually designed with relatively thin airfoils. (The development of the supercritical airfoil has somewhat loosened this criterion, as discussed in Sec. 11.8.) For example, the Gates Lear jet high-speed jet executive transport utilizes a 9 percent thick airfoil; contrast this with the low-speed Piper Aztec, a twin-engine propeller-driven general aviation aircraft designed with a 14 percent thick airfoil.

### 11.7 DRAG-DIVERGENCE MACH NUMBER: THE SOUND BARRIER

Imagine that we have a given airfoil at a fixed angle of attack in a wind tunnel, and we wish to measure its drag coefficient  $c_d$  as a function of  $M_\infty$ . To begin with, we measure the drag coefficient at low subsonic speed to be  $c_{d,0}$ , shown in Fig. 11.8. Now, as we gradually increase the freestream Mach number, we observe that  $c_d$  remains relatively constant all the way to the critical Mach number, as illustrated in Fig. 11.8. The flow fields associated with points a, b, and c in Fig. 11.8 are represented by Fig. 11.5a, b, and c, respectively. As we very carefully increase  $M_\infty$  slightly above  $M_{cr}$ , say to point d in Fig. 11.8, a finite region of supersonic flow appears on the airfoil, as shown in Fig. 11.5d. The Mach number in this bubble of supersonic flow is only slightly above Mach 1, typically 1.02 to 1.05. However, as we continue to nudge  $M_\infty$  higher, we encounter a point where the drag coefficient suddenly starts to increase. This is given as point e in Fig. 11.8. The value of  $M_\infty$  at which this sudden increase in drag starts is defined as the *drag-divergence Mach number*. Beyond the drag-divergence Mach number, the drag coefficient can become very large, typically increasing by a factor of 10 or more. This large increase in drag is associated with an extensive region of supersonic flow over the airfoil, terminating in a shock wave, as sketched in the insert in Fig. 11.8. Corresponding to point f on the drag curve, this insert shows that as  $M_\infty$  approaches unity, the flow on both the top and bottom surfaces can be supersonic, both terminated by shock waves. For example, consider the case of a reasonably thick airfoil,

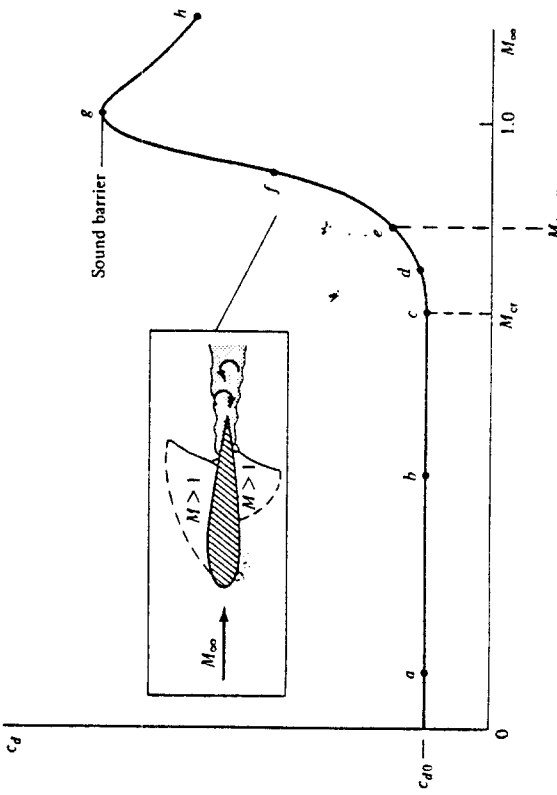


Figure 11.8 Sketch of the variation of profile drag coefficient with freestream Mach number, illustrating the critical and drag-divergence Mach numbers and showing the large drag rise near Mach one.

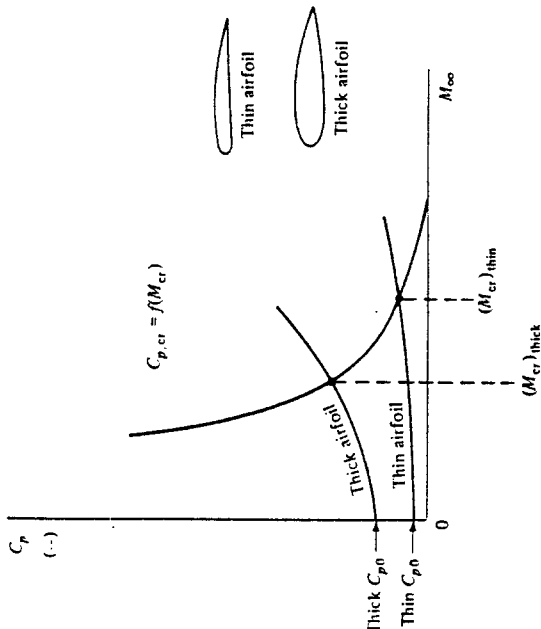


Figure 11.7 Effect of airfoil thickness on critical Mach number.

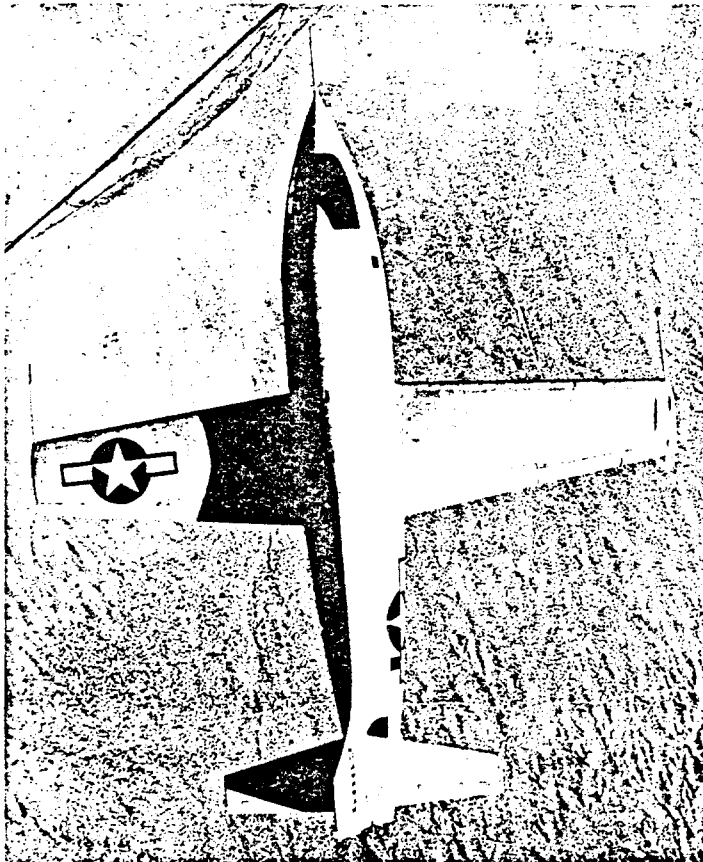


Figure 11.9 The Bell XS-1—the first manned airplane to fly faster than sound. October 14, 1947. (Courtesy of the National Air and Space Museum.)

designed originally for low-speed applications, when  $M_x$  is beyond drag-divergence; in such a case, the local Mach number can reach 1.2 or higher. As a result, the terminating shock waves can be relatively strong. These shocks generally cause severe flow separation downstream of the shocks, with an attendant large increase in drag.

Now, put yourself in the place of an aeronautical engineer in 1936. You are familiar with the Prandtl-Glauert rule, given by Eq. (11.51). You recognize that as  $M_x \rightarrow 1$ , this equation shows the absolute magnitude of  $C_r$  approaching infinity. This hints at some real problems near Mach 1. Furthermore, you know of some initial high-speed subsonic wind-tunnel tests that have generated drag curves which resemble the portion of Fig. 11.8 from points *a* to *f*. How far will the drag coefficient increase as we get closer to  $M_x = 1$ ? Will  $c_d$  go to infinity? At this stage, you might be pessimistic. You might visualize the drag increase to be so large that no airplane with the power plants existing in 1936, or even envisaged for the future, could ever overcome this "barrier." It was this type of thought that led to the popular concept of a sound barrier and that prompted many people to claim that humans would never fly faster than the speed of sound.

Of course, today we know the sound barrier was a myth. We cannot use the Prandtl-Glauert rule to argue that  $c_d$  will become infinite at  $M_x = 1$ , because the Prandtl-Glauert rule is invalid at  $M_x = 1$  (see Secs. 11.3 and 11.4). Moreover, early transonic wind-tunnel tests carried out in the late 1940s clearly indicated that  $c_d$  peaks at or around Mach 1 and then actually decreases as we enter the supersonic regime, as shown by points *g* and *h* in Fig. 11.8. All we need is an aircraft with an engine powerful enough to overcome the large drag rise at Mach 1. The myth of the sound barrier was finally put to rest on October 14, 1947, when Captain Charles (Chuck) Yeager became the first human being to fly faster than sound in the sleek, bullet-shaped Bell XS-1. This rocket-propelled research aircraft is shown in Fig. 11.9. Of course, today supersonic flight is a common reality; we have jet engines powerful enough to accelerate military fighters through Mach 1 flying straight up! Such airplanes can fly at Mach 3 and beyond. Indeed, we are limited only by aerodynamic heating at high speeds (and the consequent structural problems). Right now, NASA is conducting research on supersonic combustion ramjet engines for flight in the Mach 4 to 7 range. Keep in mind, however, that because of the large power requirements for very high speed flight, the fuel consumption becomes large. In today's energy-conscious world, this constraint can be as much a barrier to high-speed flight as the sound barrier was once envisaged.

Since 1945, research in transonic aerodynamics has focused on reducing the large drag rise shown in Fig. 11.8. Instead of living with a factor of 10 increase in drag at Mach 1, can we reduce it to a factor of 2 or 3? This is the subject of the remaining sections of this chapter.

## 11.8 THE AREA RULE

For a moment, let us expand our discussion from two-dimensional airfoils to a consideration of a complete airplane. In this section, we introduce a design concept which has effectively reduced the drag rise near Mach 1 for a complete airplane.

As stated before, the first practical jet-powered aircraft appeared at the end of World War II in the form of the German Me 262. This was a subsonic fighter plane with

a top speed near 550 mi/h. The next decade saw the design and production of many types of jet aircraft—all limited to subsonic flight by the large drag near Mach 1. Even the "century" series of fighter aircraft designed to give the U.S. Air Force supersonic capability in the early 1950s, such as the Convair F-102 delta-wing airplane, ran into difficulty and could not at first readily penetrate the sound barrier in level flight. The thrust of jet engines at that time simply could not overcome the large peak drag near Mach 1.

A planview, cross section, and area distribution (cross-sectional area versus distance along the axis of the airplane) for a typical airplane of that decade are sketched in Fig. 11.10. Let  $A$  denote the total cross-sectional area at any given station. Note that the cross-sectional area distribution experiences some abrupt changes along the axis, with discontinuities in both  $A$  and  $dA/dx$  in the regions of the wing.

In contrast, for almost a century, it was well known by ballisticians that the speed of a supersonic bullet or artillery shell with a smooth variation of cross-sectional area was higher than projectiles with abrupt or discontinuous area distributions. In the mid-1950s, an aeronautical engineer at the NACA Langley Aeronautical Laboratory, Richard T. Whitcomb, put this knowledge to work on the problem of transonic flight of airplanes. Whitcomb reasoned that the variation of cross-sectional area for an airplane should be smooth, with no discontinuities. This meant that, in the region of the

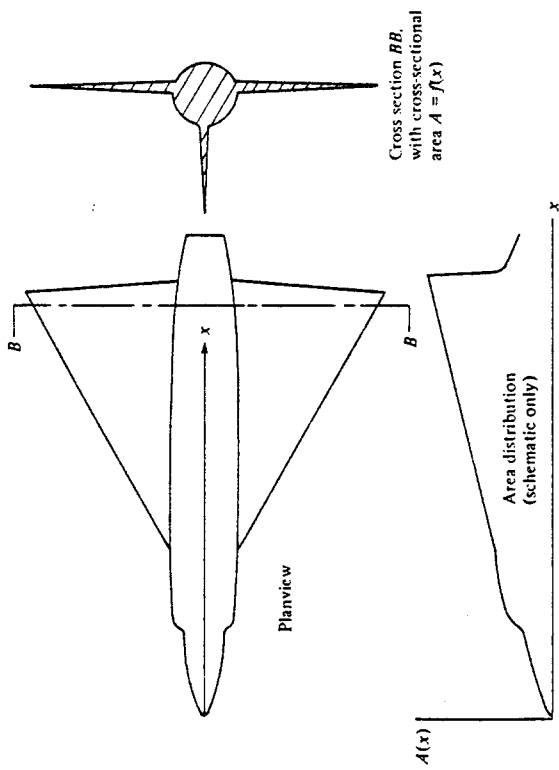


Figure 11.10 A schematic of a non-area-ruled aircraft.

wings and tail, the fuselage cross-sectional area should decrease to compensate for the addition of the wing and tail cross-sectional area. This led to a "coke bottle" fuselage shape, as shown in Fig. 11.11. Here, the planview and area distribution are shown for an aircraft with a relatively smooth variation of  $A(x)$ . This design philosophy is called the *area rule*, and it successfully reduced the peak drag near Mach 1 such that practical airplanes could fly supersonically by the mid-1950s. The variations of drag coefficient with  $M_\infty$  for an area-ruled and non-area-ruled airplane are schematically compared in Fig. 11.12; typically, the area rule leads to a factor-of-2 reduction in the peak drag near Mach 1.

The development of the area rule was a dramatic breakthrough in high-speed flight, and it earned a substantial reputation for Richard Whitcomb — a reputation which was to be later garnished by a similar breakthrough in transonic airfoil design, to be discussed in Sec. 11.9. The original work on the area rule was presented by Whitcomb in Ref. 31, which should be consulted for more details.

## 11.9 THE SUPERCRITICAL AIRFOIL

Let us return to a consideration of two-dimensional airfoils. A natural conclusion from the material in Sec. 11.6, and especially from Fig. 11.8, is that an airfoil with a high critical Mach number is very desirable, indeed necessary, for high-speed subsonic aircraft. If we can increase  $M_{cr}$ , then we can increase  $M_{drag\ divergence}$  which follows closely after  $M_{cr}$ . This was the philosophy employed in aircraft design from 1945 to approximately 1965. Almost by accident, the NACA 64-series airfoils (see Sec. 4.2), although

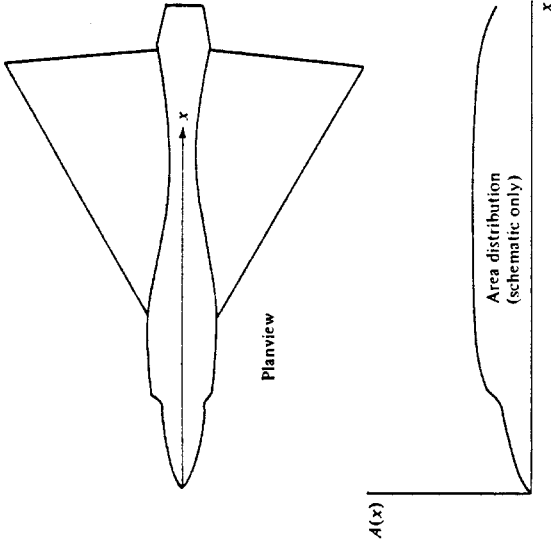


Figure 11.11 A schematic of an area-ruled aircraft.

originally designed to encourage laminar flow, turned out to have relative high values of  $M_{cr}$  in comparison with other NACA shapes. Hence, the NACA 64 series has seen wide application on high-speed airplanes. Also, we know that thinner airfoils have higher values of  $M_{cr}$  (see Fig. 11.7); hence, aircraft designers have used relatively thin airfoils on high-speed airplanes.

However, there is a limit to how thin a practical airfoil can be. For example, considerations other than aerodynamic influence the airfoil thickness; the airfoil requires a certain thickness for structural strength, and there must be room for the storage of fuel. This prompts the following question: For an airfoil of given thickness, how can we delay the large drag rise to higher Mach numbers? To increase  $M_{cr}$  is one obvious tack, as described above, but there is another approach. Rather than increasing  $M_{cr}$ , let us strive to increase the Mach number *increment* between  $M_{cr}$  and  $M_{drag\ divergence}$ . That

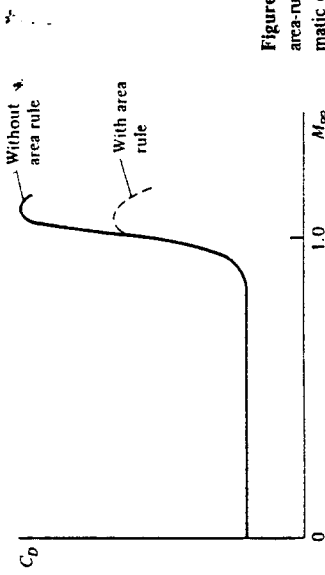


Figure 11.12 The drag-rise properties of area-ruled and non-area-ruled aircraft (schematic only).

is, referring to Fig. 11.8, let us increase the distance between points *e* and *c*. This philosophy has been pursued since 1965, leading to the design of a new family of airfoils called *supercritical airfoils*, which are the subject of this section.

The purpose of a supercritical airfoil is to increase the value of  $M_{\text{drag divergence}}$ , although  $M_{\text{cr}}$  may change very little. The shape of a supercritical airfoil is compared with an NACA 64-series airfoil in Fig. 11.13. Here, an NACA 64<sub>2</sub>-A215 airfoil is sketched in Fig. 11.13*a*, and a 15 percent thick supercritical airfoil is shown in Fig. 11.13*c*. (Note the similarity between the supercritical profile and the modern low-speed airfoils discussed in Sec. 4.10.) The supercritical airfoil has a relatively flat top, thus encouraging a region of supersonic flow with lower local values of  $M$  than the NACA 64 series. In turn, the terminating shock is weaker, thus creating less drag. Similar trends can be seen by comparing the  $C_p$  distributions for the NACA 64 series (Fig. 11.13*b*) and the supercritical airfoil (Fig. 11.13*d*). Indeed, Figs. 11.13*a* and *b* for the NACA 64-series airfoil pertain to a lower freestream Mach number,  $M_\infty = 0.69$ , than Fig. 11.13*c* and *d* which pertain to the supercritical airfoil at a higher freestream Mach number,  $M_\infty = 0.79$ . In spite of the fact that the 64-series airfoil is at a lower  $M_\infty$ , the extent of the supersonic flow reaches further above the airfoil, the local supersonic Mach numbers are higher, and the terminating shock wave is stronger. Clearly, the supercritical airfoil shows more desirable flow-field characteristics; namely, the extent of the supersonic flow is closer to the surface, the local supersonic Mach numbers are lower, and the terminating shock

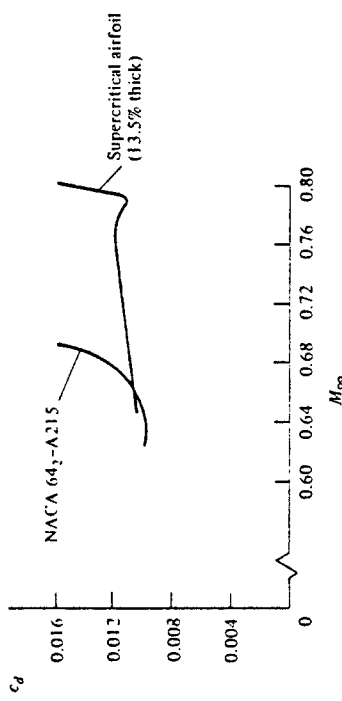


Figure 11.14 The drag divergence properties of a standard NACA 64-series airfoil and a supercritical airfoil.

wave is weaker. As a result, the value of  $M_{\text{drag divergence}}$  will be higher for the supercritical airfoil. This is verified by the experimental data given in Fig. 11.14, taken from Ref. 32. Here, the value of  $M_{\text{drag divergence}}$  is 0.79 for the supercritical airfoil in comparison with 0.67 for the NACA 64 series.

Because the top of the supercritical airfoil is relatively flat, the forward 60 percent of the airfoil has negative camber, which lowers the lift. To compensate, the lift is increased by having extreme positive camber on the rearward 30 percent of the airfoil. This is the reason for the cusplike shape of the bottom surface near the trailing edge.

The supercritical airfoil was developed by Richard Whitcomb in 1965 at the NASA Langley Research Center. A detailed description of the rationale as well as some early experimental data for supercritical airfoils is given by Whitcomb in Ref. 32, which should be consulted for more details. The supercritical airfoil, and many variations of such, are now used by the aircraft industry on modern high-speed airplane designs. Examples are the Boeing 757 and 767, and the latest model Lear jets. The supercritical airfoil is one of two major breakthroughs made in transonic airplane aerodynamics since 1945, the other being the area rule discussed in Sec. 11.8. It is a testimonial to the man that Richard Whitcomb was mainly responsible for both.

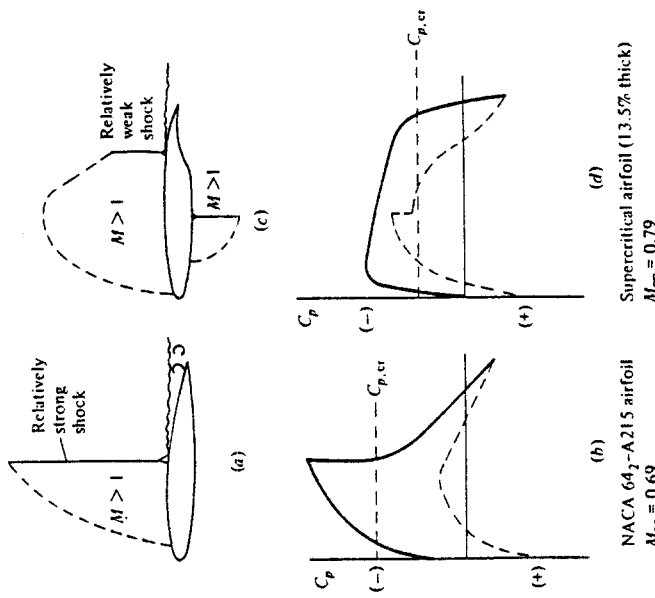


Figure 11.13 Standard NACA 64-series airfoil compared with a supercritical airfoil at cruise lift conditions.  
(From Ref. 32.)

## 11.10 HISTORICAL NOTE: HIGH-SPEED AIRFOILS—EARLY RESEARCH AND DEVELOPMENT

Twentieth-century aerodynamics does not have the exclusive rights to the observation of the large drag rise on bodies flying at near the speed of sound; rather, in the eighteenth century the Englishman Benjamin Robins, inventor of the ballistic pendulum, reported that "the velocity at which the body shifts its resistance (from a  $V^2$  to a  $V^3$  relation) is nearly the same with which sound is propagated through air." His statement was based on a large number of experiments during which projectiles were fired into his ballistic pendulum. However, these results had little relevance to the early aerodynamicists of this century, who were struggling to push aircraft speeds to 150 mi/h

during and just after World War I. To these people, flight near the speed of sound was just fantasy.

With one exception! World War I airplanes such as the Spad and Nieuport had propeller blades where the tips were moving at near the speed of sound. By 1919, British researchers had already observed the loss in thrust and large increase in blade drag for a propeller with tip speeds up to 1180 ft/s—slightly above the speed of sound. To examine this effect further, F. W. Caldwell and E. N. Fales, both engineers at the U.S. Army's Engineering Division at McCook Field near Dayton, Ohio (the forerunner of the massive Air Force research and development facilities at Wright-Patterson Air Force Base today), conducted a series of high-speed airfoil tests. They designed and built the first high-speed wind tunnel—a facility with a 14-in-diameter test section capable of velocities up to 675 ft/s. In 1918, they conducted the first wind-tunnel tests involving the high-speed flow over a stationary airfoil. Their results showed large decreases in lift coefficient and major increases in drag coefficient for the thicker airfoils at angle of attack. These were the first measured "compressibility effects" on an airfoil in history. Caldwell and Fales noted that such changes occurred at a certain air velocity, which they denoted as the "critical speed"—a term that was to evolve into the critical Mach number at a later date. It is interesting to note that Orville Wright was a consultant to the Army at this time (Wilbur had died prematurely in 1912 of typhoid fever) and observed some of the Caldwell and Fales tests. However, a fundamental understanding and explanation of this critical-speed phenomenon was completely lacking. Nobody at that time had even the remotest idea of what was really happening in this high-speed flow over the airfoil.

Members of the National Advisory Committee for Aeronautics were well aware of the Caldwell-Fales results. Rather than let the matter die, in 1922 the NACA contracted with the National Bureau of Standards (NBS) for a study of high-speed flows over airfoils, with an eye toward improved propeller sections. The work at NBS included the building of a high-speed wind tunnel with a 12-in diameter test section, capable of producing a Mach number of 0.95. The aerodynamic testing was performed by Lyman J. Briggs (soon to become director of NBS) and Hugh Dryden (soon to become one of the leading aerodynamicists of the twentieth century). In addition to the usual force data, Briggs and Dryden also measured pressure distributions over the airfoil surface. These pressure distributions allowed more insight into the nature of the flow and definitely indicated flow separation on the top surface of the airfoil. We now know that such flow separation is induced by a shock wave, but these early researchers did not at that time know about the presence of such shocks.

During the same period, the only meaningful theoretical work on high-speed airfoil properties was carried out by Ludwig Prandtl in Germany and Herman Glauert in England—work which led to the Prandtl-Glauert compressibility correction, given by Eq. (11.51). As early as 1922, Prandtl is quoted as stating that the lift coefficient increased according to  $(1 - M_x^2)^{-1/2}$ ; he mentioned this conclusion in his lectures at Göttingen, but without written proof. This result was mentioned again 6 years later by Jacob Ackeret, a colleague of Prandtl, in the famous German series *Handbuch der Physik*, again without proof. Subsequently, in 1928 the concept was formally established by Herman Glauert, a British aerodynamicist working for the Royal Aircraft

Establishment. (See chapter 9 of Ref. 21 for a biographical sketch of Glauert.) Using only six pages in the *Proceedings of the Royal Society*, vol. 118, p. 113), Glauert presented a derivation based on linearized small-perturbation theory (similar to that described in Sec. 11.4) which confirmed the  $(1 - M_x^2)^{-1/2}$  variation. In this paper, entitled "The Effect of Compressibility on the Lift of an Airfoil," Glauert derived the famous Prandtl-Glauert compressibility correction given here as Eqs. (11.51) to (11.53). This result was to stand alone, unaltered, for the next 10 years.

Hence, in 1930 the state of the art of high-speed subsonic airfoil research was characterized by experimental proof of the existence of the drag-divergence phenomenon, some idea that it was caused by flow separation, but no fundamental understanding of the basic flow field. In turn, there was virtually no theoretical background outside of the Prandtl-Glauert rule. Also, keep in mind that all the above work was paced by the need to understand propeller performance, because in that day the only component of airplanes to encounter compressibility effects was the propeller tips.

All this changed in the 1930s. In 1928, the NACA had constructed its first rudimentary high-speed subsonic wind tunnel at the Langley Aeronautical Laboratory, utilizing a 1-ft-diameter test section. With Eastman Jacobs as tunnel director and John Stack as the chief researcher, a series of tests were run on various standard airfoil shapes. Frustrated by their continual lack of understanding about the flow field, they turned to optical techniques, following in the footsteps of Ernst Mach (see Sec. 9.8). In 1933 they assembled a crude schlieren optical system consisting of 3-in-diameter reading-glass quality lenses and a short-duration-spark light source. In their first test using the schlieren system, dealing with flow over a cylinder, the results were spectacular. Shock waves were seen, along with the resulting flow separation. Visitors flocked to the wind tunnel to observe the results, including Theodore Theodorsen, one of the ranking theoretical aerodynamicists of that period. An indicator of the psychology at that time is given by Theodorsen's comment that since the freestream flow was subsonic, what appeared as shock waves must be an "optical illusion." However, Eastman Jacobs and John Stack knew differently. They proceeded with a major series of airfoil testing, using standard NACA sections. Their schlieren pictures revealed the secrets of flow over the airfoils above the critical Mach number. (See Fig. 1.26b and its attendant discussion of such supercritical flow.) In 1935, Jacobs traveled to Italy, where he presented results of the NACA high-speed airfoil research at the fifth Volta Conference (see Sec. 7.1). This is the first time in history that photographs of the transonic flow field over standard-shaped airfoils were presented in a large public forum.

During the course of such work in the 1930s, the incentive for high-speed aerodynamic research shifted from propeller applications to concern about the airframe of the airplane itself. By the mid-1930s, the possibility of the 550 mi/h airplane was more than a dream—reciprocating engines were becoming powerful enough to consider such a speed regime for propeller-driven aircraft. In turn, the entire airplane itself (wings, cowling, tail, etc.) would encounter compressibility effects. This led to the design of a large 8-ft high-speed tunnel at Langley, capable of test section velocities above 500 mi/h. This tunnel, along with the earlier 1-ft tunnel, established the NACA's dominance in high-speed subsonic research in the late 1930s.

In the decade following 1930, the picture had changed completely. By 1940, the high-speed flow over airfoils was relatively well understood. During this period, Stack and Jacobs had not only highlighted the experimental aspects of such high-speed flow, but they also derived the expression for  $C_{p,\sigma}$  as a function of  $M_\infty$  given by Eq. (11.60), and had shown how to estimate the critical Mach number for a given airfoil as discussed in Sec. 11.6. Figure 11.15 shows some representative schlieren photographs taken by the NACA of the flow over standard NACA airfoils. Although these photographs were taken in 1949, they are similar to the results obtained by Stack and Jacobs in the 1930s.

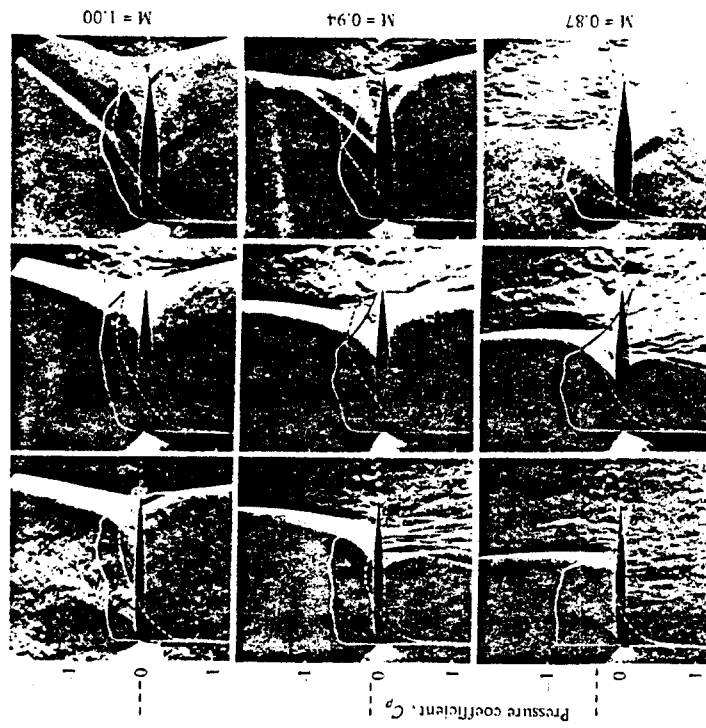


Figure 11.15 Schlieren pictures and pressure distributions for transonic flows over several NACA airfoils. These pictures were taken by the NACA in 1949. (From John V. Becker, "The High-Speed Frontier," NASA SP-445, 1980.)

Superimposed on these photographs are the measured pressure distributions over the top (solid curve) and bottom (dashed curve) surfaces of the airfoil. Study these pictures carefully. Moving from bottom to top, you can see the influence of increasing free-stream Mach number, and going from left-to-right, you can observe the effect of increasing airfoil thickness. Note how the shock wave moves downstream as  $M_\infty$  is increased, finally reaching the trailing edge at  $M_x = 1.0$ . For this case, the top row of pictures shows almost completely supersonic flow over the airfoil. Note also the large regions of separated flow downstream of the shock waves for the Mach numbers of 0.79, 0.87, and 0.94 — this separated flow is the primary reason for the large increase in drag near Mach 1. By 1940, it was well-understood that the almost discontinuous pressure increase across the shock wave creates a strong adverse pressure gradient on the airfoil surface, and this adverse pressure gradient is responsible for separating the flow.

The high-speed airfoil research program continues today within NASA. It led to the supercritical airfoils in the 1960s (see Secs. 11.9 and 11.11). It has produced a massive effort in modern times to use computational techniques for theoretically solving the transonic flow over airfoils. Such efforts are beginning to be successful, and in many respects, today we have the capability to design transonic airfoils on the computer. However, such abilities today have roots which reach all the way back to Caldwell and Fales in 1918.

For a more detailed account of the history of high-speed airfoil research, you are encouraged to read the entertaining story portrayed by John V. Becker in *The High-Speed Frontier*, NASA SP-445, 1980.

### 11.11 HISTORICAL NOTE: RICHARD T. WHITCOMB — ARCHITECT OF THE AREA RULE AND THE SUPERCRITICAL WING

The developments of the area rule (Sec. 11.8) and the supercritical airfoil (Sec. 11.9) are two of the most important advancements in aerodynamics since 1950. That both developments were made by the same man — Richard T. Whitcomb — is remarkable. Who is this man? What qualities lead to such accomplishments? Let us pursue these matters further.

Richard Whitcomb was born on February 21, 1921, in Evanston, Illinois. At an early age, he was influenced by his grandfather, who had known Thomas A. Edison. In an interview with *The Washington Post* on August 31, 1969, Whitcomb is quoted as saying: "I used to sit around and hear stories about Edison. He sort of developed into my idol." Whitcomb entered the Worcester Polytechnic Institute in 1939. (This is the same school from which the rocket pioneer, Robert H. Goddard, had graduated 31 years earlier.) Whitcomb distinguished himself in college and graduated with a mechanical engineering degree with honors in 1943. Informed by a *Fortune* magazine article on the research facilities at the NACA Langley Memorial Laboratory, Whitcomb immediately joined the NACA. He became a wind-tunnel engineer, and as an early assignment he worked on design problems associated with the Boeing B-29 Superfortress. He remained with the NACA and later its successor, the NASA, until his retirement in

1980 — spending his entire career with the wind tunnels at the Langley Research Center. In the process, he rose to become head of the Eight-foot Tunnel Branch at Langley. Whitcomb conceived the idea of the area rule as early as 1951. He tested his idea in the transonic wind tunnel at Langley. The results were so promising that the aeronautical industry changed designs in midstream. For example, the Convair F-102 delta-wing fighter had been designed for supersonic flight, but was having major difficulty even exceeding the speed of sound — the increase in drag near Mach 1 was simply too large. The F-102 was redesigned to incorporate Whitcomb's area rule and afterward was able to achieve its originally intended supersonic Mach number. The area rule was such an important aerodynamic breakthrough that it was classified "secret" from 1952 to 1954, when airplanes incorporating the area rule began to roll off the production line. In 1954, Whitcomb was given the Collier Trophy — an annual award for the "greatest achievement in aviation in America."

In the early 1960s, Whitcomb turned his attention to airfoil design, with the objective again of decreasing the large drag rise near Mach 1. Using the existing knowledge about airfoil properties, a great deal of wind-tunnel testing, and intuition honed by years of experience, Whitcomb produced the supercritical airfoil. Again, this development had a major impact on the aeronautical industry, and today virtually all new commercial transport and executive aircraft designs are incorporating a supercritical wing. Because of his development of the supercritical airfoil, in 1974 NASA gave Whitcomb a cash award of \$25,000 — the largest cash award ever given by NASA to a single individual.

There are certain parallels between the personalities of the Wright brothers and Richard Whitcomb: (1) they all had powerful intuitive abilities which they brought to bear on the problem of flight, (2) they were totally dedicated to their work (none of them ever married), and (3) they did a great deal of their work themselves, trusting only their own results. For example, here is a quote from Whitcomb which appears in the same *Washington Post* interview mentioned above. Concerning the detailed work on the development of the supercritical airfoil, Whitcomb says:

"I modified the shape of the wing myself as we tested it. It's just plain easier this way. In fact my reputation for filing the wing's shape has become so notorious that the people at North American have threatened to provide me with a 10-foot file to work on the real airplane, also."

Perhaps the real ingredient for Whitcomb's success is his personal philosophy, as well as his long hours at work daily. In his own words:

"There's been a continual drive in me ever since I was a teenager to find a better way to do everything. A lot of very intelligent people are willing to adapt, but only to a certain extent. If a human mind can figure out a better way to do something, let's do it. I can't just sit around. I have to think."

Students take note!

Review the road map in Fig. 11.1, and make certain that you have all the concepts listed on this map well in mind. Some of the highlights of this chapter are as follows.

For two-dimensional, irrotational, isentropic, steady flow of a compressible fluid, the exact velocity potential equation is

$$\left[ 1 - \frac{1}{a^2} \left( \frac{\partial \phi}{\partial x} \right)^2 \right] \frac{\partial^2 \phi}{\partial x^2} + \left[ 1 - \frac{1}{a^2} \left( \frac{\partial \phi}{\partial y} \right)^2 \right] \frac{\partial^2 \phi}{\partial y^2} - \frac{2}{a^2} \left( \frac{\partial \phi}{\partial x} \right) \left( \frac{\partial \phi}{\partial y} \right) \frac{\partial^2 \phi}{\partial x \partial y} = 0 \quad (11.12)$$

$$\text{where } a^2 = a_0^2 + \frac{\gamma - 1}{2} \left[ \left( \frac{\partial \phi}{\partial x} \right)^2 + \left( \frac{\partial \phi}{\partial y} \right)^2 \right] \quad (11.13)$$

This equation is exact, but it is nonlinear and hence difficult to solve. At present, no general analytical solution to this equation exists.

For the case of small perturbations (slender bodies at low angles of attack), the exact velocity potential equation can be approximated by

$$(1 - M_\infty^2) \frac{\partial^2 \phi}{\partial x^2} + \frac{\partial^2 \phi}{\partial y^2} = 0 \quad (11.18)$$

This equation is approximate, but linear, and hence more readily solved. This equation holds for subsonic ( $0 \leq M_\infty \leq 0.8$ ) and supersonic ( $1.2 \leq M_\infty \leq 5$ ) flows; it does not hold for transonic ( $0.8 \leq M_\infty \leq 1.2$ ) or hypersonic ( $M_\infty > 5$ ) flows.

The Prandtl-Glauert rule is a compressibility correction that allows the modification of existing incompressible flow data to take into account compressibility effects.

$$C_p = \frac{C_{p,0}}{\sqrt{1 - M_\infty^2}} \quad (11.51)$$

$$C_l = \frac{C_{l,0}}{\sqrt{1 - M_\infty^2}} \quad (11.52)$$

$$C_m = \frac{C_{m,0}}{\sqrt{1 - M_\infty^2}} \quad (11.53)$$

The critical Mach number is that freestream Mach number at which sonic flow is first obtained at some point on the surface of a body. For thin airfoils, the critical Mach number can be estimated as shown in Fig. 11.6.

The drag-divergence Mach number is that freestream Mach number at which a large rise in the drag coefficient occurs, as shown in Fig. 11.8.

The area rule for transonic flow states that the cross-sectional area distribution of an airplane, including fuselage, wing, and tail, should have a smooth distribution along the axis of the airplane.

Supercritical airfoils are specially designed profiles to increase the drag-divergence Mach number.

### PROBLEMS

11.1 Consider a subsonic compressible flow in cartesian coordinates where the velocity potential is given by

$$\phi(x, y) = V_\infty x + \frac{70}{\sqrt{1 - M_\infty^2}} e^{-2\pi\sqrt{1 - M_\infty^2} y} \sin 2\pi x$$

If the freestream properties are given by  $V_\infty = 700 \text{ ft/s}$ ,  $p_\infty = 1 \text{ atm}$ , and  $T_\infty = 519^\circ\text{R}$ , calculate the following properties at the location  $(x, y) = (0.2 \text{ ft}, 0.2 \text{ ft})$ ,  $M_\infty$ ,  $p$ , and  $T$ .

11.2 Using the Prandtl-Glauert rule, calculate the lift coefficient for an NACA 2412 airfoil at  $5^\circ$  angle of attack in a Mach 0.6 freestream. (Refer to Fig. 4.5 for the original airfoil data.)

11.3 Under low-speed incompressible flow conditions, the pressure coefficient at a given point on an airfoil is  $-0.54$ . Calculate  $C_p$  at this point when the freestream Mach number is 0.58, using

(a) The Prandtl-Glauert rule  
(b) The Karmen-Tsien rule  
(c) Laitone's rule

11.4 In low-speed incompressible flow, the peak pressure coefficient (at the minimum pressure point) on an NACA 0012 airfoil is  $-0.41$ . Estimate the critical Mach number for this airfoil, using the Prandtl-Glauert rule.

11.5 For a given airfoil, the critical Mach number is 0.8. Calculate the value of  $p/p_\infty$  at the minimum pressure point when  $M_\infty = 0.8$ .

*With the stabilizer setting at  $2^\circ$  the speed was allowed to increase to approximately 0.98 in 0.99 Mach number where elevator and rudder effectiveness were regained and the airplane seemed to smooth out to normal flying characteristics. This development item added confidence and the airplane was allowed to continue until an indication of 1.02 on the cockpit Mach meter was obtained. At this indication the motor momentarily stopped and then jumped at 1.06, and this hesitation was assumed to be caused by the effect of shock waves on the static source. At this time the power units were cut and the airplane allowed to decelerate back to the subsonic flight condition.*

*Captain Charles Yeager, describing his flight on October 14, 1947—the first manned flight to exceed the speed of sound.*

## 12.1 INTRODUCTION

The linearized perturbation velocity potential equation derived in Chap. 11, Eq. (11.18), is

$$(1 - M_\infty^2) \frac{\partial^2 \hat{\phi}}{\partial x^2} + \frac{\partial^2 \hat{\phi}}{\partial y^2} = 0 \quad (11.18)$$

and holds for both subsonic and supersonic flow. In Chap. 11, we treated the case of subsonic flow, where  $1 - M_\infty^2 > 0$  in Eq. (11.18). However, for supersonic flow,  $1 - M_\infty^2 < 0$ . This seemingly innocent change in sign on the first term of Eq. (11.18) is, in reality, a very dramatic change. Mathematically, when  $1 - M_\infty^2 > 0$  for subsonic flow, Eq. (11.18) is an *elliptic* partial differential equation, whereas when  $1 - M_\infty^2 < 0$  for supersonic flow, Eq. (11.18) becomes a *hyperbolic* differential equation. The details of this mathematical difference are beyond the scope of this book; however, the important point is that there is a difference. Moreover, this portends a fundamental difference in the physical aspects of subsonic and supersonic flow—something we have already demonstrated in previous chapters.

The purpose of this chapter is to obtain a solution of Eq. (11.18) for supersonic flow and to apply this solution to the calculation of supersonic airfoil properties. Since

## LINEARIZED SUPERSONIC FLOW

# CHAPTER TWELVE

our purpose is straightforward, and since this chapter is relatively short, there is no need for a chapter road map to provide guidance on the flow of our ideas.

## 12.2 DERIVATION OF THE LINEARIZED SUPERSONIC PRESSURE COEFFICIENT FORMULA

For the case of supersonic flow, let us write Eq. (11.18) as

$$\lambda^2 \frac{\partial^2 \hat{\phi}}{\partial x^2} - \frac{\partial^2 \hat{\phi}}{\partial y^2} = 0 \quad (12.1)$$

where  $\lambda = \sqrt{M_s^2 - 1}$ . A solution to this equation is the functional relation

$$\hat{\phi} = f(x - \lambda y) \quad (12.2)$$

We can demonstrate this by substituting Eq. (12.2) into Eq. (12.1) as follows. The partial derivative of Eq. (12.2) with respect to  $x$  can be written as

$$\frac{\partial \hat{\phi}}{\partial x} = f'(x - \lambda y) \frac{\partial(x - \lambda y)}{\partial x} \quad (12.4)$$

$$\text{or} \quad \frac{\partial \hat{\phi}}{\partial x} = f' \quad (12.5)$$

In Eq. (12.3), the prime denotes differentiation of  $f$  with respect to its argument,  $x - \lambda y$ . Differentiating Eq. (12.3) again with respect to  $x$ , we obtain

$$\frac{\partial^2 \hat{\phi}}{\partial x^2} = f'' \quad (12.6)$$

Similarly,

$$\frac{\partial \hat{\phi}}{\partial y} = f'(x - \lambda y) \frac{\partial(x - \lambda y)}{\partial y} \quad (12.7)$$

$$\text{or} \quad \frac{\partial \hat{\phi}}{\partial y} = f'(-\lambda) \quad (12.8)$$

Differentiating Eq. (12.5) again with respect to  $y$ , we have

$$\lambda^2 f'' - \lambda^2 f'' = 0 \quad (12.9)$$

Substituting Eqs. (12.4) and (12.6) into (12.1), we obtain the identity

$$\lambda^2 f'' - \lambda^2 f'' = 0$$

Hence, Eq. (12.2) is indeed a solution of Eq. (12.1).

Examine Eq. (12.2) closely. This solution is not very specific, because  $f$  can be any function of  $x - \lambda y$ . However, Eq. (12.2) tells us something specific about the flow, namely, that  $\hat{\phi}$  is constant along lines of  $x - \lambda y = \text{constant}$ . The slope of these lines is obtained from

our purpose is straightforward, and since this chapter is relatively short, there is no need for a chapter road map to provide guidance on the flow of our ideas.

From Eq. (9.31) and the accompanying Fig. 9.22, we know that

$$\tan \mu = \frac{1}{\sqrt{M_s^2 - 1}} \quad (12.8)$$

where  $\mu$  is the Mach angle. Therefore, comparing Eqs. (12.7) and (12.8), we see that a line along which  $\hat{\phi}$  is constant is a *Mach line*. This result is sketched in Fig. 12.1, which shows supersonic flow over a surface with a small hump in the middle, where  $\theta$  is the angle of the surface relative to the horizontal. According to Eqs. (12.1) to (12.8), all disturbances created at the wall (represented by the perturbation potential  $\hat{\phi}$ ) propagate unchanged away from the wall along Mach waves. All the Mach waves have the same slope, namely,  $dy/dx = (M_s^2 - 1)^{-1/2}$ . Note that the Mach waves slope *downstream* above the wall. Hence, *any disturbance at the wall cannot propagate upstream*; its effect is limited to the region of the flow downstream of the Mach wave emanating from the point of the disturbance. This is a further substantiation of the major difference between subsonic and supersonic flows mentioned in previous chapters, namely, that disturbances propagate *everywhere* throughout a subsonic flow, whereas they cannot propagate upstream in a steady supersonic flow.

Keep in mind that the above results, as well as the picture in Fig. 12.1, pertain to *linearized* supersonic flow [because Eq. (12.1) is a linear equation]. Hence, these results assume *small perturbations*, i.e., the hump in Fig. 12.1 is small, and thus  $\theta$  is small. Of course, we know from Chap. 9 that in reality a shock wave will be induced by the forward part of the hump, and an expansion wave will emanate from the rearward part of the hump. These are waves of finite strength and are not a part of linearized theory. Linearized theory is approximate; one of the consequences of this approximation is that waves of finite strength (shock and expansion waves) are not admitted. The above results allow us to obtain a simple expression for the pressure coefficient in supersonic flow, as follows. From Eq. (12.3),

$$\hat{u} = \frac{\partial \hat{\phi}}{\partial x} = f' \quad (12.9)$$

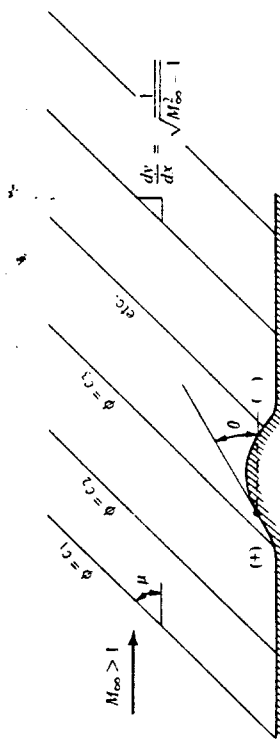


Figure 12.1 Linearized supersonic flow.

and from Eq. (12.5),

$$\dot{v} = \frac{\partial \dot{\phi}}{\partial y} = -\lambda f' \quad (12.10)$$

Eliminating  $f'$  from Eqs. (12.9) and (12.10), we obtain

$$\dot{u} = -\frac{\dot{v}}{\lambda} \quad (12.11)$$

Recall the linearized boundary condition given by Eq. (11.34), repeated below.

$$\dot{v} = \frac{\partial \dot{\phi}}{\partial y} = V_x \tan \theta \quad (12.12)$$

We can further reduce Eq. (12.12) by noting that, for small perturbations,  $\theta$  is small. Hence,  $\tan \theta \approx \theta$ , and Eq. (12.12) becomes

$$\dot{v} = V_x \theta \quad (12.13)$$

Substituting Eq. (12.13) into (12.11), we obtain

$$\dot{u} = -\frac{V_x \theta}{\lambda} \quad (12.14)$$

Recall the linearized pressure coefficient given by Eq. (11.32):

$$C_p = -\frac{2\dot{u}}{V_x} \quad (11.32)$$

Substituting Eq. (12.14) into (11.32), and recalling that  $\lambda \equiv \sqrt{M_x^2 - 1}$ , we have

$$C_p = \frac{2\theta}{\sqrt{M_x^2 - 1}} \quad (12.15)$$

Equation (12.15) is important. It is the linearized supersonic pressure coefficient, and it states that  $C_p$  is directly proportional to the local surface inclination with respect to the freestream. It holds for any slender two-dimensional body where  $\theta$  is small. Return again to Fig. 12.1. Note that  $\theta$  is positive when measured above the horizontal, and negative when measured below the horizontal. Hence, from Eq. (12.15),  $C_p$  is positive on the forward portion of the hump, and negative on the rear portion. This is denoted by the (+) and (-) signs in front of and behind the hump shown in Fig. 12.1. This is also somewhat consistent with our discussions in Chap. 9; in the real flow over the hump, a shock wave forms above the front portion where the flow is being turned into itself, and hence  $p > p_\infty$ , whereas an expansion wave occurs over the remainder of the hump, and the pressure decreases. Think about the picture shown in Fig. 12.1; the pressure is higher on the front section of the hump, and lower on the rear section. As a result, a drag force exists on the hump. This drag is called *wave drag* and is a characteristic of supersonic flows. Wave drag was discussed in Sec. 9.7 in conjunction with shock-expansion theory applied to supersonic airfoils. It is interesting that linear-

ized supersonic theory also predicts a finite wave drag, although shock waves themselves are not treated in such linearized theory.

Examining Eq. (12.15), we note that  $C_p \propto (M_x^2 - 1)^{-1/2}$ ; hence, for supersonic flow,  $C_p$  decreases as  $M_x$  increases. This is in direct contrast with subsonic flow, where Eq. (11.51) shows that  $C_p \propto (1 - M_x^2)^{-1/2}$ ; hence for subsonic flow,  $C_p$  increases as  $M_x$  increases. These trends are illustrated in Fig. 12.2. Note that both results predict  $C_p \rightarrow \infty$  as  $M_x \rightarrow 1$  from either side. However, keep in mind that neither Eq. (12.15) nor (11.51) is valid in the transonic range around Mach 1.

### 12.3 APPLICATION TO SUPERSONIC AIRFOILS

Equation (12.15) is very handy for estimating the lift and wave drag for thin supersonic airfoils, such as sketched in Fig. 12.3. When applying Eq. (12.15) to any surface, one can follow a formal sign convention for  $\theta$ , which is different for regions of left-running waves (such as above the airfoil in Fig. 12.3) than for regions of right-running waves (such as below the airfoil in Fig. 12.3). This sign convention is developed in detail in Ref. 21. However, for our purpose here, there is no need to be concerned about the sign associated with  $\theta$  in Eq. (12.15). Rather, keep in mind that when the surface is inclined *into* the freestream direction, linearized theory predicts a positive  $C_p$ . For example, points A and B in Fig. 12.3 are on surfaces inclined into the freestream, and hence  $C_{p,A}$  and  $C_{p,B}$  are positive values given by

$$C_{p,A} = \frac{2\theta_A}{\sqrt{M_x^2 - 1}} \quad \text{and} \quad C_{p,B} = \frac{2\theta_B}{\sqrt{M_x^2 - 1}}$$

In contrast, when the surface is inclined *away from* the freestream direction, linearized theory predicts a negative  $C_p$ . For example, points C and D in Fig. 12.3 are on surfaces inclined away from the freestream, and hence  $C_{p,C}$  and  $C_{p,D}$  are negative values, given by

$$C_{p,C} = -\frac{2\theta_C}{\sqrt{M_x^2 - 1}} \quad \text{and} \quad C_{p,D} = -\frac{2\theta_D}{\sqrt{M_x^2 - 1}}$$

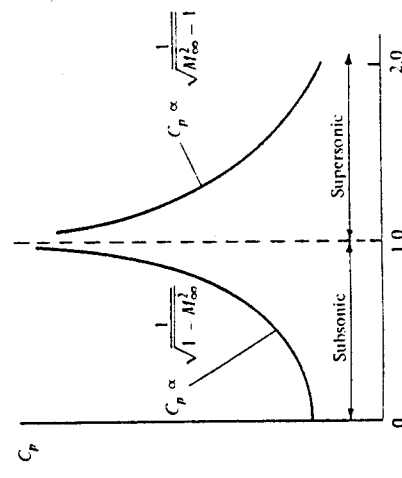


Figure 12.2 Variation of the linearized pressure coefficient with Mach number (schematic).

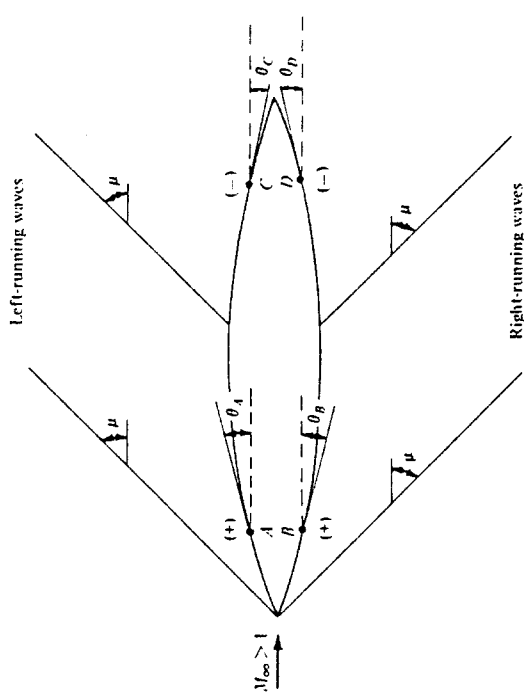


Figure 12.3 Linearized supersonic flow over an airfoil.

In the above expressions,  $\theta$  is always treated as a positive quantity, and the sign of  $C_p$  is determined simply by looking at the body and noting whether the surface is inclined into or away from the freestream.

With the distribution of  $C_p$  over the airfoil surface given by Eq. (12.15), the lift and drag coefficients,  $c_l$  and  $c_d$ , respectively, can be obtained from the integrals given by Eqs. (12.16) to (12.19).

Let us consider the simplest possible airfoil, namely, a flat plate at a small angle of attack,  $\alpha$ , as shown in Fig. 12.4. Looking at this picture, the lower surface of the plate is a compression surface inclined at the angle  $\alpha$  into the freestream, and from Eq. (12.15),

$$C_{p,l} = \frac{2\alpha}{\sqrt{M_s^2 - 1}} \quad (12.16)$$

Since the surface inclination angle is constant along the entire lower surface,  $C_{p,l}$  is a constant value over the lower surface. Similarly, the top surface is an expansion surface inclined at the angle  $\alpha$  away from the freestream, and from Eq. (12.15),

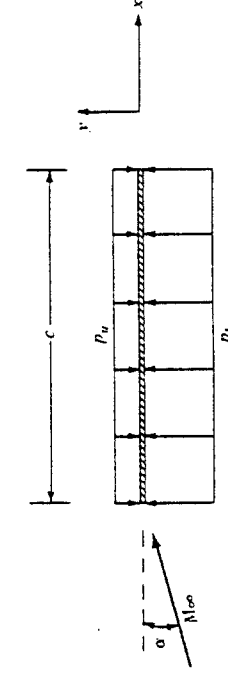


Figure 12.4 A flat plate at angle of attack in a supersonic flow.

$$C_{p,u} = -\frac{2\alpha}{\sqrt{M_s^2 - 1}} \quad (12.17)$$

$C_{p,u}$  is constant over the upper surface. The normal force coefficient for the first plate can be obtained from Eq. (1.15),

$$c_n = -\frac{1}{c} \int_0^r (C_{p,l} - C_{p,u}) dx \quad (12.18)$$

Substituting Eqs. (12.16) and (12.17) into (12.18),

$$c_n = \frac{4\alpha}{\sqrt{M_s^2 - 1}} \frac{1}{c} \int_0^r dx = \frac{4\alpha}{\sqrt{M_s^2 - 1}} \quad (12.19)$$

The axial force coefficient is given by Eq. (1.16),

$$c_a = -\frac{1}{c} \int_{LE}^{TE} (C_{p,u} - C_{p,l}) dy \quad (12.20)$$

However, the flat plate has (theoretically) zero thickness. Hence, in Eq. (12.20),  $dy = 0$ , and as a result,  $c_a = 0$ . This is also clearly seen in Fig. 12.4; the pressures act normal to the surface, and hence there is no component of the pressure force in the  $x$  direction. From Eqs. (1.18) and (1.19),

$$c_l = c_n \cos \alpha - c_a \sin \alpha \quad (1.18)$$

$$c_d = c_n \sin \alpha + c_a \cos \alpha \quad (1.19)$$

along with the assumption that  $\alpha$  is small and hence  $\cos \alpha \approx 1$  and  $\sin \alpha \approx \alpha$ , we have

$$c_l = c_n - c_a \sin \alpha \quad (12.21)$$

$$c_d = c_n \sin \alpha + c_a \quad (12.22)$$

Substituting Eq. (12.19) and the fact that  $c_a = 0$  into Eqs. (12.21) and (12.22), we obtain

$$\boxed{c_l = \frac{4\alpha}{\sqrt{M_s^2 - 1}}} \quad (12.23)$$

$$\boxed{c_d = \frac{4\alpha^2}{\sqrt{M_s^2 - 1}}} \quad (12.24)$$

Equations (12.23) and (12.24) give the lift and wave-drag coefficients, respectively, for the supersonic flow over a flat plate. Keep in mind that they are results from linearized theory and therefore are valid only for small  $\alpha$ .

For a thin airfoil of arbitrary shape at small angle of attack, linearized theory gives an expression for  $c_l$  identical to Eq. (12.23), that is,

$$c_l = \frac{4\alpha}{\sqrt{M_s^2 - 1}}$$

Within the approximation of linearized theory,  $c_l$  depends only on  $\alpha$  and is independent of the airfoil shape and thickness. However, the same linearized theory gives a wave-drag coefficient in the form of

$$c_d = \frac{4}{\sqrt{M_\infty^2 - 1}} (\alpha^2 + g_r^2 + g_t^2)$$

where  $g_r$  and  $g_t$  are functions of the airfoil camber and thickness, respectively. For more details, see Refs. 25 and 26.

#### 12.4 SUMMARY

In linearized supersonic flow, information is propagated along Mach lines where the Mach angle  $\mu = \sin^{-1}(1/M_\infty)$ . Since these Mach lines are all based on  $M_\infty$ , they are straight, parallel lines which propagate away from and downstream of a body. For this reason, disturbances cannot propagate upstream in a steady supersonic flow.

The pressure coefficient, based on linearized theory, on a surface inclined at a small angle  $\theta$  to the freestream is

$$C_p = \frac{2\theta}{\sqrt{M_\infty^2 - 1}} \quad (12.15)$$

If the surface is inclined into the freestream,  $C_p$  is positive; if the surface is inclined away from the freestream,  $C_p$  is negative.

Based on linearized supersonic theory, the lift and wave-drag coefficients for a flat plate at an angle of attack are

$$c_l = \frac{4\alpha}{\sqrt{M_\infty^2 - 1}} \quad (12.23)$$

$$c_d = \frac{4\alpha^2}{\sqrt{M_\infty^2 - 1}} \quad (12.24)$$

Equation (12.23) also holds for a thin airfoil of arbitrary shape. However, for such an airfoil, the wave-drag coefficient depends on both the shape of the mean camber line and the airfoil thickness.

### PROBLEMS

P12.1 Using the results of linearized theory, calculate the lift and wave-drag coefficients for an infinitely thin flat plate in a Mach 2.6 freestream at angles of attack of

$$(a) \alpha = 5^\circ$$

$$(b) \alpha = 15^\circ$$

Compare these approximate results with those from the exact shock-expansion theory obtained in Prob. 9.13. What can you conclude about the accuracy of linearized theory in this case?

P12.2 For the conditions of Prob. 12.1, calculate the pressures (in the form of  $p/p_\infty$ ) on the top and bottom surfaces of the flat plate, using linearized theory. Compare these approximate results with those obtained from exact shock-expansion theory in Prob. 9.13. Make some appropriate conclusions regarding the accuracy of linearized theory for the calculation of pressures.

P12.3 Consider a diamond-wedge airfoil such as shown in Fig. 9.24, with a half-angle  $\epsilon = 10^\circ$ . The airfoil is at an angle of attack  $\alpha = 15^\circ$  to a Mach 3 freestream. Using linear theory, calculate the lift and wave-drag coefficients for the airfoil. Compare these approximate results with those from the exact shock-expansion theory obtained in Prob. 9.14.

## CHAPTER THIRTEEN

### INTRODUCTION TO NUMERICAL TECHNIQUES FOR NONLINEAR SUPERSONIC FLOW

*A numerical simulation of the flow over an airfoil using the Reynolds averaged Navier-Stokes equations can be conducted on today's supercomputers in less than a half hour for less than \$1000 cost in computer time. If just one such simulation had been attempted 20 years ago on computers of that time (e.g., the IBM 704 class) and with algorithms then known, the cost in computer time would have amounted to roughly \$10 million, and the results for that single flow would not be available until 10 years from now, since the computation would have taken about 30 years to complete.*

Dean R. Chapman, NASA, 1977

#### 13.1 INTRODUCTION: PHILOSOPHY OF COMPUTATIONAL FLUID DYNAMICS

The above quotation underscores the phenomenally rapid increase in computer power available to engineers and scientists during the two decades between 1960 and 1980. This explosion in computer capability is still going on, with no specific limits in sight. As a result, an entirely new discipline in aerodynamics has evolved over the past two decades, namely, computational fluid dynamics (CFD). CFD is a new "third dimension" in aerodynamics, complementing the previous dimensions of both pure experiment and pure theory. It allows us to obtain answers to fluid dynamic problems which heretofore were intractable by classical analytical methods. Consequently, CFD is revolutionizing the airplane design process, and in many ways is modifying the way we conduct modern aeronautical research and development. For these reasons, every modern student of aerodynamics should be aware of the overall philosophy of CFD, because you are bound to be affected by it to some greater or lesser degree in your education and professional life.

Computational fluid dynamics is the art of replacing the governing partial differential equations of fluid flow with numbers, and advancing these numbers in space and/or time to obtain a final numerical description of the complete flow field of interest. The end product of CFD is indeed a collection of numbers, in contrast to a closed-form analytical solution. However, in the long run the objective of most engineering analy-

ses, closed form or otherwise, is a quantitative description of the problem, i.e., numbers (sec, for example, Ref. 33).

The purpose of this chapter is to provide an introduction to some of the basic ideas of CFD as applied to inviscid supersonic flows. More details are given in Ref. 21. Because CFD has developed so rapidly in recent years, we can only scratch the surface here. Indeed, the present chapter is intended to give you only some basic background as well as the incentive to pursue the subject further in the modern literature.

The road map for this chapter is given in Fig. 13.1. We begin by introducing the classical method of characteristics — a numerical technique that has been available in aerodynamics since 1929, but which had to wait on the modern computer for practical, everyday implementation. For this reason, the author classifies the method of characteristics under the general heading of numerical techniques, although others may prefer to list it under a more classical heading. We also show how the method of characteristics is applied to design the divergent contour of a supersonic nozzle. Then we move to a discussion of the finite-difference approach. Finite-difference methods are the "bread and butter" of modern CFD. A special, but very powerful, finite-difference technique called the *time-dependent technique* is used to illustrate the application of CFD to nozzle flows and the flow over a supersonic blunt body.

In contrast to the linearized solutions discussed in Chaps. 11 and 12, CFD represents numerical solutions to the exact nonlinear governing equations, i.e., the equations without simplifying assumptions such as small perturbations, and which apply to all speed regimes, transonic and hypersonic as well as subsonic and supersonic. Although numerical roundoff and truncation errors are always present in any numerical representation of the governing equations, we still think of CFD solutions as being "exact solutions."

Both the method of characteristics and finite-difference methods have one thing in common: they represent a continuous flow field by a series of distinct grid points in

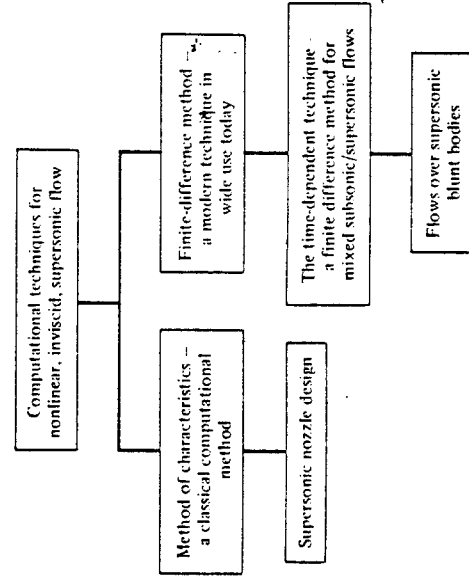


Figure 13.1 Road map for Chap. 13.

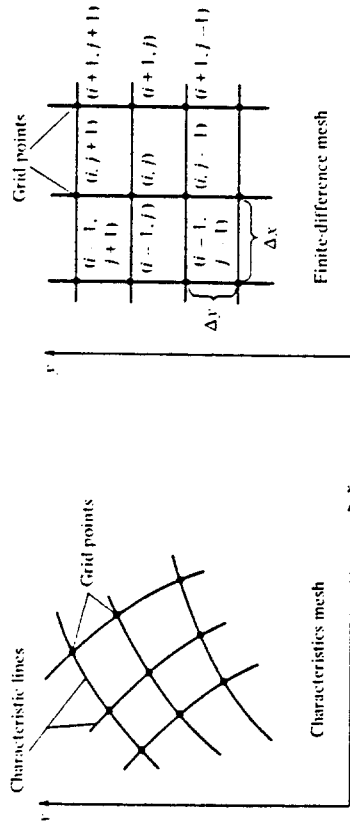


Figure 13.2 Grid points.

space, as shown in Fig. 13.2. The flow-field properties ( $u$ ,  $v$ ,  $p$ ,  $T$ , etc.) are calculated at each one of these grid points. The mesh generated by these grid points is generally skewed for the method of characteristics, as shown in Fig. 13.2a, but is usually rectangular for finite-difference solutions, as shown in Fig. 13.2b. We will soon appreciate why these different meshes occur.

## 13.2. ELEMENTS OF THE METHOD OF CHARACTERISTICS

In this section, we only introduce the basic elements of the method of characteristics. A full discussion is beyond the scope of this book; see Refs. 21, 25, and 34 for more details.

Consider a two-dimensional, steady, inviscid, supersonic flow in  $xy$  space, as given in Fig. 13.2a. The flow variables ( $p$ ,  $u$ ,  $T$ , etc.) are continuous throughout this space. However, there are certain lines in  $xy$  space along which the derivatives of the flow-field variables ( $\partial p/\partial x$ ,  $\partial u/\partial y$ , etc.) are *indeterminate* and across which may even be discontinuous. Such lines are called *characteristic lines*. This may sound strange at first; however, let us prove that such lines exist, and let us find their precise directions in the  $xy$  plane.

In addition to the flow being supersonic, steady, inviscid, and two-dimensional, assume that it is also irrotational. The exact governing equation for such a flow is given by Eq. (11.12):

$$\left[1 - \frac{1}{a^2} \left(\frac{\partial \phi}{\partial x}\right)^2\right] \frac{\partial^2 \phi}{\partial x^2} + \left[1 - \frac{1}{a^2} \left(\frac{\partial \phi}{\partial y}\right)^2\right] \frac{\partial^2 \phi}{\partial y^2} - \frac{2}{a^2} \frac{\partial \phi}{\partial x} \frac{\partial \phi}{\partial y} = 0 \quad (11.12)$$

[Keep in mind that we are dealing with the full velocity potential  $\phi$  in Eq. (11.12), not the perturbation potential.] Since  $\partial \phi/\partial x = u$  and  $\partial \phi/\partial y = v$ , Eq. (11.12) can be written as

$$\left(1 - \frac{u^2}{a^2}\right) \frac{\partial^2 \phi}{\partial x^2} + \left(1 - \frac{v^2}{a^2}\right) \frac{\partial^2 \phi}{\partial y^2} - \frac{2uv}{a^2} \frac{\partial^2 \phi}{\partial x \partial y} = 0 \quad (13.1)$$

The velocity potential and its derivatives are functions of  $x$  and  $y$ , for example,

$$\frac{\partial \phi}{\partial x} = f(x, y)$$

Hence, from the relation for an exact differential,

$$df = \frac{\partial f}{\partial x} dx + \frac{\partial f}{\partial y} dy$$

we have

$$d\left(\frac{\partial \phi}{\partial x}\right) = du = \frac{\partial^2 \phi}{\partial x^2} dx + \frac{\partial^2 \phi}{\partial x \partial y} dy \quad (13.2)$$

Similarly,

$$d\left(\frac{\partial \phi}{\partial y}\right) = dv = \frac{\partial^2 \phi}{\partial y^2} dy + \frac{\partial^2 \phi}{\partial x \partial y} dx \quad (13.3)$$

Examine Eqs. (13.1) to (13.3) closely. Note that they contain the second derivatives  $\partial^2 \phi/\partial x^2$ ,  $\partial^2 \phi/\partial y^2$ , and  $\partial^2 \phi/\partial x \partial y$ . If we imagine these derivatives as "unknowns," then Eqs. (13.1), (13.2), and (13.3) represent three equations with three unknowns. For example, to solve for  $\partial^2 \phi/\partial x \partial y$ , use Cramer's rule as follows:

$$\frac{\partial^2 \phi}{\partial x \partial y} = \frac{\begin{vmatrix} 1 - \frac{u^2}{a^2} & 0 & 1 - \frac{v^2}{a^2} \\ dx & du & 0 \\ 0 & dv & dy \end{vmatrix}}{\begin{vmatrix} 1 - \frac{u^2}{a^2} & -\frac{2uv}{a^2} & 1 - \frac{v^2}{a^2} \\ dx & dy & 0 \\ 0 & dx & dy \end{vmatrix}} = \frac{N}{D} \quad (13.4)$$

where  $N$  and  $D$  represent the numerator and denominator determinants, respectively.

The physical meaning of Eq. (13.4) can be seen by considering point  $A$  and its surrounding neighborhood in the flow, as sketched in Fig. 13.3. The derivative  $\partial^2 \phi/\partial x \partial y$  has a specific value at point  $A$ . Equation (13.4) gives the solution for  $\partial^2 \phi/\partial x \partial y$  for an arbitrary choice of  $dx$  and  $dy$ . The combination of  $dx$  and  $dy$  defines an arbitrary direction  $ds$  away from point  $A$ , as shown in Fig. 13.3. In general, this direction is different than the streamline direction going through point  $A$ . In Eq. (13.4), the differentials  $du$  and  $dv$  represent the changes in velocity that take place over the increments  $dx$  and  $dy$ . Hence, although the choice of  $dx$  and  $dy$  is arbitrary, the values of  $du$  and  $dv$  in Eq. (13.4) must correspond to this choice. No matter what values of  $dx$  and  $dy$

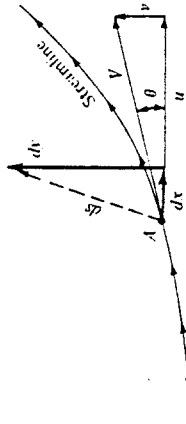


Figure 13.3 An arbitrary direction,  $ds$ , away from point A.

are arbitrarily chosen, the corresponding values of  $du$  and  $dv$  will always ensure obtaining the same value of  $\partial^2\phi/\partial x \partial y$  at point A from Eq. (13.4).

The single exception to the above comments occurs when  $dx$  and  $dy$  are chosen so that  $D = 0$  in Eq. (13.4). In this case,  $\partial^2\phi/\partial x \partial y$  is not defined. This situation will occur for a specific direction  $ds$  away from point A in Fig. 13.3, defined for that specific combination of  $dx$  and  $dy$  for which  $D = 0$ . However, we know that  $\partial^2\phi/\partial x \partial y$  has a specific defined value at point A. Therefore, the only consistent result associated with  $D = 0$  is that  $N = 0$ , also, that is,

$$\frac{\partial^2\phi}{\partial x \partial y} = \frac{N}{D} = \frac{0}{0} \quad (13.5)$$

Here,  $\partial^2\phi/\partial x \partial y$  is an indeterminate form, which is allowed to be a finite value, i.e., that value of  $\partial^2\phi/\partial x \partial y$  which we know exists at point A. *The important conclusion here is that there is some direction (or directions) through point A along which  $\partial^2\phi/\partial x \partial y$  is indeterminate.* Since  $\partial u/\partial y = \partial v/\partial x$ , this implies that the derivatives of the flow variables are indeterminate along these lines. Hence, we have proven that lines do exist in the flow field along which derivatives of the flow variables are indeterminate; earlier, we defined such lines as *characteristic lines*.

Consider again point A in Fig. 13.3. From our previous discussion, there are one or more characteristic lines through point A. *Question:* How can we calculate the precise direction of these characteristic lines? The answer can be obtained by setting  $D = 0$  in Eq. (13.4). Expanding the denominator determinant in Eq. (13.4), and setting it equal to zero, we have

$$\begin{aligned} \left(1 - \frac{u^2}{a^2}\right)(dy)^2 + \frac{2uv}{a^2}dx dy + \left(1 - \frac{v^2}{a^2}\right)(dx)^2 &= 0 \\ \left(1 - \frac{u^2}{a^2}\right)\left(\frac{dy}{dx}\right)_{\text{char}}^2 + \frac{2uv}{a^2}\left(\frac{dy}{dx}\right)_{\text{char}} + \left(1 - \frac{v^2}{a^2}\right) &= 0 \end{aligned} \quad (13.6)$$

In Eq. (13.6),  $dy/dx$  is the slope of the characteristic lines; hence the subscript "char" has been added to emphasize this fact. Solving Eq. (13.6) for  $(dy/dx)_{\text{char}}$  by means of the quadratic formula, we obtain

$$\begin{aligned} \left(\frac{dy}{dx}\right)_{\text{char}} &= \frac{-2uv/a^2 \pm \sqrt{(2uv/a^2)^2 - 4(1 - u^2/a^2)(1 - v^2/a^2)}}{2(1 - u^2/a^2)} \\ \text{or } \left(\frac{dy}{dx}\right)_{\text{char}} &= \frac{-uv/a^2 \pm \sqrt{(u^2 + v^2)/a^2 - 1}}{1 - u^2/a^2} \end{aligned} \quad (13.7)$$

From Fig. 13.3, we see that  $u = V \cos\theta$  and  $v = V \sin\theta$ . Hence, Eq. (13.7) becomes

$$\left(\frac{dy}{dx}\right)_{\text{char}} = \frac{(-V^2 \cos\theta \sin\theta)/a^2 \pm \sqrt{(V^2/a^2)(\cos^2\theta + \sin^2\theta) - 1}}{1 - [(V^2/a^2) \cos^2\theta]} \quad (13.8)$$

Recall that the local Mach angle  $\mu$  is given by  $\mu = \sin^{-1}(1/M)$ , or  $\sin\mu = 1/M$ . Thus,  $V^2/a^2 = M^2 = 1/\sin^2\mu$ , and Eq. (13.8) becomes

$$\left(\frac{dy}{dx}\right)_{\text{char}} = \frac{(-\cos\theta \sin\theta)/\sin^2\mu \pm \sqrt{(\cos^2\theta + \sin^2\theta)/\sin^2\mu - 1}}{1 - (\cos^2\theta)/\sin^2\mu} \quad (13.9)$$

After considerable algebraic and trigonometric manipulation, Eq. (13.9) reduces to

$$\boxed{\left(\frac{dy}{dx}\right)_{\text{char}} = \tan(\theta \mp \mu)} \quad (13.10)$$

Equation (13.10) is an important result; it states that *two* characteristic lines run through point A in Fig. 13.3, namely, one line with a slope equal to  $\tan(\theta - \mu)$  and the other with a slope equal to  $\tan(\theta + \mu)$ . The physical significance of this result is illustrated in Fig. 13.4. Here, a streamline through point A is inclined at the angle  $\theta$  with respect to the horizontal. The velocity at point A is  $V$ , which also makes the angle  $\theta$  with respect to the streamline direction by the angle  $\mu$ ; this characteristic line is inclined *below* the streamline direction by the angle  $\mu$ ; this characteristic line is labeled as  $C_-$  in Fig. 13.4. Equation (13.10) also states that the other characteristic line at point A is inclined *above* the streamline direction by the angle  $\mu$ ; this characteristic line is labeled as  $C_+$  in Fig. 13.4. Examining Fig. 13.4, we see that the characteristic lines through point A are simply the left- and right-running *Mach lines*. In Fig. 13.4, the left-running Mach wave is denoted by  $C_-$ , and the right-running Mach wave is denoted by  $C_+$ . Hence,

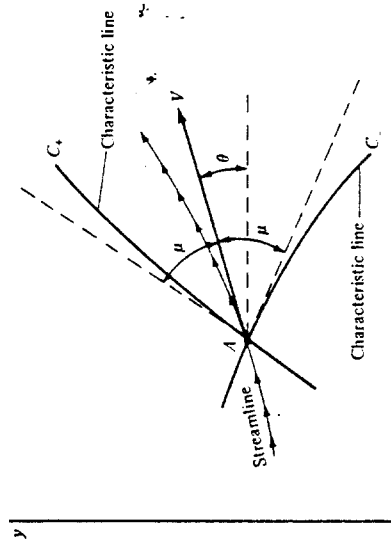


Figure 13.4 Left- and right-running characteristic lines through point A.

returning to Fig. 13.2a, the characteristics mesh consists of left- and right-running Mach waves which crisscross the flow field. There are an infinite number of these waves; however, for practical calculations we deal with a finite number of waves, the intersections of which define the grid points shown in Fig. 13.2a. Note that the characteristic lines are curved in space because (1) the local Mach angle depends on the local Mach number, which is a function of  $x$  and  $y$ , and (2) the local streamline direction  $\theta$  varies throughout the flow.

The characteristic lines in Fig. 13.2a are of no use to us by themselves. The practical consequence of these lines is that *the governing partial differential equations which describe the flow reduce to ordinary differential equations along the characteristic lines*. These equations are called the *compatibility equations*, which can be found by setting  $N = 0$  in Eq. (13.4), as follows. When  $N = 0$ , the numerator determinant yields

$$\left(1 - \frac{u^2}{a^2}\right) du dy + \left(1 - \frac{v^2}{a^2}\right) dx dv = 0 \quad (13.11)$$

or

$$\frac{dv}{du} = \frac{-(1 - u^2/a^2) dy}{1 - v^2/a^2} \quad (13.11)$$

Keep in mind that  $N$  is set to zero only when  $D = 0$  in order to keep the flow-field derivatives finite, albeit of the indeterminate form 0/0. When  $D = 0$ , we are restricted to considering directions *only* along the characteristic lines, as explained earlier. Hence, when  $N = 0$ , we are held to the same restriction. Therefore, Eq. (13.11) holds only along the characteristic lines. Therefore, in Eq. (13.11),

$$\frac{dy}{dx} \equiv \left(\frac{dy}{dx}\right)_{\text{char}} \quad (13.12)$$

Substituting Eqs. (13.12) and (13.7) into (13.11), we obtain

$$\frac{dv}{du} = -\frac{1 - u^2/a^2 - uv/a^2 \pm \sqrt{(u^2 + v^2)/a^2 - 1}}{1 - v^2/a^2} \quad (13.13)$$

or

$$\frac{dv}{du} = \frac{uv/a^2 \mp \sqrt{(u^2 + v^2)/a^2 - 1}}{1 - v^2/a^2} \quad (13.13)$$

Recall from Fig. 13.3 that  $u = V \cos \theta$  and  $v = V \sin \theta$ . Also,  $(u^2 + v^2)/a^2 = V^2/a^2 = M^2$ . Hence, Eq. (13.13) becomes

$$\frac{d(V \sin \theta)}{d(V \cos \theta)} = \frac{M^2 \cos \theta \sin \theta \mp \sqrt{M^2 - 1}}{1 - M^2 \sin^2 \theta} \quad (13.14)$$

which, after some algebraic manipulations, reduces to

$$d\theta = \mp \sqrt{M^2 - 1} \frac{dV}{V} \quad (13.14)$$

### Internal Points

Consider the internal grid points 1, 2, and 3 as shown in Fig. 13.5. Assume that we know the location of points 1 and 2, as well as the flow properties at these points.

Examine Eq. (13.14). It is an *ordinary differential equation* obtained from the original governing partial differential equation, Eq. (13.1). However, Eq. (13.14) contains the restriction given by Eq. (13.12); that is, Eq. (13.14) holds *only* along the characteristic lines. Hence, Eq. (13.14) gives the *compatibility relations* along the characteristic lines. In particular, comparing Eq. (13.14) with Eq. (13.10), we see that

$$d\theta = -\sqrt{M^2 - 1} \frac{dV}{V} \quad (\text{applies along the } C_- \text{ characteristic}) \quad (13.15)$$

$$d\theta = \sqrt{M^2 - 1} \frac{dV}{V} \quad (\text{applies along the } C_+ \text{ characteristic}) \quad (13.16)$$

Examine Eq. (13.14) further. It should look familiar; indeed, Eq. (13.14) is identical to the expression obtained for Prandtl-Meyer flow in Sec. 9.6, namely, Eq. (9.32). Hence, Eq. (13.14) can be integrated to obtain a result in terms of the Prandtl-Meyer function, given by Eq. (9.42). In particular, the integration of Eqs. (13.15) and (13.16) yields

$$\theta + \nu(M) = \text{const} = K_- \quad (\text{along the } C_- \text{ characteristic}) \quad (13.17)$$

$$\theta - \nu(M) = \text{const} = K_+ \quad (\text{along the } C_+ \text{ characteristic}) \quad (13.18)$$

In Eq. (13.17),  $K_-$  is a constant along a given  $C_-$  characteristic; it has different values for different  $C_-$  characteristics. In Eq. (13.18),  $K_+$  is a constant along a given  $C_+$  characteristic; it has different values for different  $C_+$  characteristics. Note that our compatibility relations are now given by Eqs. (13.17) and (13.18), which are *algebraic* equations which hold only along the characteristic lines. In a general inviscid, supersonic, steady flow, the compatibility equations are ordinary differential equations; only in the case of two-dimensional irrotational flow do they further reduce to algebraic equations.

What is the advantage of the characteristic lines and their associated compatibility equations discussed above? Simply this—to solve the nonlinear supersonic flow, we need deal only with ordinary differential equations (or in the present case, algebraic equations) instead of the original partial differential equations. Finding the solution of such ordinary differential equations is usually much simpler than dealing with partial differential equations.

How do we use the above results to solve a practical problem? The purpose of the next section is to give such an example, namely, the calculation of the supersonic flow inside a nozzle and the determination of a proper wall contour so that shock waves do not appear inside the nozzle. To carry out this calculation, we deal with two types of grid points: (1) internal points, away from the wall, and (2) wall points. Characteristics calculations at these two sets of points are carried out as follows.

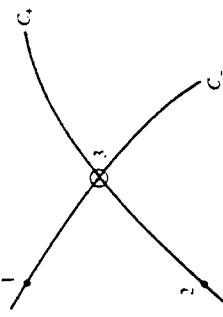


Figure 13.5 Characteristic mesh used for the location of point 3 and the calculation of flow conditions at point 3, knowing the locations and flow properties at points 1 and 2.

Define point 3 as the intersection of the  $C_-$  characteristic through point 1 and the  $C_+$  characteristic through point 2. From our previous discussion,  $(K_-)_1 = (K_-)_3$ , because  $K_-$  is constant along a given  $C_-$  characteristic. The value of  $(K_-)_1 = (K_-)_3$  is obtained from Eq. (13.17) evaluated at point 1:

$$(K_-)_3 = (K_-)_1 = \theta_1 + v_1 \quad (13.19)$$

Similarly,  $(K_+)_2 = (K_+)_3$ , because  $K_+$  is constant along a given  $C_+$  characteristic. The value of  $(K_+)_2 = (K_+)_3$  is obtained from Eq. (13.18) evaluated at point 2:

$$(K_+)_3 = (K_+)_2 = \theta_2 - v_2 \quad (13.20)$$

Now evaluate Eqs. (13.17) and (13.18) at point 3.

$$\theta_3 + v_3 = (K_-)_3 \quad (13.21)$$

$$\theta_3 - v_3 = (K_+)_3 \quad (13.22)$$

In Eqs. (13.21) and (13.22),  $(K_-)_3$  and  $(K_+)_3$  are known values, obtained from Eqs. (13.19) and (13.20). Hence, Eqs. (13.21) and (13.22) are two algebraic equations for two unknowns,  $\theta_3$  and  $v_3$ . Solving these equations, we obtain

$$\theta_3 = \frac{1}{2}[(K_-)_1 + (K_+)_2] \quad (13.23)$$

$$v_3 = \frac{1}{2}[(K_-)_1 - (K_+)_2] \quad (13.24)$$

Knowing  $\theta_3$  and  $v_3$ , all other flow properties at point 3 can be obtained as follows:

- From  $v_3$ , obtain the associated  $M_3$  from App. C.
- From  $M_3$  and the known  $p_0$  and  $T_0$  for the flow (recall that for inviscid, adiabatic flow, the total pressure and total temperature are constants throughout the flow), find  $p_3$  and  $T_3$  from App. A.
- Knowing  $T_3$ , compute  $a_3 = \sqrt{\gamma RT_3}$ . In turn,  $V_3 = M_3 a_3$ .

As stated earlier, point 3 is located by the intersection of the  $C_-$  and  $C_+$  characteristics through points 1 and 2, respectively. These characteristics are curved lines; however, for purposes of calculation, we assume that the characteristics are straight line segments between points 1 and 3 and between points 2 and 3. For example, the slope of the  $C_-$  characteristic between points 1 and 3 is assumed to be the average value between these two points, i.e.,  $\frac{1}{2}(\theta_1 + \theta_3) - \frac{1}{2}(\mu_1 + \mu_3)$ . Similarly, the slope of the  $C_+$  characteristic between points 2 and 3 is approximated by  $\frac{1}{2}(\theta_2 + \theta_3) + \frac{1}{2}(\mu_2 + \mu_3)$ .

### Wall Points

In Fig. 13.6, point 4 is an internal flow point near a wall. Assume that we know all the flow properties at point 4. The  $C_-$  characteristic through point 4 intersects the wall at point 5. At point 5, the slope of the wall,  $\theta_5$ , is known. The flow properties at the wall point, point 5, can be obtained from the known properties at point 4 as follows. Along the  $C_-$  characteristic,  $K_-$  is constant. Hence,  $(K_-)_4 = (K_-)_5$ . Moreover, the value of  $K_-$  is known from Eq. (13.17) evaluated at point 4:

$$(K_-)_4 = (K_-)_5 = \theta_4 + v_4 \quad (13.25)$$

Evaluating Eq. (13.17) at point 5, we have

$$(K_-)_5 = \theta_5 + v_5 \quad (13.26)$$

In Eq. (13.26),  $(K_-)_5$  and  $\theta_5$  are known; thus  $v_5$  follows directly. In turn, all other flow variables at point 5 can be obtained from  $v_5$  as explained earlier. The characteristic line between points 4 and 5 is assumed to be a straight line segment with average slope given by  $\frac{1}{2}(\theta_4 + \theta_5) - \frac{1}{2}(\mu_4 + \mu_5)$ .

From the above discussion of both internal and wall points, we see that properties at the grid points are calculated from *known* properties at other grid points. Hence, in order to start a calculation using the method of characteristics, we have to know the flow properties along some *initial* data line. Then we piece together the characteristics mesh and associated flow properties by "marching downstream" from the initial data line. This is illustrated in the next section.

We emphasize again that the method of characteristics is an exact solution of inviscid, nonlinear supersonic flow. However, in practice, there are numerical errors associated with the finite grid; the approximation of the characteristics mesh by straight line segments between grid points is one such example. In principle, the method of characteristics is truly exact only in the limit of an infinite number of characteristic lines.

We have discussed the method of characteristics for two-dimensional, irrotational, steady flow. The method of characteristics can also be used for rotational and three-dimensional flows, as well as unsteady flows. See Ref. 21 for more details.

### 13.3 SUPERSONIC NOZZLE DESIGN

In Chap. 10 we demonstrated that a nozzle designed to expand a gas from rest to supersonic speeds must have a convergent-divergent shape. Moreover, the quasi-one-

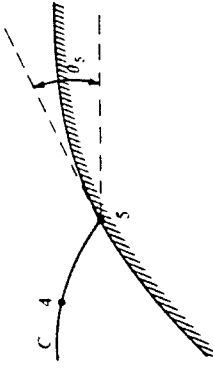


Figure 13.6 Wall point.

dimensional analysis of Chap. 10 led to the prediction of flow properties as a function of  $x$  through a nozzle of specified shape (see, for example, Fig. 10.10). The flow properties at any  $x$  station obtained from the quasi-one-dimensional analysis represent an average of the flow over the given nozzle cross section. The beauty of the quasi-one-dimensional approach is its simplicity. On the other hand, its disadvantages are (1) it cannot predict the details of the actual three-dimensional flow in a convergent-divergent nozzle and (2) it gives no information on the proper wall contour of such nozzles.

The purpose of the present section is to describe how the method of characteristics can supply the above information which is missing from a quasi-one-dimensional analysis. For simplicity, we treat a two-dimensional flow, as sketched in Fig. 13.7. Here, the flow properties are a function of  $x$  and  $y$ . Such a two-dimensional flow is applicable to supersonic nozzles of rectangular cross section, such as sketched in the insert at the top of Fig. 13.7. Two-dimensional (rectangular) nozzles are used in many supersonic wind tunnels. They are also the heart of gas-dynamic lasers (see Ref. 1). In addition, there is current discussion of employing rectangular exhaust nozzles on advanced military jet airplanes envisaged for the future.

Consider the following problem. We wish to design a convergent-divergent nozzle to expand a gas from rest to a given supersonic Mach number at the exit,  $M_r$ . How do we design the proper contour so that we have shock-free, isentropic flow in the nozzle? The answer to this question is discussed in the remainder of this section.

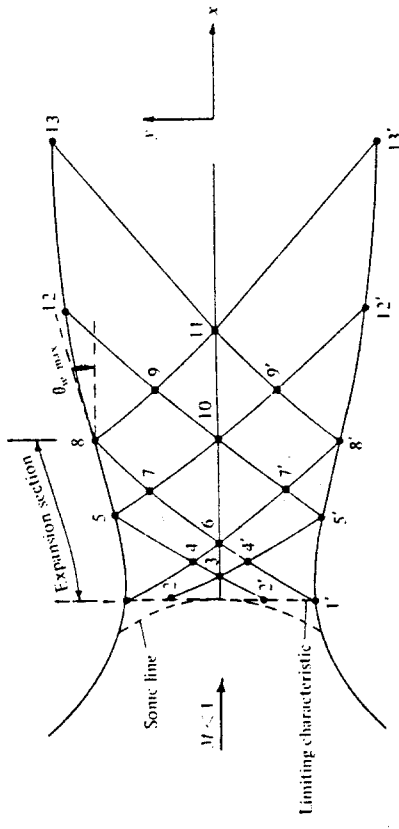
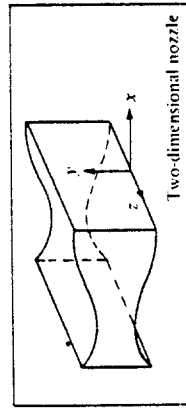


Figure 13.7 Schematic of supersonic nozzle design by the method of characteristics.

For the convergent, subsonic section, there is no specific contour which is better than any other. There are rules of thumb based on experience and guided by subsonic flow theory; however, we are not concerned with the details here. We simply assume that we have a reasonable contour for the subsonic section.

Due to the two-dimensional nature of the flow in the throat region, the sonic line is generally curved, as sketched in Fig. 13.7. A line called the *limiting characteristic* is sketched just downstream of the sonic line. The limiting characteristic is defined such that any characteristic line originating downstream of the limiting characteristic does not intersect the sonic line; in contrast, a characteristic line originating in the small region between the sonic line and the limiting characteristic can intersect the sonic line (for more details on the limiting characteristic, see Ref. 21). To begin a method of characteristics solution, we must use an initial data line which is either the limiting characteristic itself or downstream of the limiting characteristic.

Let us assume that by independent calculation of the subsonic-transonic flow in the throat region, we know the flow properties at all points on the limiting characteristic. That is, we use the limiting characteristic as our initial data line. For example, we know the flow properties at points 1 and 2 on the limiting characteristic in Fig. 13.7. Moreover, consider the nozzle contour just downstream of the throat. Letting  $\theta$  denote the angle between a tangent to the wall and the horizontal, the section of the divergent nozzle where  $\theta$  is increasing is called the *expansion section*, as shown in Fig. 13.7. The end of the expansion section occurs where  $\theta = \theta_{\max}$  (point 8 in Fig. 13.7). Downstream of this point,  $\theta$  decreases until it equals zero at the nozzle exit. The portion of the contour where  $\theta$  decreases is called the *straightening section*. The shape of the expansion section is somewhat arbitrary; typically, a circular arc of large radius is used for the expansion section of many wind-tunnel nozzles. Consequently, in addition to knowing the flow properties along the limiting characteristic, we also have an expansion section of specified shape, i.e., we know  $\theta_1$ ,  $\theta_3$ , and  $\theta_8$  in Fig. 13.7. The purpose of our application of the method of characteristics now becomes the proper design of the contour of the straightening section (from points 8 to 13 in Fig. 13.7).

The characteristics mesh sketched in Fig. 13.7 is very coarse—this is done intentionally to keep our discussions simple. In an actual calculation, the mesh should be much finer. The characteristics mesh and the flow properties at the associated grid points are calculated as follows:

1. Draw a  $C_-$  characteristic from point 2, intersecting the centerline at point 3. Evaluating Eq. (13.17) at point 3, we have

$$\theta_3 + \nu_3 = (K_-)_3$$

In the above equation,  $\theta_3 = 0$  (the flow is horizontal along the centerline). Also,  $(K_-)_3$  is known because  $(K_-)_3 = (K_-)_2$ . Hence, the above equation can be solved for  $\nu_3$ .

2. Point 4 is located by the intersection of the  $C_-$  characteristic from point 1 and the  $C_+$  characteristic from point 3. In turn, the flow properties at the internal point 4 are determined as discussed in the last part of Sec. 13.2.

3. Point 5 is located by the intersection of the C<sub>1</sub> characteristic from point 4 with the wall. Since  $\theta_2$  is known, the flow properties at point 5 are determined as discussed in Sec. 13.2 for wall points.
4. Points 6 through 11 are located in a manner similar to the above, and the flow properties at these points are determined as discussed before, using the internal point or wall point method as appropriate.
5. Point 12 is a wall point on the straightening section of the contour. The purpose of the straightening section is to cancel the expansion waves generated by the expansion section. Hence, there are no waves which are reflected from the straightening section. In turn, no right-running waves cross the characteristic line between points 9 and 12. As a result, the characteristic line between points 9 and 12 is a straight line, along which  $\theta$  is constant, that is,  $\theta_{12} = \theta_6$ . The section of the wall contour between points 8 and 12 is approximated by a straight line with an average slope of  $\frac{1}{2}(\theta_8 + \theta_{12})$ .
6. Along the centerline, the Mach number continuously increases. Let us assume that at point 11, the design exit Mach number  $M_r$  is reached. The characteristic line from points 11 to 13 is the last line of the calculation. Again,  $\theta_{13} = \theta_{11}$ , and the contour from point 12 to point 13 is approximated by a straight line segment with an average slope of  $\frac{1}{2}(\theta_{12} + \theta_{13})$ .

The above description is intended to give you a "feel" for the application of the method of characteristics. If you wish to carry out an actual nozzle design, and/or if you are interested in more details, read the more complete treatments in Refs. 21 and 34. Note in Fig. 13.7 that the nozzle flow is symmetrical about the centerline. Hence the points below the centerline (1', 2', 3', etc.) are simply mirror images of the corresponding points above the centerline. In making a calculation of the flow through the nozzle, we need to concern ourselves only with those points in the upper half of Fig. 13.7, above and on the centerline.

Finite-difference techniques for the solution of partial differential equations have been discussed by mathematicians for at least a century; however, it was not until the advent of the high-speed digital computer that finite-difference solutions became practical.

Today, the vast majority of computational fluid dynamic applications are based on finite-difference techniques. Finite-difference solutions of various flow problems are used as design tools by industry and abound in modern aerodynamic research and development. In particular, they have revolutionized the analysis of compressible flow.

The purpose of this section is to give you just the flavor of such finite-difference techniques. The intensive work in this area since 1960 has produced a multitude of different algorithms and philosophies, and it is far beyond the scope of this book to go into the details of such work. See Ref. 21 for an expanded discussion of finite-difference methods. In addition you are strongly encouraged to read the current literature in this regard, in particular, the *AIAA Journal, Computers and Fluids*, and the

*Journal of Computational Physics*. Also, Ref. 7 is a modern text on the subject of computational fluid dynamics.

What are finite differences? They are algebraic difference quotients which represent the various partial derivatives that occur in our governing equations. Hence, the solution of the governing partial differential equations involves the manipulation of algebraic quantities—just the sort of operation that digital computers are designed to handle. For example, consider the rectangular grid shown in Fig. 13.2b. The various grid points are denoted by the index  $i$  in the  $x$  direction and by  $j$  in the  $y$  direction. If we consider point  $(i, j)$ , then immediately to its right is point  $(i + 1, j)$ , and to its left is point  $(i - 1, j)$ . Similarly, directly above and below point  $(i, j)$  are points  $(i, j + 1)$  and  $(i, j - 1)$ , respectively. The spacing between points in the  $x$  direction is  $\Delta x$ , and that in the  $y$  direction is  $\Delta y$ . We will deal with a uniform grid, that is,  $\Delta x$  is the same everywhere, and  $\Delta y$  is also the same everywhere; however, in general  $\Delta x \neq \Delta y$ . Consider a Taylor series expansion of the velocity component  $u$  about point  $(i, j)$  taken in the positive  $x$  direction,

$$u_{i+1,j} = u_{i,j} + \left( \frac{\partial u}{\partial x} \right)_{i,j} \Delta x + \left( \frac{\partial^2 u}{\partial x^2} \right)_{i,j} \frac{(\Delta x)^2}{2} + \dots \quad (13.27)$$

In its present form, Eq. (13.27) is of "second-order accuracy" because terms involving  $(\Delta x)^3$ ,  $(\Delta x)^4$ , etc., have been assumed small and are neglected. If we are interested in only first-order accuracy, Eq. (13.27) can be written as

$$u_{i+1,j} = u_{i,j} + \left( \frac{\partial u}{\partial x} \right)_{i,j} \Delta x + \dots \quad (13.28)$$

Solving Eq. (13.28) for  $(\partial u / \partial x)_{i,j}$ ,

$$\left( \frac{\partial u}{\partial x} \right)_{i,j} = \frac{u_{i+1,j} - u_{i,j}}{\Delta x} \quad (13.29)$$

Examine Eq. (13.29) carefully. It is an algebraic difference quotient which represents (to first-order accuracy) the partial derivative  $(\partial u / \partial x)_{i,j}$ . The particular form of the finite difference in Eq. (13.29) is called a *forward difference*. Similarly, if Eq. (13.27) is written for a negative  $\Delta x$ , we have

$$u_{i-1,j} = u_{i,j} + \left( \frac{\partial u}{\partial x} \right)_{i,j} (-\Delta x) + \left( \frac{\partial^2 u}{\partial x^2} \right)_{i,j} \frac{(-\Delta x)^2}{2} + \dots \quad (13.30)$$

which, for first-order accuracy, can be written as

$$u_{i-1,j} = u_{i,j} - \left( \frac{\partial u}{\partial x} \right)_{i,j} \Delta x + \dots \quad (13.31)$$

Solving Eq. (13.31) for  $(\partial u / \partial x)_{i,j}$ , we obtain

$$\left( \frac{\partial u}{\partial x} \right)_{i,j} = \frac{u_{i,j} - u_{i-1,j}}{\Delta x} \quad (13.32)$$

Equation (13.32) gives a *backward difference* for the derivative. Both Eqs. (13.29) and (13.32) are finite-difference representations of the derivative  $\partial u / \partial x$  evaluated at point  $(i, j)$  in Fig. 13.2b. They are both of first-order accuracy. A finite-difference of second-order accuracy can be obtained by subtracting Eq. (13.30) from (13.27), yielding

$$u_{i+1,j} - u_{i-1,j} = 0 + 2 \left( \frac{\partial u}{\partial x} \right)_{i,j} \Delta x + 0 + \dots \quad (13.33)$$

Solving Eq. (13.33) for  $(\partial u / \partial x)_{i,j}$ , we have

$$\left( \frac{\partial u}{\partial x} \right)_{i,j} = \frac{u_{i+1,j} - u_{i-1,j}}{2 \Delta x} \quad (13.34)$$

Equation (13.34) is called a *central difference*. Because it was obtained from Eqs. (13.30) and (13.27) which are of second-order accuracy, the central difference defined by Eq. (13.34) is also second-order accurate.

Analogous expressions for the derivatives in the  $y$  direction are as follows:

$$\left( \frac{\partial u}{\partial y} \right)_{i,j} = \begin{cases} \frac{u_{i,j+1} - u_{i,j}}{\Delta y} & \text{(forward difference)} \\ \frac{u_{i,j} - u_{i,j-1}}{\Delta y} & \text{(backward difference)} \\ \frac{u_{i,j+1} - u_{i,j-1}}{2 \Delta y} & \text{(central difference)} \end{cases}$$

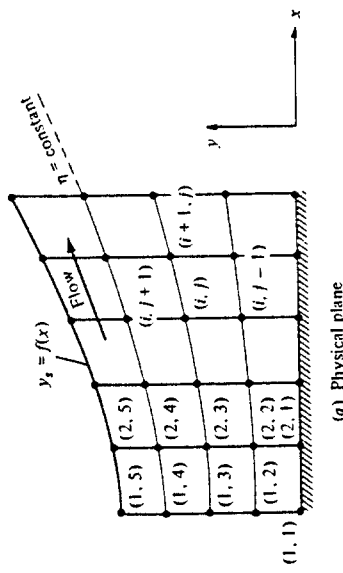
How do we use the finite differences obtained here? Imagine that a flow in  $xy$  space is covered by the mesh shown in Fig. 13.2b. Assume there are  $N$  grid points. At each one of these grid points, evaluate the continuity, momentum, and energy equations with their partial derivatives replaced by the finite-difference expressions derived above. For example, replacing the derivatives in Eqs. (7.40), (7.42a and b), and (7.44) with finite differences, along with Eqs. (7.1) and (7.6a), we obtain a system (over all  $N$  grid points) of  $6N$  simultaneous nonlinear algebraic equations in terms of the  $6N$  unknowns, namely,  $\rho$ ,  $u$ ,  $v$ ,  $p$ ,  $T$ , and  $c$ , at each of the  $N$  grid points. In principle, we could solve this system for the unknown flow variables at all the grid points. In practice, this is easier said than done. There are severe problems in solving such a large number of simultaneous nonlinear equations. Moreover, we have to deal with problems associated with numerical instabilities that sometimes cause such attempted solutions to "blow up" on the computer. Finally, and most importantly, we must properly account for the boundary conditions. These considerations make all finite-difference solutions a non-trivial endeavor. As a result, a number of specialized finite-difference techniques have evolved, directed at solving different types of flow problems and attempting to increase computational efficiency and accuracy. It is beyond the scope of this book to describe these difference techniques in detail. However, one technique in particular was widely used during the 1970s. This is an approach developed in 1969 by Robert Mac-

Cormack at the NASA Ames Research Center. Because of its widespread use and acceptance, as well as its relative simplicity, we will describe MacCormack's technique in enough detail to give you a reasonable understanding of the method. This description will be carried out in the context of the following example.

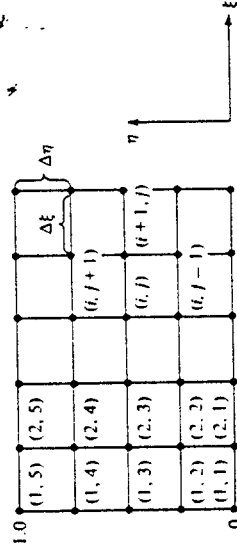
Consider the two-dimensional supersonic flow through the divergent duct shown in Fig. 13.8a. Assume the flow is supersonic at the inlet, and that all properties are known at the inlet. That is, the flow-field variables at grid points  $(1, 1)$ ,  $(1, 2)$ ,  $(1, 3)$ ,  $(1, 4)$ , and  $(1, 5)$  are known. The duct is formed by a flat surface at the bottom and a specified contour,  $y_s = f(x)$ , at the top. In addition, assume that the flow is inviscid, adiabatic, and steady, with no body forces. It can be rotational or irrotational—the method of solution is the same. The governing equations are obtained from Eqs. (7.40), (7.42a and b), (7.44), (7.1), and (7.6a) as, respectively,

$$\frac{\partial(\rho u)}{\partial x} + \frac{\partial(\rho v)}{\partial y} = 0 \quad (13.35)$$

$$\rho u \frac{\partial u}{\partial x} + \rho v \frac{\partial u}{\partial y} = - \frac{\partial p}{\partial x} \quad (13.36)$$



(a) Physical plane



(b) Computational plane

Figure 13.8 Finite-difference meshes in both the physical and computational planes.

$$\rho u \frac{\partial v}{\partial x} + \rho v \frac{\partial v}{\partial y} = -\frac{\partial p}{\partial y} \quad (13.37)$$

$$\rho u \frac{\partial(e + V^2/2)}{\partial x} + \rho v \frac{\partial(e + V^2/2)}{\partial y} = -\frac{\partial(\rho u)}{\partial x} - \frac{\partial(\rho v)}{\partial y} \quad (13.38)$$

$$p = \rho R T \quad (13.39)$$

$$e = c_v T \quad (13.40)$$

Let us express these equations in slightly different form, as follows. Multiplying Eq. (13.35) by  $u$ , and adding the result to Eq. (13.36), we have

$$u \frac{\partial(\rho u)}{\partial x} + \rho u \frac{\partial u}{\partial x} + u \frac{\partial(\rho v)}{\partial y} + \rho v \frac{\partial u}{\partial y} = -\frac{\partial p}{\partial x}$$

$$\text{or } \frac{\partial(\rho u^2)}{\partial x} + \frac{\partial(\rho u v)}{\partial y} = -\frac{\partial p}{\partial x} \quad (13.41)$$

$$\text{or } \frac{\partial}{\partial x} (\rho u^2 + p) = -\frac{\partial(\rho u v)}{\partial y} \quad (13.42)$$

Similarly, multiplying Eq. (13.35) by  $v$ , and adding the result to Eq. (13.37), we obtain

$$\frac{\partial(\rho u v)}{\partial x} = -\frac{\partial(p v^2 + p)}{\partial y} \quad (13.43)$$

Multiplying Eq. (13.35) by  $e + V^2/2$ , and adding the result to Eq. (13.38), we obtain

$$\frac{\partial}{\partial x} \left[ \rho u \left( e + \frac{V^2}{2} \right) + p u \right] = -\frac{\partial}{\partial y} \left[ \rho v \left( e + \frac{V^2}{2} \right) + p v \right] \quad (13.44)$$

Define the following symbols:

$$F = \rho u \quad (13.44a)$$

$$G = \rho u^2 + p \quad (13.44b)$$

$$H = \rho u v \quad (13.44c)$$

$$K = \rho u \left( e + \frac{V^2}{2} \right) + p u \quad (13.44d)$$

Then, Eqs. (13.35), (13.41) to (13.43) become

$$\frac{\partial F}{\partial x} = -\frac{\partial(p v)}{\partial y} \quad (13.45)$$

$$\frac{\partial G}{\partial x} = -\frac{\partial(p u v)}{\partial y} \quad (13.46)$$

$$\frac{\partial H}{\partial x} = -\frac{\partial(p v^2 + p)}{\partial y} \quad (13.47)$$

$$\frac{\partial K}{\partial x} = -\frac{\partial}{\partial y} \left[ \rho v \left( e + \frac{V^2}{2} \right) + p v \right] \quad (13.48)$$

Equations (13.45) to (13.48) are the continuity,  $x$ - and  $y$ -momentum, and energy equations, respectively—but in a slightly different form than we are used to seeing.

The above form of these equations is frequently called the *conservation form*. Let us now treat  $F$ ,  $G$ ,  $H$ , and  $K$  as our primary dependent variables; these quantities are called *flux variables*, in contrast to the usual  $p$ ,  $\rho$ ,  $T$ ,  $u$ ,  $v$ ,  $e$ , etc., which are called *primitive variables*. It is important to note that once the values of  $F$ ,  $G$ ,  $H$ , and  $K$  are known at a given grid point, the primitive variables at that point can be found from Eqs. (13.44a) to (13.44d) and

$$p = \rho R T \quad (13.49)$$

$$e = c_v T \quad (13.50)$$

$$V^2 = u^2 + v^2 \quad (13.51)$$

That is, Eqs. (13.44a) to (d) and (13.49) to (13.51) constitute seven algebraic equations for the seven primitive variables,  $\rho$ ,  $u$ ,  $v$ ,  $p$ ,  $e$ ,  $T$ , and  $V$ .

Let us return to the physical problem given in Fig. 13.8a. Because the duct diverges, it is difficult to deal with an orthogonal, rectangular mesh, rather, a mesh which conforms to the boundary of the system will be curved, as shown in Fig. 13.8a. On the other hand, to use our finite-difference quotients as given in Eqs. (13.29), (13.32), or (13.34), we desire a rectangular computational mesh. Therefore, we must "transform" the curved mesh shown in Fig. 13.8a, known as the *physical plane*, to a rectangular mesh shown in Fig. 13.8b, known as the *computational plane*. This transformation can be carried out as follows. Define

$$\xi = x \quad (13.52a)$$

$$\eta = \frac{y}{y_s} \quad (13.52b)$$

where

$$y_s = f(x) \quad (13.52c)$$

In the above transformation,  $\eta$  ranges from 0 at the bottom wall to 1.0 at the top wall.

In the computational plane (Fig. 13.8b),  $\eta = \text{constant}$  is a straight horizontal line, whereas in the physical plane,  $\eta = \text{constant}$  corresponds to the curved line shown in Fig. 13.8. Because we wish to apply our finite differences in the computational plane, we need the governing equations in terms of  $\xi$  and  $\eta$  rather than  $x$  and  $y$ . To accomplish this transformation, apply the chain rule of differentiation, using Eqs. (13.52a and b) as follows:

$$\frac{\partial}{\partial x} = \frac{\partial}{\partial \xi} \frac{\partial \xi}{\partial x} + \frac{\partial}{\partial \eta} \frac{\partial \eta}{\partial x} = \frac{\partial}{\partial \xi} - \frac{y}{y_s^2} \frac{dy}{dx} \frac{\partial}{\partial \eta} \quad (13.53)$$

$$\frac{\partial}{\partial x} = \frac{\partial}{\partial \xi} - \left( \frac{\eta}{y_s} \frac{dy_s}{dx} \right) \frac{\partial}{\partial \eta} \quad \text{or} \quad (13.53)$$

$$\text{and} \quad \frac{\partial}{\partial y} = \frac{\partial}{\partial \xi} \frac{\partial \xi}{\partial y} + \frac{\partial}{\partial \eta} \frac{\partial \eta}{\partial y} = \frac{1}{y} \frac{\partial}{\partial \eta} \quad (13.54)$$

Using Eqs. (13.53) and (13.54), Eqs. (13.45) to (13.48) become

$$\frac{\partial F}{\partial \xi} = \left( \frac{\eta}{y} \frac{\partial y}{\partial x} \right) \left( \frac{\partial F}{\partial \eta} \right) - \frac{1}{y} \frac{\partial(pv)}{\partial \eta} \quad (13.55)$$

$$\frac{\partial G}{\partial \xi} = \left( \frac{\eta}{y} \frac{\partial y}{\partial x} \right) \frac{\partial G}{\partial \eta} - \frac{1}{y} \frac{\partial(puv)}{\partial \eta} \quad (13.56)$$

$$\frac{\partial H}{\partial \xi} = \left( \frac{\eta}{y} \frac{\partial y}{\partial x} \right) \frac{\partial H}{\partial \eta} - \frac{1}{y} \frac{\partial(pvu^2 + p)}{\partial \eta} \quad (13.57)$$

$$\frac{\partial K}{\partial \xi} = \left( \frac{\eta}{y} \frac{\partial y}{\partial x} \right) \frac{\partial K}{\partial \eta} - \frac{1}{y} \frac{\partial}{\partial \eta} \left[ \rho v \left( e + \frac{V^2}{2} \right) + pv \right] \quad (13.58)$$

Note in the above equations that the  $\xi$  derivatives are on the left and the  $\eta$  derivatives are all grouped on the right.

Let us now concentrate on obtaining a numerical, finite-difference solution of the problem shown in Fig. 13.8. We will deal exclusively with the computational plane, Fig. 13.8b, where the governing continuity,  $x$ - and  $y$ -momentum, and energy equations are given by Eqs. (13.55) to (13.58), respectively. Grid points (1, 1), (2, 1), (1, 2), (2, 2), etc., in the computational plane are the same as grid points (1, 1), (2, 1), (1, 2), (2, 2), etc., in the physical plane. All the flow variables are known at the inlet, including  $F$ ,  $G$ ,  $H$ ,  $K$ . The solution for the flow variables downstream of the inlet can be found by using MacCormack's method, which is based on Taylor's series expansions for  $F$ ,  $G$ ,  $H$ , and  $K$  as follows:

$$F_{i+1,j} = F_{i,j} + \left( \frac{\partial F}{\partial \xi} \right)_{ave} \Delta \xi \quad (13.59a)$$

$$G_{i+1,j} = G_{i,j} + \left( \frac{\partial G}{\partial \xi} \right)_{ave} \Delta \xi \quad (13.59b)$$

$$H_{i+1,j} = H_{i,j} + \left( \frac{\partial H}{\partial \xi} \right)_{ave} \Delta \xi \quad (13.59c)$$

$$K_{i+1,j} = K_{i,j} + \left( \frac{\partial H}{\partial \xi} \right)_{ave} \Delta \xi \quad (13.59d)$$

In Eqs. (13.59a to d),  $F$ ,  $G$ ,  $H$ , and  $K$  at point  $(i, j)$  are considered known, and these equations are used to find  $F$ ,  $G$ ,  $H$ , and  $K$  at point  $(i+1, j)$  assuming that we can calculate the values of  $(\partial F / \partial \xi)_{ave}$ ,  $(\partial G / \partial \xi)_{ave}$ , etc. The main thrust of MacCormack's method is the calculation of these average derivatives. Examining Eqs. (13.59a to d), this finite-difference method is clearly a "downstream marching" method; given the flow at point  $(i, j)$ , we use Eqs. (13.59a to d) to find the flow at point  $(i+1, j)$ . Then the process is repeated to find the flow at point  $(i+2, j)$ , etc. This downstream marching is similar to that performed with the method of characteristics.

The average derivatives in Eqs. (13.59a to d) are found by means of a "predictor-corrector" approach, outlined below. In carrying out this approach, we assume that the flow properties are known at grid point  $(i, j)$ , as well as at all points directly above and below  $(i, j)$ , namely, at  $(i, j+1)$ ,  $(i, j+2)$ ,  $(i, j-1)$ ,  $(i, j-2)$ , etc.

### Predictor Step

First, predict the value of  $F_{i+1,j}$  by using a Taylor series where  $\partial F / \partial \xi$  is evaluated at point  $(i, j)$ . Denote this predicted value by  $\bar{F}_{i+1,j}$ .

$$\bar{F}_{i+1,j} = F_{i,j} + \left( \frac{\partial F}{\partial \xi} \right)_{i,j} \Delta \xi \quad (13.60)$$

In Eq. (13.60),  $(\partial F / \partial \xi)_{i,j}$  is obtained from the continuity equation, Eq. (13.55), using forward differences for the  $\eta$  derivatives, that is,

$$\left( \frac{\partial F}{\partial \xi} \right)_{i,j} = \left( \frac{\eta}{y_s} \frac{dy_s}{dx} \right)_{i,j} \left( \frac{F_{i,j+1} - F_{i,j}}{\Delta \eta} \right) - \frac{1}{y_s} \left[ \frac{(\rho v)_{i,j+1} - (\rho v)_{i,j}}{\Delta \eta} \right] \quad (13.61)$$

In Eq. (13.61), all quantities on the right-hand side are known and allow the calculation of  $(\partial F / \partial \xi)_{i,j}$ , which is, in turn, inserted into Eq. (13.60). A similar procedure is used to find predicted values of  $G$ ,  $H$ , and  $K$ , namely,  $\bar{G}_{i+1,j}$ ,  $\bar{H}_{i+1,j}$ , and  $\bar{K}_{i+1,j}$ , using forward differences in Eqs. (13.56) to (13.58). In turn, predicted values of the primitive variables,  $\bar{p}_{i+1,j}$ ,  $\bar{\rho}_{i+1,j}$ , etc., can be obtained from Eqs. (13.44a to d) and (13.49) to (13.51).

### Corrector Step

The predicted values obtained above are used to obtain predicted values of the derivative  $(\partial \bar{F} / \partial \xi)_{i+1,j}$ , using rearward differences in Eq. (13.55):

$$\left( \frac{\partial \bar{F}}{\partial \xi} \right)_{i+1,j} = \left( \frac{\eta}{y_s} \frac{dy_s}{dx} \right)_{i+1,j} \frac{\bar{F}_{i+1,j} - \bar{F}_{i+1,j-1}}{\Delta \eta} - \frac{1}{y_s} \frac{(\bar{\rho} v)_{i+1,j} - (\bar{\rho} v)_{i+1,j-1}}{\Delta \eta} \quad (13.62)$$

In turn, the results from Eqs. (13.61) and (13.62) allow the calculation of the average derivative

$$\left( \frac{\partial \bar{F}}{\partial \xi} \right)_{ave} = \frac{1}{2} \left[ \left( \frac{\partial \bar{F}}{\partial \xi} \right)_{i,j} + \left( \frac{\partial \bar{F}}{\partial \xi} \right)_{i+1,j} \right] \quad (13.63)$$

Finally, this average derivative is used in Eq. (13.59a) to obtain the corrected value of  $F_{i+1,j}$ . The same process is followed to find the corrected values of  $\bar{G}_{i+1,j}$ ,  $\bar{H}_{i+1,j}$ , and  $\bar{K}_{i+1,j}$  using rearward differences in Eqs. (13.56) to (13.58) and calculating the average derivatives  $(\partial \bar{G} / \partial \xi)_{ave}$ , etc., in the same manner as Eq. (13.63).

The above finite-difference procedure allows the step-by-step calculation of the flow field, marching downstream from some initial data line. In the flow given in Fig. 13.8, the initial data line is the inlet, where properties are considered known. Although all the calculations are carried out in the transformed, computational plane,

the flow-field results obtained at points (2, 1), (2, 2), etc., in the computational plane are the same values at points (2, 1), (2, 2), etc., in the physical plane.

There are other aspects of the finite-difference solution which have not been described above. For example, what values of  $\Delta\eta$  and  $\Delta\xi$  in Eqs. (13.59a to d), (13.60), (13.61), and (13.62) are allowed in order to maintain numerical stability? How is the flow tangency condition at the walls imposed on the finite-difference calculations? These are important matters, but we do not take the additional space to discuss them here. See Chapter 11 of Ref. 21 for details on these questions. Our purpose here has been to give you only a feeling for the nature of the finite-difference method.

### 13.5 THE TIME-DEPENDENT TECHNIQUE: APPLICATION TO SUPERSONIC BLUNT BODIES

The method of characteristics described in Sec. 13.2 is applicable only to supersonic flows; the characteristic lines are not defined in a practical fashion for steady, subsonic flow. Also, the particular finite-difference method outlined in Sec. 13.4 applies only to supersonic flows; if it were to be used in a locally subsonic region, the calculation would blow up. The reason for both of the above comments is that the method of characteristics and the steady flow, forward-marching finite-difference technique depend on the governing equations being mathematically "hyperbolic." In contrast, the equations for steady subsonic flow are "elliptic." (See Ref. 21 for a description of these mathematical classifications.) The fact that the governing equations change their mathematical nature in going from locally supersonic to locally subsonic flow has historically caused theoretical aerodynamicists much grief. One problem in particular, namely, the mixed subsonic-supersonic flow over a supersonic blunt body as described in Sec. 9.5, was a major research area until a breakthrough was made in the late 1960s for its proper numerical solution. The purpose of this section is to describe a numerical finite-difference solution which readily allows the calculation of mixed supersonic-supersonic flows — the *time-dependent method* — and to show how it is used to solve supersonic blunt-body flows. Time-dependent techniques are very common in modern computational fluid dynamics, and as a student of aerodynamics, you should be familiar with their philosophy.

Consider a blunt body in a supersonic stream, as sketched in Fig. 13.9a. The shape of the body is known and is given by  $b = b(y)$ . For a given freestream Mach number,  $M_\infty$ , we wish to calculate the shape and location of the detached shock wave, as well as the flow-field properties between the shock and the body. The physical aspects of this flow field were described in Sec. 9.5, which you should review before progressing further.

The flow around a blunt body in a supersonic stream is rotational. Why? Examine Fig. 13.10, which illustrates several streamlines around the blunt body. The flow is inviscid and adiabatic. In the uniform freestream ahead of the shock wave, the entropy is the same for each streamline. However, in crossing the shock wave, each streamline traverses a different part of the wave and hence experiences a different increase in entropy. That is, the streamline at point  $a$  in Fig. 13.10 crosses a normal shock and hence experiences a large increase in entropy, whereas the streamline at point  $b$  crosses

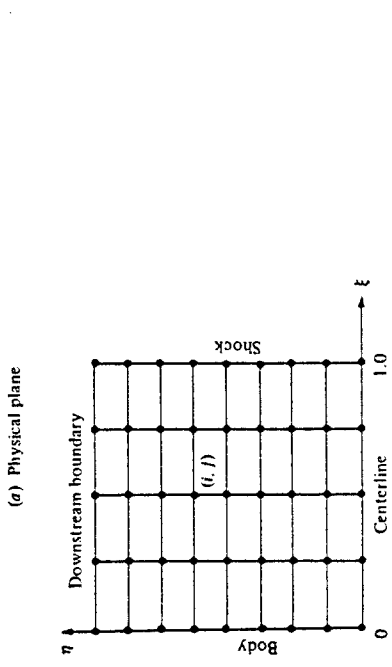
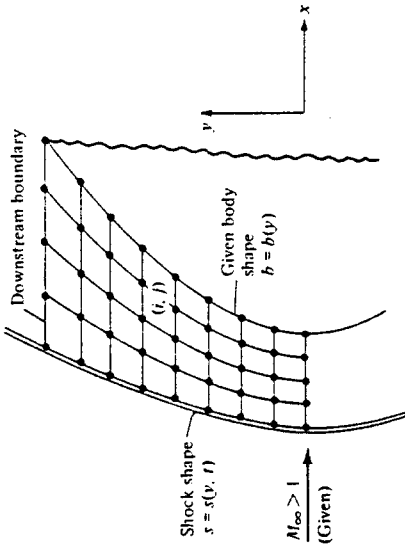


Figure 13.9 Blunt-body flow field in both the physical and computational planes.

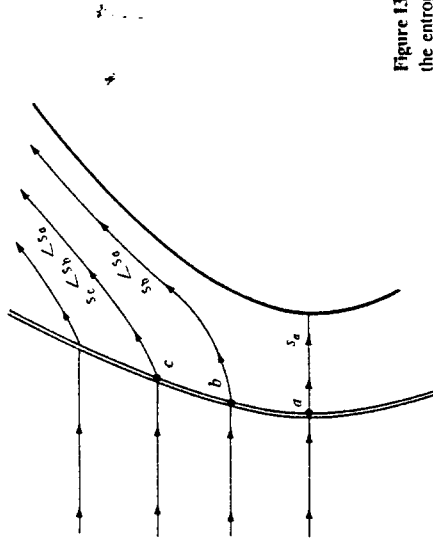


Figure 13.10 In a supersonic blunt-body flow field, the entropy is different for different streamlines.

a weaker, oblique shock and therefore experiences a smaller increase in entropy,  $s_b < s_a$ . The streamline at point  $c$  experiences an even weaker portion of the shock, and hence  $s_r < s_b < s_a$ . The net result is that in the flow between the shock and the body, the entropy along a given streamline is constant, whereas the entropy changes from one streamline to the next; i.e., an *entropy gradient* exists normal to the streamlines. It can readily be shown (see chapter 6 of Ref. 21) that an adiabatic flow with entropy gradients is *rotational*. Hence, the flow field over a supersonic blunt body is rotational.

In light of the above, we cannot use the velocity potential equation to analyze the blunt-body flow. Rather, the basic continuity, momentum, and energy equations must be employed in their fundamental form, given by Eqs. (7.40), (7.42a and b), and (7.44). With no body forces, these equations are:

$$\text{Continuity: } \frac{\partial \rho}{\partial t} = - \left( \frac{\partial(pu)}{\partial x} + \frac{\partial(pv)}{\partial y} \right) \quad (13.64)$$

$$\text{x-momentum: } \frac{\partial u}{\partial t} = - \left( u \frac{\partial u}{\partial x} + v \frac{\partial u}{\partial y} + \frac{1}{\rho} \frac{\partial p}{\partial x} \right) \quad (13.65)$$

$$\text{y-momentum: } \frac{\partial v}{\partial t} = - \left( u \frac{\partial v}{\partial x} + v \frac{\partial v}{\partial y} + \frac{1}{\rho} \frac{\partial p}{\partial y} \right) \quad (13.66)$$

$$\text{Energy: } \frac{\partial(e + V^2/2)}{\partial t} = - \left( u \frac{\partial(e + V^2/2)}{\partial x} + v \frac{\partial(e + V^2/2)}{\partial y} \right. \\ \left. + \frac{1}{\rho} \frac{\partial(\rho u)}{\partial x} + \frac{1}{\rho} \frac{\partial(\rho v)}{\partial y} \right) \quad (13.67)$$

Notice the form of the above equations; the time derivatives are on the left, and all spatial derivatives are on the right. These equations are in the form necessary for a time-dependent finite-difference solution, as described below.

Return to Fig. 13.9a. Recall that the body shape and freestream conditions are given, and we wish to calculate the shape and location of the shock wave as well as the flow field between the shock and body. We are interested in the *steady flow* over the blunt body; however, we use a time-dependent method to obtain the steady flow. The basic philosophy of this method is as follows. First assume a shock-wave shape and location. Also, cover the flow field between the shock and body with a series of grid points, as sketched in Fig. 13.9a. At each of these grid points, assume values of all the flow variables,  $\rho$ ,  $u$ ,  $v$ , etc. These assumed values are identified as *initial conditions* at time  $t = 0$ . With these assumed values, the spatial derivatives on the right sides of Eqs. (13.64) to (13.67) are known values (obtained from finite differences). Hence, Eqs. (13.64) to (13.67) allow the calculation of the time derivatives  $\partial p/\partial t$ ,  $\partial u/\partial t$ , etc. In turn, these time derivatives allow us to calculate the flow properties at each grid point at a later instant in time, say,  $\Delta t$ . The flow properties at time  $t = \Delta t$  are different than at  $t = 0$ . A repetition of this cycle gives the flow-field variables at all grid points at time  $t = 2\Delta t$ . As this cycle is repeated many hundreds of times, the flow-field properties at each grid point are calculated as a function of time. For example, the time variation of  $u_{i,j}$  is sketched in Fig. 13.11. At each time step, the value of  $u_{i,j}$  is different; however, at large times the changes in  $u_{i,j}$  from one time step

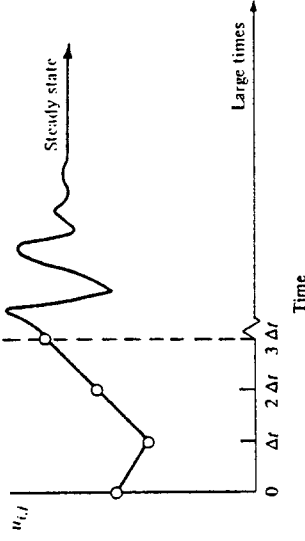


Figure 13.11 Schematic of the time variation of a typical flow variable—the time-dependent method.

to another become small, and  $u_{i,j}$  approaches a steady-state value, as shown in Fig. 13.11. It is this steady-state value that we want; the time-dependent approach is simply a means to that end. Moreover, the shock-wave shape and location will change with time; the new shock location and shape at each time step is calculated so as to satisfy the shock relations across the wave at each of the grid points immediately behind the wave. At large times, as the flow-field variables approach a steady state, the shock shape and location also approach a steady state. Because of the time-dependent motion of the shock wave, the wave shape is a function of both  $t$  and  $y$  as shown in Fig. 13.9a,  $s = s(y, t)$ .

Given the above philosophy, let us examine a few details of the method. First, note that the finite-difference grid in Fig. 13.9a is curved. We would like to apply our finite differences in a rectangular grid; hence, in Eqs. (13.64) to (13.67) the independent variables can be transformed as

$$\xi = \frac{x - b}{s - b} \quad \text{and} \quad \eta = y$$

where  $b = b(y)$  gives the abscissa of the body and  $s = s(y, t)$  gives the abscissa of the shock. The above transformation produces a rectangular grid in the computational plane, shown in Fig. 13.9b, where the body corresponds to  $\xi = 0$  and the shock corresponds to  $\xi = 1$ . All calculations are made in this transformed, computational plane.

The finite-difference calculations themselves can be carried out using MacCormack's method (see Sec. 13.4) applied as follows. The flow-field variables can be advanced in time using a Taylor series in time, for example,

$$\rho_{i,j}(t + \Delta t) = \rho_{i,j}(t) + \left[ \left( \frac{\partial \rho}{\partial t} \right)_{i,j,\text{ave}} \right] \Delta t \quad (13.68)$$

In Eq. (13.68), we know the density at grid point  $(i, j)$  at time  $t$ ; that is, we know  $\rho_{i,j}(t)$ . Then, Eq. (13.68) allows us to calculate the density at the same grid point at time  $t + \Delta t$ , that is,  $\rho_{i,j}(t + \Delta t)$ , if we know a value of the average time derivative  $[(\partial \rho / \partial t)_{i,j,\text{ave}}]$ . This time derivative is an average between times  $t$  and  $t + \Delta t$  and is obtained from a predictor-corrector process as follows.

### Predictor Step

All the flow variables are known at time  $t$  at all the grid points. This allows us to replace the spatial derivatives on the right of Eqs. (13.64) to (13.67) (suitably transformed into  $\xi, \eta$  space) with known *forward differences*. These equations then give values of the time derivatives at time  $t$ , which are used to obtain *predicted* values of the flow-field variables at time  $t + \Delta t$ , for example,

$$\bar{\rho}_{ij}(t + \Delta t) = \rho_{ij}(t) + \left[ \left( \frac{\partial \rho}{\partial t} \right)_{ij} \right] \Delta t$$

where  $\rho_{ij}(t)$  is known,  $\left[ (\partial \rho / \partial t)_{ij} \right]$ , is obtained from the governing equation, Eq. (13.64) (suitably transformed), using *forward differences* for the spatial derivatives, and  $\bar{\rho}_{ij}(t + \Delta t)$  is the predicted density at time  $t + \Delta t$ . Predicted values of all other flow variables  $\bar{u}_{ij}(t + \Delta t)$ , etc., are obtained at all the grid points in a likewise fashion.

### Corrector Step

Inserting the flow variables obtained above into the governing equations, Eqs. (13.64) to (13.67), using *backward differences* for the spatial derivatives, predicted values of the time derivatives at  $t + \Delta t$  are obtained, for example,  $\left[ (\partial \rho / \partial t)_{ij(t+\Delta t)} \right]$ . In turn, these are averaged with the time derivatives from the predictor step to obtain, for example,

$$\left[ \left( \frac{\partial \rho}{\partial t} \right)_{ij} \right]_{ave} = \frac{1}{2} \left\{ \left[ \left( \frac{\partial \rho}{\partial t} \right)_{ij} \right] + \left[ \left( \frac{\partial \rho}{\partial t} \right)_{ij(t+\Delta t)} \right] \right\} \quad (13.69)$$

Finally, the average time derivative obtained from Eq. (13.69) is inserted into Eq. (13.68) to yield the corrected value of density at time  $t + \Delta t$ . The same procedure is used for all the dependent variables,  $u$ ,  $v$ , etc.

Starting from the assumed initial conditions at  $t = 0$ , the repeated application of Eq. (13.68) along with the above predictor-corrector algorithm at each time step allows the calculation of the flow-field variables and shock shape and location as a function of time. As stated above, after a large number of time steps, the calculated flow-field variables approach a steady state, where  $\left[ (\partial \rho / \partial t)_{ij} \right]_{ave} \rightarrow 0$  in Eq. (13.68). Once again we emphasize that we are interested in the steady-state answer, and the time-dependent technique is simply a means to that end.

Note that the applications of MacCormack's technique to both the steady flow calculations described in Sec. 13.4 and the time-dependent calculations described in the present section are analogous; in the former we march forward in the spatial coordinate  $x$ , starting with known values along with a constant  $y$  line, whereas in the latter we march forward in time starting with a known flow field at  $t = 0$ .

Why do we bother with a time-dependent solution? Is it not an added complication to deal with an extra independent variable,  $t$ , in addition to the spatial variables  $x$  and  $y$ ? The answers to these questions are as follows. The governing unsteady flow equations given by Eqs. (13.64) to (13.67) are hyperbolic with respect to time, independent of whether the flow is locally subsonic or supersonic. In Fig. 13.9a, some of the grid

points are in the subsonic region and others are in the supersonic region. However, the time-dependent solution progresses in the same manner at all these points, independent of the local Mach number. Hence, the time-dependent technique is the only approach known today which allows the uniform calculation of a mixed subsonic-supersonic flow field of arbitrary extent. For this reason, the application of the time-dependent technique, although it adds one additional independent variable, allows the straightforward solution of a flow field which is extremely difficult to solve by a purely steady-state approach.

A much more detailed description of the time-dependent technique is given in chapter 12 of Ref. 21, which you should study before attempting to apply this technique to a specific problem. The intent of our description here has been to give you simply a "feeling" for the philosophy and general approach of the technique.

Some typical results for supersonic blunt-body flow fields are given in Figs. 13.12 to 13.15. These results were obtained with a time-dependent solution described in Ref. 35. Figures 13.12 and 13.13 illustrate the behavior of a time-dependent solution during its approach to the steady state. In Fig. 13.12, the time-dependent motion of the shock wave is shown for a parabolic cylinder in a Mach 4 freestream. The shock labeled  $0 \Delta t$  is the initially assumed shock wave at  $t = 0$ . At early times, the shock wave rapidly moves away from the body; however, after about 300 time steps, it has slowed considerably, and between 300 and 500 time steps, the shock wave is virtually motionless—it has reached its steady-state shape and location. The time variation of the stagnation point pressure is given in Fig. 13.13. Note that the pressure shows strong timewise oscillations at early times, but then it asymptotically approaches a steady value at large times. Again, it is this asymptotic steady state that we want, and the intermediate

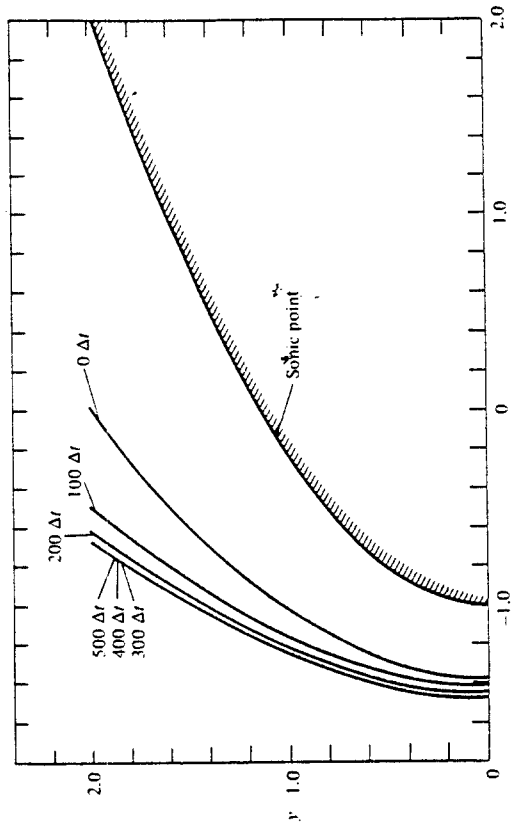
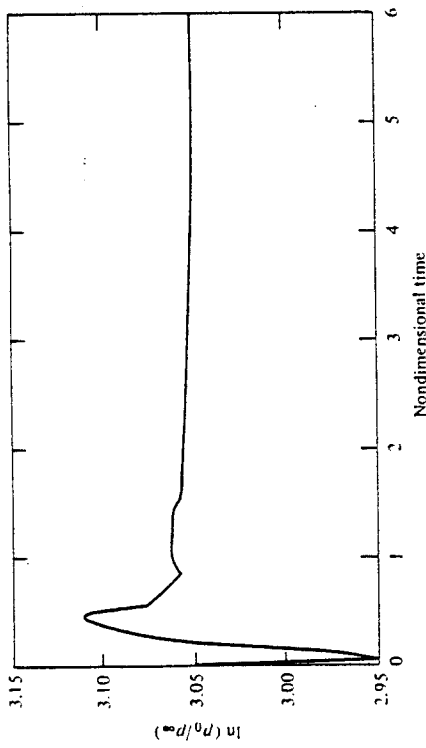


Figure 13.12 Time-dependent shock-wave motion, parabolic cylinder,  $M_\infty = 4$ .

Figure 13.13 Time variation of stagnation point pressure, parabolic cylinder,  $M_\infty = 4$ .

transient results are just a means to that end. Concentrating on just the steady-state results, Fig. 13.14 gives the pressure distribution (nondimensionalized by stagnation-point pressure) over the body surface for the cases of both  $M_\infty = 4$  and 8. The time-dependent numerical results are shown as the solid curves, whereas the open symbols are from newtonian theory, to be discussed in Chap. 14. Note that the pressure is a maximum at the stagnation point, and decreases as a function of distance away from the stagnation point — a variation that we most certainly would expect based on our previous aerodynamic experience. The steady shock shapes and sonic lines are shown

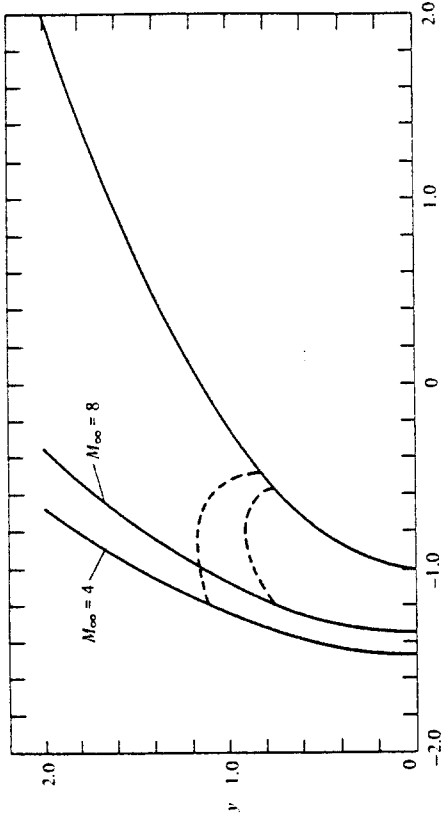


Figure 13.15 Shock shapes and sonic lines, parabolic cylinder.

in Fig. 13.15 for the cases of  $M_\infty = 4$  and 8. Note that as the Mach number increases, the shock wave moves closer to the body.

### 13.6 SUMMARY

We have now completed both branches of our road map shown in Fig. 13.1. Make certain that you feel comfortable with all the material represented by this road map. A short summary of the highlights is given below.

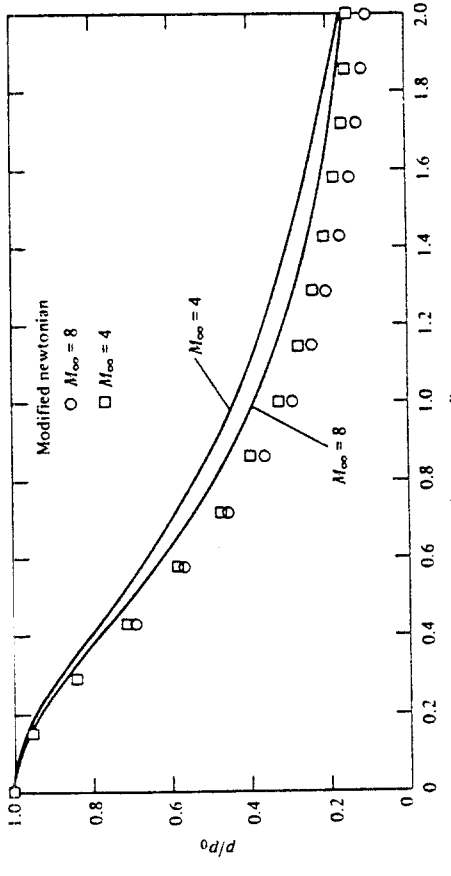


Figure 13.14 Surface pressure distributions, parabolic cylinder.

For a steady, two-dimensional, irrotational, supersonic flow, the characteristic lines are Mach lines, and the compatibility equations which hold along these characteristic lines are

$$\theta + \nu = K_- \quad (\text{along a } C_- \text{ characteristic})$$

and

$$\theta - \nu = K_+ \quad (\text{along a } C_+ \text{ characteristic})$$

The numerical solution of such a flow can be carried out by solving the compatibility equations along the characteristic lines in a step-by-step fashion, starting from an appropriate initial data line.

The contour of a supersonic nozzle can be obtained by applying the method of characteristics downstream of the limiting characteristic (which is usually downstream of the geometric throat).

The essence of finite-difference methods is to replace the partial derivatives in the governing flow equations with finite-difference quotients. For supersonic steady flows, this allows us to march downstream, starting from known data along an initial data line in the supersonic flow. For the solution of mixed subsonic-supersonic flows, a time-dependent technique can be used which allows us to march forward in time, starting with assumed initial conditions at time  $t = 0$  and achieving a steady-state result in the limit of large times.

A popular technique for carrying out finite-difference solutions, whether for supersonic steady flow or for a time-dependent solution of mixed subsonic and supersonic flow, is the predictor-corrector technique by MacCormack.

### PROBLEM

**Note:** The purpose of the following problem is to provide an exercise in carrying out a unit process for the method of characteristics. A more extensive application to a complete flow field is left to your specific desires. Also, an extensive practical problem utilizing the finite-difference method requires a large number of arithmetic operations and is practical only on a digital computer. You are encouraged to set up such a problem at your leisure. The main purpose of the present chapter is to present the essence of several numerical methods, not to burden the reader with a lot of calculations or the requirement to write an extensive computer program.

**13.1** Consider two points in a supersonic flow. These points are located in a cartesian coordinate system at  $(x_1, y_1) = (0, 0.0684)$  and  $(x_2, y_2) = (0.0121, 0)$ , where the units are meters. At point  $(x_1, y_1)$ :  $u_1 = 639 \text{ m/s}$ ,  $v_1 = 232.6 \text{ m/s}$ ,  $p_1 = 1 \text{ atm}$ ,  $T_1 = 288 \text{ K}$ . At point  $(x_2, y_2)$ :  $u_2 = 680 \text{ m/s}$ ,  $v_2 = 0$ ,  $p_2 = 1 \text{ atm}$ ,  $T_2 = 288 \text{ K}$ . Consider point 3 downstream of points 1 and 2 located by the intersection of the  $C_s$  characteristic through point 2 and the  $C_-$  characteristic through point 1. At point 3, calculate: " $u$ ",  $v$ ,  $p$ , and  $T$ . Also, calculate the location of point 3, assuming the characteristics between these points are straight lines.

## CHAPTER FOURTEEN

### ELEMENTS OF HYPERSONIC FLOW

*Isaac Newton, from the preface of his Principia, 1687.*

### 14.1 INTRODUCTION

The history of aviation has always been driven by the philosophy of "faster and higher," starting with the Wright brothers' sea level flights at 35 mi/h in 1903, and progressing exponentially to the manned space flight missions of the 1960s and 1970s. The current altitude and speed records for manned flight are the moon and 36,000 ft/s — more than 36 times the speed of sound — set by the Apollo lunar capsule in 1969. Although most of the flight of the Apollo took place in space, outside the earth's atmosphere, one of its most critical aspects was reentry into the atmosphere after completion of the lunar mission. The aerodynamic phenomena associated with very high speed flight, such as encountered during atmospheric reentry, are classified as *hypersonic aerodynamics* — the subject of this chapter. In addition to reentry vehicles, both manned and unmanned, there are other hypersonic applications on the horizon, such as ramjet-powered hypersonic missiles now under consideration by the military and the concept of a hypersonic transport, the basic technology of which is now being studied by NASA. Therefore, although hypersonic aerodynamics is at one extreme end of the whole flight spectrum (see Sec. 1.10), it is important enough to justify one small chapter in our presentation of the fundamentals of aerodynamics.

This chapter is short; its purpose is to simply introduce some basic considerations of hypersonic flow. Therefore, we have no need for a chapter road map or a summary at the end. Also, before progressing further, return to Chap. 1 and review the short discussion on hypersonic flow given in Sec. 1.10.

### 14.2 QUALITATIVE ASPECTS OF HYPERSONIC FLOW

Consider a  $15^\circ$  half-angle wedge flying at  $M_\infty = 36$ . From Fig. 9.7, we see that the wave angle of the oblique shock is only  $18^\circ$ ; that is, the oblique shock wave is very close

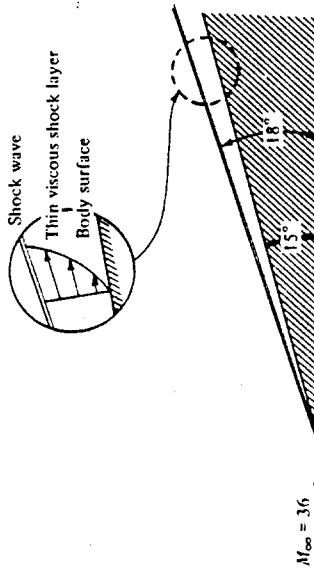


Figure 14.1 For hypersonic flow, the shock layers are thin and viscous.

to the surface of the body. This situation is sketched in Fig. 14.1. Clearly, the shock layer between the shock wave and the body is very thin. Such thin shock layers are one characteristic of hypersonic flow. A practical consequence of a thin shock layer is that a major interaction frequently occurs between the inviscid flow behind the shock and the viscous boundary layer on the surface. Indeed, hypersonic vehicles generally fly at high altitudes where the density, hence Reynolds number, is low, and therefore the boundary layers are thick. Moreover, at hypersonic speeds, the boundary-layer thickness on slender bodies is approximately proportional to  $M_x^2$ ; hence, the high Mach numbers further contribute to a thickening of the boundary layer. In many cases, the boundary-layer thickness is of the same magnitude as the shock-layer thickness, such as sketched in the insert at the top of Fig. 14.1. Here, the shock layer is fully viscous, and the shock-wave shape and surface pressure distribution are affected by such viscous effects. These phenomena are called *viscous interaction phenomena* — where the viscous flow greatly affects the external inviscid flow, and of course the external inviscid flow affects the boundary layer. A graphic example of such viscous interaction occurs on a flat plate at hypersonic speeds, as sketched in Fig. 14.2. If the flow were com-

pletely inviscid, then we would have the case shown in Fig. 14.2a, where a Mach wave trails downstream from the leading edge. Since there is no deflection of the flow, the pressure distribution over the surface of the plate is constant and equal to  $p_\infty$ . In contrast, in real life there is a boundary layer over the flat plate, and at hypersonic conditions this boundary layer can be thick, as sketched in Fig. 14.2b. The thick boundary layer deflects the external, inviscid flow, creating a comparably strong, curved shock wave which trails downstream from the leading edge. In turn, the surface pressure from the leading edge is considerably higher than  $p_\infty$ , and only approaches  $p_\infty$  far downstream of the leading edge, as shown in Fig. 14.2b. In addition to influencing the aerodynamic force, such high pressures increase the aerodynamic heating at the leading edge. Therefore, hypersonic viscous interaction can be important, and this has been one of the major areas of modern hypersonic aerodynamic research.

There is a second and frequently more dominant aspect of hypersonic flow, namely, high temperatures in the shock layer, along with large aerodynamic heating of the vehicle. For example, consider a blunt body reentering the atmosphere at Mach 36, as sketched in Fig. 14.3. Let us calculate the temperature in the shock layer immediately behind the normal portion of the bow shock wave. From App. B, we find that the static temperature ratio across a normal shock wave with  $M_x = 36$  is 252.9; this is denoted by  $T_s/T_\infty$  in Fig. 14.3. Moreover, at a standard altitude of 59 km,  $T_s = 258$  K. Hence, we obtain  $T_s = 65,248$  K — an incredibly high temperature, which is more than six times hotter than the surface of the sun! This is, in reality, an incorrect value, because we have used App. B which is good only for a calorically perfect gas with  $\gamma = 1.4$ . However, at high temperatures, the gas will become chemically reacting;  $\gamma$  will no longer equal 1.4 and will no longer be constant. Nevertheless, we get the impression from this calculation that the temperature in the shock layer will be very high, albeit something less than 65,248 K. Indeed, if a proper calculation of  $T_s$  is made taking into account the chemically reacting gas, we would find that  $T_s \approx 11,000$  K — still a very high value. Clearly, high-temperature effects are very important in hypersonic flow.

Let us examine these high-temperature effects in more detail. If we consider air at  $p = 1$  atm and  $T = 288$  K (standard sea level), the chemical composition is essentially 20% O<sub>2</sub> and 80% N<sub>2</sub> by volume. The temperature is too low for any significant chemical reaction to take place. However, if we were to increase  $T$  to 2000 K, we would observe that the O<sub>2</sub> begins to dissociate, that is,

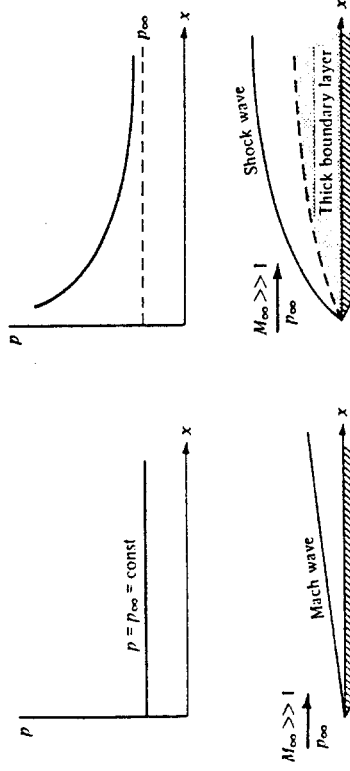


Figure 14.2 The viscous interaction on a flat plate at hypersonic speeds.  
(a) No viscous interaction  
(b) Viscous interaction

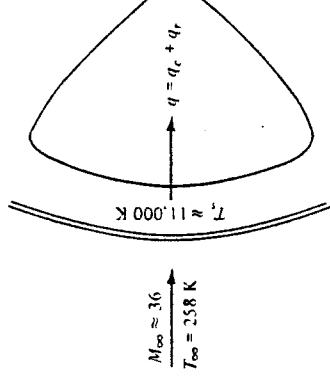


Figure 14.3 High-temperature shock layer.

$$O_2 \rightarrow 2O \quad 2000 \text{ K} < T < 4000 \text{ K}$$

If the temperature were increased to 4000 K, most of the O<sub>2</sub> would be dissociated, and N<sub>2</sub> dissociation would commence.

$$N_2 \rightarrow 2N \quad 4000 \text{ K} < T < 9000 \text{ K}$$

If the temperature were increased to 9000 K, most of the N<sub>2</sub> would be dissociated, and ionization would commence.



Hence, returning to Fig. 14.3, the shock layer in the nose region of the body is a partially ionized plasma, consisting of the atoms N and O, the ions N<sup>+</sup> and O<sup>+</sup>, and electrons, e<sup>-</sup>. Indeed, the presence of these free electrons in the shock layer is responsible for the "communications blackout" experienced over portions of the trajectory of a reentry vehicle.

One consequence of these high-temperature effects is that all our equations and tables obtained in Chaps. 7 to 13 which depended on a constant  $\gamma = 1.4$  are no longer valid. Indeed, the governing equations for the high-temperature, chemically reacting shock layer in Fig. 14.3 must be solved numerically, taking into account the proper physics and chemistry of the gas itself. The analysis of aerodynamic flows with such real physical effects is discussed in detail in chapters 13 and 14 of Ref. 21; such matters are beyond the scope of this book.

Associated with the high-temperature shock layers is a large amount of heat transfer to the surface of a hypersonic vehicle. Indeed, for reentry velocities, aerodynamic heating dominates the design of the vehicle, as explained at the end of Sec. 1.1. (Recall that the third historical example discussed in Sec. 1.1 was the evolution of the blunt-body concept to reduce aerodynamic heating; review this material before progressing further.) The usual mode of aerodynamic heating is the transfer of energy from the hot shock layer to the surface by means of thermal conduction at the surface; i.e., if  $\partial T / \partial n$  represents the temperature gradient in the gas normal to the surface, then  $q_r = -k(\partial T / \partial n)$  is the heat transfer into the surface. Because  $\partial T / \partial n$  is a flow-field property generated by the flow of the gas over the body,  $q_r$  is called *convective heating*. For reentry velocities associated with ICBMs (about 28,000 ft/s), this is the only meaningful mode of heat transfer to the body. However, at higher velocities, the shock-layer temperature becomes even hotter. From experience, we know that all bodies emit thermal radiation, and from physics you know that blackbody radiation varies as  $T^4$ ; hence, radiation becomes a dominant mode of heat transfer at high temperatures. (For example, the heat you feel by standing beside a fire in a fireplace is radiative heating from the flames.) When the shock layer reaches temperatures on the order of 11,000 K, as for the case given in Fig. 14.3, thermal radiation from the hot gas becomes a substantial portion of the total heat transfer to the body surface. Denoting radiative heating by  $q_r$ , we can express the total aerodynamic heating  $q$  as the sum of convective and radiative heating:  $q = q_r + q_r$ . For Apollo reentry,  $q_r/q \approx 0.3$ , and hence radiative heating was an important consideration in the design of the Apollo heat shield. For the entry of a space

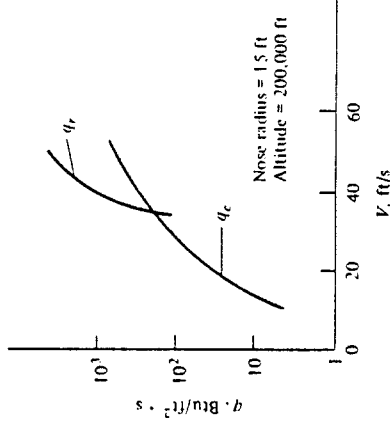


Figure 14.4 Convective and radiative heating rates of a blunt reentry vehicle as a function of flight velocity. (From Ref. 36.)

probe into the atmosphere of Jupiter, the velocities will be so high and the shock-layer temperatures so large that the convective heating is negligible, and in this case  $q \approx q_r$ . For such a vehicle, radiative heating becomes the dominant aspect in its design. Figure 14.4 illustrates the relative importance of  $q_r$  and  $q_r$  for a typical manned reentry vehicle in the earth's atmosphere; note how rapidly  $q_r$  dominates the aerodynamic heating of the body as velocities increase above 36,000 ft/s. The details of shock-layer radiative heating are interesting and important; however, they are beyond the scope of this book. For a thorough survey of the engineering aspects of shock-layer radiative heat transfer, see Ref. 36.

In summary, the aspects of thin shock-layer viscous interaction and high-temperature, chemically reacting and radiative effects distinguish hypersonic flow from the more moderate supersonic regime. Hypersonic flow has been the subject of several complete books; see, for example, Refs. 37 to 41.

### 14.3 NEWTONIAN THEORY

Return to Fig. 14.1; note how close the shock wave lies to the body surface. This figure is redrawn in Fig. 14.5 with the streamlines added to the sketch. When viewed from afar, the straight, horizontal streamlines in the freestream appear to almost impact the body, and then move tangentially along the body. Return to Fig. 1.1, which illustrates Isaac Newton's model for fluid flow, and compare it with the hypersonic flow field shown in Fig. 14.5; they have certain distinct similarities. (Also, review the discussion surrounding Fig. 1.1 before progressing further.) Indeed, the thin shock layers around hypersonic bodies are the closest example in fluid mechanics to Newton's model. Therefore, we might expect that results based on Newton's model would have some applicability in hypersonic flows. This is indeed the case; newtonian theory is used frequently to estimate the pressure distribution over the surface of a hypersonic body. The purpose of this section is to derive the famous newtonian sine-squared law first mentioned in Sec. 1.1 and to show how it is applied to hypersonic flows.

Consider a surface inclined at the angle  $\theta$  to the freestream, as sketched in

Fig. 14.6. According to the newtonian model, the flow consists of a large number of

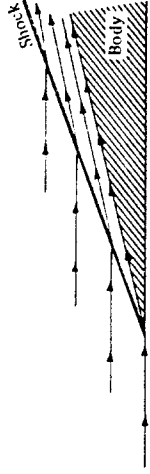


Figure 14.5 Streamlines in a hypersonic flow.

individual particles which impact the surface and then move tangentially to the surface. During collision with the surface, the particles lose their component of momentum normal to the surface, but the tangential component is preserved. The time rate of change of the normal component of momentum equals the force exerted on the surface by the particle impacts. To quantify this model, examine Fig. 14.6. The component of the freestream velocity normal to the surface is  $V_x \sin \theta$ . If the area of the surface is  $A$ , the mass flow incident on the surface is  $\rho_s A \sin \theta V_x$ . Hence, the time rate of change of momentum is

Mass flow  $\times$  change in normal component of velocity

$$\text{or } (\rho_s V_x A \sin \theta) (V_x \sin \theta) = \rho_s V_x^2 A \sin^2 \theta$$

In turn, from Newton's second law, the force on the surface is

$$N = \rho_s V_x^2 A \sin^2 \theta \quad (14.1)$$

This force acts along the same line as the time rate of change of momentum, i.e., normal to the surface, as sketched in Fig. 14.6. From Eq. (14.1), the normal force per unit area is

$$\frac{N}{A} = \rho_s V_x^2 \sin^2 \theta \quad (14.2)$$

Let us now interpret the physical meaning of the normal force per unit area in Eq. (14.2),  $N/A$ , in terms of our modern knowledge of aerodynamics. Newton's model assumes a stream of individual particles all moving in straight, parallel paths toward the surface; i.e., the particles have a completely directed, rectilinear motion. There is no random motion of the particles — it is simply a stream of particles such as pellets from a shotgun. In terms of our modern concepts, we know that a moving gas has molecular

motion that is a composite of random motion of the molecules as well as a directed motion. Moreover, we know that the freestream static pressure  $p_s$  is simply a measure of the purely random motion of the molecules. Therefore, when the purely directed motion of the particles in Newton's model results in the normal force per unit area,  $N/A$  in Eq. (14.2), this normal force per unit area must be construed as the pressure difference above  $p_s$ , namely,  $p - p_s$  on the surface. Hence, Eq. (14.2) becomes

$$p - p_s = \rho_s V_x^2 \sin^2 \theta \quad (14.3)$$

Equation (14.3) can be written in terms of the pressure coefficient  $C_p = (p - p_s)/(\rho_s V_x^2)$ , as follows

$$\frac{p - p_s}{\rho_s V_x^2} = 2 \sin^2 \theta$$

or

$$C_p = 2 \sin^2 \theta \quad (14.4)$$

Equation (14.4) is Newton's sine-squared law; it states that the pressure coefficient is proportional to the sine squared of the angle between a tangent to the surface and the direction of the freestream. This angle,  $\theta$ , is illustrated in Fig. 14.7. Frequently, the results of newtonian theory are expressed in terms of the angle between a normal to the surface and the freestream direction, denoted by  $\phi$  as shown in Fig. 14.7. In terms of  $\phi$ , Eq. (14.4) becomes

$$C_p = 2 \cos^2 \phi \quad (14.5)$$

which is an equally valid expression of newtonian theory.

Consider the blunt body sketched in Fig. 14.7. Clearly the maximum pressure, hence the maximum value of  $C_p$ , occurs at the stagnation point, where  $\theta = \pi/2$  and  $\phi = 0$ . Equation (14.4) predicts  $C_p = 2$  at the stagnation point. Contrast this hypersonic result with the result obtained for incompressible flow theory in Chap. 3, where  $C_p = 1$  at a stagnation point. Indeed, the stagnation pressure coefficient increases continuously from 1.0 at  $M_\infty = 0$  to 1.28 at  $M_\infty = 1.0$  to 2.0 as  $M_\infty \rightarrow \infty$ . (Prove this to yourself.)

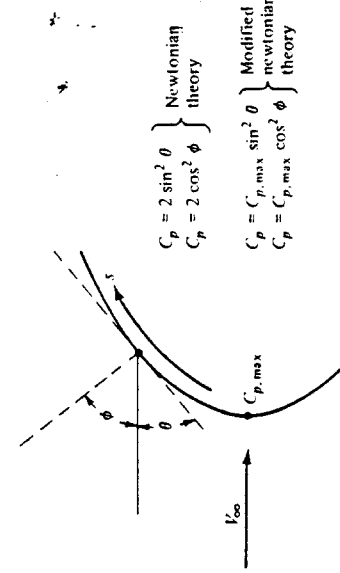


Figure 14.7 Definition of angles for newtonian theory.

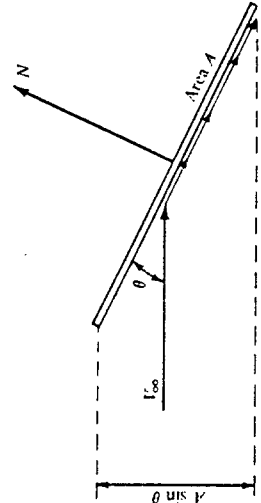


Figure 14.6 Schematic for newtonian impact theory.

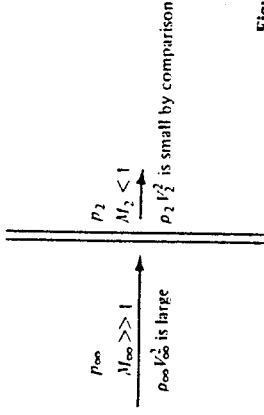


Figure 14.8 Hypersonic flow across a normal shock wave.

The result that the maximum pressure coefficient approaches 2 at  $M_\infty \rightarrow \infty$  can be obtained independently from the one-dimensional momentum equation, namely, Eq. (8.6). Consider a normal shock wave at hypersonic speeds, as sketched in Fig. 14.8. For this flow, Eq. (8.6) gives

$$p_\infty + \rho_\infty V_\infty^2 = p_2 + \rho_2 V_2^2 \quad (14.6)$$

Recall that across a normal shock wave the flow velocity decreases,  $V_2 < V_\infty$ ; indeed, the flow behind the normal shock is subsonic. This change becomes more severe as  $M_\infty$  increases. Hence, at hypersonic speeds, we can assume that  $(\rho_\infty V_\infty^2) \gg (\rho_2 V_2^2)$ , and we can neglect the latter term in Eq. (14.6). As a result, Eq. (14.6) becomes, at hypersonic speeds in the limiting case as  $M_\infty \rightarrow \infty$ ,

$$p_2 - p_\infty = \rho_\infty V_\infty^2$$

$$\text{or} \quad C_p = \frac{p_2 - p_\infty}{\frac{1}{2} \rho_\infty V_\infty^2} = 2$$

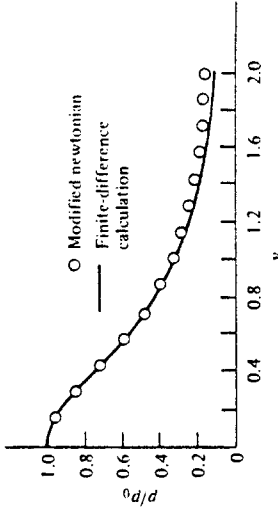
thus confirming the newtonian results from Eq. (14.4).

As stated above, the result that  $C_p = 2$  at a stagnation point is a limiting value as  $M_\infty \rightarrow \infty$ . For large but finite Mach numbers, the value of  $C_p$  at a stagnation point is less than 2. Return again to the blunt body shown in Fig. 14.7. Considering the distribution of  $C_p$  as a function of distance  $s$  along the surface, the largest value of  $C_p$  will occur at the stagnation point. Denote the stagnation point value of  $C_p$  by  $C_{p,\max}$ , as shown in Fig. 14.7.  $C_{p,\max}$  for a given  $M_\infty$  can be readily calculated from normal shock-wave theory. [If  $\gamma = 1.4$ , then  $C_{p,\max}$  can be obtained from  $p_{0,2}/p_\infty = p_{0,2}/p_\infty = (2/\gamma M_\infty^2)(p_{0,2}/p_\infty - 1)$ .] Downstream of the stagnation point,  $C_p$  can be assumed to follow the sine-squared variation predicted by newtonian theory; that is,

$$C_p = C_{p,\max} \sin^2 \theta \quad (14.7)$$

Equation (14.7) is called the *modified newtonian law*. For the calculation of the  $C_p$  distribution around blunt bodies, Eq. (14.7) is more accurate than Eq. (14.4).

Return to Fig. 13.14, which gives the numerical results for the pressure distributions around a blunt, parabolic cylinder at  $M_\infty = 4$  and 8. The open symbols in this figure represent the results of modified newtonian theory, namely, Eq. (14.7). For this

Figure 14.9 Surface pressure distribution, paraboloid,  $M_\infty = 4$ . Comparison of modified newtonian theory and time-dependent finite-difference calculations.

two-dimensional body, modified newtonian theory is reasonably accurate only in the nose region, although the comparison improves at the higher Mach numbers. It is generally true that newtonian theory is more accurate at larger values of both  $M_\infty$  and  $\theta$ . The case for an axisymmetric body, a paraboloid at  $M_\infty = 4$ , is given in Fig. 14.9. Here, although  $M_\infty$  is relatively low, the agreement between the time-dependent numerical solution (see Chap. 13) and newtonian theory is much better. It is generally true that newtonian theory works better for three-dimensional bodies. In general, the modified newtonian law, Eq. (14.7), is sufficiently accurate that it is used very frequently in the preliminary design of hypersonic vehicles. Indeed, extensive computer codes have been developed to apply Eq. (14.7) to three-dimensional hypersonic bodies of general shape. Therefore, we can be thankful to Isaac Newton for supplying us with a law which holds reasonably well at hypersonic speeds, although such an application most likely never crossed his mind. Nevertheless, it is fitting that three centuries later, Newton's fluid mechanics has finally found a reasonable application.

## PROBLEMS

### 14.1 Repeat Prob. 9.13 using

(a) Newtonian theory

(b) Modified newtonian theory

Compare these results with those obtained from exact shock-expansion theory (Prob. 9.13). From this comparison, what comments can you make about the accuracy of newtonian and modified newtonian theories at few supersonic Mach numbers?

14.2 Consider a flat plate at  $\alpha = 20^\circ$  in a Mach 20 freestream. Using straight newtonian theory, calculate the lift and wave-drag coefficients. Compare these results with exact shock-expansion theory.

## CHAPTER FIFTEEN

### INTRODUCTION TO THE FUNDAMENTAL PRINCIPLES AND EQUATIONS OF VISCOUS FLOW

*I do not see then, I admit, how one can explain the resistance of fluids by the theory in a satisfactory manner. It seems to me on the contrary that this theory, dealt with and studied with profound attention gives, at least in most cases, resistance absolutely zero: a singular paradox which I leave to geometers to explain.*

*Jean LeRond d'Alembert, 1768*

#### 15.1 INTRODUCTION

In the above quotation, the “theory” referred to by d’Alembert is inviscid, incompressible flow theory; we have seen in Chap. 3 that such theory leads to a prediction of zero drag on a closed two-dimensional body — this is d’Alembert’s paradox. In reality, there is always a finite drag on any body immersed in a moving fluid. Our earlier predictions of zero drag are a result of the inadequacy of the theory rather than some fluke of nature. With the exception of induced drag and supersonic wave drag, which can be obtained from inviscid theory, the calculation of all other forms of drag must explicitly take into account the presence of viscosity, which has not been included in our previous inviscid analyses. The purpose of the remaining chapters in this book is to discuss the basic aspects of viscous flows, thus “rounding out” our overall presentation of the fundamentals of aerodynamics. In so doing, we address the predictions of aerodynamic drag and aerodynamic heating. To help put our current discussion in perspective, return to the block diagram of flow categories given in Fig. 1.27. All of our previous discussions have focused on blocks *D*, *E*, and *F* — inviscid, incompressible and compressible flows. Now, for the remaining two chapters, we move to the left branch in Fig. 1.27, and deal with blocks, *C*, *E*, and *F* — *viscous*, incompressible and compressible flows.

Our treatment of viscous flows will be intentionally brief — our purpose is to present enough of the fundamental concepts and equations to give you the flavor of viscous flows. A thorough presentation of viscous flow theory would double the size of this book (at the very least) and is clearly beyond our scope. A study of viscous flow

Figure 15.1 Road map for Chap. 15.

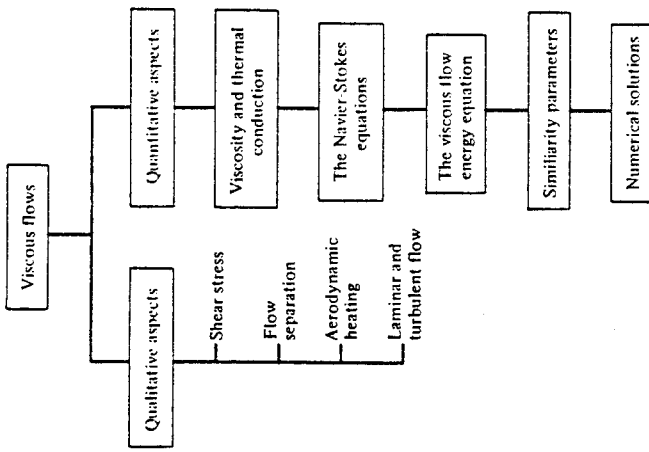


Figure 15.1 Road map for Chap. 15.

is an essential part of any serious study of aerodynamics. Many books have been exclusively devoted to the presentation of viscous flows; Refs. 42 and 43 are two good examples. You are encouraged to examine these references closely.

The road map for the present chapter is given in Fig. 15.1. Our course is to first examine some qualitative aspects of viscous flow as shown on the left branch of Fig. 15.1. Then we quantify some of these aspects as given on the right branch. In the process, we obtain the governing equations for a general viscous flow — in particular, the Navier-Stokes equations (the momentum equations) and the viscous flow energy equation. Finally, we examine a numerical solution to these equations.

#### 15.2 QUALITATIVE ASPECTS OF VISCOUS FLOW

What is a viscous flow? Answer: A flow where the effects of viscosity, thermal conduction, and mass diffusion are important. The phenomenon of mass diffusion is important in a gas with gradients in its chemical species, e.g., the flow of air over a surface through which helium is being injected or the chemically reacting flow through a jet engine or over a high-speed reentry body. In this book, we are not concerned with the effects of diffusion, and therefore we treat a viscous flow as one where only viscosity and thermal conduction are important.

First, consider the influence of viscosity. Imagine two solid surfaces slipping over each other, such as this book being pushed across a table. Clearly, there will be a

frictional force between these objects which will retard their relative motion. The same is true for the flow of a fluid over a solid surface; the influence of friction between the surface and the fluid adjacent to the surface acts to create a frictional force which retards the relative motion. This has an effect on both the surface and the fluid. The surface feels a "tugging" force in the direction of the flow, tangential to the surface. This tangential force per unit area is defined as the *shear stress*  $\tau$ , first introduced in Sec. 1.5 and illustrated in Fig. 15.2. As an equal and opposite reaction, the fluid adjacent to the surface feels a retarding force which decreases its local flow velocity, as shown in insert *a* of Fig. 15.2. Indeed, the influence of friction is to create  $V = 0$  right at the body surface — this is called the *no-slip* condition which dominates viscous flow. In any real continuum fluid flow over a solid surface, the flow velocity is zero at the surface. Just above the surface, the flow velocity is finite, but retarded, as shown in insert *a*. If  $n$  represents the coordinate normal to the surface, then in the region near the surface,  $V = V(n)$ , where  $V = 0$  at  $n = 0$ , and  $V$  increases as  $n$  increases. The plot of  $V$  versus  $n$  as shown in insert *a* is called a *velocity profile*. Clearly, the region of flow near the surface has velocity gradients,  $\partial V / \partial n$ , which are due to the frictional force between the surface and the fluid.

In addition to the generation of shear stress, friction also plays another (but related) role in dictating the flow over the body in Fig. 15.2. Consider a fluid element moving in the viscous flow near a surface, as sketched in Fig. 15.3. Assume that the flow is in its earliest moments of being started. At the station  $s_1$ , the velocity of the fluid element is  $V_1$ . Assume that the flow over the surface produces an increasing pressure distribution in the flow direction; i.e., assume  $p_3 > p_2 > p_1$ . Such a region of increasing pressure is called an *adverse pressure gradient*. Now follow the fluid element as it moves downstream. The motion of the element is already retarded by the effect of friction; in addition, it must work its way against an increasing pressure, which tends to further reduce its velocity. Consequently, at station 2 along the

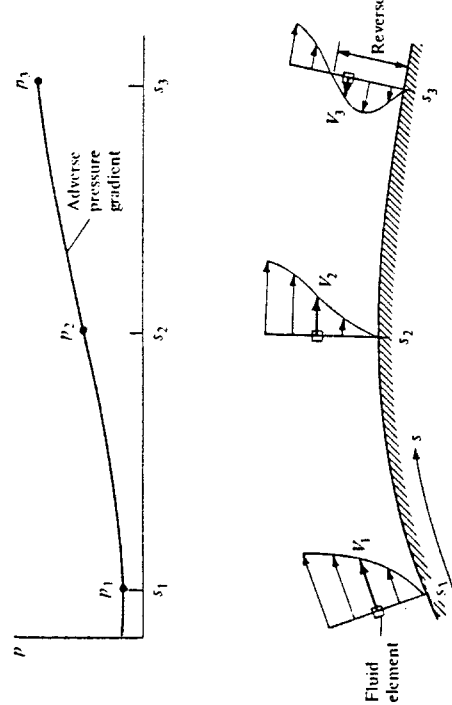


Figure 15.3 Separated flow induced by an adverse pressure gradient. This picture corresponds to the early evolution of the flow; once the flow separates from the surface between points 2 and 3, the fluid element shown at  $s_1$  is in reality different than shown at  $s_1$  and  $s_2$  because the primary flow moves away from the surface, as shown in Figure 15.2.

surface, its velocity  $V_2$  is less than  $V_1$ . As the fluid element continues to move downstream, it may completely "run out of steam," come to a stop, and then, under the action of the adverse pressure gradient, actually reverse its direction and start moving back upstream. This "reversed flow" is illustrated at station  $s_3$  in Fig. 15.3, where the fluid element is now moving upstream at the velocity  $V_3$ . The picture shown in Fig. 15.3 is meant to show the flow details very near the surface at the very initiation of the flow. In the bigger picture of this flow at later times shown in Fig. 15.2, the consequence of such reversed-flow phenomena is to cause the flow to *separate from the surface* and create a large wake of recirculating flow downstream of the surface. The point of separation on the surface in Fig. 15.2 occurs where  $\partial V / \partial n = 0$  at the surface, as sketched in insert *b* of Fig. 15.2. Beyond this point, reversed flow occurs. Therefore, in addition to the generation of shear stress, the influence of friction can cause the flow over a body to separate from the surface. When such separated flow occurs, the pressure distribution over the surface is greatly altered. The primary flow over the body in Fig. 15.2 no longer sees the complete body shape; rather, it sees the body shape upstream of the separation point, but downstream of the separation point it sees a greatly deformed "effective body" due to the large separated region. The net effect is to create a pressure distribution over the actual body surface which results in an integrated force in the flow direction, i.e., a drag. To see this more clearly, consider the pressure distribution over the upper surface of the body as sketched in Fig. 15.4. If the flow were attached, the pressure over the downstream portion of the body would be given by the dashed curve. However, for separated flow, the pressure over the downstream portion of the body is smaller, given by the solid curve in Fig. 15.4. Now return to Fig. 15.2. Note that the pressure over the upper rearward surface contributes a force in the negative drag direction; that is,  $p$  acting over the element of surface  $dS$  shown in Fig. 15.2.

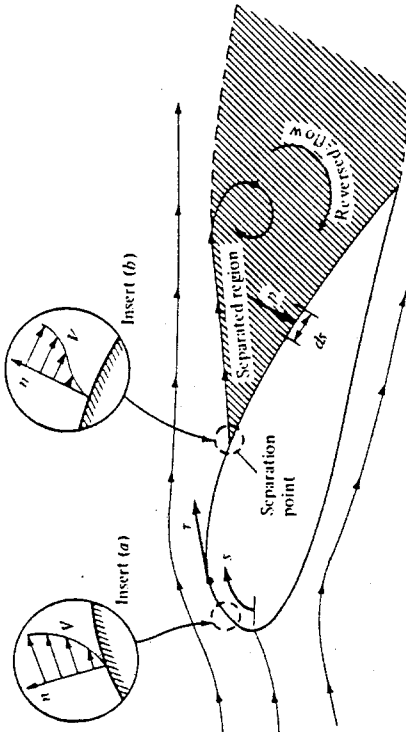


Figure 15.2 Effect of viscosity on a body in a moving fluid: shear stress and separated flow.

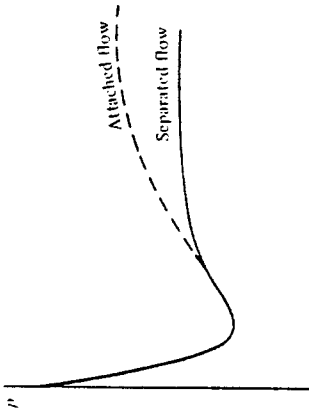


Figure 15.4 Schematic of the pressure distributions for attached and separated flow over the upper surface of the body illustrated in Fig. 15.2.

has a horizontal component in the upstream direction. If the flow were inviscid, subsonic, and attached and the body were two-dimensional, the forward-acting components of the pressure distribution shown in Fig. 15.2 would exactly cancel the rearward-acting components due to the pressure distribution over other parts of the body such that the net, integrated pressure distribution would give zero drag. This would be d'Alembert's paradox discussed in Chap. 3. However, for the viscous, separated flow, we see that  $p$  is reduced in the separated region; hence, it can no longer fully cancel the pressure distribution over the remainder of the body. The net result is the production of drag; this is called the *pressure drag due to flow separation* and is denoted by  $D_p$ .

In summary, we see that the effects of viscosity are to produce two types of drag as follows:

$D_f$  is the skin friction drag, i.e., the component in the drag direction of the integral of the shear stress  $\tau$  over the body.

$D_p$  is the pressure drag due to separation, i.e., the component in the drag direction of the integral of the pressure distribution over the body.

$D_p$  is sometimes called *form drag*. The sum  $D_f + D_p$  is called the *profile drag* of a two-dimensional body. For a three-dimensional body such as a complete airplane, the sum  $D_f + D_p$  is frequently called *parasite drag*. (See Ref. 2 for a more extensive discussion of the classification of different drag contributions.)

The occurrence of separated flow over an aerodynamic body not only increases the drag but also results in a substantial loss of lift. Such separated flow is the cause of airfoil stall as discussed in Sec. 4.3. For these reasons, the study, understanding, and prediction of separated flow is an important aspect of viscous flow.

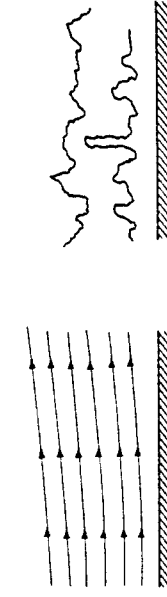
Let us turn our attention to the influence of thermal conduction — another overall physical characteristic of viscous flow in addition to friction. Again, let us draw an analogy from two solid bodies slipping over each other, such as the motion of this book over the top of a table. If we would press hard on the book, and vigorously rub it back and forth over the table, the cover of the book as well as the table top would soon become warm. Some of the energy we expend in pushing the book over the table will be dissipated by friction, and this shows up as a form of heating of the bodies. The same phenomenon occurs in the flow of a fluid over a body. The moving fluid has a certain

amount of kinetic energy, in the process of flowing over a surface, the flow velocity is decreased by the influence of friction, as discussed earlier, and hence the kinetic energy is decreased. This lost kinetic energy reappears in the form of internal energy of the fluid, hence causing the temperature to rise. This phenomenon is called *viscous dissipation* within the fluid. In turn, when the fluid temperature increases, there is an overall temperature difference between the warmer fluid and the cooler body. We know from experience that heat is transferred from a warmer body to a cooler body; therefore, heat will be transferred from the warmer fluid to the cooler surface. This is the mechanism of *aerodynamic heating* of a body. Aerodynamic heating becomes more severe as the flow velocity increases, because more kinetic energy is dissipated by friction, and hence the overall temperature difference between the warm fluid and the cool surface increases. As discussed in Chap. 14, at hypersonic speeds, aerodynamic heating becomes a dominant aspect of the flow.

All the aspects discussed above — shear stress, flow separation, aerodynamic heating, etc. — are dominated by a single major question in viscous flow, namely, is the flow laminar or turbulent? Consider the viscous flow over a surface as sketched in Fig. 15.5. If the path lines of various fluid elements are smooth and regular, as shown in Fig. 15.5a, the flow is called *laminar flow*. In contrast, if the motion of a fluid element is very irregular and tortuous, as shown in Fig. 15.5b, the flow is called *turbulent flow*. Because of the agitated motion in a turbulent flow, the higher-energy fluid elements from the outer regions of the flow are pumped close to the surface. Hence, the average flow velocity near a solid surface is larger for a turbulent flow in comparison with laminar flow. This comparison is shown in Fig. 15.6, which gives velocity profiles for laminar and turbulent flow. Note that immediately above the surface, the turbulent flow velocities are much larger than the laminar values. If  $(\partial V / \partial n)_{n=0}$  denotes the velocity gradient at the surface, we have

$$\left[ \left( \frac{\partial V}{\partial n} \right)_{n=0} \right]_{\text{laminar}} > \left[ \left( \frac{\partial V}{\partial n} \right)_{n=0} \right]_{\text{turbulent}}$$

Because of this difference, the frictional effects are more severe for a turbulent flow; both the shear stress and aerodynamic heating are larger for the turbulent flow in comparison with laminar flow. However, turbulent flow has a major redeeming value; because the energy of the fluid elements close to the surface is larger in a turbulent flow, a turbulent flow does not separate from the surface as readily as a laminar flow. If the flow over a body is turbulent, it is less likely to separate from the body surface,



(a) Laminar flow  
(b) Turbulent flow

Figure 15.5 Path lines for laminar and turbulent flows.

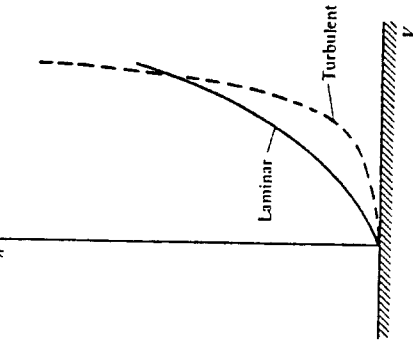


Figure 15.6 Schematic of velocity profiles for laminar and turbulent flows.

and if flow separation does occur, the separated region will be smaller. As a result, the pressure drag due to flow separation,  $D_p$ , will be smaller for turbulent flow.

The above discussion points out one of the great compromises in aerodynamics. For the flow over a body, is laminar or turbulent flow preferable? There is no pat answer; it depends on the shape of the body. In general, if the body is slender, as sketched in Fig. 15.7a, the friction drag  $D_f$  is much greater than  $D_p$ . For this case, because  $D_f$  is smaller for laminar than for turbulent flow, laminar flow is desirable for slender bodies. In contrast, if the body is blunt, as sketched in Fig. 15.7b,  $D_p$  is much greater than  $D_f$ . For this case, because  $D_p$  is smaller for turbulent than for laminar flow, turbulent flow is desirable for blunt bodies. The above comments are not all-inclusive; they simply state general trends, and for any given body, the aerodynamic virtues of laminar versus turbulent flow must always be assessed.

Although, from the above discussion, laminar flow is preferable for some cases, and turbulent flow for other cases, in reality we have little control over what actually happens. Nature makes the ultimate decision as to whether a flow will be laminar or turbulent. There is a general principle in nature that a system, when left to itself, will always move toward its state of maximum disorder. To bring order to the system, we

$$D = D_f + D_p$$

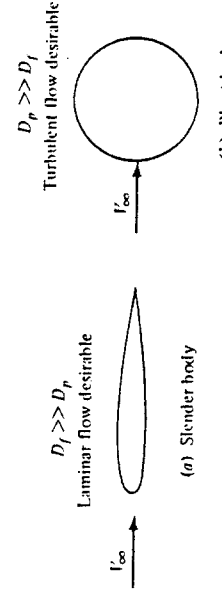


Figure 15.7 Drag on slender and blunt bodies.

generally have to exert some work on the system or expend energy in some manner. (This analogy can be carried over to daily life; a room will soon become cluttered and disordered unless we exert some effort to keep it clean.) Since turbulent flow is much more "disordered" than laminar flow, nature will always favor the occurrence of turbulent flow. Indeed, in the vast majority of practical aerodynamic problems, turbulent flow is usually present.

Let us examine this phenomenon in more detail. Consider the viscous flow over a flat plate, as sketched in Fig. 15.8. The flow immediately upstream of the leading edge is uniform at the freestream velocity. However, downstream of the leading edge, the influence of friction will begin to retard the flow adjacent to the surface, and the extent of this retarded flow will grow higher above the plate as we move downstream, as shown in Fig. 15.8. To begin with, the flow just downstream of the leading edge will be laminar. However, after a certain distance, instabilities will appear in the laminar flow; these instabilities rapidly grow, causing transition to turbulent flow. The transition from laminar to turbulent flow takes place over a finite region, as sketched in Fig. 15.8. However, for purposes of analysis, we frequently model the transition region as a single point, called the *transition point*, upstream of which the flow is laminar and downstream of which the flow is turbulent. The distance from the leading edge to the transition point is denoted by  $x_{cr}$ . The value of  $x_{cr}$  depends on a whole host of phenomena. For example, some characteristics which encourage transition from laminar to turbulent flow, and hence reduce  $x_{cr}$ , are

1. Increased surface roughness. Indeed, to promote turbulent flow over a body, rough grit can be placed on the surface near the leading edge to "trip" the laminar flow into turbulent flow. This is a frequently used technique in wind-tunnel testing. Also, the dimples on the surface of a golf ball are designed to encourage turbulent flow, thus reducing  $D_p$ . In contrast, in situations where we desire large regions of laminar flow, such as the flow over the NACA six-series laminar-flow airfoils, the surface should be as smooth as possible. The main reason why such airfoils do not produce in actual flight the large regions of laminar flow observed in the laboratory is that manufacturing irregularities and bug spots (believe it or not) roughen the surface and promote early transition to turbulent flow.
2. Increased turbulence in the freestream. This is particularly a problem in wind-tunnel testing; if two wind tunnels have different levels of freestream turbulence, then data generated in one tunnel are not repeatable in the other.

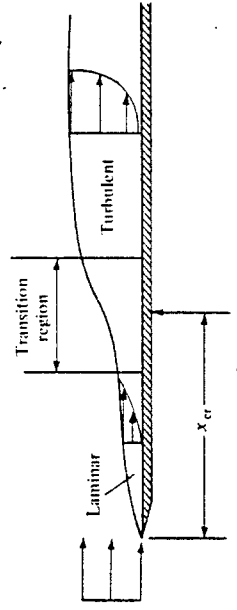


Figure 15.8 Transition from laminar to turbulent flow.

3. Adverse pressure gradients. In addition to causing flow-field separation as discussed earlier, an adverse pressure gradient strongly favors transition to turbulent flow. In contrast, strong favorable pressure gradients (where  $p$  decreases in the downstream direction) tend to preserve initially laminar flow.
4. Heating of the fluid by the surface. If the surface temperature is warmer than the adjacent fluid, such that heat is transferred to the fluid from the surface, the instabilities in the laminar flow will be amplified, thus favoring early transition. In contrast, a cold wall will tend to encourage laminar flow.

There are many other parameters which influence transition; see Ref. 42 for a more extensive discussion. Among these are the similarity parameters of the flow, principally Mach number and Reynolds number. High values of  $M_\infty$  and low values of  $Re$  tend to encourage laminar flow; hence, for high-altitude hypersonic flight, laminar flow can be quite extensive. The Reynolds number itself is a dominant factor in transition to turbulent flow. Referring to Fig. 15.8, we define a *critical* Reynolds number,  $Re_{cr}$ , as

$$Re_{cr} \equiv \frac{\rho_\infty V_\infty x_{cr}}{\mu_\infty}$$

The value of  $Re_{cr}$  for a given body under specified conditions is difficult to predict; indeed, the analysis of transition is still a very active area of modern aerodynamic research. As a rule of thumb in practical applications, we frequently take  $Re_{cr} \approx 500,000$ ; if the flow at a given  $x$  station is such that  $Re = \rho_\infty V_\infty x / \mu_\infty$  is considerably below 500,000, then the flow at that station is most likely laminar, and if the value of  $Re$  is much larger than 500,000, then the flow is most likely turbulent.

To obtain a better feeling for  $Re_{cr}$ , let us imagine that the flat plate in Fig. 15.8 is a wind-tunnel model. Assume that we carry out an experiment under standard sea level conditions [ $\rho_\infty = 1.23 \text{ kg/m}^3$  and  $\mu_\infty = 1.79 \times 10^{-5} \text{ kg/(m} \cdot \text{s)}$ ] and measure  $x_{cr}$  for a certain freestream velocity; for example, say that  $x_{cr} = 0.05 \text{ m}$  when  $V_\infty = 120 \text{ m/s}$ . In turn, this measured value of  $x_{cr}$  determines the measured  $Re_{cr}$  as

$$Re_{cr} = \frac{\rho_\infty V_\infty x_{cr}}{\mu_\infty} = \frac{1.23(120)(0.05)}{1.79 \times 10^{-5}} = 412,000$$

Hence, for the given flow conditions and the surface characteristics of the flat plate, transition will occur whenever the local  $Re$  exceeds 412,000. For example, if we double  $V_\infty$ , that is,  $V_\infty = 240 \text{ m/s}$ , then we will observe transition to occur at  $x_{cr} = 0.05/2 = 0.025 \text{ m}$ , such that  $Re_{cr}$  remains the same value of 412,000.

This brings to an end our introductory qualitative discussion of viscous flow. The physical principles and trends discussed in this section are very important, and you should study them carefully and feel comfortable with them before progressing further.

### 15.3 VISCOSITY AND THERMAL CONDUCTION

The basic physical phenomena of viscosity and thermal conduction in a fluid are due to the transport of momentum and energy via random molecular motion. Each molecule

in a fluid has momentum and energy, which it carries with it when it moves from one location to another in space before colliding with another molecule. The transport of molecular momentum gives rise to the macroscopic effect we call viscosity, and the transport of molecular energy gives rise to the macroscopic effect we call thermal conduction. This is why viscosity and thermal conduction are labeled as *transport phenomena*. A study of these transport phenomena at the molecular level is part of kinetic theory, which is beyond the scope of this book. Instead, in this section we simply state the macroscopic results of such molecular motion.

Consider the flow sketched in Fig. 15.9. For simplicity, we consider a one-dimensional shear flow, i.e., a flow with horizontal streamlines in the  $x$  direction but with gradients in the  $y$  direction of velocity,  $du/dy$ ; and temperature,  $\partial T/\partial y$ . Consider a plane  $ab$  perpendicular to the  $y$  axis, as shown in Fig. 15.9. The shear stress exerted on plane  $ab$  by the flow is denoted by  $\tau_{yx}$  and is proportional to the velocity gradient in the  $y$  direction,  $\tau_{yx} \propto du/dy$ . The constant of proportionality is defined as the *viscosity coefficient*  $\mu$ . Hence

$$\tau_{yx} = \mu \frac{du}{dy} \quad (15.1)$$

The subscripts on  $\tau_{yx}$  denote that the shear stress is acting in the  $x$  direction and is being exerted on a plane perpendicular to the  $y$  axis. The velocity gradient  $du/dy$  is also taken perpendicular to this plane, i.e., in the  $y$  direction. The dimensions of  $\mu$  are mass/length  $\times$  time, as originally stated in Sec. 1.7 and as can be seen from Eq. (15.1). In addition, the time rate of heat conducted per unit area across plane  $ab$  in Fig. 15.9 is denoted by  $\dot{q}_y$  and is proportional to the temperature gradient in the  $y$  direction,  $\dot{q}_y \propto \partial T/\partial y$ . The constant of proportionality is defined as the *thermal conductivity*  $k$ . Hence

$$\dot{q}_y = -k \frac{\partial T}{\partial y} \quad (15.2)$$

where the minus sign accounts for the fact that the heat is transferred from a region of high temperature to a region of lower temperature; that is,  $\dot{q}_y$  is in the opposite direction

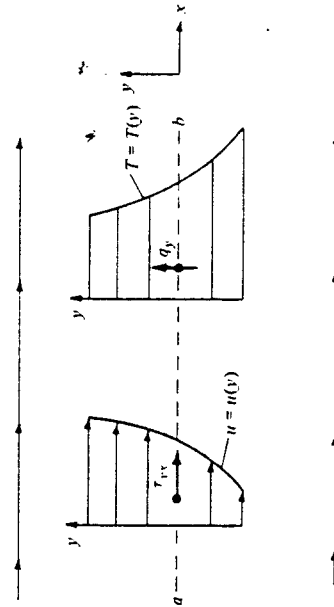


Figure 15.9 Relationship of shear stress and thermal conduction to velocity and temperature gradients, respectively.

of the temperature gradient. The dimensions of  $k$  are mass  $\times$  length/( $s^2 \cdot K$ ), which can be obtained from Eq. (15.2) keeping in mind that  $\dot{q}_v$  is energy per second per unit area.

Both  $\mu$  and  $k$  are physical properties of the fluid and, for most normal situations, are functions of temperature only. A conventional relation for the temperature variation of  $\mu$  for air is given by Sutherland's law,

$$\frac{\mu}{\mu_0} = \left( \frac{T}{T_0} \right)^{m_2} \frac{T_0 + 110}{T + 110} \quad (15.3)$$

where  $T$  is in kelvin and  $\mu_0$  is a reference viscosity at a reference temperature,  $T_0$ . For example, if we choose reference conditions to be standard sea level values, then  $\mu_0 = 1.7894 \times 10^{-5} \text{ kg}/(\text{m} \cdot \text{s})$  and  $T_0 = 288.16 \text{ K}$ . The temperature variation of  $k$  is analogous to Eq. (15.3) because the results of elementary kinetic theory show that  $k \propto \mu c_p$ ; for air at standard conditions,

$$k = 1.45\mu c_p \quad (15.4)$$

where  $c_p = 1000 \text{ J}/(\text{kg} \cdot \text{K})$ .

Equations (15.3) and (15.4) are only approximate and do not hold at high temperatures. They are given here as representative expressions which are handy to use. For any detailed viscous flow calculation, you should consult the published literature for more precise values of  $\mu$  and  $k$ .

In order to simplify our introduction of the relation between shear stress and viscosity, we considered the case of a one-dimensional shear flow in Fig. 15.9. In this picture, the  $y$  and  $z$  components of velocity,  $v$  and  $w$ , respectively, are zero. However, in a general three-dimensional flow,  $u$ ,  $v$ , and  $w$  are finite, and this requires a generalization of our treatment of stress in the fluid. Consider the fluid element sketched in Fig. 15.10. In a three-dimensional flow, each face of the fluid element experiences both tangential and normal stresses. For example, on face  $abcd$ ,  $\tau_{yy}$  and  $\tau_{xz}$  are the tangential stresses, and  $\tau_{zz}$  is the normal stress. As before, the nomenclature  $\tau_{ij}$  denotes a stress

in the  $j$  direction exerted on a plane perpendicular to the  $i$  axis. Similarly, on face  $abfe$ , we have the tangential stresses  $\tau_{yy}$  and  $\tau_{xz}$ , and the normal stress  $\tau_{yy}$ . On face  $adge$ , we have the tangential stresses  $\tau_{yy}$  and  $\tau_{yz}$ , and the normal stress  $\tau_{yz}$ . Now recall the discussion in the last part of Sec. 2.12 concerning the *strain* of a fluid element, i.e., the change in the angle  $\kappa$  shown in Fig. 2.26. What is the force which causes this deformation shown in Fig. 2.26? Returning to Fig. 15.10, we have to say that the strain is caused by the tangential shear stress. However, in contrast to solid mechanics where stress is proportional to strain, in fluid mechanics the stress is proportional to the *time rate of strain*. The time rate of strain in the  $xy$  plane was given in Sec. 2.12 as Eq. (2.126a):

$$\epsilon_{yy} = \frac{\partial v}{\partial x} + \frac{\partial u}{\partial y} \quad (2.126a)$$

Examining Fig. 15.10, the strain in the  $xy$  plane must be carried out by  $\tau_{yy}$  and  $\tau_{xz}$ . Moreover, we assume that moments on the fluid element in Fig. 15.10 are zero; hence  $\tau_{yy} = \tau_{yz}$ . Finally, from the above, we know that  $\tau_{yy} = \tau_{xz} \propto \epsilon_{yy}$ . The proportionality constant is the viscosity coefficient  $\mu$ . Hence, from Eq. (2.126a), we have

$$\tau_{yy} = \tau_{xz} = \mu \left( \frac{\partial v}{\partial x} + \frac{\partial u}{\partial y} \right) \quad (15.5)$$

which is a generalization of Eq. (15.1), extended to the case of multidimensional flow. For the shear stresses in the other planes, Eqs. (2.126b and c) yield

$$\tau_{yz} = \tau_{xy} = \mu \left( \frac{\partial w}{\partial y} + \frac{\partial v}{\partial z} \right) \quad (15.6)$$

and

$$\tau_{zx} = \tau_{zy} = \mu \left( \frac{\partial u}{\partial z} + \frac{\partial w}{\partial x} \right) \quad (15.7)$$

The normal stresses  $\tau_{xx}$ ,  $\tau_{yy}$ , and  $\tau_{zz}$  shown in Fig. 15.10 may at first seem strange. In our previous treatments of inviscid flow, the only force normal to a surface in a fluid is the pressure force. However, if the gradients in velocity  $\partial u/\partial x$ ,  $\partial v/\partial y$ , and  $\partial w/\partial z$  are *extremely large* on the faces of the fluid element, there can be a meaningful viscous-induced normal force on each face which acts *in addition to* the pressure. These normal stresses act to compress or expand the fluid element, hence changing its volume. Recall from Sec. 2.12 that the derivatives  $\partial u/\partial x$ ,  $\partial v/\partial y$ , and  $\partial w/\partial z$  are related to the dilatation of a fluid element, that is, to  $\nabla \cdot \mathbf{V}$ . Hence, the normal stresses should in turn be related to these derivatives. Indeed, it can be shown that

$$\tau_{xx} = \lambda (\nabla \cdot \mathbf{V}) + 2\mu \frac{\partial u}{\partial x} \quad (15.8)$$

$$\tau_{yy} = \lambda (\nabla \cdot \mathbf{V}) + 2\mu \frac{\partial v}{\partial y} \quad (15.9)$$

$$\tau_{zz} = \lambda (\nabla \cdot \mathbf{V}) + 2\mu \frac{\partial w}{\partial z} \quad (15.10)$$

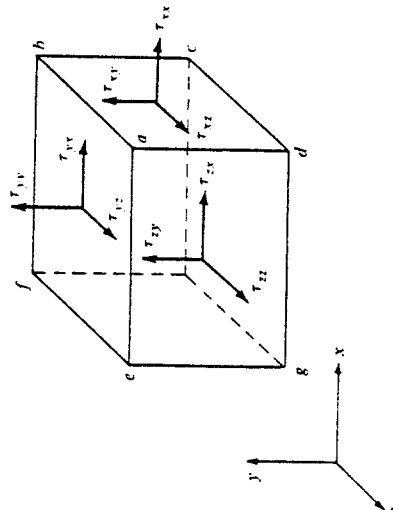


Figure 15.10 Shear and normal stresses caused by viscous action on a fluid element.

In Eqs. (15.8) to (15.10),  $\lambda$  is called the *bulk viscosity coefficient*. In 1845, the Englishman George Stokes hypothesized that

$$\lambda = -\frac{2}{3}\mu \quad (15.11)$$

To this day, the correct expression for the bulk viscosity is still somewhat controversial, and so we continue to use the above expression given by Stokes. Once again, the normal stresses are important only where the derivatives  $\partial u / \partial x$ ,  $\partial v / \partial y$ , and  $\partial w / \partial z$  are very large. For most practical flow problems,  $\tau_{xx}$ ,  $\tau_{yy}$ , and  $\tau_{zz}$  are small, and hence the uncertainty regarding  $\lambda$  is essentially an academic question. An example where the normal stress is important is inside the internal structure of a shock wave. Recall that, in real life, shock waves have a finite but small thickness. If we consider a normal shock wave across which large changes in velocity occur over a small distance (typically  $10^{-5}$  cm), then clearly  $\partial u / \partial x$  will be very large, and  $\tau_{xx}$  becomes important inside the shock wave.

To this point in our discussion, the transport coefficients  $\mu$  and  $\kappa$  have been considered molecular phenomena, involving the transport of momentum and energy by random molecular motion. This molecular picture prevails in a laminar flow. The values of  $\mu$  and  $\kappa$  are physical properties of the fluid; i.e., their values for different gases can be found in standard reference sources, such as the *Handbook of Chemistry and Physics* (The Chemical Rubber Co.). In contrast, for a turbulent flow the transport of momentum and energy can also take place by random motion of large turbulent eddies, or globs of fluid. This turbulent transport gives rise to effective values of viscosity and thermal conductivity defined as *eddy viscosity*,  $\epsilon$ , and *eddy thermal conductivity*,  $\kappa$ , respectively (Please do not confuse this use of the symbols  $\epsilon$  and  $\kappa$  with the time rate of strain and strain itself, as used earlier.) These turbulent transport coefficients  $\epsilon$  and  $\kappa$  can be much larger (typically 10 to 100 times larger) than the respective molecular values  $\mu$  and  $\kappa$ . Moreover,  $\epsilon$  and  $\kappa$  predominantly depend on characteristics of the flow field, such as velocity gradients; they are not just a molecular property of the fluid such as  $\mu$  and  $\kappa$ . The proper calculation of  $\epsilon$  and  $\kappa$  for a given flow has remained a state-of-the-art research question for the past 80 years; indeed, the attempt to model the complexities of turbulence by defining an eddy viscosity and thermal conductivity is even questionable. The details and basic understanding of turbulence remain one of the greatest unsolved problems in physics today. For our purpose here, we simply adopt the ideas of eddy viscosity and eddy thermal conductivity, and for the transport of momentum and energy in a turbulent flow, we replace  $\mu$  and  $\kappa$  in Eqs. (15.1) to (15.10) by the combination  $\mu + \epsilon$  and  $\kappa + \kappa$ , that is,

$$\tau_{xy} = (\mu + \epsilon) \left( \frac{\partial v}{\partial x} + \frac{\partial u}{\partial y} \right)$$

$$q_y = -(k + \kappa) \frac{\partial T}{\partial y}$$

An example of the calculation of  $\epsilon$  and  $\kappa$  is as follows. In 1925, Prandtl suggested that

$$\epsilon = \rho l^2 \left| \frac{\partial u}{\partial y} \right| \quad (15.12)$$

for a flow where the dominant velocity gradient is in the  $y$  direction. In Eq. (15.12),  $l$  is called the *mixing length*, which is different for different applications; it is an empirical constant which must be obtained from experiment. Indeed, *all* turbulence models require the input of empirical data; no self-contained purely theoretical turbulence model exists today. Prandtl's mixing length theory, embodied in Eq. (15.12), is a simple relation which appears to be adequate for a number of engineering problems. For these reasons, the mixing length model for  $\epsilon$  has been used extensively since 1925. In regard to  $\kappa$ , a relation similar to Eq. (15.4) can be assumed (using 1.0 for the constant), that is,

$$\kappa = \epsilon c_p \quad (15.13)$$

The above comments on eddy viscosity and thermal conductivity are purely introductory. The modern aerodynamicist has a whole stable of turbulence models to choose from, and before tackling the analysis of a turbulent flow, you should be familiar with the modern approaches described in such books as Refs. 42 to 45.

#### 15.4 THE NAVIER-STOKES EQUATIONS

In Chap. 2, Newton's second law was applied to obtain the fluid-flow momentum equation in both integral and differential forms. In particular, recall Eqs. (2.104a to c), where the influence of viscous forces was expressed simply by the generic terms  $(\mathcal{F}_x)_{\text{viscous}}$ ,  $(\mathcal{F}_y)_{\text{viscous}}$ , and  $(\mathcal{F}_z)_{\text{viscous}}$ . The purpose of this section is to obtain the analogous forms of Eqs. (2.104a to c) where the viscous forces are expressed explicitly in terms of the appropriate flow-field variables. The resulting equations are called the *Navier-Stokes equations* — probably the most pivotal equations in all of theoretical fluid dynamics.

In Sec. 2.3 we discussed the philosophy behind the derivation of the governing equations, namely, that certain physical principles are applied to a suitable *model* of the fluid flow. Moreover, we saw that such a model could be either a finite control volume (moving or fixed in space) or an infinitesimally small element (moving or fixed in space). In Chap. 2, we chose the fixed, finite control volume for our model and obtained integral forms of the continuity, momentum, and energy equations directly from this model. Then, indirectly, we went on to extract partial differential equations from the integral forms. Before progressing further, it would be wise for you to review these matters from Chap. 2.

For the sake of variety, let us not use the fixed, finite control volume employed in Chap. 2; rather, in this section, let us adopt an infinitesimally small moving fluid element of fixed mass as our model of the flow, as sketched in Fig. 15.11. To this model let us apply Newton's second law in the form  $\mathbf{F} = m\mathbf{a}$ . Moreover, for the time being consider only the  $x$  component of Newton's second law:

$$F_x = ma_x \quad (15.14)$$

In Eq. (15.14),  $F_x$  is the sum of all the body and surface forces acting on the fluid element in the  $x$  direction. Let us ignore body forces; hence, the net force acting on the element in Fig. 15.11 is simply due to the pressure and viscous stress distributions over

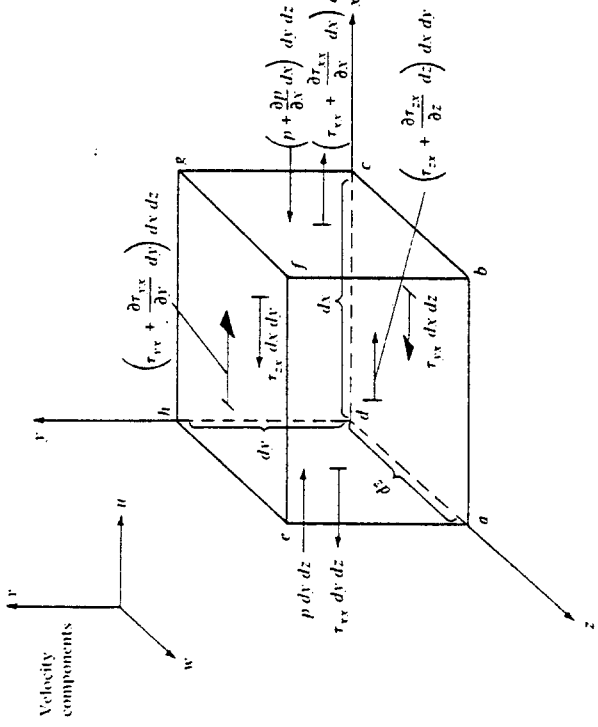


Figure 15.11 Infinitesimally small, moving fluid element. Only the forces in the  $x$  direction are shown.

the surface of the element. For example, on face  $abcd$ , the only force in the  $x$  direction is that due to shear stress,  $\tau_{xy} dy dz$ . Face  $efgh$  is a distance  $dy$  above face  $abcd$ ; hence, the shear force in the  $x$  direction on face  $efgh$  is  $[\tau_{yy} + (\partial \tau_{yy}/\partial y) dy] dx dz$ . Note the directions of the shear stress on faces  $abcd$  and  $efgh$ ; on the bottom face,  $\tau_{xy}$  is to the left (the negative  $x$  direction), whereas on the top face,  $\tau_{yy} + (\partial \tau_{yy}/\partial y) dy$  is to the right (the positive  $x$  direction). These directions are due to the convention that positive increases in all three components of velocity,  $u$ ,  $v$ , and  $w$ , occur in the positive directions of the axes. For example, in Fig. 15.11,  $u$  is higher just above the face than on the face; this causes a "jutting" action which tries to pull the fluid element in the positive  $x$  direction (to the right) as shown in Fig. 15.11. In turn, concentrating on face  $abcd$ ,  $u$  is lower just beneath the face than on the face; this causes a retarding or dragging action on the fluid element, which acts in the negative  $x$  direction (to the left), as shown in Fig. 15.11. The directions of all the other viscous stresses shown in Fig. 15.11, including  $\tau_{zz}$ , can be justified in a like fashion. Specifically, on face  $degh$ ,  $\tau_{zz}$  acts in the negative  $x$  direction, whereas on face  $abfe$ ,  $\tau_{xx} + (\partial \tau_{xx}/\partial z) dz$  acts in the positive  $x$  direction. On face  $adhe$ , which is perpendicular to the  $x$  axis, the only forces in the  $x$  direction are the pressure force  $p dy dz$ , which always acts in the direction *into* the fluid element, and  $\tau_{xx} dy dz$ , which is in the negative  $x$  direction. In Fig. 15.11, the reason why  $\tau_{xx}$  on face  $adhe$  is to the left hinges on the convention mentioned earlier for the direction of increasing velocity. Here, by convention, a positive increase in  $u$  takes place in the positive  $x$  direction. Hence, the value of  $u$  just to the left of face  $adhe$  is smaller than the value of  $u$  on the face itself. As a result, the viscous action of the

normal stress acts as a "suction" on face  $adhe$ , i.e., there is a dragging action toward the left that wants to retard the motion of the fluid element. In contrast, on face  $bcgf$ , the pressure force  $[p + (\partial p/\partial x) dx] dy dz$  presses inward on the fluid element (in the negative  $x$  direction), and because the value of  $u$  just to the right of face  $bcgf$  is larger than the value of  $u$  on the face, there is a "suction" due to the viscous normal stress which tries to pull the element to the right (in the positive  $x$  direction) with a force equal to  $[\tau_{xx} + (\partial \tau_{xx}/\partial x) dx] dy dz$ .

Return to Eq. (15.14). Examining Fig. 15.11 in light of our previous discussion, we can write for the net force in the  $x$  direction acting on the fluid element:

$$\begin{aligned} F_x &= \left[ p - \left( p + \frac{\partial p}{\partial x} dx \right) \right] dy dz + \left[ \left( \tau_{xx} + \frac{\partial \tau_{xx}}{\partial x} dx \right) - \tau_{xx} \right] dy dz \\ &\quad + \left[ \left( \tau_{yx} + \frac{\partial \tau_{yx}}{\partial y} dy \right) - \tau_{yx} \right] dx dz + \left[ \left( \tau_{zx} + \frac{\partial \tau_{zx}}{\partial z} dz \right) - \tau_{zx} \right] dx dy \\ \text{or } F_x &= \left( -\frac{\partial p}{\partial x} + \frac{\partial \tau_{xx}}{\partial x} + \frac{\partial \tau_{yx}}{\partial y} + \frac{\partial \tau_{zx}}{\partial z} \right) dx dy dz \end{aligned} \quad (15.15)$$

Equation (15.15) represents the left-hand side of Eq. (15.14). Considering the right-hand side of Eq. (15.14), recall that the mass of the fluid element is fixed and is equal to

$$m = \rho dx dy dz \quad (15.16)$$

Also, recall that the acceleration of the fluid element is the time rate of change of its velocity. Hence, the component of acceleration in the  $x$  direction, denoted by  $a_x$ , is simply the time rate of change of  $u$ ; since we are following a moving fluid element, this time rate of change is given by the *substantial derivative* (see Sec. 2.9 for a review of the meaning of substantial derivative). Thus,

$$a_x = \frac{Du}{Dt} \quad (15.17)$$

Combining Eqs. (15.14) to (15.17), we obtain

$$\rho \frac{Du}{Dt} = -\frac{\partial p}{\partial x} + \frac{\partial \tau_{xx}}{\partial x} + \frac{\partial \tau_{yx}}{\partial y} + \frac{\partial \tau_{zx}}{\partial z} \quad (15.18a)$$

which is the  $x$  component of the momentum equation for a viscous flow. In a similar fashion, the  $y$  and  $z$  components can be obtained as

$$\rho \frac{Dv}{Dt} = -\frac{\partial p}{\partial y} + \frac{\partial \tau_{xy}}{\partial x} + \frac{\partial \tau_{yy}}{\partial y} + \frac{\partial \tau_{yz}}{\partial z} \quad (15.18b)$$

$$\rho \frac{Dw}{Dt} = -\frac{\partial p}{\partial z} + \frac{\partial \tau_{xz}}{\partial x} + \frac{\partial \tau_{yz}}{\partial y} + \frac{\partial \tau_{zz}}{\partial z} \quad (15.18c)$$

Equations (15.18a to c) are the momentum equations in the  $x$ ,  $y$ , and  $z$  directions, respectively. They are scalar equations and are called the *Navier-Stokes* equations in honor of two men—the Frenchman M. Navier and the Englishman G. Stokes—who independently obtained the equations in the first half of the nineteenth century.

With the expressions for  $\tau_{xy} = \tau_{yx}$ ,  $\tau_{yz} = \tau_{zy}$ ,  $\tau_{zx} = \tau_{xz}$ ,  $\tau_{yy} = \tau_{yy}$ , and  $\tau_{zz}$  from Eqs. (15.5) to (15.10), the Navier-Stokes equations, Eqs. (15.18a to c) can be written as

$$\begin{aligned} \rho \frac{\partial u}{\partial t} + \rho u \frac{\partial u}{\partial x} + \rho v \frac{\partial u}{\partial y} + \rho w \frac{\partial u}{\partial z} &= -\frac{\partial p}{\partial x} + \frac{\partial}{\partial x} \left( \lambda \nabla \cdot \mathbf{V} + 2\mu \frac{\partial u}{\partial x} \right) \\ &+ \frac{\partial}{\partial y} \left[ \mu \left( \frac{\partial v}{\partial x} + \frac{\partial u}{\partial y} \right) \right] + \frac{\partial}{\partial z} \left[ \mu \left( \frac{\partial w}{\partial z} + \frac{\partial u}{\partial x} \right) \right] \end{aligned} \quad (15.19a)$$

$$\begin{aligned} \rho \frac{\partial v}{\partial t} + \rho u \frac{\partial v}{\partial x} + \rho v \frac{\partial v}{\partial y} + \rho w \frac{\partial v}{\partial z} &= -\frac{\partial p}{\partial y} + \frac{\partial}{\partial y} \left[ \mu \left( \frac{\partial v}{\partial x} + \frac{\partial u}{\partial y} \right) \right] \\ &+ \frac{\partial}{\partial z} \left( \lambda \nabla \cdot \mathbf{V} + 2\mu \frac{\partial v}{\partial y} \right) + \frac{\partial}{\partial x} \left[ \mu \left( \frac{\partial w}{\partial y} + \frac{\partial v}{\partial z} \right) \right] \end{aligned} \quad (15.19b)$$

$$\begin{aligned} \rho \frac{\partial w}{\partial t} + \rho u \frac{\partial w}{\partial x} + \rho v \frac{\partial w}{\partial y} + \rho w \frac{\partial w}{\partial z} &= -\frac{\partial p}{\partial z} + \frac{\partial}{\partial z} \left[ \mu \left( \frac{\partial w}{\partial z} + \frac{\partial u}{\partial x} \right) \right] \\ &+ \frac{\partial}{\partial y} \left[ \mu \left( \frac{\partial w}{\partial y} + \frac{\partial v}{\partial z} \right) \right] + \frac{\partial}{\partial x} \left( \lambda \nabla \cdot \mathbf{V} + 2\mu \frac{\partial w}{\partial z} \right) \end{aligned} \quad (15.19c)$$

Equations (15.19a to c) represent the complete Navier-Stokes equations for an unsteady, compressible, three-dimensional viscous flow. To analyze incompressible viscous flow, Eqs. (15.19a to c) and the continuity equation [say, Eq. (2.43)] are sufficient. However, for a compressible flow, we need an additional equation, namely, the energy equation to be discussed in the next section.

In the above form, the Navier-Stokes equations are suitable for the analysis of laminar flow. For a turbulent flow, the flow variables in Eqs. (15.19a to c) can be assumed to be time-mean values over the turbulent fluctuations, and  $\mu$  can be replaced by  $\mu + \epsilon$ , as discussed in Sec. 15.3. For more details, see Refs. 42 and 43.

## 15.5 THE VISCOUS FLOW ENERGY EQUATION

The energy equation was derived in Sec. 2.7, where the first law of thermodynamics was applied to a finite control volume fixed in space. The resulting integral form of the energy equation was given by Eq. (2.86), and differential forms were obtained in Eqs. (2.87) and (2.105). In these equations, the influence of viscous effects were

expressed generically by such terms as  $\dot{Q}'_{viscous}$  and  $\dot{W}'_{viscous}$ . It is recommended that you review Sec. 2.7 before progressing further.

In the present section, we derive the energy equation for a viscous flow using as our model an infinitesimal moving fluid element. This will be in keeping with our derivation of the Navier-Stokes equation in Sec. 15.4, where the infinitesimal element was shown in Fig. 15.11. In the process, we obtain explicit expressions for  $\dot{Q}'_{viscous}$  and  $\dot{W}'_{viscous}$  in terms of the flow-field variables. That is, we once again derive Eq. (2.105), except the viscous terms are now displayed in detail.

Consider again the moving fluid element shown in Fig. 15.11. To this element, apply the first law of thermodynamics, which states

$$\text{Rate of change of energy inside fluid element} = \text{heat into element} + \text{done on element due to pressure and stress forces on surface} \quad (15.20)$$

or

where  $A$ ,  $B$ , and  $C$  denote the respective terms above.

Let us first evaluate  $C$ , i.e., let us obtain an expression for the rate of work done on the moving fluid element due to the pressure and stress forces on the surface of the element. (Note that we are neglecting body forces in this derivation.) These surface forces are illustrated in Fig. 15.11, which for simplicity shows only the forces in the  $x$  direction. Recall from Sec. 2.7 that the rate of doing work by a force exerted on a moving body is equal to the product of the force and the component of velocity in the direction of the force. Hence, the rate of work done on the moving fluid element by the forces in the  $x$  direction shown in Fig. 15.11 is simply the  $x$  component of velocity,  $u$ , multiplied by the forces; e.g., on face  $abcd$  the rate of work done by  $\tau_{yx} dx dz$  is  $\tau_{yx} dx dz$ , with similar expressions for the other faces. To emphasize these energy considerations, the moving fluid element is redrawn in Fig. 15.12, where the rate of work done on each face by forces in the  $x$  direction is shown explicitly. Study this figure carefully, referring frequently to its companion in Fig. 15.11, until you feel comfortable with the work terms given in each face. To obtain the net rate of work done on the fluid element by the forces in the  $x$  direction, note that forces in the positive  $x$  direction do positive work and that forces in the negative  $x$  direction do negative work. Hence, comparing the pressure forces on face  $adhe$  and  $bcef$  in Fig. 15.12, the net rate of work done by pressure in the  $x$  direction is

$$\left[ up - \left( up + \frac{\partial(u\tau_y)}{\partial x} dx \right) \right] dy dz = -\frac{\partial(up)}{\partial x} dy dz$$

Similarly, the net rate of work done by the shear stresses in the  $x$  direction on faces  $abcd$  and  $efgh$  is

$$\left[ \left( u\tau_x + \frac{\partial(u\tau_y)}{\partial y} dy \right) - u\tau_y \right] dx dz = \frac{\partial(u\tau_y)}{\partial y} dx dy dz$$

Considering all the forces shown in Fig. 15.12, the net rate of work done on the moving fluid element is simply

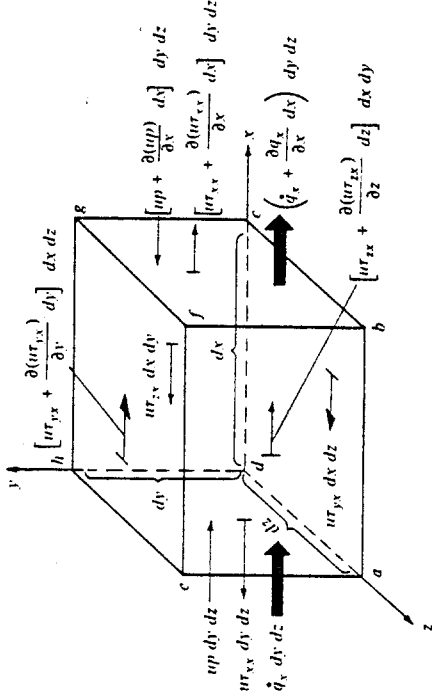


Figure 15.12 Energy fluxes associated with an infinitesimally small, moving fluid element. For simplicity, only the fluxes in the  $x$  direction are shown.

$$\left[ -\frac{\partial(up)}{\partial x} + \frac{\partial(ur_x)}{\partial x} + \frac{\partial(ur_{xy})}{\partial y} + \frac{\partial(ur_{xz})}{\partial z} \right] dx dy dz$$

The above expression considers only forces in the  $x$  direction. When the forces in the  $y$  and  $z$  directions are also included, similar expressions are obtained (draw some pictures and obtain these expressions yourself). In total, the net rate of work done on the moving fluid element is the sum of all contributions in the  $x$ ,  $y$ , and  $z$  directions; this is denoted by  $C$  in Eq. (15.20) and is given by

$$C = \left[ -\left( \frac{\partial(up)}{\partial x} + \frac{\partial(vp)}{\partial y} + \frac{\partial(wp)}{\partial z} \right) + \frac{\partial(ur_x)}{\partial x} + \frac{\partial(ur_{xy})}{\partial y} + \frac{\partial(ur_{xz})}{\partial z} \right. \\ \left. + \frac{\partial(ur_{xy})}{\partial x} + \frac{\partial(vr_y)}{\partial x} + \frac{\partial(vr_{yz})}{\partial y} + \frac{\partial(vr_z)}{\partial z} + \frac{\partial(wr_x)}{\partial x} \right. \\ \left. + \frac{\partial(wr_{yz})}{\partial y} + \frac{\partial(wr_z)}{\partial z} \right] dx dy dz \quad (15.21)$$

Note in Eq. (15.21) that the term in large parentheses is simply  $\nabla \cdot p \mathbf{V}$ .

Let us turn our attention to  $B$  in Eq. (15.20), i.e., the net flux of heat into the element. This heat flux is due to (1) volumetric heating such as absorption or emission of radiation and (2) heat transfer across the surface due to temperature gradients (i.e., thermal conduction). Let us treat the volumetric heating the same as was done in Sec. 2.7; that is, define  $\dot{q}$  as the rate of volumetric heat addition per unit mass. Noting that the mass of the moving fluid element in Fig. 15.12 is  $\rho dx dy dz$ , we obtain

$$\text{Volumetric heating of element} = \dot{q} \rho dx dy dz \quad (15.22)$$

Thermal conduction was discussed in Sec. 15.3. In Fig. 15.12, the heat transferred by thermal conduction into the moving fluid element across face  $adhe$  is  $\dot{q}_v dx dy dz$ , and

the heat transferred out of the element across face  $bcef$  is  $[\dot{q}_v + (\partial q_x / \partial x) dx] dy dz$ . Thus, the net heat transferred in the  $x$  direction into the fluid element by thermal conduction is

$$\left[ \dot{q}_v - \left( \dot{q}_v + \frac{\partial q_x}{\partial x} dx \right) \right] dy dz = - \frac{\partial q_x}{\partial x} dx dy dz \quad (15.23)$$

Taking into account heat transfer in the  $y$  and  $z$  direction across the other faces in Fig. 15.12, we obtain

$$\begin{aligned} \text{Heating of fluid element by thermal conduction} &= - \left( \frac{\partial \dot{q}_v}{\partial x} + \frac{\partial \dot{q}_y}{\partial y} + \frac{\partial \dot{q}_z}{\partial z} \right) dx dy dz \end{aligned} \quad (15.23)$$

The term  $B$  in Eq. (15.20) is the sum of Eqs. (15.22) and (15.23). Also, recalling that thermal conduction is proportional to temperature gradient, as exemplified by Eq. (15.2), we have

$$B = \left[ \rho \dot{q} + \frac{\partial}{\partial x} \left( k \frac{\partial T}{\partial x} \right) + \frac{\partial}{\partial y} \left( k \frac{\partial T}{\partial y} \right) + \frac{\partial}{\partial z} \left( k \frac{\partial T}{\partial z} \right) \right] dx dy dz \quad (15.24)$$

Finally, the term  $A$  in Eq. (15.20) denotes the time rate of change of energy of the fluid element. In Sec. 2.7, we stated that the energy of a moving fluid per unit mass is the sum of the internal and kinetic energies, for example,  $e + V^2/2$ . Since we are following a moving fluid element, the time rate of change of energy per unit mass is given by the substantial derivative (see Sec. 2.9). Since the mass of the fluid element is  $\rho dx dy dz$ , we have

$$A = \rho \frac{D}{Dt} \left( e + \frac{V^2}{2} \right) dx dy dz \quad (15.25)$$

The final form of the energy equation for a viscous flow is obtained by substituting Eqs. (15.21), (15.24), and (15.25) into Eq. (15.20), obtaining

$$\rho \frac{D(e + V^2/2)}{Dt} = \rho \dot{q} + \frac{\partial}{\partial x} \left( k \frac{\partial T}{\partial x} \right) + \frac{\partial}{\partial y} \left( k \frac{\partial T}{\partial y} \right) + \frac{\partial}{\partial z} \left( k \frac{\partial T}{\partial z} \right) - \nabla \cdot p \mathbf{V} + \frac{\partial(u\tau_{xx})}{\partial x} + \frac{\partial(v\tau_{yy})}{\partial y} + \frac{\partial(w\tau_{zz})}{\partial z} \\ + \frac{\partial(u\tau_{xy})}{\partial x} + \frac{\partial(v\tau_{yz})}{\partial y} + \frac{\partial(w\tau_{zx})}{\partial z} + \frac{\partial(u\tau_{xz})}{\partial z} + \frac{\partial(v\tau_{yz})}{\partial y} + \frac{\partial(w\tau_{xy})}{\partial x} \quad (15.26)$$

Equation (15.26) is the general energy equation for unsteady, compressible, three-dimensional, viscous flow. Compare Eq. (15.26) with Eq. (2.105); the viscous terms are now explicitly spelled out in Eq. (15.26). [Note that the body force term in Eq. (15.26) has been neglected.] Moreover, the normal and shear stresses that appear

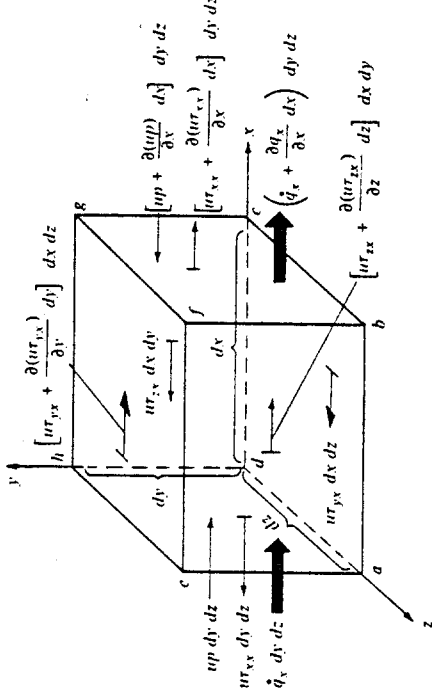


Figure 15.12 Energy fluxes associated with an infinitesimally small, moving fluid element. For simplicity, only the fluxes in the  $x$  direction are shown.

$$\left[ -\frac{\partial(up)}{\partial x} + \frac{\partial(ur_x)}{\partial x} + \frac{\partial(ur_{xy})}{\partial y} + \frac{\partial(ur_{xz})}{\partial z} \right] dx dy dz$$

The above expression considers only forces in the  $x$  direction. When the forces in the  $y$  and  $z$  directions are also included, similar expressions are obtained (draw some pictures and obtain these expressions yourself). In total, the net rate of work done on the moving fluid element is the sum of all contributions in the  $x$ ,  $y$ , and  $z$  directions; this is denoted by  $C$  in Eq. (15.20) and is given by

$$C = \left[ -\left( \frac{\partial(up)}{\partial x} + \frac{\partial(vp)}{\partial y} + \frac{\partial(wp)}{\partial z} \right) + \frac{\partial(ur_x)}{\partial x} + \frac{\partial(ur_{xy})}{\partial y} + \frac{\partial(ur_{xz})}{\partial z} \right. \\ \left. + \frac{\partial(ur_{xy})}{\partial x} + \frac{\partial(vr_y)}{\partial x} + \frac{\partial(vr_{yz})}{\partial y} + \frac{\partial(vr_z)}{\partial z} + \frac{\partial(wr_x)}{\partial x} \right. \\ \left. + \frac{\partial(wr_{yz})}{\partial y} + \frac{\partial(wr_z)}{\partial z} \right] dx dy dz \quad (15.21)$$

Note in Eq. (15.21) that the term in large parentheses is simply  $\nabla \cdot p \mathbf{V}$ .

Let us turn our attention to  $B$  in Eq. (15.20), i.e., the net flux of heat into the element. This heat flux is due to (1) volumetric heating such as absorption or emission of radiation and (2) heat transfer across the surface due to temperature gradients (i.e., thermal conduction). Let us treat the volumetric heating the same as was done in Sec. 2.7; that is, define  $\dot{q}$  as the rate of volumetric heat addition per unit mass. Noting that the mass of the moving fluid element in Fig. 15.12 is  $\rho dx dy dz$ , we obtain

$$\text{Volumetric heating of element} = \dot{q} \rho dx dy dz \quad (15.22)$$

Thermal conduction was discussed in Sec. 15.3. In Fig. 15.12, the heat transferred by thermal conduction into the moving fluid element across face  $adhe$  is  $\dot{q}_v dy dz$ , and

the heat transferred out of the element across face  $bcef$  is  $[\dot{q}_v + (\partial q_x / \partial x) dx] dy dz$ . Thus, the net heat transferred in the  $x$  direction into the fluid element by thermal conduction is

$$\left[ \dot{q}_v - \left( \dot{q}_v + \frac{\partial q_x}{\partial x} dx \right) \right] dy dz = - \frac{\partial q_x}{\partial x} dx dy dz \quad (15.23)$$

Taking into account heat transfer in the  $y$  and  $z$  direction across the other faces in Fig. 15.12, we obtain

$$\begin{aligned} \text{Heating of fluid element by thermal conduction} &= - \left( \frac{\partial \dot{q}_v}{\partial x} + \frac{\partial \dot{q}_y}{\partial y} + \frac{\partial \dot{q}_z}{\partial z} \right) dx dy dz \end{aligned} \quad (15.23)$$

The term  $B$  in Eq. (15.20) is the sum of Eqs. (15.22) and (15.23). Also, recalling that thermal conduction is proportional to temperature gradient, as exemplified by Eq. (15.2), we have

$$B = \left[ \rho \dot{q} + \frac{\partial}{\partial x} \left( k \frac{\partial T}{\partial x} \right) + \frac{\partial}{\partial y} \left( k \frac{\partial T}{\partial y} \right) + \frac{\partial}{\partial z} \left( k \frac{\partial T}{\partial z} \right) \right] dx dy dz \quad (15.24)$$

Finally, the term  $A$  in Eq. (15.20) denotes the time rate of change of energy of the fluid element. In Sec. 2.7, we stated that the energy of a moving fluid per unit mass is the sum of the internal and kinetic energies, for example,  $e + V^2/2$ . Since we are following a moving fluid element, the time rate of change of energy per unit mass is given by the substantial derivative (see Sec. 2.9). Since the mass of the fluid element is  $\rho dx dy dz$ , we have

$$A = \rho \frac{D}{Dt} \left( e + \frac{V^2}{2} \right) dx dy dz \quad (15.25)$$

The final form of the energy equation for a viscous flow is obtained by substituting Eqs. (15.21), (15.24), and (15.25) into Eq. (15.20), obtaining

$$\rho \frac{D(e + V^2/2)}{Dt} = \rho \dot{q} + \frac{\partial}{\partial x} \left( k \frac{\partial T}{\partial x} \right) + \frac{\partial}{\partial y} \left( k \frac{\partial T}{\partial y} \right) + \frac{\partial}{\partial z} \left( k \frac{\partial T}{\partial z} \right) - \nabla \cdot p \mathbf{V} + \frac{\partial(u\tau_{xx})}{\partial x} + \frac{\partial(v\tau_{yy})}{\partial y} + \frac{\partial(w\tau_{zz})}{\partial z} \\ + \frac{\partial(u\tau_{xy})}{\partial x} + \frac{\partial(v\tau_{yz})}{\partial y} + \frac{\partial(w\tau_{zx})}{\partial z} + \frac{\partial(u\tau_{xz})}{\partial z} + \frac{\partial(v\tau_{yz})}{\partial y} + \frac{\partial(w\tau_{xy})}{\partial x} \quad (15.26)$$

Equation (15.26) is the general energy equation for unsteady, compressible, three-dimensional, viscous flow. Compare Eq. (15.26) with Eq. (2.105); the viscous terms are now explicitly spelled out in Eq. (15.26). [Note that the body force term in Eq. (15.26) has been neglected.] Moreover, the normal and shear stresses that appear



velocity as a function of the *nondimensional* coordinates is the same for the two flows. How did we obtain Eq. (15.30)? Simply by saying that  $\gamma$ ,  $M_x$ , and  $RC_x$  are the same for the two flows and that the two bodies are geometrically similar. *These are precisely the criteria for two flows to be dynamically similar*, as originally stated in Sec. 1.8.

What we have seen in the above derivation is a formal mechanism to identify governing similarity parameters for a flow. By couching the governing flow equations in terms of nondimensional variables, the coefficients of the derivatives in these equations are dimensionless similarity parameters or combinations thereof.

To see this more clearly, and to extend our analysis further, consider the energy equation for a steady, two-dimensional, viscous, compressible flow, which from Eq. (15.26) can be written as (assuming no volumetric heating and neglecting the normal stresses)

$$\begin{aligned} \rho u \frac{\partial(e + V^2/2)}{\partial x} + \rho v \frac{\partial(e + V^2/2)}{\partial y} &= \frac{\partial}{\partial x} \left( k \frac{\partial T}{\partial y} \right) + \frac{\partial}{\partial y} \left( k \frac{\partial T}{\partial x} \right) - \frac{\partial(u p)}{\partial x} \\ &\quad - \frac{\partial(v p)}{\partial y} + \frac{\partial(v \tau_v)}{\partial x} + \frac{\partial(u \tau_u)}{\partial y} \end{aligned} \quad (15.31)$$

Substituting Eq. (15.5) into (15.31), we have

$$\begin{aligned} \rho u \frac{\partial(e + V^2/2)}{\partial x} + \rho v \frac{\partial(e + V^2/2)}{\partial y} &= \frac{\partial}{\partial x} \left( k \frac{\partial T}{\partial x} \right) + \frac{\partial}{\partial y} \left( k \frac{\partial T}{\partial y} \right) \\ &\quad - \frac{\partial(u p)}{\partial x} - \frac{\partial(v p)}{\partial y} \\ &\quad + \frac{\partial}{\partial x} \left[ \mu u \left( \frac{\partial v}{\partial x} + \frac{\partial u}{\partial y} \right) \right] \\ &\quad + \frac{\partial}{\partial y} \left[ \mu u \left( \frac{\partial v}{\partial x} + \frac{\partial u}{\partial y} \right) \right] \end{aligned} \quad (15.32)$$

Using the same nondimensional variables as before, and introducing

$$\begin{aligned} e' &= \frac{e}{c_v T_x}, \quad k' = \frac{k}{k_x}, \quad V'^2 = \frac{V^2}{V_x^2} = \frac{u'^2 + v'^2}{V_x^2} = (u')^2 + (v')^2 \\ \text{Eq. (15.32) can be written as} \quad \frac{\rho_x V_x^3}{c} \left( \rho' u' \frac{\partial e'}{\partial x} + \rho' v' \frac{\partial e'}{\partial y} \right) &= \\ &\quad - \frac{\rho_x V_x^3}{c} \left[ \rho' u' \frac{\partial}{\partial x} \left( u'^2 + v'^2 \right) + \rho' v' \frac{\partial}{\partial y} \left( u'^2 + v'^2 \right) \right] \\ &\quad + \frac{k_x T_x}{c^2} \left[ \frac{\partial}{\partial x} \left( k' \frac{\partial T'}{\partial x} \right) + \frac{\partial}{\partial y} \left( k' \frac{\partial T'}{\partial y} \right) \right] - \frac{V_x \rho_x}{c} \left( \frac{\partial(u' p')}{\partial x} + \frac{\partial(v' p')}{\partial y} \right) \\ &\quad + \frac{\mu_x V_x^2}{c^2} \left\{ \frac{\partial}{\partial x} \left[ \mu' u' \left( \frac{\partial v'}{\partial x} + \frac{\partial u'}{\partial y} \right) \right] + \frac{\partial}{\partial y} \left[ \mu' u' \left( \frac{\partial v'}{\partial x} + \frac{\partial u'}{\partial y} \right) \right] \right\} \end{aligned} \quad (15.33)$$

How did we obtain Eq. (15.30)? Simply by saying that  $\gamma$ ,  $M_x$ , and  $RC_x$  are the same for the two flows and that the two bodies are geometrically similar. *These are precisely the criteria for two flows to be dynamically similar*, as originally stated in Sec. 1.8.

What we have seen in the above derivation is a formal mechanism to identify governing similarity parameters for a flow. By couching the governing flow equations in terms of nondimensional variables, the coefficients of the derivatives in these equations are dimensionless similarity parameters or combinations thereof.

To see this more clearly, and to extend our analysis further, consider the energy equation for a steady, two-dimensional, viscous, compressible flow, which from Eq. (15.26) can be written as (assuming no volumetric heating and neglecting the normal stresses)

Examining the coefficients of each term on the right-hand side of Eq. (15.32a), we find consecutively

$$\begin{aligned} \frac{V_x^2}{c_v T_x} &= \frac{(\gamma - 1)V_x^2}{R T_x} = \frac{\gamma(\gamma - 1)V_x^2}{\gamma R T_x} = \frac{\gamma(\gamma - 1)V_x^2}{a_x^2} = \gamma(\gamma - 1)M_x^2 \\ \frac{k_x}{c_p V_x c_v} &= \frac{k_x \gamma \mu_{x,p}}{c_p V_x c_p \mu_\infty} = \frac{\gamma}{\Pr_x \Re_x} \end{aligned}$$

*Note:* In the above, we have introduced a new dimensionless parameter, the *Prandtl number*,  $\Pr_x \equiv \mu_{x,p}/k_\infty$ , the significance of which will be discussed later.

$$\begin{aligned} \frac{p_x}{\rho_x c_v T_x} &= \frac{(\gamma - 1)p_x}{\rho_x R T_x} = \frac{(\gamma - 1)p_x}{p_\infty} = \gamma - 1 \\ \frac{\mu_x V_x}{c \rho_x c_v T_x} &= \frac{\mu_x}{c \rho_x V_x c_v} \left( \frac{V_x^2}{c_v T_x} \right) = \frac{1}{R \epsilon_x} (\gamma - 1) \frac{V_x^2}{R T_x} = \gamma(\gamma - 1) \frac{M_x^2}{R \epsilon_x} \end{aligned}$$

Hence, Eq. (15.32) can be written as

$$\rho' u' \frac{\partial e'}{\partial x} + \rho' v' \frac{\partial e'}{\partial y} = \gamma(\gamma - 1) M_x^2 \left[ \rho' u' \frac{\partial}{\partial x} (u'^2 + v'^2) \right. \\ \left. + \rho' v' \frac{\partial}{\partial y} (u'^2 + v'^2) \right]$$

$$\begin{aligned} &\quad + \frac{\gamma}{\Pr_x \Re_x} \left[ \frac{\partial}{\partial x} \left( k' \frac{\partial T'}{\partial x} \right) + \frac{\partial}{\partial y} \left( k' \frac{\partial T'}{\partial y} \right) \right] \\ &\quad - (\gamma - 1) \left( \frac{\partial(u' p')}{\partial x} + \frac{\partial(v' p')}{\partial y} \right) \\ &\quad + \gamma(\gamma - 1) \frac{M_x^2}{R \epsilon_x} \left\{ \frac{\partial}{\partial x} \left[ \mu' u' \left( \frac{\partial v'}{\partial x} + \frac{\partial u'}{\partial y} \right) \right] \right. \\ &\quad \left. + \frac{\partial}{\partial y} \left[ \mu' u' \left( \frac{\partial v'}{\partial x} + \frac{\partial u'}{\partial y} \right) \right] \right\} \end{aligned} \quad (15.33)$$

Examine Eq. (15.33). It is a nondimensional equation which, in principle, can be solved for  $e' = f(x', y')$ . If we have two different flows, but with the same values  $M_\infty$ ,  $Re_x$ , and  $Pr_x$ , Eq. (15.33) will be numerically identical for the two flows, and if we are considering geometrically similar bodies, then the solution  $e' = f(x', y')$  will be identical for the two flows.

Reflecting upon Eqs. (15.29) and (15.33), which are the nondimensional  $x$ -momentum and energy equations, respectively, we clearly see that the governing similarity parameters for a viscous, compressible flow are  $\gamma$ ,  $M_\infty$ ,  $Re_x$ , and  $Pr_x$ . If the above parameters are the same for two different flows with geometrically similar bodies, then the flows are dynamically similar. We obtained these results by considering the  $x$ -momentum equation and the energy equation, both in two dimensions. The same results would have occurred if we had considered three-dimensional flow and the  $y$ - and  $z$ -momentum equations.

Note that the similarity parameters  $\gamma$ ,  $M_\infty$ , and  $Re_x$  were obtained from the momentum equation. When the energy equation is considered, an additional similarity parameter is introduced, namely, the Prandtl number. On a physical basis, the Prandtl number is an index which is proportional to the ratio of energy dissipated by friction to the energy transported by thermal conduction; that is,

$$Pr = \frac{\mu_x C_p}{k} \frac{\text{frictional dissipation}}{\text{thermal conduction}}$$

In the study of compressible, viscous flow, Prandtl number is just as important as  $\gamma$ ,  $Re_x$ , or  $M_\infty$ . For air at standard conditions,  $Pr_x = 0.71$ . Note that  $Pr_x$  is a property of the gas. For different gases,  $Pr_x$  is different. Also, like  $\mu$  and  $k$ ,  $Pr_x$  is in general a function of temperature; however, for air over a reasonable temperature range (up to  $T_x = 600$  K), it is safe to assume  $Pr_x = \text{constant} = 0.71$ .

## 15.7 SOLUTIONS OF VISCOUS FLOWS

The governing continuity, momentum, and energy equations for a general unsteady, compressible, viscous, three-dimensional flow are given by Eqs. (2.43), (15.19a to c), and (15.26). Historically, only the momentum equations were called the Navier-Stokes equations; however, today the complete system of viscous flow equations listed above—the continuity, momentum, and energy equations—is frequently referred to in the modern literature as the “complete Navier-Stokes equations.” We adopt this nomenclature throughout the remainder of our discussions.

Examine these equations closely. They are nonlinear partial differential equations. There is no known general analytic solution to these equations. There do exist exact analytical solutions of the Navier-Stokes equations to a very few highly specialized flow geometries; such solutions are discussed in Ref. 42. However, for the vast bulk of practical viscous flow problems, aerodynamicists have had to make assumptions which simplify the Navier-Stokes equations. The boundary-layer assumption discussed in Chap. 16 is one of the most important and frequently used assumption which leads to tractable solutions.

On the other hand, the advent of computational fluid dynamics (CFD) during the past decade has revolutionized the solution of the complete Navier-Stokes equations. We are now able to obtain “exact” numerical solutions to these equations for laminar flows applied to a wide range of flow geometries and conditions. It is beyond the scope of this book to detail such numerical solutions. However, many viscous flows have been solved by means of the time-dependent technique discussed in Sec. 13.5. Here, the flow field of interest is covered with a mesh of grid points, and values for all the flow-field variables are assumed at all the grid points. These assumed values are the initial conditions at time  $t = 0$ . Now examine Eqs. (2.43), (15.19a to c), and (15.26); all the spatial derivatives in these equations can be replaced by finite differences using the known (in this case, the assumed) flow variables at  $t = 0$ . Hence, values of the time derivatives of the flow-field variables,  $\partial\rho/\partial t$ ,  $\partial u/\partial t$ , etc., can be obtained from these equations. In turn, these time derivatives are used to obtain new values of the flow variables at time  $t = \Delta t$ . The actual algorithm can be any one of several; however, MacCormack’s technique discussed in Sec. 13.5 has been a popular choice. This cycle is repeated over many time steps until the flow field converges to a steady state. The philosophy and implementation of such time-dependent solutions of viscous flows is exactly the same as discussed in Sec. 13.5—only the equations are different.

An example of the type of viscous flow that can readily be solved by such a time-dependent technique is the supersonic flow over a rearward-facing step. Results for the separated flow downstream of the step are shown in Figs. 15.13 and 15.14. These results are taken from Ref. 46, which utilized a time-dependent finite-difference solution of the complete two-dimensional Navier-Stokes equations by means of MacCormack’s technique. Such results are typical of modern CFD solutions to complicated viscous flow problems.

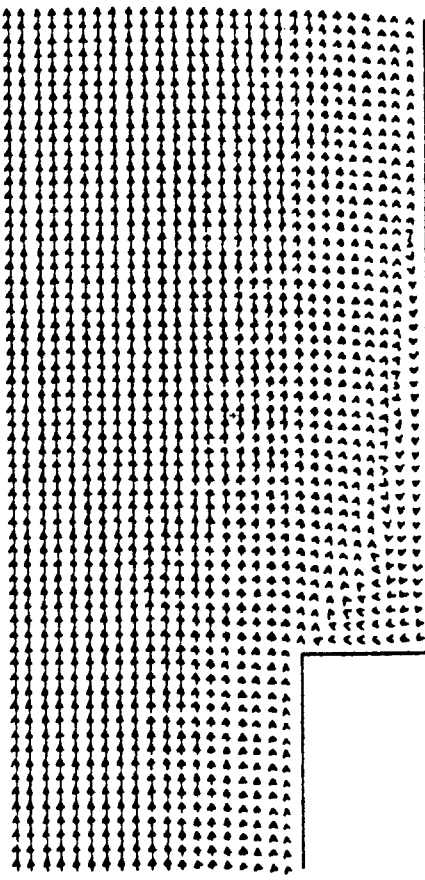


Figure 15.13 Velocity vector diagram for the flow over a rearward-facing step,  $M = 2.19$ ,  $T = 1005$  K,  $Re = 70,000$  (based on step height) (Ref. 46). Note the recirculating, separated flow region downstream of the step.

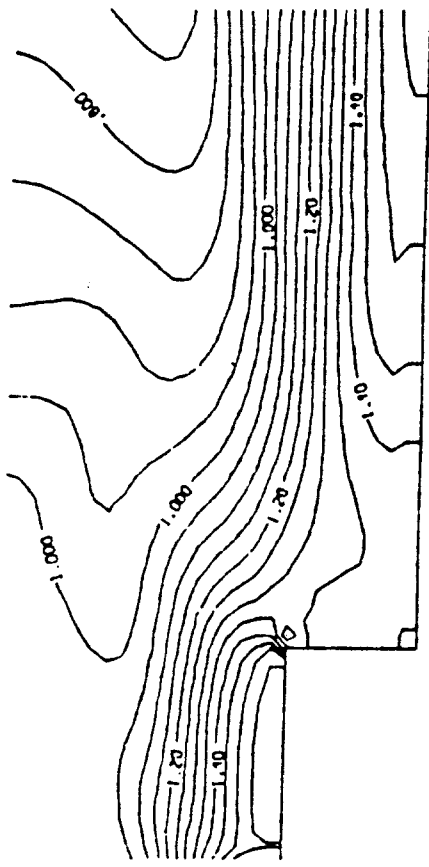


Figure 15.14 Temperature contours for the flow shown in Fig. 15.13. The separated region just downstream of the step is a reasonably constant pressure, constant temperature region.

As mentioned earlier, for the solution of turbulent flows, an effective eddy viscosity [such as  $\epsilon$  given in Eq. (15.12)] and eddy thermal conductivity [such as  $\kappa$  given in Eq. (15.13)] can be defined. In Eqs. (15.19a to c) and (15.26), the flow variables can be assumed to be time-mean values over the turbulent fluctuations, and  $\mu$  and  $k$  can be replaced by  $\mu + \epsilon$  and  $k + \kappa$ , respectively. Indeed, the numerical results shown in Figs. 15.13 and 15.14 assume an algebraic turbulence model similar to but more sophisticated than the simple model discussed in Sec. 15.3. It can be argued that numerical solutions of the complete time-averaged (sometimes called the *Reynolds averaged*) — see the quotation at the beginning of Chap. 13) Navier-Stokes equations using a turbulence model is not an exact solution of the flow due to uncertainty in the turbulence model. However, this is simply a matter of semantics; the equations using a given turbulence model are being solved exactly, although the true physics of the turbulent flow are only being approximated. Any numerical solution of a turbulent flow, today or in the future, will always be a slave to the existing state of the art of turbulence modeling.

## 15.8 SUMMARY

We have now completed the road map given in Fig. 15.1. The main results of this chapter are summarized below.

Shear stress and flow separation are two major ramifications of viscous flow. Shear stress is the cause of skin friction drag  $D_f$ , and flow separation is the source of pressure drag  $D_p$ , sometimes called form drag. Transition from laminar to turbulent flow causes  $D_f$  to increase and  $D_p$  to decrease.

Shear stress in a flow is due to velocity gradients, for example,  $\tau_{xy} = \mu \frac{\partial u}{\partial y}$  for a flow with gradients in the  $y$  direction. Similarly, heat conduction is due to temperature gradients, for example,  $\dot{q}_y = -k \frac{\partial T}{\partial y}$ , etc. Both  $\mu$  and  $k$  are physical properties of the gas and are functions of temperature.

The general equations of viscous flow are

$$x \text{ momentum: } \rho \frac{Du}{Dt} = -\frac{\partial p}{\partial x} + \frac{\partial \tau_{xx}}{\partial x} + \frac{\partial \tau_{xy}}{\partial y} + \frac{\partial \tau_{xz}}{\partial z} \quad (15.18a)$$

$$y \text{ momentum: } \rho \frac{Dv}{Dt} = -\frac{\partial p}{\partial y} + \frac{\partial \tau_{xy}}{\partial x} + \frac{\partial \tau_{yy}}{\partial y} + \frac{\partial \tau_{yz}}{\partial z} \quad (15.18b)$$

$$z \text{ momentum: } \rho \frac{Dw}{Dt} = -\frac{\partial p}{\partial z} + \frac{\partial \tau_{xz}}{\partial x} + \frac{\partial \tau_{yz}}{\partial y} + \frac{\partial \tau_{zz}}{\partial z} \quad (15.18c)$$

Energy:

$$\begin{aligned} \rho \frac{D(e + V^2/2)}{Dt} &= \rho \dot{q} + \frac{\partial}{\partial x} \left( k \frac{\partial T}{\partial x} \right) + \frac{\partial}{\partial y} \left( k \frac{\partial T}{\partial y} \right) + \frac{\partial}{\partial z} \left( k \frac{\partial T}{\partial z} \right) - \nabla \cdot p \mathbf{V} \\ &\quad + \frac{\partial(u\tau_{xx})}{\partial x} + \frac{\partial(u\tau_{xy})}{\partial y} + \frac{\partial(u\tau_{xz})}{\partial z} + \frac{\partial(v\tau_{yx})}{\partial x} + \frac{\partial(v\tau_{yy})}{\partial y} + \frac{\partial(v\tau_{yz})}{\partial z} \\ &\quad + \frac{\partial(w\tau_{zx})}{\partial x} + \frac{\partial(w\tau_{zy})}{\partial y} + \frac{\partial(w\tau_{zz})}{\partial z} \end{aligned} \quad (15.26)$$

where

$$\tau_{xy} = \tau_{yx} = \mu \left( \frac{\partial v}{\partial x} + \frac{\partial u}{\partial y} \right)$$

$$\tau_{yz} = \tau_{zy} = \mu \left( \frac{\partial w}{\partial y} + \frac{\partial v}{\partial z} \right)$$

$$\tau_{zx} = \tau_{xz} = \mu \left( \frac{\partial u}{\partial z} + \frac{\partial w}{\partial x} \right)$$

$$\tau_{yy} = \lambda(\nabla \cdot \mathbf{V}) + 2\mu \frac{\partial v}{\partial y}$$

$$\tau_{zz} = \lambda(\nabla \cdot \mathbf{V}) + 2\mu \frac{\partial w}{\partial z}$$

$$\tau_{xx} = \lambda(\nabla \cdot \mathbf{V}) + 2\mu \frac{\partial u}{\partial x}$$

The similarity parameters for a flow can be obtained by nondimensionalizing the governing equations; the coefficients in front of the nondimensionalized derivatives give the similarity parameters or combinations thereof. For a viscous, compressible flow, the main similarity parameters are  $\gamma$ ,  $M_\infty$ ,  $Re_\infty$ , and  $Pr_\infty$ .

---

CHAPTER  
**SIXTEEN**  
INTRODUCTION TO BOUNDARY LAYERS

---

Exact analytical solutions of the complete Navier-Stokes equations exist for only a few very specialized cases. Instead, the equations are frequently simplified by making appropriate approximations about the flow. In modern times, exact solutions of the complete Navier-Stokes equations for many practical problems can be obtained numerically, using various techniques of computational fluid dynamics.

### PROBLEMS

15.1 Consider the incompressible viscous flow of air between two infinitely long parallel plates separated by a distance  $h$ . The bottom plate is stationary, and the top plate is moving at the constant velocity  $u_e$  in the direction of the plate. Assume that no pressure gradient exists in the flow direction.

(a) Obtain an expression for the variation of velocity between the plates.

(b) If  $T = \text{constant} = 320\text{ K}$ ,  $u_e = 30\text{ m/s}$ , and  $h = 0.01\text{ m}$ , calculate the shear stress on the top and bottom plates.

15.2 Assume that the two parallel plates in Prob. 15.1 are both stationary but that a constant pressure gradient exists in the flow direction, that is,  $dp/dx = \text{constant}$ .

(a) Obtain an expression for the variation of velocity between the plates.

(b) Obtain an expression for the shear stress on the plates in terms of  $dp/dx$ .

*A very satisfactory explanation of the physical process in the boundary layer between a fluid and a solid body could be obtained by the hypothesis of an adhesion of the fluid to the walls, that is, by the hypothesis of a zero relative velocity between fluid and wall. If the viscosity was very small and the fluid path along the wall not too long, the fluid velocity ought to resume its normal value at a very short distance from the wall. In the thin transition layer however, the sharp changes of velocity, even with small coefficient of friction, produce marked results.*

*Ludwig Prandtl, 1904*

### 16.1 INTRODUCTION

The above quotation is taken from an historic paper given by Ludwig Prandtl at the third Congress of Mathematicians at Heidelberg, Germany, in 1904. In this paper, the concept of the boundary layer was first introduced — a concept which eventually revolutionized the analysis of viscous flows in the twentieth century and which allowed the practical calculation of drag and flow separation over aerodynamic bodies. Before Prandtl's 1904 paper, the Navier-Stokes equations discussed in Chap. 15 were well known, but fluid dynamicists were frustrated in their attempts to solve these equations for practical engineering problems. After 1904, the picture changed completely. Using Prandtl's concept of a boundary layer adjacent to an aerodynamic surface, the Navier-Stokes equations can be reduced to a more tractable form called the *boundary-layer equations*. In turn, these boundary-layer equations can be solved to obtain the distributions of shear stress and aerodynamic heat transfer to the surface. Prandtl's boundary-layer concept was an advancement in the science of fluid mechanics of the caliber of a Nobel prize, although he never received that honor. The purpose of this chapter is to present the general concept of the boundary layer and to give a few representative samples of its application. Our purpose here is to provide only an introduction to boundary-layer theory; consult Ref. 42 for a rigorous and thorough discussion of boundary-layer analysis and applications.

What is a boundary layer? We have used this term in several places in our previous chapters, first introducing the idea in Sec. 1.10 and illustrating the concept in

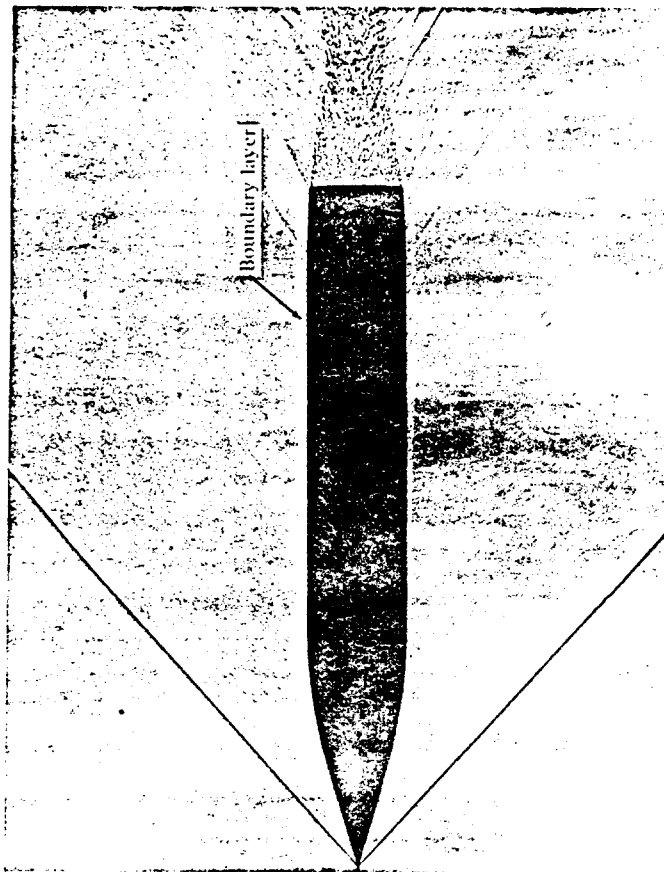


Figure 16.1 The boundary layer on an aerodynamic body. (Courtesy of the U.S. Army Ballistics Laboratory, Aberdeen, Maryland.)

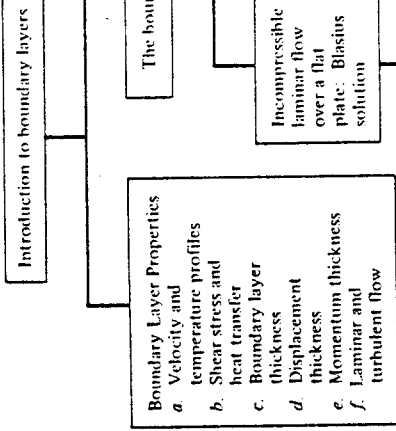


Figure 16.2 Road map for Chap. 16.

## 16.2 BOUNDARY-LAYER PROPERTIES

Consider the viscous flow over a flat plate as sketched in Fig. 16.3. The viscous effects are contained within a thin layer adjacent to the surface; the thickness is exaggerated in Fig. 16.3 for clarity. Immediately at the surface, the flow velocity is zero; this is the "no-slip" condition discussed in Sec. 15.2. In addition, the temperature of the fluid immediately at the surface is equal to the temperature of the surface; this is called the *wall temperature*  $T_w$ , as shown in Fig. 16.3. Above the surface, the flow velocity increases in the  $y$  direction until, for all practical purposes, it equals the freestream velocity. This will occur at a height above the wall equal to  $\delta$ , as shown in Fig. 16.3. More precisely,  $\delta$  is defined as that distance above the wall where  $u = 0.99u_\infty$ ; here,  $u$  is the velocity at the outer edge of the boundary layer. In Fig. 16.3, which illustrates

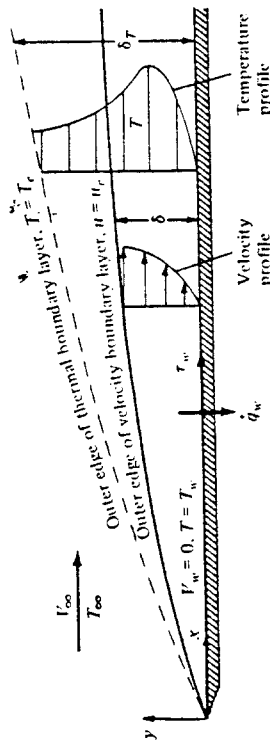


Figure 16.3 Boundary-layer properties.

Fig. 1.24. The boundary layer is the thin region of flow adjacent to a surface where the flow is retarded by the influence of friction between a solid surface and the fluid. For example, a photograph of the flow over a supersonic body is shown in Fig. 16.1, where the boundary layer (along with shock and expansion waves and the wake) is made visible by a special optical technique called a *shadowgraph* (see Refs. 25 and 26 for discussions of the shadowgraph method). Note how thin the boundary layer is in comparison with the size of the body; however, although the boundary layer occupies geometrically only a small portion of the flow field, its influence on the drag and heat transfer to the body is immense—in Prandtl's own words as quoted above, it produces "marked results."

The purpose of this chapter is to examine these "marked results." The road map for the present chapter is given in Fig. 16.2. In the next section we discuss some fundamental properties of boundary layers. This is followed by a development of the boundary-layer equations, with specific solutions of these equations for the incompressible and compressible laminar flow over a flat plate. Finally, some comments are made on the effects of turbulent flow. As we progress through this chapter, refer to the road map in Fig. 16.2 for orientation on the flow of ideas.

the flow over a flat plate, the velocity at the edge of the boundary layer will be  $V_x$ ; that is,  $u_e = V_x$ . For a body of general shape,  $u_e$  is the velocity obtained from an inviscid flow solution evaluated at the body surface (or at the "effective body" surface, as discussed later). The quantity  $\delta$  is called the *velocity boundary-layer thickness*. At any given  $x$  station, the variation of  $u$  between  $y = 0$  and  $y = \delta$ , that is,  $u = u(y)$ , is defined as the *velocity profile* within the boundary layer, as sketched in Fig. 16.3. This profile is different for different  $x$  stations. Similarly, the flow temperature will change above the wall, ranging from  $T = T_w$  at  $y = 0$  to  $T = 0.99T_e$  at  $y = \delta_T$ . Here,  $\delta_T$  is defined as the *thermal boundary-layer thickness*. At any given  $x$  station, the variation of  $T$  between  $y = 0$  and  $y = \delta_T$ , that is,  $T = T(y)$ , is called the *temperature profile* within the boundary layer, as sketched in Fig. 16.3. (In the above,  $T_e$  is the temperature at the edge of the thermal boundary layer. For the flow over a flat plate, as sketched in Fig. 16.3,  $T_e = T_\infty$ . For a general body,  $T_e$  is obtained from an inviscid flow solution evaluated at the body surface, or at the "effective body" surface, to be discussed later.)

Hence, two boundary layers can be defined: a velocity boundary layer with thickness  $\delta$  and a temperature boundary layer with thickness  $\delta_T$ . In general,  $\delta_T \neq \delta$ . The relative thicknesses depend on the Prandtl number: it can be shown that if  $Pr = 1$ , then  $\delta = \delta_T$ ; if  $Pr > 1$ , then  $\delta_T < \delta$ ; if  $Pr < 1$ , then  $\delta_T > \delta$ . For air at standard conditions,  $Pr = 0.71$ ; hence, the thermal boundary layer is thicker than the velocity boundary layer, as shown in Fig. 16.3. Note that both boundary layer thicknesses increase with distance from the leading edge, that is,  $\delta = \delta(x)$  and  $\delta_T = \delta_T(x)$ .

The consequence of the velocity gradient at the wall is the generation of shear stress at the wall,

$$\tau_w = \mu \left( \frac{\partial u}{\partial y} \right)_w \quad (16.1)$$

where  $(\partial u / \partial y)_w$  is the velocity gradient evaluated at  $y = 0$ , that is, at the wall. Similarly, the temperature gradient at the wall generates heat transfer at the wall,

$$\dot{q}_w = -k \left( \frac{\partial T}{\partial y} \right)_w \quad (16.2)$$

where  $(\partial T / \partial y)_w$  is the temperature gradient evaluated at  $y = 0$ , that is, at the wall. In general, both  $\tau_w$  and  $\dot{q}_w$  are functions of distance from the leading edge; that is,  $\tau_w = \tau_w(x)$  and  $\dot{q}_w = \dot{q}_w(x)$ . One of the central purposes of boundary-layer theory is to compute  $\tau_w$  and  $\dot{q}_w$ .

A frequently used boundary-layer property is the *displacement thickness*  $\delta^*$ , defined as

$$\delta^* = \int_0^y \left( 1 - \frac{\rho u}{\rho_e u_e} \right) dy \quad \delta \leq y_i \rightarrow \infty \quad (16.3)$$

The displacement thickness has two physical interpretations:

1.  $\delta^*$  is an index proportional to the "missing mass flow" due to the presence of the boundary layer. Let us explain. Consider point  $y_i$  above the boundary layer, as

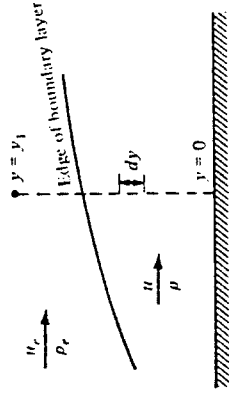


Figure 16.4 Construction for the discussion of displacement thickness.

shown in Fig. 16.4. Consider also the mass flow (per unit depth perpendicular to the page) across the vertical line connecting  $y = 0$  and  $y = y_i$ . Then

$$A = \text{actual mass flow between } 0 \text{ and } y_i = \int_0^{y_i} \rho u dy$$

hypothetical mass flow

$$B = \text{between } 0 \text{ and } y_i \text{ if boundary layer were not present}$$

decrement in mass flow due to

$$B - A = \text{presence of boundary layer, i.e., } = \int_0^{y_i} (\rho_e u_e - \rho u) dy \quad (16.4)$$

missing mass flow

Express this missing mass flow as the product of  $\rho_e u_e$  and a height,  $\delta^*$ ; that is,

$$\text{Missing mass flow} = \rho_e u_e \delta^* \quad (16.5)$$

Equating Eqs. (16.4) and (16.5), we have

$$\rho_e u_e \delta^* = \int_0^{y_i} (\rho_e u_e - \rho u) dy$$

or

$$\delta^* = \int_0^{y_i} \left( 1 - \frac{\rho u}{\rho_e u_e} \right) dy \quad (16.6)$$

Equation (16.6) is identical to the definition of  $\delta^*$  given in Eq. (16.3). Hence, clearly  $\delta^*$  is a height proportional to the missing mass flow. If this missing mass flow were crammed into a streamtube where the flow properties were constant at  $\rho_e$  and  $u_e$ , then Eq. (16.5) says that  $\delta^*$  is the height of this hypothetical streamtube. 2. The second physical interpretation of  $\delta^*$  is more practical than the one discussed above. Consider the flow over a flat surface as sketched in Fig. 16.5. At the left is a picture of the hypothetical inviscid flow over the surface; a streamline through point  $y_i$  is straight and parallel to the surface. The actual viscous flow is shown at the right of Fig. 16.5; here, the retarded flow inside the boundary layer acts as a partial obstruction to the freestream flow. As a result, the streamline external to the boundary layer passing through point  $y_i$  is deflected upward through a distance  $\delta^*$ .

We now prove that this  $\delta^*$  is precisely the displacement thickness defined by Eq. (16.3). At station 1 in Fig. 16.5, the mass flow (per unit depth perpendicular to the page) between the surface and the external streamline is

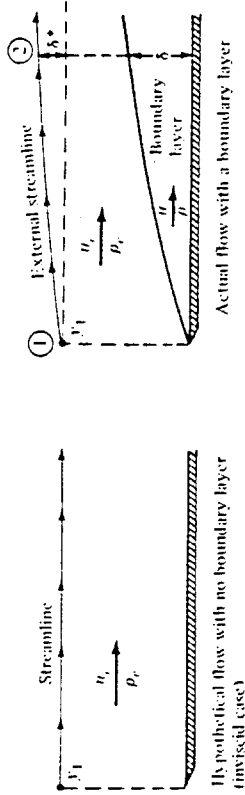


Figure 16.5 Displacement thickness is the distance by which an external flow streamline is displaced by the presence of the boundary layer.

$$\dot{m} = \int_0^{y_1} \rho_r u_r dy \quad (16.8)$$

At station 2, the mass flow between the surface and the external streamline is

$$\dot{m} = \int_0^{y_1} \rho u dy + \rho_r u_r \delta^* \quad (16.8)$$

Since the surface and the external streamline form the boundaries of a streamtube, the mass flows across station 1 and 2 are equal. Hence, equating Eqs. (16.7) and (16.8), we have

$$\int_0^{y_1} \rho_r u_r dy = \int_0^{y_1} \rho u dy + \rho_r u_r \delta^* \quad (16.9)$$

$$\text{or } \delta^* = \int_0^{y_1} \left( 1 - \frac{\rho u}{\rho_r u_r} \right) dy \quad (16.9)$$

Hence, the height by which the streamline in Fig. 16.5 is displaced upward by the presence of the boundary layer, namely  $\delta^*$ , is given by Eq. (16.9). However, Eq. (16.9) is precisely the definition of the displacement thickness given by Eq. (16.3). Thus, the displacement thickness, first defined by Eq. (16.3), is physically the distance through which the external inviscid flow is displaced by the presence of the boundary layer.

This second interpretation of  $\delta^*$  gives rise to the concept of an *effective body*. Consider the aerodynamic shape sketched in Fig. 16.6. The actual contour of the body is given by curve  $ab$ . However, due to the displacement effect of the boundary layer, the shape of the body effectively seen by the freestream is not given by curve  $ab$ ; rather, the freestream sees an effective body given by curve  $ac$ . In order to obtain the conditions  $\rho_r$ ,  $u_r$ ,  $T_r$ , etc., at the outer edge of the boundary layer on the actual body  $ab$ , an inviscid flow solution should be carried out for the effective body, and  $\rho_e$ ,  $u_e$ ,  $T_e$ , etc., are obtained from this inviscid solution evaluated along curve  $ac$ .

Note that in order to solve for  $\delta^*$  from Eq. (16.3), we need the profiles of  $u$  and  $\rho$  from a solution of the boundary layer flow. In turn, to solve the boundary layer flow,

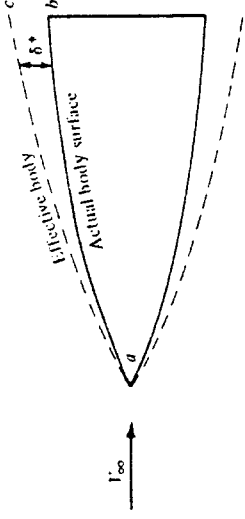


Figure 16.6 The "effective body," equal to the actual body shape plus the displacement thickness distribution.

we need  $\rho_e$ ,  $u_e$ ,  $T_e$ , etc. However,  $\rho_e$ ,  $u_e$ ,  $T_e$ , etc., depend on  $\delta^*$ . This leads to an iterative solution. To accurately calculate the boundary-layer properties as well as the pressure distribution over the surface of the body in Fig. 16.6, we proceed as follows:

1. Carry out an inviscid solution for the given body shape  $ab$ . Evaluate  $\rho_r$ ,  $u_r$ ,  $T_r$ , etc., along curve  $ab$ .
2. Using these values of  $\rho_r$ ,  $u_r$ ,  $T_r$ , etc., solve the boundary-layer equations (discussed in Secs. 16.3 to 16.6) for  $u = u(y)$ ,  $\rho = \rho(y)$ , etc., at various stations along the body.
3. Obtain  $\delta^*$  at these stations from Eq. (16.3). This will not be an accurate  $\delta^*$  because  $\rho_r$ ,  $u_r$ ,  $T_r$ , etc., were evaluated on curve  $ab$ , not the proper effective body. Using this intermediate  $\delta^*$ , calculate an effective body, given by a curve  $ac'$  (not shown in Fig. 16.6).
4. Carry out an inviscid solution for the flow over the intermediate effective body  $ac'$ , and evaluate new values of  $\rho_r$ ,  $u_r$ ,  $T_r$ , etc., along  $ac'$ .
5. Repeat steps 2 to 4 above until the solution at one iteration essentially does not deviate from the solution at the previous iteration. At this stage, a converged solution will be obtained, and the final results will pertain to the flow over the proper effective body  $ac$  shown in Fig. 16.6.

In some cases, the boundary layers are so thin that the effective body can be ignored, and a boundary-layer solution can proceed directly from  $\rho_r$ ,  $u_r$ ,  $T_r$ , etc., obtained from an inviscid solution evaluated on the actual body surface ( $ab$  in Fig. 16.6). However, for highly accurate solutions, and for cases where the boundary-layer thickness is relatively large (such as for hypersonic flow as discussed in Chap. 14), the iterative procedure described above should be carried out. Also, we note parenthetically that  $\delta^*$  is usually smaller than  $\delta$  typically,  $\delta \approx 0.3\delta$ . Another boundary-layer property of importance is the *momentum thickness*  $\theta$ , defined as

$$\theta = \int_0^{y_1} \frac{\rho u}{\rho_r u_r} \left( 1 - \frac{u}{u_r} \right) dy \quad \delta \leq y_1 \rightarrow \infty \quad (16.10)$$

To understand the physical interpretation of  $\theta$ , return again to Fig. 16.4. Consider the mass flow across a segment  $dy$ , given by  $d\dot{m} = \rho u dy$ . Then

$$A = \text{momentum flow across } dy = dm u = \rho u^2 dy$$

If this same elemental mass flow were associated with the freestream, where the velocity is  $u_\infty$ , then

$$B = \begin{cases} \text{momentum flow at freestream} \\ \text{velocity associated with mass } dm = dm u_\infty = (\rho u_\infty^2) dy \end{cases}$$

Hence,  $B - A = \begin{cases} \text{decrement in momentum flow} \\ \text{(missing momentum flow) associated with mass } dm \end{cases}$

The total decrement in momentum flow across the vertical line from  $y = 0$  to  $y = y_1$  in Fig. 16.4 is the integral of Eq. (16.11),

$$\text{Total decrement in momentum flow, or missing momentum flow} = \int_0^{y_1} \rho u(u_\infty - u) dy \quad (16.12)$$

Assume that the missing momentum flow is the product of  $\rho u_\infty^2$  and a height  $\theta$ . Then,

$$\text{Missing momentum flow} = \rho u_\infty^2 \theta \quad (16.13)$$

Equating Eqs. (16.12) and (16.13), we obtain

$$\rho u_\infty^2 \theta = \int_0^{y_1} \rho u(u_\infty - u) dy$$

$$\text{or} \quad \theta = \int_0^{y_1} \frac{\rho u}{\rho u_\infty} \left( 1 - \frac{u}{u_\infty} \right) dy \quad (16.14)$$

Equation (16.14) is precisely the definition of the momentum thickness given by Eq. (16.10). Therefore,  $\theta$  is an index that is proportional to the decrement in momentum flow due to the presence of the boundary layer. It is the height of a hypothetical streamtube which is carrying the missing momentum flow at freestream conditions.

Note that  $\theta = \theta(x)$ . In more detailed discussions of boundary-layer theory, it can be shown that  $\theta$  evaluated at a given station  $x = x_1$  is proportional to the integrated friction drag coefficient from the leading edge to  $x_1$ ; that is,

$$\theta(x_1) \propto \frac{1}{x_1} \int_0^{x_1} c_f dx = C_f$$

where  $c_f$  is the local skin friction coefficient defined in Sec. 1.5 and  $C_f$  is the total skin friction drag coefficient for the length of surface from  $x = 0$  to  $x = x_1$ . Hence, the concept of momentum thickness is useful in the prediction of drag coefficient.

All the boundary-layer properties discussed above are general concepts; they apply to compressible as well as incompressible flows, and to turbulent as well as laminar flows. The differences between turbulent and laminar flows were introduced in Sec. 15.2. Here, we extend that discussion by noting that the increased momentum and energy exchange that occur within a turbulent boundary layer cause a turbulent boundary layer to be thicker than a laminar boundary layer. That is, for the same edge conditions,  $\rho_\infty$ ,  $u_\infty$ ,

$T_c$ , etc., we have  $\delta_{\text{turbulent}} > \delta_{\text{laminar}}$  and  $(\delta_r)_{\text{turbulent}} > (\delta_r)_{\text{laminar}}$ . When a boundary layer transits from laminar to turbulent flow, as sketched in Fig. 15.8, the boundary-layer thickness markedly increases. Similarly,  $\delta^*$  and  $\theta$  are larger for turbulent flows.

### 16.3 THE BOUNDARY-LAYER EQUATIONS

For the remainder of this chapter, we consider two-dimensional, steady flow. The nondimensionalized form of the  $x$ -momentum equation (one of the Navier-Stokes equations) was developed in Sec. 15.6 and was given by Eq. (15.29):

$$\rho' u' \frac{\partial u'}{\partial x} + \rho' v' \frac{\partial u'}{\partial y} = - \frac{1}{\rho M_\infty^2} \frac{\partial p'}{\partial x} + \frac{1}{Re_x} \frac{\partial}{\partial y} \left[ \mu' \left( \frac{\partial v'}{\partial x} + \frac{\partial u'}{\partial y} \right) \right] \quad (15.29)$$

Let us now reduce Eq. (15.29) to an approximate form which holds reasonably well within a boundary layer.

Consider the boundary layer along a flat plate of length  $c$  as sketched in Fig. 16.7. The basic assumption of boundary-layer theory is that a boundary layer is very thin in comparison with the scale of the body; that is,

$$\delta \ll c \quad (16.15)$$

Consider the continuity equation for a steady, two-dimensional flow,

$$\frac{\partial(\rho u)}{\partial x} + \frac{\partial(\rho v)}{\partial y} = 0 \quad (16.16)$$

In terms of the nondimensional variables defined in Sec. 15.6, Eq. (16.16) becomes

$$\frac{\partial(\rho' u')}{\partial x'} + \frac{\partial(\rho' v')}{\partial y'} = 0 \quad (16.17)$$

Because  $u'$  varies from 0 at the wall to 1 at the edge of the boundary layer, let us say that  $u'$  is of the *order of magnitude* equal to 1, symbolized by  $O(1)$ . Similarly,  $\rho' = O(1)$ . Also, since  $x$  varies from 0 to  $c$ ,  $x' = O(1)$ . However, since  $y$  varies from 0 to  $\delta$ , where  $\delta \ll c$ , then  $y'$  is of the *smaller order of magnitude*, denoted by  $y' = O(\delta/c)$ . Without loss of generality, we can assume that  $c$  is a unit length. Therefore,  $y' = O(\delta)$ . Putting these orders of magnitude in Eq. (16.17), we have

$$\frac{O(1)[O(1)]}{O(1)} + \frac{[O(1)][v']}{O(\delta)} = 0 \quad (16.18)$$

$$\delta \ll c$$

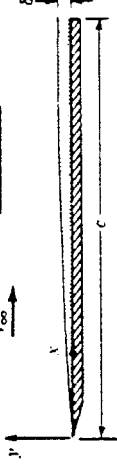


Figure 16.7 The basic assumption of boundary-layer theory: a boundary layer is very thin in comparison with the scale of the body.

Hence, from Eq. (16.18), clearly  $v'$  must be of an order of magnitude equal to  $\delta$ , that is,  $v = O(\delta)$ . Now examine the order of magnitude of the terms in Eq. (15.29). We have,

$$\begin{aligned} \rho' u' \frac{\partial u'}{\partial x'} &= O(1) & \rho' v' \frac{\partial u'}{\partial y'} &= O(1) & \frac{\partial p'}{\partial x'} &= O(1) \\ \frac{\partial}{\partial y'} \left( \mu' \frac{\partial v'}{\partial x'} \right) &= O(1) & \frac{\partial}{\partial y'} \left( \mu' \frac{\partial u'}{\partial y'} \right) &= O\left(\frac{1}{\delta^2}\right) \end{aligned}$$

Hence, the order-of-magnitude equation for Eq. (15.29) can be written as

$$O(1) + O(1) = -\frac{1}{\gamma M_*^2} O(1) + \frac{1}{Re_x} \left[ O(1) + O\left(\frac{1}{\delta^2}\right) \right] \quad (16.19)$$

Let us now introduce another assumption of boundary-layer theory, namely, that *Reynolds number is large, indeed large enough such that*

$$\boxed{\frac{1}{Re_x} = O(\delta^2)} \quad (16.20)$$

Then, Eq. (16.19) becomes

$$O(1) + O(1) = -\frac{1}{\gamma M_*^2} O(1) + O(\delta^2) \left[ O(1) + O\left(\frac{1}{\delta^2}\right) \right] \quad (16.21)$$

In Eq. (16.21), there is one term with an order of magnitude that is much smaller than the rest, namely, the product  $O(\delta^2)[O(1)] = O(\delta^2)$ . This term corresponds to  $(1/Re_x) \partial/\partial y' (\mu' \partial v'/\partial x')$  in Eq. (15.29). Hence, *neglect this term in comparison to the remaining terms in Eq. (15.29)*. We obtain

$$\rho' u' \frac{\partial u'}{\partial x'} + \rho' v' \frac{\partial u'}{\partial y'} = -\frac{1}{\gamma M_*^2} \frac{\partial p'}{\partial x'} + \frac{1}{Re_x} \frac{\partial}{\partial y'} \left( \mu' \frac{\partial u'}{\partial y'} \right) \quad (16.22)$$

In terms of dimensional variables, Eq. (16.22) is

$$\boxed{\mu u \frac{\partial u}{\partial x} + \rho v \frac{\partial u}{\partial y} = -\frac{\partial p}{\partial x} + \frac{\partial}{\partial y} \left( \mu \frac{\partial u}{\partial y} \right)} \quad (16.23)$$

Equation (16.23) is the approximate x-momentum equation which holds for flow in a thin boundary layer at high Reynolds number.

Consider the y-momentum equation for two-dimensional, steady flow, obtained from Eq. (15.19b) as (neglecting the normal stress  $\tau_{yy}$ )

$$\boxed{\frac{\partial v}{\partial x} + \rho v \frac{\partial v}{\partial y} = -\frac{\partial p}{\partial y} + \frac{\partial}{\partial x} \left[ \mu \left( \frac{\partial v}{\partial x} + \frac{\partial u}{\partial y} \right) \right]} \quad (16.24)$$

In terms of the nondimensional variables, Eq. (16.24) becomes

$$\boxed{\rho' u' \frac{\partial v'}{\partial x'} + \rho' v' \frac{\partial v'}{\partial y'} = -\frac{1}{\gamma M_*^2} \frac{\partial p'}{\partial y'} + \frac{1}{Re_x} \frac{\partial}{\partial x'} \left[ \mu' \left( \frac{\partial v'}{\partial x'} + \frac{\partial u'}{\partial y'} \right) \right]} \quad (16.25)$$

The order-of-magnitude equation for Eq. (16.25) is

$$O(\delta) + O(\delta) = -\frac{1}{\gamma M_*^2} \frac{\partial p'}{\partial y'} + O(\delta^2) \left[ O(\delta) + O\left(\frac{1}{\delta}\right) \right] \quad (16.26)$$

From Eq. (16.26), we see that  $\partial p'/\partial y' = O(\delta)$  or smaller, assuming that  $\gamma M_*^2 = O(1)$ . Since  $\delta$  is very small, this implies that  $\partial p'/\partial y'$  is very small. Therefore, from the y-momentum equation specialized to a boundary layer, we have

$$\boxed{\frac{\partial p}{\partial y} = 0} \quad (16.26a)$$

Equation (16.26a) is important; it states that at a given x-station, *the pressure is constant through the boundary layer in a direction normal to the surface*. This implies that the pressure distribution at the outer edge of the boundary layer is impressed directly to the surface without change. Hence, throughout the boundary layer,  $p = p(x) = p_s(x)$ .

It is interesting to note that if  $M_*^2$  is very large, as in the case of large hypersonic Mach numbers, then from Eq. (16.26)  $\partial p'/\partial y'$  does not have to be small. For example, if  $M_*$  were large enough such that  $1/\gamma M_*^2 = O(\delta)$ , then  $\partial p'/\partial y'$  could be as large as  $O(1)$ , and Eq. (16.26) would still be satisfied. Thus, for very large hypersonic Mach numbers, the assumption that  $p$  is constant in the normal direction through a boundary layer is not always valid.

Consider the general energy equation given by Eq. (15.26). The nondimensional form of this equation for two-dimensional, steady flow is given in Eq. (15.33). Inserting  $e = h - p/\rho$  into this equation, subtracting the momentum equation multiplied by velocity, and performing an order-of-magnitude analysis similar to those above, we can obtain the boundary-layer energy equation as

$$\boxed{\rho u \frac{\partial h}{\partial x} + \rho v \frac{\partial h}{\partial y} = \frac{\partial}{\partial y} \left( k \frac{\partial T}{\partial y} \right) + u \frac{\partial p}{\partial x} + \mu \left( \frac{\partial u}{\partial y} \right)^2} \quad (16.27)$$

The details are left to you.

In summary, by making the combined assumptions of  $\delta \ll c$  and  $Re \geq 1/\delta^2$ , the complete Navier-Stokes equations derived in Chap. 15 can be reduced to simpler forms which apply to a boundary layer. These boundary-layer equations are

$$\boxed{\text{Continuity: } \frac{\partial(\rho u)}{\partial x} + \frac{\partial(\rho v)}{\partial y} = 0} \quad (16.28)$$

$$\boxed{x \text{ momentum: } \mu u \frac{\partial u}{\partial x} + \rho v \frac{\partial u}{\partial y} = -\frac{\partial p}{\partial x} + \frac{\partial}{\partial y} \left( \mu \frac{\partial u}{\partial y} \right)} \quad (16.29)$$

$$\boxed{y \text{ momentum: } \frac{\partial p}{\partial y} = 0} \quad (16.30)$$

$$\boxed{\text{Energy: } \rho u \frac{\partial h}{\partial x} + \rho v \frac{\partial h}{\partial y} = \frac{\partial}{\partial y} \left( k \frac{\partial T}{\partial y} \right) + u \frac{dp_e}{dx} + \mu \left( \frac{\partial u}{\partial y} \right)^2} \quad (16.31)$$

Note that, as in the case of the Navier-Stokes equations, the boundary-layer equations are nonlinear. However, the boundary-layer equations are simpler and therefore are more readily solved. Also, since  $p = p(x)$ , the pressure gradient expressed as  $\partial p / \partial x$  in Eqs. (16.23) and (16.27) is reexpressed as  $dp_e / dx$  in Eqs. (16.29) and (16.31). In the above equations, the unknowns are  $u$ ,  $v$ ,  $\rho$ , and  $h$ ;  $p$  is known from  $p = p_e(x)$ , and  $\mu$  and  $k$  are properties of the fluid which vary with temperature. To complete the system, we have

$$p = \rho R T \quad (16.32)$$

$$h = c_p T \quad (16.33)$$

Hence, Eqs. (16.28), (16.29), and (16.31 to 16.33) are five equations for the five unknowns,  $u$ ,  $v$ ,  $\rho$ ,  $T$ , and  $h$ .

The boundary conditions for the above equations are as follows:

*At the wall:*  $y = 0 \quad u = 0 \quad v = 0 \quad T = T_w$

*At the boundary layer edge:*  $y \rightarrow \infty \quad u \rightarrow u_\infty \quad T \rightarrow T_\infty$

Note that since the boundary layer thickness is not known a priori, the boundary condition at the edge of the boundary layer is given at large  $y$ , essentially  $y$  approaching infinity.

In general, the boundary-layer equations given by Eqs. (16.28) to (16.31) must be solved numerically. Modern boundary-layer techniques utilize sophisticated finite-difference solutions to obtain the boundary-layer profiles and the resulting distributions of  $\tau_w$  and  $q_w$  over bodies of general shapes. Such techniques are beyond the scope of this book. However, in order to give you a feeling for the nature of boundary-layer solutions, the following two sections treat the case of flow over a flat plate, first dealing with incompressible flow in Sec. 16.4, and extending our considerations to compressible flow in Sec. 16.5. The flat plate is a special case among the whole inventory of boundary-layer solutions. It is one of a special class of solutions called *self-similar solutions*, the nature of which is discussed in the remaining sections.

$$\boxed{\text{Energy: } \frac{\partial u}{\partial x} + \frac{\partial v}{\partial y} = 0} \quad (16.34)$$

$$\boxed{u \frac{\partial u}{\partial x} + v \frac{\partial u}{\partial y} = v \frac{\partial^2 u}{\partial y^2}} \quad (16.35)$$

Note that, as in the case of the Navier-Stokes equations, the boundary-layer equations are nonlinear. However, the boundary-layer equations are simpler and therefore are more readily solved. Also, since  $p = p(x)$ , the pressure gradient expressed as  $\partial p / \partial x$  in Eqs. (16.23) and (16.27) is reexpressed as  $dp_e / dx$  in Eqs. (16.29) and (16.31). In the above equations, the unknowns are  $u$ ,  $v$ ,  $\rho$ , and  $h$ ;  $p$  is known from  $p = p_e(x)$ , and  $\mu$  and  $k$  are properties of the fluid which vary with temperature. To complete the system, we have

$$p = \rho R T \quad (16.32)$$

$$h = c_p T \quad (16.33)$$

Hence, Eqs. (16.28), (16.29), and (16.31 to 16.33) are five equations for the five unknowns,  $u$ ,  $v$ ,  $\rho$ ,  $T$ , and  $h$ .

The boundary conditions for the above equations are as follows:

*At the wall:*  $y = 0 \quad u = 0 \quad v = 0 \quad T = T_w$

*At the boundary layer edge:*  $y \rightarrow \infty \quad u \rightarrow u_\infty \quad T \rightarrow T_\infty$

Note that since the boundary layer thickness is not known a priori, the boundary condition at the edge of the boundary layer is given at large  $y$ , essentially  $y$  approaching infinity.

In general, the boundary-layer equations given by Eqs. (16.28) to (16.31) must be solved numerically. Modern boundary-layer techniques utilize sophisticated finite-difference solutions to obtain the boundary-layer profiles and the resulting distributions of  $\tau_w$  and  $q_w$  over bodies of general shapes. Such techniques are beyond the scope of this book. However, in order to give you a feeling for the nature of boundary-layer solutions, the following two sections treat the case of flow over a flat plate, first dealing with incompressible flow in Sec. 16.4, and extending our considerations to compressible flow in Sec. 16.5. The flat plate is a special case among the whole inventory of boundary-layer solutions. It is one of a special class of solutions called *self-similar solutions*, the nature of which is discussed in the remaining sections.

## 16.4 INCOMPRESSIBLE FLOW OVER A FLAT PLATE: THE BLASIUS SOLUTION

Consider the incompressible, two-dimensional flow over a flat plate at  $0^\circ$  angle of attack, such as sketched in Fig. 16.7. For such a flow,  $\rho = \text{constant}$ ,  $\mu = \text{constant}$ , and  $d\rho_e / dx = 0$  (because the inviscid flow over a flat plate at  $x = 0$  yields a constant pressure over the surface.) Moreover, recall that the energy equation is not needed to calculate the velocity field for an incompressible flow. Hence, the boundary-layer equations, Eqs. (16.28) to (16.31), reduce to

$$\boxed{u = \frac{\partial \psi}{\partial y} = \sqrt{\frac{V_s}{\nu x}} \frac{\partial \psi}{\partial y} = V_s f'(\eta)} \quad (16.45)$$

$$\boxed{\psi = \sqrt{\nu x V_s} f(\eta)} \quad (16.44)$$

where  $f(\eta)$  is strictly a function of  $\eta$  only. This expression for  $\psi$  identically satisfies the continuity equation, Eq. (16.34); therefore, it is a physically possibly streamfunction. [Show yourself that  $\psi$  satisfies Eq. (16.34); to do this, you will have to carry out many of the same manipulations described below.] From the definition of the stream function, and using Eqs. (16.41), (16.42), and (16.44), we have

$$\boxed{\frac{\partial \xi}{\partial x} = 1 \quad \frac{\partial \xi}{\partial y} = 0 \quad \frac{\partial \eta}{\partial y} = \sqrt{\frac{V_s}{\nu x}}} \quad (16.40)$$

$$\boxed{\frac{\partial}{\partial x} = \frac{\partial}{\partial \xi} - \frac{\partial \xi}{\partial x} \frac{\partial}{\partial \eta} \quad \frac{\partial}{\partial y} = \sqrt{\frac{V_s}{\nu x}} \frac{\partial}{\partial \eta}} \quad (16.41)$$

$$\boxed{\frac{\partial^2}{\partial y^2} = \frac{V_s}{\nu x} \frac{\partial^2}{\partial \eta^2}} \quad (16.43)$$

$$\boxed{\text{Also, let us define a stream function } \psi \text{ such that:}}$$

$$\boxed{\psi = \sqrt{\nu x V_s} f(\eta)} \quad (16.44)$$

where  $f(\eta)$  is strictly a function of  $\eta$  only. This expression for  $\psi$  identically satisfies the continuity equation, Eq. (16.34); therefore, it is a physically possibly streamfunction. [Show yourself that  $\psi$  satisfies Eq. (16.34); to do this, you will have to carry out many of the same manipulations described below.] From the definition of the stream function, and using Eqs. (16.41), (16.42), and (16.44), we have

$$v = -\frac{\partial \psi}{\partial x} = -\left(\frac{\partial \psi}{\partial \xi} + \frac{\partial \eta}{\partial x} \frac{\partial \psi}{\partial \eta}\right) = -\frac{1}{2} \sqrt{\frac{\nu V_s}{x}} f - \sqrt{\nu x V_s} \frac{\partial \eta}{\partial x} f' \quad (16.46)$$

Equation (16.45) is of particular note. The function  $f(\eta)$  defined in Eq. (16.44) has the property that its derivative,  $f'$ , gives the  $x$  component of velocity as

$$f'(\eta) = \frac{u}{V_s}$$

Substitute Eqs. (16.41) to (16.43), (16.45), and (16.46) into the momentum equation, Eq. (16.35). Writing each term explicitly so that you can see what is happening, we have

$$V_s f \left( V_s \frac{\partial \eta}{\partial x} f' \right) - \left( \frac{1}{2} \sqrt{\frac{\nu V_s}{x}} f + \sqrt{\nu x V_s} \frac{\partial \eta}{\partial x} f' \right) V_s \sqrt{\frac{V_s}{\nu x}} f'' = \nu V_s \frac{V_s}{\nu x} f''' \quad (16.47)$$

Simplifying,

$$V_s^2 \frac{\partial \eta}{\partial x} f f'' - \frac{1}{2} \frac{V_s^2}{x} f f'' - V_s^2 \left( \frac{\partial \eta}{\partial x} \right) f f'' = \frac{V_s^2}{x} f''' \quad (16.47)$$

The first and third terms cancel, and Eq. (16.47) becomes

$$2f''' + ff'' = 0 \quad (16.48)$$

Equation (16.48) is important; it is called *Blasius's equation*, after H. Blasius, who obtained it in his Ph.D. dissertation in 1908. Blasius was a student of Prandtl, and his flat-plate solution using Eq. (16.48) was the first practical application of Prandtl's boundary-layer hypothesis since its announcement in 1904. Examine Eq. (16.48) closely. Amazingly enough it is an *ordinary differential equation*. Look what has happened! Starting with the partial differential equations for a flat-plate boundary layer given by Eqs. (16.34) to (16.36), and transforming *both* the independent and dependent variables through Eqs. (16.37) and (16.44), we obtain an ordinary differential equation for  $f(\eta)$ . In the same breath, we can say that Eq. (16.48) is also an equation for the velocity  $u$ , because  $u = V_s f'(\eta)$ . Because Eq. (16.48) is a single ordinary differential equation, it is simpler to solve than the original boundary-layer equations. However, it is still a nonlinear equation and must be solved numerically, subject to the transformed boundary conditions,

$$\text{At } \eta = 0: \quad f = 0, f' = 0$$

$$\text{At } \eta \rightarrow \infty: \quad f' = 1$$

[Note that at the wall where  $\eta = 0$ ,  $f' = 0$  because  $u = 0$ , and therefore  $f = 0$  from Eq. (16.46) evaluated at the wall.]

The solution of Eq. (16.48) is plotted in Fig. 16.8 in the form of  $f'(\eta) = u/V_s$  as a function of  $\eta$ . Note that this curve is the *velocity profile* and that it is a function of  $\eta$  only. Think about this for a moment. Consider two different  $x$  stations along the plate, as shown in Fig. 16.9. In general,  $u = u(x, y)$ , and the velocity profiles in terms

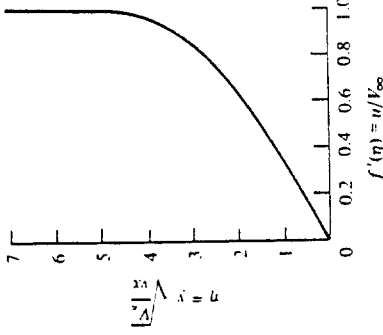


Figure 16.8 Incompressible velocity profile for a flat plate; solution of the Blasius equation.

of  $u = u(x)$  at given  $x$  stations will be *different*. Clearly, the variation of  $u$  normal to the wall will change as the flow progresses downstream. However, when plotted versus  $\eta$ , we see that the profile,  $u = u(\eta)$ , is the same for *all*  $x$  stations, as illustrated in Fig. 16.9. This result is an example of a *self-similar solution*—solutions where the boundary-layer profiles, when plotted versus a similarity variable,  $\eta$ , are the same for all  $x$  stations. For such self-similar solutions, the governing boundary-layer equations reduce to one or more ordinary differential equations in terms of a transformed independent variable. Self-similar solutions occur only for certain special types of flows—the flow over a flat plate is one such example. In general, for the flow over an arbitrary body, the boundary-layer solutions are nonsimilar; the governing partial differential equations cannot be reduced to ordinary differential equations.

Numerical values of  $f$ ,  $f'$ , and  $f''$  tabulated versus  $\eta$  can be found in Ref. 42. Of particular interest is the value of  $f''$  at the wall;  $f''(0) = 0.332$ . Consider the local

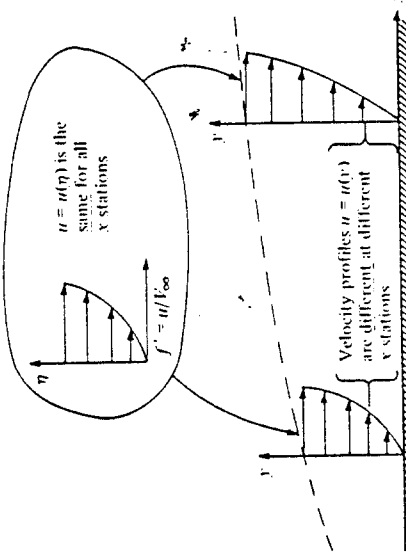


Figure 16.9 Velocity profiles in physical and transformed space, demonstrating the meaning of self-similar solutions.

skin friction coefficient defined as  $c_f = \tau_w / (\rho_s V_s^2)$ . From Eq. (15.1), the shear stress at the wall is given by

$$\tau_w = \mu \left( \frac{\partial u}{\partial y} \right)_{y=0} \quad (16.49)$$

However, from Eqs. (16.42) and (16.44)

$$\frac{\partial u}{\partial y} = V_s \frac{\partial f'}{\partial \eta} = V_s \sqrt{\frac{V_s}{\nu x}} \frac{\partial f'}{\partial \eta} = V_s \sqrt{\frac{V_s}{\nu x}} f'' \quad (16.50)$$

Evaluating Eq. (16.50) at the wall, where  $y = \eta = 0$ ,

$$\left( \frac{\partial u}{\partial y} \right)_{y=0} = V_s \sqrt{\frac{V_s}{\nu x}} f''(0) \quad (16.51)$$

Combining Eqs. (16.49) and (16.51),

$$\begin{aligned} c_f &= \frac{\tau_w}{\frac{1}{2} \rho_s V_s^2} = \frac{2\mu}{\rho_s V_s^2} V_s \sqrt{\frac{V_s}{\nu x}} f''(0) \\ &= 2 \sqrt{\frac{\mu}{\rho_s V_s x}} f''(0) = \frac{2f''(0)}{\sqrt{R e_x}} \end{aligned} \quad (16.52)$$

where  $R e_x$  is the local Reynolds number. Since  $f''(0) = 0.332$  from the numerical solution of Eq. (16.48), then Eq. (16.52) yields

$$c_f = \frac{0.664}{\sqrt{R e_x}} \quad (16.53)$$

which is a classic expression for the local skin-friction coefficient for the incompressible laminar flow over a flat plate — a result that stems directly from boundary-layer theory. Its validity has been amply verified by experiment. Note that  $c_f \propto R e_x^{-1/2} \propto x^{-1/2}$ , that is,  $c_f$  decreases inversely proportional to the square root of distance from the leading edge. Examining the flat plate sketched in Fig. 16.7, the total drag on the top surface of the entire plate is the integrated contribution of  $\tau_s(x)$  from  $x = 0$  to  $x = c$ . Letting  $C_f$  denote the skin friction drag coefficient, we obtain from Eq. (1.16)

$$C_f = \frac{1}{c} \int_0^c c_f dx \quad (16.54)$$

Substituting Eq. (16.53) into (16.54), we obtain

$$C_f = \frac{1}{c} (0.664) \sqrt{\frac{\mu}{\rho_s V_s}} \int_0^c x^{-1/2} dx = \frac{1.328}{c} \sqrt{\frac{\mu c}{\rho_s V_s}} \quad (16.55)$$

$$C_f = \frac{1.328}{\sqrt{R e_x}} \quad (16.56)$$

where  $R e_x$  is the Reynolds number based on the total plate length  $c$ .

An examination of Fig. 16.8 shows that  $f' = 0.99$  at approximately  $\eta = 5.0$ . Hence, the boundary-layer thickness, which was defined earlier as that distance above the surface where  $u = 0.99u_\infty$ , is

$$\eta = y \sqrt{\frac{V_s}{\nu x}} = \delta \sqrt{\frac{V_s}{\nu x}} = 5.0 \quad (16.57)$$

$$\delta = \frac{5.0x}{\sqrt{R e_x}} \quad (16.58)$$

Note that the boundary-layer thickness is inversely proportional to the square root of the Reynolds number (based on the local distance  $x$ ). Also,  $\delta \propto x^{1/2}$ , the laminar boundary layer over a flat plate grows parabolically with distance from the leading edge.

The displacement thickness  $\delta^*$ , defined by Eq. (16.3), becomes for an incompressible flow

$$\delta^* = \int_0^\eta \left( 1 - \frac{u}{u_\infty} \right) dy \quad (16.59)$$

In terms of the transformed variables  $f'$  and  $\eta$  given by Eqs. (16.37) and (16.45), the integral in Eq. (16.57) can be written as

$$\delta^* = \sqrt{\frac{\nu x}{V_s}} \int_0^\eta [1 - f'(\eta)] d\eta = \sqrt{\frac{\nu x}{V_s}} [\eta_1 - f(\eta_1)] \quad (16.58)$$

where  $\eta_1$  is an arbitrary point above the boundary layer. The numerical solution for  $f(\eta)$  obtained from Eq. (16.48) shows that, amazingly enough,  $\eta_1 - f(\eta_1) = 1.72$  for all values of  $\eta$  above 5.0. Therefore, from Eq. (16.58), we have

$$\delta^* = 1.72 \sqrt{\frac{\nu x}{V_s}} \quad (16.59)$$

or

$$\delta^* = \frac{1.72x}{\sqrt{R e_x}} \quad (16.59)$$

Note that, as in the case of the boundary-layer thickness itself,  $\delta^*$  varies inversely with the square root of the Reynolds number, and  $\delta^* \propto x^{1/2}$ . Also, comparing Eqs. (16.56) and (16.59), we see that  $\delta^* = 0.34\delta$ ; the displacement thickness is smaller than the boundary-layer thickness, confirming our earlier statement in Sec. 16.2.

The momentum thickness for an incompressible flow is, from Eq. (16.10),

$$\theta = \int_0^{\eta_1} \frac{u}{u_\infty} \left( 1 - \frac{u}{u_\infty} \right) dy$$

or in terms of our transformed variables,

$$\theta = \sqrt{\frac{\nu x}{V_s}} \int_0^{\eta_1} f'(1 - f') d\eta \quad (16.60)$$

Equation (16.60) can be integrated numerically from  $\eta = 0$  to any arbitrary point  $\eta_1 > 5.0$ . The result gives

$$\theta = \sqrt{\frac{\eta_x}{V_x}} (0.664) \quad (16.61)$$

or

$$\theta = \frac{0.664x}{\sqrt{Re_c}} \quad (16.61)$$

Note that, as in the case of our previous thicknesses,  $\theta$  varies inversely with the square root of the Reynolds number and that  $\theta \propto x^{1/2}$ . Also,  $\theta = 0.398^*$ , and  $\theta = 0.136$ . Another property of momentum thickness can be demonstrated by evaluating  $\theta$  at the trailing edge of the flat plate sketched in Fig. 16.7. In this case,  $x = c$ , and from Eq. (16.61), we obtain

$$\theta_{x=c} = \frac{0.664c}{\sqrt{Re_c}} \quad (16.62)$$

Comparing Eqs. (16.55) and (16.62), we have

$$C_f = \frac{2\theta_{x=c}}{c} \quad (16.63)$$

*Exercise 16.52:* Demonstrate that the integrated skin friction coefficient for the flat plate is directly proportional to the value of  $\theta$  evaluated at the trailing edge.

## 16.5 COMPRESSIBLE FLOW OVER A FLAT PLATE

The properties of the incompressible, laminar, flat-plate boundary layer were developed in Sec. 16.4. These results hold at low Mach numbers where the density is essentially constant through the boundary layer. However, what happens to these properties at high Mach numbers where the density becomes a variable, i.e., what are the compressibility effects? The purpose of the present section is to briefly outline the effects of compressibility on both the derivations and the final results for laminar flow over a flat plate. We do not intend to present much detail; rather, we examine some of the salient aspects which distinguish compressible from incompressible boundary layers.

The compressible boundary-layer equations were derived in Sec. 16.3, and were presented as Eqs. (16.28) to (16.31). For flow over a flat plate, where  $dp_x/dx = 0$ , these equations become

$$\frac{\partial(pu)}{\partial x} + \frac{\partial(\rho v)}{\partial y} = 0 \quad (16.64)$$

$$\mu \frac{\partial u}{\partial x} + \rho v \frac{\partial u}{\partial y} = \frac{\partial}{\partial y} \left( \mu \frac{\partial u}{\partial y} \right) \quad (16.65)$$

Equation (16.60) can be integrated numerically from  $\eta = 0$  to any arbitrary point  $\eta_1 > 5.0$ . The result gives

$$\frac{\partial p}{\partial y} = 0 \quad (16.66)$$

$$\rho u \frac{\partial h}{\partial x} + \rho v \frac{\partial h}{\partial y} = \frac{\partial}{\partial y} \left( k \frac{\partial T}{\partial y} \right) + \mu \left( \frac{\partial u}{\partial y} \right)^2 \quad (16.67)$$

Compare these equations with those for the incompressible case given by Eqs. (16.34) to (16.36). Note that, for a compressible boundary layer, (1) the energy equation must be included, (2) the density is treated as a variable, and (3) in general,  $\mu$  and  $k$  are functions of temperature and hence also must be treated as variables. As a result, the system of equations for the compressible case, Eqs. (16.64) to (16.67), is more complex than for the incompressible case, Eqs. (16.34) to (16.36).

It is sometimes convenient to deal with total enthalpy,  $h_0 = h + V^2/2$ , as the dependent variable in the energy equation, rather than the static enthalpy as given in Eq. (16.67). Note that, consistent with the boundary-layer approximation, where  $v$  is small,  $h_0 = h + V^2/2 = h + (u + v^2)/2 \approx h + u^2/2$ . To obtain the energy equation in terms of  $h_0$ , multiply Eq. (16.65) by  $u$ , and add to Eq. (16.67), as follows. From Eq. (16.65) multiplied by  $u$ ,

$$\rho u \frac{\partial(u^2/2)}{\partial x} + \rho v \frac{\partial(u^2/2)}{\partial y} = u \frac{\partial}{\partial y} \left( \mu \frac{\partial u}{\partial y} \right) \quad (16.68)$$

Adding Eq. (16.68) to (16.67),

~~$$\rho u \frac{\partial(h - u^2/2)}{\partial x} + \rho v \frac{\partial(h - u^2/2)}{\partial y} = \frac{\partial}{\partial y} \left( k \frac{\partial T}{\partial y} \right) + \mu \left( \frac{\partial u}{\partial y} \right)^2 + \mu \left( \frac{\partial u}{\partial y} \right)^2 + \mu \left( \frac{\partial u}{\partial y} \right)^2 \quad (16.69)$$~~

Recall that for a calorically perfect gas,  $dh = c_p dT$ ; hence,

$$\frac{\partial T}{\partial y} = \frac{1}{c_p} \frac{\partial h}{\partial y} = \frac{1}{c_p} \frac{\partial}{\partial y} \left( h_0 - \frac{u^2}{2} \right) \quad (16.70)$$

Substituting Eq. (16.70) into (16.69), we obtain

$$\rho u \frac{\partial h_0}{\partial x} + \rho v \frac{\partial h_0}{\partial y} = \frac{\partial}{\partial y} \left[ \frac{k}{c_p} \frac{\partial}{\partial y} \left( h_0 - \frac{u^2}{2} \right) \right] + \mu \left( \frac{\partial u}{\partial y} \right)^2 + u \frac{\partial}{\partial y} \left( \mu \frac{\partial u}{\partial y} \right) \quad (16.71)$$

Note that

$$\frac{k}{c_p} \frac{\partial}{\partial y} \left( h_0 - \frac{u^2}{2} \right) = \frac{\mu k}{\mu c_p} \frac{\partial}{\partial y} \left( h_0 - \frac{u^2}{2} \right) = \frac{\mu}{Pr} \left( \frac{\partial h_0}{\partial y} - u \frac{\partial u}{\partial y} \right) \quad (16.72)$$

and

$$\mu \left( \frac{\partial u}{\partial y} \right)^2 + u \frac{\partial}{\partial y} \left( \mu \frac{\partial u}{\partial y} \right) = \frac{\partial}{\partial y} \left( \mu u \frac{\partial u}{\partial y} \right) \quad (16.73)$$

Substituting Eqs. (16.72) and (16.73) into (16.71), we obtain

$$\rho u \frac{\partial h_0}{\partial x} + \rho v \frac{\partial h_0}{\partial y} = \frac{\partial}{\partial y} \left[ \frac{\mu}{Pr} \frac{\partial h_0}{\partial y} + \left( 1 - \frac{1}{Pr} \right) \mu u \frac{\partial u}{\partial y} \right] \quad (16.74)$$

which is an alternate form of the boundary-layer energy equation. In this equation,  $\Pr$  is the local Prandtl number, which, in general, is a function of  $T$  and hence varies throughout the boundary layer.

For the laminar, compressible flow over a flat plate, the system of governing equations can now be considered to be Eqs. (16.64) to (16.66) and (16.74). These are nonlinear partial differential equations. As in the incompressible case, let us seek a self-similar solution; however, the transformed independent variables must be defined differently:

$$\xi = \rho_c \mu_c t_c x \quad \xi = \xi(x)$$

$$\eta = \frac{u_c}{\sqrt{2\xi}} \int_0^y \rho_c dy \quad \eta = \eta(x, y)$$

The dependent variables are transformed as follows:

$$f' = \frac{u}{u_c} \quad (\text{which is consistent with defining stream function } \psi = \sqrt{2\xi} f)$$

$$g = \frac{h_0}{(h_0)_c}$$

The mechanics of the transformation using the chain rule are similar to that described in Sec. 16.4. Hence, without detailing the precise steps (which are left for your entertainment), Eqs. (16.65) and (16.74) transform to

$$\left( \frac{\rho\mu}{\rho_c\mu_c} f' \right)' + ff' = 0 \quad (16.75)$$

$$\text{and} \quad \left( \frac{\rho\mu}{\rho_c\mu_c} \frac{1}{\Pr} g' \right)' + fg' + \frac{u_c^2}{(h_0)_c} \left[ \left( 1 - \frac{1}{\Pr} \right) \frac{\rho\mu}{\rho_c\mu_c} f' f'' \right]' = 0 \quad (16.76)$$

Examine Eqs. (16.75) and (16.76) closely. They are ordinary differential equations—recall that the primes denote differentiation with respect to  $\eta$ . Therefore, the compressible, laminar flow over a flat plate does lend itself to a self-similar solution, where  $f = f(\eta)$  and  $g = g(\eta)$ . That is, the velocity and total enthalpy profiles plotted versus  $\eta$  are the same at any station. Furthermore, the product  $\rho\mu$  is a variable and depends in part on temperature. Hence, Eq. (16.75) is coupled to the energy equation, Eq. (16.76), via  $\rho\mu$ . Of course, the energy equation is strongly coupled to Eq. (16.75) via the appearance of  $f, f'$ , and  $f''$  in Eq. (16.76). Hence, we are dealing with a system of coupled ordinary differential equations which must be solved simultaneously. The boundary conditions for these equations are

At  $\eta = 0$ :

$$f = f' = 0 \quad g = g_w$$

$$f' = 1 \quad g = 1$$

Note that the coefficient  $u_c^2/(h_0)_c$  appearing in Eq. (16.76) is simply a function of Mach number:

$$\begin{aligned} \frac{u_c^2}{(h_0)_c} &= \frac{u_c^2}{h_c + u_c^2/2} = \frac{1}{h_c/u_c^2 + \frac{1}{2}} = \frac{1}{c_p h_c/u_c^2 + \frac{1}{2}} = \frac{1}{RT_c/(\gamma - 1)M_c^2 + \frac{1}{2}} \\ &= \frac{1}{1/(\gamma - 1)M_c^2 + \frac{1}{2}} = \frac{2(\gamma - 1)M_c^2}{2 + (\gamma - 1)M_c^2} \end{aligned}$$

Therefore, Eq. (16.76) involves as a parameter the Mach number of the flow at the outer edge of the boundary layer, i.e., for the flat plate case, the freestream Mach number. Hence, we can explicitly see that the compressible boundary-layer solutions will depend on the Mach number. Moreover, because of the appearance of the local  $\Pr$  in Eq. (16.76), the solutions will also depend on the freestream Prandtl number as a parameter. Finally, note from the boundary conditions that the value of  $g$  at the wall,  $g_w$ , is a given quantity. Note that at the wall where  $u = 0$ ,  $g_w = h_w/(h_0)_c = c_p T_w/(h_0)_c$ . Hence, instead of referring to a given enthalpy at the wall,  $g_w$ , we usually deal with a given wall temperature,  $T_w$ . An alternative to a given value of  $T_w$  is the assumption of an *adiabatic wall*, i.e., a case where there is no heat transfer to the wall. If  $\dot{q}_w = k(\partial T/\partial y)_w = 0$ , then  $(\partial T/\partial y)_w = 0$ . Hence, for an adiabatic wall, the boundary condition at the wall becomes simply  $(\partial T/\partial y)_w = 0$ .

In short, we see from the above discussion that a numerical self-similar solution can be obtained for the compressible, laminar flow over a flat plate. However, this solution depends on the Mach number, the Prandtl number, and the condition of the wall (whether it is adiabatic or a constant temperature wall with  $T_w$  given). Such numerical solutions have been carried out; see Ref. 4.3 for details. Return to Eq. (16.55) for the friction drag coefficient for incompressible flow. The analogous compressible result can be written as

$$C_f = \frac{1.328}{\sqrt{\text{Re}_c}} F(M_c, \Pr, T_w) \quad (16.77)$$

In Eq. (16.77), the function  $F$  must be determined numerically. Sample results are given in Fig. 16.10, which shows that the product  $C_f \sqrt{\text{Re}_c}$  decreases as  $M_c$  increases.

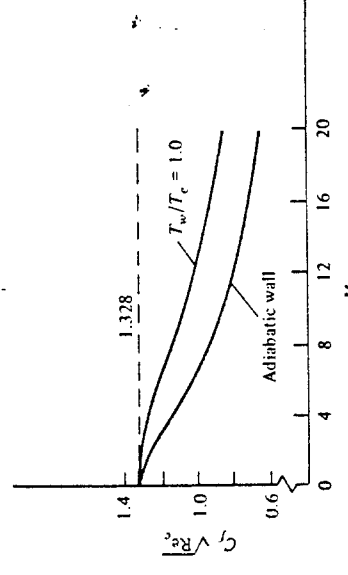
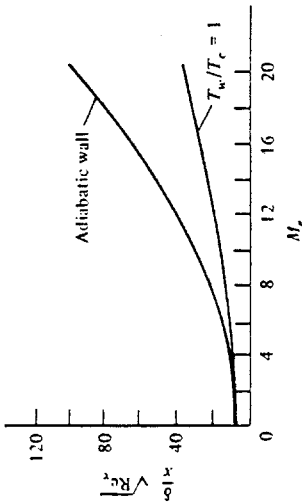


Figure 16.10 Friction drag coefficient for laminar, compressible flow over a flat plate, illustrating the effect of Mach number and wall temperature.  $\Pr = 0.75$ . (Calculations by E. R. van Driest, NACA Tech. Note 2597.)



**Figure 16.11** Boundary-layer thickness  $\delta$  versus Mach number  $M_w$  for laminar, compressible flow over a flat plate, illustrating the effect of Mach and wall temperature.  $\Pr = 0.75$ . (Calculations by E.R. van Driest, NACA Tech. Note 2597.)

Moreover, the adiabatic wall is warmer than the wall in the case of  $T_w/T_e = 1.0$ . Hence, Fig. 16.10 demonstrates that a hot wall also reduces  $C_f \sqrt{Re_c}$ .

Return to Eq. (16.56) for the thickness of the incompressible flat plate boundary layer. The analogous result for compressible flow is

$$\delta = \frac{5.0x}{\sqrt{Re}} G(M_\infty, \Pr, T_w) \quad (16.78)$$

In Eq. (16.78), the function  $G$  must be determined numerically. Sample results are given in Fig. 16.11, which shows that the product  $(\delta \sqrt{Re}/x)$  increases as  $M_\infty$  increases. Everything else being equal, boundary layers are thicker at higher Mach numbers. This fact was stated earlier, in Chap. 14 dealing with hypersonic flow. Note also from Fig. 16.11 that a hot wall thickens the boundary layer.

## 16.6 RESULTS FOR TURBULENT BOUNDARY LAYERS

The basic nature of turbulent flow and the transition of laminar to turbulent flow was discussed in Chap. 15. The analysis of turbulent boundary layers is a constantly evolving and heavily worked subject; it is not our purpose to even introduce such analyses here. Rather, in this section we discuss a few results for the turbulent boundary layer on a flat plate, both incompressible and compressible, simply to provide a basis of comparison with the laminar results described in the previous section. For considerably more detail on the subject of turbulent boundary layers, consult Refs. 42 to 44.

For incompressible flow over a flat plate, the boundary-layer thickness is given approximately by

$$\delta = \frac{0.37x}{Re_c^{1/5}} \quad (16.79)$$

Note from Eq. (16.79) that the turbulent boundary-layer thickness varies approximately as  $Re_c^{-1/5}$  in contrast to  $Re_c^{-1/2}$  for a laminar boundary layer. Also, turbulent values of  $\delta$  grow more rapidly with distance along the surface;  $\delta \propto x^{4/5}$  for a turbulent flow in contrast to  $\delta \propto x^{1/2}$  for a laminar flow. With regard to skin friction drag, for incompressible turbulent flow over a flat plate, we have

$$C_f = \frac{0.074}{Re_c^{1/5}} \quad (16.80)$$

Note that for turbulent flow,  $C_f$  varies as  $Re_c^{-1/5}$  in comparison with the  $Re_c^{-1/2}$  variation for laminar flow. Hence, Eq. (16.80) yields larger friction drag coefficients for turbulent flow in comparison with Eq. (16.55) for laminar flow.

The effects of compressibility on Eq. (16.80) are shown in Fig. 16.12, where  $C_f$  is plotted versus  $Re_c$  with  $M_\infty$  as a parameter. The turbulent flow results are shown toward the right of Fig. 16.12, at the higher values of Reynolds numbers where turbulent conditions are expected to occur, and laminar flow results are shown toward the left of the figure, at lower values of Reynolds numbers. This type of figure — friction drag coefficient for both laminar and turbulent flow as a function of  $Re$  on a log-log plot — is a classic picture, and it allows a ready contrast of the two types of flow. From this figure, we can see that, for the same  $Re_c$ , turbulent skin friction is higher than laminar; also, the slopes of the turbulent curves are smaller than the slopes of the laminar curves — a graphic comparison of the  $Re^{-1/5}$  variation in contrast to the laminar  $Re^{-1/2}$  variation. Note that the effect of increasing  $M_\infty$  is to reduce  $C_f$  at constant  $Re$  and that this effect is stronger on the turbulent flow results. Indeed,  $C_f$  for the turbulent results decreases by almost an order of magnitude (at the higher values of  $Re_c$ ) when  $M_\infty$  is increased from 0 to 10. For the laminar flow, the decrease in  $C_f$  as  $M_\infty$  is increased through the same Mach number range is far less pronounced.

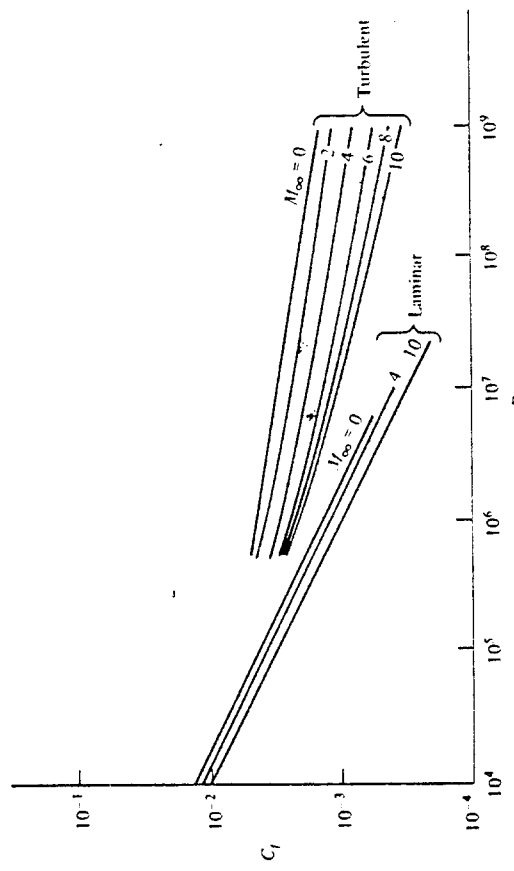


**Figure 16.12** Turbulent friction coefficient for a flat plate as a function of Reynolds and Mach numbers. Adiabatic wall.  $\Pr = 0.75$ . For contrast, some laminar results are shown. (Data are from the calculations of van Driest, Ref. 47.)

## 16.7 FINAL COMMENTS

This brings to an end our discussion of boundary-layer flows in particular and of viscous flow in general. Our purpose has been to introduce some basic ideas and concepts of viscous flow in such a fashion as to put our earlier studies of inviscid flows in proper perspective. By no means have we presented a picture even resembling a complete story of viscous flow. Rather, we hope only to have whetted your appetite for further study, and again, Refs. 42 to 44 are reasonable sources for such further reading. We are also out of our allotted space for this book. Therefore, we hope that you have enjoyed and benefited from our presentation of the fundamentals of aerodynamics. However, before closing the cover, it might be useful to return once again to Fig. 1.27, which is the block diagram categorizing the different general types of aerodynamic flows. Recall the curious, uninitiated thoughts you might have had when you first examined this figure during your study of Chap. 1, and compare these with your informed and mature thoughts that you now have—honed by the aerodynamic knowledge packed into the intervening pages. Hopefully, each block in Fig. 1.27 has substantially more meaning for you now than when we first started. If this is true, then my efforts as an author have not gone in vain.

## 16.8 SUMMARY

Return to the road map given in Fig. 16.2, and make certain that you feel at home with the material represented by each box. The highlights of our discussion of boundary layers are summarized as follows.

The basic quantities of interest from boundary-layer theory are the velocity and thermal boundary-layer thicknesses,  $\delta$  and  $\delta_t$ , respectively, the shear stress at the wall,  $\tau_w$ , and heat transfer to the surface,  $q_w$ . In the process, we can define two additional thicknesses: the displacement thickness

$$\delta^* \equiv \int_0^\infty \left(1 - \frac{\rho u}{\rho_s u_s}\right) dy \quad \delta \leq y \rightarrow \infty \quad (16.3)$$

and the momentum thickness

$$\theta \equiv \int_0^\infty \frac{\rho u}{\rho_s u_s} \left(1 - \frac{u}{u_s}\right) dy \quad \delta \leq y \rightarrow \infty \quad (16.10)$$

Both  $\delta^*$  and  $\theta$  are related to decrements in the flow due to the presence of the boundary layer;  $\delta^*$  is proportional to the decrement in mass flow, and  $\theta$  is proportional to the decrement in momentum flow. Moreover,  $\delta^*$  is the distance away from the body surface through which the outer inviscid flow is displaced due to the boundary layer. The body shape plus  $\delta^*$  defines a new effective body seen by the inviscid flow.

By an order-of-magnitude analysis, the complete Navier-Stokes equations for two-dimensional flow reduce to the following boundary-layer equations:

$$\text{Continuity:} \quad \frac{\partial(\rho u)}{\partial x} + \frac{\partial(\rho v)}{\partial y} = 0 \quad (16.28)$$

$$\text{x momentum:} \quad \mu u \frac{\partial u}{\partial x} + \rho v \frac{\partial u}{\partial y} = -\frac{dp_e}{dx} + \frac{\partial}{\partial y} \left( \mu \frac{\partial u}{\partial y} \right) \quad (16.29)$$

$$\text{y momentum:} \quad \frac{\partial p}{\partial y} = 0 \quad (16.30)$$

$$\text{Energy:} \quad \rho u \frac{\partial h}{\partial x} + \rho v \frac{\partial h}{\partial y} = \frac{\partial}{\partial y} \left( k \frac{\partial T}{\partial y} \right) + u \frac{dp_e}{dx} + \mu \left( \frac{\partial u}{\partial y} \right)^2 \quad (16.31)$$

These equations are subject to the boundary conditions:

$$\text{At the wall:} \quad y = 0 \quad u = 0 \quad v = 0 \quad h = h_w$$

$$\text{At the boundary-layer edge:} \quad y \rightarrow \infty \quad u \rightarrow u_\infty \quad h \rightarrow h_\infty$$

Inherent in the above boundary-layer equations are the assumptions that  $\delta \ll c$ ,  $Re$  is large, and  $M_\infty$  is not inordinately large.

For incompressible laminar flow over a flat plate, the boundary-layer equations reduce to the Blasius equation

$$2f''' + ff'' = 0 \quad (16.48)$$

where  $f' = u/u_\infty$ . This produces a self-similar solution where  $f' = f'(\eta)$ , independent of any particular  $x$  station along the surface. A numerical solution of Eq. (16.48) yields numbers which lead to the following results. ,

*Local skin friction coefficient:*

$$c_f = \frac{\tau_w}{\frac{1}{2} \rho_s V_\infty^2} = \frac{0.664}{\sqrt{Re_x}} \quad (16.53)$$

*Integrated friction drag coefficient:*  $C_f = \frac{1.328}{\sqrt{Re_x}}$   $c_f = \frac{1.328}{\sqrt{Re_x}}$   $(16.55)$

*Boundary-layer thickness:*  $\delta = \frac{5.0x}{\sqrt{Re_x}}$   $(16.56)$

*Displacement thickness:*  $\delta^* = \frac{1.72x}{\sqrt{Re_x}}$   $(16.59)$

*Momentum thickness:*  $\theta = \frac{0.664x}{\sqrt{Re_x}}$   $(16.61)$

Compressibility effects are such as to make boundary-layer solutions a function of Mach number, Prandtl number, and wall-to-freestream temperature ratio. Typical compressibility effects are shown in Figs. 16.10 to 16.12. Generally, compressibility reduces  $C_f$  and increases  $\delta$ .

## APPENDIX A

### ISENTROPIC FLOW PROPERTIES

Approximations for turbulent, incompressible flow over a flat plate are

$$\delta = \frac{0.37x}{Re_x^{1/5}} \quad (16.79)$$

$$C_f = \frac{0.074}{Re_t^{1/5}} \quad (16.80)$$

and

### PROBLEMS

*Note:* The standard sea level value of viscosity coefficient for air is  $\mu = 1.7894 \times 10^{-5} \text{ kg}/(\text{m} \cdot \text{s}) = 3.7373 \times 10^{-7} \text{ slug}/(\text{ft} \cdot \text{s})$ .

16.1 The wing on a Piper Cherokee general aviation aircraft is rectangular, with a span of 9.75 m and a chord of 1.6 m. The aircraft is flying at cruising speed (141 mi/h) at sea level. Assume that the skin friction drag on the wing can be approximated by the drag on a flat plate of the same dimensions. Calculate the skin friction drag.

- (a) If the flow were completely laminar (which is not the case in real life)
- (b) If the flow were completely turbulent (which is more realistic)

Compare the two results.

16.2 For the case in Prob. 16.1, calculate the boundary-layer thickness at the trailing edge for

- (a) Completely laminar flow
- (b) Completely turbulent flow

16.3 For the case in Prob. 16.1, calculate the skin friction drag accounting for transition. Assume the transition Reynolds number  $= 5 \times 10^4$ .

16.4 Consider Mach 4 flow at standard sea level conditions over a flat plate of chord 5 in. Assuming all laminar flow and adiabatic wall conditions, calculate the skin friction drag on the plate per unit span.

16.5 Repeat Prob. 16.4 for the case of all turbulent flow.

16.6 Consider a compressible, laminar boundary layer over a flat plate. Assuming  $Pr = 1$  and a calorically perfect gas, show that the profile of total temperature through the boundary layer is a function of the velocity profile via

$$T_0 = T_w + (T_{\infty} - T_w) \frac{u}{u_*}$$

where  $T_w$  = wall temperature and  $T_{\infty}$  and  $u_*$  are the total temperature and velocity, respectively, at the outer edge of the boundary layer. [Hint: Compare Eqs. (16.65) and (16.74).]

$M$	$\frac{P_0}{P}$	$\frac{\rho_0}{\rho}$	$\frac{T_0}{T}$	$\frac{A}{A^*}$
0.2000 -0.01	0.1000 +0.01	0.1000 +0.01	0.1000 +0.01	0.2894 +0.02
0.4000 -0.01	0.1001 +0.01	0.1001 +0.01	0.1001 +0.01	0.1448 +0.02
0.6000 -0.01	0.1003 +0.01	0.1002 +0.01	0.1001 +0.01	0.9686 +0.01
0.8000 -0.01	0.1004 +0.01	0.1003 +0.01	0.1001 +0.01	0.7262 +0.01
1.0000 +0.00	0.1007 +0.01	0.1005 +0.01	0.1002 +0.01	0.5822 +0.01
1.2000 +0.00	0.1010 +0.01	0.1007 +0.01	0.1003 +0.01	0.4854 +0.01
1.4000 +0.00	0.1014 +0.01	0.1010 +0.01	0.1004 +0.01	0.4182 +0.01
1.6000 +0.00	0.1018 +0.01	0.1013 +0.01	0.1005 +0.01	0.3673 +0.01
1.8000 +0.00	0.1023 +0.01	0.1016 +0.01	0.1006 +0.01	0.3278 +0.01
2.0000 +0.00	0.1028 +0.01	0.1020 +0.01	0.1008 +0.01	0.2964 +0.01
2.2000 +0.00	0.1034 +0.01	0.1024 +0.01	0.1010 +0.01	0.2708 +0.01
2.4000 +0.00	0.1041 +0.01	0.1029 +0.01	0.1012 +0.01	0.2496 +0.01
2.6000 +0.00	0.1048 +0.01	0.1034 +0.01	0.1014 +0.01	0.2317 +0.01
2.8000 +0.00	0.1056 +0.01	0.1040 +0.01	0.1016 +0.01	0.2166 +0.01
3.0000 +0.00	0.1064 +0.01	0.1046 +0.01	0.1018 +0.01	0.2035 +0.01
3.2000 +0.00	0.1074 +0.01	0.1052 +0.01	0.1020 +0.01	0.1922 +0.01
3.4000 +0.00	0.1083 +0.01	0.1059 +0.01	0.1023 +0.01	0.1823 +0.01
3.6000 +0.00	0.1094 +0.01	0.1066 +0.01	0.1026 +0.01	0.1736 +0.01
3.8000 +0.00	0.1105 +0.01	0.1074 +0.01	0.1029 +0.01	0.1659 +0.01
4.0000 +0.00	0.1117 +0.01	0.1082 +0.01	0.1032 +0.01	0.1590 +0.01
4.2000 +0.00	0.1129 +0.01	0.1091 +0.01	0.1035 +0.01	0.1529 +0.01
4.4000 +0.00	0.1142 +0.01	0.1100 +0.01	0.1039 +0.01	0.1474 +0.01
4.6000 +0.00	0.1156 +0.01	0.1109 +0.01	0.1042 +0.01	0.1425 +0.01
4.8000 +0.00	0.1171 +0.01	0.1119 +0.01	0.1046 +0.01	0.1380 +0.01
5.0000 +0.00	0.1186 +0.01	0.1130 +0.01	0.1050 +0.01	0.1340 +0.01
5.2000 +0.00	0.1202 +0.01	0.1141 +0.01	0.1054 +0.01	0.1303 +0.01
5.4000 +0.00	0.1219 +0.01	0.1152 +0.01	0.1058 +0.01	0.1270 +0.01
5.6000 +0.00	0.1237 +0.01	0.1164 +0.01	0.1063 +0.01	0.1240 +0.01
5.8000 +0.00	0.1256 +0.01	0.1177 +0.01	0.1067 +0.01	0.1213 +0.01
6.0000 +0.00	0.1276 +0.01	0.1190 +0.01	0.1072 +0.01	0.1188 +0.01

$M$	$\frac{p_e}{p}$	$\frac{\rho_e}{\rho}$	$\frac{T_e}{T}$	$\frac{A}{A^*}$	$M$	$\frac{p_e}{p}$	$\frac{\rho_e}{\rho}$	$\frac{T_e}{T}$	$\frac{A}{A^*}$
0.6200+00	0.1296+01	0.1203+01	0.1077+01	0.1166+01	0.1620+01	0.4378+01	0.2871+01	0.1525+01	0.1267+01
0.6400+00	0.1317+01	0.1218+01	0.1082+01	0.1145+01	0.1640+01	0.4511+01	0.2933+01	0.1538+01	0.1284+01
0.6600+00	0.1340+01	0.1232+01	0.1087+01	0.1127+01	0.1660+01	0.4648+01	0.2996+01	0.1551+01	0.1301+01
0.6800+00	0.1363+01	0.1247+01	0.1092+01	0.1110+01	0.1680+01	0.4790+01	0.3061+01	0.1564+01	0.1319+01
0.7000+00	0.1387+01	0.1263+01	0.1094+01	0.1098+01	0.1700+01	0.4936+01	0.3128+01	0.1578+01	0.1338+01
0.7200+00	0.1412+01	0.1280+01	0.1104+01	0.1081+01	0.1720+01	0.5087+01	0.3196+01	0.1592+01	0.1357+01
0.7400+00	0.1439+01	0.1297+01	0.1110+01	0.1068+01	0.1740+01	0.5244+01	0.3266+01	0.1606+01	0.1376+01
0.7600+00	0.1466+01	0.1314+01	0.1116+01	0.1057+01	0.1760+01	0.5406+01	0.3338+01	0.1620+01	0.1397+01
0.7800+00	0.1495+01	0.1333+01	0.1122+01	0.1047+01	0.1780+01	0.5573+01	0.3411+01	0.1634+01	0.1418+01
0.8000+00	0.1524+01	0.1351+01	0.1128+01	0.1038+01	0.1800+01	0.5746+01	0.3487+01	0.1648+01	0.1439+01
0.8200+00	0.1553+01	0.1371+01	0.1134+01	0.1030+01	0.1820+01	0.5924+01	0.3564+01	0.1662+01	0.1461+01
0.8400+00	0.1587+01	0.1391+01	0.1141+01	0.1024+01	0.1840+01	0.6109+01	0.3643+01	0.1677+01	0.1484+01
0.8600+00	0.1621+01	0.1412+01	0.1148+01	0.1018+01	0.1860+01	0.6300+01	0.3723+01	0.1692+01	0.1507+01
0.8800+00	0.1655+01	0.1433+01	0.1155+01	0.1013+01	0.1880+01	0.6497+01	0.3806+01	0.1707+01	0.1531+01
0.9000+00	0.1691+01	0.1456+01	0.1162+01	0.1009+01	0.1900+01	0.6701+01	0.3891+01	0.1722+01	0.1555+01
0.9200+00	0.1729+01	0.1478+01	0.1169+01	0.1006+01	0.1920+01	0.6911+01	0.3978+01	0.1737+01	0.1580+01
0.9400+00	0.1767+01	0.1502+01	0.1177+01	0.1003+01	0.1940+01	0.7138+01	0.4067+01	0.1753+01	0.1606+01
0.9600+00	0.1808+01	0.1526+01	0.1184+01	0.1001+01	0.1960+01	0.7353+01	0.4158+01	0.1768+01	0.1633+01
0.9800+00	0.1850+01	0.1552+01	0.1192+01	0.1000+01	0.1980+01	0.7585+01	0.4251+01	0.1784+01	0.1660+01
0.1000+01	0.1893+01	0.1577+01	0.1200+01	0.1000+01	0.2000+01	0.7824+01	0.4347+01	0.1800+01	0.1687+01
0.1020+01	0.1938+01	0.1604+01	0.1208+01	0.1000+01	0.2050+01	0.8458+01	0.4596+01	0.1840+01	0.1760+01
0.1040+01	0.1995+01	0.1632+01	0.1216+01	0.1001+01	0.2100+01	0.9145+01	0.4859+01	0.1882+01	0.1837+01
0.1060+01	0.2033+01	0.1660+01	0.1225+01	0.1003+01	0.2150+01	0.9888+01	0.5138+01	0.1924+01	0.1919+01
0.1080+01	0.2083+01	0.1689+01	0.1233+01	0.1005+01	0.2200+01	0.1069+02	0.5413+01	0.1968+01	0.2005+01
0.1100+01	0.2135+01	0.1719+01	0.1242+01	0.1008+01	0.2250+01	0.1156+02	0.5746+01	0.2012+01	0.2096+01
0.1120+01	0.2189+01	0.1750+01	0.1251+01	0.1011+01	0.2300+01	0.1250+02	0.6076+01	0.2058+01	0.2193+01
0.1140+01	0.2245+01	0.1782+01	0.1260+01	0.1015+01	0.2350+01	0.1352+02	0.6425+01	0.2104+01	0.2295+01
0.1160+01	0.2303+01	0.1814+01	0.1269+01	0.1020+01	0.2400+01	0.1462+02	0.6794+01	0.2152+01	0.2403+01
0.1180+01	0.2363+01	0.1848+01	0.1278+01	0.1025+01	0.2450+01	0.1581+02	0.7183+01	0.2200+01	0.2517+01
0.1200+01	0.2425+01	0.1883+01	0.1288+01	0.1040+01	0.2500+01	0.1709+02	0.7594+01	0.2250+01	0.2637+01
0.1220+01	0.2489+01	0.1918+01	0.1298+01	0.1037+01	0.2550+01	0.1847+02	0.8027+01	0.2300+01	0.2763+01
0.1240+01	0.2556+01	0.1955+01	0.1308+01	0.1043+01	0.2600+01	0.1995+02	0.8384+01	0.2352+01	0.2896+01
0.1260+01	0.2625+01	0.1992+01	0.1318+01	0.1050+01	0.2650+01	0.2156+02	0.8865+01	0.2404+01	0.3016+01
0.1280+01	0.2697+01	0.2031+01	0.1328+01	0.1058+01	0.2700+01	0.2228+02	0.9472+01	0.2458+01	0.3183+01
0.1300+01	0.2771+01	0.2071+01	0.1338+01	0.1066+01	0.2750+01	0.2314+02	0.1001+02	0.2512+01	0.3338+01
0.1320+01	0.2847+01	0.2112+01	0.1348+01	0.1075+01	0.2800+01	0.2714+02	0.1057+02	0.2568+01	0.3500+01
0.1340+01	0.2927+01	0.2153+01	0.1359+01	0.1084+01	0.2850+01	0.2829+02	0.1116+02	0.2624+01	0.3671+01
0.1360+01	0.3009+01	0.2197+01	0.1370+01	0.1094+01	0.2900+01	0.3159+02	0.1178+02	0.2682+01	0.3850+01
0.1380+01	0.3094+01	0.2241+01	0.1381+01	0.1104+01	0.2950+01	0.3407+02	0.1243+02	0.2740+01	0.4018+01
0.1400+01	0.3182+01	0.2286+01	0.1392+01	0.1115+01	0.3000+01	0.3673+02	0.1312+02	0.2800+01	0.4225+01
0.1420+01	0.3273+01	0.2333+01	0.1403+01	0.1126+01	0.3050+01	0.3959+02	0.1384+02	0.2860+01	0.4441+01
0.1440+01	0.3368+01	0.2381+01	0.1415+01	0.1138+01	0.3100+01	0.4265+02	0.1459+02	0.2922+01	0.4657+01
0.1460+01	0.3465+01	0.2430+01	0.1426+01	0.1150+01	0.3150+01	0.4593+02	0.1539+02	0.2984+01	0.4884+01
0.1480+01	0.3566+01	0.2480+01	0.1438+01	0.1163+01	0.3200+01	0.4944+02	0.1622+02	0.3048+01	0.5121+01
0.1500+01	0.3671+01	0.2532+01	0.1450+01	0.1176+01	0.3250+01	0.5320+02	0.1709+02	0.3112+01	0.5369+01
0.1520+01	0.3779+01	0.2585+01	0.1462+01	0.1190+01	0.3300+01	0.5722+02	0.1800+02	0.3178+01	0.5629+01
0.1540+01	0.3891+01	0.2619+01	0.1474+01	0.1204+01	0.3350+01	0.6152+02	0.1896+02	0.3244+01	0.5900+01
0.1560+01	0.4007+01	0.2695+01	0.1487+01	0.1219+01	0.3400+01	0.6612+02	0.1996+02	0.3312+01	0.6184+01
0.1580+01	0.4127+01	0.2752+01	0.1499+01	0.1234+01	0.3450+01	0.7103+02	0.2101+02	0.3380+01	0.6480+01
0.1600+01	0.4250+01	0.2811+01	0.1512+01	0.1250+01	0.3500+01	0.7627+02	0.2211+02	0.3450+01	0.6790+01

$M$	$\frac{p_e}{p}$	$\frac{\rho_e}{\rho}$	$\frac{T_e}{T}$	$\frac{A}{A^*}$	$M$	$\frac{p_e}{p}$	$\frac{\rho_e}{\rho}$	$\frac{T_e}{T}$	$A$
0.3550+01	0.8187+02	0.2125+02	0.3520+01	0.7113+01	0.7100+01	0.4531+04	0.4088+03	0.1108+02	0.1109+03
0.3600+01	0.8784+02	0.2445+02	0.3392+01	0.7450+01	0.7200+01	0.4953+04	0.4357+03	0.1137+02	0.1181+03
0.3650+01	0.9420+02	0.2571+02	0.3664+01	0.7802+01	0.7300+01	0.5410+04	0.4640+03	0.1166+02	0.1256+03
0.3700+01	0.1010+03	0.2701+02	0.3738+01	0.8169+01	0.7400+01	0.5903+04	0.4939+03	0.1195+02	0.1335+03
0.3750+01	0.1082+03	0.2838+02	0.3812+01	0.8552+01	0.7500+01	0.6434+04	0.5252+03	0.1225+02	0.1418+03
0.3800+01	0.1159+03	0.2981+02	0.3888+01	0.8851+01	0.7600+01	0.7006+04	0.5582+03	0.1255+02	0.1506+03
0.3850+01	0.1241+03	0.3129+02	0.3964+01	0.9366+01	0.7700+01	0.7623+04	0.5928+03	0.1286+02	0.1598+03
0.3900+01	0.1328+03	0.3285+02	0.4042+01	0.9799+01	0.7800+01	0.8285+04	0.6292+03	0.1317+02	0.1694+03
0.3950+01	0.1420+03	0.3446+02	0.4120+01	0.1025+02	0.7900+01	0.8998+04	0.6674+03	0.1348+02	0.1795+03
0.4000+01	0.1518+03	0.3615+02	0.4200+01	0.1072+02	0.8000+01	0.9763+04	0.7075+03	0.1380+02	0.1901+03
0.4050+01	0.1623+03	0.3791+02	0.4280+01	0.1121+02	0.9000+01	0.2110+05	0.1227+04	0.1720+02	0.3272+03
0.4100+01	0.1733+03	0.3974+02	0.4362+01	0.1171+02	0.1000+02	0.4244+05	0.2021+04	0.2100+02	0.5339+03
0.4150+01	0.1851+03	0.4164+02	0.4444+01	0.1224+02	0.1100+02	0.8033+05	0.3188+04	0.2520+02	0.8419+03
0.4200+01	0.1975+03	0.4363+02	0.4528+01	0.1279+02	0.1200+02	0.1445+06	0.4648+04	0.2980+02	0.1276+04
0.4250+01	0.2108+03	0.4569+02	0.4612+01	0.1336+02	0.1300+02	0.2486+06	0.7144+04	0.3480+02	0.1876+04
0.4300+01	0.2247+03	0.4784+02	0.4698+01	0.1395+02	0.1400+02	0.4119+06	0.1025+05	0.4020+02	0.2685+04
0.4350+01	0.2396+03	0.5007+02	0.4784+01	0.1457+02	0.1500+02	0.6602+06	0.1435+05	0.4600+02	0.3735+04
0.4400+01	0.2553+03	0.5239+02	0.4872+01	0.1521+02	0.1600+02	0.1028+07	0.1969+05	0.5220+02	0.5145+04
0.4450+01	0.2719+03	0.5480+02	0.4960+01	0.1587+02	0.1700+02	0.1559+07	0.2651+05	0.5880+02	0.6921+04
0.4500+01	0.2894+03	0.5731+02	0.5050+01	0.1656+02	0.1800+02	0.2311+07	0.3512+05	0.6580+02	0.9159+04
0.4550+01	0.3080+03	0.5991+02	0.5140+01	0.1728+02	0.1900+02	0.3356+07	0.4584+05	0.7320+02	0.1195+05
0.4600+01	0.3276+03	0.6261+02	0.5232+01	0.1802+02	0.2000+02	0.4783+07	0.5905+05	0.8100+02	0.1538+05
0.4650+01	0.3483+03	0.6545+02	0.5324+01	0.1879+02	0.2200+02	0.9251+07	0.9459+05	0.9780+02	0.2461+05
0.4700+01	0.3702+03	0.6833+02	0.5418+01	0.1958+02	0.2400+02	0.1691+08	0.1456+06	0.1162+03	0.3783+05
0.4750+01	0.3913+03	0.7135+02	0.5512+01	0.2041+02	0.2600+02	0.2949+08	0.2165+06	0.1362+03	0.5624+05
0.4800+01	0.4177+03	0.7448+02	0.5608+01	0.2126+02	0.2800+02	0.4936+08	0.3128+06	0.1578+03	0.8121+05
0.4850+01	0.4434+03	0.7772+02	0.5704+01	0.2215+02	0.3000+02	0.7978+08	0.4408+06	0.1810+03	0.1144+06
0.4900+01	0.4705+03	0.8109+02	0.5802+01	0.2307+02	0.3200+02	0.1250+09	0.6076+06	0.2058+03	0.1576+06
0.4950+01	0.4990+03	0.8457+02	0.5900+01	0.2402+02	0.3400+02	0.1908+09	0.8216+06	0.2322+03	0.2131+06
0.5000+01	0.5291+03	0.8818+02	0.6000+01	0.2500+02	0.3600+02	0.2842+09	0.1092+07	0.2602+03	0.2832+06
0.5100+01	0.5941+03	0.9579+02	0.6202+01	0.2707+02	0.3800+02	0.4143+09	0.1430+07	0.2898+03	0.1707+06
0.5200+01	0.6661+03	0.1039+03	0.6408+01	0.2928+02	0.4000+02	0.5926+09	0.1846+07	0.3210+03	0.4785+06
0.5300+01	0.7457+03	0.1127+03	0.6618+01	0.3165+02	0.4200+02	0.8330+09	0.2354+07	0.3538+03	0.6102+06
0.5400+01	0.8335+03	0.1220+03	0.6832+01	0.3417+02	0.4400+02	0.1153+10	0.2969+07	0.3882+03	0.7694+06
0.5500+01	0.9204+03	0.1320+03	0.7050+01	0.3687+02	0.4600+02	0.1572+10	0.3706+07	0.4242+03	0.9603+06
0.5600+01	0.1037+04	0.1426+03	0.7272+01	0.3974+02	0.4800+02	0.2116+10	0.4583+07	0.4618+03	0.1187+07
0.5700+01	0.1154+04	0.1539+03	0.7489+01	0.4280+02	0.5000+02	0.2815+10	0.5618+07	0.5010+03	0.1455+07
0.5800+01	0.1283+04	0.1660+03	0.7728+01	0.4605+02					
0.5900+01	0.1424+04	0.1789+03	0.7962+01	0.4951+02					
0.6000+01	0.1579+04	0.1925+03	0.8200+01	0.5318+02					
0.6100+01	0.1748+04	0.2071+03	0.8442+01	0.5708+02					
0.6200+01	0.1913+04	0.2225+03	0.8688+01	0.6121+02					
0.6300+01	0.2135+04	0.2388+03	0.8938+01	0.6559+02					
0.6400+01	0.2355+04	0.2562+03	0.9192+01	0.7023+02					
0.6500+01	0.2594+04	0.2745+03	0.9450+01	0.7513+02					
0.6600+01	0.2835+04	0.2939+03	0.9712+01	0.8032+02					
0.6700+01	0.3138+04	0.3145+03	0.9978+01	0.8580+02					
0.6800+01	0.3445+04	0.3362+03	0.1023+02	0.9159+02					
0.6900+01	0.3779+04	0.3591+03	0.1052+02	0.9770+02					
0.7000+01	0.4140+04	0.3833+03	0.1080+02	0.1041+03					

## NORMAL SHOCK PROPERTIES

$M$	$\frac{p_2}{p_1}$	$\frac{\rho_2}{\rho_1}$	$\frac{T_2}{T_1}$	$\frac{p_{\infty}}{p_1}$	$M_2$	$\frac{p_{\infty}}{p_1}$	$\frac{p_{\infty}}{p_1}$	$\frac{T_1}{T_1}$	$M_2$
						$\frac{p_{\infty}}{p_1}$	$\frac{p_{\infty}}{p_1}$	$\frac{T_1}{T_1}$	$M_2$
0.1600+01	0.2820+01	0.2032+01	0.1388+01	0.8952+00	0.3805+01	0.3805+01	0.3887+01	0.3887+01	0.6684+00
0.1620+01	0.2895+01	0.2065+01	0.1402+01	0.8877+00	0.3887+01	0.3887+01	0.3887+01	0.3887+01	0.6625+00
0.1640+01	0.2971+01	0.2099+01	0.1416+01	0.8799+00	0.3969+01	0.3969+01	0.3969+01	0.3969+01	0.6568+00
0.1660+01	0.3048+01	0.2132+01	0.1430+01	0.8720+00	0.4053+01	0.4053+01	0.4053+01	0.4053+01	0.6512+00
0.1680+01	0.3126+01	0.2165+01	0.1444+01	0.8639+00	0.4138+01	0.4138+01	0.4138+01	0.4138+01	0.6458+00
0.1700+01	0.3205+01	0.2198+01	0.1458+01	0.8557+00	0.4224+01	0.4224+01	0.4224+01	0.4224+01	0.6405+00
0.1720+01	0.3285+01	0.2230+01	0.1473+01	0.8474+00	0.4311+01	0.4311+01	0.4311+01	0.4311+01	0.6355+00
0.1740+01	0.3366+01	0.2263+01	0.1487+01	0.8389+00	0.4399+01	0.4399+01	0.4399+01	0.4399+01	0.6305+00
0.1760+01	0.3447+01	0.2295+01	0.1502+01	0.8302+00	0.4488+01	0.4488+01	0.4488+01	0.4488+01	0.6257+00
0.1780+01	0.3530+01	0.2327+01	0.1517+01	0.8215+00	0.4578+01	0.4578+01	0.4578+01	0.4578+01	0.6210+00
0.1800+01	0.3613+01	0.2359+01	0.1532+01	0.8127+00	0.4670+01	0.4670+01	0.4670+01	0.4670+01	0.6165+00
0.1820+01	0.3698+01	0.2391+01	0.1547+01	0.8038+00	0.4762+01	0.4762+01	0.4762+01	0.4762+01	0.6121+00
0.1840+01	0.3783+01	0.2422+01	0.1562+01	0.7948+00	0.4855+01	0.4855+01	0.4855+01	0.4855+01	0.6078+00
0.1860+01	0.3870+01	0.2454+01	0.1577+01	0.7857+00	0.4950+01	0.4950+01	0.4950+01	0.4950+01	0.6036+00
0.1880+01	0.3957+01	0.2485+01	0.1592+01	0.7765+00	0.5045+01	0.5045+01	0.5045+01	0.5045+01	0.5996+00
0.1900+01	0.4045+01	0.2516+01	0.1608+01	0.7674+00	0.5142+01	0.5142+01	0.5142+01	0.5142+01	0.5956+00
0.1920+01	0.4134+01	0.2546+01	0.1624+01	0.7581+00	0.5239+01	0.5239+01	0.5239+01	0.5239+01	0.5918+00
0.1940+01	0.4224+01	0.2577+01	0.1639+01	0.7488+00	0.5338+01	0.5338+01	0.5338+01	0.5338+01	0.5880+00
0.1960+01	0.4315+01	0.2607+01	0.1655+01	0.7395+00	0.5438+01	0.5438+01	0.5438+01	0.5438+01	0.5844+00
0.1980+01	0.4407+01	0.2637+01	0.1671+01	0.7302+00	0.5539+01	0.5539+01	0.5539+01	0.5539+01	0.5808+00
0.2000+01	0.4500+01	0.2667+01	0.1687+01	0.7209+00	0.5640+01	0.5640+01	0.5640+01	0.5640+01	0.5774+00
0.2020+01	0.4673+01	0.2740+01	0.1729+01	0.6975+00	0.5900+01	0.5900+01	0.5900+01	0.5900+01	0.5691+00
0.2040+01	0.4978+01	0.2812+01	0.1770+01	0.6744+00	0.6165+01	0.6165+01	0.6165+01	0.6165+01	0.5613+00
0.2060+01	0.5226+01	0.2882+01	0.1813+01	0.6511+00	0.6438+01	0.6438+01	0.6438+01	0.6438+01	0.5540+00
0.2080+01	0.5480+01	0.2951+01	0.1857+01	0.6281+00	0.6716+01	0.6716+01	0.6716+01	0.6716+01	0.5471+00
0.2100+01	0.5740+01	0.3019+01	0.1901+01	0.6055+00	0.7002+01	0.7002+01	0.7002+01	0.7002+01	0.5406+00
0.2120+01	0.6005+01	0.3085+01	0.1947+01	0.5833+00	0.7294+01	0.7294+01	0.7294+01	0.7294+01	0.5344+00
0.2140+01	0.6276+01	0.3149+01	0.1993+01	0.5615+00	0.7592+01	0.7592+01	0.7592+01	0.7592+01	0.5286+00
0.2160+01	0.6553+01	0.3212+01	0.2040+01	0.5401+00	0.7897+01	0.7897+01	0.7897+01	0.7897+01	0.5231+00
0.2180+01	0.6836+01	0.3273+01	0.2088+01	0.5193+00	0.8208+01	0.8208+01	0.8208+01	0.8208+01	0.5179+00
0.2200+01	0.7125+01	0.3333+01	0.2137+01	0.4990+00	0.8526+01	0.8526+01	0.8526+01	0.8526+01	0.5130+00
0.2220+01	0.7420+01	0.3392+01	0.2187+01	0.4793+00	0.8830+01	0.8830+01	0.8830+01	0.8830+01	0.5083+00
0.2240+01	0.7720+01	0.3449+01	0.2238+01	0.4601+00	0.9181+01	0.9181+01	0.9181+01	0.9181+01	0.5039+00
0.2260+01	0.8026+01	0.3505+01	0.2290+01	0.4416+00	0.9519+01	0.9519+01	0.9519+01	0.9519+01	0.4996+00
0.2280+01	0.8338+01	0.3559+01	0.2343+01	0.4236+00	0.9862+01	0.9862+01	0.9862+01	0.9862+01	0.4956+00
0.2300+01	0.8656+01	0.3612+01	0.2397+01	0.4062+00	0.1021+02	0.1021+02	0.1021+02	0.1021+02	0.4918+00
0.2320+01	0.8980+01	0.3664+01	0.2451+01	0.3895+00	0.1057+02	0.1057+02	0.1057+02	0.1057+02	0.4882+00
0.2340+01	0.9310+01	0.3714+01	0.2507+01	0.3733+00	0.1093+02	0.1093+02	0.1093+02	0.1093+02	0.4847+00
0.2360+01	0.9645+01	0.3763+01	0.2563+01	0.3577+00	0.1130+02	0.1130+02	0.1130+02	0.1130+02	0.4844+00
0.2380+01	0.9986+01	0.3811+01	0.2621+01	0.3428+00	0.1168+02	0.1168+02	0.1168+02	0.1168+02	0.4782+00
0.2400+01	0.1023+02	0.3857+01	0.2679+01	0.3283+00	0.1206+02	0.1206+02	0.1206+02	0.1206+02	0.4752+00
0.2420+01	0.1049+02	0.3902+01	0.2718+01	0.3145+00	0.1245+02	0.1245+02	0.1245+02	0.1245+02	0.4723+00
0.2440+01	0.1075+02	0.3947+01	0.2759+01	0.3012+00	0.1285+02	0.1285+02	0.1285+02	0.1285+02	0.4695+00
0.2460+01	0.1101+02	0.3990+01	0.1141+02	0.2885+00	0.1325+02	0.1325+02	0.1325+02	0.1325+02	0.4669+00
0.2480+01	0.1127+02	0.4031+01	0.1178+02	0.2950+00	0.1374+02	0.1374+02	0.1374+02	0.1374+02	0.4643+00
0.2500+01	0.1153+02	0.4071+01	0.1203+02	0.2980+00	0.1422+02	0.1422+02	0.1422+02	0.1422+02	0.4552+00
0.2520+01	0.1179+02	0.4111+01	0.1229+02	0.2980+00	0.1463+02	0.1463+02	0.1463+02	0.1463+02	0.4531+00
0.2540+01	0.1205+02	0.4151+01	0.1255+02	0.2980+00	0.1504+02	0.1504+02	0.1504+02	0.1504+02	0.4511+00
0.2560+01	0.1231+02	0.4191+01	0.1281+02	0.2980+00	0.1545+02	0.1545+02	0.1545+02	0.1545+02	0.4491+00
0.2580+01	0.1257+02	0.4231+01	0.1311+02	0.2980+00	0.1586+02	0.1586+02	0.1586+02	0.1586+02	0.4471+00
0.2600+01	0.1283+02	0.4271+01	0.1341+02	0.2980+00	0.1627+02	0.1627+02	0.1627+02	0.1627+02	0.4451+00
0.2620+01	0.1309+02	0.4311+01	0.1371+02	0.2980+00	0.1668+02	0.1668+02	0.1668+02	0.1668+02	0.4431+00
0.2640+01	0.1335+02	0.4351+01	0.1401+02	0.2980+00	0.1709+02	0.1709+02	0.1709+02	0.1709+02	0.4411+00
0.2660+01	0.1361+02	0.4391+01	0.1431+02	0.2980+00	0.1750+02	0.1750+02	0.1750+02	0.1750+02	0.4391+00
0.2680+01	0.1387+02	0.4431+01	0.1461+02	0.2980+00	0.1791+02	0.1791+02	0.1791+02	0.1791+02	0.4371+00
0.2700+01	0.1413+02	0.4471+01	0.1491+02	0.2980+00	0.1832+02	0.1832+02	0.1832+02	0.1832+02	0.4351+00

$M$	$\frac{p_2}{p_1}$	$\frac{\rho_2}{\rho_1}$	$\frac{T_2}{T_1}$	$\frac{P_{21}}{P_{11}}$	$\frac{P_{22}}{P_{11}}$	$M_2$
0.3500 + 01	0.1412 + 02	0.4261 + 01	0.3315 + 01	0.2129 + 00	0.1624 + 02	0.4512 + 00
0.3550 + 01	0.1454 + 02	0.4296 + 01	0.3384 + 01	0.2039 + 00	0.1670 + 02	0.4492 + 00
0.3600 + 01	0.1495 + 02	0.4310 + 01	0.3454 + 01	0.1953 + 00	0.1716 + 02	0.4474 + 00
0.1650 + 01	0.1538 + 02	0.4163 + 01	0.1525 + 01	0.1871 + 00	0.1762 + 02	0.4356 + 00
0.1700 + 01	0.1580 + 02	0.4195 + 01	0.2596 + 01	0.1792 + 00	0.1810 + 02	0.4419 + 00
0.1750 + 01	0.1624 + 02	0.4426 + 01	0.3669 + 01	0.1717 + 00	0.1857 + 02	0.4423 + 00
0.3800 + 01	0.1668 + 02	0.4457 + 01	0.3743 + 01	0.1645 + 00	0.1906 + 02	0.4407 + 00
0.3850 + 01	0.1713 + 02	0.4487 + 01	0.3817 + 01	0.1576 + 00	0.1955 + 02	0.4392 + 00
0.3900 + 01	0.1758 + 02	0.4516 + 01	0.3893 + 01	0.1510 + 00	0.2005 + 02	0.4377 + 00
0.3950 + 01	0.1804 + 02	0.4544 + 01	0.3969 + 01	0.1448 + 00	0.2036 + 02	0.4363 + 00
0.4000 + 01	0.1850 + 02	0.4571 + 01	0.4047 + 01	0.1388 + 00	0.2107 + 02	0.4350 + 00
0.4050 + 01	0.1897 + 02	0.4598 + 01	0.4125 + 01	0.1330 + 00	0.2159 + 02	0.4336 + 00
0.4100 + 01	0.1944 + 02	0.4624 + 01	0.4205 + 01	0.1276 + 00	0.2211 + 02	0.4324 + 00
0.4150 + 01	0.1993 + 02	0.4650 + 01	0.4285 + 01	0.1223 + 00	0.2264 + 02	0.4311 + 00
0.4200 + 01	0.2041 + 02	0.4675 + 01	0.4367 + 01	0.1173 + 00	0.2318 + 02	0.4299 + 00
0.4250 + 01	0.2091 + 02	0.4699 + 01	0.4449 + 01	0.1126 + 00	0.2372 + 02	0.4288 + 00
0.4300 + 01	0.2140 + 02	0.4723 + 01	0.4512 + 01	0.1080 + 00	0.2427 + 02	0.4277 + 00
0.4350 + 01	0.2191 + 02	0.4746 + 01	0.4616 + 01	0.1036 + 00	0.2483 + 02	0.4266 + 00
0.4400 + 01	0.2242 + 02	0.4768 + 01	0.4702 + 01	0.9948 - 01	0.2539 + 02	0.4255 + 00
0.4450 + 01	0.2294 + 02	0.4790 + 01	0.4788 + 01	0.9950 - 01	0.2596 + 02	0.4245 + 00
0.4500 + 01	0.2346 + 02	0.4812 + 01	0.4875 + 01	0.9170 - 01	0.2654 + 02	0.4236 + 00
0.4550 + 01	0.2399 + 02	0.4833 + 01	0.4963 + 01	0.8806 - 01	0.2712 + 02	0.4226 + 00
0.4600 + 01	0.2452 + 02	0.4853 + 01	0.5032 + 01	0.8459 - 01	0.2771 + 02	0.4217 + 00
0.4650 + 01	0.2506 + 02	0.4873 + 01	0.5142 + 01	0.8126 - 01	0.2831 + 02	0.4208 + 00
0.4700 + 01	0.2560 + 02	0.4893 + 01	0.5233 + 01	0.7809 - 01	0.2891 + 02	0.4199 + 00
0.4750 + 01	0.2616 + 02	0.4912 + 01	0.5325 + 01	0.7505 - 01	0.2952 + 02	0.4191 + 00
0.4800 + 01	0.2671 + 02	0.4930 + 01	0.5418 + 01	0.7214 - 01	0.3013 + 02	0.4183 + 00
0.4850 + 01	0.2728 + 02	0.4948 + 01	0.5512 + 01	0.6936 - 01	0.3075 + 02	0.4175 + 00
0.4900 + 01	0.2784 + 02	0.4966 + 01	0.5607 + 01	0.6670 - 01	0.3118 + 02	0.4167 + 00
0.4950 + 01	0.2842 + 02	0.4983 + 01	0.5703 + 01	0.6415 - 01	0.3201 + 02	0.4160 + 00
0.5000 + 01	0.2900 + 02	0.5000 + 01	0.5800 + 01	0.6172 - 01	0.3265 + 02	0.4152 + 00
0.5100 + 01	0.3018 + 02	0.5033 + 01	0.5997 + 01	0.5715 - 01	0.3395 + 02	0.4138 + 00
0.5200 + 01	0.3138 + 02	0.5064 + 01	0.6197 + 01	0.5297 - 01	0.3528 + 02	0.4125 + 00
0.5300 + 01	0.3260 + 02	0.5093 + 01	0.6401 + 01	0.4913 - 01	0.3663 + 02	0.4113 + 00
0.5400 + 01	0.3385 + 02	0.5122 + 01	0.6610 + 01	0.4560 - 01	0.3801 + 02	0.4101 + 00
0.5500 + 01	0.3512 + 02	0.5149 + 01	0.6822 + 01	0.4236 - 01	0.3941 + 02	0.4090 + 00
0.5600 + 01	0.3642 + 02	0.5175 + 01	0.7038 + 01	0.3938 - 01	0.4084 + 02	0.4079 + 00
0.5700 + 01	0.3774 + 02	0.5200 + 01	0.7258 + 01	0.3664 - 01	0.4230 + 02	0.4069 + 00
0.5800 + 01	0.3908 + 02	0.5224 + 01	0.7481 + 01	0.3412 - 01	0.4378 + 02	0.4059 + 00
0.5900 + 01	0.4044 + 02	0.5246 + 01	0.7709 + 01	0.3180 - 01	0.4528 + 02	0.4050 + 00
0.6000 + 01	0.4183 + 02	0.5268 + 01	0.7941 + 01	0.2965 - 01	0.4682 + 02	0.4042 + 00
0.6100 + 01	0.4324 + 02	0.5289 + 01	0.8176 + 01	0.2767 - 01	0.4837 + 02	0.4033 + 00
0.6200 + 01	0.4468 + 02	0.5309 + 01	0.8415 + 01	0.2584 - 01	0.4996 + 02	0.4025 + 00
0.6300 + 01	0.4614 + 02	0.5329 + 01	0.8658 + 01	0.2416 - 01	0.5157 + 02	0.4018 + 00
0.6400 + 01	0.4762 + 02	0.5347 + 01	0.8905 + 01	0.2259 - 01	0.5320 + 02	0.4011 + 00
0.6500 + 01	0.4912 + 02	0.5363 + 01	0.9156 + 01	0.2115 - 01	0.5486 + 02	0.4004 + 00
0.6600 + 01	0.5065 + 02	0.5382 + 01	0.9411 + 01	0.1981 - 01	0.5655 + 02	0.3997 + 00
0.6700 + 01	0.5212 + 02	0.5599 + 01	0.9670 + 01	0.1857 - 01	0.5826 + 02	0.3991 + 00
0.6800 + 01	0.5378 + 02	0.5415 + 01	0.9933 + 01	0.1741 - 01	0.6000 + 02	0.3985 + 00
0.6900 + 01	0.5538 + 02	0.5430 + 01	0.1020 + 02	0.1635 - 01	0.6176 + 02	0.3979 + 00

$M$	$\frac{p_2}{p_1}$	$\frac{\rho_2}{\rho_1}$	$\frac{T_2}{T_1}$	$\frac{P_{21}}{P_{11}}$	$\frac{P_{22}}{P_{11}}$	$M_2$
0.7000 + 01	0.5700 + 02	0.5444 + 01	0.1047 + 02	0.1535 - 01	0.6355 + 02	0.3974 + 00
0.7100 + 01	0.5864 + 02	0.5659 + 01	0.1074 + 02	0.1443 - 01	0.6537 + 02	0.3968 + 00
0.7200 + 01	0.6011 + 02	0.5872 + 01	0.1102 + 02	0.1357 - 01	0.6721 + 02	0.3963 + 00
0.7300 + 01	0.6200 + 02	0.5885 + 01	0.1130 + 02	0.1277 - 01	0.6908 + 02	0.3958 + 00
0.7400 + 01	0.6372 + 02	0.5498 + 01	0.1159 + 02	0.1202 - 01	0.7097 + 02	0.3954 + 00
0.7500 + 01	0.6546 + 02	0.5510 + 01	0.1188 + 02	0.1133 - 01	0.7289 + 02	0.3949 + 00
0.7600 + 01	0.6722 + 02	0.5522 + 01	0.1217 + 02	0.1068 - 01	0.7481 + 02	0.3945 + 00
0.7700 + 01	0.6900 + 02	0.5533 + 01	0.1247 + 02	0.1008 - 01	0.7680 + 02	0.3941 + 00
0.7800 + 01	0.7080 + 02	0.5544 + 01	0.1277 + 02	0.9510 - 02	0.7880 + 02	0.3937 + 00
0.7900 + 01	0.7264 + 02	0.5555 + 01	0.1308 + 02	0.8982 - 02	0.8082 + 02	0.3933 + 00
0.8000 + 01	0.7450 + 02	0.5656 + 01	0.1339 + 02	0.8488 - 02	0.8287 + 02	0.3929 + 00
0.9000 + 01	0.9433 + 02	0.5651 + 01	0.1669 + 02	0.4964 - 02	0.1048 + 01	0.3898 + 00
0.1000 + 02	0.1165 + 03	0.5714 + 01	0.2039 + 02	0.3045 - 02	0.1292 + 03	0.3876 + 00
0.1100 + 02	0.1410 + 03	0.5762 + 01	0.2447 + 02	0.1945 - 02	0.1563 + 03	0.3859 + 00
0.1200 + 02	0.1678 + 03	0.5799 + 01	0.2894 + 02	0.1287 - 02	0.1859 + 03	0.3847 + 00
0.1300 + 02	0.1970 + 03	0.5878 + 01	0.3380 + 02	0.8771 - 03	0.2181 + 03	0.3837 + 00
0.1400 + 02	0.2285 + 03	0.5851 + 01	0.3905 + 02	0.6138 - 03	0.2528 + 03	0.3829 + 00
0.1500 + 02	0.2623 + 03	0.5870 + 01	0.4469 + 02	0.4395 - 03	0.2902 + 03	0.3823 + 00
0.1600 + 02	0.2985 + 03	0.5885 + 01	0.5072 + 02	0.3212 - 03	0.3301 + 03	0.3817 + 00
0.1700 + 02	0.3370 + 03	0.5898 + 01	0.5714 + 02	0.2390 - 03	0.3726 + 03	0.3813 + 00
0.1800 + 02	0.3778 + 03	0.5909 + 01	0.6190 + 02	0.1807 - 03	0.4176 + 03	0.3810 + 00
0.1900 + 02	0.4210 + 03	0.5918 + 01	0.7114 + 02	0.1386 - 03	0.4653 + 03	0.3806 + 00
0.2000 + 02	0.4665 + 03	0.5926 + 01	0.7872 + 02	0.1078 - 03	0.5155 + 03	0.3804 + 00
0.2200 + 02	0.5645 + 03	0.5939 + 01	0.9506 + 02	0.6741 - 04	0.6236 + 03	0.3800 + 00
0.2400 + 02	0.6718 + 03	0.5948 + 01	0.1129 + 03	0.4388 - 04	0.7421 + 03	0.3796 + 00
0.2600 + 02	0.7885 + 03	0.5956 + 01	0.1324 + 03	0.2953 - 04	0.8709 + 03	0.3794 + 00
0.2800 + 02	0.9145 + 03	0.5962 + 01	0.1534 + 03	0.2046 - 04	0.1010 + 04	0.3792 + 00
0.3000 + 02	0.1050 + 04	0.5967 + 01	0.1759 + 03	0.1453 - 04	0.1159 + 04	0.3790 + 00
0.3200 + 02	0.1194 + 04	0.5971 + 01	0.2001 + 03	0.1055 - 04	0.1319 + 04	0.3789 + 00
0.3400 + 02	0.1348 + 04	0.5974 + 01	0.2257 + 03	0.7804 - 05	0.1489 + 04	0.3788 + 00
0.3600 + 02	0.1512 + 04	0.5977 + 01	0.2529 + 03	0.5874 - 05	0.1669 + 04	0.3787 + 00
0.3800 + 02	0.1684 + 04	0.5979 + 01	0.2817 + 03	0.4488 - 05	0.1860 + 04	0.3786 + 00
0.4000 + 02	0.1856 + 04	0.5981 + 01	0.3121 + 03	0.3477 - 05	0.2061 + 04	0.3785 + 00
0.4200 + 02	0.2058 + 04	0.5983 + 01	0.3439 + 03	0.2727 - 05	0.2277 + 04	0.3785 + 00
0.4400 + 02	0.2258 + 04	0.5985 + 01	0.3774 + 03	0.2163 - 05	0.2493 + 04	0.3785 + 00
0.4600 + 02	0.2468 + 04	0.5986 + 01	0.4000 + 03	0.1669 + 04	0.3787 + 00	0.3784 + 00
0.4800 + 02	0.2688 + 04	0.5987 + 01	0.4124 + 03	0.1402 - 05	0.2967 + 04	0.3784 + 00
0.5000 + 02	0.2916 + 04	0.5988 + 01	0.4811 + 03	0.1144 - 05	0.3219 + 04	0.3784 + 00

## PRANDTL-MEYER FUNCTION AND MACH ANGLE

<i>M</i>	<i>v</i>	<i>μ</i>	<i>M</i>	<i>v</i>	<i>μ</i>
0.2700 + 01	0.4362 + 02	0.2174 + 02	0.5600 + 01	0.8203 + 02	0.1029 + 02
0.2750 + 01	0.4469 + 02	0.2132 + 02	0.5700 + 01	0.8280 + 02	0.1010 + 02
0.2800 + 01	0.4575 + 02	0.2092 + 02	0.5800 + 01	0.8354 + 02	0.9928 + 01
0.2850 + 01	0.4678 + 02	0.2054 + 02	0.5900 + 01	0.8426 + 02	0.9758 + 01
0.2900 + 01	0.4779 + 02	0.2017 + 02	0.6000 + 01	0.8496 + 02	0.9594 + 01
0.2950 + 01	0.4878 + 02	0.1981 + 02	0.6100 + 01	0.8563 + 02	0.9435 + 01
0.3000 + 01	0.4976 + 02	0.1947 + 02	0.6200 + 01	0.8629 + 02	0.9282 + 01
0.3050 + 01	0.5071 + 02	0.1914 + 02	0.6300 + 01	0.8694 + 02	0.9133 + 01
0.3100 + 01	0.5165 + 02	0.1882 + 02	0.6400 + 01	0.8756 + 02	0.8989 + 01
0.3150 + 01	0.5257 + 02	0.1851 + 02	0.6500 + 01	0.8817 + 02	0.8850 + 01
0.3200 + 01	0.5347 + 02	0.1821 + 02	0.6600 + 01	0.8876 + 02	0.8715 + 01
0.3250 + 01	0.5435 + 02	0.1792 + 02	0.6700 + 01	0.8931 + 02	0.8584 + 01
0.3300 + 01	0.5522 + 02	0.1764 + 02	0.6800 + 01	0.8989 + 02	0.8457 + 01
0.3350 + 01	0.5607 + 02	0.1737 + 02	0.6900 + 01	0.9044 + 02	0.8333 + 01
0.3400 + 01	0.5691 + 02	0.1710 + 02	0.7000 + 01	0.9097 + 02	0.8213 + 01
0.3450 + 01	0.5773 + 02	0.1685 + 02	0.7100 + 01	0.9149 + 02	0.8097 + 01
0.3500 + 01	0.5853 + 02	0.1660 + 02	0.7200 + 01	0.9200 + 02	0.7984 + 01
0.3550 + 01	0.5932 + 02	0.1636 + 02	0.7300 + 01	0.9249 + 02	0.7873 + 01
0.3600 + 01	0.6009 + 02	0.1613 + 02	0.7400 + 01	0.9297 + 02	0.7766 + 01
0.3650 + 01	0.6085 + 02	0.1590 + 02	0.7500 + 01	0.9344 + 02	0.7662 + 01
0.3700 + 01	0.6160 + 02	0.1568 + 02	0.7600 + 01	0.9390 + 02	0.7561 + 01
0.3750 + 01	0.6233 + 02	0.1547 + 02	0.7700 + 01	0.9434 + 02	0.7462 + 01
0.3800 + 01	0.6304 + 02	0.1526 + 02	0.7800 + 01	0.9478 + 02	0.7366 + 01
0.3850 + 01	0.6375 + 02	0.1505 + 02	0.7900 + 01	0.9521 + 02	0.7272 + 01
0.3900 + 01	0.6444 + 02	0.1486 + 02	0.8000 + 01	0.9562 + 02	0.7181 + 01
0.3950 + 01	0.6512 + 02	0.1466 + 02	0.9000 + 01	0.9932 + 02	0.6379 + 01
0.1120 + 01	0.1755 + 01	0.6323 + 02	0.1760 + 01	0.1956 + 02	0.1023 + 03
0.1140 + 01	0.2160 + 01	0.6131 + 02	0.1780 + 01	0.2015 + 02	0.1048 + 03
0.1160 + 01	0.2607 + 01	0.5955 + 02	0.1800 + 01	0.2073 + 02	0.1200 + 02
0.1180 + 01	0.3074 + 01	0.5794 + 02	0.1820 + 01	0.2130 + 02	0.1367 + 02
0.1200 + 01	0.3558 + 01	0.5644 + 02	0.1840 + 01	0.2188 + 02	0.1329 + 02
0.1220 + 01	0.4057 + 01	0.5505 + 02	0.1860 + 01	0.2245 + 02	0.1382 + 02
0.1240 + 01	0.4569 + 01	0.5375 + 02	0.1880 + 01	0.2320 + 02	0.1442 + 02
0.1260 + 01	0.5093 + 01	0.5253 + 02	0.1900 + 01	0.2359 + 02	0.1501 + 02
0.1280 + 01	0.5627 + 01	0.5138 + 02	0.1920 + 01	0.2415 + 02	0.1560 + 02
0.1300 + 01	0.6170 + 01	0.5028 + 02	0.1940 + 01	0.2471 + 02	0.1619 + 02
0.1320 + 01	0.6721 + 01	0.4925 + 02	0.1960 + 01	0.2527 + 02	0.1678 + 02
0.1340 + 01	0.7279 + 01	0.4827 + 02	0.1980 + 01	0.2583 + 02	0.1737 + 02
0.1360 + 01	0.7844 + 01	0.4733 + 02	0.2000 + 01	0.2638 + 02	0.1794 + 02
0.1380 + 01	0.8413 + 01	0.4644 + 02	0.2020 + 01	0.2775 + 02	0.1853 + 02
0.1400 + 01	0.8987 + 01	0.4558 + 02	0.2040 + 01	0.2910 + 02	0.1912 + 02
0.1420 + 01	0.9565 + 01	0.4477 + 02	0.2060 + 01	0.3043 + 02	0.1971 + 02
0.1440 + 01	0.1015 + 02	0.4398 + 02	0.2080 + 01	0.3173 + 02	0.2030 + 02
0.1460 + 01	0.1073 + 02	0.4323 + 02	0.2100 + 01	0.3302 + 02	0.2090 + 02
0.1480 + 01	0.1132 + 02	0.4251 + 02	0.2130 + 01	0.3428 + 02	0.2157 + 02
0.1500 + 01	0.1191 + 02	0.4181 + 02	0.2150 + 01	0.3553 + 02	0.2226 + 02
0.1520 + 01	0.1249 + 02	0.4114 + 02	0.2170 + 01	0.3675 + 02	0.2294 + 02
0.1540 + 01	0.1309 + 02	0.4049 + 02	0.2190 + 01	0.3795 + 02	0.2363 + 02
0.1560 + 01	0.1368 + 02	0.3987 + 02	0.2210 + 01	0.3912 + 02	0.2438 + 02
0.1580 + 01	0.1427 + 02	0.3927 + 02	0.2230 + 01	0.4028 + 02	0.2309 + 02
0.1600 + 01	0.1486 + 02	0.3868 + 02	0.2250 + 01	0.4141 + 02	0.2262 + 02
0.1620 + 01	0.1545 + 02	0.3812 + 02	0.2270 + 01	0.4251 + 02	0.2217 + 02

## REFERENCES

---

1. Anderson, John D., Jr.: "Gasdynamic Lasers: An Introduction," Academic Press, New York, 1976.
2. Anderson, John D., Jr.: "Introduction to Flight," McGraw-Hill Book Company, New York, 1978.
3. Durand, W. F. (ed.): "Aerodynamic Theory," vol. 1, Springer, Berlin, 1934.
4. Wylie, C. R.: "Advanced Engineering Mathematics," 4th ed., McGraw-Hill Book Company, New York, 1975.
5. Kreyzig, E.: "Advanced Engineering Mathematics," John Wiley & Sons, Inc., New York, 1962.
6. Hillebrand, F. B.: "Advanced Calculus for Applications," 2d ed., Prentice-Hall, Inc., Englewood Cliffs, N.J., 1976.
7. Anderson, D. A., J. C. Tanchill, and R. H. Pletcher: "Computational Fluid Mechanics and Heat Transfer," McGraw-Hill Book Company, New York, 1984.
8. Prandtl, L., and O. G. Tietjens: "Applied Hydro- and Aeromechanics," United Engineering Trustees, Inc., 1934; also, Dover Publications, Inc., New York, 1957.
9. Karamcheti, K.: "Principles of Ideal Fluid Aerodynamics," John Wiley & Sons, Inc., New York, 1975.
10. Prentop, P. K.: "Bringing Wings of Change," *Astronaut. Aeronaut.*, vol. 13, no. 10, pp. 20-27, October 1979.
11. Abbott, I. H., and A. E. von Doenhoff: "Theory of Wing Sections," McGraw-Hill Book Company, New York, 1949; also, Dover Publications, Inc., New York, 1959.
12. Munk, Max M.: "General Theory of Thin Wing Sections," NACA report no. 142, 1922.
13. Berlin, John J., and M. L. Smith: "Aerodynamics for Engineers," Prentice-Hall, Inc., Englewood Cliffs, N.J., 1979.
14. Hess, J. L., and A. M. O. Smith: Calculation of potential flow about arbitrary bodies, in "Progress in Aeronautical Sciences," vol. 8, D. Kuchemann (ed.), Pergammon Press, New York, pp. 1-138.
15. Chow, C. Y.: "An Introduction to Computational Fluid Dynamics," John Wiley & Sons, Inc., New York, 1979.
16. McGhee, R. J., and W. D. Basley: "Low-Speed Aerodynamic Characteristics of a 17-Percent-Thick Airfoil Section Designed for General Aviation Applications," NASA TN D-7428, December 1973.
17. McGhee, R. J., W. D. Basley, and R. T. Whitcomb: NASA low- and medium-speed airfoil development, in "Advanced Technology Airfoil Research," vol. II, NASA CP 2046, March 1980.
18. Glauert, H.: "The Elements of Aerofoil and Airscrew Theory," Cambridge University Press, London 1926.
19. Winkelmann, A. E., J. B. Barlow, S. Agrawal, J. K. Saini, J. D. Anderson, Jr., and E. Jones: "The Effects of Leading Edge Modifications on the Post-Stall Characteristics of Wings," AIAA paper no. 80-0199, American Institute of Aeronautics and Astronautics, New York, 1980.
20. Anderson, John D., Jr., Stephen Corda, and David M. Van Wie: "Numerical Lifting Line Theory Applied to Dropped Leading-Edge Wings Below and Above Stall," *J. Aircraft*, vol. 17, no. 12, December 1980, pp. 898-904.
21. Anderson, John D., Jr.: "Modern Compressible Flow: With Historical Perspective," McGraw-Hill Book Company, New York, 1982.
22. Sears, F. W.: "An Introduction to Thermodynamics. The Kinetic Theory of Gases, and Statistical Mechanics," 2d ed., Addison-Wesley Publishing Company, Inc., Reading, Mass., 1959.
23. Van Wylen, G. J., and R. E. Sonntag: "Fundamentals of Classical Thermodynamics," 2d ed., John Wiley & Sons, Inc., New York, 1973.
24. Reynolds, W. C., and H. C. Perkins: "Engineering Thermodynamics," 2d ed., McGraw-Hill Book Company, New York, 1977.
25. Shapiro, A. H.: "The Dynamics and Thermodynamics of Compressible Fluid Flow," vols. 1 and 2, The Ronald Press Company, New York, 1953.
26. Leipmann, H. W., and A. Roshko: "Elements of Gasdynamics," John Wiley & Sons, Inc., New York, 1957.
27. Tsien, H. S.: Two-Dimensional Subsonic Flow of Compressible Fluids, *J. Aeronaut. Sci.*, vol. 6, no. 10, October 1939, p. 399.
28. von Karman, T. H.: Compressibility Effects in Aerodynamics, *J. Aeronaut. Sci.*, vol. 8, no. 9, September 1941, p. 337.
29. Laitone, E. V.: New Compressibility Correction for Two-Dimensional Subsonic Flow, *J. Aeronaut. Sci.*, vol. 18, no. 5, May 1951, p. 350.
30. Stack, John, W. F. Lindsey, and R. E. Littell: "The Compressibility Burble and the Effect of Compressibility on Pressures and Forces Acting on an Airfoil," NACA report no. 646, 1938.
31. Whitcomb, R. T.: "A Study of the Zero-Lift Drag-Rise Characteristics of Wing-Body Combinations Near the Speed of Sound," NACA Report 1273, 1936.
32. Whitcomb, R. T., and L. R. Clark: "An Airfoil Shape for Efficient Flight at Supercritical Mach Numbers," NASA TMX-1109, July 1965.
33. Anderson, J. D., Jr.: Computational fluid dynamics — an engineering tool? in "Numerical/Laboratory Computer Methods in Fluid Dynamics," A. A. Pouring (ed.), ASME: New York, 1976, pp. 1-12.
34. Owczarczak, Jerzy A.: "Fundamentals of Gas Dynamics," International Textbook Company, Scranton, Pa., 1964.
35. Anderson, J. D., Jr., L. M. Albacker, and A. E. Winkelmann: "On Hyperersonic Blunt Body Flow Fields Obtained with a Time-Dependent Technique," Naval Ordnance Laboratory NOL TR 68-129, 1968.
36. Anderson, J. D., Jr.: An Engineering Survey of Radiating Shock Layers, *AIAA J.*, vol. 7, no. 9, September 1969, pp. 1665-1675.
37. Chemi, G. G.: "Introduction to Hypersonic Flow," Academic Press, New York, 1961.
38. Truitt, R. W.: "Hyperersonic Aerodynamics," The Ronald Press Company, New York, 1959.
39. Dornance, H. W.: "Viscous Hypersonic Flow," McGraw-Hill Book Company, New York, 1962.
40. Hayes, W. D., and R. F. Probstein: "Hypersonic Flow Theory," 2d ed., Academic Press, New York, 1966.
41. Vinh, N. X., A. Bussemann, and R. D. Culp: "Hypersonic and Planetary Entry Flight Mechanics," University of Michigan Press, Ann Arbor, 1980.
42. Schlichting, H.: "Boundary Layer Theory," 7th ed., McGraw-Hill Book Company, New York, 1979.
43. White, F. M.: "Viscous Fluid Flow," McGraw-Hill Book Company, New York, 1974.
44. Cebeci, T., and A. M. O. Smith: "Analysis of Turbulent Boundary Layers," Academic Press, New York, 1974.
45. Bradshaw, P., T. Cebeci, and J. Whitehead: "Engineering Calculation Methods for Turbulent Flow," Academic Press, New York, 1981.
46. Berman, H. A., J. D. Anderson, Jr., and J. P. Drummond: A Numerical Solution of the Supersonic Flow over a Rearward-Facing Step with Transverse Non-reacting Hydrogen Injection, AIAA paper no. 82-1002, American Institute of Aeronautics and Astronautics, 1982.
47. Van Driest, E. R.: Turbulent Boundary Layer in Compressible Fluids, *J. Aeronaut. Sci.*, vol. 18, no. 3, March 1951, p. 145.

# INDEX

- Ackeret, Jacob, 273, 287, 288, 434  
Adiabatic process, definition of, 292  
Adverse pressure gradient, 490  
Aerodynamic center, 192-193, 212  
Aerodynamic force, calculation of, 12-19  
Aerodynamic heating, 481, 493  
Aerodynamics, definition of, 8  
Aerodynamic twist, 237  
Airfoil:  
definition of, 186-187  
geometric properties, 187-190  
modern low-speed, 222-224  
NACA nomenclature for, 189  
supercritical, 430-433  
symmetric, 189, 204-212  
thin, theory of (*see* Thin airfoil theory)  
Airfoil Design Center (Ohio State University), 224  
Airspeed measurement:  
incompressible flow, 126-129  
subsonic compressible flow, 337-338  
supersonic flow, 338-339  
Alembert, Jean Le Rond' (*see* d'Alembert; d'Alembert's paradox)  
Allen, H. Julian, 5-6  
Angle of attack:  
definition of, 14  
effective, 232, 242  
geometric, 231  
induced, 231, 242, 246  
zero lift, 191, 215  
Archimedes principle, 33  
Area-Mach number relation, 388  
Area rule, 428-430  
Area-velocity relation, 385  
Aspect ratio, 246, 252-258
- Attack, angle of (*see* Angle of attack)  
Axial force, definition of, 8  
Axisymmetric flow, 280  
Back pressure, 395  
Becker, John V., 437  
Bernoulli, Daniel, 115, 176-180  
Bernoulli's equation, 115-118, 301  
Biot-Savart law, 235, 264  
Blasius, H., 530  
Blasius's equation, 530  
Blunt body, 5, 362-364, 470-477  
Body forces, 69  
Bound vortex, 238  
Boundary conditions, 133-135  
Boundary layer approximation, 525  
Boundary layer equations, 517, 525-528  
Boundary layer thickness, 520, 533, 538  
Boundary layers, 35, 512, 517-540  
Briggs, Lyman J., 434  
Buckingham pi theorem, 21-26  
Bulk viscosity coefficient, 500  
Buoyancy force, 32-34  
Busemann, Adolf, 273, 287, 377  
Caldwell, F. W., 434  
Calorically perfect gas, 291  
Camber, 188, 212-217  
Camber line, mean, 187  
Cartesian coordinate system, 50, 53, 55, 56  
Cayley, George, 40-41  
Center of pressure, 19-21, 40-43, 211, 216

- Centered expansion wave, 365  
 Chapman, Dean R., 450  
 Characteristic lines, 452, 454–455  
 Characteristics, method of, 451–462  
 Chemically reacting flow, 481–482  
 Choked flow, 392  
 Chord line, 188  
 Circular cylinder flow:  
     lifting, 155–164  
     non-lifting, 147–152  
 Circulation:  
     definition of, 98–100  
     around a vortex sheet, 196  
 Compatibility equations, 456–457  
 Compressibility, 22, 297–299, 322  
 Compressibility corrections, 408, 417–423  
 Compressible flow:  
     definition of, 36, 299, 328–329  
     through diffusers, 397–399  
     through nozzles, 397–397  
     through wind tunnels, 399–404  
 Compressible quasi-one-dimensional  
     flow, 377–404  
 Computational fluid dynamics, 450–477,  
     513–514  
 Computational plane, 467  
 Conduction, thermal, 492  
 Conductivity, thermal, 26, 497  
     eddy, 500  
 Continuity equation:  
     boundary layer, 527  
     derivation of, 63–68  
     normal shock, 316  
     oblique shock, 348  
 quasi-one-dimensional flow, 120, 380,  
     383  
     with substantial derivative, 87  
 Continuum flow, definition of, 34  
 Control point, 168  
 Convective derivative, 86  
 Convective heating, 482  
 Convergent-divergent duct, 386  
 Convergent-divergent nozzle (*see* Nozzle  
     flow)  
 Coordinate systems:  
     cartesian, 50, 53, 55, 56  
     cylindrical, 50–51, 53–57  
     spherical, 51–52, 54–57  
 Coordinate transformations, 51–52
- Critical Mach number, 422–426  
 Critical pressure coefficient, 424, 425  
 Critical Reynolds number, 496  
 Crocco, Arturo, 287  
 Curl of a vector:  
     cartesian coordinates, 56  
     cylindrical coordinates, 57  
     definition of, 56  
     spherical coordinates, 57  
 Cylindrical coordinate system, 50–51,  
     53–57
- Critical Mach number, 422–426  
 Critical pressure coefficient, 424, 425  
 Critical Reynolds number, 496  
 Crocco, Arturo, 287  
 Curl of a vector:  
     cartesian coordinates, 56  
     cylindrical coordinates, 57  
     definition of, 56  
     spherical coordinates, 57  
 Cylindrical coordinate system, 50–51,  
     53–57
- Drag (*Cont.*):  
     induced drag, 232–233, 243–244, 246  
     due to lift, 246  
     parasite drag, 492  
     pressure drag, 192, 233, 492  
     profile drag, 192, 233, 492  
     wave drag, 372, 444  
     Drag coefficient, definition of, 17  
     Drag-divergence Mach number, 427–428  
     Drag polar, 192  
     Dryden, Hugh, 434  
     Dynamic pressure, 17  
     Dynamic similarity, 27–29  
     Friction drag, 192, 233, 532, 537, 539
- Eddy thermal conductivity, 500  
 Eddy viscosity, 500  
 Effective angle of attack, 232, 242  
 Elliptic lift distribution, 244, 245  
 Elliptic partial differential equation, 441  
 Energy:  
     internal, 290–291  
     total, 81  
 Energy equation:  
     alternate forms, 323–328  
     boundary layer, 528  
     derivation of, 78–83  
     normal shock, 317  
     oblique shock, 350  
     quasi-one-dimensional flow, 382, 384  
     for viscous flow, 504–508
- Enthalpy, 290–291  
 total, 301
- Entropy, 293, 295
- Equation of state, 289–290
- Euler, Leonhard, 2–3  
 Euler's equations, 117, 178
- Expansion section, 461
- Expansion waves, 343–344, 364–370  
     441
- Fales, E. N., 434
- Finite control volume, 60–61
- Finite difference methods, 462–477
- Finite differences:  
     central, 464  
     forward, 463  
     backward, 463–464
- First law of thermodynamics, 292–293
- Flow (*see specific entries, for example:*):
- Incompressible flow
  - Flow separation, 35, 491
  - Flow similarity, 27–29, 508–512
  - Fluid, definition of, 7–8
  - Fluid dynamics, computational, 450–477,  
         513–514
  - Fluid element, 12, 61–62
  - strain of, 97, 499
  - Fluid statics, 29–34
  - Flux variables, 467
  - Form drag, 192, 492
  - Free molecule flow, 34
  - Free vortex, 238
  - Freestream, definition of, 13
  - Friction drag, 192, 233, 532, 537, 539
- Gas, perfect, 289–291
- Geometric angle of attack, 231
- Geometric twist, 237
- Glauert, Herman, 252, 434
- Gradient of a scalar field:  
     cartesian coordinates, 55  
     cylindrical coordinates, 55  
     definition of, 54  
     spherical coordinates, 55
- Gradient theorem, 59
- Heating:  
     aerodynamic, 481, 493  
     convective, 482  
     radiative, 482–483
- Helmholtz, Hermann, 236
- Helmholtz's vortex theorem, 237
- High temperature effects, 481–483
- Horseshoe vortex, 238
- Hydrostatic equation, 30
- Hyperbolic partial differential equation,  
     441
- Hypersonic flow, 39, 479–487
- Incompressible flow:  
     in airspeed measurement, 126–129  
     definition of, 36  
     pressure coefficient for, 130
- Incompressible quasi-one-dimensional  
     flow, 118–125

- Induced angle of attack, 231, 242, 246  
 Induced drag, 232–233, 243–244, 246  
 Initial data line, 459  
   Intermolecular force, 289  
   Internal energy, 290–291  
   Inviscid flow, definition of, 35  
   Irrational flow, definition of, 95  
   Isentropic process:  
     definition of, 292  
     equations for, 295–297  
   Jacobs, Eastman, 287, 288, 435  
   Joukowski, Nikolai E., 161, 225–226  
  
   Kármán, Theodore von, 268, 273, 287  
   Kármán-Tsien rule, 422  
   Kelvin's theorem, 202–203  
   Kinematic viscosity, 529  
   Kutta, Wilhelm, 199, 225–226  
   Kutta condition, 198–201  
   Kutta-Joukowski theorem, 161, 164–166,  
     225–226  
  
   Laitone's rule, 422  
   Laminar flow, 493  
   Lanchester, Frederick W., 224, 267–270  
   Langley, Samuel Pierpoint, 3, 41–42  
   Laplace's equation, 131–133, 277  
   Leading edge, moment coefficient about:  
     19, 211, 216  
   Lift:  
     definition of, 13  
     drag due to, 246  
   Lift coefficient:  
     definition of, 17  
     design, 189  
     for finite wings, 243  
       maximum, 191, 223  
       for thin airfoils, 210, 215  
   Lift distribution, 237–245  
   Lift slope, 190, 210  
   Lifting circular cylinder flow, 155–164  
   Lifting line, 239  
     Lifting line theory:  
       classical, 237–258  
       fundamental equation, 243  
       numerical, 258–261
- Newton's sine-squared law, 2, 485  
 No-slip condition, 490  
 Non-lifting circular cylinder flow, 147–152  
 Normal force, definition of, 13  
 Normal flow coefficient, definition of, 17  
 Normal shock wave, 313–318, 329–336  
 Normal stress, 498  
 Nozzle flow:  
     compressible flow, 377–397  
     supersonic nozzle design, 459–462  
     underexpanded, 395  
  
   Oblique shock charts, 351–352  
   Oblique shocks, 243–264  
   One-dimensional flow, 315–336  
   Over-expanded nozzle flow, 395  
  
   Panel technique, 114, 166–176, 217–222,  
     283–285  
   Parasite drag, 492  
   Pathlines, 88–90  
   Perfect gas, 289–291  
   Perturbations:  
     general, 412  
     small, 414  
   Phillips, Horatio, 187  
   Physical plane, 467  
   Pi products, 23–25  
   Pistolesi, Enrico, 287  
   Pitot-static tube, 128  
   Pitot tube, 77–78, 126–129, 336–339  
   Position vector, 50  
   Prandtl, Ludwig, 43, 186, 198, 237, 253,  
     260, 268–273, 287, 288, 377, 434,  
     517, 530  
   Prandtl-Glauert rule, 420, 435  
   Prandtl-Meyer expansion waves, 364–370  
   Prandtl-Meyer function, 368  
   Prandtl number, 26, 511, 512  
   Prandtl relation, 330  
   Prandtl's lifting-line theory, 237–258  
   Pressure:  
     back, 395  
     center of, 19–21, 40–43, 211, 216  
     definition of, 10  
     dynamic, 17  
     stagnation, 127
- Pressure (*Cont.*):  
   static, 126  
   total, 127, 304, 325  
 Pressure coefficient:  
   critical, 424, 425  
   cylinder, 151  
   definition of, 18, 129  
   for incompressible flow, 130  
   linearized, 416  
   in terms of Mach number, 415  
 Modified Newtonian, 486  
 Newtonian, 485  
 sphere, 282  
   for supersonic flow, 444  
 Pressure drag, 192, 233, 492  
 Pressure gradient, adverse, 490  
 Profile drag, 192, 233, 492  
  
   Quarter chord, moment coefficient  
     about, 191, 211, 216  
 Quasi-one-dimensional flow:  
   compressible, 377–404  
   continuity equation, 120, 380, 383  
   definition of, 119, 379  
   energy equation, 382, 384  
   incompressible, 118–125  
   momentum equation, 381, 384  
  
   Radiative heating, 482–483  
   Rayleigh-Pitot tube formula, 339  
   Reflected shock, 359–361  
   Relative wind, 13  
   Reversed flow, 491  
   Reversible process, definition of, 292  
   • Reynolds number, definition of, 25  
   critical, 496  
   Robins, Benjamin, 433  
   Rotational flow, definition of, 95  
  
   Scalar field, gradient of (*see* Gradient of  
     a scalar field)  
 Scalar product:  
   cartesian coordinates, 53  
   cylindrical coordinates, 53–54  
   definition of, 49  
   spherical coordinates, 54

## Index

- Second law of thermodynamics, 293–295  
 Second throat, 402  
 Self-similar solutions, 528–531  
 Separated flow, 35, 491  
 Shear stress, 13, 490  
 Shock detachment distance, 363  
 Shock expansion theory, 370–372  
 Shock intersection, 361–362  
 Shock reflection, 359–361  
 Shock wave:  
     detached, 354, 362–364  
     general description, 305–308  
     normal shocks, 313–318, 329–336  
     oblique shocks, 343–364  
 Similarity of flow, 27–29, 508–512  
 Similarity parameters, 27–29, 508–512  
 Sine-squared law of Newton, 2, 485  
 Sink flow, 138–141, 277–278  
 Skin friction coefficient, 18, 532, 537, 539  
 Sonic flow, definition of, 37  
 Sonic line, 364  
 Sound wave, 319  
 speed of (*see* Speed of sound)  
 Source flow, 138–141, 277–278  
 Source panel method, 166–176  
 Source sheet, 167  
 Specific heat, 26, 291  
 Speed of sound:  
     calculation of, 318–323  
     role in dimensional analysis, 22  
     Spherical coordinate system, 51–52,  
     54–57  
     Spherical flow, 280–283  
     Stack, John, 435  
     Stagnation point, 127  
     Stagnation pressure, 127  
     Stall, 35, 191  
     Starting vortex, 203–204  
     Static pressure, 126  
     Static temperature, 301  
     Stokes' theorem, 39  
     Straightening section, 461  
     Strain of a fluid element, 97, 499  
     Streamfunction:  
         definition of, 101–104  
         for doublet flow, 146  
         for lifting circular cylinder, 156  
         for non-lifting circular cylinder, 148  
         for source flow, 141
- Streamfunction (*Cont.*):  
     for uniform flow, 136  
     velocity potential, relation with,  
     106–107  
     for vortex flow, 154  
     Streamline, 12, 88–92  
     Streamtube, 91  
     Subsonic flow:  
         compressible, in airspeed  
         measurement, 337–338  
         definition of, 37  
     Substantial derivative, 83–88  
     Supercritical airfoil, 430–433  
     Supersonic flow:  
         in airspeed measurement, 338–339  
         definition of, 37–38  
     pressure coefficient for, 444  
     Supersonic nozzle design, 459–462  
     Supersonic wind tunnels, 399–404  
     Surface forces, 69  
     Surface integrals, definition of, 58  
     Sutherland's law, 498  
     Symmetric airfoil, 189, 204–212  
 Taylor, G. I., 287  
 Temperature:  
     definition of, 12  
     static, 301  
     total, 301, 303, 325  
     wall, 519  
 Temperature profile, 520  
 Thermal conduction, 492  
 Thermal conductivity, 26, 497  
 eddy, 500  
 Thermodynamics:  
     first law, 292–293  
     second law, 293–295  
 Thickness, displacement, 520–522, 533  
 Thin airfoil theory:  
     for cambered airfoil, 212–217  
     fundamental equation, 207  
     general development, 204–217  
     for symmetric airfoil, 204–212  
     Three-dimensional relieving effect, 282,  
     358  
 Throat, 120, 386, 402  
 Time-dependent technique, 451, 470–477  
 Total density, 304, 325
- Viscous interaction, 480  
 Volta Conference, 287–288, 407  
 Volume, finite control, 60–61  
 Volume integrals, definition of, 58–59  
 Von Karman, Theodore, 268, 273, 287  
 Vortex:  
     starting, 203–204  
     trailing, 230  
     wing-tip, 230–231  
 Vortex filament, 194  
 Vortex flow, 152–155  
 Vortex lattice method, 267  
 Vortex panel method, 217–222  
 Vortex sheet, 195–198  
 Vortex theorem of Helmholtz, 237  
 Vortices, types of, 238
- Wall temperature, 519  
 Washin, 237  
 Washout, 237  
 Wave angle, 347  
 Wave drag, 372, 444  
 Waves:  
     expansion, 343–344, 364–370  
     Mach waves, 346  
     Whitcomb, Richard, 223, 429, 433,  
     437–438  
     Whittle, Frank, 407  
     Wind, relative, 13  
     Wind tunnel:  
         low-speed, 123–125  
         supersonic, 399–404  
     Wing-tip vortex, 230–231  
     Wings, finite, lift coefficient for, 243  
     Wright Brothers (Wilbur and Orville),  
     345, 42–43, 112
- Yeager, Charles, 407, 441
- Viscous dissipation, 493  
 Viscous flow:  
     definition of, 35, 489  
     energy equation, 504–508  
     momentum equation, 501–504